STRUCTURAL, CORROSION INHIBITION AND BIOLOGICAL INVESTIGATIONS OF SCHIFF BASES CONTAINING SULPHUR AND THEIR METAL CHELATES

Submitted to
University of Calicut
in partial fulfillment of the requirements
for the award of the Degree of

Doctor of Philosophy
in
Chemistry

By

REEJA JOHNSON

Under the guidance of

Dr. Joby Thomas K

RESEARCH AND POSTGRADUATE DEPARTMENT OF CHEMISTRY
ST. THOMAS' COLLEGE (AUTONOMOUS)
(UNIVERSITY OF CALICUT)
THRISSUR, KERALA – 680001
AUGUST – 2021

Estd. 1889

Research and PG Department of Chemistry
ST.THOMAS COLLEGE *(Autonomous)*
THRISSUR - 680 001, KERALA, INDIA
(Affiliated to University of Calicut, NAAC with 'A' Grade and College with Potential for Excellence)
Web:- http://stthomas.ac.in
Email:- stcthrissur@gmail.com
Phone:- +91 487 2420435
Fax:- +91 487 2421510

Dr. JOBY THOMAS K. M.Sc., M.Phil., MBA, Ph.D
Retired Vice Principal & HOD

24-11-2021

CERTIFICATE

*I hereby certify that, this is the revised version of the thesis entitled "**Structural, corrosion inhibition and biological investigations of Schiff bases containing sulphur and their metal chelates**" submitted by **Ms. REEJA JOHNSON** under my guidance after incorporating the necessary corrections/suggestions made by the adjudicators. Also certify that the contents in the thesis and the soft copy are one and the same.*

Dr. Joby Thomas. K
(Supervising Teacher)

Estd. 1889

Research and PG Department of Chemistry
ST.THOMAS COLLEGE *(Autonomous)*
THRISSUR - 680 001, KERALA, INDIA
(Affiliated to University of Calicut, NAAC with 'A' Grade and College with Potential for Excellence)
Web:- http://stthomas.ac.in Email:- stcthrissur@gmail.com
Phone:- +91 487 2420435 Fax:- +91 487 2421510

Dr. JOBY THOMAS K. M.Sc., M.Phil., MBA, Ph.D
Retired Vice Principal & HOD

05-08-2021

CERTIFICATE

*This is to certify that the thesis entitled "**Structural, corrosion inhibition and biological investigations of Schiff bases containing sulphur and their metal chelates**" is an authentic record of research work carried out by **Ms. REEJA JOHNSON** under my supervision in partial fulfillment of the requirements for the degree of Doctor of Philosophy in Chemistry of University of Calicut and further that no part thereof has been presented before for any other degree.*

Dr. Joby Thomas. K
(Supervising Teacher)

DECLARATION

I hereby declare that the thesis entitled, **"Structural, corrosion inhibition and biological investigations of Schiff bases containing sulphur and their metal chelates",** submitted to the University of Calicut in partial fulfillment of the requirements for the award of the Degree of Doctor of Philosophy in Chemistry is a bonafide research work done by me under the supervision and guidance of Dr. Joby Thomas. K, Retired Vice Principal & Head, Department of Chemistry, St. Thomas' College (Autonomous), Thrissur, Kerala.

I further declare that this thesis has not previously formed the basis of any degree, diploma or any other similar title.

05-08-2021

REEJA JOHNSON

ACKNOWLEDGEMENT

First of all I thank God Almighty, for His showers of blessing throughout my research to complete the work successfully. I would also like to express my deep and sincere gratitude to my Research Supervisor and my Mentor Dr. Joby Thomas K for giving me the opportunity to do research and providing invaluable guidance throughout this research. I would always cherish this experience in the rest of my life and it was a great privilege and honour to work and study under his guidance.

I recall at this juncture with reverence, my parents Mr. Stanley Johnson M.M (Late), Mrs Rosy Stanley and my sister Mrs. Reji Denny whose selfless sacrificial life, great efforts with pain and tears, unceasing prayers and immense concern, established me make this thesis possible.

The support rendered by the St. Thomas College Team – Rev. Dr. Martin Kolambrath, Principal, Dr. Joy K. L, Dr. Jenson P. O and Dr. Ignatius Antony, former Principals, all the faculty members of the Chemistry Department, especially Dr. Joshy C.L (HoD), Dr. C.V Jose, Dr. Joy Anto, Dr. Babu Joseph and Lab Assistants and Office Staffs has been really high. They served as a lighthouse in my journey towards the completion of this voyage.

I would like to express my sincere gratitude to the support and help rendered by my seniors Dr. Vinod P. Raphael, Dr. Shaju K.S, Dr. Nimmy Kuriakose and Dr. Aby Paul. Special thanks to Dr. Vinod P. Raphael for his constant guidance and support which helped me a lot during the entire research period.

The support and help rendered by my research colleagues Dr. Sini, Dr. Ragi, Dr. Binsi, Vidhya, Ramesh, Dr. Dinoop, Anju, Martin, Savitha, Dr. Sr. Jisha, Raji, Cinu, Memcy, Swathy, Rohini, Dr. Drishya, Aji, Siji, Nithya and Neera, helped me a lot in completing this thesis, they sincerely worked as a unit. Really it was an honour to work with them.

A memorable support in the completion of this work came from the former Bursar of St. Thomas College, Thrissur, Rev. Dr. Martin Kolambrath, Right from arranging the infrastructure and in providing a well equipped laboratory were the real turning point in my work which saved a lot of time and money.

The help given by the Biotechnology lab of St. Joseph College, Irinjalakuda was really appreciable. I would like to express my sincere thanks to Naijil George and Kavya for the successful completion of the antimicrobial studies.

I hereby acknowledge the help rendered by the STIC-CUSAT, NIT Calicut and Mr. Vishnu of IISER Trivandrum in analysing the compounds, which were really worthwhile to mention. I would like express huge, warm thanks to Fredy Francis, National Tsing Hua University, Taiwan whose brotherly concern supported me in various stages of my research work.

It is my fortune to grateful express the support of some special friends who are special in my life and shaped me to the present stage

I also thank the staff of CHMK Library of Calicut University for helping me frame a smooth bibliography.

Last but not the least, I sincerely thank the hard work of Mr. M. I. Pauly of Educare, Thrissur who did the DTP work for this project.

I have no valuable words to express my thanks, but my heart is still full of the favours received from every person.

Reeja johnson

Dedicated to

My Parents

I am forever grateful and indebted to them for their parental guidance, patience, caring, and prayers which is the reason for what I have become today.

PREFACE

Schiff bases are a class of compounds which have profound use as ligands as well as in the form of complexes. The versatile use of Schiff bases is due to its ability to coordinate to the metal ions via the azomethine nitrogen. Multidentate Schiff base ligands and their coordination with metals attract much attention because of their biological relevance. Heterocyclic Schiff bases have wide application in therapeutic fields either as potential drug or diagnostic probes and also in analytical tools. Since the polarizability of lone pairs on the sulphur atom is high one can expect an escalated chance for the chelation and other related properties. Heterocyclic ligands especially 'S' containing Schiff bases have wide application in therapeutic fields either as potential drug or diagnostic probes and also in analytical tools. Checking the chelating ability of the newly synthesized sulphur compounds may lead to open a new series of novel metal complexes which may have some pharmacological activity. To ensure the drug ability of the newly synthesized organic molecules and their metal chelates, it is decided to conduct the molecular docking studies and antimicrobial studies.

The presence of heteroatoms in such ligands gives them excellent characteristics like corrosion inhibition property. Till now, several review articles have been published depicting elaborately the application of P, N and O atoms; but, a thorough literature survey revealed that corrosion inhibition studies of organic molecules bearing sulphur atoms are scarce. Sulphur containing compounds are greatly preferred for preventing metallic dissolution due to the high polarisability of the sulphur atom. So the present investigation is intended to realize novel potential sulphur containing Schiff base ligands.

During the present course of study seven novel 'S' containing Schiff base ligands and their transition metal complexes were prepared and characterized. Molecular

docking studies of these potential 'S' containing heterocyclic Schiff bases were conducted. Antimicrobial studies on the metal chelates and corrosion inhibition capacity of the newly synthesized Schiff bases have been carried out in different acid media. For convenience and better understanding, the entire work has been presented in this thesis as three parts.

In the first part of the thesis, seven novel heterocyclic Schiff bases namely (E)-(N-anthracene-9-ylmethylene)-5-(4-nitrophenyl)-1,3,4-thiadiazol-2-amine (A9CNPTDA), N-(anthracen-9(10H)-ylidene)-5-(4-nitrophenyl)-1,3,4-thiadiazol-2-amine (ANNPTDA), (E)-5-(4-nitrophenyl)-N-((pyridine-2-yl)methylene)-1,3,4-thiadia zol-2-amine (P2CNPTDA), (E)-5-(4-nitrophenyl)-N-(1(pyridine-3-yl)ethylidene)-1,3,4-thiadiazol-2-amine (3APNPTDA), (E)-5-(4-nitrophenyl)-N-(1(pyridin-2-yl) ethylidene)-1,3,4-thiadiazol-2-amine (2APNPTDA), N-((1H-indol-3-yl)methylene) thiazol-2-amine (I3A2AT) and (13E)-N1,N2-bis((thiophene-2-yl)methylene)cyclohexane-1,2-diamine (T2CDACH) were synthesized and characterized by different techniques like CHNS analysis and spectral studies such as FTIR, UV-visible, Mass, NMR etc. The chelating abilities of these Schiff bases were investigated by synthesizing a number of transition metal complexes. Elemental analysis shows that majority of the metal complexes obey 1:1 stoichiometry between the metal and ligand. Then these complexes were also subjected to characterization studies by elemental analysis, magnetic moment measurements, molar conductance studies and spectral analysis.

This part is divided into five chapters. The first chapter includes details of literature survey and the scope of present investigation. Various physicochemical methods employed for the elucidation of the structures of the Schiff bases and their metal chelates are discussed in chapter 2. Details of synthesis and characterization of two novel sulphur containing polynuclear derivatives of Schiff bases, (E)-(N-anthracene-9-yl

methylene)-5-(4-nitrophenyl)-1,3,4-thiadiazol-2-amine (A9CNPTDA) and N-(anthracen-9(10H)-ylidene)-5-(4-nitrophenyl)-1,3,4-thiadiazol-2-amine (ANNPTDA), and their transition metal complexes are presented in the chapters 3. Synthesis and characterization of thiadiazole based pyridine derivatives of Schiff bases, (E)-5-(4-nitrophenyl)-N-((pyridine-2-yl)methylene)-1,3,4-thiadiazol-2-amine (P2CNPTDA), (E)-5-(4-nitrophenyl) -N-(1(pyridine-3-yl)ethylidene)-1,3,4-thiadiazol-2-amine (3APNPTDA), (E)-5-(4-nitro phenyl)-N-(1(pyridin-2-yl)ethylidene)-1,3,4-thiadiazol-2-amine (2APNPTDA) are explained in chapter 4. Preparation and physicochemical properties on Schiff base derived from indole-3-carbaldehyde and thiophene 2-carbaldehyde and their transition metal chelates are explained in chapter 5. This part ends with a brief summary and references.

Second part of thesis mainly focused on the biological investigations. The studies were extended to the computational evaluation of the drug ability of the newly synthesized 'S' containing Schiff bases on the target proteins like SARS-CoV-2 Main protease (PDB code: **6lu7**) causing COVID-19, HIV-1 protease (PDB code: **1mui**) causing HIV/AIDS, HER2 protease (PDB code: **3rcd**) responsible for Breast cancer, and Human acetylcholine esterase (AChE) (PDB code:**1b41**) causing Alzheimer's disease and the ligands were ranked on the binding score with these target proteins (Molecular docking studies). *In vitro* antibacterial studies of transition metal chelates of these 'S' containing Schiff bases were also conducted. The drug-likeness (Bioavailability) of these ligands were also to be checked using Lipinski rule of five.

This part is divided into four chapters. The first chapter in this part (chapter 6) includes details of literature survey and the scope of present investigation. The method employed for *in silico* molecular docking studies and *in vitro* antibacterial studies of these novel ligands and its transition metal complexes are discussed in chapter 7. In the 8th

chapter, antibacterial performances of these 'S' containing Schiff base ligands and their transition metal complexes were explored against five clinically important pathogens such as *staphylococcus aureus, Bacillus subtilis, Escherichia coli, Proteus vulgaris and Klebsiella pneumonia. T*he results generated of these synthesized Schiff base ligands and their transition metal complexes were compared with the antibacterial data obtained for standard antibiotics Vancomycin, Erythromycin, Chloramphenicol, Streptomycin, Tetracycline, Ampicillin and Gentamicin.

In the ninth chapter, attention was made to focus on newly synthesized' S' containing Schiff bases docked into the active binding cavity of the main proteases accessed from RCSB Protein Data Bank (**PDB codes**: **6lu7, 1mui**, **3rcd**, **1b41**) leading to diseases like Covid-19, HIV, Breast cancer and Alzheimer's respectively. The drug likeness (Bioavailability) of these ligands were also checked using Lipinski rule of five. All the results are briefly summarized at the end of this part followed by references.

Part III deals with the detailed investigations of the corrosion inhibition capacity of these newly synthesized 'S' containing Schiff bases on carbon steel in hydrochloric acid and sulphuric acid media. The corrosion inhibition studies were carried out with conventional gravimetric method and electrochemical methods such as electrochemical impedance spectroscopy (EIS), potentiodynamic polarization studies and electrochemical noise measurements. Surface morphological analysis and quantum chemical parameters were also studied. In the polarization analysis, Tafel extrapolation method and Linear polarization method were performed separately. Both Nyquist plot and Bode plot analysis were utilized to get much density on the inhibitory action of the novel Schiff bases by EIS method. Adsorption isotherms were plotted from the results of gravimetric weight loss studies in order to predict the mechanism of corrosion inhibition by the Schiff bases. In order to establish the nature of inhibitor adsorption on carbon steel surface,

thermodynamic parameters like free energy of adsorption and adsorption equilibrium constant were determined and interpreted. Weight loss method was followed to compare the inhibition efficiencies of Schiff bases and their respective parent amines in acid medium. Corrosion studies clearly established that all the studied Schiff bases were excellent corrosion inhibitors on carbon steel in hydrochloric acid medium. Generally the corrosion inhibition efficiency was relatively less in H_2SO_4 medium which may be due to the aggressive nature of sulphuric acid towards CS corrosion. Surface morphological analysis was also conducted to establish the mechanism of corrosion inhibition of these inhibitors. Energy difference of HOMO and LUMO, number of electrons transferred, electronegativity, chemical hardness, and so forth were evaluated by quantum chemical studies.

This part is comprised of four chapters. Chapter 10 details the different aspects of corrosion and corrosion inhibitors. A report of thorough literature survey on corrosion inhibition studies and the scope of the present study are also included in this chapter. The details of different corrosion monitoring techniques such as Conventional gravimetric studies, Electrochemical studies, Quantum chemical studies, Temperature studies, Surface morphological studies are discussed in chapter 11. Results and discussion of corrosion inhibition investigations of the newly synthesized Schiff bases in different acid media, 1M HCl and 0.5M H_2SO_4 have been reported well in chapter 12 and chapter 13 respectively. The quantum chemical studies were also included. Carbon Steel specimens were employed to investigate corrosion inhibitory power of the synthesized Schiff bases. A brief summary of the corrosion studies along with the references are followed thereafter.

LIST OF ABBREVIATIONS

NPTDA	5-(4-nitrophenyl)-1,3,4-thiadiazol-2-amine
A9CNPTDA	(E)-(N-anthracene-9-ylmethylene)-5-(4-nitrophenyl)-1,3,4-thiadiazol-2-amine
ANNPTDA	N-(anthracen-9(10H)-ylidene)-5-(4-nitrophenyl)-1,3,4-thiadiazol-2-amine
P2CNPTDA	(E)-5-(4-nitrophenyl)-N-((pyridine-2-yl)methylene)-1,3,4-thiadiazol-2-amine
3APNPTDA	(E)-5-(4-nitrophenyl)-N-(1(pyridine-3-yl)ethylidene)-1,3,4-thiadiazol-2-amine
2APNPTDA	(E)-5-(4-nitrophenyl)-N-(1(pyridin-2-yl)ethylidene)-1,3,4-thiadiazol-2-amine
I3A2AT	N-((1H-indol-3-yl)methylene)thiazol-2amine
T2CDACH	(13E)-N1,N2-bis((thiophene-2-yl)methylene)cyclohexane-1,2-diamine
A9C	Anthracene 9-carbaldehyde
AN	Anthrone
P2C	Pyridine-2-carbaldehyde
3ACP	3-acetylpyridine
2ACP	2-acetylpyridine
I3A	Indole-3-carbaldehyde
2AT	2-Aminothiazole
T2C	Thiophene-2-carbaldehyde
DMSO	Dimethyl sulphoxide
L	Ligand moiety in the complex
M	Central metal ion in the complex
BM	Bohr magneton
EDTA	Ethylenediaminetetraacetic acid
Ac	Acetate part in the complex
BM	Bohr magneton
UV-Vis	Ultraviolet-visible
FTIR	Fourier-transform infrared
NMR	Nuclear magnetic resonance
PDB	Protein data bank
MHA	Mueller-Hinton agar
CS	Carbon steel
EIS	Electrochemical impedance spectroscopy
PDP	Potentiodynamic polarization
SCE	Saturated calomel electrode
OCP	Open circuit potential
CPE	Constant phase element

ECN	Electrochemical noise
PSD	Power spectral density
FFT	Fast Fourier transform
MEM	Maximum entropy method
DFT	Density functional theory
SEM	Scanning electron microscopy
HOMO	Highest occupied molecular orbital
LUMO	Lowest unoccupied molecular orbital
HSAB	Hard and soft acid and base

ABSTRACT

Schiff bases containing heteroatoms and their metal complexes have found multidimensional applications in various fields. Researchers had investigated the biological importance of heterocyclic derivatives of the Schiff bases and their impressive biological activities attributed to the presence of aromatic ring containing heteroatoms such as nitrogen, sulphur and oxygen. Since the polarizability of lone pairs on the sulphur atom is high one can expect an escalated chance for the chelation and other related properties. Here novel potential 'S' containing Schiff bases were synthesized and characterized. Checking the chelating ability of the newly synthesized sulphur compounds lead to open a new series of novel metal complexes which have some pharmacological activity. Here evaluated the biological activities of Schiff bases and their metal chelates and computational studies ensure the druggability of these newly synthesized compounds using Lipinski's rule. The antimicrobial activity analysis, *in silico* molecular docking studies and evaluation of corrosion inhibition efficiency of these potential compounds were explored in this thesis. The entire work is presented in this thesis as three parts.

In the first part, seven novel 'S' containing Schiff bases were synthesized and characterized using elemental analysis and spectral studies such as FTIR, UV-Vis, NMR (^{1}H and ^{13}C) and Mass spectroscopy. The chelating ability of these Schiff bases were proved by synthesizing various transition metal complexes. Elemental (CHNS) analysis, FTIR and UV-Vis spectroscopy, magnetic moment measurements, estimation of metal content and molar conductance studies were employed for the characterization of the complexes. 1:1 stoichiometry exists between metal and ligand in almost all complexes except few.

In the second part antibacterial activity of these novel heterocyclic ligands and their transition metal complexes were analysed against bacterial strains such as *Staphylococcus aureus*, *Bacillus subtilis*, *Escherichia coli, Proteus vulgaris* and *Klebsiella pneumonia*. Disc diffusion method is employed for the antibacterial screening. All the compounds have appreciable growth inhibitory power on comparing with the activity of the standard drugs. As a preliminary test Lipinski rule of five was evaluated to check the drug ability of the molecule. The studies were extended to the computational evaluation of the drug ability of the newly synthesized 'S' containing Schiff bases on the target proteins like SARS CoV-2 main protease (PDB code: **6lu7**) causing COVID-19, HIV-1 protease (PDB code: **1mui**) causing HIV/AIDS, HER2 protease (PDB code: **3rcd**) responsible for Breast cancer and Human acetylcholinesterase (AChE) (PDB code: **1b41**) causing Alzheimer's disease.

The corrosion inhibition efficiency of these novel sulphur containing Schiff bases on carbon steel in 1M HCl and 0.5M H_2SO_4 was also evaluated. The corrosion monitoring techniques employed for the analysis include weight loss, electrochemical impedance spectroscopy (EIS), potentiodynamic polarization studies and electrochemical noise measurements. Adsorption and surface morphological studies were also carried out to determine the mechanism of adsorption. Thermodynamic parameters of corrosion on carbon steel were determined based on temperature studies at varied temperatures 301, 313, 323 and 333K. Quantum chemical studies followed evaluation and optimization of geometries of these inhibitors were carried out using DFT method.

LIST OF CONTENTS

CHAPTER	TITLE	PAGE NO.
PART I SYNTHESIS AND CHARACTERIZATION		
CHAPTER 1	**INTRODUCTION AND REVIEW**	**1**
	Sulphur Compounds - An Outlook	1
	Sulphur Heterocycles	2
	Schiff Base Ligands	3
	Transition Metal Complexes	5
	Schiff base Complexes	6
	Transition Metal Complexes of Schiff Bases - A Review	11
	Sulphur Containing Schiff Bases and Their Transition Metal Complexes: A Review	16
	Schiff Bases Derived From Polynuclear Carbonyl Compounds and its Transition Metal Complexes: A Review	20
	Schiff Bases Derived From Pyridine Derivatives and its Transition Metal Complexes: A Review	21
	Schiff Bases Derived From Indole and its Transition Metal Complexes: A Review	23
	Scope and Objectives of Present Investigations	25
CHAPTER 2	**MATERIALS AND METHODS**	**27**
CHAPTER 3	**TRANSITION METAL COMPLEXES OF SCHIFF BASES DERIVED FROM 5-(4-NITROPHENYL)-1,3,4 -THIADIAZOL-2-AMINE (NPTDA) AND POLY NUCLEAR CARBONYL COMPOUNDS**	**32**
	Synthesis of 5-(4-nitrophenyl)-1,3,4-thiadiazol-2-amine (NPTDA)	33
	Characterization of Parent Amine (NPTDA)	33
SECTION I	***STUDIES ON SCHIFF BASE, (E)-N-(ANTHRACEN-9-YLMETHYLENE)-5-(4-NITROPHENYL)-1,3,4-THIA DIAZOL-2-AMINE (A9CNPTDA) AND ITS TRANSITION METAL COMPLEXES***	**36**
	Synthesis of A9CNPTDA	36
	Characterization of A9CNPTDA	37
	Synthesis of Complexes	41
	Characterization of Complexes	41
SECTION II	***STUDIES ON SCHIFF BASE, N-(ANTHRACEN-10 (9H)-YLIDENE)-5-(4-NITROPHENYL)-1,3,4-THIA DIAZOL-2-AMINE (ANNPTDA) AND ITS TRANSITION METAL COMPLEXES***	**48**
	Synthesis of ANNPTDA	48
	Characterization of ANNPTDA	48
	Synthesis of Complexes	52

	Characterization of Complexes	53
CHAPTER 4	**TRANSITION METAL COMPLEXES OF SCHIFF BASES DERIVED FROM 5-(4-NITROPHENYL)-1,3,4-THIADIAZOL-2-AMINE (NPTDA) AND CARBONYL COMPOUNDS WITH PYRIDINE RING**	**59**
SECTION I	***STUDIES ON SCHIFF BASE,(E)-5-(4-NITRO PHENYL)-N-((PYRIDINE-2-YL)METHYLENE)-1,3,4-THIADIAZOL-2AMINE (P2CNPTDA) AND ITS TRANSITION METAL COMPLEXES***	**60**
	Synthesis of P2CNPTDA	60
	Characterisation of P2CNPTDA	61
	Synthesis of Complexes	64
	Characterisation of Complexes	64
SECTION II	***STUDIES ON SCHIFF BASE (E)-5-(4-NITRO PHENYL)-N-(1(PYRIDINE-3-YL)ETHYLIDENE)-1,3,4-THIADIAZOL-2-AMINE (3APNPTDA) AND ITS TRANSITION METAL COMPLEXES***	**70**
	Synthesis of 3APNPTDA	70
	Characterisation of 3APNPTDA	71
	Synthesis of Complexes	74
	Characterisation of Complexes	74
SECTION III	***STUDIES ON SCHIFF BASE (E)-5-(4-NITRO PHENYL)-N-(1(PYRIDIN-2-YL)ETHYLIDENE)-1,3,4-THIADIAZOL-2-AMINE (2APNPTDA) AND ITS TRANSITION METAL COMPLEXES***	**80**
	Synthesis of 2APNPTDA	80
	Characterisation of 2APNPTDA	80
	Synthesis of Complexes	84
	Characterisation of Complexes	84
CHAPTER 5	**TRANSITION METAL COMPLEXES OF SCHIFF BASES DERIVED FROM INDOLE-3-CARBALDEHYDE AND THIOPHENE-2-CARBALDEHYDE**	**90**
SECTION I	***STUDIES ON SCHIFF BASE, N-((1H-INDOL-3-YL) METHYLENE)THIAZOL-2-AMINE (I3A2AT) AND ITS TRANSITION METAL COMPLEXES***	**91**
	Synthesis of I3A2AT	91
	Characterization of I3A2AT	92
	Synthesis of Complexes	95
	Characterization of Complexes	96
SECTION II	***STUDIES ON SCHIFF BASE, (13E)-N1,N2-BIS((THIO PHENE-2-YL)METHYLENE)CYCLOHEXANE-1,2-DIAMINE (T2CDACH) AND ITS TRANSITION METAL COMPLEXES***	**102**
	Synthesis of T2CDACH	102

	Characterization of T2CDACH	103
	Synthesis of Complexes	106
	Characterization of Complexes	107
	SUMMARY	**113**
	REFERENCES	**118**
PART II BIOLOGICAL STUDIES		
CHAPTER 6	**INTRODUCTION AND REVIEW**	**127**
	Pharmacological Properties of Schiff Bases	127
	Antibacterial Studies	129
	Important Pathogens	129
	Metal Complexes in Pharmacology	136
	Metal Chelates Containing Schiff Bases as Antibacterial Agents - A Review	136
	Sulphur Containing Schiff Base Complexes as Antibacterial agent - A Review	140
	Mechanism of Action of Antibiotics in Microbial Cell	143
	Molecular Docking Aided Drug Discovery (*In Silico* Studies)	144
	Molecular Docking – A Review	147
	Scope and Objectives of Present Investigation	149
CHAPTER 7	**MATERIALS AND METHODS**	**151**
CHAPTER 8	***IN VITRO* ANTIBACTERIAL STUDIES ON SULPHUR CONTAINING SCHIFF BASES AND THEIR METAL COMPLEXES**	**162**
	In vitro Antibacterial Studies of A9CNPTDA and its Transition Metal Chelates	162
	In vitro Antibacterial Studies of P2CNPTDA and its Transition Metal Chelates	164
	In vitro Antibacterial Studies of 3APNPTDA and its Transition Metal Chelates	165
	In vitro Antibacterial Studies of 2APNPTDA and its Transition Metal Chelates	165
	In vitro Antibacterial Studies of ANNPTDA and its Transition Metal Complexes	166
	In vitro Antibacterial Studies of I3A2AT and its Transition Metal Chelates	166
	In vitro Antibacterial Studies of T2CDACH and its Transition Metal Chelates	167
CHAPTER 9	***IN SILICO* MOLECULAR DOCKING STUDIES ON SULPHUR CONTAINING SCHIFF BASES**	**180**
	Druglikeness and Toxicity of Schiff Bases	180
SECTION I	***MOLECULAR DOCKING STUDIES OF SARS-CoV-2 MAIN PROTEASE (COVID-19) WITH SULPHUR CONTAINING SCHIFF BASES***	**182**
	A9CNPTDA-**6lu7** Complex	182
	P2CNPTDA-**6lu7** Complex	183
	3APNPTDA-**6lu7** Complex	184

	2APNPTDA-**6lu7** Complex	184
	ANNPTDA-**6lu7** Complex	185
	I3A2AT-**6lu7** Complex	186
	T2CDACH-**6lu7** Complex	187
SECTION II	***MOLECULAR DOCKING STUDIES OF HIV-1 PROTEASE (HIV/AIDS) WITH SULPHUR CONTAINING SCHIFF BASES***	**190**
	A9CNPTDA-**1mui** Complex	191
	P2CNPTDA-**1mui** Complex	192
	3APNPTDA-**1mui** Complex	193
	2APNPTDA-**1mui** Complex	193
	ANNPTDA-**1mui** Complex	194
	I3A2AT-**1mui** Complex	195
	T2CDACH-**1mui** Complex	196
SECTION III	***MOLECULAR DOCKING STUDIES OF HER2 PROTEASE (BREAST CANCER) WITH SULPHUR CONTAINING SCHIFF BASES***	**198**
	A9CNPTDA-**3rcd** Complex	198
	P2CNPTDA-**3rcd** Complex	199
	3APNPTDA-**3rcd** Complex	200
	2APNPTDA-**3rcd** Complex	200
	ANNPTDA-**3rcd** Complex	201
	I3A2AT-**3rcd** Complex	202
	T2CDACH-**3rcd** Complex	202
SECTION IV	***MOLECULAR DOCKING STUDIES OF ACETYL CHOLINESTERASE (ALZHEIMER'S DISEASE) WITH SULPHUR CONTAINING SCHIFF BASES***	**205**
	A9CNPTDA-**1b41** Complex	205
	P2CNPTDA-**1b41** Complex	206
	3APNPTDA-**1b41** Complex	207
	2APNPTDA-**1b41** Complex	207
	ANNPTDA-**1b41** Complex	208
	I3A2AT-**1b41** Complex	209
	T2CDACH-**1b41** Complex	210
	SUMMARY	**212**
	REFERENCES	**216**
PART III CORROSION INHIBITION STUDIES		
CHAPTER 10	**INTRODUCTION AND REVIEW**	**221**
	Factors Responsible for Corrosion	225
	Types of Corrosion	225
	Prevention of Corrosion	229
	Schiff Base Corrosion Inhibitors - A Review	233
	Heterocyclic Schiff Base Inhibitors- A Review	237
	Sulphur Containing Schiff Base Inhibitors-A Review	240
	Polynuclear Schiff Base Inhibitors– A Review	242
	Pyridine Derivatives of Schiff Base Inhibitors- A Review	243
	Indole Derivatives of Schiff Base Inhibitors- A Review	246

	Scope and Objective of Present Investigation	248
CHAPTER 11	**MATERIALS AND METHODS**	**251**
CHAPTER 12	**CORROSION INHIBITION STUDIES OF SULPHUR CONTAINING SCHIFF BASES ON CARBON STEEL IN 1M HCl**	**268**
	Gravimetric Weight Loss Investigations	268
	Comparison of Corrosion Inhibition Efficiencies of Schiff Bases with their parent compounds	276
	Adsorption Isotherms	277
	Impact of Temperature	280
	Surface Morphological Investigations	285
	Electrochemical Impedance Spectroscopic Studies (EIS)	286
	Potentiodynamic Polarization Studies	292
	Mechanism of Inhibition	297
	Electrochemical Noise Studies	299
	Quantum Chemical Studies	303
CHAPTER 13	**CORROSION INHIBITION STUDIES OF SULPHUR CONTAINING SCHIFF BASES ON CARBON STEEL IN 0.5M H_2SO_4**	**308**
	Gravimetric Weight Loss Measurements	308
	Adsorption Isotherms	312
	Surface Morphological Investigations	314
	Electrochemical Impedance Spectroscopic Studies (EIS)	315
	Potentiodynamic Polarization Studies	321
	SUMMARY	**328**
	REFERENCES	**332**
LIST OF PUBLICATIONS AND CONFERENCE PAPERS		**343**

LIST OF TABLES

TABLE No.	TITLE	PAGE No.
PART I SYNTHESIS AND CHARACTERIZATION		
1.1	^{1}H NMR and ^{13}C NMR spectral data of A9CNPTDA	39
1.2	Electronic spectral data of parent amine (NPTDA), Schiff base (A9CNPTDA) and its transition metal complexes	42
1.3	Microanalytical, magnetic and conductance data of the ligand A9CNPTDA and its transition metal complexes	45
1.4	Characteristic infrared absorption frequencies (cm^{-1}) of A9CNPTDA and its transition metal complexes	46
1.5	Electronic spectral data of Schiff base, ANNPTDA and its transition metal complexes	53
1.6	Microanalytical, magnetic and conductance data of the ligand ANNPTDA and its transition metal complexes	56
1.7	Characteristic infrared absorption frequencies (cm^{-1}) of ANNPTDA and its transition metal complexes	57
1.8	Electronic spectral data of Schiff base, P2CNPTDA and its transition metal complexes	65
1.9	Microanalytical, magnetic and conductance data of the ligand P2CNPTDA and its transition metal complexes	67
1.10	Characteristic infrared absorption frequencies (cm^{-1}) of P2CNPTDA and its transition metal complexes	68
1.11	Electronic spectral data of Schiff base, 3APNPTDA and its transition metal complexes	74
1.12	Microanalytical, magnetic and conductance data of the ligand 3APNPTDA and its transition metal complexes	77
1.13	Characteristic infrared absorption frequencies (cm^{-1}) of 3APNPTDA and its transition metal complexes	78
1.14	Electronic spectral data of Schiff base, 2APNPTDA and its transition metal complexes	85
1.15	Microanalytical, magnetic and conductance data of the ligand 2APNPTDA and its transition metal complexes	87
1.16	Characteristic infrared absorption frequencies (cm^{-1}) of 2APNPTDA and its transition metal complexes	88
1.17	Electronic spectral data of Schiff base, I3A2AT and its transition metal complexes	96
1.18	Microanalytical, magnetic and conductance data of the ligand I3A2AT and its transition metal complexes	99

1.19	Characteristic infrared absorption frequencies (cm^{-1}) of I3A2AT and its transition metal complexes	100
1.20	^{1}H NMR and ^{13}C NMR spectral data of T2CDACH	105
1.21	Electronic spectral data of Schiff base T2CDACH and its transition metal complexes	107
1.22	Microanalytical, magnetic and conductance data of the ligand T2CDACH and its transition metal complexes	110
1.23	Characteristic infrared absorption frequencies (cm^{-1}) of T2CDACH and its transition metal complexes	111
PART II BIOLOGICAL STUDIES		
2.1	Crystallographic features of proteins	161
2.2	Antibacterial activity of standard antibiotics and the solvent DMSO	172
2.3	Antibacterial activity of 'S' containing heterocyclic Schiff base, (E)-(N-anthracene-9-ylmethylene)-5-(4-nitrophenyl)-1,3,4-thia diazol-2-amine (A9CNPTDA) and its transition metal complexes	173
2.4	Antibacterial activity of 'S' containing heterocyclic Schiff base, (E)-5-(4-nitrophenyl)-N-((pyridine-2-yl)methylene)-1,3,4-thia diazol-2-amine (P2CNPTDA) and its transition metal complexes	174
2.5	Antibacterial activity of 'S' containing heterocyclic Schiff base, (E)-5-(4-nitrophenyl)-N-(1(pyridine-3-yl)ethylidene)-1,3,4-thia diazol-2-amine (3APNPTDA) and its transition metal complexes	175
2.6	Antibacterial activity of 'S' containing heterocyclic Schiff base, (E)-5-(4-nitrophenyl)-N-(1(pyridin-2-yl)ethylidene)-1,3,4-thia diazol-2-amine (2APNPTDA)and its transition metal complexes	176
2.7	Antibacterial activity of 'S' containing heterocyclic Schiff base, N-(anthracen-9(10H)-ylidene)-5-(4-nitrophenyl)-1,3,4-thiadiazol-2-amine (ANNPTDA) and its transition metal complexes	177
2.8	Antibacterial activity of 'S' containing heterocyclic Schiff base, N-((1H-indol-3-yl)methylene)thiazol-2amine (I3A2AT) and its transition metal complexes	178
2.9	Antibacterial activity of 'S' containing heterocyclic Schiff base, (13E)-N1,N2-bis((thiophene-2-yl)methylene)cyclohexane-1,2-diamine (T2CDACH) and its transition metal complexes	179
2.10	Lipinski's parameters for analysing druglikeness of Schiff bases	181
2.11	Binding energies and interactions of seven novel 'S' containing heterocyclic Schiff bases with SARS CoV-2 main protease (PDB code: **6lu7**)	189
2.12	Binding energies and interactions of seven novel 'S' containing heterocyclic Schiff bases with HIV-1protease (PDB code: **1mui**)	197
2.13	Binding energies and interactions of seven novel 'S'containing heterocyclic Schiff bases with HER2 protease (PDB code: **3rcd**)	204

2.14	Binding energies and interactions of seven novel 'S' containing heterocyclic with Acetylcholinesterase(AChE) (PDB code: **1b41**)	211
PART III CORROSION INHIBITION STUDIES		
3.1	Corrosion rate of carbon steel in mmy^{-1} in the absence and presence of 'S' containing heterocyclic Schiff bases in 1M HCl at 28^0C for 24h	269
3.2	Corrosion inhibition efficiencies of 'S' containing heterocyclic Schiff bases in 1M HCl at 28^0C for 24h	271
3.3	Effect of time on the corrosion inhibition efficiency of 'S' containing heterocyclic corrosion inhibitors (1mM) on CS in 1M HCl	274
3.4	Corrosion inhibition efficiencies (η_w%) of parent compounds NPTDA, A9C, P2C, 3ACP, 2ACP, ANT, I3A, 2AT, T2C and DAC on CS in 0.5M HCl for a period 24h	277
3.5	Adsorption parameters of 'S' containing heterocyclic Schiff bases on CS corrosion in 1M HCl	279
3.6	Thermodynamic parameters of CS corrosion, in the presence and absence of 'S' containing heterocyclic Schiff bases in 1M HCl	284
3.7	Electrochemical Impedance parameters of CS corrosion in the presence and absence of 'S' containing heterocyclic Schiff base inhibitors in 1M HCl at 303K	290
3.8	Potentiodynamic polarisation parameters of CS corrosion in the presence and absence of 'S' containing heterocyclic inhibitors in 1M HCl at 303K	293
3.9	Quantum chemical parameters of 'S' containing heterocyclic inhibitors	304
3.10	Corrosion rates (mmy^{-1}) of CS in the presence of 'S' containing heterocyclic Schiff bases in 0.5M H_2SO_4 at 28^0C for 24h	309
3.11	Corrosion inhibition efficiencies (η_w%) of 'S' containing heterocyclic Schiff bases on CS in 0.5M H_2SO_4 at 28^0C for 24h	310
3.12	Corrosion inhibition efficiencies (η_w%) of parent compounds NPTDA, A9C, P2C, 3ACP, 2ACP, ANT, I3A, 2AT, T2C and DAC on CS corrosion in 0.5M H_2SO_4 for a period 24h	312
3.13	Adsorption parameters of 'S' containing heterocyclic Schiff base inhibitors on CS in 0.5M H_2SO_4	314
3.14	Electrochemical impedance parameters of CS corrosion in the presence and absence of 'S' containing heterocyclic Schiff bases in 0.5M H_2SO_4 at 303K	320
3.15	Potentiodynamic polarization parameters of CS corrosion in the presence and absence of 'S' containing heterocyclic Schiff bases in 0.5M H_2SO_4 at 303K	325

LIST OF FIGURES

FIG. No.	TITLE	PAGE No.
PART I SYNTHESIS AND CHARACTERIZATION		
1.1	Schematic representation of the synthesis of parent amine 5-(4-nitro phenyl) -1,3,4-thiadiazole-2-amine (NPTDA)	33
1.2	^{1}H NMR spectrum of NPTDA	35
1.3	Mass spectrum of NPTDA	35
1.4	Synthesis of A9CNPTDA	36
1.5	^{1}H NMR spectrum of A9CNPTDA	38
1.6	^{13}Cnmr spectrum of A9CNPTDA	39
1.7	Mass spectrum of A9CNPTDA	40
1.8	Structure of A9CNPTDA	40
1.9	Structures of transition metal complexes of A9CNPTDA	47
1.10	Synthesis of ANNPTDA	48
1.11	^{1}H NMR spectrum of ANNPTDA	50
1.12	DEPT-135 spectrum of ANNPTDA	50
1.13	^{13}C NMR spectrum of ANNPTDA	51
1.14	Mass spectrum of ANNPTDA	51
1.15	Structure of ANNPTDA	52
1.16	Structures of transition metal complexes of ANNPTDA	58
1.17	Synthesis of P2CNPTDA	60
1.18	^{1}H NMR spectrum of P2CNPTDA	62
1.19	^{13}C NMR spectrum of P2CNPTDA	63
1.20	Mass spectrum of P2CNPTDA	63
1.21	Structure of P2CNPTDA	64
1.22	Structures of transition metal complexes of P2CNPTDA	69
1.23	Synthesis of 3APNPTDA	70
1.24	^{1}H NMR spectrum of 3APNPTDA	72
1.25	^{13}C NMR spectrum of 3APNPTDA	72
1.26	Mass spectrum of 3APNPTDA	73
1.27	Structure of 3APNPTDA	73
1.28	Structures of transition metal complexes of 3APNPTDA	79
1.29	Synthesis of 2APNPTDA	80
1.30	^{1}H NMR spectrum of 2APNPTDA	82
1.31	^{13}C NMR spectrum of 2APNPTDA	83
1.32	Mass spectrum of 2APNPTDA	83
1.33	Structure of 2APNPTDA	84
1.34	Structures of transition metal complexes of 2APNPTDA	89
1.35	Synthesis of I3A2AT	91

1.36	^{1}H NMR spectrum of I3A2AT	93
1.37	DEPT 135 spectrum of I3A2AT	94
1.38	^{13}C NMR spectrum of I3A2AT	94
1.39	Mass spectrum of I3A2AT	95
1.40	Structure of I3A2AT	95
1.41	Structures of transition metal complexes of I3A2AT	101
1.42	Synthesis of T2CDACH	102
1.43	^{1}H NMR spectrum of T2CDACH	104
1.44	^{13}C NMR spectrum of T2CDACH	104
1.45	Mass spectrum of T2CDACH	106
1.46	Structure of T2CDACH	106
1.47	Structures of transition metal complexes of T2CDACH	112
PART II BIOLOGICAL STUDIES		
2.1	Micrograph of *S. aureus*	130
2.2	Micrograph of *Bacillus subtilis*	131
2.3	Micrograph of *Escherichia coli*	132
2.4	Micrograph of *Proteus vulgaris*	133
2.5	Micrograph of *Klebsiella pneumonia*	134
2.6	Structure of Penicillin	135
2.7	Structure of Cephalosporin	135
2.8	Structure of Quinolones	135
2.9	Mechanism of antibiotic (drugs) resistance	144
2.10	Pictorial representation of Disc diffusion method	154
2.11	Structures of target proteins (a) **6lu7** (b) **1mui** (c) **3rcd** and (d) **1b41**	161
2.12	Antibacterial activity of 'S' containing heterocyclic Schiff bases against gram-positive strains *Staphylococcus aureus*, *Bacillus subtilis* and gram-negative bacterial strain *Escherichia coli* at a concentration 200µgdisc^{-1}	168
2.13	Antibacterial activity of 'S' containing heterocyclic Schiff bases against gram-negative bacterial strains *Proteus vulgaris, Klebsiella pneumonia* at a concentration 200µgdisc^{-1}	169
2.14	Antibacterial activity of transition metal complexes of A9CNPTDA against *Escherichia coli* and *Klebsiella pneumonia* at a concentration 50µgdisc^{-1}	169
2.15	Antibacterial activity of transition metal complexes of P2CNPTDA against *Staphylococcus aureus* and *Klebsiella pneumonia* at a concentration 50µgdisc^{-1}	170
2.16	Antibacterial activity of transition metal complexes of 3APNPTDA against *Staphylococcus aureus*, *Escherichia coli, Proteus vulgaris* and *Klebsiella pneumonia* at a concentration 50µgdisc^{-1}	170
2.17	Antibacterial activity of transition metal complexes of 2APNPTDA	171

	against *Escherichia coli* at a concentration 50µgdisc^{-1}	
2.18	Antibacterial activity of transition metal complexes of ANNPTDA against *Bacillus subtilis* at a concentration 50µgdisc^{-1}	171
2.19	Antibacterial activity of transition metal complexes of T2CDACH against *S. aureus* at a concentration 50µgdisc^{-1}	171
2.20	Antibacterial activity of P2CNPTDA-Cd^{2+} at different concentrations against *S. aureus*	171
2.21	(a) 2D and (b) 3D interaction diagrams of A9CNPTDA with M^{pro}	183
2.22	(a) 2D and (b) 3D interaction diagrams of P2CNPTDA with M^{pro}	183
2.23	(a) 2D and (b) 3D interaction diagrams of 3APNPTDA with M^{pro}	184
2.24	(a) 2D and (b) 3D interaction diagrams of 2APNPTDA with M^{pro}	185
2.25	(a) 2D and (b) 3D interaction diagrams of ANNPTDA with the M^{pro}	186
2.26	(a) 2D and (b) 3D interaction diagrams of I3A2AT with the M^{pro}	187
2.27	(a) 2D and (b) 3D interaction diagrams of T2CDACH with the M^{pro}	187
2.28	(a) 2D and (b) 3D interaction diagrams of A9CNPTDA with HIV-1 protease	191
2.29	(a) 2D and (b) 3D interaction diagrams of P2CNPTDA with HIV-1 protease	192
2.30	(a) 2D and (b) 3D interaction diagrams of 3APNPTDA with HIV-1 protease	193
2.31	(a) 2D and (b) 3D interaction diagrams of 2APNPTDA with HIV-1 protease	194
2.32	(a) 2D and (b) 3D interaction diagrams of ANNPTDA with HIV-1 protease	195
2.33	(a) 2D and (b) 3D interaction diagrams of I3A2AT with HIV-1 protease	195
2.34	(a) 2D and (b) 3D interaction diagrams of T2CDACH with HIV-1 protease	196
2.35	(a) 2D and (b) 3D interaction diagrams of A9CNPTDA with HER2 protease	199
2.36	(a) 2D and (b) 3D interaction diagrams of P2CNPTDA with HER2 protease	199
2.37	(a) 2D and (b) 3D interaction diagrams of 3APNPTDA with HER2 protease	200
2.38	(a) 2D and (b) 3D interaction diagrams of 2APNPTDA with HER2 protease	201
2.39	(a) 2D and (b) 3D interaction diagrams of ANNPTDA with HER2 protease	201
2.40	(a) 2D and (b) 3D interaction diagrams of I3A2AT with HER2 protease	202
2.41	(a) 2D and (b) 3D interaction diagrams of T2CDACH with HER2 protease	203
2.42	(a) 2D and (b) 3D interaction diagrams of A9CNPTDA with	206

	acetylcholinesterase	
2.43	(a) 2D and (b) 3D interaction diagrams of P2CNPTDA with acetylcholinesterase	207
2.44	(a) 2D and (b) 3D interaction diagrams of 3APNPTDA with acetylcholinesterase	208
2.45	(a) 2D and (b) 3D interaction diagrams of 2APNPTDA with acetylcholinesterase	208
2.46	(a) 2D and (b) 3D interaction diagrams of ANNPTDA with acetylcholinesterase	209
2.47	(a) 2D and (b) 3D interaction diagrams I3A2AT with acetylcholinesterase	210
2.48	(a) 2D and (b) 3D interaction diagrams of T2CDACH with acetylcholinesterase	210
PART III CORROSION INHIBITION STUDIES		
3.1	Demonstration of components of corrosion	221
3.2	Corrosion impacts in various areas	222
3.3	Application of carbon steel/mild steel in various areas	223
3.4	Reactions occurring throughout the corrosion of steel	224
3.5	Galvanic corrosion	226
3.6	Pitting corrosion in steel	227
3.7	Mechanism of crevice corrosion	227
3.8	Microbiologically influenced corrosion (MIC) or bio-corrosion	228
3.9	Inter-granular corrosion of stainless steel	229
3.10	Schematic representation of stress corrosion cracking	229
3.11	Equivalent circuit	257
3.12	Nyquistplot	258
3.13	Bode and impedance plots	258
3.14	Linear polarization plot	260
3.15	Tafel plot	262
3.16	Noise current Vs time	264
3.17	Pitting index curve	264
3.18	PSD plot	265
3.19	Corrosion rates of CS with different concentration of 'S' containing heterocyclic Schiff base inhibitors in 1M HCl at 28^0C for 24h.	270
3.20	Comparison of corrosion inhibition efficiencies (η_w%) of 'S' containing heterocyclic Schiff bases on CS in 1M HCl at 28^0C for 24h	272
3.21	Variation of corrosion inhibition efficiencies of 'S' containing Schiff base inhibitors (1mM) with time on CS in 1M HCl	275
3.22	UV-Visible spectra of a) Thiophene 2-carbaldehyde (T2C) b) 1,2 Diaminocyclohexane (DAC) c) T2CDACH at 0h and (d)	275

	T2CDACH at 48h 1M HCl	
3.23	Comparison study of corrosion inhibition efficiencies (η_w%) of 'S' containing heterocyclic Schiff bases with their parent compounds	276
3.24	Langmuir adsorption isotherms of (a) A9CNPTDA (b) P2CNPT 3APNPTDA (d) 2APNPTDA (e) ANNPTDA (f) I3A2AT (g) T2CDACH on CS in 1M HCl	278
3.25	a) Arrhenius plots and b) log (K/T) vs 1000/T plots of CS corrosion in the presence and absence of A9CNPTDA in 1M HCl	281
3.26	a) Arrhenius plots and b) log (K/T) vs 1000/T plots of CS corrosion in the presence and absence of P2CNPTDA in 1M HCl	281
3.27	a) Arrhenius plots and b) log (K/T) vs 1000/T plots of CS corrosion in the presence and absence of 3APNPTDA in 1M HCl	281
3.28	a) Arrhenius plots and b) log (K/T) vs 1000/T plots of CS corrosion in the presence and absence of 2APNPTDA in 1M HCl	282
3.29	a) Arrhenius plots and b) log (K/T) vs 1000/T plots of CS corrosion in the presence and absence of ANNPTDA in 1M HCl	282
3.30	a) Arrhenius plots and b) log (K/T) vs 1000/T plots of CS corrosion in the presence and absence of I3A2AT in 1M HCl	282
3.31	a) Arrhenius plots and b) log (K/T) vs 1000/T plots of CS corrosion in the presence and absence of T2CDACH in 1M HCl	283
3.32	SEM images of (a) bare CS (b) CS treated with 1M HCl (c) CS treated with A9CNPTDA (1mM) (d) CS treated with T2CDACH (1mM) for 48h.	285
3.33	a) Nyquist plots and b) Bode plots of CS corrosion in the presence and absence of A9CNPTDA in 1M HCl	287
3.34	a) Nyquist plots and b) Bode plots of CS corrosion in the presence and absence of P2CNPTDA in 1M HCl	287
3.35	a) Nyquist plots and b) Bode plots of CS corrosion in the presence and absence of 3APNPTDA in 1M HCl	287
3.36	a) Nyquist plots and b) Bode plots of CS corrosion in the presence and absence of 2APNPTDA in 1M HCl	288
3.37	a) Nyquist plots and b) Bode plots of CS corrosion in the presence and absence of ANNPTDA in 1M HCl	288
3.38	a) Nyquist plots and b) Bode plots of CS corrosion in the presence and absence of I3A2AT in 1M HCl	288
3.39	a) Nyquist plots and b) Bode plots of CS corrosion in the presence and absence of T2CDACH in 1M HCl	290
3.40	Comparison of the corrosion inhibition efficiencies ($\eta_{EIS\%}$) of 'S' containing heterocyclic in 1M HCl on CS in 1M HCl at 28^0C	291
3.41	a) Tafel plots and b) Linear polarization plots of CS corrosion in the presence and absence of A9CNPTDA in 1M HCl.	294
3.42	a) Tafel plots and b) Linear polarization plots of CS corrosion in the presence and absence of P2CNPTDA in 1M HCl	294

3.43	a) Tafel plots and b) Linear polarization plots of CS corrosion in the presence and absence of 3APNPTDA in 1M HCl	294
3.44	a) Tafel plots and b) Linear polarization plots of CS corrosion in the presence and absence of 2APNPTDA in 1M HCl	295
3.45	a) Tafel plots and b) Linear polarization plots of CS corrosion in the presence and absence of ANNPTDA in 1M HCl	295
3.46	a) Tafel plots and b) Linear polarization plots of CS corrosion in the presence and absence of I3A2AT in 1M HCl	295
3.47	a) Tafel plots and b) Linear polarization plots of CS corrosion in the presence and absence of T2CDACH in 1M HCl	296
3.48	Comparison study of corrosion inhibition efficiencies ($\eta_{pol\%}$) of 'S' containing heterocyclic Schiff base inhibitors on CS in 1M HCl at 28^0C	297
3.49	Corrosion inhibition mechanism of A9CNPTDA molecules on metallic surface	299
3.50	Noise current for CS with and without 'S' containing heterocyclic inhibitors in 1M HCl solution	300
3.51	PSD curves of CS in a) blank b) A9CNPTDA c) P2CNPTDA d) 3APNPTDA e) 2APNPTDA f) ANNPTDA g) I3A2AT h) T2CDACH (1mM) in 1M HCl)	301
3.52	Pitting index curves of CS in a) blank b) A9CNPTDA c) P2CNPTDA d) 3APNPTDA e) 2APNPTDA f) ANNPTDA g) I3A2AT and h) T2CDACH	302
3.53	a) HOMO and b) LUMO of A9CNPTDA	305
3.54	a) HOMO and b) LUMO of P2CNPTDA	305
3.55	a) HOMO and b) LUMO of 3APNPTDA	305
3.56	a) HOMO and b) LUMO of 2APNPTDA	306
3.57	a) HOMO and b) LUMO of ANNPTDA	306
3.58	a) HOMO and b) LUMO of I3A2AT	306
3.59	a) HOMO and b) LUMO of T2CDACH	306
3.60	Optimised geometries of 'S' containing Schiff bases	307
3.61	Variation of corrosion rates of CS with the concentration of 'S' containing heterocyclic Schiff base inhibitors in 0.5M H_2SO_4 for 24h	309
3.62	Comparison of corrosion inhibition efficiencies ($\eta_w\%$) of 'S' containing heterocyclic Schiff base inhibitors on CS in 0.5M H_2SO_4 for 24h	310
3.63	Langmuir adsorption isotherms of (a) A9CNPTDA (b) P2CNPTDA (c) 3APNPTDA (d) 2APNPTDA (e) ANNPTDA (f) I3A2AT (g) T2CDACH on CS in 0.5M H_2SO_4	313
3.64	SEM images of (a) bare CS (b) CS treated with 0.5M H_2SO_4 (c) CS treated with A9CNPTDA (1mM) (d) CS treated with ANNPTDA	315

	(1mM) for 24h	
3.65	a) Nyquist plots and b) Bode plots of CS corrosion in the presence and absence of A9CNPTDA in 0.5M H_2SO_4	316
3.66	a) Nyquist plots and b) Bode plots of CS corrosion in the presence and absence of P2CNPTDA in 0.5M H_2SO_4	316
3.67	a) Nyquist plots and b) Bode plots of CS corrosion in the presence and absence of 3APNPTDA in 0.5M H_2SO_4	316
3.68	a) Nyquist plots and b) Bode plots of CS corrosion in the presence and absence of 2APNPTDA in 0.5M H_2SO_4	317
3.69	a) Nyquist plots and b) Bode plots of CS corrosion in the presence and absence of ANNPTDA in 0.5M H_2SO_4	317
3.70	a) Nyquist plots and b) Bode plots of CS corrosion in the presence and absence of I3A2AT in 0.5M H_2SO_4	317
3.71	a) Nyquist plots and b) Bode plots of CS corrosion in the presence and absence of T2CDACH in 0.5M H_2SO_4	318
3.72	Comparison of Corrosion inhibition efficiencies ($\eta_{EIS\%}$) of 'S' containing heterocyclic Schiff base inhibitors on CS in 0.5M H_2SO_4 at 28^0C	319
3.73	a) Tafel plots and b) Linear polarization curves of CS corrosion in the presence and absence of A9CNPTDA in 0.5M H_2SO_4	322
3.74	a) Tafel plots and b) Linear polarization curves of CS corrosion in the presence and absence of P2CNPTDA in 0.5M H_2SO_4	322
3.75	a) Tafel plots and b) Linear polarization curves of CS corrosion in the presence and absence of 3APNPTDA in 0.5M H_2SO_4	323
3.76	a) Tafel plots and b) Linear polarization curves of CS corrosion in the presence and absence of 2APNPTDA in 0.5M H_2SO_4	323
3.77	a) Tafel plots and b) Linear polarization curves of CS corrosion in the presence and absence of ANNPTDA in 0.5M H_2SO_4	323
3.78	a) Tafel plots and b) Linear polarization curves of CS corrosion in the presence and absence of I3A2AT in 0.5M H_2SO_4	324
3.79	a) Tafel plots and b) Linear polarization curves of CS corrosion in the presence and absence of T2CDACH in 0.5M H_2SO_4	324
3.80	Comparison study of corrosion inhibition potencies ($\eta_{pol}\%$) of 'S' containing heterocyclic Schiff bases on CS in 0.5M H_2SO_4 at 28^0C	324

PART I

SYNTHESIS AND CHARACTERIZATION

CHAPTER 1

INTRODUCTION AND REVIEW

Sulphur, is a nonmetal and one of the first ten most abundant elements in universe. There are not much compounds which got a mention in the Bible. Of the fifteen compounds which were established during that time, sulphur, is clearly mentioned in the the context of the destruction of Sodom and Gomorrah.

"*On the wicked he will rain fiery coals and burning sulfur; a scorching wind will be their lot.*" – Genesis 19:24

This again establishes the significance of the element sulphur. Sulphur's natural occurrence is often associated with hot springs or volcanoes as a stinky yellow material which relates it to hellfire and wrath. The element was isolated in its pure form in1809 by Louis-Josef Gay-Lussac and Louis-Jacques Thénard. There exists several allotropes of sulphur and most common form appears as yellow powder or even crystals. It is considered to be one of the most important inorganic element; it is incorporated into proteins, enzymes, vitamins, amino acids, and other crucial biomolecules. It is used as a fungicide, fumigant, in the vulcanization of rubber and in explosives. Most of the element produced goes into the production of sulfuric acid.

Sulphur Compounds- An Outlook

In all living things, sulphur compounds are present and they can be divided into two groups: the essential primary metabolites and the non-essential secondary metabolites. A wide variety of compounds, ranging from simple gases to complex polycyclic aromatics, constitute the family of sulfur compounds, both of biogenic and anthropogenic origin. These compounds can be observed in numerous, typically complex matrices, such as air (gas), water (aqueous systems), different fractions of petroleum

(gas, liquid and solid), beverages, foodstuffs and pharmaceutical formulations. Gas fumigants used as insecticides are sulfur-containing compounds such as carbonyl sulphide and sulfuryl fluoride. They have been developed to substitute methyl bromide, the ozone-depleting insecticide. Vikane, Zythor, Termafume, sulfuryl fluoride fumigant, sulfuryl fluoride (Master fume) and Dow AgroSciences/Profume gas fumigants include sulfuryl fluoride (CAS no.2699-79-8) as the active ingredient. The reduction of sulfoxides into their corresponding sulfides utilizes a variety of Sulfur-containing compounds.

Sulphur Heterocycles

Heterocycles constitute a vast area of research in both organic and inorganic chemistry. They play a key role in biochemical processes since the side groups and active sites of many living cells comprise of aromatic heterocycles, eg: DNA, RNA and various enzymes [1]. Literature survey reveal that if sulphur containing heterocyclic molecules act as ligands, they are well known for its pharmacological actions include anticancer, antimicrobial, antiviral, antitubercular anti-inflammatory etc. and the most commonly found motifs in sulfur containing drugs are thiadiazole, thiazole, isothiazole, thiophene, thiopyran, thiazepine and thiazolidine.

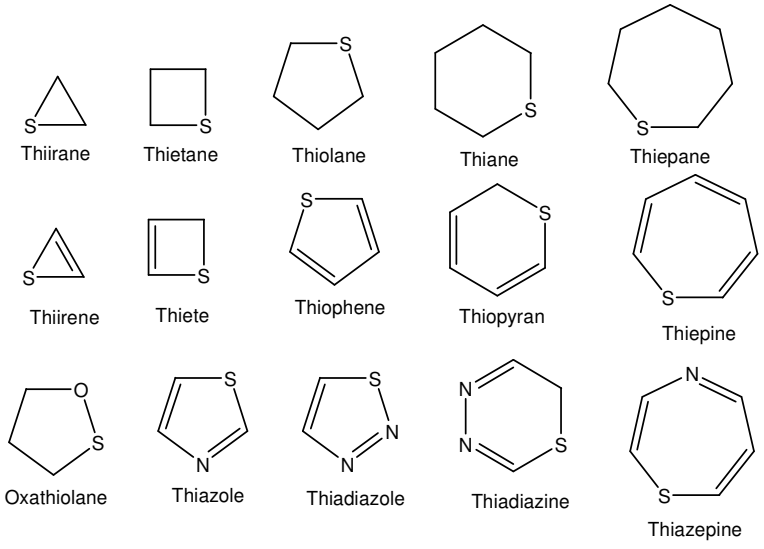

These S-heterocycles, compared to the N-heterocycles, are less reported but have enhanced prospects in pharmaceutical industry due to their superior therapeutic potential. This is also as a result of the improvements in the feasible synthesis reported recently. The field of S-heterocyclic demands much higher attention to counteract the issues of toxicity and various pathological targets.

Schiff Base Ligands

Schiff bases are named after Hugo Schiff, and is a nitrogen analogue of carbonyl compounds like aldehydes or ketones in which carbonyl (C=O) is replaced by an azomethine or imine group. Schiff base (SB) ligands are one of the most commonly used ligands because of their ease of formation and remarkable flexibility. Schiff bases, the versatile pioneer for organic synthesis and later researches proved that it has wide variety of applications in pharmaceutical fields and that was due to the biological activities expressed. Aromatic Schiff bases have shown more potential in activity due to free electron delocalization within the ring structure. Likewise Schiff base derived from heterocyclic ring containing sulphur atom also showed more advantage in this regard.

The general synthetic method involves the condensation of primary amines with a carbonyl precursor usually in an alcoholic medium or on reflux conditions. This reversible reaction proceeds via a carbinolamine intermediate produces water as an additional product and provides excellent yield. The reaction is acid catalyzed and the products resulting from these reactions features an imine or an azomethine group (C=N) and is commonly called a Schiff base.

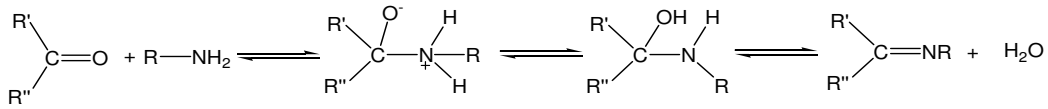

The majority of the heterocyclic SB ligands comprise N, O, P and S. Heterocyclic Schiff base containing sulphur atom shows impressive biological activities due to the

presence of aromatic ring containing the highly polarisable sulphur atom. Various publications had covered the antibacterial, anticancer, antifungal, anti-inflammatory and antiviral properties, hence researches had proved that Schiff bases containing heteroatoms especially sulphur atoms are highly potential drugs [2]. Making certain modification in the structure of Schiff base by thiadiazole and thiazole moieties, its would influence on biological activity may be improved. A versatile moiety, thiadiazole attracted as a privileged scaffold because of its potential therapeutic significance [3]. Superior liposolubility and mesoionic character of thiadiazole moiety are due to the presence of sulphur in the thiadiazole ring that allows them to move across the cell membrane and facilitating the interaction with biological targets. Diverse applications of thiadiazole derivatives and their varying pharmacological activities like antidepressants [4], anticancer [5], antidiabetic [6], antianxiety [7], antiviral [8], antifungal [9], antimicrobial [10], anti-inflammatory [11], anticonvulsant [12], anti-tubercular [13] etc., have attracted widespread attention in the recent years. Many drugs containing thiadiazole derivatives such as sulphamethoxazole, acetazolamide, cefazoline and methazolamide are available in the market [14]. Previous studies indicate that the biological activity exhibited by the thiadiazole ring system is due to the presence of N=C-S bonding where the sulphur atom acts as hydrogen binding domain and two nitrogen atoms are electron donors [15].

It is interesting to investigate sulphur containing Schiff bases which have broad applications in pharmaceutical fields. Computer-based drug discovery is the most appreciable method in the field of pharmaceutics. More efficient approach in drug discovery is examining the effectiveness of the drug for a specific disease by studying the type of interactions between the target protein and the drug at its molecular level.

Accurate fast docking protocol and visualizing ability of the binding geometries

and drug-protein interactions increases the systematic understanding of ligand-receptor complex strength, bond length and structural principles. Proteins associated with specific diseases are identified by understanding the mechanistic aspects of causing diseases. For a systematic understanding of the structural principles that establish the strength of a ligand/protein complex both, an accurate and fast docking protocol and the ability to visualize binding geometries and interactions are mandatory. Here we present an interface between the popular molecular graphics system PyMOL and the molecular docking suites Autodock and Vina and demonstrate how the combination of docking and visualizationcan aid structure-based drug design efforts [16].

One of the most outstanding applications of Schiff bases are their use as an efficient corrosion inhibitor and it is mainly based on its ability to get adsorbed on the surface to be protected spontaneously to form a monolayer. Organic molecules having electron lone pairs on the heteroatoms such as P, S, N and O atoms have proved, both theoretically and practically, that they can perform as admirable corrosion inhibitors in aggressive solutions by improved adsorption on the metal surface [17]. Different Schiff base ligands have been used as carriers of cation in potentiometric sensors because they have exhibits excellent sensitivity, stability and selectivity for specific metal ions [18–21].

Transition Metal Complexes

The modern studies of metal complexes begin with the work of Werner and Jorgenson. In 1893, Werner put forward his famous theory of coordination to explain the formation and structures of complex compounds. In recognition of his work in this field; he was awarded the Nobel Prize in 1913 in chemistry. Werner is rightly called the father of coordination chemistry. Sixty years later in 1973, E.O. Fischer and G. Wilkinson shared the Nobel Prize for their work on Ferrocene. As more complexes were discovered

in the 19th century, numerous theories were arised to account the formation of metal complexes and its properties. Later, more reliable explanation regarding the structure, formation and stability of complexes was given by valence bond theory (VBT), crystal field theory (CFT), ligand field theory (LFT) and molecular orbital theory (MOT). A sudden change in solubility, drop in conductivity or colour change indicates the formation of complex between a metal ion and ligand. According to Werner a metal ion tries to satisfy both its primary and secondary valencies. The secondary valencies are directed towards fixed positions in space so that each complex possesses a definite stereochemistry. Now majority of research papers being published every year in inorganic chemistry are on coordination chemistry. The scope of the subject is due to the various applications of coordination compounds in science and industry.

The use of coordination compounds in medicinal field is inevitable. Complexes of transition metals can be used in MRI scan. Cis platinum complexes for the treatment of cancer and gold complexes are used for the treatment of arthritis. Barium sulphate and triiodobenzene moiety can be applied in gastrointestinal tract imaging. Many catalytic enzymes in living systems are coordination compounds. Coordination compounds are involved in processes like photosynthesis, nitrogen fixation, oxygen transport etc.

Schiff Base Complexes

They played an important role in the development of coordination chemistry. Free Schiff base have heteroatom show biological activity whereas in metal complexes with such ligands show better activity than free ligand because of chelation. With majority of transition metals, they readily form stable complexes. Bioinorganic chemistry, catalysis, and magnetochemistry are potential interdisciplinary avenues including their applications. Synthetic models for the metal-containing sites in metalloproteins and enzymes are often provided by the metal complexes supported by

SB ligands. Yamanda *et al.* has reviewed the developments in stereochemistry of metal complexes prepared by Schiff base ligands [22]. A number of Schiff base macrocycles have been utilized as metal containing liquid crystal polymers. They are also used as odouring agents, superconductors and for the formulation of semiconductors. Currently several Schiff-base complexes have been explored as effective scavengers of reactive oxygen species (ROS) and they act as efficient antioxidants [23].

Metal complexes are important constituents of industrial processes in pharma, industrial and agricultural chemistry. Schiff bases by virtue of their lone pairs and azomethine moieties are capable of coordinating to metals and form complexes. These complexes find use in many fields including catalysis, industrial processes and various biological uses as antimicrobial, antifungal, antibacterial, insecticidal, anti-inflammatory, antitumor and cytotoxic agents. They are also useful as dyes and enzymatic regulatory agents.

The chelating properties of ligands are used to transport across membranes or to attach to specific site, thus it can hinder the growth of the organism. The antibacterial activity is based on the selective toxicity of agents on the microbial cells. In transition metal complexes with ligand Schiff base i.e., azomethine group possess (C=N) bond, positive charge of metal ion is partially shared among hetero atoms (S, N and O) present in the Schiff base ligand. Due to the presence of lone pair of electrons in it cause delocalization of π–electrons over the whole chelating system. Hence this increase the lipophilic character of metal complexes which favours its permeation through the lipid layer of the bacterial membrane and inhibiting metal binding sites in enzymes of that organism and finally, inhibit its growth.

Due to synthetic flexibility and relative easiness in synthesis, Schiff base complexes are very much interesting in the field of fundamental and applied research. In

magnetochemistry, dinuclear SB complexes demonstrate and facilitate the study of the exchange coupling process between two metal ions. Chiral SB complexes have also been shown to be excellent catalysts for certain organic reactions. They have also been used as catalysts for small molecules activation. Tetra coordinate cobalt(II) Schiff base complexes can catalyze mono oxygenation of alkenes in primary or secondary alcohols under atmospheric oxygen pressure at 60°C, without a carbon-carbon bond cleavage. This happens via proposed mechanism which involves the decomposition of a benzylalcoholato cobalt(III) complex [24].

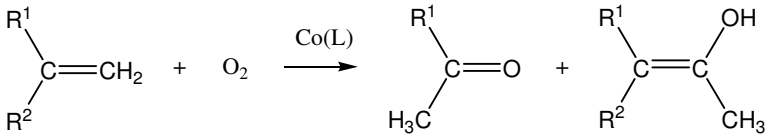

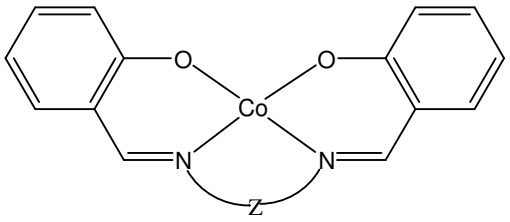

Z = $(CH_2)_2$, $(CH_2)_3$, $(CH_2)_4$,

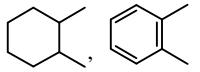

,

$(CH_2)_3NH(CH_2)_3$, $(CH_2)_3NMe(CH_2)_3$,

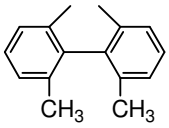

Low spin cobalt(II) square pyramidal complexes were reported from a polymer based Schiff base ligand derived from crosslinked polystyrene bound benzaldehyde and 2-aminobenzimidazole coordinated to a [Co(TPP)] (TPP= *meso*-tetraphenylporphyrin) and tetrahedral complexes of cobalt. The resulted complexes all exhibited square pyramidal structures irrespective of square planar or tetrahedral structure of starting material [25].

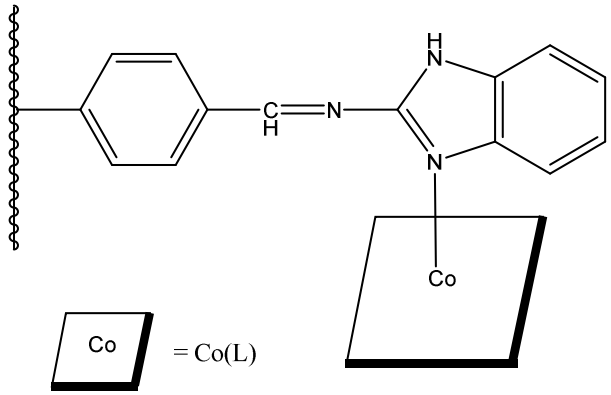

Salicylaldehyde and 2-amino-4-phenyl-5-methyl thiazole was subjected to a condensation reaction in ethanol solution in presence of a few drops of glacial acetic acid resulting in the formation of a Schiff base ligand.

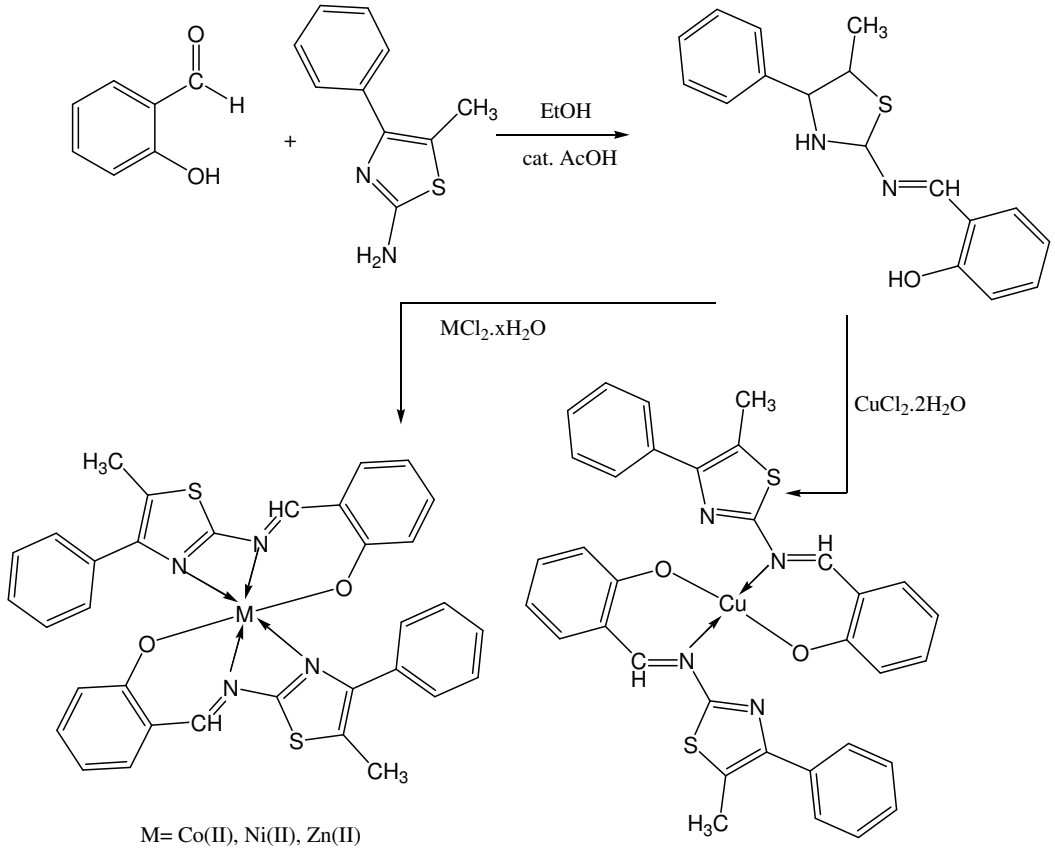

This ligand was in turn utilized to synthesize Cu, Ni, Co, Zn(II) complexes via reactions of $CuCl_2.2H_2O$, $NiCl_2.6H_2O$, $CoCl_2.6H_2O$, and $ZnCl_2$ in ethanol-reflux

conditions. Zn(II) complex exhibited anticancer activity against MCF-7, HepG2, A549 and HCT116 cell lines. Molecular docking studies were also conducted against tyrosine kinases receptor (PDB1t46) [26].

A Co(III) chiral complex supported by a Schiff base comprised from tryptophan and salicylaldehyde was reported to catalyze the trimethylsilylcynation of benzaldehyde. (R)-trytophan was used in the synthesis of ligand. The reaction of this ligand with $Na_3[Co(CO)_3]$ yielded a mixture of diastereomeric complexes Λ-bis-[N-salicylidene-(R)-tryptophanato]cobaltate sodium and Δ-bis[N-salicylidene-(R)-tryptophanato]cobaltate sodium. The counter cations were substituted by other metal ions and the complexes exhibited catalytic activity [27].

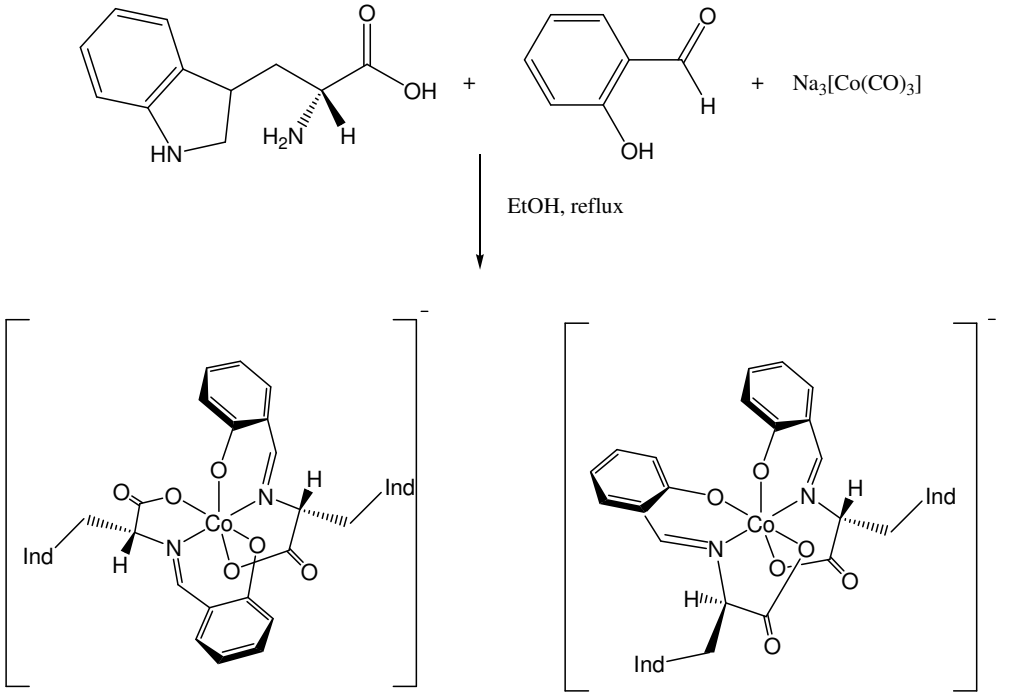

Δ-bis[N-salicylidene-(R)-tryptophanato]cobaltate

Λ-bis- [N-salicylidene-(R)-tryptophanato]cobaltate

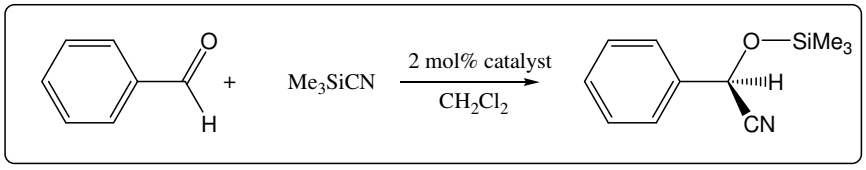

Bidentate Schiff base ligands with sulphur and nitrogen donors were synthesized via condensation of heterocyclic aldehydes with S-benzyldithiocarbazate. These ligands on reaction with diphenyltin dichloride afforded Sn(IV) organometallic complexes.

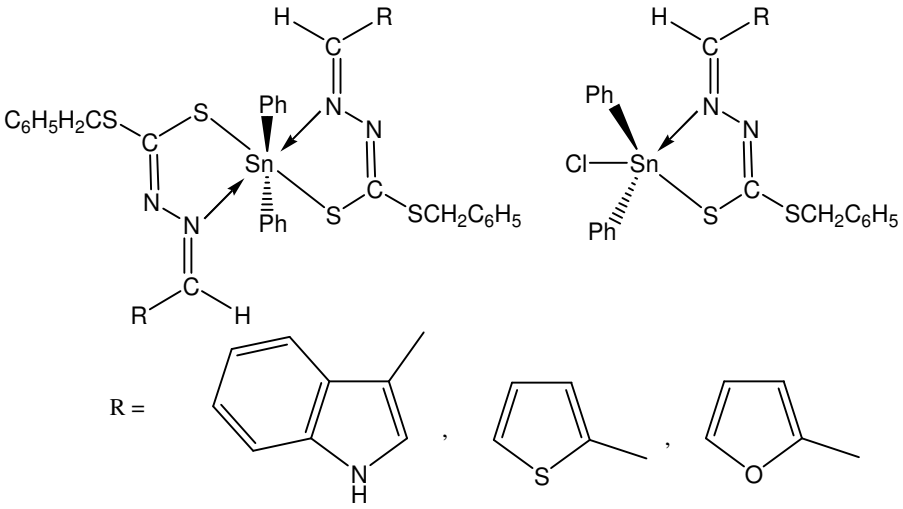

The anti-bacterial and anti-fungal properties were screened for both the complexes and free ligands in which the complexes showed higher inhibitory action. This was proposed due to the metal chelation and solubility [28].

Transition Metal Complexes of Schiff Bases –A Review

The versatile compounds, Schiff bases and their complexes exhibit a broad range of catalytical activities, corrosion inhibition activities and pharmaceutical activities including anticancer, antimalarial, antibacterial, antifungal, antiproliferative, antipyretic antiviral, anti-inflammatory properties. The influence of metals on their intrinsic chemical interest as multidentate ligands and the biological activity of these compounds has encouraged a considerable increase in their coordination behaviour investigations.

In 1990, N. K. Rao and M. R. Reddy synthesized Co(II), Ni(II) and Zn(II) complexes with indane-1,3-dione-2-imine-N-acetic acid, an intermediate Schiff base obtained by the condensation of glycine and ninhydrin [29]. IR, NMR, electronic spectrum, magnetic susceptibility, elemental analysis, thermogravimetric

analyses/differential thermal analysis and molar conductivity studies evaluated these coloured complexes and put forward a mechanism for their formation. The nature of Schiff base as a monobasic tridentates ligand whereas its complexes possess octahedral stereochemistry in this case. A comparative antimicrobial study was done with the complexes and ninhydrin against *Staphylococcus aureus, Streptococcus faecalis Escherichia coli* and *Proteus mirabilis.*

In 2007, N. Raman, et al. synthesized transition metal complexes of Hg(II), Mn(II), Cu(II), VO(IV), Zn(II), Co(II), Cd(II) and Ni(II) from Schiff base derivative of 3-hydroxy-4-nitrobenzaldehyde, 4-aminoantipyrine and o-phenylenediamine [30]. Structural features of these complexes were studied from their IR, UV-Vis, ^{1}H NMR, elementary analyses, ESR spectrum and magnetic susceptibility. Cyclic voltammetry studies explained the redox behaviour of vanadyl and copper complexes and these complexes showed good results in antimicrobial screening tests. From the nuclease activity study of these complexes reveals that Ni(II), Cu(II) and Co(II) complexes cleave DNA by redox chemistry were others not.

In 2008, Monica Soni and A. P. Mishra synthesized new bidentate/tridentate Schiff bases and their Co(II) and VO(II) complexes by the condensation reaction of 2-hydroxyacetophenone with nicotinamide (han)/isoniazide (hai) and methyl isobutyl ketone with nicotinamide (mna)/2-amino-4-chlorophenol (map). Structure of the complexes were determined by physicochemical studies [31]. From the thermal data and FAB mass, degradation pattern of the complexes were obtained. XRD analysis showed the results that these complexes crystallized as a tetragonal crystal system. Well diffusion technique is used to evaluate antimicrobial activity of the complex using DMSO as a solvent on different bacterias/fungi *A. niger, E. coli, S. fecalis, T. polysporum* and

S. aureus. The studies concluded that metal chelation affects the antimicrobial activity of all complexes and they have better antimicrobial activity than free ligands

In 2009, R.D. Deshmukh, et al. synthesized novel Schiff base from glycine and 2-hydroxy-5-methyl acetophenone and it's coordination with metals like Cd(II), Mn(II), Co(II), Zn(II), Fe(II), Ni(II), UO_2(VI), Cu(II) results a series of new transition metal complexes [32]. Characterization of the ligand and complexes done on the basis of magnetic susceptibility measurements, electrical conductance, analytical measurements, ESR, IR, electronic spectra and thermogravimetric analysis. In all the complexes, ligand behaves as a dibasic tridentate –ONO- donor, but in Zn(II) complex, the ligand behaves as monobasic bidentate –OO- donor. In the range, 313–398 K, DC electrical conductivity of ligand and its complexes the solid state have been measured and found that complexes were semiconducting. Various Gram (+) and Gram (−) bacterial strains are used for screening studies of the ligand and complexes.

In 2011, Mehmet Tümer, et al. synthesized Pd(II), Cu(II), Ni(II), Co(II) and Ru(III) metal complexes with two Schiff base ligands (HL_1 and HL_2). By analytical and spectroscopic methods these complexes were characterized [33]. Using cyclohexane as substrate, metal complexes alkane oxidation activities were studied. These complexes were checked for their antimicrobial performance against *Bacillus cereus, Micrococcus luteus, Bacillus brevis, Bacillus megaterium, Staphylococcus aureus, Enterococcus faecalis, Corynebacteriumxerosis* and *Mycobacterium smegmatis* (Gram-positive bacterias) and *Saccharomyces cerevisiae, Pseudomonas aeruginosa, Yersinia enterocolitica, Klebsiellafragilis, Escherichia coli, Candida albicans* and *Klebsiella pneumonia* (Gram-negative bacterias). Thermal and electrochemical properties of these complexes are also studied. By using reducing power action of superoxide anion radical

generated in non-enzymatic systems and free radical scavenging by DPPH (1,1-diphenyl-2-picrylhydrazyl), the antioxidant properties of Schiff base ligands were also evaluated.

In 2012, Zhang et al. synthesized transition metal coordination complexes $Zn(C_{18}H_{16}N_3O_2)_2 \cdot 2CH_3CH_2OH$, $Cu(C_{18}H_{16}N_3O_2)_2 \cdot 2CH_3OH$, and $Cd(C_{18}H_{16}N_3O_2)_2 \cdot 2CH_3OH$ derived from the same ligand of L-tryptophan and 2-acetylpyridine are prepared and investigated the anticancer performances on MDA-MB-231 breast cancer cells. All three complexes can inhibit the cellular proliferation, but Cd-complex showed highest anti-proliferative activity. In addition to this, the same complex can inhibit proteasomal chymotrypsin like activity. [34]

In 2013, A. Kiruthika, et al. synthesized Schiff base ligands from acetylacetone/2-hydroxynaphthaldehyde/isatin with salicylaldehyde and o-phenylene diamine and Fe(III) complexes were synthesized [35]. These were characterized by different spectral studies and analytical techniques. From the spectral data, octahedral geometry is assigned to Fe(III) complexes and these complexes were converted to its nano metal oxides. Using 3D modelling molecular picture, the possible geometries of complexes were evaluated. The results of antibacterial investigations show that they are excellent antibacterial and antifungal agents with their MIC values 62.5 and 125µg / litre.

In 2013, Shakuntala. M synthesized new Schiff base ligand from 2-hydroxy1-naphthaldehyde with 8-amino 2-naphthol, 1, 8-diaminonaphthalene, and 4-Bromo-1-naphthylamine, 5-amino1-naphthol [36]. The ligand and its complexes with Zn(II), Cu(II), Ni(II), Mn(II) and ions characterized by using electronic and IR spectra, elementary analysis, cyclic voltammetry, ^1H NMR, molar conductance, thermal and magnetic analysis. The ligands and complexes tested for their antimicrobial activity against one positive bacterium (*Klebsiella pneumonia*) and two negative bacterias (*Staphylococcus aureus* and *Escherichia coli*). Comparison between zones of inhibition

of complexes and ligands shows that complexes have higher activity than ligands. From the studies, concluded that the antibacterial activity is dependent on the molecular structure of the compound, solvent used and bacterial strains under consideration.

In 2014, K.R. Joshi, et al. synthesized nickel(II) and copper(II) complexes with Schiff bases 2-((3,4-difluorophenylimino)methyl)-6-methoxy-4-nitrophenol and 2-((2,4-dimethylphenylimino)methyl)-6-methoxy-4-nitrophenol [37]. The above Schiff bases are derived from the condensation reaction of 2,4-dimethylaniline/ 3,4-difluoroaniline with 2-hydroxy-3-methoxy-5-nitrobenzaldehyde. Characterization of these ligands and their metal complexes was done by IR, ^{1}H NMR, electronic, mass spectra and TG analysis. Using Broth dilution method, these Schiff bases and their metal complexes were checked for antimicrobial activity against *Streptococcus pyogenes, Staphylococcus aureus*, *Pseudomonas aeruginosa*, *Escherichia coli*, *Aspergillus clavatus*, *Candida Albicans* and *Aspergillus niger*. Results shows that metalation increases with chelation.

In 2015, A. Pradhan et al. carried out a review based on the Schiff bases derived from2-aminobenzthiazole, 4-aminobenzene, sulphonamide, 4-aminophenol, 4-amino salicylic acid, semicarbazide, aniline, 4-aminoantipyrine, thiosemicarbazide, o-phenyl enediamine, 2-aminopyrazine, 2-aminothiophenol, s-benzyldithiocarbamate and p-anisidine and its complexes Co(II), Ni(II), Cu(II), Mn(II), Zn(II), Cd(II), Hg(II), VO(II), Pt(II), Pd(II), U(IV), Sb(II) and ZrO(II) [38]. Antimicrobial activity of the Schiff bases and the complexes were also discussed

In 2016, Geetha Kannappan and S. Syed Tajudeen synthesized Schiff Base–copper(II) complex. Their work includes synthesis, spectral characterization of Schiff base complexes of pyrazinamide (an anti-tubercular drug), isoniazid, nicotinohydrazide and benzhydrazide with benzadehyde and dimethoxybenzaldehyde [39]. The copper complexes synthesized and isolated in powdered form and their 1:1 electrolytic nature

obtained from molar conductance values. Analytical data agreed that they have the composition of type $[L_2CuClO_4]ClO_4$. The stoichiometry and analytical data were further supported by magnetic susceptibility, mass spectrometry-liquid chromatography, Fourier transform infrared spectra, electronic spectra, electron paramagnetic resonance studies and cyclic voltammetry. They also made a preliminary attempt to compare the potencies of complexes with parent drug and significant results are obtained from copper(II) complexes.

In 2017, Hmeed, et al. carried out a review covers patented Schiff bases and their metal complexes having different therapeutic applications such as antialzheimer, antimicrobial, anticancer, urease inhibition, antituberculosis, detoxification, pesticidal activity, antiglycation and they used as antimicrobial wound dressing agents, imaging reagents and for quantitative determination of homocysteine in biological fluids [40].

Zhu, et al. investigated that when fluorination done at aldehyde part of the Schiff base, that will enhance its activity against insects [41]. Schiff bases derived from thiazole, aminothiazole, furfural, salicylaldehyde, pyridine aldehydes, taurine, amino acids, glucosamine, pyrazolone, aminopyridine, benzaldehyde and indole their metal chelates are found to be efficient inhibitors towards the growth of different pathogen.

Sulphur Containing Schiff Bases and Their Transition Metal Complexes: A Review

In many fields, the presence of sulphur in the ligand backbone imparts unique properties in terms of selectivity, activity and the catalyst precursor's stability. Metal complexes of ‘S’ containing Schiff bases and their relevant metal complexes have received extensive attention during recent years, mostly due to the outstanding antitumor, antibacterial and antiviral properties. Metal-sulphur centres play a vital role in activity of metalloproteins in enzymatic reactions. The systematic search for M-S model

compounds led to discovering an interesting and novel structural chemistry, which stems from the numerous possibilities of coordination of sulphur containing ligands.

Schiff base complexes derived from salicyladehyde and thiophene-2-aldehyde and sulfanethiadiazole displayed toxicities against insects [4,42]. Many pyran, quinazole, thiazole and benzothiazole derived Schiff bases possess efficient antifungal activity and the activity is enhanced when groups such as naphthyl, methoxy and halogen are attached [43,44]. In 1985, Vasilev and Devarski derived and studied herbicidal growth regulating activity of Zn(II) complexes of 2-aminobenzothiazole, 2- aminothiazole, 5-methoxybenzothiazole and 5-methyl benzothiazole [45]. Rhodium complexes of 2-amino-6-bromothiazole and 2-aminobenzothiazole exhibited antitumor activity.

In 1977, Ali and Tarafdar synthesized and characterized a benzoin derivative of Schiff base, H_2BBDT and its transition metal complexes [M= Ni(II), Mn(II), Co(II), Cd(II) and Zn(II)] which is derived from S-benzyldithiocarbazate, having the general formula $M(HBBDT)_2$ by means of elemental analyses, IR and electronic spectra, magnetic susceptibility and conductivity measurements [46]. The Schiff base functions as a uninegative, tridentate ligand formed by deprotonation and enethiolization of the thioamide group and bonds through the thiolate sulphur, hydroxyl oxygen and azomethine nitrogen. Based on magnetic and spectral studies, a distorted octahedral geometry or octahedral is proposed for the complexes.

In 2002 A. P. Mishra, et al. synthesized complexes of Co, Ni, Cu in +2 oxidation state with Schiff bases salicylidene-N-phenylthiourea (HSNPTU), furfurylidene-N-phenylthiourea (FNPTU) and salicylidene-2-aminophenol (H2SAPh). Using microanalytical data, IR, Conductance, UV-Vis, ESR spectroscopy, magnetic susceptibility measurements and TGA their physical-chemical properties have been investigated [47]. Ligand field parameters of complexes and also the non-isothermal

kinetic have been calculated. Salicylidene-2-aminophenol Ni(II) and Co(II) complexes have the general formula $[ML(H_2O)_3]\cdot 2H_2O$.Cu(II) complexes have the formula $[CuL(H_2O)]\cdot H_2O$. The general formulae $[ML_2]\cdot 2H_2O$ and $[ML_2Cl_2]\cdot 2H_2O$ are respectively for Salicylidene-N-phenylthiourea and Furfurylidene-N-phenylthiourea complexes. The antibacterial properties of these complexes were also screened and some of the complexes have been tested against tubercular bacteria.

In 2010, Shahriar Ghammamy et al. synthesized and the antitumour properties of two Fe complexes, [Fe(pythsal Br)]$Cl_2$and [Fe(pythsalI)]Cl_2 with the NSNO-donor tetradentate ligands of Schiff bases pythsal HX [(5-X-N-(2-Pyridylethylsufanyl ethyl)salicylidenemine] where 'X' is I or Br. These are obtained from the inserted condensation of (1,2-pyridyl)-3-thia-5-aminopentane with the respective derivative of salicyladehyde in molar ratio 1:1.molar ratio and their iron (III) complexes were studied for their antitumor properties. These new complexes showed anti-tumour activity against two kinds of cancer cells Jurkat (human T lymphocyte carcinoma) and K562 (human chronic myeloid leukaemia).

In 2012, Anjali Jha, synthesized 2,5-disubstituted thiadiazole by both microwave irradiation methods and conventional and then this these thiadiazole derivative is coupled with ethyl cyanoacetate (ECA), 2,4-pentanedione (AcAc) and malanodinitrile (MN) and these nucleated ligands were condensed with Ru(III), Cu(II) and Ni(II) [48]. These complexes were screened with U-937 lymphoma and HL-60 leukaemia cell lines. Ru complexes showed promising activity whereas Cu and Ni complexes exhibited moderate activity. On comparing their MIC values of ligand and complexes indicates that complexes display higher performance than ligands. Ru(III) complexes are better anticancer compounds

In 2014, Mohammad Nasir Uddin and coworkers prepared Schiff base by

condensing Thiophene-2-carbaldehyde with propane-1,2-diamine and 2-aminothiophenol [49] and synthesized its copper(II), cadmium(II), zinc(II) and nickel(II) complexes. Characterization conducted by elemental analysis, spectroscopic and magnetic measurements. Ligand is coordinated through nitrogen atom of the azomethine (-HC=N-) linkage and through sulfur atom of the thiophene moiety and it was recognized by NMR and IR spectra. Conductance measurements and magnetic susceptibility suggested non-electrolytic nature and octahedral geometry of the synthesized complexes. Antibacterial screening (*in vitro)* against different human pathogenic bacteria demonstrated that Cu(II) chelates shows high antibacterial activity and ligands exhibit only moderate activity.

In 2016, Abdel-Hady, et.al, synthesized new series of complexes of Schiff base (E)-N-(4-(2-hydroxybenzylideneamino) phenylsulfonyl) (S.S) with metal ions Cr(III), Pb(II), Ag(I), Cd(II), Fe(III), Co(II), Ni(II) and Ce(III) [50]. Characterization of these novel complexes were carried out by physico-chemical techniques like magnetic susceptibility, melting point, FT-IR, elemental analysis, ^{1}H NMR spectroscopy, conductance measurements, UV spectroscopy and mass spectral analysis. By using ICP-MS (Inductively Coupled Plasma-Mass Spectrometry), the metal ions concentrations have been determined. Complexes have been tested for antimicrobial performance against gram positive bacteria like *Streptococcus pneumonia, Bacillus subtilis* and gram negative bacteria like *Pseudomonas aeruginosa* and *Escherichia coli* and fungus like *Aspergillus fumigates* and *Candida albicans*. Spectroscopic studies revealed that coordination of most of complexes of (E)-N-(4-(2-hydroxybenzylideneamino) phenylsulfonyl) by two OH phenolic and 'N' azomethine in a regular octahedral arrangement in 2L:1M molar ratio in the form of $[ML_2(H_2O)_2]$.

In 2017, Shambuling Karabasannavar, et al. synthesized five metal complexes of Cd(II), Cu(II), Zn(II), Ni(II), and Co(II) with Schiff-base ligand, 3-((4-phenylthiazol-2-

ylimino)methyl)-2-hydroxybenzoic acid with metal ions [51]. Reaction proceeded through condensation reaction between 2-amino-4-phenyl thiazole and 3-aldehydo salicylic acid. Molar conductance, ^{1}H NMR, TGA/TDA, FT-IR and ESI mass studies are used for structural elucidation. The square planar geometry of the complex and bidentate O-O donor atom is determined by spectral studies and the antimicrobial and antifungal activity is detected. In order to investigate the *in vitro* cytotoxicity properties, the brine shrimp biological assay was carried out against Artemiasalina. Experimental results of DNA cleavage show that Co(II), Zn(II) and Cu(II) complexes exhibited outstanding DNA cleavage performances by the generation of radical of hydroxyl group.

In 2017, Emad Yousif, et.al; synthesized five novel complexes of Pd(II), Vo(II), Au(III), Co(II), and Rh(III) with Schiff base derivatives of 2N-salicylidene-5-(p-nitrophenyl)-1,3,4-thiadiazole, HL in alcohol medium [52]. These complexes characterized both by qualitatively and quantitatively by mass spectroscopy, FTIR, ^{1}H, ^{13}C NMR and UV–Vis spectroscopies and magnetic susceptibility, micro elemental analysis and conductivity measurements etc., These different metal ions coordinated to the ligand, HL through oxygen and nitrogen atoms. Most of these complexes exhibit square planar geometry except two complexes which are square pyramidal and tetrahedral in structure. In vitro antibacterial studies of these complexes gives that all these show moderate activity towards bacterial strains and slightly higher activity compared to HL ligand.

Schiff Bases Derived From Polynuclear Carbonyl Compounds and its Transition Metal Complexes: A Review

In 2002, Joby Thomas, et al. synthesized and characterized Mn(II), Co(II) and Ni(II) chelates of anthracene-9-carboxaldehyde thiosemicarbazone and carried out thermoanalytical and antitumour studies on the obtained complexes [53].

In 2009, Anant Prakash et al. synthesised novel Schiff bases derived from anthracene-9-carboxaldehyde with different amino acids like L-glycine, L-tryptophan, L-histidine, L-methionine and L-valine. These newly developed ligands and their transition metal complexes Cr(III), Ni(II) and Ti(III) are characterised by physicochemical techniques like elemental analysis, magnetic susceptibility measurement, Molar conductance, thermogravimetric analysis and spectrchemical studies like electronic spectral investigations [54]. The stoichiometry of metal ligand ratio found to possess 1:2. These novel Schiff bases and these Cr(III), Ni(II) and Ti(III) complexes were screened for antimicrobial studies.

In 2013, Devi, et al. synthesized and characterized Ni(II), Co(II) and Cu(II) complexes of the Schiff base derivatives from anthracene-9-carboxaldehyde with tyrosine on the basis of different physic chemical techniques [55]. To determine the decomposition pattern and thermal stability, Ni(II), Co(II) and Cu(II) complexes were subjected to thermal analysis. From TG curves, kinetic parameters like frequency factor (A), activation energy (ΔE) and entropy of activation (ΔS) were determined. The thermal stability of studied complexes are in the order Co(II) > Cu(II) > Ni(II). In TG curve, Co(II) and Ni(II) complexes showed a one stage decomposition pattern and Cu(II) complex showed a pattern of two stage decomposition.

In 2018, Shaju, et.al., synthesized, characterised novel Schiff base derivative and its Cu(II) complex from anthracene-9-(10H)-one and 3-phenyl propanoic acid. Also investigated the redox nature of these complexes with the help of cyclic voltammetry [56]. The effect of scan rate on the behaviour of redox reactions was evaluated.

Schiff Bases Derived From Pyridine Derivatives and its Transition Metal Complexes: A Review

In 2004, N. Raman, et.al. prepared Schiff bases derived from salicylidene-4-aminoantipyrine with substituted anilines/ $PhNH_2$ and their neutral Cu(II) complexes.

Structural features of these complexes were studied by microanalytical, IR, UV-Visible, ^{1}H NMR, ESR and mass spectral data [57]. The antimicrobial performance of the ligands and the copper complexes against the bacteria *Klebsiella pneumonia, Staphylococcus aureus, Salmonella typhi, Pseudomonas aerugenosa* and *Bacillus subtilis* are also reported. These complexes show higher activity than those of the free Schiff bases. They have higher activity than the control except for *Klebsiella pneumonia* and *Pseudomonas aeruginous*

In 2012, Y.K. Gupta, et al. synthesized complexes of transition metals like Ni(II), Co(II), Zn(II), Cu(II), Hg(II) and Cd(II) with bis(2-pyridylcarboxyl aldehyde)ethylene diamine (a bidentate ligand) formed by the condensation of ethylenediamine and 2-pyridylcarboxyl aldehyde [58]. On the basis of different analytical techniques like elemental analysis, magnetic moment data, conductance measurements, infrared and ^{1}H NMR spectroscopic datas, metal complexes have been characterized. From that, it has been found that complexes are in the ratio 1:2 (metal: ligand). Based on this data, they proposed a geometry which is octahedral for the metal(ll) complexes. Physiological activities against *Staphylococcus aureus, E. coli, Salmonella typhi* and *Bacillus subtilis* for the ligand and metal complexes were also screened.

In 2012, Krishnan Pothiraj, et al. synthesized four mononuclear Zn(II) and Cu(II) complexes of Schiff-base ligand and 2,2′-bipyridine/1,10-phenanthroline [59]. Characterization was also done on these complexes. Octahedral geometry has been proposed to complexes based on the data obtained from magnetic susceptibility and electronic spectral data. By absorption filtration, viscosity and electrochemical methods DNA binding behaviour of these complexes were evaluated and found that complexes bind to calf thymus DNA in an interactive mode. The antimicrobial studies reveal that complexes are superior antimicrobial agents than ligands.

In 2012, A. Angel, et al. synthesized and characterized [Cu(2AcpClPh)Cl]2H_2O, [Cu(2AcPh)Cl]2H_2O, [Cu(2BzpNO_2Ph)Cl], [Cu(2AcpNO_2Ph)Cl], [Cu(2BzpClPh)Cl] and [Cu(2BzPh)Cl] with 2-acetylpyridine-para-chloro-phenylhydrazone (H_2AcpClPh), 2-acetylpyridine-para-nitro-phenylhydrazone (H_2AcpNO_2Ph), 2-acetylpyridine-phenyl hydrazone (H_2AcPh), 2-benzoylpyridine-phenylhydrazone (H_2BzPh), 2-benzoyl pyridine -para-nitro-phenylhydrazone (H_2BzpNO2Ph) and 2-benzoylpyridineparachloro-phenyl hydrazone (H_2BzpClPh) [60]. Hydrazone derivatives exhibit poor antibacterial effect against *Enterococcus faecalis*, *Staphylococcus aureus* and *Pseudomonas aeruginosa*. But they demonstrated significant antifungal performance against the bacterial strain *Candida albicans*. The antifungal and antibacterial activities are appreciably increased by complexation with copper.

In 2012, N. S. Gwaram, et al. synthesized transition metal complexes of Schiff base derivatives 4-(2-aminoethyl)morpholine and 4-(2-aminoethyl)piperazine with 2-acetylpyridne and characterized using elemental analysis, UV-Vis spectral studies, NMR and FT-IR [61]. Cd(II) complexes displayed polymeric structure Zn(II) complex exhibited square pyramidal geometry while Ni(II) complexes showed an octahedral geometry.

In 2014, Raphael P. Vinod, et al. synthesized and investigated copper chelate of heterocyclic Schiff base 3-acetylpyridine phenylhydrazone (APPH) and are characterized by elemental, spectral, magnetic and conductance measurements [56]. Results showed that during chelation, APPH performed as bidentate ligand. The electrochemical response of this Schiff base and its chelate were reported. The square planar geometry of the chelate was confirmed by optical spectral studies and magnetic studies.

Schiff bases Derived From Indole and its Transition Metal Complexes: A Review

In 2012, Ibrahim, et al. evaluated the gastroprotective activity of nickel(II)

complex of Schiff base ligand derived from the condensation reaction of 5-nitro salicylaldehyde (TNS) and an indole derivative of tryptamine against ethanol-induced gastric ulcer in rats [62]. The results showed that these Schiff base ligand and nickel(II) complex showed effective gastric protection and leucocyte infiltration of the submucosal layer and reduced edema.

In 2014, Rhaman, et al. synthesized and characterised transition metal complexes of Zn(II), Co(II), Ni(II), Cu(II), Hg(II) and Cd(II) with a tridentate (Oxygen-Nitrogen-Nitrogen) ligand 3,5-dimethyl-*N*′-[(1*E*)-1′-pyridin-2′-ylethylidene]-1*H*-indole-2-carbo hydrazide on the basis of analytical, infrared, nuclear magnetic resonance, magnetic susceptibility, electron paramagnetic resonance spectral studies, fast atom bombardment-mass, UV-and visible spectral data and X-ray powder diffraction [63]. Based on molar conductance and analytical data, the complexes may be formulated as $[M(L)Cl_2].(H_2O)_n$, where M=Zn, Hg and Cd and $[M(L)_2]\cdot(H_2O)_n$, where 'M' can be Cu, Ni and Co and. The spectral studies revealed that, an square pyramidal geometry for Zn(II), Cd(II) and Hg(II) complexes whereas octahedral geometry for Co(II), Ni(II) and Cu(II) complexes, Their antifungal activity against *Candida albicans and Aspergillus niger* and antibacterial activity against *Staphylococcus aureus* and *Escherichia coli* were screened.

In 2019, Tadele and Tsega studied the anticancer activity of the novel Schiff bases and their metal complexes was studied using different assays such as PI staining, 3-[4,5-dimethyltiazol-2-yl]-2,5-diphenyl-tetrazolium bromide (MTT), Allium cepa, Sulforhodamine, Sulfo- Rhodamine-B-stain (SRB), viability and potato disc against various animal and human cancer cell lines [64]. They exhibited very high activity against MCF-7 and HepG2 cell lines.

In 2019, E.L. Gammal, et al. synthesized novel mononuclear Cu(II), Cd(II),

Sn(IV), Fe(III) and binuclear Hg(II), Ni(II) and complexes with the Schiff base ligand: (E)-N'-((4-methyl-1H-indol-3-yl)methylene)nicotinohydrazide [65]. The structures of the prepared compounds were elucidated by elemental analyses, magnetic measurements, 3D molecular modeling, Thermogravimetry and molar conductance techniques were by conducted by diverse spectroscopic (^{1}H NMR, IR, UV–Visible and EPR) techniques. Antioxidant activities of ligand and metal complexes were studied by DPPH scanning *(in vitro)* technique. Highest antioxidant activity shown by $[Sn(HL)Cl_2(OH)_2].2H_2O$ complex. Ligand and its metal complexes were screened for antibacterial activities against two strains of fungi *Aspergillus flavus* and *Candida albicans* and two bacterial strains *Staphylococcus aureus* and *Escherichia coli.* The binuclear complex, $[Hg_2(HL)Cl_4]\cdot EtOH$ showed excellent antifungal performance against *Aspergillusflavus* and excellent antibacterial activity higher than the standard drug Ampicillin.

Scope and Objectives of Present Investigation

Many Schiff bases have been checked for their chelating ability with different transition and inner transition metals. The quest for novel Schiff bases and their metal chelates are continuing in the present decades. Literature survey revealed that there is a wide scope still remains for the investigation of novel Schiff bases and its metal chelates. In the present investigation, it is proposed to synthesize novel Schiff bases containing sulphur and its transition metal chelates. Since the polarizability of lone pairs on the sulphur atom is high one can expect an escalated chance for the chelation and other related properties. Exploring the structure and geometries of newly synthesized Schiff bases and metal chelates with the help of various analytical techniques will be helpful in explaining the significant properties and applications by correlating to their molecular structure.

Checking the chelating ability of the newly synthesized sulphur compounds may lead to open a new series of novel metal complexes which may have some pharmacological activity. To ensure the drug ability of the newly synthesized organic molecules and their metal chelates, it is decided to conduct the antimicrobial studies and molecular docking studies.

A thorough literature survey revealed that many Schiff base molecules bearing sulphur atoms is infrequently subjected to the corrosion inhibition studies on various metals in acidic medium. So in the present investigation it is proposed to screen corrosion inhibition properties of the newly synthesized Schiff bases on various metals in acidic media.

CHAPTER 2
MATERIALS AND METHODS

In this chapter, a brief sketch of the common reagents and general methods adopted for the preparation, purification and characterization of heterocyclic Schiff bases containing 'S' and their transition metal complexes are explained.

Reagents Used

For the preparation of amine, analar grade samples of para nitro benzoic acid, potassium hydroxide, thiosemicarbazide and phosphorous oxychloride were used. Analar grade samples of anthracene-9-carbaldehyde (synthetic material), anthrone, pyridine-2-carbaldehyde, 3-acetyl pyridine, 2-acetyl pyridine, indole-3-carbaldehyde, 2-aminothiazole, thiophene-2-carbaldehyde, 1,2-diaminocyclohexane were purchased from Fluka for the synthesis of heterocyclic ligands.

Solvents, rectified spirit and ethanol were purchased from E. Merck in pure form was used as the medium used for the synthesis of the 'S' containing heterocyclic ligands. Solvent DMSO purchased from E. Merck was used for the analysis of UV-Visible spectral studies and electrolytic conductance measurements. Metal salts like acetates, chlorides and nitrates from Qualigens (AR samples) were used for the synthesis of the heterocyclic Schiff base complexes. Almost all transition metal chelates were synthesized in pure ethanol medium.

Metal salts used for the analysis were the acetates or chlorides of copper, chromium, manganese, cobalt, nickel and zinc and nitrates of zirconium. For the preparation of Fe(III) complexes, ferric chloride (analar grade from Ranbaxy) was used, while nitrates of zirconium were used for the synthesis of Zirconium chelates/ complexes. The entire metal salts were purchased from Qualigens and E. Merck

The general preparation procedure for the synthesis of the heterocyclic ligands and their transition metal complexes with various metal salts and other details are given in the subsequent chapters.

Analytical Techniques

CHNS analysis

Elementar make Vario EL III model CHNS analyzer is used for the microanalysis of the heterocyclic Schiff bases and their transition metal chelates by assessing carbon, hydrogen, nitrogen and Sulphur.

Metal content analysis

Pyrolytic method was used as the preliminary estimation of metal percentage in the heterocyclic Schiff base complexes [66]. An electric Bunsen was used for heating the metal complexes. About 0.2g of the transition metal complex was weighed, transferred in a previously weighed silica crucible and heated for 2h. Metal oxides were produced by the decomposition of their consequent metal complexes. The metal oxide left behind was weighed after cooling and the metal percentage of for each complex was estimated.

For conducting further estimations, a known amount of the metal chelates were digested for 1h with a mixture of concentrated perchloric-nitric acid. After the digestion or decomposition of the metal complexes, the mixture was further extracted with concentrated HCl and the resultant solution was then quantitatively transferred into a volumetric flask. Different analyses were carried out for finding out the percentage of the metal by taking a definite volume of the solutions.

Estimation of chromium was done by photometric method using 1,5-diphenyl carbazide; a violet colour of chromium complex was formed with this reagent.

Thiocyanate method was used for the estimation of iron complexes. The cobalt metal ion can be estimated by both volumetrically and complexometrically. (Standard EDTA, hexamine buffer solution and xylenol orange indicator were mainly used for the complexometric estimation)

Complexometric titration was also employed for the estimations of nickel and zinc by using complexing agent as EDTA; Murexide and Eriochrome black-T were used as indicators for nickel and zinc metal ions respectively [67]. Iodometric titration was used for copper estimation by means of sodium thiosulphate as titrant and starch as indicator. Nickel content was estimated by the precipitation of the complex of nickel dimethyl glyoxime [$Ni(C_4H_7O_2N_2)_2$], using dimethylglyoxime as the precipitating agent.

Spectral studies

To confirm the structures and geometry of the heterocyclic Schiff base ligands and their complexes, spectral tools like UV-Visible, GCMS, Infrared, ^{1}H NMR and ^{13}C NMR were used.

- ***UV-Visible spectra:*** Electronic spectra of these molecules and its transition metal complexes were traced in the range of 200-800nm in DMSO on a Shimadzu UV-Visible-1800 spectrophotometer. These spectra play an important role as a confirmation to magnetic moment studies to formulate the geometry of the complexes. Structural identification was also the main perspective of UV-Visible spectra.
- ***Infrared spectra*****:** Infrared spectra of all synthesized heterocyclic compounds and metal complexes were traced in the range 4000-400cm^{-1} by KBr disc technique. FT-IR spectrometer made by Shimadzu, Japan, specially indicated model IR affinity-1, was utilized for the analysis of the infrared spectra of all synthesized heterocyclic ligands and metal complexes. The IR spectroscopy is important since

it exhibits a characteristic absorption band for a particular group irrespective of the ligands and complexes in which the group is present. Thus it becomes a fingerprint for identification and a powerful tool for studying molecular structure. Moreover, the coordination of the metal ion with the ligands can be reputable with the corresponding spectra. Prediction of the coordination sites of these heterocyclic ligands to the metal ion can be done by the comparison between the infrared spectrum of these ligands with the metal chelates.

- ***NMR spectra*:** The performance of ^{1}H NMR and ^{13}C NMR spectral studies of ligands and complexes were carried out in DMSO as the solvent and studies were done using the instrument Bruker Avancelll, 400MHz model.
- ***Mass spectra*:** GCMS Qp-2010 plus model Shimadzu at a source temperature of $300^{0}C$ were used for recording the mass spectra of the synthesized heterocyclic ligands. Before the mass spectral studies, gas chromatography was conducted on these synthesized Schiff bases for the confirmation of purities of the ligands.

Physicochemical studies such as molar conductance studies and magnetic susceptibility measurements were conducted to clarify the structure and geometry of the synthesized complexes

Molar conductance measurements

ELICO conductivity meter was used to measure the molar conductivities of the metal complex solutions at room temperature which helps to ascertain the charge of the complex.In all measurements, the solution concentration was maintained as $10^{-3}M$ at 30±2°C and cell constant as '1'. By measuring this parameter, the electrolytic behavior of the compounds could understand [68].

Magnetic susceptibility measurements

By adapting Gouy method, the magnetic susceptibilities of the complexes could

be measured. The apparatus UK (Mark 1) from Sherwood and $Hg[Co(NCS)_4]$ as the calibrant (do not decompose or absorb moisture, easy to prepare and pack well in the sample tube) were used for this purpose. "The molar susceptibility, a measure of magnetic field of a substance, is the algebraic summation of the susceptibilities of the constituent ions, atoms or molecules". By using Pascal's constants, diamagnetic corrections were applied [69]. It is done by taking in to the deliberation of the magnetic contribution of different atoms and structural units. From the corrected susceptibilities, the effective magnetic moments were calculating using the equation.

$$\mu_{eff} = 2.84\sqrt{\chi_m \times T} \quad (1)$$

where χ_m= Molar susceptibility (corrected for diamagnetism); T = Absolute temperature

$$\chi_m = \chi_g \times \text{Molecular mass} \quad (2)$$

where, χ_g= Gram susceptibility

$$\chi_g = C \times L \times (R\text{-}R_0)/W \times 10^9 \quad (3)$$

Where, C = Tube calibration constant; L = Length of the complex (sample); R_0 = Value of empty glass tube; R = Value of sample + glass tube; W = Weight of sample.

The theoretical magnetic moment values were calculated using the formula,

$$\mu_{eff} = g\sqrt{S(S+1)} \quad (4)$$

where 'g' is the Lande splitting factor or gyromagnetic ratio and '*S*' is the total spin quantum number.

CHAPTER 3

TRANSITION METAL COMPLEXES OF SCHIFF BASES DERIVED FROM 5-(4-NITROPHENYL)-1,3,4-THIADIAZOL-2-AMINE (NPTDA) AND POLYNUCLEAR CARBONYL COMPOUNDS

Nowadays, the transition metal complexes with thiadiazole moieties have great commercial value and this has aroused considerable interest in the field coordination chemistry. However, there is no information available in the literature on metal complexes of Schiff base ligands synthesized from 5-(4-nitrophenyl)-1,3,4-thiadiazole-2-amine and its polynuclear carbonyl compounds. Therefore it was considered to be very useful and interesting to study the donor properties of novel 'S' containing Schiff bases (E)-N-(anthracen-9-ylmethylene)-5-(4-nitrophenyl)-1,3,4-thiadiazol-2-amine) (A9CNPTDA) and N-(anthracen-10(9H)-ylidene)-5-(4-nitrophenyl)-1,3,4-thiadiazol-2-amine) (ANNPTDA) and their transition metal complexes. An attempt for the characterization of the ligands and complexes were done with the aid of analytical tools such as elemental (CHNS) analysis, estimation of metal percentage, magnetic moment, molar conductance and various spectroscopic techniques.

The detailed synthesis and characterization of these two novel 'S' containing polynuclear derivatives of Schiff bases and their metallic complexes are discussed as two separate sections. Section I deals with synthesis and characterization of polynuclear Schiff base ligand, A9CNPTDA derived from the parent amine 5-(4-nitrophenyl)-1,3,4-thiadiazol-2-amine (NPTDA) and anthracene-9-carbaldehyde and its transition metal complexes. Section II consists of synthesis and characterization of another polynuclear 'S' containing Schiff base, ANNPTDA derived from the parent amine, NPTDA and anthrone and its transition metal complexes

Synthesis of 5-(4-nitrophenyl)-1,3,4-thiadiazol-2-amine (NPTDA)

Parent amine, 5-(4-nitrophenyl)-1,3,4-thiadiazol-2-amine (NPTDA) was synthesized using the standard procedure by Yousif et al. [70] and the schematic representation of the synthesis is shown in Fig. 1.1. It was synthesized by refluxing equimolar mixture of 4-nitrobenzoic acid and thiosemicarbazide in phosphorus oxychloride solution for 3h. To the cooled mixture, distilled water was added and further refluxed for 5h. The solution obtained was neutralized with potassium hydroxide and the formed yellow precipitate was filtered, washed with cold distilled water, dried and melting point was found to be 247^{o}C (Yield: 56%)

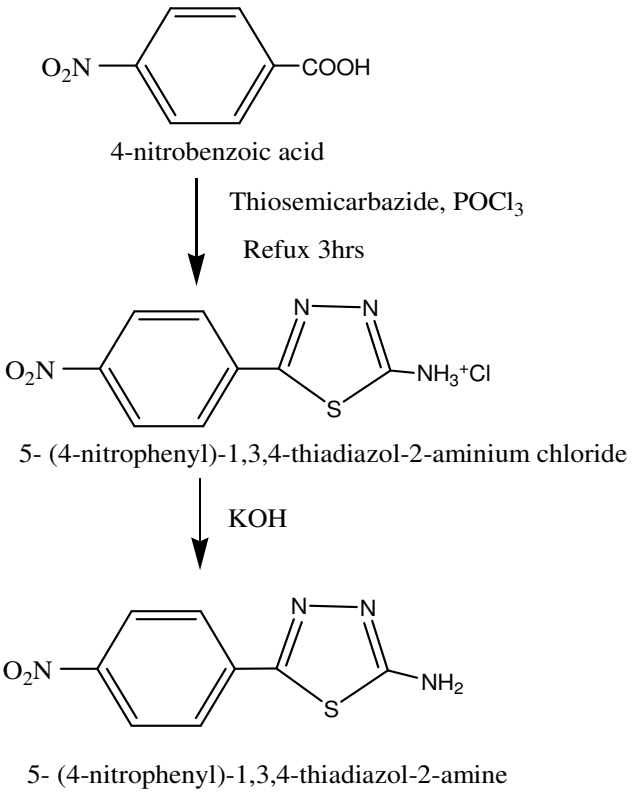

Fig. 1.1: Schematic representation of the synthesis of parent amine 5-(4-nitrophenyl)-1,3,4-thiadiazole-2-amine (NPTDA)

Characterization of Parent Amine (NPTDA)

Characterization of amine was done by spectral studies. Electronic spectrum of 5-(4-nitrophenyl)-1,3,4-thiadiazol-2-amine exhibited a band at 39215cm^{-1} which can be

consigned to $\pi \rightarrow \pi^*$ transition and the $n \rightarrow \pi^*$ transition band was appeared at lower frequency of 27173cm^{-1}. The K-band is found to have more intensity compared to R-band, which is spectroscopically forbidden.

FTIR spectral analysis

Infrared spectrum of amine showed broad bands of medium intensity at about 3422cm^{-1} and 3309cm^{-1} which may be attributed to the asymmetric and symmetric N-H stretching frequency of amino part. Another peak appeared at 1615cm^{-1} can be assigned to the C=N stretching in the ring. Strong peaks displayed at 1603cm^{-1} and 1526cm^{-1} are due to C=C stretching frequencies. There were also characteristic peaks at 3121cm^{-1} and 1105cm^{-1} because of the aromatic C-H and C-S stretching vibrations respectively. Also the C-N vibrational frequency was emerged at 1280cm^{-1}. The presence of nitro group was confirmed by the presence of peaks at 1463cm^{-1} and 1349$cm^{-1}$and the in plane bending vibrations appeared at 1012cm^{-1}. Also the peaks obtained at 871cm^{-1} and 714cm^{-1} can be assigned as out of plane bending vibrations.

NMR spectral analysis

A broad singlet peak that appeared at 4.14δ was consigned to the protons of the free terminal NH_2 group present in the parent amine NPTDA and the spread in the peak may be attributed to quadrupole broadening (Fig. 1.2). The aromatic protons of both anthracene and benzenoid rings resonated as multiplets at 8.1δ and 8.24δ.

Mass spectral analysis

Molecular ion peak of NPTDA was observed at m/z 222 $[C_8H_6N_4O_2S^{32}]^+$ as a strong peak, which establishes the stability of molecule. The emergence of the M+2 peak (isotopic peak) in the spectrum of parent amine at m/z 224 $[C_8H_6N_2S]^+$, is due to the presence of the S^{34} atom present in it. [M]:[M+2] ratio indicates one 'S' atom in the molecule. The base peak was displayed at m/z 74 due to the fragment $[CH_2N_2O_2S]^+$. The

fragments $[C_8H_6N_2S]^+$, $[C_7H_4NS]^+$, $[C_7H_4S]^+$ and $[C_7H_7]^+$, $[CH_2NS]^+$ displayed corresponding signals at m/z 162, 134, 120, 91 and 60 respectively (Fig. 1.3).

The characterization records obtained were in excellent correlation with the reported data in literature. From the spectral data and synthetic route adopted, the amine was assumed the structure represented in Fig. 1.1.

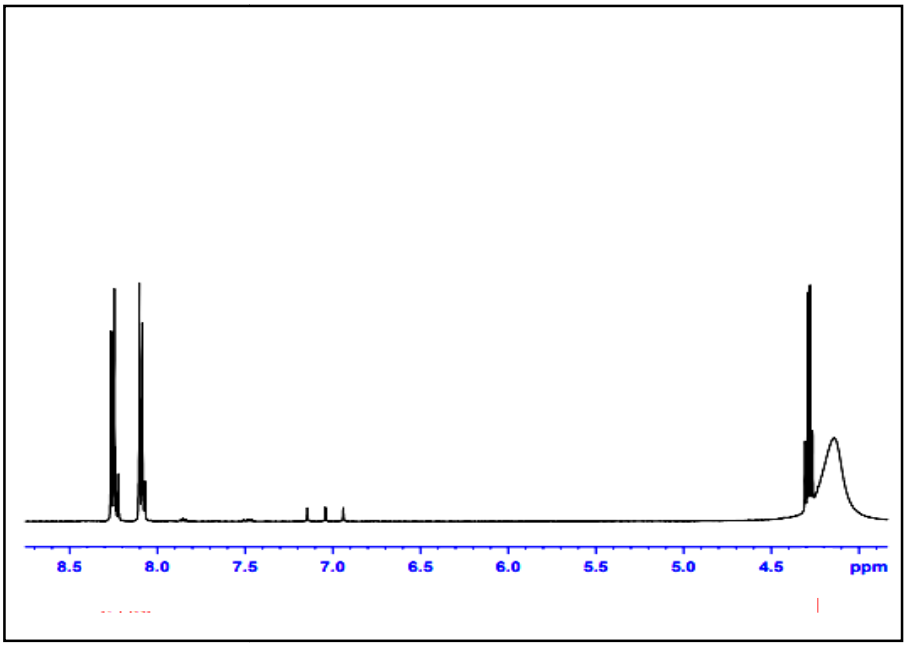

Fig. 1.2: ^{1}H NMR spectrum of NPTDA

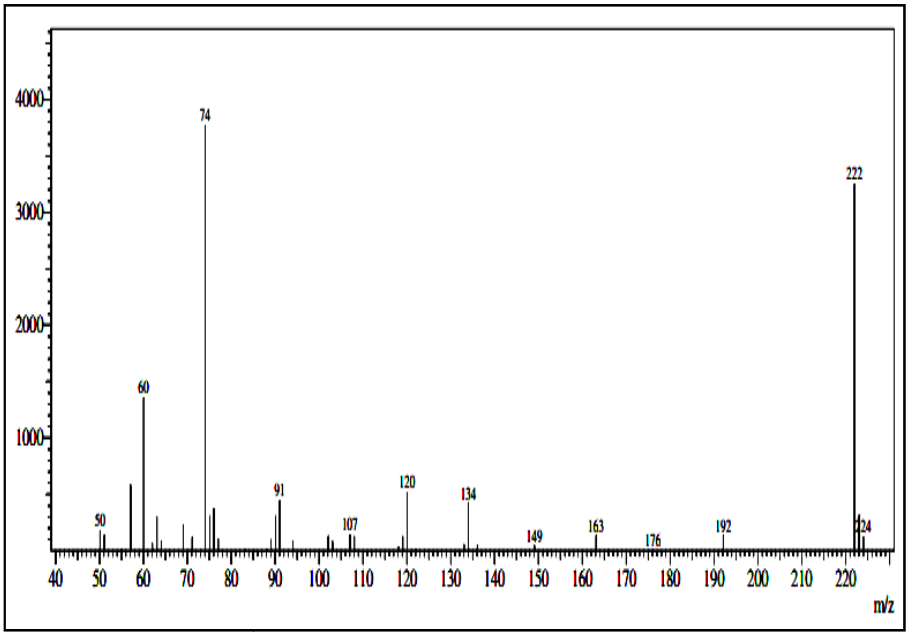

Fig. 1.3: Mass spectrum of NPTDA

SECTION I

STUDIES ON SCHIFF BASE, (E)-N-(ANTHRACEN-9-YLMETHYLENE)-5-(4-NITROPHENYL)-1,3,4 THIADIAZOL-2-AMINE) (A9CNPTDA) AND ITS TRANSITION METAL COMPLEXES

A novel 'S' containing polynuclear Schiff base (E)-N-(anthracen-9-ylmethylene)-5-(4-nitrophenyl)-1,3,4-thiadiazol-2-amine (A9CNPTDA) was synthesized and characterized by elemental analysis and various spectroscopic techniques. The structure of A9CNPTDA and its transition metal complexes with chromium, manganese, iron, cobalt, nickel, copper, zinc and zirconium ions were established based on spectroscopic, magnetic and electrical studies. In this section, the detailed synthesis and characterization of both the ligand and complexes are discussed.

Synthesis of A9CNPTDA

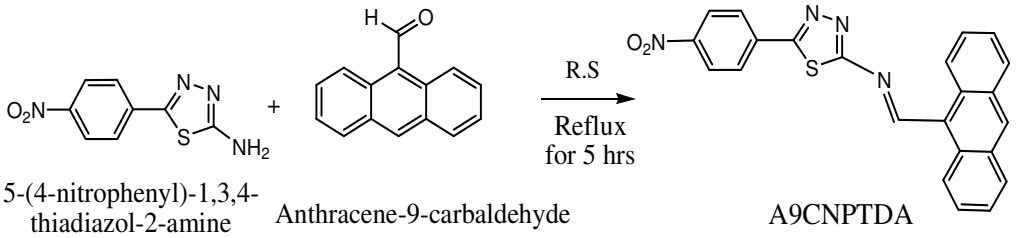

5-(4-nitrophenyl)-1,3,4-thiadiazol-2-amine Anthracene-9-carbaldehyde A9CNPTDA

Fig. 1.4: Synthesis of A9CNPTDA

Polynuclear 'S' containing Schiff base, (E)-N-(anthracen-9-ylmethylene)-5-(4-nitrophenyl)-1,3,4-thiadiazol-2-amine (A9CNPTDA) was synthesized by adding a hot ethanolic solution of anthracene-9-carbaldehyde (2mM) in dropwise to stirred solution containing equimolar concentration of 5-(4-nitrophenyl)-1,3,4-thiadiazol-2-amine in ethanol medium. The mixture was refluxed for 5h, cooled and concentrated to derive reddish orange coloured needle-shaped crystals of A9CNPTDA. MP is 279^0C (Yield: 73%).

Characterization of A9CNPTDA

Elemental analysis

The elemental analysis data of 'S' containing polynuclear Schiff base A9CNPTDA is given in Table 1.3. The experimentally obtained percentages of elements like carbon, hydrogen, nitrogen and sulphur were in good agreement with the calculated values.

Electronic spectral analysis

Characterization of ligand, (E)-N-(anthracen-9-ylmethylene)-5-(4-nitrophenyl)-1, 3,4-thiadiazol-2-amine (A9CNPTDA) was done using UV, IR, NMR and Mass spectral data. Electronic spectrum of the ligand showed important two peaks at 39062 (strong) and 27100cm^{-1} (weak), due to $\pi \rightarrow \pi^*$ and $n \rightarrow \pi^*$ transitions respectively. The decrease in the values compared to the parent amine is an indication of extension of conjugation during the formation of ligands.

FTIR spectral analysis

The absorption bands in the IR spectrum of parent amine NPTDA, due to N-H stretching frequency of amino group at 3600-3300cm^{-1} were disappeared in the spectrum of Schiff base, which confirms the formation of A9CNPTDA. Another important band emerged at 1691cm^{-1} was due to the stretching mode of azomethine linkage. There was an aromatic C-H stretching frequency at 3102cm^{-1} and C-N stretching at 1274cm^{-1} and band at 1104cm^{-1}corresponds to $\upsilon_{C\text{-}S.}$ Two important peaks appeared at 1527$cm^{-1}$and 1347cm^{-1} indicated the presence of nitro group in this polynuclear Schiff base A9CNPTDA. C=C present in the aromatic rings displayed peaks at 1556cm^{-1} and 1445cm^{-1} and in plane bending vibrations appeared at 1008cm^{-1}. Also the peaks obtained at 854cm^{-1} and 607cm^{-1} can be assigned as out of plane bending vibrations. Characteristic

infrared absorption frequencies (cm^{-1}) of this polynuclear sulphur containing Schiff base A9CNPTDA is represented in Table 1.4.

NMR spectral analysis

The ^{1}H NMR spectrum of the 'S' containing Schiff base, A9CNPTDA are shown in Fig. 1.5. Six non equivalent protons which are in different electronic environments gave their characteristic peaks in the PMR spectrum. The detailed assignments of peaks are shown in Table 1.1. A peak at 11.5δ (s) can be assigned to the azomethine proton. The aromatic protons of the anthracene ring resonated as multiplets between 7.75-9.03δ. Doublet protons appeared at 8.02δ and 8.30δ was due to the proton in the benzene ring.

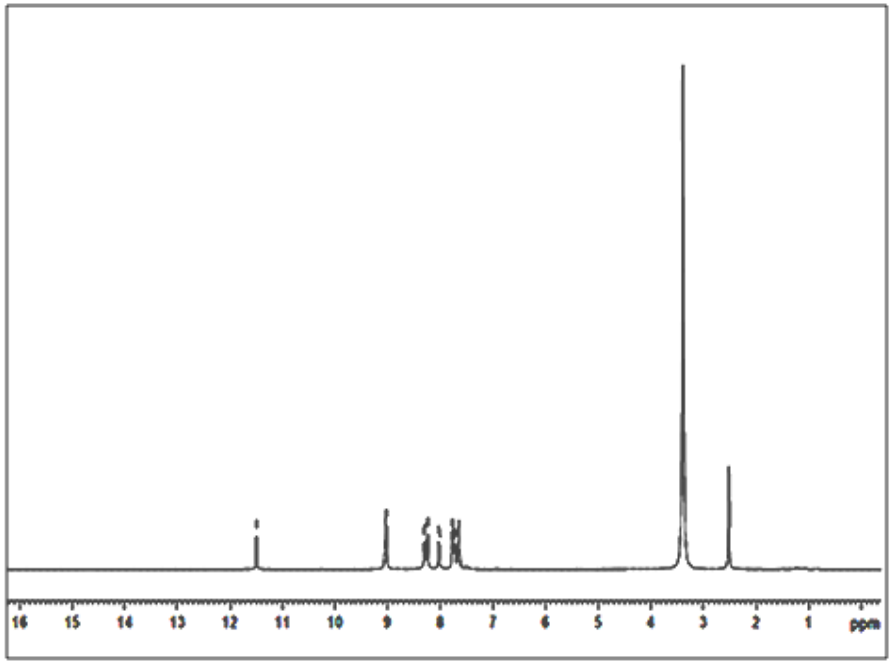

Fig. 1.5: ^{1}H NMR spectrum of A9CNPTDA

Fifteen chemically different carbon atoms present in A9CNPTDA showed 15 distinct signals in the ^{13}C NMR spectrum (Fig. 1.6). Peak at 136ppm corresponds to the carbon atom of azomethine linkage and labelled carbon atoms present in the anthracene

and benzene rings observed between 123-154ppm. The details of the peaks corresponding to different carbon atoms are expressed in Table 1.1.

Table 1.1: ^{1}H NMR and ^{13}C NMR spectral data of A9CNPTDA

^{1}H NMR			^{13}C NMR		
	δ value	Labelled proton	δ value	Labelled carbon	
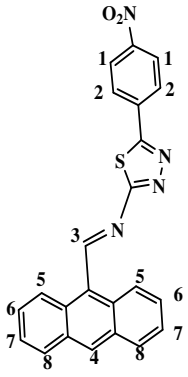	8.02(d,2H)	1	131	1	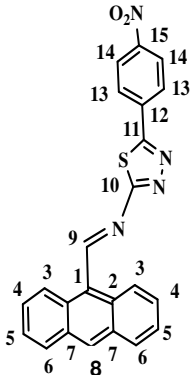
	8.30(d,2H)	2	130	2	
	11.5(s,1H)	3	129.5	3	
	7.75(m,3H)	4&8	129.2	4	
	9.03(m,4H)	5&6	127	5	
	8.24(m,2H)	7	125	6	
			127	7	
			124	8	
			136	9	
			194	10	
			169	11	
			147	12	
			123	13	
			135	14	
			154	15	

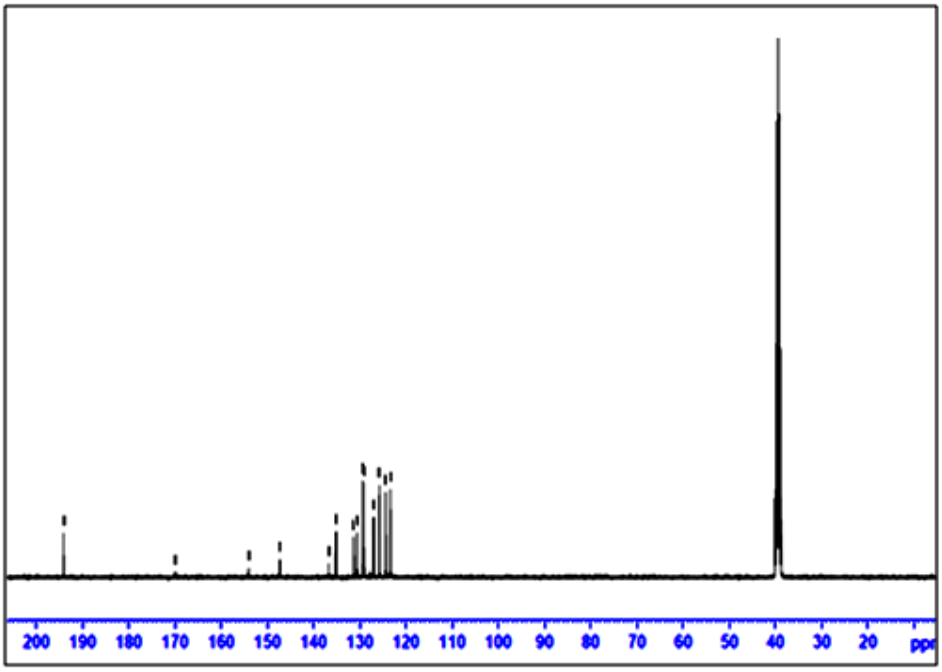

Fig. 1.6: ^{13}C NMR spectrum of A9CNPTDA

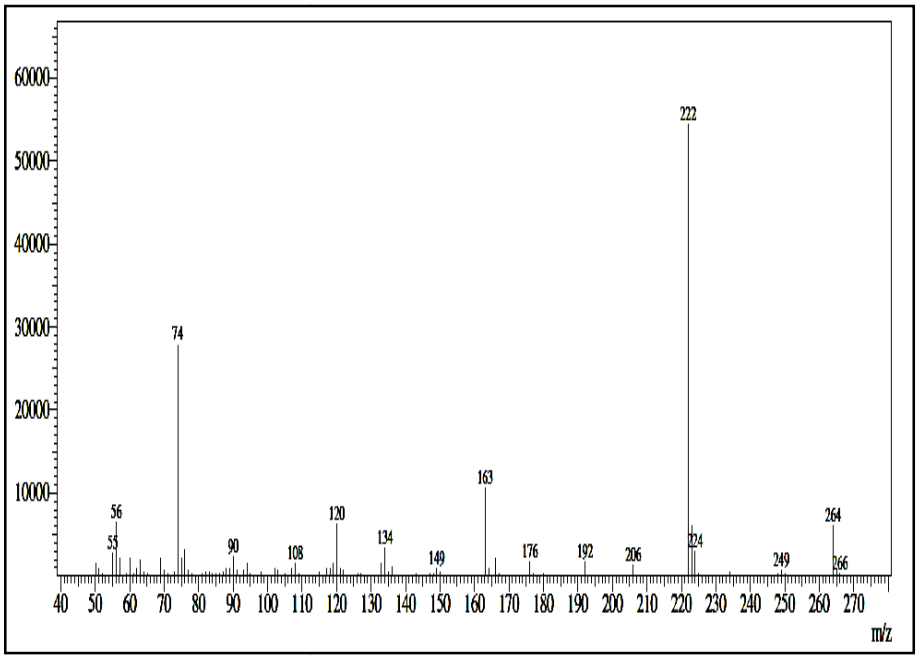

Fig. 1.7: Mass spectrum of A9CNPTDA

Mass spectral analysis

The separation of Schiff base was ascertained by the single sharp signal in GCMS showing the purity of the ligand A9CNPTDA. The mass spectrum of A9CNPTDA is represented in Fig. 1.7. In the spectrum, molecular ion peak was absent and the base peak was shown at m/z 222 due to the fragment $[C_8H_6N_4O_2S]^+$, originated by the loss of A9C part from the molecule. The fragments $[C_8H_7N_2S]^+$, $[C_7H_4S]^+$, $[C_7H_7]^+$ and $[CH_2N_2S]^+$ displayed signals at m/z 163, 120, 91 and 74 respectively.

From the above discussions the structure of polynuclear Schiff base A9CNPTDA can be assigned and given in Fig 1.8

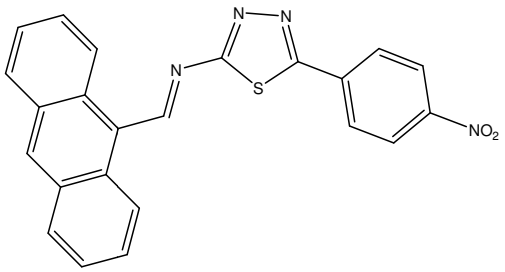

Fig. 1.8: Structure of A9CNPTDA

Synthesis of Complexes

Cr(III), Mn(II), Fe(III), Co(II), Ni(II), Cu(II), Zn(II) and ZrO(II) complexes of polynuclear 'S' containing Schiff base, (E)-N-(anthracen-9-ylmethylene)-5-(4-nitro phenyl)-1,3,4-thiadiazol-2-amine (A9CNPTDA) were synthesized as follows.

Acetate salts of chromium, manganese, nickel and copper were used for the synthesis of corresponding metal complexes. Chloride salts of iron and zinc were used for the preparation of Fe(III) and Zn(II) complexes. For the synthesis of Co(II) and ZrO(II) complexes, metal nitrates were employed.

2mM solution of the polynuclear 'S' containing Schiff base, A9CNPTDA in 10ml ethanol was refluxed on a water bath. To the boiling solution, 2mM hot ethanolic solution of the corresponding metal salt (acetates/chlorides/nitrates) was added and again refluxed for 6h. The pH of the mixture was adjusted to 7-8 by adding a few drops of sodium acetate solution (CH_3COONa). Then reduced its volume by evaporation, cooled and the crystallized metal complexes were collected, washed and dried over $CaCl_2$.

Zirconyl nitrate solution in ethanol medium was added dropwise to the hot ethanolic solution of Schiff base ligand (molar ratio 1:1) and refluxed for five hours at 80ºC [71]. The resulting orange coloured precipitate was collected by filtration, washed with ethanol and hot water and finally dried. Melting points of the complexes were noted, and these were higher than that of ligand A9CNPTDA.

Characterization of Complexes

All the complexes of this ligand were amorphous solids and stable to light and air. They are insoluble in water and soluble in organic solvents like DMSO and DMF. They are characterized by elemental analysis, spectral studies, molar conductance studies, magnetic moment measurements etc;

Elemental analysis

This analysis provides an important key to structural elucidation of complexes. Percentage of C, H, N and S as well as the metal content were estimated by microanalytical methods. There is a good correlation between observed and calculated values of elemental analysis. 1:1 stoichiometry exists between metal and this polynuclear Schiff base derivative A9CNPTDA in all complexes.

The elemental and metal percentage data of A9CNPTDA-complexes obtained theoretically and experimentally are listed in Table 1.3.

Electronic spectral analysis

In the case of complexes, bathochromic shift was occurred for both $\pi \rightarrow \pi^*$ and $n \rightarrow \pi^*$ bands which is a clear evidence for the complex formation. The electronic spectra of all complexes of A9CNPTDA showed two peaks with red shift with respect to that of ligand, which confirms the complexation. The electronic spectral bands of polynuclear sulphur containing Schiff base A9CNPTDA and its metal complexes are summarized in Table 1.2.

Table 1.2: Electronic spectral data of parent amine (NPTDA), Schiff base (A9CNPTDA) and its transition metal complexes

Compound	Electronic bands in cm^{-1}	
	$\pi \rightarrow \pi^*$	$n \rightarrow \pi^*$
NPTDA	39215	27173
A9CNPTDA	39062	27100
$[CrL(Ac)_3H_2O]$	37878	26666
$[MnL(Ac)_2(H_2O)_2]$	38759	26954
$[FeLCl_3(H_2O)]$	37878	27027
$[CoL(NO_3)_2(H_2O)_2]$	38910	27027
$[NiL(Ac_2)_2(H_2O)_2]$	38910	26881
$[CuL(Ac)_2(H_2O)_2]$	38759	26954
$[ZnLCl_2]$	38610	26954
$[ZrOL(NO_3)_2]$	37735	25252, 26954

Magnetic moment analysis

The geometry of the complexes can be predicted from the magnetic moment measurements. Magnetic moment values of Cr(III) complex was found to be 3.83BM (Calculated μ_{eff} value of d^3 system by spin only formula is 3.87BM), which clearly indicate octahedral geometry of A9CNPTDA-Cr^{3+}complex. The observed magnetic moment value for the Mn(II) complex was 6.56BM which clearly establishes its octahedral geometry. The increase in the value compared to expected spin only value of Mn(II) chelate (5.9BM) is an indication of orbital contribution towards the effective magnetic moment [72]. Fe(III), Co(II) and Ni(II) complexes were found to be in distorted octahedral geometry since they exhibited magnetic moment values 5.15BM, 3.23BM and 2.14BM respectively [73,74]. μ_{eff} value of Cu(II) chelate was 2.19BM, which is reliable with data accessible from the literature review, for distorted octahedral geometry Cu(II) chelates [75]. Diamagnetic character was observed for Zn(II) and ZrO(II) complexes, which is quite justifiable with their d^{10} or d^0 configuration respectively and hence tetrahedral and square pyramidal geometry respectively were ascertained for them [32,76]. Magnetic moments of all synthesized metal complexes of A9CNPTDA are listed in Table 1.3.

Molar conductance analysis

Molar conductance measurement was done for all complexes and the data is given in Table 1.3. The molar conductance value of the complexes was very low, in the range of 2.5-7$\Omega^{-1}cm^2mol^{-1}$. These values suggest non-electrolytic behaviour and absence of counter ions outside the coordination sphere of metal chelates.

FTIR spectral analysis

In complexes, the involvement of azomethine group in coordination with metal ion was confirmed by shifting its stretching frequency to lower value [60,77]. The

presence of new broad band signal around 3400cm^{-1} in Cr(II), Mn(II), Fe(III), Co(II), Ni(II) and Cu(II) complexes of A9CNPTDA confirmed the presence of coordinated water molecule. In Co(II) and ZrO(II) complexes, three bands appeared for N-O bond with a difference of 130cm^{-1} correspond to monodentate nitrate group. Also, the emergence of stretching frequencies in the range 614-694cm^{-1} and 489-543cm^{-1} confirmed the formation of M-N bonds and M-S bond. Cr(II), Mn(II), Ni(II) and Cu(II) complexes were showed two characteristic infrared absorption bands in the range 1670-1540cm^{-1} with a difference of <150cm^{-1} corresponds to asymmetric and symmetric stretching frequency of monodentate –COO (acetate) group. An additional new band emerged at 989cm^{-1} in the IR spectrum of Zirconium - A9CNPTDA complex assigned to the stretching frequency of the Zr=O bond. Important and characteristic IR spectral data of A9CNPTDA and its transition metal complexes are reported and compared in Table1.4.

Based on the physicochemical analysis, structures were derived for the metal complexes of A9CNPTDA and given in Fig. 1.9.

Table 1.3: Microanalytical, magnetic and conductance data of the ligand A9CNPTDA and its transition metal complexes

Complex	Colour	Yield (%)	Mol. Wt.	M.P (^{0}C)	Metal % Found (Cald.)	C % Found (Cald.)	H % Found (Cald.)	N % Found (Cald.)	S % Found (Cald.)	μ_{eff} (BM)	Molar Conductance ($\Omega^{-1}cm^2mol^{-1}$)	Geometry
A9CNPTDA (L)	Dark brown	83	410	279	-	67.02 (67.3)	3.31 (3.44)	13.25 (13.65)	7.34 (7.81)	-	-	-
$[CrL(Ac)_3H_2O]$	Green	50	657	>300	7.64 (7.91)	48.56 (49.73)	3.82 (3.89)	7.15 (7.73)	4.18 (4.43)	3.83	3.9	Octahedral
$[MnL(Ac)_2(H_2O)_2]$	Brown	55	619	>310	8.24 (8.88)	51.16 (52.35)	3.88 (3.9)	8.97 (9.04)	4.98 (5.18)	6.56	4.58	Octahedral
$[FeLCl_3(H_2O)]$	Black	50	590	280	10.28 (9.49)	46.3 (47.59)	3.03 (3.16)	9.11 (9.25)	5.12 (5.29)	5.15	2.91	Distorted Octahedral
$[CoL(NO_3)_2(H_2O)_2]$	Yellow	55	629	>300	9.99 (9.38)	42.29 (43.89)	2.56 (2.88)	11.96 (13.35)	4.84 (5.09)	3.23	5.2	Distorted Octahedral
$[NiL(Ac_2)_2(H_2O)_2]$	Yellow	50	623	270	9.69 (9.47)	51.16 (52.03)	3.43 (3.88)	8.15 (8.99)	5.01 (5.14)	2.14	2.6	Distorted Octahedral
$[CuL(Ac)_2(H_2O)_2]$	Black	55	628	>310	9.89 (10.19)	48.49 (50.77)	3.26 (3.77)	8.02 (9.11)	4.78 (5.21)	2.19	6.52	Distorted Octahedral
$[ZnLCl_2]$	Creamish orange	60	545	>300	11.39 (11.93)	50.28 (50.53)	2.46 (2.58)	9.96 (10.25)	5.59 (5.86)	D	4.12	Tetrahedral
$[ZrOL(NO_3)_2]$	Orange	60	641	>300	13.82 (14.2)	40.64 (43.05)	2.06 (2.2)	12.29 (13.1)	4.77 (5)	D	5.7	Square Pyramidal

Table 1.4: Characteristic infrared absorption frequencies (cm^{-1}) of A9CNPTDA and its transition metal complexes

Complex	υ_{H_2O}	υ_{C-H}	υ_{COOasy}	$\upsilon_{C=N}$	υ_{COOsy}	$\upsilon_{C=C}$	υ_{NO_2/NO_3}	υ_{M-N}	υ_{M-S}
A9CNPTDA (L)	-	3102	-	1691	-	1508	1436 1347	-	-
$[CrL(Ac)_3H_2O]$	3390(br)	3118	1662	1627	1512	1595 1502	1428 1336	648	534
$[MnL(Ac)_2(H_2O)_2]$	3340(br)	3110	1680	1649	1555	1595 1510	1454 1342	623	516
$[FeLCl_3(H_2O)]$	3387(br)	3118	-	1614	-	1593 1494	1454 1327	682	523
$[CoL(NO_3)_2(H_2O)_2]$	3394(br)	3112	-	1629	-	1588 1502	1470 1437 1340	692	543
$[NiL(Ac_2)_2(H_2O)_2]$	3388(br)	3118	1664	1627	1529	1589 1500	1492 1330	694	538
$[CuL(Ac)_2(H_2O)_2]$	3400(br)	3109	1689	1591	1538	1599 1521	1469 1342	624	489
$[ZnLCl_2]$	-	3115	-	1658	-	1600 1514	1444 1432	614	525
$[ZrOL(NO_3)_2]$	-	3110	-	1629	-	1588 1506	1468 1400 1340	665	534

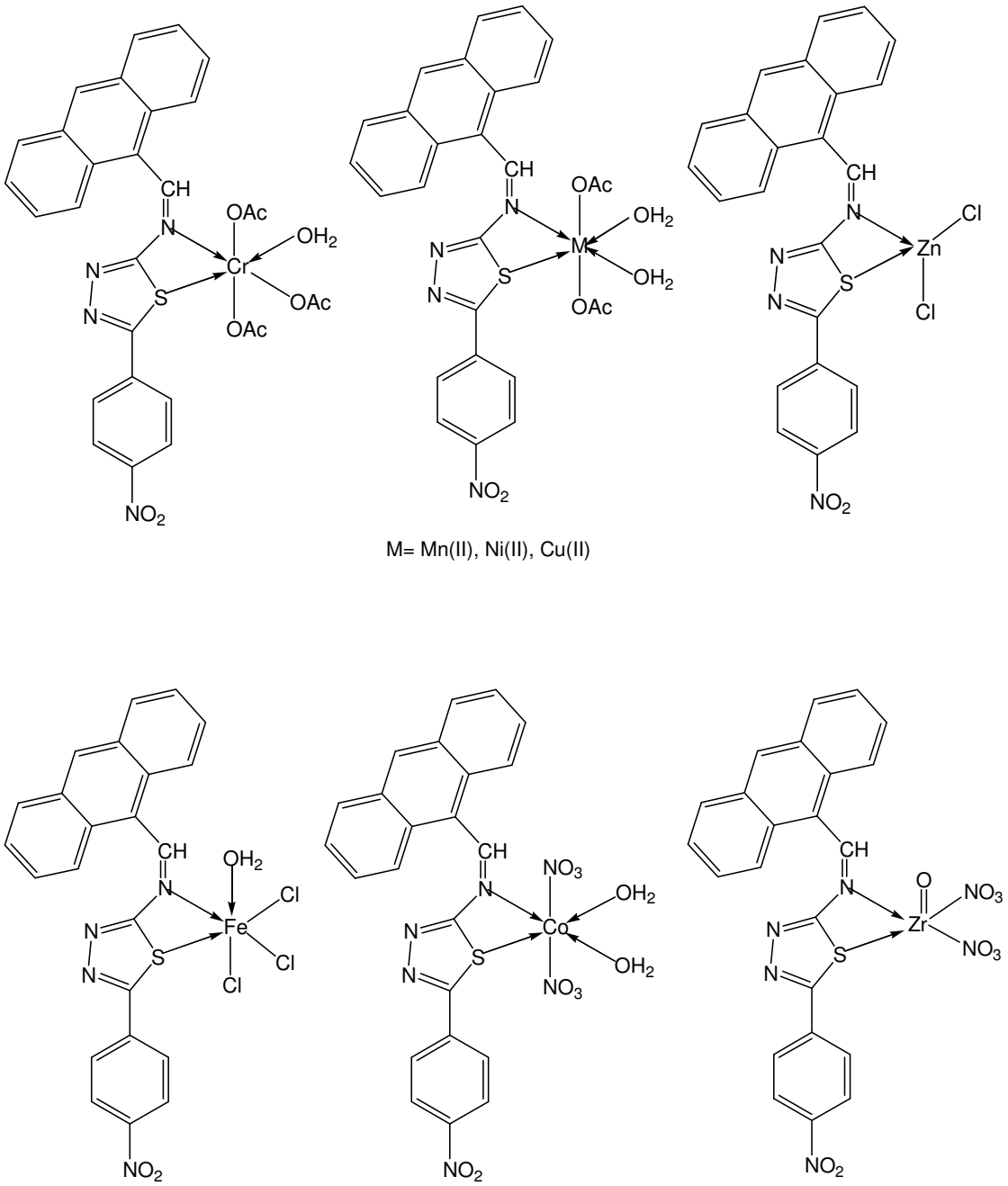

Fig. 1.9: Structures of transition metal complexes of A9CNPTDA

SECTION II

STUDIES ON SCHIFF BASE, N-(ANTHRACEN-10(9H)-YLIDENE)-5-(4-NITROPHENYL)-1, 3, 4-THIADIAZOL-2-AMINE (ANNPTDA) AND ITS TRANSITION METAL COMPLEXES

Another polynuclear Schiff base, N-(anthracen-9(10H)-ylidene)-5-(4-nitro phenyl)-1,3,4-thiadiazol-2-amine (ANNPTDA) derived from NPTDA and anthrone was synthesized and characterized using physico chemical techniques such as elemental and spectral analysis. The chelation ability of this ligand was explored by preparing transition metal complexes of Cr(II), Ni(II), Cu(II), Zn(II) and ZrO(II). Based on elemental, spectroscopic, magnetic and electrical studies, the geometry of the complexes derived, which are discussed in detail in this section.

Synthesis of ANNPTDA

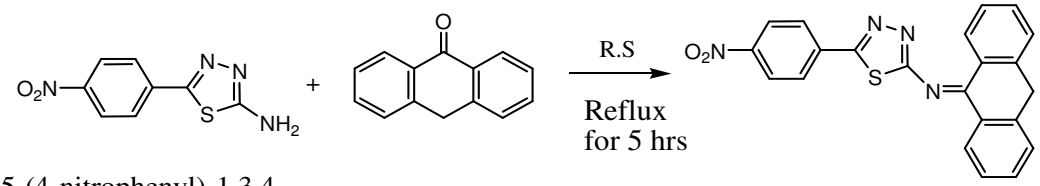

5-(4-nitrophenyl)-1,3,4-thiadiazol-2-amine

Anthrone

ANNPTDA

Fig. 1.10: Synthesis of ANNPTDA

Polynuclear Schiff base N-(anthracen-9(10H)-ylidene)-5-(4-nitrophenyl)-1,3,4-thiadiazol-2-amine (ANNPTDA) was synthesized by the condensation of equimolar mixture of 5-(4-nitrophenyl)-1,3,4-thiadiazol-2-amine and anthrone in ethanol medium. The reaction mixture was refluxed for 5h, concentrated, and cooled. Off-white coloured crystals of ANNPTDA was filtered, washed and dried and MP was 212^0C (Yield: 75%)

Characterization of ANNPTDA

Elemental analysis

The elemental analysis data of polynuclear thiadiazole Schiff base ANNPTDA is

given in Table 1.6. The experimentally obtained percentages of elements like carbon, hydrogen, nitrogen and sulphur were in good agreement with the calculated values.

Electronic spectral analysis

The electronic spectra of ANNPTDA contain two peaks; one at 39062cm^{-1} corresponds to $\pi \rightarrow \pi^*$ transition and the other at 27174cm^{-1} corresponds to $n \rightarrow \pi^*$ transition.

FTIR spectral analysis

Stretching frequencies corresponding to different bonds in ANNPTDA were observed in its IR spectrum. Formation of C=N linkage was proved by the stretching vibration shown at 1662cm^{-1}. υ_{C-H} stretching frequencies of methylene group of anthrone ring were observed at 2924 and 2875cm^{-1}. Two important peaks appeared at 1480 and 1400cm^{-1} indicated the presence of nitro group in the molecule. υ_{C-H} of aromatic ring was observed at 3066cm^{-1}. C=C present in the aromatic rings displayed distinct peaks at 1597 and 1510cm^{-1}. A clear broad signal obtained at 3425cm^{-1} was due to the presence of N-H stretching frequency (tautomer). Emergence of new peaks appeared at 1317cm^{-1} and 1101cm^{-1} is a clear indication of C-N and C-S bond in the molecule. In plane and out of plane deformations were shown at 933cm^{-1} and 842,705cm^{-1} respectively.

NMR spectral analysis

The ^{1}H NMR spectrum of the Schiff base, ANNPTDA is shown in Fig. 1.11. All the ten different aromatic protons gave multiplets between 7.34-8.3δ in the NMR spectrum. Sharp singlet at 4.3δ can be assigned to the CH_2 (methylene) proton in the anthrone ring. In DEPT-135 spectrum (Fig. 1.12), only one CH_2 group in the anthrone ring gave an inverse peak at 62.13ppm. All other CH groups gave upward peaks

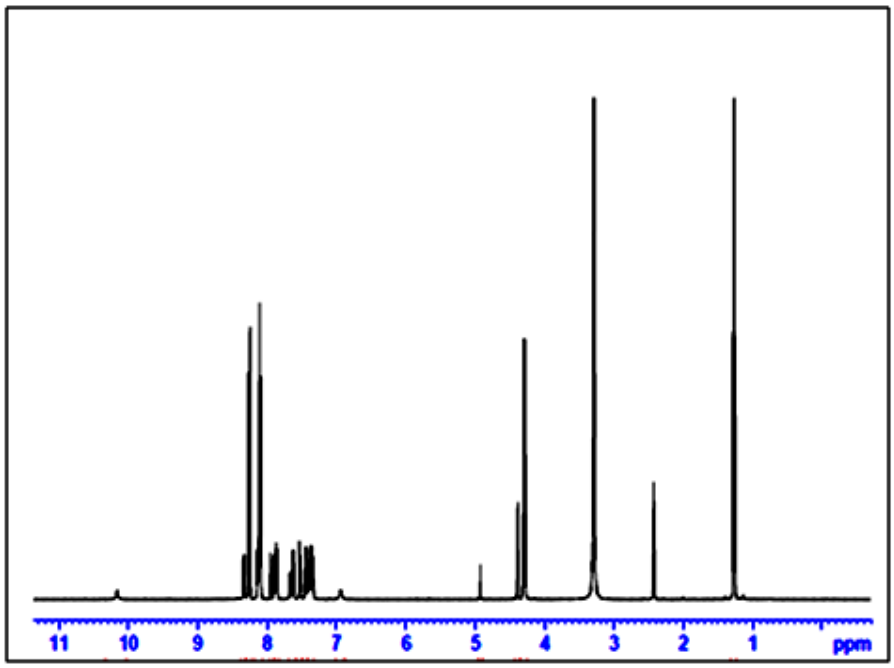

Fig. 1.11: ^{1}H NMR spectrum of ANNPTDA

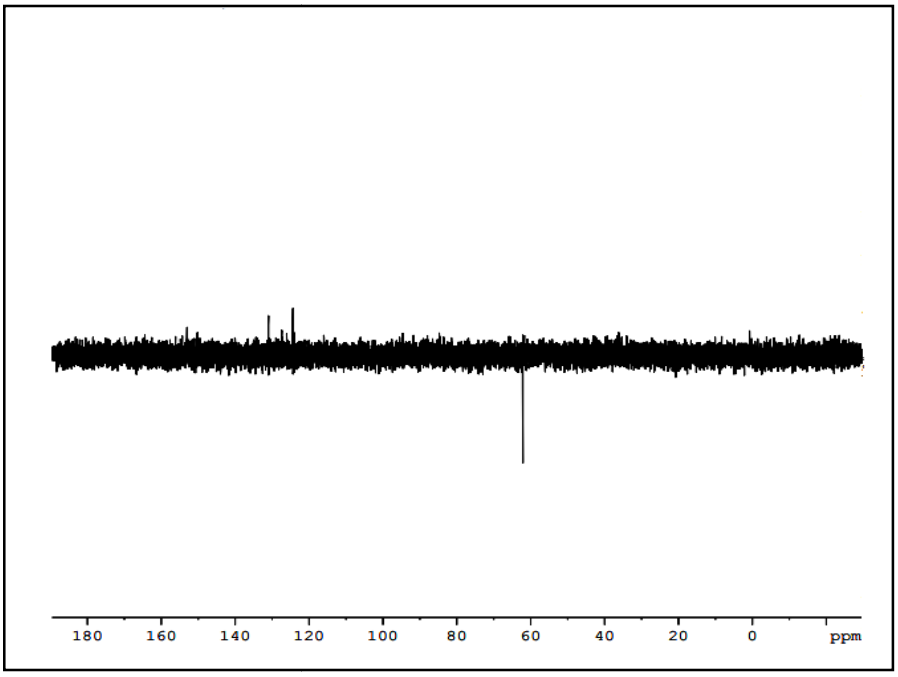

Fig. 1.12: DEPT-135 spectrum of ANNPTDA

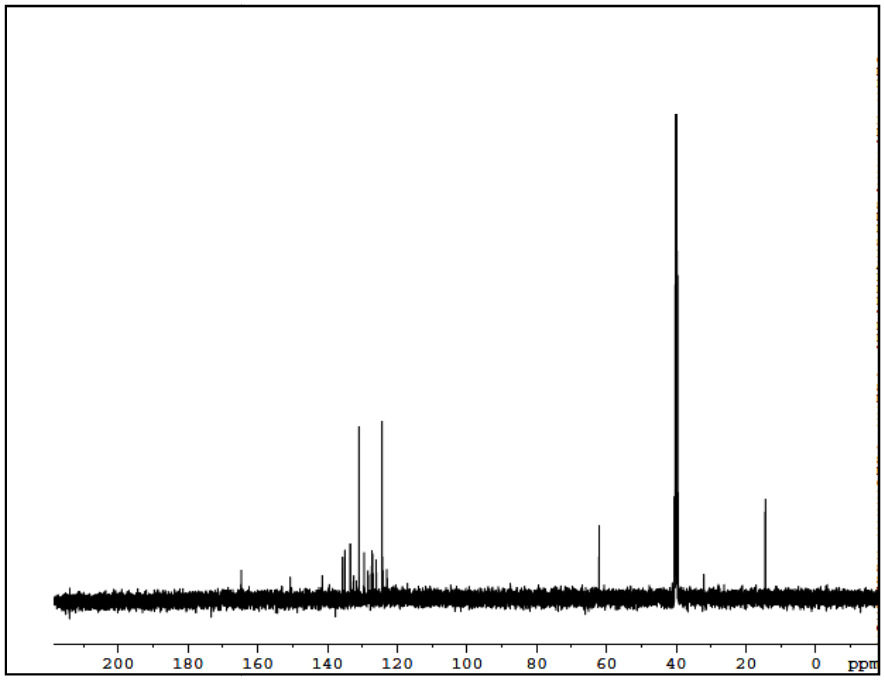

Fig. 1.13: ^{13}C NMR spectrum of ANNPTDA

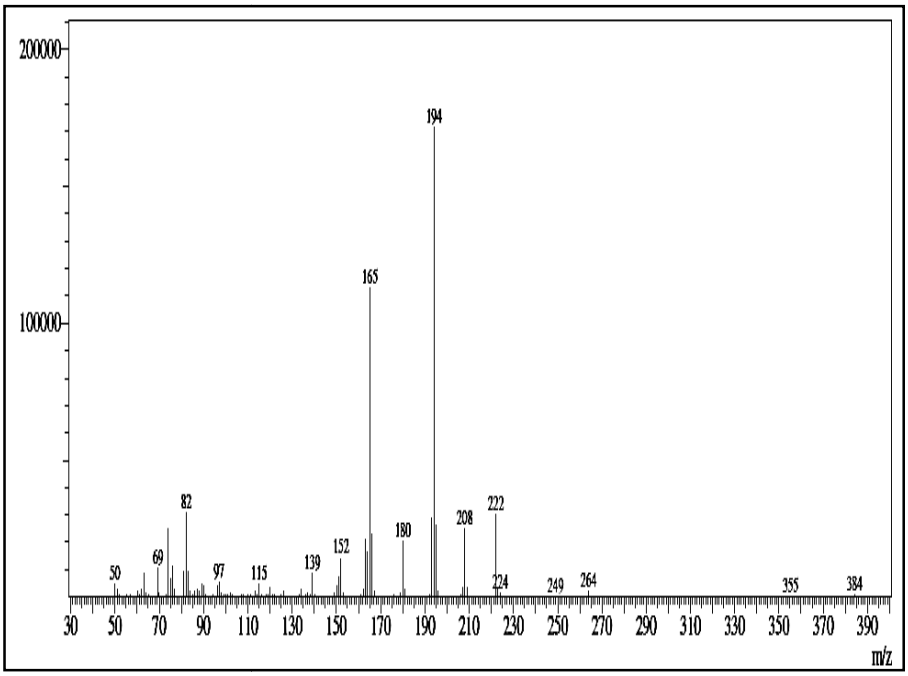

Fig. 1.14: Mass spectrum of ANNPTDA

The ^{13}C NMR spectrum of the Schiff base ANNPTDA is provided in Fig. 1.13. All seventeen different carbon atoms, which are sp^2 hybridized, gave 17 different peaks between 123-164ppm (17 different aromatic sp^2 'C' atoms). Peak at 128ppm corresponds

to the carbon atom of azomethine group. Sharp peak at 39ppm corresponds to the carbon atom of CH_2 group in the anthrone ring.

Mass spectral analysis

In the mass spectrum of Schiff base ANNPTDA, signal of molecular ion was absent. A sharp base peak appeared at m/z 194 was due to the fragment $[C_{14}H_{13}N]^+$. The fragment $[C_8H_9N_2S]^+$ displayed signal at m/z 165. Mass spectrum of ligand is presented in Fig. 1.14.

From the above discussions, the structure of 'S' containing polynuclear Schiff base ANNPTDA was assigned and given in Fig. 1.15.

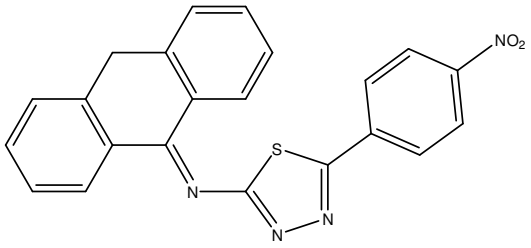

Fig. 1.15: Structure of ANNPTDA

Synthesis of Complexes

The complexing capability of polynuclear thiadiazole Schiff base, ANNPTDA were checked with Cr(III), Ni(II), Cu(II), Zn(II) and ZrO(II) ions. Zirconyl nitrate is used for the synthesis of Zirconium complex. Acetate salts of other metal ions were used for the synthesis of respective complexes. The Schiff base ligand ANNPTDA (3mmol) was dissolved in minimum quantity of ethanol (15ml) and refluxed on a water bath (30min). Hot ethanolic solution of appropriate amount corresponding metal salt (acetate/nitrate) was added to the boiling medium and again refluxed for 6h. Then reduced its volume by evaporation, cooled and kept overnight and the crystallized metal complexes were collected, washed with water ethanol mixture and dried over $CaCl_2$.

Characterization of Complexes

Almost all the metal complexes of ANNPTDA were seen to be stable in air and light. They were soluble in aprotic polar solvents like DMF and DMSO. But their solubility was very less in organic solvents like diethyl ether, ethanol, chloroform, benzene, etc.

Elemental analysis

Percentage of C, H, N and S as well as the metal content were estimated by microanalytical methods. 1:2 stoichiometry exist between Cr(III), Ni(II) and Cu(II) metal ions with the ligand ANNPTDA while 1:1 stoichiometry was displayed by Zn(II) and ZrO(II) ions with this ligand. The elemental and metal percentage data of the complexes obtained theoretically and experimentally are listed in Table 1.6. These values obtained are in good agreement with theoretical explanations.

Electronic spectral analysis

In the case of complexes bathochromic shift occurred for these bands which are a clear evidence for the complex formation. The electronic bands are summarized in Table 1.5.

Table 1.5: Electronic spectral data of Schiff base, ANNPTDA and its transition metal complexes

Compound	Electronic bands in cm^{-1}	
	$\pi \rightarrow \pi^*$	$n \rightarrow \pi^*$
ANNPTDA	39062	27174
$[CrL_2(Ac)_3H_2O]$	38461	26881
$[NiL_2(Ac)_2(H_2O)_2]$	38610	26595
$[CuL_2(Ac)_2(H_2O)_2]$	38610	26809
$[ZnL(Ac)_2(H_2O)]$	38461	27027
$[ZrOL(NO_3)_2(H_2O)]$	38610	27027

The electronic spectra of all complexes of ANNPTDA mainly showed two peaks, $n \rightarrow \pi^*$ and $\pi \rightarrow \pi^*$, which showed increase in λ_{max} as compared to that of the ligand. This red shift confirms the extension of conjugation and hence the complexation. Other peaks due to charge transfer, π bonding etc. were less significant in the spectra.

Magnetic moment analysis

Informations regarding the geometry of transition metal complexes were obtained by magnetic moment measurements. Effective magnetic moments of ANNPTDA-Complexes are displayed in Table 1.6. Cr(III), Ni(II) and Cu(II) complexes showed a slight increase in their μ_{eff} values (4.02BM, 2.92BM and 2.25 BM respectively) compared to the theoretical values which lead to octahedral geometries of these complexes. This slight change in magnetic moment observed may due to the contribution from the magnetic moment due to orbital motion of electrons. Diamagnetic magnetic moment are expected and confirmed for Zn(II) and ZrO(II) complexes due to d^{10} or d^0 configuration respectively and assumed tetrahedral and square pyramidal geometry respectively.

Molar conductance analysis

Molar conductance measurement was done for all complexes and is given in Table 1.6. The molar conductance values of all the complexes were in the range of 2-13$\Omega^{-1}cm^2mol^{-1}$. These values suggest non-electrolytic behaviour and absence of counter ions outside the coordination sphere of metal complexes.

FTIR spectral analysis

Significant infrared absorption frequencies (cm^{-1}) of ANNPTDA and its transition metal complexes are summarized and distinguished in Table 1.7. In ANNPTDA-complexes the involvement of 'N' atom of azomethine linkage in coordination with metal was confirmed by the downward frequency shift from 1662cm^{-1}. The presence of broad bands observed at 3360 and 3319cm^{-1}in the infrared spectra of

Cr(III) and Ni(II) complexes respectively and new signals around 3485cm^{-1}, 3391cm^{-1} and 3347cm^{-1} in the spectra of Cu(II), Zn(II) and ZrO(II) complexes respectively confirmed the presence of coordinated water molecule in these complexes. Also, the appearance of stretching frequencies in the range 690-694cm^{-1} and 458-572cm^{-1} respectively corresponding to M-O and M-N bonds, confirmed the formation of ANNPTDA complexes. Cr(III), Ni(II), Cu(II) and Zn(II) complexes of ANNPTDA showed peaks around 1595cm^{-1} and 1700cm^{-1} due to symmetric and asymmetric stretching of monodentate acetate moieties. New additional bands displayed at 1317-133cm^{-1} and 1058-1101cm^{-1} indicated the stretching frequencies of C-N and C-S bonds in complexes.

Structures of transition metal complexes of ANNPTDA are depicted in Fig. 1.16. Ligand ANNPTDA was found to act as zerovalent unidentate moiety in all the complexes, coordinating only through azomethine nitrogen.

Table 1.6: Microanalytical, magnetic and conductance data of the ligand ANNPTDA and its transition metal complexes

Complex	Colour	Yield (%)	Mol. Wt.	M.P (^{0}C)	Metal% Found (Cald.)	C % Found (Cald.)	H % Found (Cald.)	N % Found (Cald.)	S % Found (Cald.)	μ_{eff} (BM)	Molar Conductance ($\Omega^{-1}cm^2mol^{-1}$)	Geometry
ANNPTDA (L)	Flesh coloured	75	398	212	-	65.18 (66.32)	3.12 (3.54)	14.83 (14.06)	7.98 (8.05)	-	-	-
$[CrL_2(Ac)_3H_2O]$	Black	70	1043	280	5.4 (4.99)	55.19 (57.52)	3.01 (3.77)	10.18 (10.73)	5.66 (6.14)	4.02	9.7	Octahedral
$[NiL_2(Ac)_2(H_2O)_2]$	Orange	50	1009	280	5.8 (5.84)	56.15 (57.1)	3.34 (3.79)	10.12 (11.1)	5.68 (6.35)	2.92	12.1	Octahedral
$[CuL_2(Ac)_2(H_2O)_2]$	Brownish green	80	1014	>300	6.82 (6.31)	55.78 (56.83)	2.95 (3.78)	10.83 (11.04)	6.25 (6.32)	2.25	5.8	Octahedral
$[ZnL(Ac)_2(H_2O)]$	Black	70	599	240	9.99 (10.85)	51.52 (52.05)	2.81 (3.70)	8.37 (9.34)	4.44 (5.34)	D	10.9	Tetrahedral
$[ZrOL(NO_3)_2(H_2O)]$	Yellow	70	647	220	14.01 (14.07)	39.9 (40.8)	2.21 (2.49)	11.56 (12.98)	4.16 (4.95)	D	2.8	Square Pyramidal

Table 1.7: Characteristic infrared absorption frequencies (cm^{-1}) of ANNPTDA and its transition metal complexes

Complex	υ_{H_2O}	υ_{COOasy}	$\upsilon_{C=N}$	υ_{COOsy}	$\upsilon_{C=C}$	υ_{NO_2/NO_3}	υ_{C-N}	υ_{C-S}	υ_{M-O}	υ_{M-N}
ANNPTDA (L)	-	-	1662	-	1510	1480 1400	1317	1101	-	-
$[CrL_2(Ac)_3H_2O]$	3360(br)	1714	1660	1597	1522	1450 1411	1319	1101	694	506
$[NiL_2(Ac)_2(H_2O)_2]$	3319(br)	1677	1661	1591	1512	1463 1401	1319	1095	692	458
$[CuL_2(Ac)_2(H_2O)_2]$	3485	1686	1659	1595	1513	1462 1402	1318	1107	690	572
$[ZnL(Ac)_2(H_2O)]$	3391	1702	1627	1592	1497	1450 1393	1335	1058	690	491
$[ZrOL(NO_3)_2(H_2O)]$	3347	-	1658	-	1505	1462 1401 1349	1317	1093	688	571

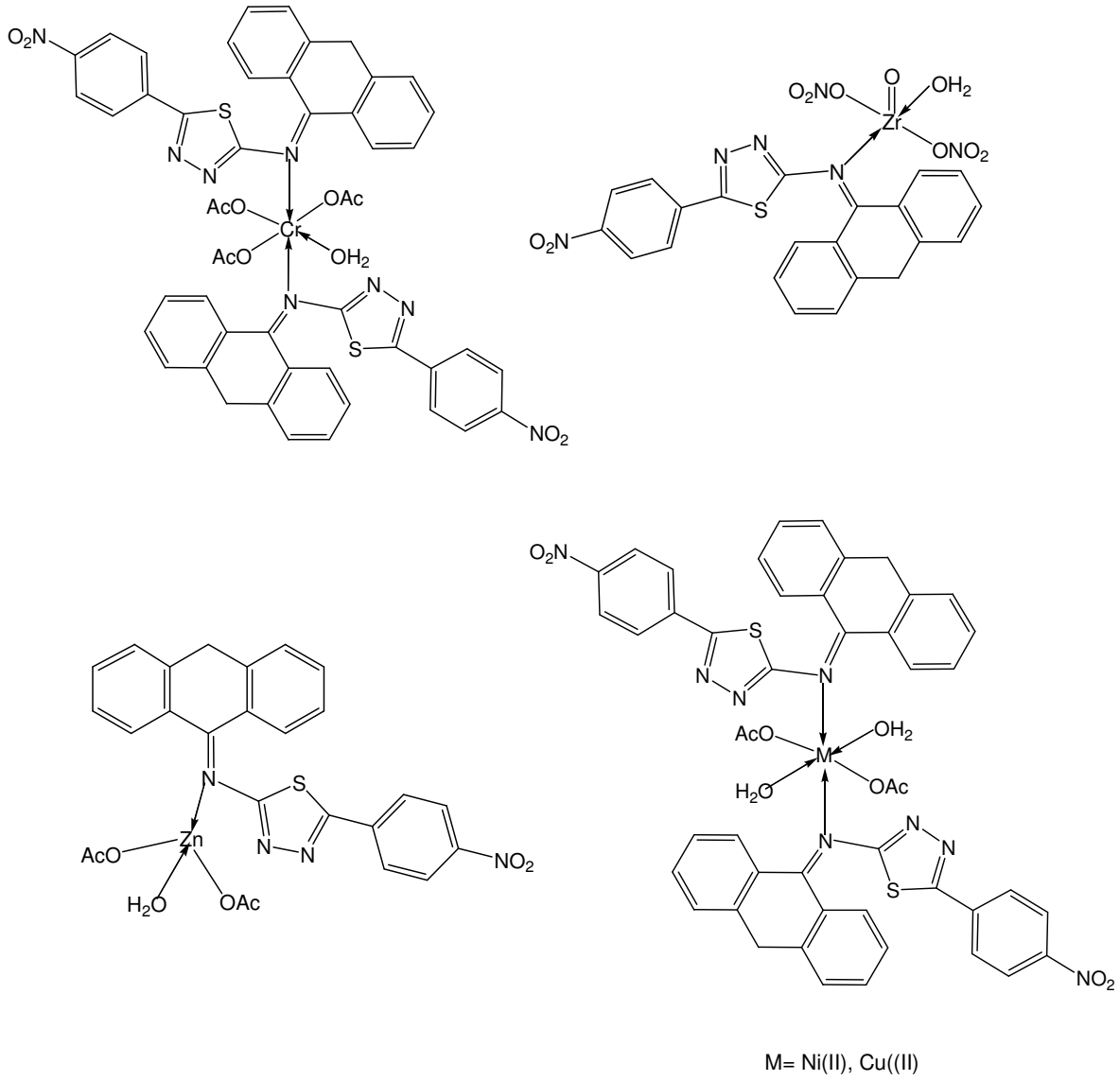

Fig. 1.16: Structures of transition metal complexes of ANNPTDA

CHAPTER 4

TRANSITION METAL COMPLEXES OF SCHIFF BASES DERIVED FROM 5-(4-NITROPHENYL)-1,3,4-THIADIAZOL-2-AMINE (NPTDA) AND CARBONYL COMPOUNDS WITH PYRIDINE RING

This chapter deals with the synthesis and characterization of novel 'S' containing pyridine derivative of thiadiazole Schiff bases (E)-5-(4-nitrophenyl)-N-((pyridine-2-yl)methylene)-1,3,4-thiadiazol-2-amine (P2CNPTDA), (E)-5-(4-nitrophenyl)-N-(1-(pyridine-3-yl)ethylidene)-1,3,4-thiadiazol-2-amine (3APNPTDA), (E)-5-(4-nitro phenyl)-N-(1(pyridin-2-yl)ethylidene)-1,3,4-thiadiazol-2-amine (2APNPTDA) and their transition metal complexes. Attempts to characterize the ligands and complexes were done with the aid of analytical tools such as elemental analysis, spectral studies such as Fourier transform infrared, UV-visible, NMR (^{1}H and ^{13}C), and mass spectroscopy. The detailed synthesis and characterization of these three novel 'S' containing pyridine derivatives of Schiff bases and their metallic complexes are discussed in detail as three separate sections in this chapter.

SECTION I

STUDIES ON SCHIFF BASE, (E)-5-(4-NITROPHENYL)-N-((PYRIDINE-2-YL)METHYLENE)-1,3,4-THIADIAZOL-2AMINE (P2CNPTDA) AND ITS TRANSITION METAL COMPLEXES

A novel thiadiazole based pyridine deivative of Schiff base (E)-5-(4-nitrophenyl)-N-((pyridine-2-yl)methylene)-1,3,4-thiadiazol-2amine (P2CNPTDA) was synthesized and characterized by elemental analysis and various spectroscopic techniques. The structure of the Schiff base, P2CNPTDA derived from NPTDA (parent amine) and pyridine 2-carbaldehyde and its transition metal complexes were established based on spectroscopic, magnetic and electrical studies. The detailed synthesis and characterization of the ligand P2CNPTDA and their transition metal complexes are discussed in this section..

Synthesis of P2CNPTDA

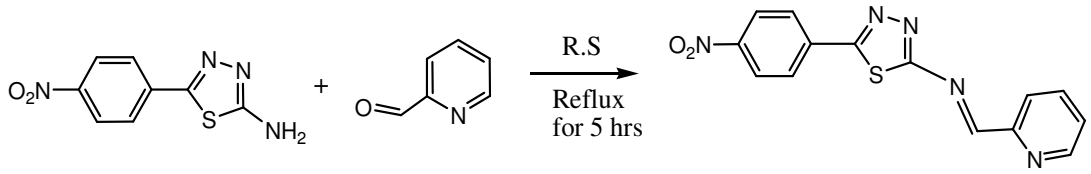

5-(4-nitrophenyl)-1,3,4-thiadiazol-2-amine

Pyridine-2-aldehyde

P2CNPTDA

Fig. 1.17: Synthesis of P2CNPTDA

A hot ethanolic solution of pyridine 2-carbaldehyde was added to a refluxing solution of 5-(4-nitrophenyl)-1,3,4-thiadiazol-2-amine in ethanol and refluxed 5h on a water bath. The resulting solution was concentrated to obtain dark brown crystals of P2CNPTDA, which was filtered, washed and dried. Recrystallization from methanol gave 80 % yield of the desired product MP: 210^0C

Characterisation of P2CNPTDA

Elemental analysis

Percentage of C, H, N and S were estimated by microanalytical methods. Calculated values of P2CNPTDA were in close agreement with experimental results.

Electronic spectral analysis

In electronic spectrum recorded at a concentration of 10^{-4}M in Schimadzu UV-Visible spectra, the ligand P2CNPTDA showed peaks at 39062cm^{-1} and 27560cm^{-1} due to $\pi \rightarrow \pi^*$ and $n \rightarrow \pi^*$ transitions. The decrease in the values compared to the parent amine, NPTDA indicates the extension of conjugation during the formation of the Schiff base P2CNPTDA.

FTIR spectral analysis

Characterization of ligand, (E)-5-(4-nitrophenyl)-N-((pyridine-2-yl)methylene)-1,3,4-thiadiazol-2-amine was done using IR spectral data. The IR spectrum of this thiadiazole Schiff base, P2CNPTDA recognized the unique stretching and bending vibrational frequencies, as depicted in Table 1.9. The absorption bands due to N-H stretching frequency of amino group at 3500-3200cm^{-1} was absent in the IR spectra of the P2CNPTDA, which proved the formation of Schiff base. An intense band observed at 1629cm^{-1} was assigned to the stretching mode of azomethine linkage (C=N). The peaks at 1595cm^{-1} and 1510cm^{-1} can be consigned to C=C vibrations in aromatic rings. The aromatic C-H stretching frequency at 3097cm^{-1}, C-S stretching frequencies at 1103cm^{-1} and C-N stretching at 1271cm^{-1}were clearly appeared in the spectra. There is a small change in the presence of nitro group by Schiff base formation; two peaks were present at 1493cm^{-1} and 1338cm^{-1} corresponds to N-O stretching frequency. In plane bending vibrations of the Schiff base P2CNPTDA were sighted at 1082cm^{-1}. Also the peaks gained at 850cm^{-1} and 970cm^{-1} can be consigned as out of plane bending vibrations.

NMR spectral analysis

Characteristics peak at 7.126δ can be assigned to the azomethine proton. The aromatic protons both in the pyridine and benzene rings gave characteristic peaks between 8.02-8.32δ. The ^{1}H NMR spectrum of P2CNPTDA recorded in dmso-d_6 solvent on 400MHz-NMR instrument is displayed as Fig. 1.18.

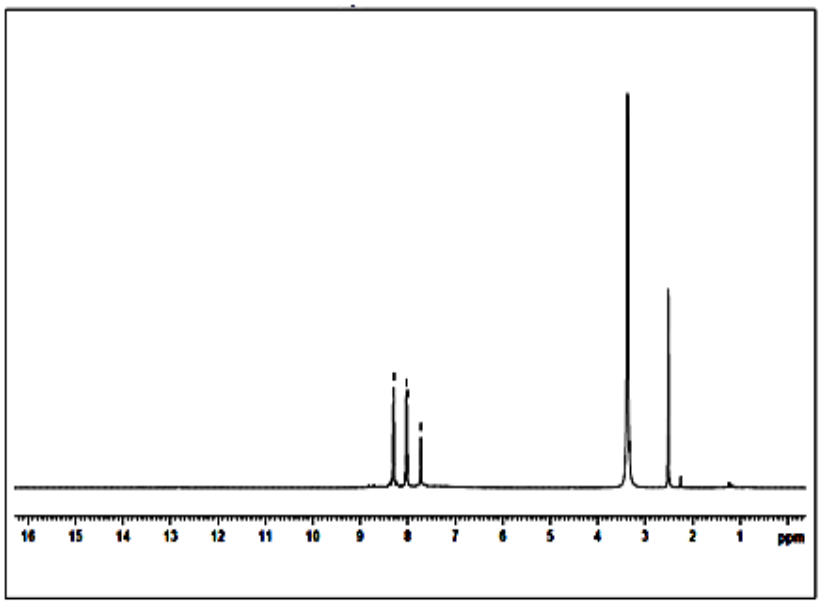

Fig. 1.18: ^{1}H NMR spectrum of P2CNPTDA

The proton decoupled ^{13}C NMR spectrum of P2CNPTDA is shown in Fig. 1.19. The carbon atom of the azomethine linkage was recognized at 147ppm. The aromatic carbons of the thiadiazole, benzene and pyridine rings exhibited four signals in the range 124-169ppm. The assignment of peaks to diverse carbon atoms of P2CNPTDA were shown in the ^{13}C NMR spectrum.

Mass spectral analysis

In gas chromatogram, there was only one distinct peak which authenticates the purity of the sample P2CNPTDA. Molecular ion peak (M^+ peak) was absent but a clear base peak at m/z 222 with high intensity observed corresponding to the fragment

$[C_8H_6N_4O_2S]^+$, which is formed due to the loss of $[C_6H_5N]^+$ from the ligand. The clear signal with high intensity appeared at m/z 74 corresponding to the fragment, $[CH_2N_2S]^+$. The fragments $[C_7H_4NS]^+$ and $[CH_2N_2S]^+$ appeared at m/z 134 and 120 respectively. Mass spectrum of P2CNPTDA is given as Fig. 1.20.

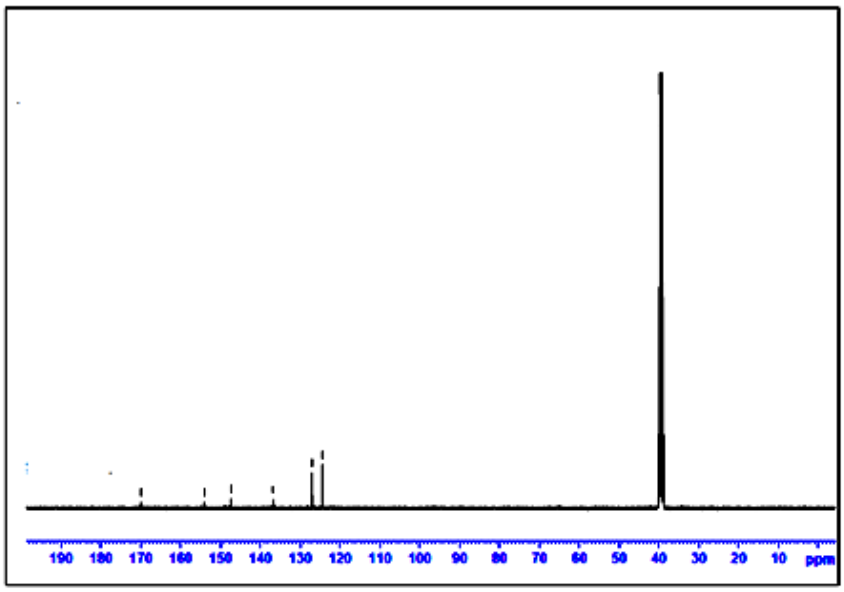

Fig. 1.19: ^{13}C NMR spectrum of P2CNPTDA

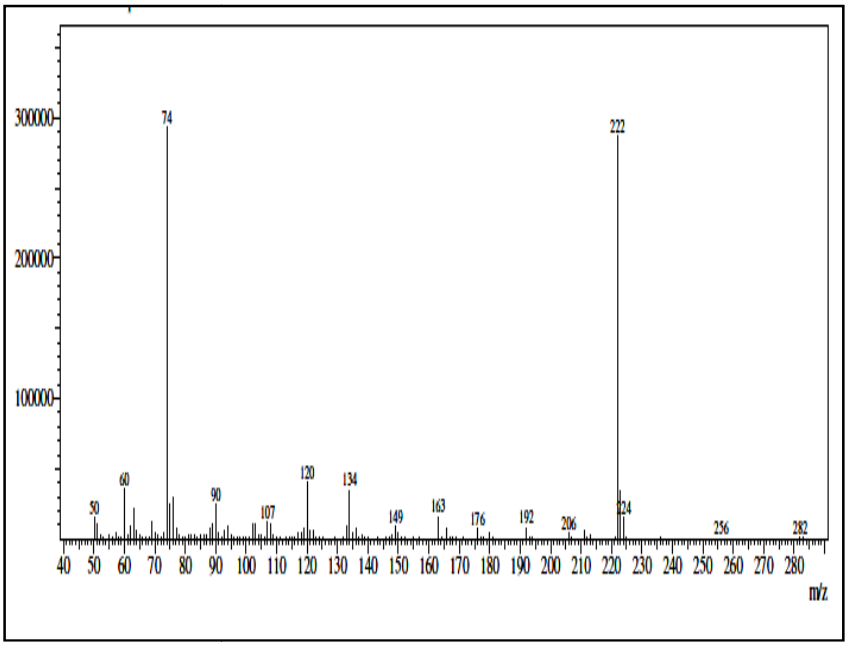

Fig. 1.20: Mass spectrum of P2CNPTDA

From the above discussions, the structure of 'S containing Schiff base P2CNPTDA, derived from pyridine 2-carbaldehyde and NPTDA can be assigned and it is given in Fig. 1.21

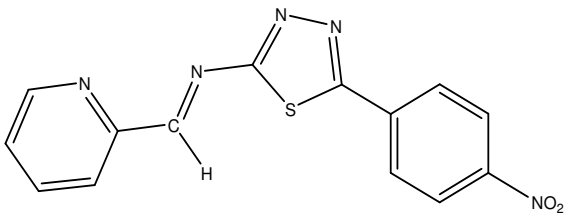

Fig. 1.21: Structure of P2CNPTDA

Synthesis of Complexes

Copper complex was prepared by using cupric acetate. 2mmol ethanolic solution of NPTDA (5-(4-nitrophenyl)-1,3,4-thiadiazol-2-amine) and P2C (Pyridine2-carbaldehyde) (2mmol) were mixed together and adjusted the pH to 7-8 by the addition of sodium acetate to this mixture and the solution was then refluxed for 5h. The reaction mixture was kept overnight and the complex was precipitated as brown coloured crystals. Filtered, washed with ethanol and warm water, dried and melting point was determined.

Nickel acetate, zinc acetate, ferric chloride, zirconyl nitrate and cadmium nitrate were used for the preparation of Ni(II), Zn(II), Fe (III), ZrO(II) and Cd(II) complexes. The procedure taken up for the preparation of the complexes was the same as that employed for Cu(II) complex synthesis. (Yield: 40-80%).

Characterisation of Complexes

All complexes of P2CNPTDA are stable amorphous powder having high melting points and they are highly soluble in organic solvents (DMSO, DMF, $CHCl_3$) and insoluble in water. There is a good correlation between observed and calculated values of elemental analysis and 1:1 stoichiometry exists between metal and ligand

Electronic spectral analysis

In the case of complexes the electronic bands due to K band and R band are found to shift to higher wavelength. This is a clear proof for the formation of complexes. The electronic spectral bands of the Schiff base, P2CNPTDA and its complexes are summarized in Table 1.8.

Table 1.8: Electronic spectral data of Schiff base, P2CNPTDA and its transition metal complexes

Compound	Electronic bands in cm^{-1}	
	$\pi \rightarrow \pi^*$	$n \rightarrow \pi^*$
P2CNPTDA	39062	31949
$[FeLCl_3(H_2O)]$	38167	27472
$[NiL(Ac)_2(H_2O)_2]$	37878	27777
$[CuL(Ac)_2(H_2O)_2]$	38167	30487
$[ZnL(Ac)_2]$	38610	26954
$[CdL(NO_3)_2]$	38610	27548
$[ZrOL(NO_3)_2]$	38610	27027

Magnetic moment analysis

Measurements of the values of magnetic susceptibility of the complexes offered strong support for determining the exact geometry. The effective magnetic moment data of P2CNPTDA-complexes are shown in Table 1.9. Ni(II) and Cu(II) complexes of P2CNPTDA were assigned octahedral structure because they showed magnetic moment values 2.43BM and 1.92BM respectively. Fe-P2CNPTDA chelate displayed magnetic moment value of 4.84BM, which may be due to antiferromagnetic exchange in this complex. Diamagnetic character was found for Zn(II), Cd(II) and ZrO(II) complexes, which is quite justifiable with the absence of unpaired electron (d^{10} or d^0) in their electronic configuration

Molar conductance analysis

Molar conductance measurement was done for all complexes and is given in Table 1.9. Molar conductance values of the complexes are in the range of 3.3-17.4$\Omega^{-1}cm^2mol^{-1}$. These values suggest the non-electrolytic behavior of the complexes.

FTIR spectral analysis

In complexes a considerable lowering of stretching frequencies of the azomethine group (from 1629cm^{-1}) was observed due to the involvement of azomethine nitrogen of this heterocyclic ligand P2CNPTDA in complexation. Additional broad bands appeared in Fe(III), Ni(II) and Cu(II) complexes in the range 3280-3421cm^{-1} implies the coordination of water molecules in the complexes. In ZrO(II) and Cd(II)complexes of P2CNPTDA, three additional bands were observed for N-O stretching frequency, which corresponds to monodentate nitrate group. Appearance of additional M-N and M-O bands in the spectrum of complexes proves the coordination of N and O atom to the metal. Ni(II), Cu(II) and Zn(II) complexes of P2CNPTDA showed peaks in the range 1683-1698cm^{-1} and 1593-1599cm^{-1} due to asymmetric and symmetric stretching of monodentate acetate moieties respectively. In Cd(II) and ZrO(II) complexes, three bands appeared for N-O bond with a difference of 145cm^{-1} correspond to monodentate nitrate group. A peak at 494cm^{-1} in the spectrum of iron complex can be assigned to M-Cl stretching. In all complexes, peaks due to C-N and C-S stretching frequencies were appeared in the range 1271-1272cm^{-1} and 1095-1108cm^{-1} respectively. Characteristic infrared absorption frequencies of P2CNPTDA and its transition metal complexes are given in Table 1.10.

Structures of the transition metal complexes of P2CNPTDA derived based on elemental, spectral, magnetic and electronic studies are represented in Fig. 1.22.

Table 1.9: Microanalytical, magnetic and conductance data of the ligand P2CNPTDA and its transition metal complexes

Complex	Colour	Yield (%)	Mol. Wt.	M.P (^{0}C)	Metal% Found (Cald.)	C % Found (Cald.)	H % Found (Cald.)	N % Found (Cald.)	S% Found (Cald.)	μ_{eff} (BM)	Molar Conductance ($\Omega^{-1}cm^2mol^{-1}$)	Geometry
P2CNPTDA (L)	Dark brown	70	311	208	-	52.23 (54.01)	2.07 (2.91)	21.18 (22.5)	9.66 (10.3)	-	-	-
$[FeLCl_3(H_2O)]$	Dark Brown	40	492	280	10.96 (11.38)	33.88 (34.21)	2.19 (2.26)	13.26 (14.25)	6.52 (6.52)	4.84	9.2	Distorted Octahedral
$[NiL(Ac)_2(H_2O)_2]$	Dark Yellow	50	524	280	11.07 (11.26)	41.54 (43.59)	3.35 (3.49)	10.94 (11.55)	4.68 (5.29)	2.43	8.8	Octahedral
$[CuL(Ac)_2(H_2O)_2]$	Coffee brown	80	529	>300	12.48 (12.1)	42.07 (43.24)	3.38 (3.46)	11.12 (11.46)	5.32 (5.25)	1.92	5.7	Octahedral
$[ZnL(Ac)_2]$	Yellow	85	494	250	15.12 (13.68)	26.15 (28.31)	1.71 (1.78)	10.24 (10.32)	4.64 (4.72)	D	3.3	Tetrahedral
$[CdL(NO_3)_2]$	Yellow	60	547	235	21.14 (20.48)	30.82 (32.01)	2.12 (2.15)	17.45 (17.42)	5.56 (5.7)	D	17.4	Tetrahedral
$[ZrOL(NO_3)_2]$	Slight yellow	80	542	>310	17.15 (16.79)	30.18 (33.56)	2.18 (2.64)	15.95 (17.12)	15.68 (15.93)	D	4.4	Square Pyramidal

Table 1.10: Characteristic infrared absorption frequencies (cm^{-1}) of P2CNPTDA and its transition metal complexes

Complex	υ_{H_2O}	υ_{COOasy}	$\upsilon_{C=N}$	υ_{COOsy}	$\upsilon_{C=C}$	υ_{NO_2/NO_3}	υ_{M-O}	υ_{C-N}	υ_{C-S}	υ_{M-N}
P2CNPTDA (L)	-	-	1629	-	1510	1493 1338	-	1271	1103	-
$[FeLCl_3(H_2O)]$	3280	-	1626	-	1504	1340	638	1264	1108	494
$[NiL(Ac)_2(H_2O)_2]$	3421	1683	1625	1595	1505	1498 1339	610	1271	1104	493
$[CuL(Ac)_2(H_2O)_2]$	3410	1698	1624	1593	1516	1437 1333	634	1247	1095	490
$[ZnL(Ac)_2]$	-	1689	1625	1599	1523	1490 1348	646	1271	1103	495
$[CdL(NO_3)_2]$	-	-	1621	-	1539	1503 1487 1363	657	1271	1108	476
$[ZrOL(NO_3)_2]$	-	-	1595	-	1504	1496 1428 1339	687	1272	1103	464

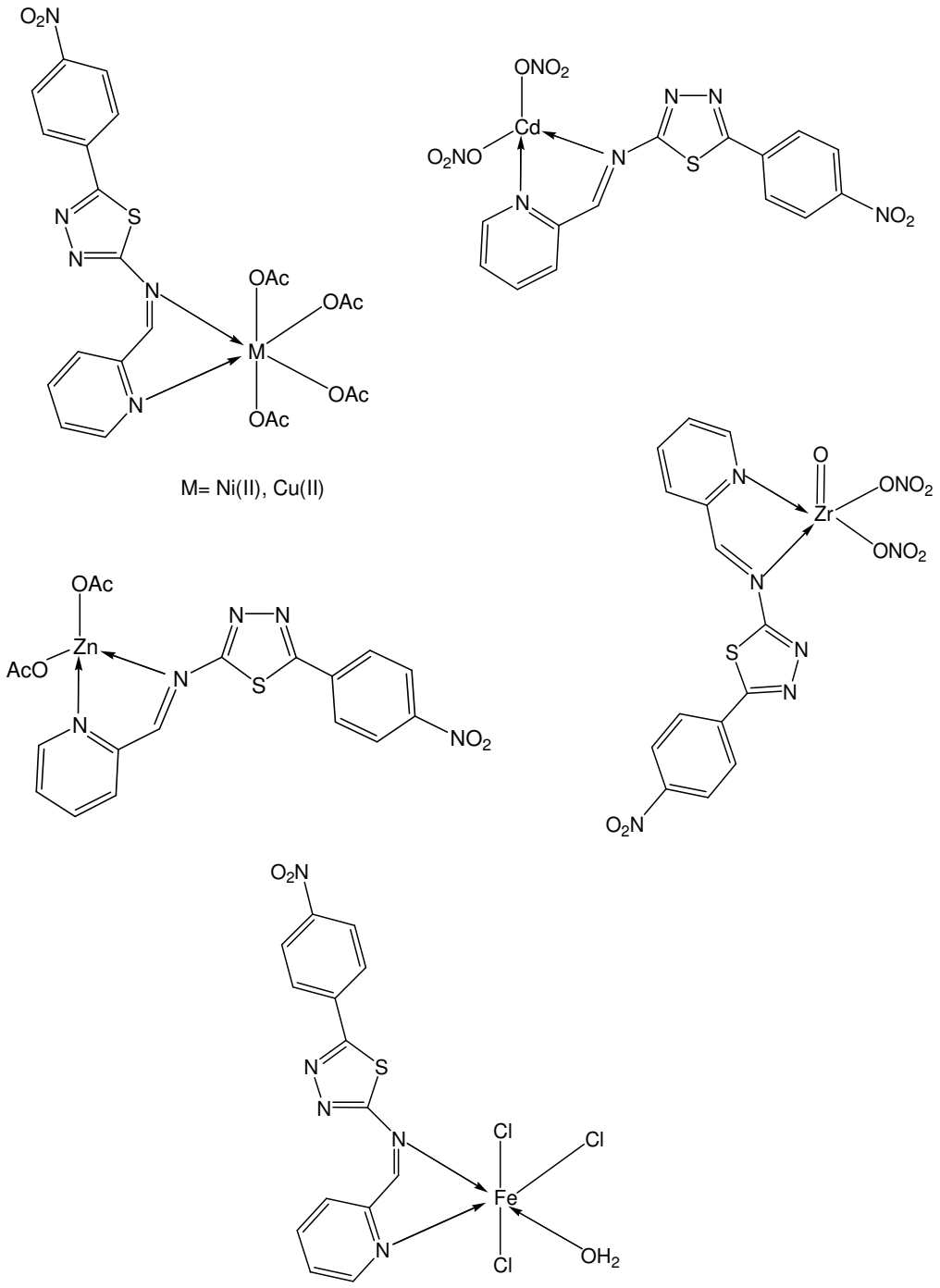

Fig. 1.22: Structures of transition metal complexes of P2CNPTDA

SECTION II

STUDIES ON SCHIFF BASE (E)-5-(4-NITROPHENYL)-N-(1(PYRIDINE-3-YL)ETHYLIDENE)-1,3,4THIADIAZOL-2-AMINE (3APNPTDA) AND ITS TRANSITION METAL COMPLEXES

Heterocyclic sulphur containing Schiff base, (E)-5-(4-nitrophenyl)-N-(1-(pyridine-3-yl)ethylidene)-1,3,4-thiadiazol-2-amine (3APNPTDA), derived from 3-acetyl pyridine and the parent amine NPTDA was prepared and its ability to form metal chelates was established by synthesizing transition metal complexes. Formulation of the structures and geometries of the synthesized ligand and complexes were made based on spectral, magnetic, electronic and elemental data.

Synthesis of 3APNPTDA

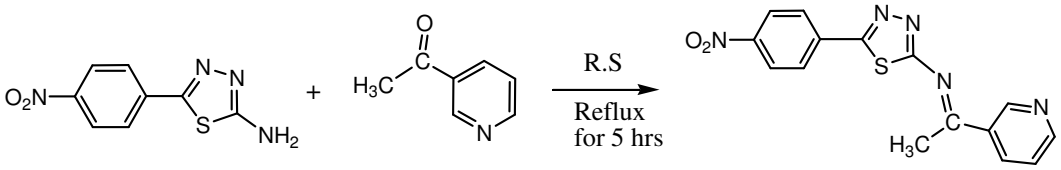

5-(4-nitrophenyl)-1,3,4-thiadiazol-2-amine

3-Acetylpyridine

3APNPTDA

Fig. 1.23: Synthesis of 3APNPTDA

A hot ethanolic solution of 3-acetylpyridine was added to a refluxing solution of 5-(4-nitrophenyl)-1,3,4-thiadiazol-2-amine in ethanol and refluxed 5h on a water bath. The resulting solution was concentrated in order to obtain yellow crystals, which was collected and washed with ethanol. Recrystallization from ethanol gave 70% yield of the desired product. MP: 235°C.

Characterisation of 3APNPTDA

Elemental analysis

The elemental analysis data of thiadiazole pyridine derivative, 3APNPTDA is given in Table 1.12. The experimentally obtained percentages of elements like carbon, hydrogen, nitrogen and sulphur were in good agreement with the calculated

Electronic spectral analysis

Two characteristic absorption bands were observed in the UV-visible spectrum of the Schiff base, 3APNPTDA. In the $\pi \rightarrow \pi^*$ region one characteristics band exhibited at 38910cm^{-1}. The $n \rightarrow \pi^*$ electronic transition was observed at 26954cm^{-1} with relatively low intensity, as it is spectroscopically forbidden.

FTIR spectral analysis

The characteristic group especially the functional groups of the Schiff base 3APNPTDA were established by using IR spectral data. A strong band appeared in the IR spectrum at 1593cm^{-1} can be assigned to stretching frequency of azomethine (C=N) group. The peak at 1506cm^{-1} can be consigned to C=C vibrations in aromatic rings. Aromatic C-H stretching frequency was found at 3107cm^{-1} and C-N stretching appeared as a strong band at 1232cm^{-1}. Another peak at 2924cm^{-1} was an indication of the C-H stretching frequency of CH_3 group. The presence of nitro group was confirmed by the appearance of the peaks at 1342cm^{-1} and 1301cm^{-1}. The peak found at 1105cm^{-1} was due to the C-S linkage. In plane bending vibrations come into sighted at 1068cm^{-1}. Also the peaks gained at 970cm^{-1} and 854cm^{-1} can be consigned as out of plane bending vibrations.

NMR spectral analysis

The ^1H NMR spectrum of the pyridine derivative 3APNPTDA, derived from 3-acetyl pyridine and the parent amine, NPTDA is shown in Fig. 1.24. The methyl group

at acetyl moiety appeared as a singlet signal at 2.6δ. The aromatic protons of anthracene and pyridine rings resonated between 7.75-8.30δ.

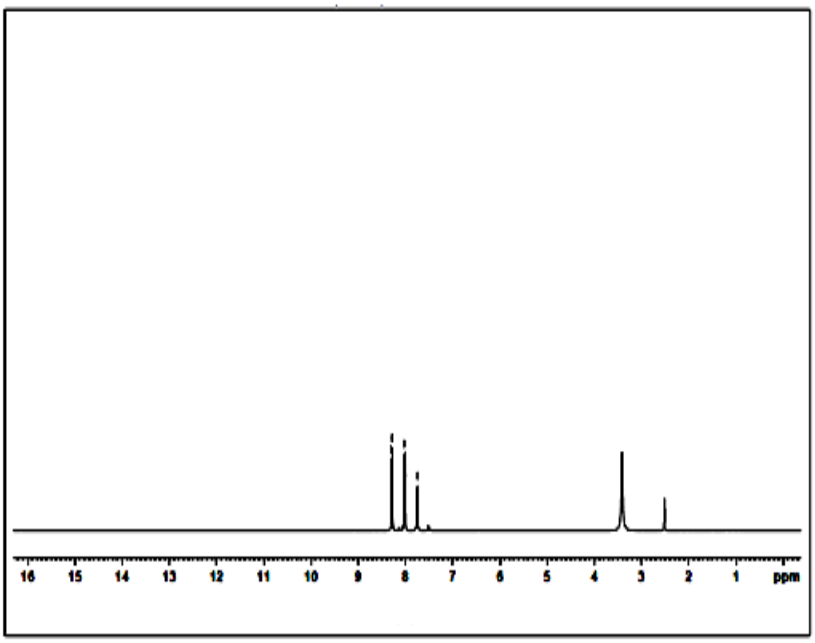

Fig. 1.24: ^{1}H NMR spectrum of 3APNPTDA

Characteristics ^{13}C NMR spectrum of Schiff base 3APNPTDA is shown in Fig. 1.25. Methyl C atom observed as a sharp signal at 39ppm. All other carbon atoms in the aromatic rings observed in the range 124-169ppm

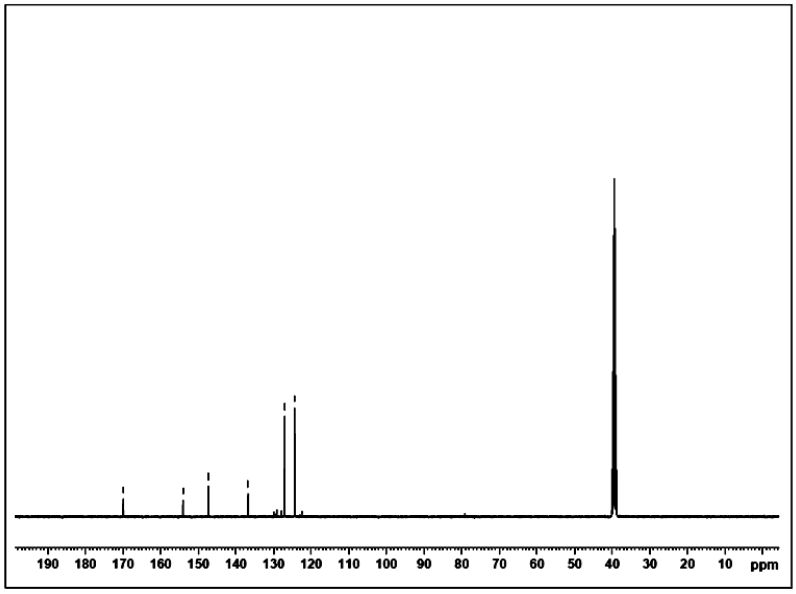

Fig. 1.25: ^{13}C NMR spectrum of 3APNPTDA

Mass spectral analysis

Only one distinct peak was appeared in the gas chromatogram of the sample which establish the purity of the compound 3APNPTDA. Molecular ion peak (M^+ peak) was absent but a clear base peak with high intensity observed at m/z 74 corresponding to the fragment $[CH_2N_2S]^+$. Another peak at m/z 222 monitored $[C_8H_6N_4O_2S]^+$ with high intensity, which is formed due to the loss of 3-acetyl pyridine part from the ligand 3APNPTDA. Other signals appeared at m/z 134, 120 and 60 were assigned due to the fragments $[C_7H_4N_2S]^+$, $[C_7H_4S]^+$ and $[CH_2NS]^+$ respectively. Mass spectrum of 3APNPTDA is shown in Fig. 1.26.

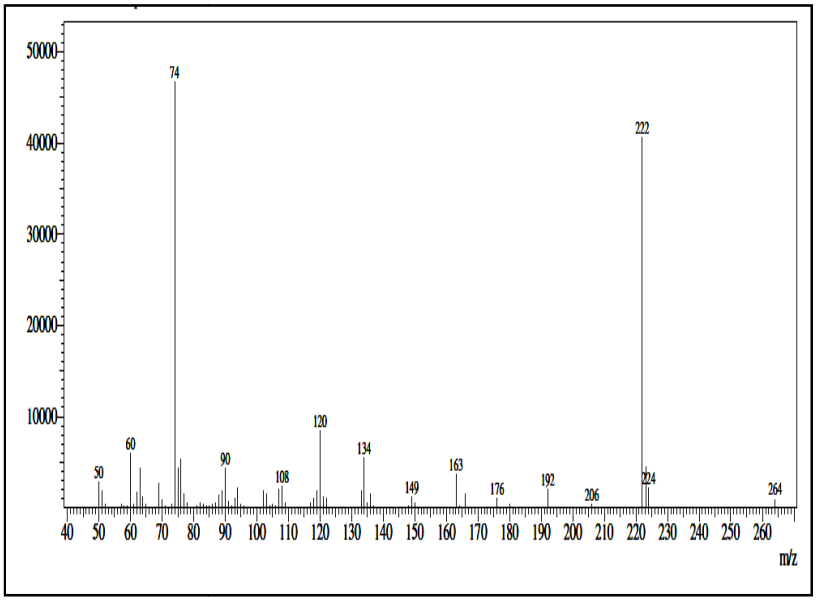

Fig. 1.26: Mass spectrum of 3APNPTDA

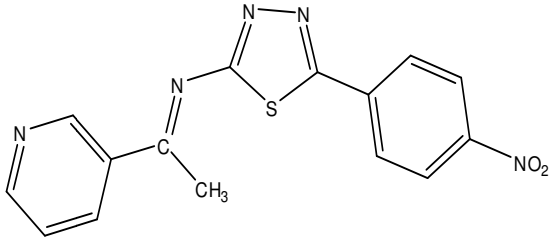

Fig. 1.27: Structure of 3APNPTDA

Synthesis of Complexes

The ethanolic solution of chromium(III) acetate, manganese(II) acetate, ferric(III) chloride, nickel(II) acetate, copper(III) acetate, zinc(II) chloride and zirconyl nitrate was added dropwise to the hot ethanolic solution of 3-acetyl pyridine derivative of 'S' containing Schiff base 3APNPTDA in 1:1 molar ratio and refluxed this mixture to about seven hours and concentrated. The resulting crystals were collected, washed with ethanol and hot water and dried (Yield = 50-75%).

Characterisation of Complexes

There is a good correlation between observed and calculated values of elemental analysis and 1:1 stoichiometry was exist between metal and ligand in all complexes. All the complexes of 3APNPTDA are stable amorphous powder and it is soluble in organic solvents like DMSO, $CHCl_3$ and DMF and insoluble in water. Physical properties of all complexes were studied and tabulated in Table 1.12.

Electronic spectral analysis

Electronic spectra of complexes prepared showed two characteristic peaks corresponding to $\pi \rightarrow \pi^*$ and $n \rightarrow \pi^*$ transitions.

Table 1.11: Electronic spectral data of Schiff base, 3APNPTDA and its transition metal complexes

Compound	Electronic bands in cm^{-1}	
	$\pi \rightarrow \pi^*$	$n \rightarrow \pi^*$
3APNPTDA	38910	26954
$[CrL(Ac)_3H_2O]$	38610	26809
$[MnL(Ac)_2(H_2O)_2]$	37313	26455
$[FeLCl_3(H_2O)]$	38610	26385
$[NiL(Ac)_2(H_2O)_2]$	37235	26455
$[CuL(Ac)_2(H_2O)_2]$	38610	26809
$[ZnLCl_2]$	37174	26666
$[ZrOL(NO_3)_2]$	38660	26455

Both the peaks exhibited a downward shift in frequency during Schiff base formation and complexation due to increased conjugation. The electronic bands are summarized and characteristic IR absorption bands are given in Table 1.11. This is clear proof for the formation of complexes.

Magnetic moment analysis

Measurements of the values of magnetic susceptibility of the complexes offered strong support for determining the exact geometry. The effective magnetic moment data of 3APNPTDA-complexes are shown in Table 1.12. Cr(III), Mn(II), Fe(III), Ni(II) and Cu(II) complexes of 3APNPTDA were assigned octahedral structure because they showed magnetic moment values 3.92BM, 5.85BM and 1.83BM respectively. Fe-3APNPTDA chelate displayed low magnetic moment value of 5.02BM, which may be due to antiferromagnetic exchange in this complex. A slight increase in the magnetic moment showed by Ni-3APNPTDA (3.15BM) from the theoretical value (2.87BM) is mainly due to spin–orbit coupling. Diamagnetic character was found for Zn(II) and ZrO(II) complexes, which is quite justifiable with the absence of unpaired electron (d^{10} or d^{0}) in its configuration

Molar conductance analysis

Molar conductance measurement was done for all complexes and is given in Table 1.12. Molar conductance values of the complexes are in the range of 6-28$\Omega^{-1}cm^{2}mol^{-1}$. These values suggest non-electrolytic behavior and absence of counter ions outside the coordination sphere of metal chelates.

FTIR spectral analysis

Infrared spectra can be utilized mainly for analyzing the coordination sites of the ligand. In 3APNPTDA complexes, the stretching frequencies of the azomethine linkage showed a downward shift during complexation due to the decreased electron density at

azomethine group. Additional bands in the range 3245-3423cm^{-1} implies the coordination of water molecules in the complexes and 1310-1472cm^{-1} implies the coordination of nitrate molecules respectively. C-N and C-S stretching frequency shown in the region of 1272-1279cm^{-1} and 1100-1126cm^{-1} respectively. Appearance of M-O and M-N bands in the spectrum clarify the coordination of O and N atom to the metal. Cr(III), Mn(II), Ni(II) and Cu(II) complexes of 3APNPTDA showed peaks in the range 1629-1693cm^{-1} and 1514-1557cm^{-1} due to asymmetric and symmetric stretching of monodentate acetate moieties. In ZrO(II) complex, three bands appeared for N-O bond with a difference of 160cm^{-1} correspond to monodentate nitrate group. A peak at 468cm^{-1} in the spectrum of 3APNPTDA-Zn complex can be assigned to Zn-Cl stretching. Characteristic infrared absorption frequencies (cm^{-1}) of 3APNPTDA and its transition metal complexes are given in Table 1.13.

Electrical,magnetic and spectral studies revealed that all these complexes are neutral having 1:1 stochiometry between ligand and metal. The structures of complexes derived are represented in Fig. 1.28.

Table 1.12: Microanalytical, magnetic and conductance data of the ligand 3APNPTDA and its transition metal complexes

Complex	Colour	Yield (%)	Mol. Wt.	M.P (^{0}C)	Metal % Found (Cald.)	C % Found (Cald.)	H % Found (Cald.)	N % Found (Cald.)	S % Found (Cald.)	μ_{eff} (BM)	Molar Conductance ($\Omega^{-1}cm^2mol^{-1}$)	Geometry
3APNPTDA (L)	Yellow	70	325	230	-	55.12 (55.38)	3.18 (3.41)	20.24 (21.53)	9.15 (9.86)	-	-	-
$[CrL(Ac)_3H_2O]$	Light Green	60	572	280	9.87 (9.09)	42.58 (44.97)	3.72 (4.29)	11.14 (11.92)	5.44 (5.46)	3.92	28.0	Octahedral
$[MnL(Ac)_2(H_2O)_2]$	Black	65	534	>320	9.98 (10.29)	41.12 (42.70)	3.41 (3.96)	12.60 (13.11)	5.38 (6.0)	5.85	19.2	Octahedral
$[FeLCl_3(H_2O)]$	Dark Yellow	70	506	>310	10.55 (11.07)	34.71 (35.64)	2.03 (2.59)	12.18 (13.85)	6.02 (6.34)	5.02	12.7	Octahedral
$[NiL(Ac)_2(H_2O)_2]$	Yellowish Orange	75	538	>320	11.66 (10.97)	41.17 (42.40)	3.65 (3.93)	12.22 (13.01)	5.77 (5.96)	3.15	19.0	Octahedral
$[CuL(Ac)_2(H_2O)_2]$	Black	70	543	>310	12.27 (11.79)	40.13 (42.03)	2.80 (3.9)	11.53 (12.9)	5.41 (5.91)	1.83	19.4	Octahedral
$[ZnLCl_2]$	Cream	60	461	260	14.73 (14.10)	36.69 (39.03)	2.16 (2.40)	13.79 (15.17)	5.64 (6.95)	D	9.7	Tetrahedral
$[ZrOL(NO_3)_2]$	Orange needle	60	556	242	17.02 (16.37)	30.00 ((32.37)	1.45 (1.99)	16.90 (17.62)	5.09 (5.76)	D	6.8	Square Pyramidal

Table 1.13: Characteristic infrared absorption frequencies (cm^{-1}) of 3APNPTDA and its transition metal complexes

Complex	υ_{H_2O}	υ_{COOAsy}	$\upsilon_{C=N}$	υ_{COOsy}	$\upsilon_{C=C}$	υ_{NO_2/NO_3}	υ_{C-N}	υ_{C-S}	υ_{M-O}	υ_{M-N}
3APNPTDA (L)	-	-	1593	-	1506	1342 1301	1232	1105	-	-
$[CrL(Ac)_3(H_2O)]$	3363	1687	1587	1557	1505	1364 1335	1272	1126	620	526
$[MnL(Ac)_2(H_2O)_2]$	3245	1647	1586	1515	1503	1340 1317	1273	1102	617	506
$[FeLCl_3(H_2O)]$	3285	-	1586	-	1505	1430 1315	1276	1104	610	494
$[NiL(Ac)_2(H_2O)_2]$	3423	1629	1590	1514	1502	1338 1310	1279	1100	618	509
$[CuL(Ac)_2(H_2O)_2]$	3385	1693	1559	1528	1505	1403 1347	1273	1106	589	478
$[ZnLCl_2]$	-	-	1572	-	1512	1428 1348	1272	1103	603	468 M-Cl
$[ZrOL(NO_3)_2]$	-	-	1544	-	1514	1472 1344 1310	1273	1105	675	586

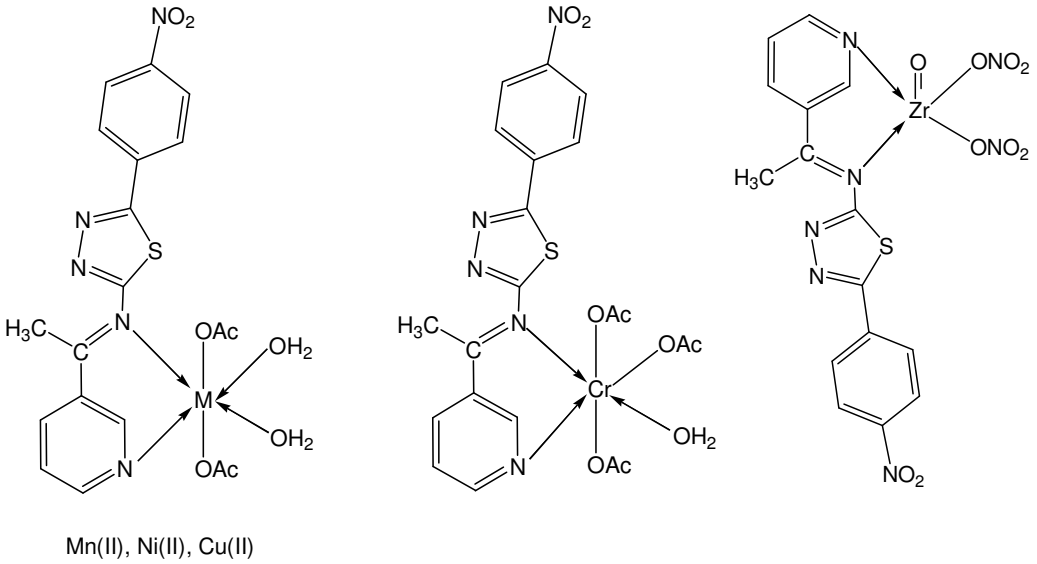

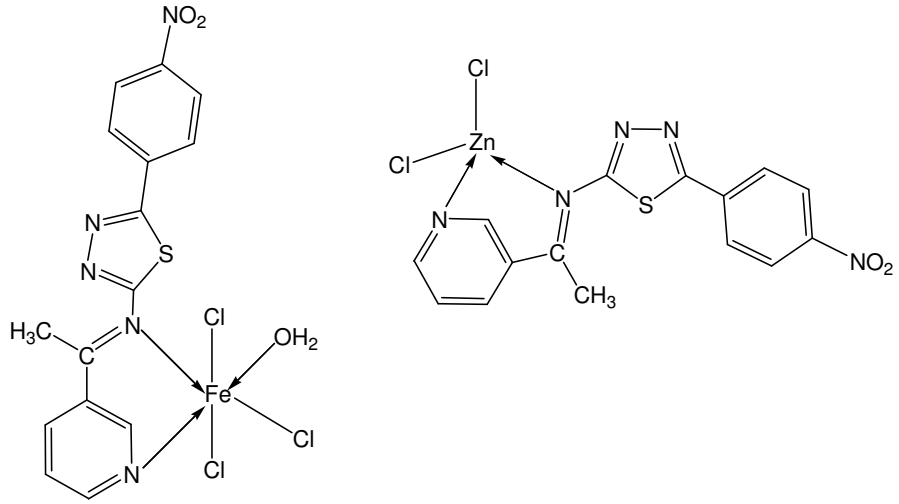

Fig. 1.28: Structures of transition metal complexes of 3APNPTDA

SECTION III

STUDIES ON SCHIFF BASE (E)-5-(4-NITROPHENYL)-N-(1(PYRIDIN-2-YL) ETHYLIDENE)-1,3,4-THIADIAZOL-2-AMINE (2APNPTDA) AND ITS TRANSITION METAL COMPLEXES

Another novel thiadiazole and pyridine based Schiff base, (E)-5-(4-nitro phenyl)-N-(1(pyridin-2-yl)ethylidene)-1,3,4-thiadiazol-2-amine (2APNPTDA) was synthesized and characterized by elemental analysis and various spectroscopic techniques. The structure of the ligand 2APNPTDA and its transition metal complexes with chromium, cobalt, nickel, copper, zinc and zirconium ions were established based on spectroscopic, magnetic and electrical studies. The detailed synthesis and characterization of both the ligand and complexes are discussed in this section**.**

Synthesis of 2APNPTDA

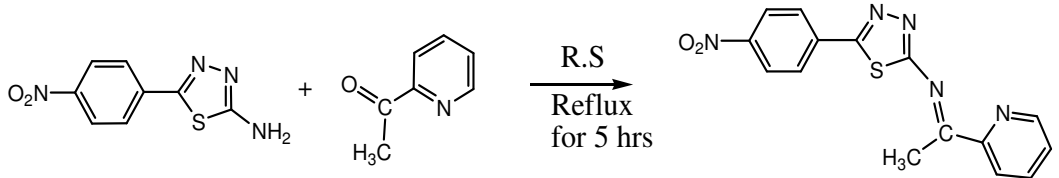

5-(4-nitrophenyl)-1,3,4-thiadiazol-2-amine

2-Acetylpyridine

2APNPTDA

Fig. 1.29: Synthesis of 2APNPTDA

Hot ethanolic solution of 2-acetyl pyridine was added to a refluxing solution of 5-(4-nitrophenyl)-1,3,4-thiadiazol-2-amine in ethanol and refluxed 5 hrs on a water bath. The resulting solution was concentrated to obtain yellowish brown crystals of 2APNPTDA, which was filtered, washed and dried. Recrystallization from methanol gave 80 % yield of the desired product. MP: 220^0C

Characterisation of 2APNPTDA

Elemental analysis

The elemental analysis data of thiadiazole and 2-acetyl pyridine derivative of

Schiff base 2APNPTDA is given in Table 1.15. The experimentally obtained percentages of elements like carbon, hydrogen, nitrogen and sulphur were in good agreement with the calculated values.

Electronic spectral analysis

Characterization of ligand, (E)-5-(4-nitrophenyl)-N-(1(pyridin-2-yl)ethylidene)-1,3,4-thiadiazol-2-amine (2APNPTDA)was done using IR and UV spectral data. Electronic spectrum of the ligand showed peaks at 39370$cm^{-1}$and 27100 cm^{-1}due to $\pi\rightarrow\pi^*$ and $n\rightarrow\pi^*$ transitions respectively. The decrease in the values compared to the parental amine is an indication of extension of conjugation during the formation of ligand 2APNPTDA.

FTIR spectral analysis

Characteristic infrared absorption frequencies (cm^{-1}) of thiadiazole pyridine derivative 2APNPTDA are represented in Table 1.15. Another important band was at 1692cm^{1}(C=N) due to the stretching mode of azomethine linkage. The peaks at 1592cm^{-1} and 1493cm^{-1} can be consigned to C=C vibrations in aromatic rings. Aromatic C-H stretching frequency was found at 3111cm^{-1} and C-N stretching appeared at 1269cm^{-1}. Another peak at 2929cm^{-1} was an indication of the C-H stretching frequency of CH_3 group. The presence of nitro group was confirmed by the appearance of the peaks at 1385cm^{-1} and 1312cm^{-1}. The peak found at 1104cm^{-1} was due to the carbon sulphur linkage and C-N stretching frequency was appeared at 1269cm^{-1}.In plane bending vibrations come into sighted at 1059cm^{-1} and the peaks gained at 983cm^{-1} and 853cm^{-1} can be consigned as out of plane bending vibrations.

NMR spectral analysis

The ^{1}H NMR spectrum of the 'S' containing Schiff base, 2APNPTDA which is derived from 2-acetyl pyridine and NPTDA are shown in Fig. 1.30. Eight non equivalent

hydrogen atoms which were in different electronic environments gave characteristic peaks in the NMR spectrum. The methyl group attached to the pyridine ring appeared as a singlet signal at 2.6δ, and the protons present in the aromatic (pyridine and benzene) rings exhibited signals in the range 7.12-8.32δ.

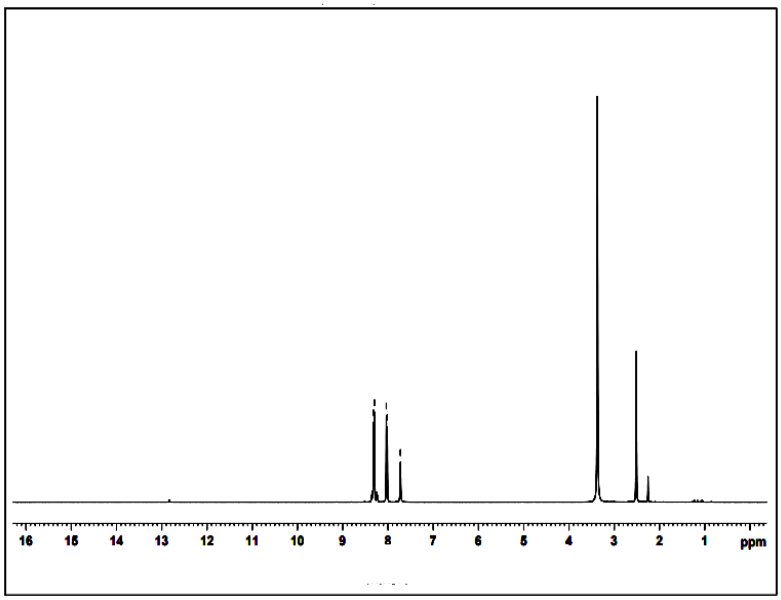

Fig. 1.30: ^{1}H NMR spectrum of 2APNPTDA

Characteristics ^{13}C NMR spectrum of Schiff base 2APNPTDA is shown in Fig. 1.31. Methyl C atom observed as a sharp signal at 38ppm. Peaks due to other carbon atoms in the aromatic rings were observed in the range 124-169ppm

Mass spectral analysis

In GCMS, the ligand 2APNPTDA shows a highly intensified base peak at m/z 222 due to the fragment $[C_8H_6N_4O_2S]^+$, which is formed due to the loss of 2-acetyl pyridine part from the ligand 2APNPTDA. Another clear signal with high intensity appeared at m/z 74 corresponding to the fragment, $[CH_2N_2S]^+$. The fragments $[C_8H_7N_2S]^+$, $[C_7H_4NS]^+$, $[C_7H_4S]^+$, $[CH_2N_2S]^+$ and $[CH_2NS]^+$ were appeared at m/z 163, 134, 120, 74, 60 respectively. The mass spectrum of the Schiff base 2APNPTDA is provided in Fig. 1.32.

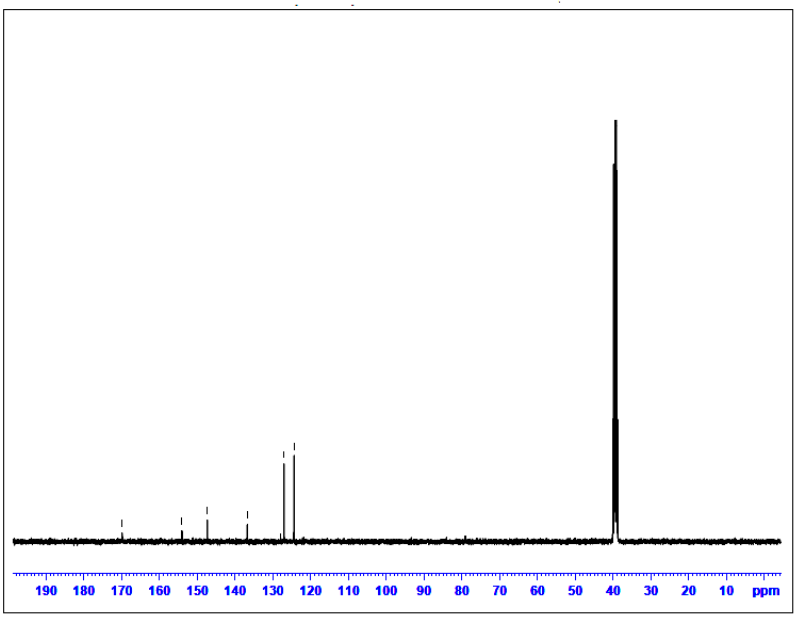

Fig. 1.31: ^{13}C NMR spectrum of 2APNPTDA

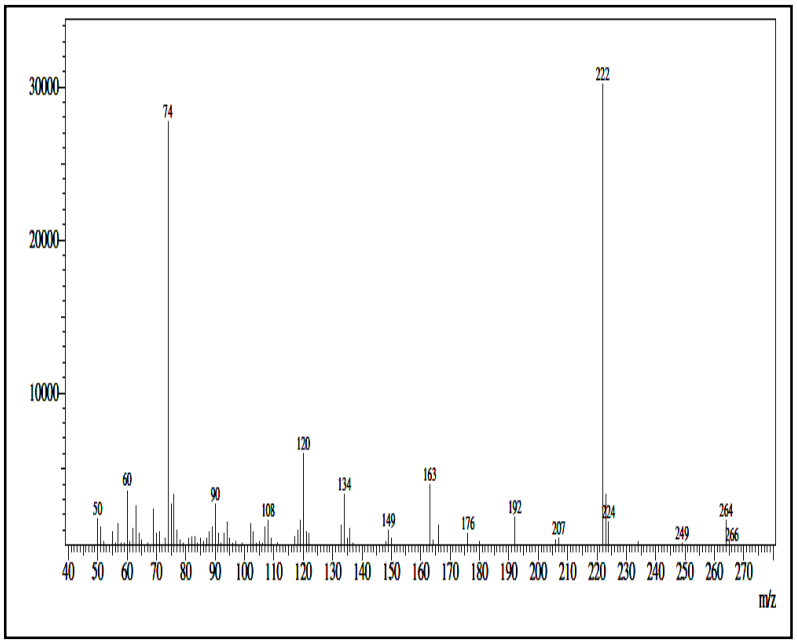

Fig. 1.32: Mass spectrum of 2APNPTDA

From the above discussions, the structure of 'S' containing pyridine derivative Schiff base, 2APNPTDA was derived and represented in Fig 1.33.

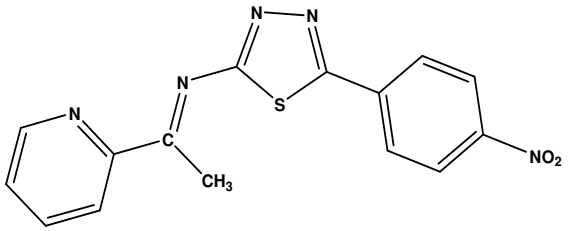

Fig. 1.33: Structure of 2APNPTDA

Synthesis of Complexes

Cr(III), Co(II), Ni(II) ,Cu(II), Zn(II) and ZrO(II) complexes of 2APNPTDA were prepared in ethanolic medium by adopting conventional refluxing method. Equimolar mixtures of NPTDA and 2-acetylpyridine were refluxed in rectified spirit or 4h. To the boiling solution, ethanolic solution of chromium acetate (2mmol) was added and again refluxed for 5h. The reaction mixture was kept overnight, and the complex was precipitated as brown coloured crystals. Filtered, washed with alcohol and warm water, dried, and melting point was determined. Cobalt nrate, nickel(II) acetate, copper(III) acetate, zinc(II) acetate and zirconyl(IV) nitrate were used for the preparation of respective complexes.(Yield = 60-90%).

Characterisation of Complexes

The metal complexes of Cr(III), Co(II), Ni(II), Cu(II), Zn(II) and ZrO(II) are coloured and stable towards light, air and they have high m.ps (above 280^{o}C). Analytical records suggested that the M:L ratio in all transition metals complexes of 2APNPTDA to be 1:1 (Table 1.15). These complexes are insoluble in water, but they are soluble in DMSO, DMF and $CDCl_3$. Molar conductivity values of 2APNPTDA-Complexes in DMSO are shown in Table 1.15. Elemental analysis provides an important key to structural elucidation of complexes. Percentage of C, H, N and S as well as the metal content were estimated by microanalytical methods. There is a good correlation between observed and calculated values.

Electronic spectral analysis

In all metal complexes of 2APNPTDA, the intra ligand electronic transitions ($n\rightarrow\pi^*$ and $\pi\rightarrow\pi^*$) were shifted to longer wavelength region. This clearly proves the occurrence of complexation. Electronic spectral data of all transition metal complexes of 2APNPTDA are provided in Table 1.14

Table 1.14: Electronic spectral data of Schiff base, 2APNPTDA and its transition metal complexes

Compounds	Electronic bands in cm^{-1}	
	$\pi\rightarrow\pi^*$	$n\rightarrow-\pi^*$
2APNPTDA	39370	27100
$[CrL(Ac)_3(H_2O)]$	38461	26666
$[CoL(NO_3)_2(H_2O)_2]$	38910	26178
$[NiL(Ac)_2(H_2O)_2]$	38610	26809
$[CuL(Ac)_2(H_2O)_2]$	39062	26954
$[ZnL(Ac)_2]$	39062	26385
$[ZrOL(NO_3)_2]$	38610	26455

Magnetic moment analysis

Magnetic moment data measurements of the complexes helped to establish their geometry. Results are shown in Table 1.15. Cr(III), Co(II) and Ni(II) complexes of 2APNPTDA were consigned octahedral configurations, as they were exhibited magnetic moment values of 3.84BM, 3.2BM and 2.82BM respectively. Cu(II)-2APNPTDA chelate displayed a higher magnetic moment of 2.16BM due to the spin-orbit coupling occurs and octahedral geometry was found to fit it. For the zinc complex diamagnetic nature was expected for Zn(II) and ZrO(II) complexes and these results were harmonized with the fact that these metal ions have d^{10} or d^0 configurations. Tetrahedral and square pyramidal geometries were therefore suggested for them.

Molar conductance analysis

Molar conductance values of the complexes are in the range of 1.8-14$\Omega^{-1}cm^2mol^{-1}$. These values suggest non-electrolytic behaviour and absence of counter ions outside the coordination sphere of metal chelates.

FTIR spectral analysis

Selected IR spectral bands for the ligand and its complexes are given in Table 1.16. The IR spectral bands of free ligand 2APNPTDA is characterized mainly by the strong bands at 1662cm^{-1}, 1592cm^{-1}, 1385cm^{-1}, 1269cm^{-1} and 1104cm^{-1} attributed the stretching frequencies of -C=N, C=C, -NO_2, C-N and C-S respectively. The FTIR spectrum of the free ligand (2APNPTDA) was compared with the spectra its transition metal complexes. Characteristic absorption bands in the range 3304-3375cm^{-1} were accredited to the coordinated water. The absorption frequencies in the range 1626–1686cm^{-1}, 1504-1585cm^{-1}, 1270–1275cm^{-1}, 1092-1106cm^{-1} were consigned to –C=N, -C=C,–C-N and -C-S bond stretching respectively in complexes. The imine peak (azomethine peak) in the metal complexes of 2APNPTDA showed change in shifts to lower region compared to the free ligand, which indicates the coordination of azomethine N atom to the metal ion. A peak at 474cm^{-1}in 2APNPTDA-Zn(II) complex can be assigned to Zn-Cl stretching. Also, the emergence of stretching frequencies in the range 615-717cm^{-1} and 420-505cm^{-1} confirmed corresponding to the formation of M-O bonds and M-N bond respectively.

From the above studies proper geometries were found for all complexes of 2APNPTDA and are given in Fig. 1.34.

Table 1.15: Microanalytical, magnetic and conductance data of the ligand 2APNPTDA and its transition metal complexes

Complex	Colour	Yield (%)	Mol. Wt.	M.P (^{0}C)	Metal% Found ((Cald.)	C % Found (Cald.)	H% Found (Cald.)	N % Found (Cald.)	S % Found (Cald.)	μ_{eff} (BM)	Molar Conductance ($\Omega^{-1}cm^2mol^{-1}$)	Geometry
2APNPTDA (L)	Yellowish brown	70	325	220	-	52.57 (55.38)	3.31 (3.41)	22.35 (21.53)	10.03 (9.86)	-	-	-
$[CrL(Ac)_3(H_2O)]$	Brown	85	572	310	9.89 (9.09)	44.13 (44.97)	3.98 (4.29)	10.77 (11.92)	5.39 (5.46)	3.84	7.2	Octahedral
$[CoL(NO_3)_2(H_2O)_2]$	Black	60	544	>310	11.5 (10.85)	31.27 (33.1)	2.54 (2.78)	17.85 (18.01)	5.69 (5.89)	3.21	8.2	Octahedral
$[NiL(Ac)_2(H_2O)_2]$	Black	80	538	>300	11.43 (10.97)	40.03 (42.4)	3.56 (3.93)	13.04 (13.01)	5.99 (5.92)	2.87	1.8	Octahedral
$[CuL(Ac)_2(H_2O)_2]$	Black	70	543	>360	12.61 (11.97)	40.37 (42.03)	2.95 (3.9)	13.04 (12.9)	5.42 (5.91)	2.16	3.5	Octahedral
$[ZnL(Ac)_2]$	Dark green	90	508	>300	11.98 (12.79)	30.13 (29.47)	1.95 (2.04)	10.33 (10.11)	4.70 (4.63)	D	14.0	Tetrahedral
$[ZrOL(NO_3)_2]$	Reddish orange	60	556	280	17.06 (16.37)	31.76 (32.37)	1.92 (1.99)	17.30 (17.62)	5.68 (5.76)	D	4.58	Square Pyramidal

Table 1.16: Characteristic infrared absorption frequencies (cm^{-1}) of 2APNPTDA and its transition metal complexes

Complex	υ_{H_2O}	υ_{COOAsy}	$\upsilon_{C=N}$	υ_{COOsy}	$\upsilon_{C=C}$	υ_{NO_2/NO_3}	υ_{C-N}	υ_{C-S}	υ_{M-O}	υ_{M-N}
2APNPTDA (L)	-	-	1692	-	1592	1385 1312	1269	1104	-	-
$[CrL(Ac)_3H_2O]$	3329	1714	1626	1522	1504	1449 1346	1273	1101	615	505
$[CoL(NO_3)_2(H_2O)_2]$	3310	-	1685	-	1584	1524 1470 1346	1274	1099	717	457
$[NiL(Ac)_2(H_2O)_2]$	3375	1690	1675	1586	1525	1485 1342	1275	1105	617	420
$[CuL(Ac)_2(H_2O)_2]$	3304	1700	1639	1596	1585	1476 1342	1270	1106	685	525
$[ZnL(Ac)_2]$	-	1699	1686	1586	1519	1382 1349	1275	1103	643	M-Cl 474
$[ZrOL(NO_3)_2]$	-	-	1633	-	1544	1508 1468 1337	1275	1092	614	462

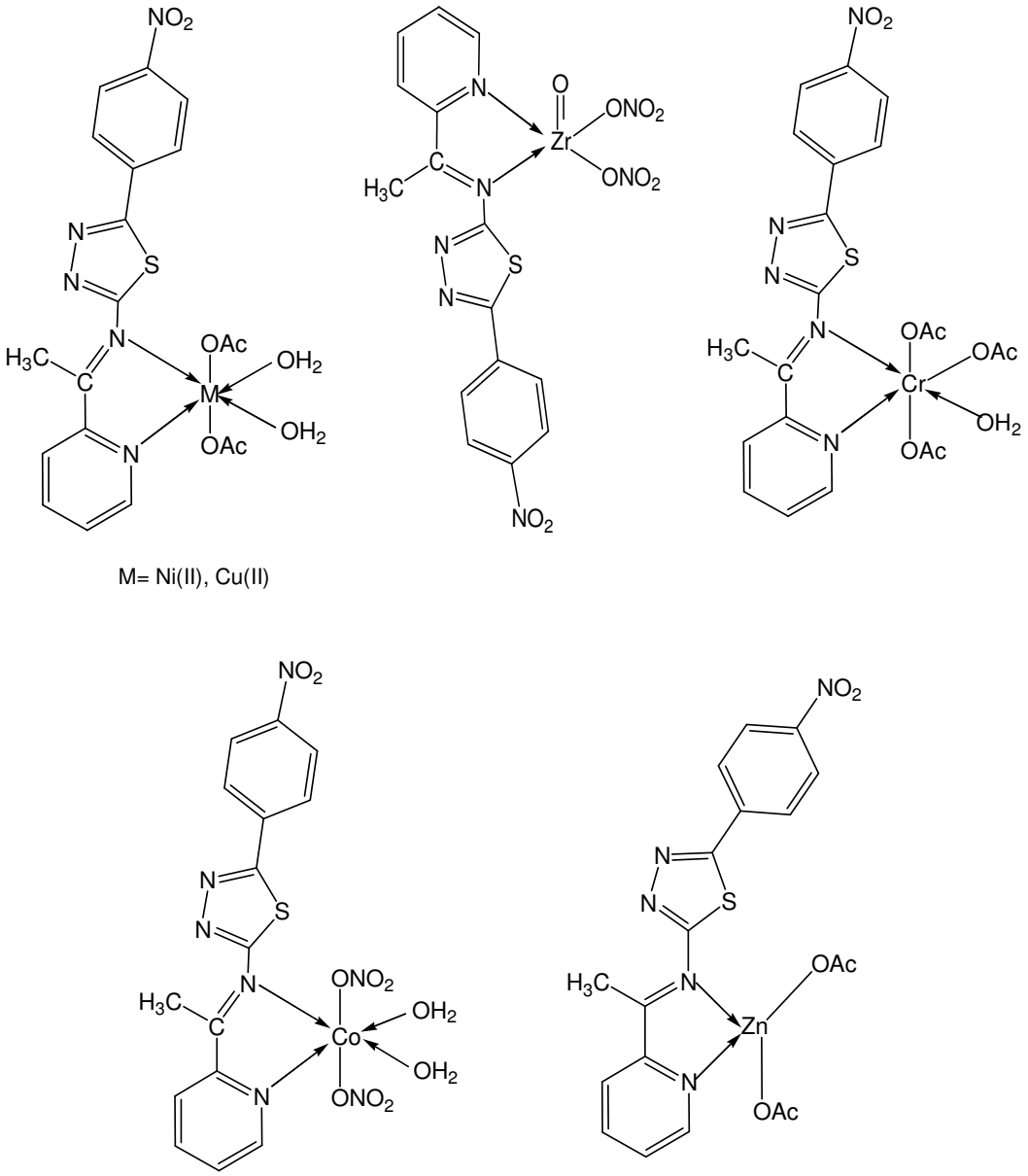

Fig. 1.34: Structures of transition metal complexes of 2APNPTDA

CHAPTER 5

TRANSITION METAL COMPLEXES OF SCHIFF BASES DERIVED FROM INDOLE-3-CARBALDEHYDE AND THIOPHENE 2-CARBALDEHYDE

Two novel sulphur containing Schiff bases such as N-((1H-indol-3 yl)methylene)thiazol-2amine (I3A2AT), which is an indole and thiazole derivative and (13E)-N1,N2-bis((thiophene-2-yl)methylene)cyclohexane-1,2-diamine (T2CDACH), which is derived from thiophene-2-carbaldehyde and 1,2-diaminocyclohexane were synthesized and characterized by means of elemental analysis and spectral studies such as FTIR, UV-visible, NMR (^{1}H and ^{13}C) and Mass spectroscopy. Chelating ability of these heterocyclic Schiff base ligands were proved by synthesizing transition metal complexes. Elemental (CHNS) analysis, FTIR, UV-visible spectroscopy, magnetic moment measurements, estimation of metal content and molar conductance studies were used to characterize the metal complexes.

This chapter is divided into two sections. Section I deals with synthesis and characterization of the indole and thiazole derived Schiff base ligand N-((1H-indol-3-yl)methylene)thiazol-2-amine (I3A2AT) and its transition metal complexes. Synthesis and characterization of the Schiff base ligand (13E)-N1,N2-bis((thiophene-2-yl) methylene) cyclohexane-1,2-diamine (T2CDACH) and its transition metal complexes were discussed in section II

SECTION I

STUDIES ON SCHIFF BASE, N-((1H-INDOL-3-YL)METHYLENE)THIAZOL-2-AMINE (I3A2AT) AND ITS TRANSITION METAL COMPLEXES

Novel thiazole and indole derivative of Schiff base, N-((1H-indol-3-yl) methylene)thiazol-2amine, (I3A2AT) was synthesized and characterized by various physicochemical techniques like UV-Visible, FTIR, NMR and Mass spectroscopy. The structure of transition metal complexes of the ligand with chromium, manganese, nickel, copper, zinc and zirconium ions were established based on elemental, spectroscopic, magnetic and electrical studies. The detailed synthesis and characterization of both the ligand I3A2AT and their complexes are discussed in this section**.**

Synthesis of I3A2AT

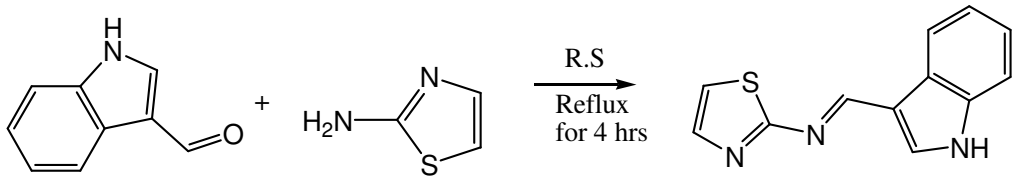

Indole 3-carboxaldehyde 2-Amino thiazole I3A2AT

Fig. 1.35: Synthesis of I3A2AT

The N-((1H-indol-3-yl)methylene)thiazol-2-amine (I3A2AT) was synthesized by adding hot ethanolic solution of 2-aminothiazole in dropwise to stirred solution containing equimolar concentration of indole-3-aldehyde in ethanol medium. The mixture was refluxed for 4h, kept for 1h to cool down to room temperature and the brown glittering crystals separated were filtered, washed with ethanol-water (1:1) mixture, and dried [78]. Yield-70% (MP: 120^0C)

Characterization of I3A2AT

Elemental analysis

The elemental analysis data of thiazole derivative of Schiff base I3A2AT is given in Table 1.18. Experimentally obtained percentages of elements like carbon, hydrogen, nitrogen and sulphur were in good agreement with the calculated values.

Electronic spectral analysis

Schiff base I3A2AT exhibited two important peaks in the UV–Visible spectrum. High intense peak at 29600cm^{-1} corresponds to allowed $\pi \rightarrow \pi^*$ and the peak at 25600cm^{-1} was assigned to the spectroscopically forbidden $n \rightarrow \pi^*$ transition.

FTIR spectral analysis

IR spectrum of I3A2AT consists of characteristic stretching frequencies corresponding to various bonds. Presence of azomethine group is proved by the peak observed at 1627cm^{-1}. Aromatic C-H stretching frequency appeared at 3114cm^{-1} and the stretching frequency due to NH vibration was identified at 3347cm^{-1} as a medium band. C=C stretching frequencies of thiazole and indole rings were observed at 1575, 1495, 1516cm^{-1} and C-S vibration and C-N stretching frequencies observed at 1112cm^{-1} and 1241cm^{-1} respectively Bands corresponding to in plane bending were observed at 1083cm^{-1} and 1027 cm^{-1} and out of plane bending bands observed at 757 and 638cm^{-1}.

NMR spectral analysis

Eight non-equivalent protons displayed their own distinct peak in the proton NMR spectrum of I3A2AT. Azomethine protons exhibited a singlet peak at 7.19δ. Weak and broad singlet appeared at 12.0δ corresponds to the proton present in the NH group in the indole moiety and the broadness can be explained by quadrupole interaction between ^{14}N and ^{1}H nuclei. Aromatic proton present in the indole ring exhibited signals in the range 7.12-7.18δ. The signals appeared at 7.43 and 8.01δ were due to the protons in the

thiazole ring and no inverse peak was observed in DEPT 135 which establish that there is no CH_2 moiety in the Schiff base.

Nine chemically different carbon atoms present in I3A2AT showed 9 distinct signals in the ^{13}C NMR spectrum. Peak at 185ppm corresponds to the carbon atom of azomethine group. Quaternary carbon atom present in the thiazole ring and indole ring displayed signals in the range 112-138ppm.^{1}H NMR, DEPT-135 and ^{13}C NMR spectral datas of indole based 'S' containing Schiff base I3A2AT are provided in Fig. 1.36, 1.37 and 1.38 respectively.

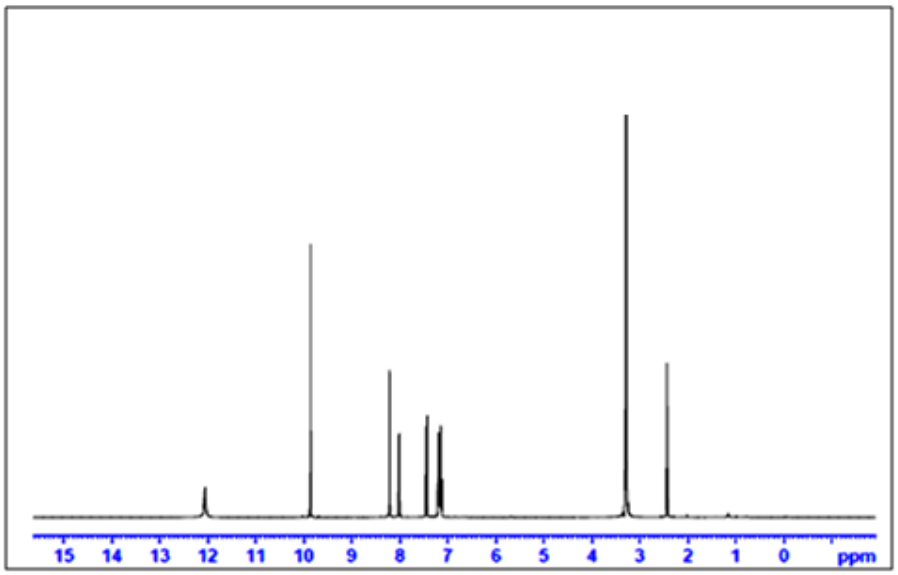

Fig. 1.36: ^{1}H NMR spectrum of I3A2AT

Mass spectral analysis

In the mass spectrum of I3A2AT, the molecular ion peak at m/z 227 was very much weak. The base peak was appeared as weak signal at m/z 144 by the fragment $[C_9H_8N_2]^+$ which is generated by the loss of thiazole part. The formation of fragments at m/z 89, m/z 100, m/z 116 and m/z 128 were due to the fragments $[C_3H_7NS]^+$, $[C_3H_4N_2S]^+$, $[C_8H_6N]^+$ and $[C_9H_6N]^+$ respectively. The electron impact mass spectrum of ligand I3A2AT is represented in Fig. 1.39.

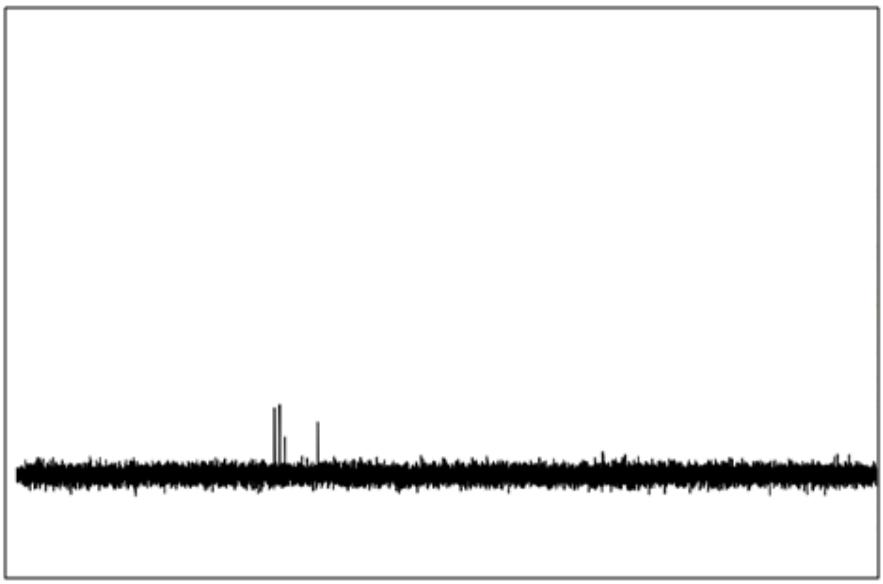

Fig. 1.37: DEPT 135 spectrum of I3A2AT

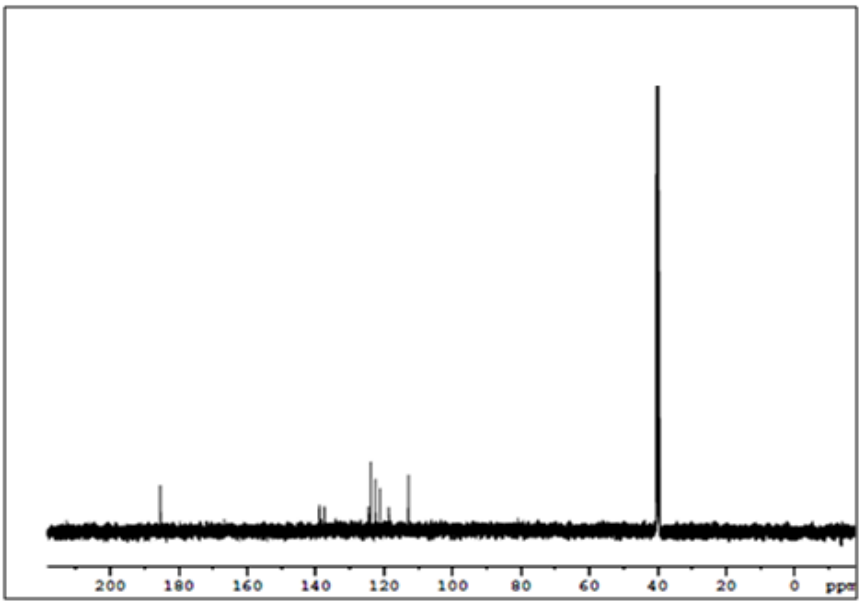

Fig. 1.38: ^{13}C NMR spectrum of I3A2AT

From the preceding discussions, the structure of 'S' containing indole derivative Schiff base I3A2AT is represented in Fig. 1.40.

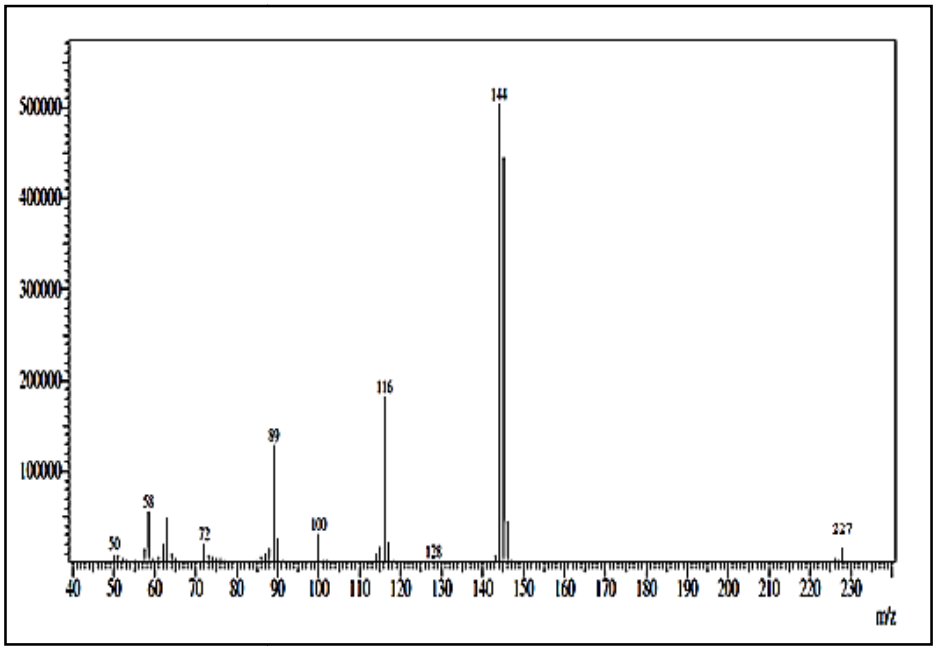

Fig. 1.39: Mass spectrum of I3A2AT

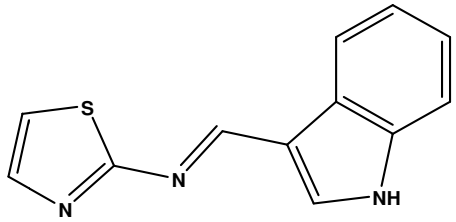

Fig. 1.40: Structure of I3A2AT

Synthesis of Complexes

The complexing capability of indole and thiazole derivative of Schiff base, I3A2AT were checked with Cr(III), Mn(II), Ni(II), Cu(II), Zn(II) and Zirconyl ions. Zirconyl nitrate is used for the synthesis of Zirconium complex. Acetate salts of other metal ions were used for the synthesis of respective complexes. Schiff base ligand I3A2AT (2mmol) was dissolved in minimum quantity of ethanol (15ml) and refluxed on a water bath (30min). Hot ethanolic solution of appropriate amount corresponding metal salt (acetate/nitrate) was added to the boiling medium and again refluxed for 4h. Then reduced its volume by evaporation, cooled and kept overnight and the crystallized metal

complexes were collected, washed with water ethanol mixture and dried over $CaCl_2$.

Characterization of Complexes

Adopted analytical techniques and the details for the characterization of I3A2AT-complexes include elemental analysis, conductance measurements, magnetic moment measurements, and spectral studies like electronic and IR spectroscopy are given in following paragraphs. All complexes were amorphous solid, coloured, non-hygroscopic, stable to light and air and highly soluble in DMSO, acids and other solvents.

A distinct idea about the precise molecular formula of complexes can be derived by the estimation of elements. It is seen that the theoretical values were very close to the observed values. Cr(III), Mn(II), Ni(II), Cu(II), Zn(II) and ZrO(II) complexes of I3A2AT were found to possess 1:1 stoichiometry. The data of CHNS analysis is listed in Table 1.18.

Electronic spectral analysis

From electronic spectra of the complexes d-d transitions and intra ligand electronic transitions were obtained. Electronic spectral data of I3A2AT and complexes are provided in Table 1.17.

Table 1.17: Electronic spectral data of Schiff base, I3A2AT and its transition metal complexes

Compound	Electronic bands in cm^{-1}	
	$\pi \rightarrow \pi^*$	$n \rightarrow \pi^*$
I3A2AT	39062	33783
$[CrL(Ac)_2(H_2O)]$	38610	33222
$[MnLAc(H_2O)_3]$	38314	32358
$[NiLCl(H_2O)_3]$	38610	26809
$[CuLAc(H_2O)_3]$	38461	33557
$[ZnLAc(H_2O)]$	38610	33557
$[ZrOLNO_3(H_2O)]$	38610	33333

A clear indication of complexation was obtained from the shift of these bands from lower to higher wavelength region.

Magnetic moment analysis

Magnetic moment data measurements gave an insight leading to the geometry of the complexes. Complexes of chromium and manganese were found to have octahedral geometry since they displayed their magnetic moment values 3.74BM and 5.91BM, respectively. Copper and nickel complexes showed their magnetic moment as 3.04BM and 1.92BM respectively, which designated high spin octahedral geometries. For zinc and zirconium complexes, observed diamagnetic characters justify their tetrahedral and square pyramidal geometries. Results are tabulated in Table 1.18.

Molar conductance analysis

For all the complexes of I3A2AT, the molar conductance measurements were done in the medium of DMSO. It was concluded from the conductance measurements that, counter ions were not present outside the coordination sphere of all complexes of I3A2AT (3.1-10.2$\Omega^{-1}cm^2mol^{-1}$) and therefore non-electrolytic character was consigned to them (Table 1.18).

FTIR spectral analysis

The downward shift in the vibrational frequencies of azomethine bond is seen in all complexes compared to the ligand I3A2AT (1627cm^{-1}) establishes the strong coordination of metal with imine nitrogen through coordinate bond. Broad bands seen in the FTIR spectra of all the chelates at the range of 3101-3325cm^{-1} can be ascribed to coordinated water molecules. In Cr(III), Mn(II), Cu(II), Zn(II) and ZrO(II) complexes, the asymmetric and symmetric stretching vibrational frequencies of the carboxylate group were observed in the range 1679-1698cm^{-1} and 1543-1590cm^{-1} respectively which indicates the monodentate nature of this group. N-H peak disappeared in all

complexes of I3A2AT indicated that the N atom was coordinated to metal atom, after protonation. Again, the new C-N and C-S stretching frequencies were observed in these complexes in the range 1237-1242cm^{-1} and 1101-1125cm^{-1} respectively. M-O and M-N bonds confirmed their presence as prominent peaks in low field area of IR spectrum. Spectral data of I3A2AT and their transition metal complexes are specified in Table 1.19.

The structures of the complexes of this heterocyclic Schiff base I3A2AT was established based on above justifications and it are represented in Fig. 1.41. In all the chelates, the Schiff base act as monovalent bidentate ligand.

Table 1.18: Microanalytical, magnetic and conductance data of the ligand I3A2AT and its transition metal complexes

Complex	Colour	Yield (%)	Mol. Wt.	M.P (^{0}C)	Metal% Found (Cald.)	C % Found (Cald.)	H % Found (Cald.)	N % Found (Cald.)	S % Found (Cald.)	μ_{eff} (BM)	Molar Conductance ($\Omega^{-1}cm^2mol^{-1}$)	Geometry
I3A2AT (LH)	Brown	70	227	120	-	60.41 (63.41)	3.90 (3.99)	16.79 (18.49)	13.43 (14.11)	-	-	-
$[CrL(Ac)_2(H_2O)_2]$	Black	55	433	>300	12.98 (12.01)	43.21 (45.63)	4.70 (4.73)	8.09 (9.39)	5.83 (7.17)	3.74	8.1	Octahedral
$[MnL(Ac)(H_2O)_3]$	Brown	70	395	250	14.85 (13.92)	41.30 (42.64)	3.98 (4.35)	8.75 (10.66)	6.90 (8.13)	5.91	4.9	Octahedral
$[NiLCl(H_2O)_3]$	Greenish red	80	376	180	14.75 (15.69)	36.46 (38.49)	3.45 (3.77)	11.01 (11.22)	8.22 (8.56)	3.04	6.6	Octahedral
$[CuL(Ac)(H_2O)_3]$	Dark brown	80	404	290	15.03 (15.84)	40.09 (41.73)	3.56 (4.25)	8.13 (10.43)	6.54 (7.96)	1.97	3.1	Octahedral
$[ZnL(Ac)(H_2O)]$	Creamish yellow	75	369	161	17.42 (17.61)	44.58 (45.6)	2.89 (3.55)	10.34 (11.4)	7.33 (8.7)	D	10.2	Tetrahedral
$[ZrOL(NO_3)(H_2O)]$	Flesh colour	90	414	>320	22.02 (21.98)	32.00 (34.85)	1.92 (2.44)	12.51 (13.55)	56.98 (7.75)	D	8.4	Square Pyramidal

Table 1.19: Characteristic infrared absorption frequencies (cm^{-1}) of I3A2AT and its transition metal complexes

Complex	υ_{H_2O}	υ_{COOasy}	$\upsilon_{C=N}$	υ_{COOsy}	$\upsilon_{C=C}$	υ_{C-N}	υ_{C-S}	υ_{M-O}	υ_{M-N}
I3A2AT (LH)	-	-	1627	-	1495	1241	1112	-	-
$[CrL(Ac)_2(H_2O)_2]$	3325	1695	1605	1550	1519	1242	1105	617	530
$[MnL(Ac)(H_2O)_3]$	3324	1679	1620	1547	1495	1240	1101	607	491
$[NiLCl(H_2O)_3]$	3166	-	1609	-	1520	1242	1125	640	430
$[CuL(Ac)(H_2O)_3]$	3312	1683	1613	1543	1503	1237	1108	598	483
$[ZnL(Ac)(H_2O)]$	3101	1698	1601	1573	1519	1241	1121	638	411
$[ZrOL(NO_3)(H_2O)]$	3241	1693	1623	1590	1511	1238	1107	607	450

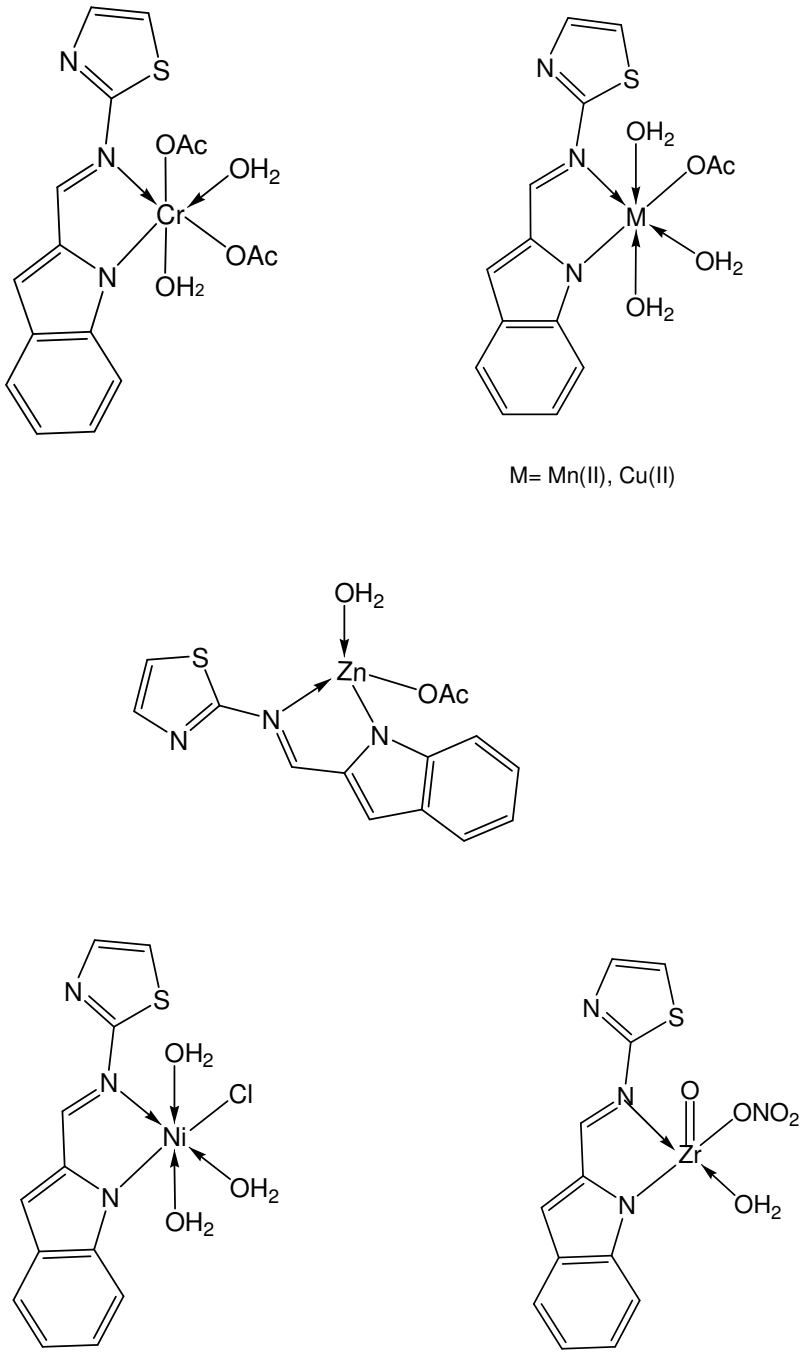

Fig. 1.41: Structures of transition metal complexes of I3A2AT

SECTION II

STUDIES ON SCHIFF BASE, (13E)-N1,N2-BIS((THIOPHENE-2-YL) METHYLENE) CYCLOHEXANE-1,2-DIAMINE (T2CDACH) AND ITS TRANSITION METAL COMPLEXES

Thiophene derivative of Schiff base, (13E)-N1,N2-bis((thiophen-2yl)methylene) cyclohexane -1,2-diamine (T2CDACH) which is a thiophene derivative, was synthesized and characterized by elemental analysis and various spectroscopic techniques. The structures of T2CDACH and its transition metal complexes with manganese, nickel, copper, zinc and zirconium of the ligand T2CDACH were established based on spectroscopic, magnetic and electrical studies. The detailed discussion on the synthesis and characterization of both the ligand and complexes are well depicted in this section.

Synthesis of T2CDACH

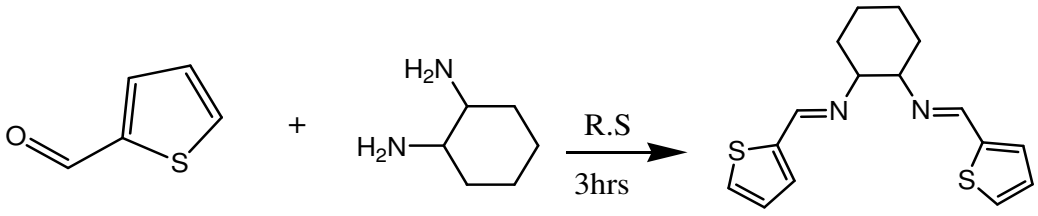

Thiophene-2-carbaldehyde 1,2-diamino cyclohexane T2CDACH

Fig. 1.42: Synthesis of T2CDACH

Heterocyclic Schiff base (13E)-N1,N2-bis((thiophen-2yl)methylene)cyclohexane -1,2-diamine (T2CDACH) was synthesized by the condensation of equimolar mixture of thiophene-2-carbaldehyde and 1,2-diaminocyclohexane, in ethanol medium and the reaction mixture was refluxed for 4 hours, concentrated, and cooled. The cream coloured solid formed was filtered, washed, and dried. Yield-90% (MP: 131^0C)

Characterization of T2CDACH

Elemental analysis

Elemental analysis data of thiophene derived Schiff base T2CDACH is given in Table 1.22. The experimentally obtained percentages of elements like carbon, hydrogen, nitrogen and sulphur were in good agreement with the calculated values.

Electronic spectral analysis

Thiophene derivative of Schiff base T2CDACH exhibited two important peaks in the UV–Visible spectrum. Peak at 39525cm^{-1}corresponds to $\pi \rightarrow \pi^*$ transitions while the peak at 35971cm^{-1} assigned to $n \rightarrow \pi^*$ transitions.

FTIR spectral analysis

Characteristics stretching frequencies of different bonds of thiophene derivative of Schiff base T2CDACH were obtained in the infrared spectrum. The stretching vibration band displayed at 1627cm^{-1} proved the formation of C=N linkage in the ligand. Aromatic C-H bond vibration and olefinic-H vibrations were observed at 3070cm^{-1}and 3008cm^{-1} respectively. The C-H stretching frequency in cyclohexane ring gave characteristics peaks at 2924cm^{-1}and 2829cm^{-1}. Aromatic C=C stretching frequency of thiophene moiety were observed at 1508cm^{-1}. A signal at 1211cm^{-1} was assignable to υ_{C-N} and a peak corresponding to υ_{C-S} was observed at 1128cm^{-1}. In plane deformations were observed at 1080cm^{-1} and 1033 cm^{-1}, while the out of plane deformations were observed at 846 and 709 cm^{-1}, respectively.

NMR spectral analysis

In the proton NMR spectrum of T2CDACH, a singlet signal at 8.30δ corresponds to the proton present in the azomethine linkage. Protons of the thiophene ring and cyclohexane ring showed their respective signals in the range 7.04-7.56δ and 1.40-3.25δ respectively. Both upward and downward peaks were observed in DEPT 135 due to the

presence of CH and CH_2 groups in the molecule.

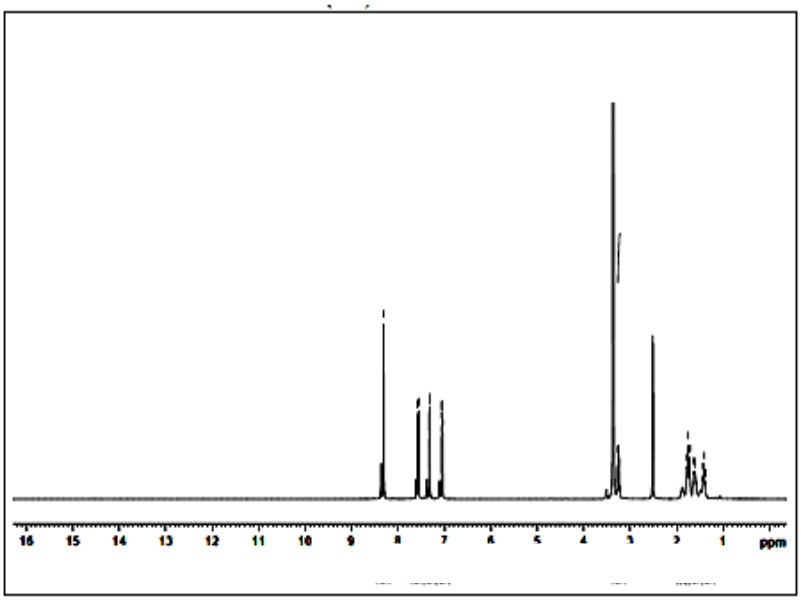

Fig. 1.43: ^{1}H NMR spectrum of T2CDACH

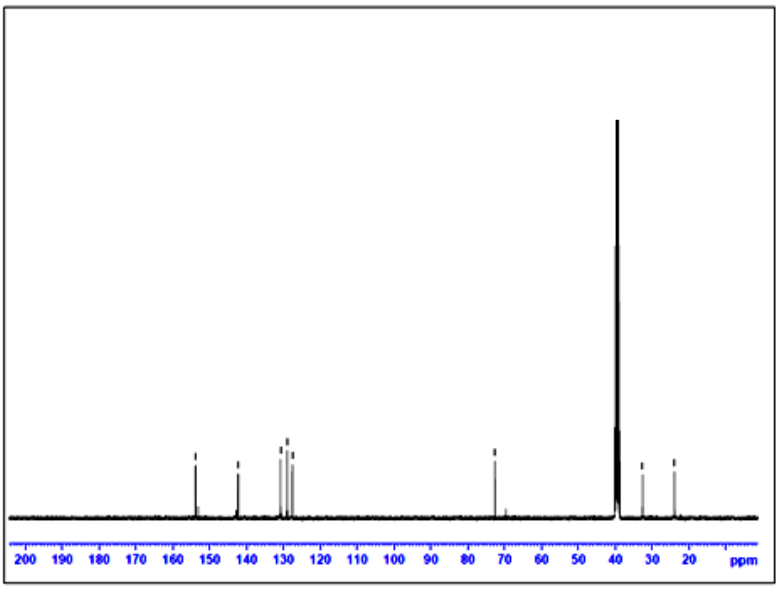

Fig. 1.44: ^{13}C NMR spectrum of T2CDACH

Eight different type carbon atoms showed 8 characteristic peaks in ^{13}C NMR spectrum of T2CDACH. Azomethine carbon displayed a peak at 153.83ppm and three different type sp^3 hybridised carbon atoms in cyclohexane ring exhibited three peaks between 23.93-72.61ppm. Five sp^2 carbons showed five peaks between 153.83-

127.58ppm. ^{1}H and ^{13}C NMR spectra of T2CDACH and the assignment signals are provided in Fig. 1.43, Fig. 1.44 and Table 1.20 respectively.

Table 1.20: ^{1}H NMR and ^{13}C NMR spectral data of T2CDACH

^{1}H NMR			^{13}C NMR		
	δ value	Labelled proton	δ value	Labelled carbon	
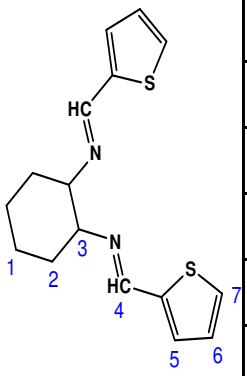	1.40 (t,4H)	1	23.93	1	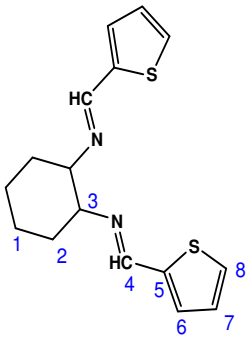
	1.76 (m,4H)	2	32.57	2	
	3.25 (t,2H)	3	72.61	3	
	8.30 (s,2H)	4	153.8	4	
	7.56 (d,2H)	5	142.2	5	
	7.04 (t,2H)	6	128.9	6	
	7.31 (d,2H)	7	127.5	7	
			130.8	8	

Mass spectral analysis

Purity of the synthesized thiophene derivative T2CDACH was proved by the appearance of only one peak in the gas chromatogram. The molecular ion peak due to $[C_{16}H_{18}N_2S_2]^+$ was appeared at m/z 302 as a very weak signal. The base peak was shown at m/z 193 due to the fragment $[C_{11}H_{15}NS]^+$ and the appearance of peak at m/z 219 was due to the loss of one thiophene moiety. Other peaks at m/z 112, 110 and 97 were due to the fragments $[C_5H_6NS]^+$, $[C_5H_4NS]^+$ and $[C_5H_5S]^+$ respectively. Mass spectrum of T2CDACH is shown in Fig. 1.45.

Above discussions, clearly establish the structure of thiophene derivative of Schiff base, T2CDACH as provided in Fig. 1.46.

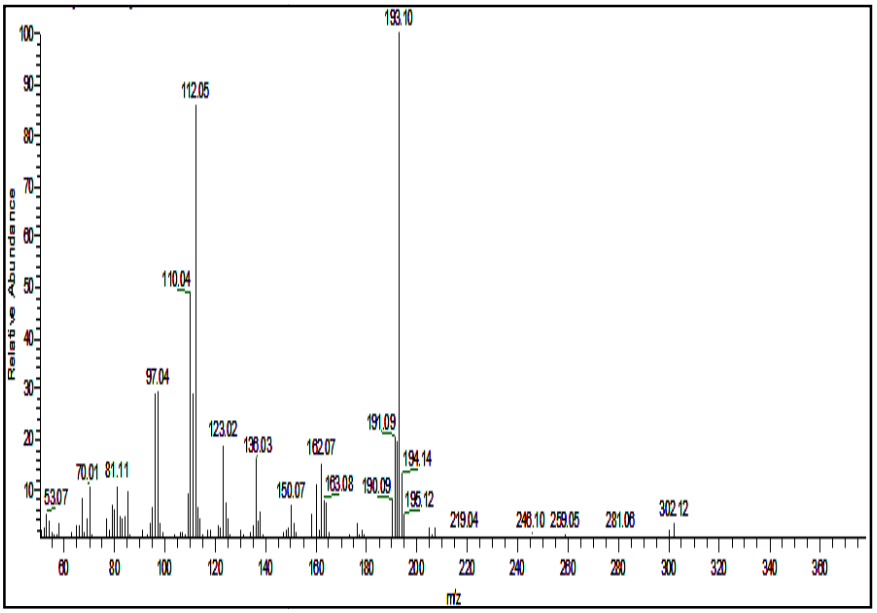

Fig. 1.45: Mass spectrum of T2CDACH

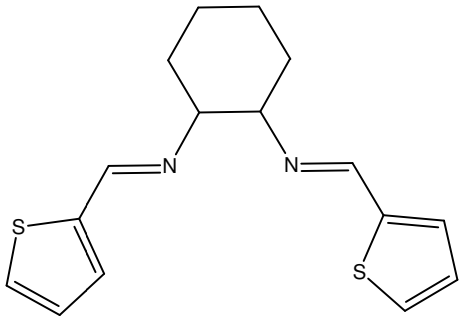

Fig. 1.46: Structure of T2CDACH

Synthesis of Complexes

Complexes of T2CDACH were synthesized by adding hot ethanolic solution of corresponding metal salts to the refluxing solution of ligand in 1:1 ratio and further refluxed for 5h. Acetates of manganese, nickel, copper and zinc were used, while nitrate salt of zirconium was employed for this purpose. Then, the mixture was cooled and the separated complexes filtered, cleaned and dried. All complexes were coloured and their melting points were found to be greater than 300^0C. Details of properties are reported in Table 1.22.

Characterization of Complexes

Elemental analysis

Microanalytical methods were employed for the estimation. The metal content in the chelates were derived by using pyrolytic, volumetric and gravimetric methods. CHNS analysis was used for determining carbon, hydrogen, nitrogen and sulphur content in the complexes. There is a good correlation between observed and calculated values of elemental analysis. The metal percentage data of the complexes obtained theoretically and experimentally are listed in Table 1.22. The results obtained are in match with theoretical explanations, which along with spectral data confirm 1:1 stoichiometry between metal and ligand in these complexes

Electronic spectral analysis

In the case of complexes, bathochromic shift was occurred for these bands which was a clear evidence for the complex formation. The electronic spectra of all complexes of T2CDACH showed mainly two peaks, due to $\pi \rightarrow \pi^*$ and $n \rightarrow \pi^*$transitions and they exhibited a downward shift in frequency in the spectra of chelates. This red shift confirms the extension of conjugation and hence the complexation.

Table 1.21: Electronic spectral data of Schiff base T2CDACH and its transition metal complexes

Compound	Electronic bands in cm^{-1}	
	$\pi \rightarrow \pi^*$	$n \rightarrow \pi^*$
T2CDACH	39525	35971
$[MnL(Ac)_2(H_2O)_2]$	38461	34602
$[NiL(Ac)_2(H_2O)_2]$	38759	35211
$[CuL(Ac)_2(H_2O)_2]$	38910	35087
$[ZnL(Ac)_2]$	38759	34602
$[ZrOL(NO_3)_2]$	38759	35460

The electronic bands of thiophene based Schiff base T2CDACH and its metal complexes are summarized in Table 1.21.

Magnetic moment analysis

The magnetic moment values of the complexes T2CDACH are represented in Table 1.22. The observed magnetic moment value for the Mn(II) complex is 5.90BM which establishes its octahedral geometry. The effective magnetic moment values of Ni(II) complex was found to be 2.21BM, which may be due to the antiferromagnetic exchange. Cu-T2CDACH complex exhibited its magnetic moment value 1.18BM which is less than the value obtained from spin only formula. Diamagnetic character was found for Zn(II) and ZrO(II) complexes, which is quite justifiable with the absence of unpaired electron (d^{10} or d^{0}) in its configuration.

Molar conductance analysis

Molar conductance measurement was done in the complexes and the data is tabulated in Table 1.22. The molar conductance values of all complexes of T2CDACH were very low and appeared in the range of 5-15$\Omega^{-1}cm^{2}mol^{-1}$. These values suggest the non-electrolytic behaviour of the chelates and absence of ionisable ions outside the coordination sphere of metal chelates

FTIR spectral analysis

In T2CDACH complexes, the involvement of azomethine groups in coordination with metal was confirmed by shift of stretching frequency to lower values. The presence of new broad signals around 3387cm^{-1}, 3442cm^{-1} and 3233 cm^{-1} in Mn(II), Ni(II) and Cu(II) complexes respectively confirmed the presence of coordinated water molecules in the complexes. Significant characteristic adsorption frequencies in the regions, 1547-1590cm^{-1} and 1681-1717cm^{-1} were accredited to the symmetric and asymmetric stretching vibrations of acetate groups respectively in complexes of T2CDACH except in

the case of Zr-T2CDACH complex. Also the appearance of stretching frequencies corresponding to M-O and M-N bonds confirmed the formation of complex. FTIR spectral informations of T2CDACH and its transition metal complexes are displayed in Table 1.23. The frequency separation between $\upsilon_{COO(asy)}$ and $\upsilon_{COO(sy)}$ was found to be above 150cm^{-1}, which confirm the monodenticity of acetate group. Based on the spectral analysis it is established that the Schiff base T2CDACH act as bidentate ligand towards chelation with transition metal ions. Fig. 1.47 depicts the structures of transition metal complexes of T2CDACH.

Table 1.22: Microanalytical, magnetic and conductance data of the ligand T2CDACH and its transition metal complexes

Complex	Colour	Yield (%)	Mol. Wt.	M.P (^{0}C)	Metal% Found (Cald.)	C % Found (Cald.)	H % Found (Cald.)	N % Found (Cald.)	S % Found (Cald.)	μ_{eff} (BM)	Molar Conductance ($\Omega^{-1}cm^2mol^{-1}$)	Geometry
T2CDACH (L)	Cream	90	302	131	-	63.30 (63.54)	6.2 (6.0)	9.25 (9.26)	19.73 (21.20)	-	-	-
$[MnL(Ac)_2(H_2O)_2]$	Black	60	511	>300	10.72 (10.76)	45.23 (46.96)	5.47 (5.52)	4.92 (5.48)	12.18 (12.54)	5.90	5.0	Octahedral
$[NiL(Ac)_2(H_2O)_2]$	Light Green	40	515	>300	12.03 (11.46)	44.12 (46.62)	4.75 (5.48)	4.58 (5.44)	11.81 (12.45)	2.21	8.0	Octahedral
$[CuL(Ac)_2(H_2O)_2]$	Dark Violet	90	520	>310	11.88 (12.31)	43.74 (46.18)	5.58 (5.43)	4.98 (5.39)	11.54 (12.33)	1.18	15.0	Octahedral
$[ZnL(Ac)_2]$	Dark Brown	80	485	>310	12.94 (13.40)	53.34 (51.31)	4.93 (5.68)	4.67 (5.44)	12.31 (12.45)	D	10.0	Tetrahedral
$[ZrOL(NO_3)_2]$	Slight Green	80	533	280	17.91 (17.07)	36.42 (37.21)	3.52 (3.86)	9.88 (10.21)	10.99 (11.69)	D	11.0	Square Pyramidal

Table 1.23: Characteristic infrared absorption frequencies (cm^{-1}) of T2CDACH and its transition metal complexes

Complex	υ_{H_2O}	$\upsilon_{COO(asy)}$	$\upsilon_{C=N}$	$\upsilon_{COO(sy)}$	$\upsilon_{C=C}$	υ_{C-S}	υ_{M-O}	υ_{M-N}
T2CDACH (L)	-	-	1627	-	1508	1128	-	-
$[MnL(Ac)_2(H_2O)_2]$	3387(br)	1715	1621	1588	1510	1127	698	521
$[NiL(Ac)_2(H_2O)_2]$	3442(br)	1698	1624	1547	1501	1126	653	513
$[CuL(Ac)_2(H_2O)_2]$	3233(br)	1681	1622	1554	1508	1135	706	474
$[ZnL(Ac)_2]$	-	1709	1621	1590	1506	1127	661	503
$[ZrOL(NO_3)_2]$	-	-	1624	-	1529	1132	650	480

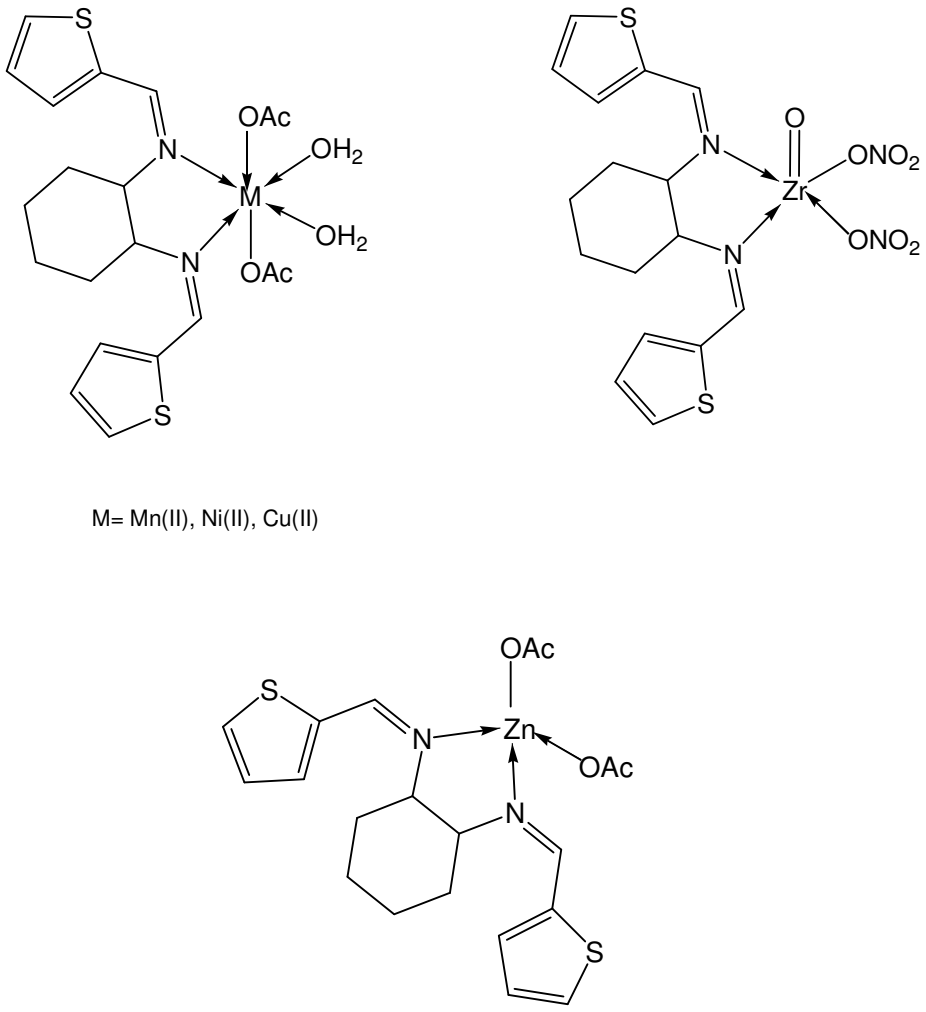

Fig. 1.47: Structures of transition metal complexes of T2CDACH

SUMMARY

Seven novel sulphur containing Schiff bases were synthesized and characterized by different techniques like CHNS analysis and spectral studies such as UV-visible, FTIR, NMR and Mass spectroscopy. Five of them are thiadiazole based Schiff bases namely (E)-(N-anthracene-9-ylmethylene)-5-(4-nitrophenyl)-1,3,4-thiadiazol-2-amine (A9CNPTDA), N-(anthracen-9(10H)-ylidene)-5-(4-nitrophenyl)-1,3,4-thiadiazol-2-amine (ANNPTDA), (E)-5-(4-nitrophenyl)-N-((pyridine-2-yl)methylene)-1,3,4-thia diazol-2-amine (P2CNPTDA), (E)-5-(4-nitrophenyl)-N-(1(pyridine-3-yl)ethylidene)-1,3,4-thiadiazol-2-amine (3APNPTDA) and (E)-5-(4-nitrophenyl)-N-(1(pyridin-2-yl) ethylidene)-1,3,4-thiadiazol-2-amine (2APNPTDA). Two of them are indole/ thiophene derivatives, N-((1H-indol-3-yl)methylene)thiazol-2-amine (I3A2AT) and (13E)-N1,N2-bis((thiophene-2-yl)methylene)cyclohexane-1,2-diamine (T2CDACH). Thiadiazole based Schiff bases were synthesized in two steps. First step is the synthesis of parent amine 5-(4-nitrophenyl)-1,3,4-thiadiazol-2-amine (NPTDA) followed by condensation reaction with corresponding carbonyl compounds. The chelating abilities of these 'S' containing Schiff bases were investigated by synthesizing a number of transition metal complexes. Then these complexes were also subjected to characterization studies by CHNS analysis, magnetic moment measurements, molar conductance studies different and spectral analysis. All the results are detailed and well discussed in this part.

Two polynuclear 'S' containing Schiff bases (E)-(N-anthracene-9-ylmethylene)-5-(4-nitrophenyl)-1,3,4-thiadiazol-2-amine (A9CNPTDA), N-(anthracen-9(10H)-yli dene) -5-(4-nitrophenyl)-1,3,4-thiadiazol-2-amine (ANNPTDA) were synthesized from 5-(4-nitrophenyl)-1,3,4-thiadiazole-2-amine (NPTDA) and polynuclear carbonyl compounds like anthracene-9-carbaldehyde and anthrone respectively. Transition metal

complexes of A9CNPTDA were prepared with Cr(III), Mn(II), Fe(III), Co(II), Ni(II), Cu(II), Zn(II) and ZrO(II) ions. 1:1 stoichiometry was found to exist between the metal and ligand in all the complexes of A9CNPTDA. The Cr(III) and Mn(II) chelates were found to have octahedral geometry. In the case of iron, cobalt, nickel and copper complexes a distorted octahedral geometry were fixed. Diamagnetic character was found for Zn(II) and ZrO(II) complexes in the magnetic studies and tetrahedral and square pyramidal geometry respectively were assigned for them. The studies establish that this polynuclear Schiff base A9CNPTDA is acting as a zerovalent bidentate ligand in the metal complexes having the active probes like highly polarisable 'S' atom of thiadiazole ring and azomethine nitrogen for coordination. The nonelectrolytic nature of these complexes was confirmed by molar conductance studies. The presence of coordinated water molecule was established from IR studies, by the presence of broad bands in the range 3340-3400cm^{-1}.

The complexing ability of another polynuclear Schiff base ANNPTDA which is derived from NPTDA and anthrone is explored with transition metal ions like Cr(III), Ni(II), Cu(II), Zn(II) and ZrO(II) ions. Various analytical techniques were employed to establish the structure and geometry. The metal content and CHNS analysis showed that all the complexes except Zn(II) and ZrO(II) possess 1:2 stoichiometry between metal ligand. Magnetic moment values and electronic spectra studies revealed that all the complexes except Zn(II) and ZrO(II) have octahedral geometry. Zn(II) complex has tetrahedral geometry and ZrO(II) hold square pyramidal structure. Spectral data also confirmed the geometry of the complexes

Three pyridine based thiadiazole derivatives of Schiff bases P2CNPTDA, 2APNPTDA and 3APNPTDA were synthesized from the coupling reactions between NPTDA and pyridine-2-carbaldehyde or 2-acetyl pyridine or 3-acetyl pyridine. The

chelating efficacy of these pyridine derivatives of Schiff bases were explored by synthesizing transition metal complexes. All the complexes of these Schiff bases were found to have 1:1 stoichiometry between the metal and ligand. Various spectral techniques established the exact coordination probes of these ligands. These ligands were bidentate in nature coordinating through azomethine group and nitrogen atom of pyridine moiety. Molar conductance data suggested that all the compounds were non-electrolytic in nature.

For nickel(II) and copper(II) complexes of P2CNPTDA, octahedral geometry were assigned according to their magnetic behaviour. Iron(III) chelate of P2CNPTDA was exhibiting distorted octahedral geometry. Tetrahedral geometry was assigned for both the zinc(II) and cadmium(II) complexes. Zirconium complexes of P2CNPTDA exhibit square pyramidal geometry. Transition metal complexes of 3APNPTDA were synthesized with Cr(III), Mn(II), Fe(II), Ni(II), Cu(II), Zn(II) and ZrO(II) ions and characterized by different analytical techniques. It was concluded that all the complexes of 3APNPTDA were of 1:1 stoichiometry between the ligand and metal ion. Cr(III), Mn(II), Fe(III), Ni(II) and Cu(II) complexes of 3APNPTDA obeyed octahedral geometry whereas Zn(II) and ZrO(II) complexes showed tetrahedral and square pyramidal geometry respectively. This Schiff base acted as a nonovalent bidentate ligand during complexation. Six transition metal complexes of Schiff base 2APNPTDA were synthesized and characterized. It is shown from the investigations that this Schiff base behaved as neutral bidentate ligand in all complexes. Spectral and magnetic studies revealed that complexes of Cr(III), Co(II), Ni(II) and Cu(II) possess octahedral nature. For the zinc and zirconium complexes, diamagnetic nature was observed and tetrahedral and square pyramidal geometry were assigned respectively for them.

The chelating efficiency of imine I3A2AT derived from 2-aminothiazole and

indole-3-carbaldehyde was fair and six transition metal complexes were synthesized with Cr(III), Mn(II), Ni(II), Cu(II), Zn(II) and ZrO(II) ions and characterized. Octahedral geometry was shown by chromium, manganese, nickel and copper complexes, while tetrahedral and square pyramidal geometry was followed by zinc and zirconium complexes. It was found that all complexes of 13A2AT were of 1:1 stoichiometry. N-H peak appeared in the IR spectrum of I3A2AT was disappeared in all complexes which indicated that the 'N' atom was coordinated to metal atom, after deprotonation. The 'N' atom of indole ring and azomethine linkage participated in complexation which was confirmed by spectral analysis especially FTIR studies.

The metal chelates of the thiophene derivative of Schiff base T2CDACH were prepared and characterized using various analytical techniques. Metal complexes of Mn(II), Ni(II), and Cu(II) exhibited octahedral geometry. But Zn(II) and ZrO(II) complexes showed tetrahedral and square pyramidal geometry respectively. All the complexes of T2CDACH were found to be non-electrolytic in nature. The presence of coordinated water molecule was established from IR studies by the presence of a broad band at about 3300cm^{-1}. The results obtained from elemental and metal content analysis are in match with the theoretical expectations, which along with spectral data confirm 1:1 stoichiometry between metal and ligand in these complexes. Based on the spectral analysis it is established that the Schiff base T2CDACH act as bidentate ligand towards chelation with transition metal ions, coordinating through nitrogen atoms of two azomethine moiety.

In short, seven potential novel 'S'containing Schiff base ligands derived from primary amines namely, 5-(4-nitrophenyl)-1,3,4-thiadiazol-2-amine, 2-aminothiazole and 1,2-diaminocyclo hexane with different carbonyl compounds such as anthracene-9-carbaldehyde, anthrone, pyridine-2-carbaldehyde or 2-acetyl pyridine, 3-acetyl pyridine,

indole-3-carbaldehyde and thiophene-2-carbaldehyde and their forty three transition metal chelates were synthesized and characterized using most modern analytical tools, which are further employed for evaluating their applications in biological and corrosion inhibition fields and discussed in subsequent parts.

REFERENCES

[1] A.T. Balaban, D.C. Oniciu, A.R. Katritzky, Aromaticity as a cornerstone of heterocyclic chemistry, Chem. Rev. 104 (2004) 2777–2812.

[2] T.Y. Fonkui, M.I. Ikhile, D.T. Ndinteh, P.B. Njobeh, Microbial activity of some heterocyclic Schiff bases and metal complexes: A review, Trop. J. Pharm. Res. 17 (2018) 2507–2518.

[3] M. Taha, M.T. Javid, S. Imran, M. Selvaraj, S. Chigurupati, H. Ullah, F. Rahim, F. Khan, J.I. Mohammad, K.M. Khan, Synthesis and study of the α-amylase inhibitory potential of thiadiazole quinoline derivatives, Bioorganic Chem. 74 (2017) 179–186.

[4] N. Siddiqui, S.B. Andalip, R. Ali, O. Afzal, M.J. Akhtar, B. Azad, R. Kumar, Antidepressant potential of nitrogen-containing heterocyclic moieties: an updated review, J. Pharm. Bioallied Sci. 3 (2011) 194-205.

[5] X.-H. Yang, L. Xiang, X. Li, T.-T. Zhao, H. Zhang, W.-P. Zhou, X.-M. Wang, H.-B. Gong, H.-L. Zhu, Synthesis, biological evaluation, and molecular docking studies of 1,3,4-thiadiazol-2-amide derivatives as novel anticancer agents, Bioorg. Med. Chem. 20 (2012) 2789–2795.

[6] Y. Vaishnav, D. Dewangan, S. Verma, A. Mishra, A.S. Thakur, P. Kashyap, S.K. Verma, PPAR gamma targeted molecular docking and synthesis of some new amide and urea substituted 1,3,4-thiadiazole derivative as antidiabetic compound, J. Heterocycl. Chem. 57 (2020) 2213–2224.

[7] M. Harfenist, D.J. Heuser, C.T. Joyner, J.F. Batchelor, H.L. White, Selective inhibitors of monoamine oxidase. 3. Structure- activity relationship of tricyclics bearing imidazoline, oxadiazole, or tetrazole groups, J. Med. Chem. 39 (1996) 1857–1863.

[8] L. Dong, B. Song, J. Wu, Z. Wu, Y. Zhu, X. Chen, D. Hu, Synthesis and antiviral activity of novel thioether derivatives containing 1,3,4-oxadiazole/thiadiazole and emodin moieties, Phosphorus Sulfur Silicon Relat. Elem. 191 (2016) 904–907.

[9] P. Li, D. Hu, D. Xie, J. Chen, L. Jin, B. Song, Design, synthesis, and evaluation of new sulfone derivatives containing a 1,3,4-oxadiazole moiety as active antibacterial agents, J. Agric. Food Chem. 66 (2018) 3093–3100.

[10] N.N. Farshori, M.R. Banday, A. Ahmad, A.U. Khan, A. Rauf, Synthesis, characterization, and in vitro antimicrobial activities of 5-alkenyl/hydroxyalkenyl-2-phenylamine-1,3,4-oxadiazoles and thiadiazoles, Bioorg. Med. Chem. Lett. 20 (2010) 1933–1938.

[11] E. Palaska, G. Şahin, P. Kelicen, N.T. Durlu, G. Altinok, Synthesis and anti-inflammatory activity of 1-acylthiosemicarbazides, 1,3,4-oxadiazoles, 1,3,4-thia diazoles and 1,2,4-triazole-3-thiones, J. Med. Farm. 57 (2002) 101–107.

[12] V. Jatav, P. Mishra, S. Kashaw, J. Stables, CNS depressant and anticonvulsant activities of some novel 3-[5-substituted 1,3,4-thiadiazole-2-yl]-2-styryl quinazoline-4(3H)-ones, Eur. J. Med. Chem. 43 (2008) 1945–1954.

[13] E.E. Oruç, S. Rollas, F. Kandemirli, N. Shvets, A.S. Dimoglo, 1,3,4-thiadiazole derivatives. Synthesis, structure elucidation, and structure- antituberculosis activity relationship investigation, J. Med. Chem. 47 (2004) 6760–6767.

[14] Y. Hu, C.-Y. Li, X.-M. Wang, Y.-H. Yang, H.-L. Zhu, 1,3,4-Thiadiazole: synthesis, reactions and applications in medicinal, agricultural, and materials chemistry, Chem. Rev. 114 (2014) 5572–5610.

[15] D.R. Kumar, M.S. Sayed, M.L. Baynosa, J.-J. Shim, 5-Amino-2-mercapto-1,3,4-thiadiazole coated nitrogen-doped-carbon sphere composite for the determination of phenolic compounds, Microchem. J. 105023 (2020) 1-11.

[16] D. Seeliger, B.L. de Groot, Ligand docking and binding site analysis with PyMOL and Autodock/Vina, J. Comput. Aided Mol. Des. 24 (2010) 417–422.

[17] A. Asan, S. Soylu, T. Kıyak, F. Yıldırım, S. Öztaş, N. Ancın, M. Kabasakaloğlu, Investigation on some Schiff bases as corrosion inhibitors for mild steel, Corros. Sci. 48 (2006) 3933–3944.

[18] M. Gholivand, F. Ahmadi, E. Rafiee, A Novel Al(III)-Selective Electrochemical sensor based on N,N′-Bis(salicylidene)-1,2-phenylenediamine complexes, Electroanal. Int. J. Devoted Fundam. Pract. Asp. Electroanal. 18 (2006) 1620–1626.

[19] W. Wróblewski, Z. Brzózka, D.M. Rudkevich, D.N. Reinhoudt, Nitrite-selective ISE based on uranyl salophen derivatives, Sens. Actuators B Chem. 37 (1996) 151–155.

[20] M.R. Ganjali, F. Mizani, M. Salavati-Niasari, Novel monohydrogenphosphate sensor based on vanadyl salophen, Anal. Chim. Acta. 481 (2003) 85–90.

[21] M. Shamsipur, S. Ershad, N. Samadi, A.R. Esmaeilbeig, R. Kia, A. Abdolmaleki, Polymeric membrane lanthanum (III)-selective electrode based on N, N′-Adipylbis (5-phenylazo salicylaldehyde hydrazone), Electroanal. Int. J. Devoted Fundam. Pract. Asp. Electroanal. 17 (2005) 1828–1834.

[22] S. Yamada, Advancement in stereochemical aspects of Schiff base metal complexes, Coord. Chem. Rev. 190 (1999) 537–555.

[23] I. Kostova, L. Saso, Advances in research of Schiff-base metal complexes as potent antioxidants, Curr. Med. Chem. 20 (2013) 4609–4632.

[24] K. Mohammed Yusuff, N. Sridevi, C. Pearly Sebastian, Characterization and catalytic activity of polymer supported ruthenium Schiff base complexes towards catechol oxidation, 105 (2007) 997-1002.

[25] K.K.M. Yusuff, R. Sreekala, Mixed ligand five coordinate cobalt(II) complexes of a polymer-bound schiff base derived from 2-aminobenzimidazole, J. Polym. Sci. Part Polym. Chem. 30 (1992) 2595–2599.

[26] M.M. Abd-Elzaher, A.A. Labib, H.A. Mousa, S.A. Moustafa, M.M. Ali, A.A. El-Rashedy, Synthesis, anticancer activity and molecular docking study of Schiff base complexes containing thiazole moiety, Beni-Suef Univ. J. Basic Appl. Sci. 5 (2016) 85–96.

[27] Y.N. Belokon, A.G. Bulychev, V.I. Maleev, M. North, I.L. Malfanov, N.S. Ikonnikov, Asymmetric synthesis of cyanohydrins catalysed by a potassium Δ-bis[N-salicylidene-(R)-tryptophanato]cobaltate complex, Mendeleev Commun. 14 (2004) 249–250.

[28] H.L. Singh, A.K. Varshney, Synthetic, structural, and biochemical studies of organotin(IV) with Schiff bases having nitrogen and sulphur donor ligands, Bioinorg. Chem. Appl. 206 (2006) 1–7.

[29] N.K. Rao, M.R. Reddy, Studies on the synthesis, characterisation and antimicrobial activity of new Co(II), Ni(II) and Zn(II) complexes of Schiff base derived from ninhydrin and glycine, Biol. Met. 3 (1990) 19–23.

[30] N. Raman, J.D. Raja, A. Sakthivel, Synthesis, spectral characterization of Schiff base transition metal complexes: DNA cleavage and antimicrobial activity studies, J. Chem. Sci. 119 (2007) 303–310.

[31] A. Mishra, M. Soni, Synthesis, structural, and biological studies of some Schiff bases and their metal complexes, Met.-Based Drugs. 7 (2008) 1-12.

[32] V. Badwaik, R. Deshmukh, A. Aswar, Transition metal complexes of a Schiff base: synthesis, characterization, and antibacterial studies, J. Coord. Chem. 62 (2009) 2037–2047.

[33] G. Ceyhan, C. Celik, S. Uruş, I. Demirtaş, M. Elmastaş, M. Tümer, Antioxidant, electrochemical, thermal, antimicrobial and alkane oxidation properties of tridentate Schiff base ligands and their metal complexes, Spectrochim. Acta. A. Mol. Biomol. Spectrosc. 81 (2011) 184–198.

[34] X. Zhang, C. Jiao, J. Wang, Q. Liu, R. Li, P. Yang, M. Zhang, Removal of uranium (VI) from aqueous solutions by magnetic Schiff base: kinetic and thermodynamic investigation, Chem. Eng. J. 198 (2012) 412–419.

[35] A. Nagajothi, A. Kiruthika, S. Chitra, K. Parameswari, Fe(III) complexes with Schiff base ligands: synthesis, characterization, antimicrobial studies, Res. J. Chem. Sci. 3 (2013) 606-613.

[36] P. Subramanian, M. Sakunthala, Antibacterial activities of new Schiff base metal complexes synthesised from 2-hydroxy-1-naphthaldehyde and 5-amino-1-naphthol, World J. Pharm. Pharm. Sci. 2 (2013) 2753–2764.

[37] K. Joshi, A. Rojivadiya, J. Pandya, Synthesis and spectroscopic and antimicrobial studies of schiff base metal complexes derived from 2-hydroxy-3-methoxy-5-nitrobenzaldehyde, Int. J. Inorg. Chem. 2014 (2014) 1-8.

[38] A. Pradhan, A. Kumar, A review: an overview on synthesis of some Schiff bases and their metal complexes with anti-microbial activity, Chem. Process Eng. Res. 35 (2015) 84–86.

[39] S.S. Tajudeen, G. Kannappan, Schiff base–copper(II) complexes: synthesis, spectral studies and anti-tubercular and antimicrobial activity, Indian J. Adv. Chem. Sci. 4 (2016) 40–48.

[40] A. Hameed, M. Al-Rashida, M. Uroos, S. Abid Ali, K.M. Khan, Schiff bases in medicinal chemistry: a patent review (2010-2015), Expert Opin. Ther. Pat. 27 (2017) 63–79.

[41] L. Zhu, N. Chen, H. Li, F. Song, X. Zhu, Synthesis, characterization and biological activities of Schiff bases of 2-amino-5-mercapto-1,3,4-thiadiazole and their Mo (VI) complexes, Huazhong Shifan Daxue Xuebao Zirankexueban. 37 (2003) 499–502.

[42] D.A. Laidler, D.J. Milner, Asymmetric synthesis of cyclopropane carboxylates: catalysis of diazoacetate reactions by copper (II) Schiff base complexes derived from α-amino acids, J. Organomet. Chem. 270 (1984) 121–129.

[43] B. Dash, P. Mahapatra, D. Panda, J. Pattnaik, Fungicidal activities and mass spectral studies of some schiff bases derived from p-hydroxybenzaldehyde and their derivatives, Chem. Informationsdienst. 16 (1985) 163-172.

[44] N. Rao, P. Rao, G. Reddy, M. Ganorkar, Metal-chelates of a new physiologically active ons tridentate schiff-base, Council Scientific Industrial Research Publ & Info Directorate, New delhi, 1987.

[45] B. Garg, R. Dixit, I. Das, Studies on the complexation behaviour of dehydroacetic acid-4-methyl-2-quinolylhydrazone with bivalent metal ions, in: Proc. Indian Acad. Sci.-Chem. Sci., (1990) 497–502.

[46] M.A. Ali, M. Tarafdar, Metal complexes of sulphur and nitrogen-containing ligands: complexes of s-benzyldithiocarbazate and a Schiff base formed by its condensation with pyridine-2-carboxaldehyde, J. Inorg. Nucl. Chem. 39 (1977) 1785–1791.

[47] A. Mishra, M. Khare, S. Gautam, Synthesis, physico-chemical characterization, and antibacterial studies of some bioactive Schiff bases and their metal chelates, Synth. React. Inorg. Met.-Org. Chem. 32 (2002) 1485–1500.

[48] A. Jha, Y. Murthy, U. Sanyal, G. Durga, Rapid synthesis, characterization, anticancer and antimicrobial activity studies of substituted thiadiazoles and their dinucleating ligand metal complexes, Med. Chem. Res. 21 (2012) 2548–2556.

[49] M.N. Uddin, D.A. Chowdhury, M.M. Rony, M.E. Halim, Metal complexes of Schiff bases derived from 2-thiophenecarboxaldehyde and mono/diamine as the antibacterial agents, Mod. Chem. 2 (2014) 6–13.

[50] A.S. Abu-Khadra, R.S. Farag, A.E.-D.M. Abdel-Hady, others, Synthesis, characterization and antimicrobial activity of Schiff base (E)-N-(4-(2-hydroxy benzylideneamino) phenylsulfonyl) acetamide metal complexes, Am. J. Anal. Chem. 7 (2016) 233-245.

[51] S. Karabasannavar, P. Allolli, I.N. Shaikh, B.M. Kalshetty, Synthesis, characterization and antimicrobial activity of some metal complexes derived from thiazole Schiff bases with in-vitro cytotoxicity and DNA cleavage studies, Indian J. Pharm. Educ. Res. 51 (2017) 490–501.

[52] E. Yousif, A. Majeed, K. Al-Sammarrae, N. Salih, J. Salimon, B. Abdullah, Metal complexes of Schiff base: preparation, characterization and antibacterial activity, Arab. J. Chem. 10 (2017) 1639–1644.

[53] J. Thomas, G. Parameswaran, Structural, thermoanalytical and antitumour studies of metal chelates of anthracene-9-carboxaldehyde thiosemicarbazone, Asian J. Chem. 14 (2002) 1354-1364.

[54] A. Prakash, S. Ahmad, Synthesis and characterisation of Schiff base complexes with Ti(III), Cr(III) and Ni(II), Orient. J. Chem. 25 (2009) 1035-1040.

[55] G.I. Devi, P. Sabu, P. Geetha, Thermal decomposition Kinetics and mechanism of Co(II), Ni(II), and Cu(II) complexes derived from Anthracene carboxaldehyde L–Tyrosine, Res. J. Chem. Sci. 2231 (2013) 606-614.

[56] K. Shaju, K. Joby Thomas, K. Vidhya Thomas, P.R. Vinod, Comparative cyclic voltammetric studies of (s)-2-(anthracen-9-(10H)-ylideneamino)-3-phenyl propanoic acid and its Cu(II) complex, J. Chem. Sci. 7 (2018) 73-84.

[57] N. Raman, A. Kulandaisamy, C. Thangaraja, P. Manisankar, S. Viswanathan, C. Vedhi, Synthesis, structural characterisation and electrochemical and antibacterial studies of Schiff base copper complexes, Transit. Met. Chem. 29 (2004) 129–135.

[58] Y. Gupta, S. Agarwal, S. Madnawat, Synthesis, characterization and antimicrobial studies of some transition metal complexes of Schiff bases, Res. J. Chem. Sci. ISSN. 2231 (2012) 606-617.

[59] K. Pothiraj, T. Baskaran, N. Raman, DNA interaction studies of d^9 and d^{10} metal complexes having Schiff base and polypyridyl ligands, J. Coord. Chem. 65 (2012) 2110–2126.

[60] A.A.R. Despaigne, F.B. Da Costa, O.E. Piro, E.E. Castellano, S.R. Louro, H. Beraldo, Complexation of 2-acetylpyridine-and 2-benzoylpyridine-derived hydrazones to copper(II) as an effective strategy for antimicrobial activity improvement, Polyhedron. 38 (2012) 285–290.

[61] N.S. Gwaram, H.M. Ali, H. Khaledi, M.A. Abdulla, A.H.A. Hadi, T.K. Lin, C.L. Ching, C.L. Ooi, Antibacterial evaluation of some Schiff bases derived from 2-acetylpyridine and their metal complexes, Molecules. 17 (2012) 5952–5971.

[62] M.M. Ibrahim, H.M. Ali, M.A. Abdullah, P. Hassandarvish, Acute toxicity and gastroprotective effect of the Schiff base ligand 1H-indole-3-ethylene-5-nitro salicylaldimine and its nickel(II) complex on ethanol induced gastric lesions in rats, Molecules. 17 (2012) 12449–12459.

[63] F. Rahaman, B. Mruthyunjayaswamy, Synthesis, spectral characterization and biological activity studies of transition metal complexes of Schiff base ligand containing indole moiety, Complex Met. 1 (2014) 88–95.

[64] K.T. Tadele, T.W. Tsega, Schiff bases and their metal complexes as potential anticancer candidates: A review of recent works, Anti-Cancer Agents Med. Chem. Former. Curr. Med. Chem.-Anti-Cancer Agents. 19 (2019) 1786–1795.

[65] O.A. EL-Gammal, H. Alshater, H.A. El-Boraey, Schiff base metal complexes of 4-methyl-1H-indol-3-carbaldehyde derivative as a series of potential antioxidants and antimicrobial: Synthesis, spectroscopic characterization and 3D molecular modeling, J. Mol. Struct. 1195 (2019) 220–230.

[66] W. Wendlandt, C. Chou, The thermal decomposition of metal complexes—XI: The hexamminechromium (III) complexes, J. Inorg. Nucl. Chem. 26 (1964) 943–949.

[67] E. Kohn, D. Venezky, R. Rice, F. Ross, G. Asbury Sr, A new electrochemical recorder paper, Naval Research Lab Washington DC, 1952.

[68] L. Coury, Conductance measurements Part I: theory, Curr. 18 (1999) 91–96.

[69] G. Maret, K. Dransfeld, Biomolecules and polymers in high steady magnetic fields, in strong ultrastrong magn. fields their Appl., (1985) 143–204.

[70] E. Yousif, A. Majeed, K. Al-Sammarrae, N. Salih, J. Salimon, B. Abdullah, Metal complexes of Schiff base: preparation, characterization and antibacterial activity, Arab. J. Chem. 10 (2017) 1639–1644.

[71] M. Tunçel, S. Serin, Synthesis and characterization of new azo-linked Schiff bases and their cobalt(II), copper(II) and nickel(II) complexes, Transit. Met. Chem. 31 (2006) 805–812.

[72] A. Paul, K. Joby Thomas, C. Sini Varghese, R. Johnson, Evaluation on Structural and Thermoanalytical Properties of a Novel Heterocyclic Schiff Base Derived from 3-Formylindole and its Metal Chelates, Chem. Sci. Rev. Lett. 4(2015), 278-284.

[73] N.H. Al-Shaalan, Synthesis, characterization and biological activities of Cu(II), Co(II), Mn(II), Fe(II), and UO_2(VI) complexes with a new Schiff base hydrazone: O-Hydroxyacetophenone-7-chloro-4-quinoline hydrazone, Molecules. 16 (2011) 8629–8645.

[74] L. Racanè, V. Tralić-Kulenović, D.W. Boykin, G. Karminski-Zamola, Synthesis of new cyano-substituted bis-benzothiazolylarylfurans and arylthiophenes, Molecules. 8 (2003) 342–348.

[75] C. Alarcón-Payer, T. Pivetta, D. Choquesillo-Lazarte, J.M. González-Pérez, G. Crisponi, A. Castiñeiras, J. Niclós-Gutiérrez, Thiodiacetato-copper (II) chelates with or without N-heterocyclic donor ligands: molecular and/or crystal structures of [Cu(tda)]n, [Cu(tda)(Him)2(H_2O)] and [Cu(tda)(5Mphen)]·2H_2O (Him= imidazole, 5Mphen= 5-methyl-1,10-phenanthroline), Inorganica Chim. Acta. 358 (2005) 1918–1926.

[76] P.S. Deshmukh, A. Yaul, J.N. Bhojane, A. Aswar, Synthesis, characterization and thermogravimetric studies of some metal complexes with N 2 O 2 Schiff base ligand, World Appl Sci J. 9 (2010) 1301–1305.

[77] G.L. Parrilha, R.P. Vieira, A.P. Rebolledo, I.C. Mendes, L.M. Lima, E.J. Barreiro, O.E. Piro, E.E. Castellano, H. Beraldo, Binuclear zinc (II) complexes with the anti-inflammatory compounds salicylaldehyde semicarbazone and salicylaldehyde-4-chlorobenzoyl hydrazone (H2LASSBio-1064), Polyhedron. 30 (2011) 1891–1898.

[78] S. Erdemir, Synthesis of novel chiral Schiff base and amino alcohol derivatives of calix[4]arene and chiral recognition properties, J. Mol. Struct. 1007 (2012) 235–241.

PART- II

BIOLOGICAL STUDIES

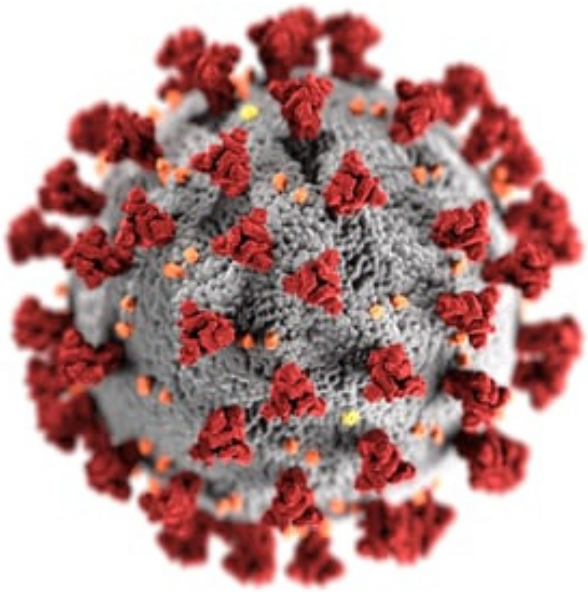

CHAPTER 6

INTRODUCTION AND REVIEW

Schiff bases, the versatile pioneer for organic synthesis and later researches proved that it has wide variety of applications in pharmaceutical fields and that was due to the biological activities expressed. Schiff bases (bearing imine or azomethine –C=N–) have shown a broad spectrum of activities including anti-diabetic, enzyme inhibition, DNA binding, cleavage activity and cytotoxicity activities [1]. Various publications had covered the antibacterial, anticancer, antifungal, anti-inflammatory and antiviral properties, hence researchers have promoted to extend their research domains on developing novel heterocyclic/ aryl derivatives of Schiff bases [2].

Schiff bases containing aromatic rings have exhibited prominent activity due to the free electron delocalisation within the ring structure. Likewise, Schiff base derived from heterocyclic rings were also shown potential activity. Researchers had investigated the biological importance of heterocyclic derivatives of the Schiff bases and their impressive biological activities attributed to the presence of aromatic ring containing heteroatoms such as nitrogen, sulphur and oxygen. Azomethine linkage present in Schiff bases makes hydrogen bond with the active centres of the cell and thereby interfere the normal processes of the cell [3]. These heterocyclic Schiff bases form the metal complexes such as Cd(II), Cu(II), Zn(II), Mn(II) and Ni(II) promises good chances in the development of antimicrobial, antiviral, anticancer drugs and also diminish the other life threatening diseases to humans.

Pharmacological Properties of Schiff Bases

Investigation have put forward that ‘S’ containing Schiff bases exhibits various pharmacological activities and medicinal applications such as anticancer, antifungal,

antimicrobial, anti-inflammatory, analgesic, antiepileptic etc. Thiadiazole is one of the most common and most important unit that is incorporated in the core structure of various natural products, array of drugs and medicinal agents. These thiadiazole derivatives of Schiff bases having five membered ring system containing hydrogen binding domain, sulphur atom and two-electron donor nitrogen system that exhibit a wide variety of biological activities. Rate of progress of studies in this field is greatly accelerated by the discovery of potent sulfa drugs containing nucleus [4]. There are several thiadiazole based drugs which are commercially available which includes, acetazolamide and methazolamide both are used for the treatment of glaucoma. Tebuthiuron is used as a non-selective broad spectrum herbicide, Megazol is used for the treatment of sleeping sickness and Sulfamethizole is useful as antibiotic [5]. In addition, Filanesib is used for the treatment of cancer, while Cefazedone is a cephalosporin antibiotic, and Cefazolin is an antibiotic used for the treatment of a number of bacterial infections.

On making certain modifications in the structure of Schiff base by heterocyclic substituent that should provide donor atoms such as 'N' and 'S' which would influence biological activity. In general, metal complex having Schiff base containing sulphur group show better biological activity due to their greater lipophilic nature. Its increased activity can be explained by overtone's concept of cell permeability and Tweed's chelation theory. According to these theories of cell permeability, lipid that surrounds the cell favours only the passage of lipid soluble materials. Thus lipid solubility is an important factor for controlling microbial activity. On chelation, the polarity of metal ion will be reduced to a greater extent due to the overlap of ligand orbital and more number of donor atoms would influence the polarity of metal ion. Further, this would increase the delocalisation of π-electrons all over the chelate ring and increases lipid solubility

(lipophilicity) of the complex. This helps to the penetration of complex into lipid membrane and thus blocks the binding sites of the microbes and inhibits its growth.

It is very important to explore the biological activities of novel 'S' containing Schiff bases and its metal chelates that have exhibited high effectiveness with lesser toxicity. Currently, researchers are more interested to evaluate the biological activities of Schiff bases using Lipinski's rule and computational studies ensure the druggability of the newly synthesized Schiff bases.

Antibacterial Studies

In the present era, chemists are very eager to synthesis drugs for diseases by microbes. The existing drugs are ineffective because, the microbes were acquired resistance by mutations. This made chemists to focus synthesis to get better drugs and to prevent the growth of microbes. The present work is proposed to monitor drug ability of newly synthesised heterocyclic 'S' containing Schiff bases and their metal chelates against various pathogens.

Important Pathogens

Bacteria are microscopic, single celled prokaryotes, which thrive in diverse environments. These live in soil, water and human gut. Even though they have important roles in human, animal and plants bodies and some of them are leads to pathogenic diseases which are harmful to human body. Bacteria like Rhizobium are useful in nitrogen fixation.

They had a simple internal structure that lacks a nucleus and contain a DNA that either floats freely in a twisted or thread like mass called nucleoid. Bacterial cells are generally covered by two protective layers: an outer cell wall and an inner membrane and certain bacteria even possess a third layer called capsule. They can be classified according on the basis of nature of cell wall, genetic makeup and their shape. The gram

stain is a test used to identify the bacteria by their morphology and differential staining properties. It was named after Hans Christian's gram, who developed this technique in 1884. In this technique slides are frequently stains with crystal violet, iodine then detained with alcohol and then by safranin. Gram-positive bacteria stain is blue-purple and gram-negative bacteria stain is red. The major difference between these groups is that, gram-positive bacteria contain cell wall. That is iodine and crystal violet precipitate in the thickened cell wall and are not eluted by alcohol whereas in gram negatives crystal violet are readily eluted.

Gram positive Bacteria

In gram-positive bacteria the single prokaryotic cell membrane is surrounded by a thick peptidoglycan layer. e.g. *Staphylococcus aureus, Bacillus subtilis* etc;

❖ ***Staphylococcus aureus***

Fig. 2.1: Micrograph of *S. aureus*

Staphylococcus aureus (S. aureus) is an important zoonotic bacteria. *S. aureus* is gram-positive opportunistic pathogen which belongs to Firmicutes family (Fig. 2.1). Scottish surgeons Alexander Ogston discovered this in 1880. They are mainly seen on the skin and upper respiratory tract. *S. aureus* is a facultative anaerobic seen as colonies. Golden appearance is the etymological root of bacterium's name: *aureus* convey golden in Latin. It coagulase and catalase positive. Golden coloured carotenoid pigment staphyloxanthina can be produced from some strains of *Staphylococcus aureus*. This pigment is a bacterial antioxidant, able to evade the reactive oxygen species which the host immune system uses to kill pathogens. Mutant strains of *S. aureus* modified with lack of staphyloxanthin are less likely to survive incubation with an oxidizing agent such as hydrogen peroxide than pigmented strains. When Mutant

colonies exposed to human neutrophils, they will quickly kill, but many of the pigmented colonies survive. Since it is an opportunistic pathogen, it cause skin infections like pimples, boils and scalded skin syndromes. They also make respiratory infections which leads to life threatening diseases like pneumonia, meningitis, toxic shock syndrome etc.

❖ ***Bacillus subtilis***

Bacillus subtilis is a spore forming, rod-shaped, motile, facultative, gram-positive aerobes (Fig. 2.2), also known to be *hay bacillus or grass bacillus* found in soil and gastrointestinal tract of ruminants and humans.

Fig. 2.2: Micrograph of *Bacillus subtilis*

It is a member of genus Bacillus. Their optimal growth temperature is about 25-35^{o}C. It lives in moist extreme conditions has endospore allowing it to live in extreme places. It was originally named as vibrio subtilis by Christian Gottfried Ehrenberg in 1935 and renamed as *Bacillus subtilis* by Ferdinand Cohn in1872. It is typically rod shaped and is 4-10μm long and 0.25-1mm with cell volume of about 4.6fl oz at stationary phase. It is an endospore forming bacteria that enable to withstand extreme temperatures as well as environment. It is not considered as pathogen or toxic disease causing agent. It contains flagellum which makes it move faster.

B. subtilis is capable of producing and secreting antibiotics. Five signal peptidase genes are present in this organism responsible for the secretion of antibiotics. They are capable of secreting subtilin, polymyxin, mycobacillin and difficidin. These antibiotics have the ability to increase the microorganism's chance of survival and kill competing microbes. Harsh environmental conditions can be tolerated by endospores of *B. subtilis*. It is considered an opportunistic pathogen. Because of their ability to produce antibiotics, they are used on vegetables plants and seeds. These strains are used by farmers to protect

their crops because of their ability to produce toxins for insects and inhibiting by competing with disease causing organisms. For all bacteria, it is used as a model organism and it is used in antibiotics for minor cuts and burns, used for desizing textiles and starching paper.

Gram-Negative Bacteria

In gram-negative bacteria, the single prokaryotic cell membrane is surrounded by a thin peptidoglycan layer that cannot retain the crystal violet stain in the Gram stain test. E.g. *Escherichia coli, Proteus vulgaris, Klebsiella pneumonia*

❖ ***Escherichia coli***

Escherichia coli is also known as *E. coli* is a gram-negative anaerobic, rod shaped coliform bacterium commonly found in lower intestine of warm blooded organism (Fig. 2.3). Most of the *E. Coli* are harmless but some serotypes cause serious food poisoning.

Fig. 2.3: Micrograph of *Escherichia coli*

It belongs to the *Enterobacteriaceae* family. *E.coli* is first found in human colon by Theodor Escherich, German bacteriologist in 1885. In olden days it was thought that *E .coli* cannot survive outside of the host, but recent studies show that the bacteria can even survive outside the host. The growth and survival of *E. coli* in natural environments can be influenced by both biotic and abiotic factors. Solar radiation, pH, water, nutrient availability and temperature are the abiotic factors. Biotic factors include the ability to acquire nutrients in the presence of other microorganisms and form biofilms in natural environments. Optimal temperature for the growth and survival of *E. coli* is from 15 to 45^0C. Nutrients such as carbon, nitrogen and phosphorus are also an important factor influencing survival and growth in the environment. Low pH is more preferred

environment for this bacteria. Sunlight can cause damage but its influence varies with environment. It is an important pathogenic, can cause variety of diseases resulting more than 2 million death per year. *E. coli* is classified according to the diseases caused by them: Asenterohaemmorrhagic *E. coli* (EHEC), Enteroinvasive *E. coli* (EIEC) and Uropathogenic *E. coli* (UPEC). Well studied intestinal pathotypes are Enteropathogenic *E. coli* (EPEC), Enteroaggregative *E. coli* (EAEC), Shiga toxin-producing *E. coli* (STEC), Enterotoxigenic *E. coli* (ETEC), Enteroinvasive *E. coli*, including Shigella strains and diffusely adherent *E. coli*. This classification was done based on virulence properties and pathogenicity mechanisms.

❖ ***Proteus vulgaris***

Proteus vulgaris is a gram-negative rod–shaped bacterium that inhabits the intestinal tracts of humans and animals (Fig. 2.4). It can be found in soil, water and faecal matter. It belongs to the family *Enterobacteria*. It was first identified and isolated from putrid meat by Hauser. Three types of organism were studied under this term. Currently, the genus Proteus consists of five named species (*P. hauseri, P. mirabilis, P. myxofaciens, P. penneri and P. vulgaris*). In animal and human small intestines, their presence can be found out. They can cause urinary tract infections under several conditions, which may lead to severe complications, such as pyelonephritis or stone formation. These bacteria can also cause severe infections like respiratory tract infections, wound infections and rheumatoid arthritis etc.

Fig. 2.4: Micrograph of *Proteus vulgaris*

❖ ***Klebsiella pneumonia***

Klebsiella pneumonia is a gram-negative rod shaped anaerobic bacteria (Fig. 2.5). It forms the part of gastrointestinal flora in humans. It may cause destructive changes to human and animal lungs.

Fig. 2.5: Micrograph of *Klebsiella pneumonia*

They have the capacity to acquire a versatile armament of antibiotic resistance genes and carry a variety of virulence genes. 30% of strain can fix nitrogen in anaerobic conditions. It was named after German microbiologist Edwin Klebs. It is also known to be *Friedlander's Bacillum* in honour of Carl Friedlander, who proposed that this bacterium is the etiological factor for pneumonia in people with chronic disease or alcoholics. It has large accessory genome of chromosomal genes and plasmids. *Klebsiella* species are found in nature, including in animals, humans and plants and this can cause deadly severe infections to some patients who are immune compromised or critically ill. Pneumonia, bloodstream infections and urinary tract infections can also be caused by these bacteria. It has wide application in producing a multitude of clinical infections resulting in morbidity and mortality. Interaction with the host lung environment during infection of *K. pneumonia* is known about its clinical significance.

Antibiotic is an agent that kills or inhibit the growth of bacteria. In 1928 Scottish bacteriologist Alexander Fleming noticed that colonies of bacteria growing on a culture plate unfavourably affected by a mold, penicillium notatum, which had contaminated the culture. A few years later British biochemist Ernst chain and others isolated penicillin and noticed that it can be used against bacterial infections. Sulphonamides, oxazolidinones etc. are some other natural compounds which form the building blocks of synthetic ones. Penicillin is a naturally occurring antibiotic agent which inhibits the

action of bacteria by forming cell wall and was used to treat skin, dental, ear infections. Its structure is depicted in Fig. 2.6.

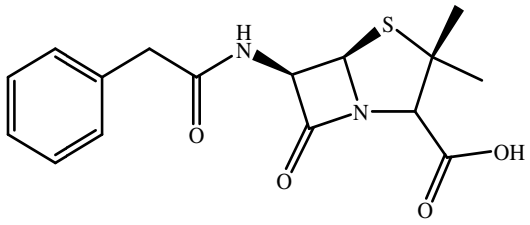

Fig. 2.6: Structure of Penicillin

In 1950's, researchers were discovered cephalosporin, which was much related to penicillin. It had an identical mechanism to that of penicillin as it interfere the synthesis of cell wall of bacteria. It is used to treat pneumonia, strep throats etc and the structure of cephalosporin is shown in Fig. 2.7. Substitution with different 'R' groups can yield different derivatives with low toxicity and high potency.

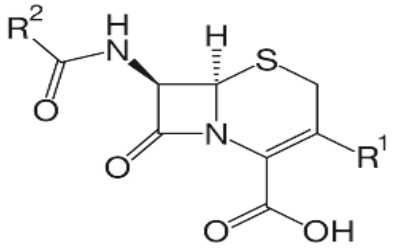

Fig. 2.7: Structure of Cephalosporin

Later discovered a new class namely quinolones, synthetic one which was chemically different from penicillin or cephalosporin. It can inhibit bacterial growth by interrupting DNA replication of bacteria and this paid light for the discovery of disease causing microbes and substances against them. Its structure is depicted in Fig. 2.8.

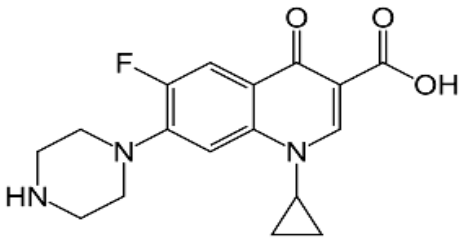

Fig. 2.8: Structure of Quinolones

Metal Complexes in Pharmacology

Antibacterial properties of metal complexes have been found long before, which paid a way to the medicinal field. The first laboratory antibacterial experiment was found by Koch through an investigation of activity of mercuric chloride on anthrax. The introduction of metalloid i.e., organ arsenical compound in 1912 by Salvarsan led for the treatment of Syphilis. Metal complexes can be used as drugs in biological systems. A significant interest on designing of metal complex as drugs and diagnostic agents were observed in the scientific era, which can be termed as medicinal chemistry.

Metal Chelates Containing Schiff Bases as Antibacterial Agents- A Review

Complexes of transition metal ions with various ligands have been exhibit antimicrobial activity against a spectrum of microbes. Among them, metal complexes of Schiff bases showed better antibacterial activity against various bacteria. The activity of metal chelates depends on steric, electronic, and pharmacokinetic factors. The mechanism of action depends on the interactive forces that bind the compound to the organism. These forces may vary from rigid covalent to weaker Van der Waal forces.

The chelating properties of Schiff bases are used to transport across membranes or to attach to specific site, thus it can hinder the growth of the organism. The antibacterial activity is based on the selective toxicity of agents on the microbial cells. The cellular structures of the bacteria or its function should influence the role of antibiotics. This includes inhibiting nucleic acid synthesis, inhibiting protein synthesis, inhibiting cell wall biosynthesis, inhibiting cell membrane etc;

Ligands in the metal complex play an important role in targeting specific tissues or enzymes or protect etc, on a metal complex. In transition metal complex, the azomethine group possess (C=N) bond is very important. In such complexes positive charge of the metal ion is partially shared among hetero atoms (S, N and O) present in

the Schiff base ligand. Due to the presence of lone pair of electron, delocalisation of π–electron over the whole chelating system will occur. This increases the lipophilic character of metal complexes favours its permeation through the lipid layer of the bacterial membrane and inhibiting metal binding sites in enzymes of that organism. Ligands containing sulphur, nitrogen and oxygen especially amide nitrogen, azomethane nitrogen, phenolic or alcoholic oxygen and carboxylate oxygen are some of the donor atoms predominantly employed in such cases. Schiff bases shown a variety of pharmacological properties such as antiviral, antibacterial, antitumor and that promises a better development in drug industry against the most dreadful disease to human lives. These pharmacological properties were studied and utilized for the drug development by researchers.

In 2008, P. Banerjee et.al. synthesized bis(cyclopentadienyl)titanium(IV) chloride with a series of Schiff bases (which were derived by the condensing 3-(phenyl/2-chlorophenyl/4-nitrophenyl)-4-amino-5-hydrazino-1,2,4-triazoles with salicylaldehyde) by both conventional stirring method and microwave assisted technology [6]. The yield of the product from conventional method was less as compared to microwave assisted one. The structure of complexes were examined on the basis of physico-chemical and spectroscopic methods. They were screened for antibacterial studies to assess the growth-inhibiting potential of the free Schiff bases and their complexes against various bacterial strains using paper disc plate method and found that the activity increases with chelation.

In 2008, Y. Prashanti, et al. synthesized metal complexes of Cu(II), Ni(II) and Co(II) with Schiff bases of 3-(2-hydroxy-3-hyoxybenzyllideneamiono)-5-methylisoxazole (HEBMI) and 3-(2-hydroxy-5-nitrobenzylideneamino)-5-methyl isoxazole (HNBMI) and were characterized on the basis of their elemental analysis,

magnetic moments, molar conductivity, thermal analysis and spectral (IR, UV-vis, NMR) studies etc; [7]. Antibacterial activities also were examined and found that activity increases upon co-ordination. The increased activity of metal chelates was explained on the basis of chelation theory.

In 2011, T. Rosu, et al. synthesised copper (II) complexes $CuLCl.H_2O$, $CuL(NO_3).2H_2O$, $(Cu(L)_2)CuL(SCN).H_2O$ and $(CuL)_2(SO_4).4H_2O$ where HL = 1-phenyl -2,3-dimethyl-4-methoxy-benzaldehyde-3-pyrazolin-5-one [8]. These complexes were characterized by NMR, UV-Vis, IR, ESR, elementary analysis and molar conductivity etc. The Cu (II) complexes were screened for *in vitro* antibacterial activity against *Klebsiella pneumonia*, *Staphylococcus aureus, Pseudomonas aeruginous* and *Escherichia Coli* and showed better activity than that of free ligand. Antibacterial activity was enhanced due to bonding of Cu(II) to two nitrogen atoms and two oxygen atoms in the Schiff base. They found that antimicrobial activity was dependent on the microbial species tested and anion used in metal salt.

In 2012, A. Jha, et.al. synthesized 2,5-disubstituted thiadiazole by both conventional and microwave irradiation methods and coupled with 2,4-pentanedione (AcAc) ethyl cyanoacetate (ECA) and malononitrile (MN) to get ligands and then complexed with Ni(II), Cu(II) and Ru(III) chlorides [9]. These complexes were screened with HL-60 leukaemia and U-937 lymphoma cell lines. Ruthenium complexes showed promising activity whereas Ni(II) and Cu(II) complexes showed moderate activity. On comparing their MIC values of ligand and complexes indicates that complexes exhibit higher activity than ligands. Ruthenium complexes are acted as better anticancer compounds comparing to other metal chelates

In 2014, L. Lekha, et al. synthesised various complexes of lanthanides as Pr(III), Sm(III), Tb(III), Er(III) and Yb(III) using sodium salt of Schiff base 2-(5- bromo-

2-hydroxy-benzlidene)-amino-3-hydroxyl-propionic acid [10]. They were characterized on the basis of NMR, UV-Vis, IR and elemental analysis. They were also screened for antibacterial study and showed better activity than free Schiff base.

In 2016, M. Salehi, et al. Synthesised certain complexes of nickel(II) with tridendate Schiff base ligand by the reaction of ligand salicylidene -2-aminophenol with $Ni(OAc)_2.4H_2O$. They were characterized on the basis of NMR, IR UV-Vis, elemental analysis etc [11]. They were also analyzed for antibacterial study and observed that higher activity than free ligand in both gram-positive and gram-negative bacteria.

In 2018, H. Keypour, et al. synthesized cadmium macrocyclic Schiff base complexes by the preparation of 2,2'-(piperazine-1,4-diylbis(methyllene)dianiline and 2,6-pyridine dicaraldehyde [12]. They were characterized on the basis of elemental analysis, mass spectroscopy and spectroscopic analysis as FT-IR, NMR etc., They were also analysed for antibacterial activity and found that the complex gives better activity than free ligand.

In 2019, N. Turan, et al. synthesised complexes of Ru(III), Co(II) and N(II) with Schiff base formed by the condensation of (E)-methyl-2-amino-6-methyl-4,5,6,7-tetra hydrotheino[2,3-c]pyridine-3-carboxylate] with 2-hydroxy-3-methyoxybenzaldehyde (o-vanillin) [13]. These were characterized by elemental analysis, magnetic susceptibility, mass spectra, UV–Vis, IR etc. They were also analysed for antibacterial activity against both gram-positive and negative bacteria and found higher activity than free ligand

In 2020, Y. Xu, et al. introduced cellulose fibres into the Schiff base and found that good antibacterial activity [14]. On complexing, this Schiff base to copper(II) showed enhanced activity than free ligand against *E. coli* and *S. aureus*.

Sulphur Containing Schiff Base Complexes as Antibacterial agent – A Review

In 2002, A. Mishra, et al. synthesized complexes of Cu(II), Ni(II), Co(II) with Schiff bases salicylidene-2-aminophenol, furfurylidene-n-phenylthiourea and salicylidene and examined them with help of microanalytical data like UV-Vis, IR, ESR spectroscopy, TGA, conductance, and magnetic susceptibility measurements etc; [15]. Non-isothermal kinetic and ligand field parameters of some complexes were measured. These complexes were checked for their antibacterial activity against *Salmonella typhi, Escheria coli* and *Bascillus subtilis* using filter paper disc method. Cu(II) complexes showed higher activity than Co(II) and Ni(II) complexes. These metal complexes were more reactive than ligands

In 2003, Z.H. Chohan, et al. synthesized Zn(II) containing metal chelates with a series of Schiff bases which were derived from the reaction of 2-acetamidobenzaldehyde with 2-amino-6-methylsufonylbenzothiazole. These complexes were characterized by physical, spectral and analytical data [16]. The Schiff bases and Zn(II) complexes were evaluated for their antibacterial properties against the strains *E. coli, S.aureus* and *P. aeruginosa* and found that anions do affect the antibacterial activity of the chelate complex.

In 2005, A. Srivastava, et al. synthesized metal complexes of bis (cyclopentadienyl) titanium(IV) dichloride with Schiff bases derived from the reaction of 2-amino-5-phenyl-1,3,4-thiadiazole (SPT), 4-nitrobenzaldehyde (SNT), 4-methoxy benzaldehyde (SMT), 2-hydroxyacetophenone (SATH) [17]. These were characterized on the basis of elemental analysis, electrical conductance, magnetic susceptibility and spectral studies. They were also screened against gram-positive *B.subtilis* and gram-negative *E.coli* bacteria using paper disk plate method at 1000ppm concentration and found that complexes were slightly more toxic than parent ligands.

In 2006, Harlal Singh, et al. synthesized a series of organotin (IV) complexes with bidendate Schiff bases having nitrogen and sulphur donor sequences (prepared by condensation of S-benzyldithiocarbazate with heterocyclic aldehyde) [18]. They were characterized on the basis of elemental analysis, conductance measurements and spectral studies. They were also screened for antibacterial activity using paper disc method and found that organo tin complexes are more active than free ligands which imply metalation increases antimicrobial activity. The increase in activity of the above complexes is attributed to the chelate formation i.e. ligands coordinated to central tin atom through thioketonic sulphur and azomethine.

In 2006, G. G. Mohamed, et al. synthesized Cu(II), Fe(II) and Ni(II) complexes of Schiff bases derived from 2-furanacarboxaladehyde and o-phenylenedamine and 2-thiophenecarboxaldehyde and 2-aminothiophenol and characterized them on the basis of elemental analyses, IR, ^{1}H-NMR, solid reflectance, magnetic moment, molar conductance and thermal analysis [19]. They were screened for antibacterial activity against bacterial strains as *E. coli*, *P. aeruginosa* and *S. pyogones* and a fungi (candida) using diffusion agar technique. Activity data showed that metal complex are potent antibacterial than parent Schiff bases.

In 2008, K. S. A. Melha synthesized complexes of Cu(II), Ni(II), Co(II), Mn(II), Fe(II), Cr(III) with N_4-(7′-chloroquinoline-4′-ylamino)-N_1(2-hydroxyl-benzylidene)thio semicarbazone (HL) (prepared by the reaction of ortho-N_4-(7′-chloroquinolin-4′-yl amino)thiosemicarbazide with 2-hydroxybenzaldehyde [20]. They were characterized by elemental analysis, spectral studies, magnetic susceptibility, molar conductivity, thermal analysis etc. They were also screened against gram-positive and gram-negative bacteria and found that chelation metal complex become more active than parent ligand.

In 2013, M. Alias, et al. synthesised metal complex of Cd(II), Mn(II), Fe(II) derived from potassium 2-carbomethoxy amino-5-trithiocarbonate 1,3,4-thiadiazole (CATT) and potassium 2-N(4-N,N-dimethylaminobenzylidene)-4-trithiocarbonate-1,3,4-thiadiazole (DBTT) [21]. They were characterized on the basis of flame atomic absorption, elemental analysis, spectral studies, thermal analysis, and magnetic susceptibility measurements. They were also screened for antibacterial activity against *P. aeruginosa* (gram -negative strain*), S. aureus* (gram- positive) in nutrient agar media and compared with standard drug ampicillin. On comparison found that complexes have higher antibacterial activity than parent ligands. At 5mM concentration, Cd(II)-DBTT complexes have higher inhibition zone than $Cd(CATT)_2$ against *S. aureus* and $Mn(CATT)_2$ complex showed better activity at 5mM concentration against *P.aeruginaous*. The higher inhibition zone of complex than ligand was due to chelation effect.

In 2013, B. K. Rai, et al. synthesized complexes of metals Cu(II), Ni(II) Co(II) with Schiff base ligand (3-amino-2-ethylquinazolinethiosemicarbazone (AEQT) [22]. They were characterized by molar mass, elemental analysis, spectral studies, magnetic susceptibility, molar conductance and thermal analysis. They were also screened for antibacterial effect by disc diffusion method against *Staphylococcus aureus and E.coli.* All the complexes were active against gram positive bacteria and less active against *E.coli* which is gram-negative. All complexes were more active than Schiff base.

In 2014, M. K. Sahaani, et al. synthesized oxovanadium (IV) complexes with Schiff bases derived from the reaction of 5-(phenyl/substituted phenyl)-2-hydrazino-1,3,4-thiadiazoles and indoline-2,3-dione in ethanol in the presence of sodium acetate. They were characterized on the basis on micro-analytical data, magnetic susceptibility, spectral studies, and predicted structure [23]. They screened the antibacterial activity of

complexes against gram-negative bacteria (*E. coli, S. typhi*) and gram-positive (*S. aureus, B. subtils*) bacterial strains and found that oxovanadium (IV) complexes have higher antibacterial effect than free ligands on the comparison with standard drug gentamycin. All the ligands and oxovanadium (IV) complex possessed varying inhibition effect as low (33%), moderate (53%), significant (above 53%).

In 2017, D. Bandyopadhyay, et al. prepared three cobalt(III) complexes using ligands N,N'-propane-1,3-diylbis[1-(pyrrol-2-yl)methaanimine, 1-[(thiophene-2-yl methylidene) amino]propan-2-amine and 1-[(3-methylthiophen-2-ylmethylidene)amino] propan-2-amine [24]. They were characterized by microanalytical, spectroscopic, single –diffraction X-ray diffraction and physicochemical studies. They were also screened for antibacterial activity against gram-positive and gram-negative bacteria.

Mechanism of Action of Antibiotics in Microbial Cell

The mechanism of action is a biochemical way in which drug is pharmacologically effective. Antibiotic or drug binds to specific target site like enzyme. Antibacterial action can be categorised as variety of mechanism, which involves the disruption of cell membrane structure.

- Inhibits an enzyme
- Interferes with cell membrane permeability
- Interferes with cell wall synthesis
- Interfere with DNA synthesis
- Interfere with protein synthesis

Bacterial cell wall is formed by partial assembly of wall components inside cell followed by transport of structures through cell membrane to the growing cell wall and finally cross linking of the strands of wall material. Antimicrobial agent or antibiotic inhibit the synthesis of cell wall have specific effect on one or another phase. This results

in alteration in cell wall and shape of the organism and eventually causes death of bacterium. These pathogens gains resistance against certain drugs and the reason can be explained in two different ways (i) Non genetic pathway: which arises due to the loss or alteration of specific receptors like cell wall (ii) Genetic reason: which results by the mutation of bacterial cell? In 2001, Fluit, et al. was effectively investigated the mechanism of bacterium achieves resistance to drug (Fig 2.9) [25].

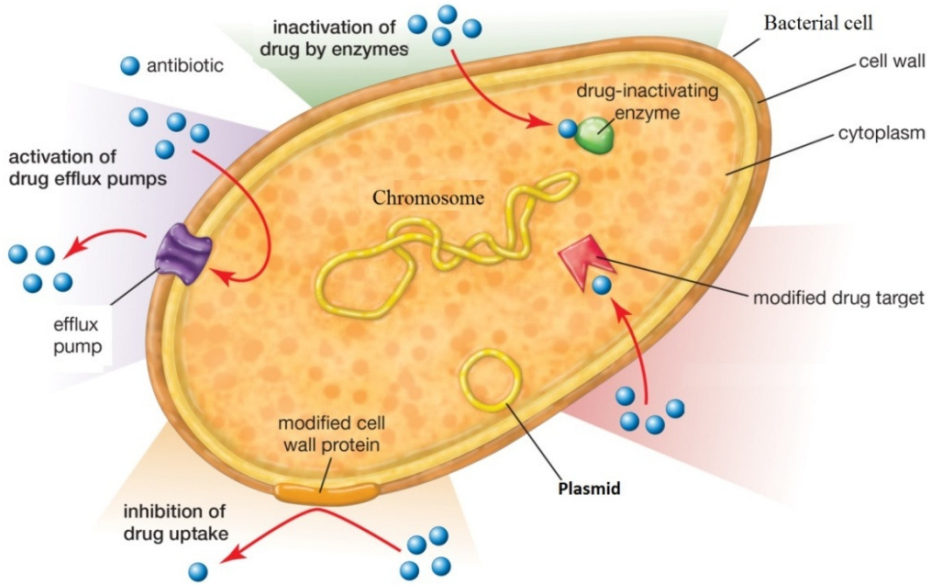

Fig. 2.9: Mechanism of antibiotic (drugs) resistance

Molecular Docking Aided Drug Discovery (*In Silico* Studies)

Computer-based drug discovery is the most appreciable method in the field of pharmaceutics. More efficient approach in drug discovery is examining the effectiveness of the drug for a specific disease by studying the type of interactions between the target protein and the drug at its molecular level. Essentially, the aim of molecular docking is to aid us in the prediction of the ligand-protein intermolecular framework or protein-protein binding complex formed and thereby suggesting the binding modes which are

responsible for inhibition of particular target proteins. Proteins associated with specific diseases are identified by understanding the mechanistic aspects of causing diseases.

Docking can be achieved mainly through two interrelated steps: (i) Sampling conformations of the ligand molecule into the active position of the protein (sampling algorithm); then (ii) Ranking these conformations by a scoring function. Preferably sampling algorithms should be able to reproduce the experimental binding mode and the scoring function should also rank it highest among all generated conformations [26].

Sampling algorithm

There are number of modes of binding between two molecules that may result in productive conformations. Different types of algorithms were developed which is based on the degree of freedom and one of the simplest algorithms introduced, in which molecules were treated as two rigid bodies thus reduces the degree of freedom to just six (three translational and three rotational). Based on this algorithm, various programs were developed to find the molecules that have a greater extent of similarity in shape with the binding site. This algorithm is based on pairing rule and it says that ligand sphere and protein sphere are paired only if their internal distances are matching by permitting some user specified acceptance. Thus, program recognises geometrically similar spheres on the protein site and the ligand.

The other type of algorithm is introduced for the ligand which is not a rigid molecule but fragmented from rotatable bonds into segments. Primary anchoring occurs between the segments to the protein receptors followed by each segment anchors in step by step with the receptor. Those fragments have the greater tendency for hydrogen bonding interaction with the receptor binding site will anchors first. Hydrogen bonding leads to more accuracy in prediction of geometry [27].

Scoring function

Scoring function has three applications involved in molecular docking. The first application involved is determining the binding mode and binding site of the ligand with protein. A specific protein target probably generates number of binding modes of ligand binding with protein active site with different orientations. Scoring function is also aided to rank these ligand-protein binding mode orientations by weighing the tightness of binding of the putative complexes. The second application of a scoring function involved in docking is that absolute binding affinity between protein-ligand complexes. A scoring function increases the optimization efficiency by computationally predicting the binding affinities between the protein and ligands. The third application is to identify the potential drug for a particular protein target in structure-based drug design by virtual database screening. The scoring function ranks the known binders in accordance with the binding scores [28].

For the thorough understanding of the structural principles that determine the strength of a protein-ligand complex, an accurate and fast docking protocol and the ability to visualize binding geometries and interactions are mandatory. And additional interactions and bond length present between the ligand–receptor complex can be obtained through Discovery studio 2016 software. Through molecular docking, we had presented the interface between the popular molecular graphics system PyMOL and the molecular docking suites AutodockVina and demonstrate how the combination of docking and visualization can aid structure-based drug design efforts.

Our work based on molecular docking studies mainly focuses the computational evaluation of the drug ability of the newly synthesized 'S' containing Schiff bases on the target proteins COVID-19 main protease (M^{pro}), HER2 protease, HIV-1 protease and human acetylcholinesterase (AChE) [29–31] and the molecules were ranked on the

binding score with these target proteins. The drug likeness and toxicity parameters of the molecules were checked using Lipinski rule.

Molecular Docking – A Review

In 1864, Emil Fischer was the pioneer of docking studies and proposed a 'lock-key' model of binding which interpret enzyme specificity; the ligand rigidly recognizes and occupies the binding site. This model could not explain the enzyme in competitive inhibition and this model was modified by Koshland and introduced a new model 'induced fit' in 1958. According to this model, the ligand is able to induce the conformational changes of the protein and it enhance the ligand-target interactions. Later in 2000, new interaction model was established known as conformation selection. According to this type of interactions, the ligands stabilize the protein conformation with a consequent shift of the protein population equilibrium and hence ligand interacts with the protein. Later on the development and modifications carried out on molecular docking theories, accuracy in calculations on ligand-receptor interaction were enhanced. This expansion in docking has ensured the profound studies on drug designing [32].

Changsheng Gan and his co-workers had synthesised benzothiazole Schiff-bases and evaluated whether the compounds display potential imaging agents that target the beta-amyloid (Ab) plaques in Alzheimer's disease (AD). When *in vitro* binding studies for ADhomogenate carried out by keeping a reference ligand 6-iodo-2-(4-dimethyl-amino)-phenyl-imidazo[1,2-a]pyridine ([125I]IMPY). It depends on the substitution on the phenyl ring; the compounds exhibited high to low binding affinities for AD homogenate at the K_i (Inhibitor constant) values ranged from 4.38 to 514.65nm. Fluorescent staining *in vitro* displayed that one compound with N,N-dimethylamino group penetratingly stained Ab plaques inside brain sections of post-mortem AD

patients. These studies infer that the derivatives having high binding affinity to amyloid plague in AD brain are potential agents for molecular imaging [33].

Recent research published by D. Wrapp, N. Wang and their crew worked on the viral protein of novel coronavirus and they were able to deposit a new structure of spike glycoprotein in perfusion conformation in protein database bank (6vsb) [34]. Based on this work, Shweta Choudhary, Yashpal S. Malik, Shailly Tomar had worked on *in silico* studies on drug repurposing for the S glycoprotein and ACE2 of 2019-nCoV.

In 2009, M. Lakshmana Doss and K. G. Lalithaa have synthesised thiazole derivatives of Schiff bases and they investigated the biological activities. The synthesised Schiff bases show prominent antimicrobial and antibacterial properties. This work mainly focuses on the molecular docking of the synthesised compounds against the target viral protein, HIV-1 protease (HIV-PR), which is an aspartic protease that is essential for the life-cycle of HIV, the retrovirus that causes AIDS. HIV PR's active site or inhibition of its activity disrupts HIV's ability to replicate and infect additional cells, making HIV-PR inhibition. This investigation established that the developed thiazole Schiff bases were the potential inhibitor of HIV-1 protease and that inactivate the retrovirus. This result enhances the chance of drug designing against the disease HIV/AIDS which is the most destructive disease to the humans. From this study, we gained an idea on developing Schiff's base based drug to inhibit the activity of the viral protein of the corona virus [35].

In 2014, Jayalakshmi Sridhar and her crew had worked on the HER2 protein inhibition studies by molecular docking studies. In their publication, their studies were based on identification of quinones that inhibit HER2 protein. HER2 overexpression is associated with aggressive breast cancer with high recurrence rate and poor patient prognosis. They also reported that the two quinone compounds show good inhibition

against the breast tumour cells expressing HER2. This work contributes to wide application in development of drugs against breast cancer. Similarly, researches are still progressing in drug development against different types of tumour growth diagnosed in human lives [36].

In 2019, Rabail Ujan and his co-workers had published their work on synthesis of novel potential inhibitors of Acetylcholinesterase causing Alzheimer's disease. In their work, a series of 5-amino-1,3,4-thiadiazole derivatives were synthesised and the likeness of the compounds were examined using Lipinski rule through ADMET software and these synthesised inhibitors were characterized and assessed for their acetylcholinesterase enzyme (AChE) inhibitory and free radical scavenging activities. The newly synthesized derivatives showed promising activities against AChE and the molecular docking studies further elucidated the non-covalent interactions between the ligands and the active site of the target protein. From their work, the newly synthesised thiadiazole derivatives exhibit good biological activities and binding affinity, suggesting a wide development in pharmaceutical applications against Alzheimer's disease [37].

Scope and Objectives of Present Investigation

Many Schiff bases have been checked for their chelating ability with different transition and inner transition metals. The quest for novel Schiff bases and their metal chelates are continuing in the present decades. Literature survey revealed that there is a wide scope still remains for the investigation of novel 'S' containing Schiff bases and its transition metal chelates. Since the polarizability of lone pairs on the sulphur atom is high, one can expect an escalated chance for the chelation and other related properties. It is very important to explore the biological activities of these 'S' containing Schiff base ligands and its metal chelates that have demonstrated high effectiveness with lesser toxicity.

To study the antibacterial performances of these studied Schiff base ligands and their transition metal complexes against five clinically important pathogens such as *Staphylococcus aureus, Bacillus subtilis, Escherichia coli, Proteus vulgaris, Klebsiella pneumonia* and to compare the data with that of standard antibiotics like Vancomycin, Erythromycin, Chloramphenicol, Streptomycin, Gentamicin, Ampicillin and Tetracycline were one of the important objective of current investigation.

Introduction of advanced computational molecular docking studies helps in probing the inhibitory competency of newly developed molecules on selectively identified target proteins. More efficient approach in drug discovery is examining the effectiveness of the drug for a specific disease by studying the type of interactions between the target protein and the drug at its molecular level. Currently, many researchers focus on discovering potential inhibitors of these target proteins which can exhibit lower side effects during drug therapy. Accordingly, the studies were extended to identify the potential inhibitors of novel coronavirus by utilizing the computational treatment for drug designing. Recent biological studies provided an extensive feature of M^{pro} protease or main protease of novel coronavirus as a potential drug target for precise treatment for COVID- 19. There are number of FDA approved drugs which are clinically tested and show high inhibition on HIV-1 protease (causing HIV/AIDS), HER2 protease (responsible for Breast cancer), and human acetylcholinesterase (causing Alzheimer's disease) respectively. Currently, many researches focus on discovering potential inhibitors of these target proteins which can exhibit lower side effects during drug therapy. Much attention was given on newly synthesized' S' containing Schiff bases docked into the active binding cavity of these main proteases leading to corresponding diseases. Checking the drug likeness (bioavailability) of these ligands using Lipinski rule of five is the another objective of the present investigation.

CHAPTER 7

MATERIALS AND METHODS

In present work, newly synthesized seven novel sulphur containing Schiff bases, (E)-(N-anthracene-9-ylmethylene)-5-(4-nitrophenyl)-1,3,4-thiadiazol-2-amine (A9CNPTDA), (E)-5-(4-nitrophenyl)-N-((pyridine-2-yl)methylene)-1,3,4-thiadiazol-2-amine (P2CNPTDA), (E)-5-(4-nitrophenyl)-N-(1(pyridine-3-yl)ethylidene)-1,3,4-thiadia zol-2-amine (3APNPTDA), (E)-5-(4-nitrophenyl)-N-(1(pyridin-2-yl)ethylidene)-1,3,4-thiadiazol-2-amine (2APNPTDA), N-(anthracen-9(10H)-ylidene)-5-(4-nitrophenyl)-1,3,4 -thiadiazol-2-amine (ANNPTDA), N-((1H-indol-3-yl)methylene)thiazol-2-amine (I3A2AT) and (13E)-N1,N2-bis((thiophene-2-yl)methylene)cyclohexane-1,2-diamine (T2CDACH) were subjected to the evaluation of Lipinski's rule of five in order to verify the druglikeness followed by structure based molecular docking studies.

These newly synthesized 'S' containing ligands and their transition metal complexes were subjected to antibacterial studies clinically important pathogens such as *Staphylococcus aureus, Bacillus subtilis, Escherichia coli, Proteus vulgaris* and *Klebsiella pneumonia.* The results obtained for Schiff base ligands and their transition metal complexes were compared with the antibacterial data obtained for standard antibiotics Vancomycin, Chloramphenicol, Gentamicin, Tetracycline. For this purpose, disk diffusion method was used. For preparing the medium, Mueller- Hinton agar was used.

For the thorough understanding of the structural principles that determine the strength of a protein-ligand complex, an accurate and fast docking protocol and the ability to visualize binding geometries and interactions are mandatory. Additional interactions and bond length present between the ligand–receptor complex can be

obtained through Discovery studio 2016 software. Through molecular docking, the interface between the popular molecular graphics system PyMOL and the molecular docking suites AutodockVina were well explained and demonstrated how the combination of docking and visualization can aid structure-based drug design efforts

The method employed for *in vitro* antibacterial studies and *in silico* molecular docking studies are discussed in detail in this chapter.

In Vitro Antibacterial Studies

Disk diffusion method

This method is used to detect the efficient antibiotics that can eliminate pathogens. This method is also called Kirby–Bauer test or agar diffusion test [38]. In this method, the first step is to prepare an agar plate and then the bacteria are spread on it [39]. Then discs containing sample is added and incubated at 37^0C for 24h. There will be zone of inhibition if the sample is effective against the bacteria. This is the region around the bacteria where there is no bacterial growth. Actual studies involve the comparison of the diameter of these zones with standard antibiotic.

Mueller-Hinton agar (MHA) plate preparation

Beef extract-300g, Casein acid hydrolysate-17.5g, Starch-1.5g, agar-17g, pH -7.3, Distilled water-1000ml were the ingredients used in this step. All these were dissolved in distilled water and autoclaved at 121^0C for 15min after closing it with sterilized cotton. It is cooled for half an hour and poured into a sterilized petri dish (diameter-90mm and depth-4mm) and placed in laminar flow hood chamber. Examined each set of plates for sterility by incubating at 30-35^0C for 24h after allowing it to solidify.

Nutrient broth for inoculum preparation

The ingredients used were Beef extract-3g, Agar-20g, Peptone -5g, NaCl-5g, pH-

7.4, Yeast extract-3g, by heating it all were dissolved in distilled water-1000ml. Take 5-7ml of the medium in separate test tubes. The test tubes were closed using cotton wool and autoclaved for 15min at 121℃.

Inoculum preparation

For this, growth method is used. Four to six isolated bacterial colonies having similar morphology was selected from an agar plate culture, and then the growth is transferred to a tube consisting of nutrient broth (5ml) at 35^0C until it gains the turbidity of 0.5 Mc Farland standards and incubation of the broth culture was done. Usually it will take 2-6h to produce turbidity.

Disc preparation

To prepare the stock solutions, newly synthesized ligands, its transition metal complexes and standard antibiotics were dissolved in DMSO. Then it is diluted to various ranges of concentrations from 100-500µgdisc^{-1}. Using a micropipette samples were inoculated to the discs. Disc containing DMSO (control) was also tested. Discs are then incubated at 37^0C for 24 h after placing it in a petridish.

Test plate inoculation

Inoculated the plate by dipping a sterile cotton swab into the inoculums. Removed the excess inoculum by pressing and rotating the swabs firmly against the side of the tube above the level of the liquid. Streaked the swab all over the surface of the medium 3 times by rotating the Mueller-Hinton agar plate through an angle of 60^0C after each application. Finally passed the swab round the edge of the agar surface then dried for 20 minutes.

Allocation of disc containing samples on inoculated agar plates

The antibiotic discs placed on the inoculated plates using a pair of sterile forceps, sterile needle tip or an antibiotic disc dispenser. Each disc gently pressed down to ensure

even contact with the medium. The plate is placed in an incubator at 35^0C within 30 min of the preparation for 24h. After overnight incubation, the diameter of each zone (including the diameter of the disc) is measured and recorded in mm. The results were then interpreted according to the critical diameters by comparing them with standard tables. Pictorial representation of Disc diffusion method is shown in Fig. 2.10.

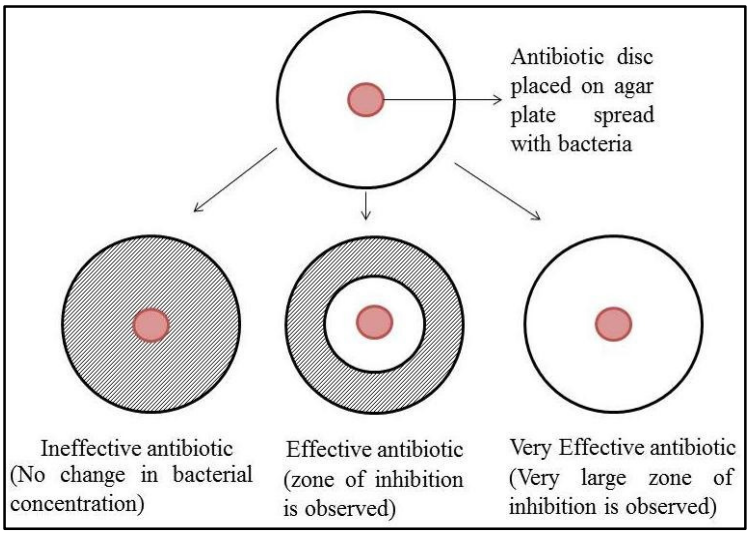

Fig. 2.10: Pictorial representation of Disc diffusion method

***In Silico* Molecular Docking Studies**

Lipinski's rule of five

In 1997, Christopher A. Lipinski pointed out that, drugs normally exhibits physicochemical and structural properties in definite ranges. The Lipinski rule-of-five concept aids in designing orally active compounds. Later this rule of five was also known as Lipinski rule of five or Pfizer's rule of five. This rule aims to compare the drug like compound describing whether the compound is orally active or not to humans. There are five certain rules that must be satisfied by drug like compounds

(i) Compound must have molecular mass less than 500 Dalton

(ii) Molecule must have high lipophilicity

(iii) Molar refractivity between 40 and 130

(iv) Number of H-bond donors must be less than five

(v) Number of hydrogen bond acceptors must be less than 10

Softwares Used in Molecular Docking

- ***Open Babel GUI 2.4.1***

It is an open source chemical tool that includes many different chemical data language. OpenBabel is a specific tool used for interconversion of 110 formats. In addition, it provides a variety of useful utilities from conformer searching, 2D depiction, filtering, batch conversion, and substructure and similarity searching. The need to represent such a wide variety of chemical and molecular data requires a library that implements a wide range of cheminformatics algorithms, from partial charge assignment and aromaticity detection, to bond order perception and canonicalization [40].

- ***PyMOL viewer1.7***

PyMOL is a graphic tool software which is used for the three dimensional visualisation of the proteins, nucleic acid, small molecules, electron densities, surfaces and trajectories [41].

- ***Autodock 4.2 software (MGL tools)***

Autodock tools are the graphical interface used to prepare input, run and analyse dockings generated from Autodock (adding atomic charges, fixing bonds, adding hydrogen, preparing the ligand and the target inconvenient PDBQT format compatible with Autodock, creating grids and docking parameter file and visualizing interactively docking results). AutoDock Tool (ADT) combines accuracy in determining the binding pose of a small-sized chemical in a corresponding receptor pocket and a free open source solution available to researchers interested in computational docking [42].

- ***AutoDock Vina***

Programme which is developed for improving the accuracy of the binding mode

predictions, judging by our tests on the training set used in AutoDock 4 development [43].

- ***Discovery studio software 2016***

This tool was also used to visualize the two dimensional and three-dimensional interaction of the ligand with the binding pocket of the receptor. The binding site coordinates of the receptor molecules were fixed using this software. It is suite software for simulating small molecules and macromolecular systems and which is suitable in providing scientific assistance for drug development. Additionally, this software provides pharmacophore modelling, structure based drug designing, QSAR, ADME, etc.

Steps Involved in Molecular Docking Approach

- ***Protein database***

The required proteins for the investigation were accessed from RCSB Protein Data Bank using the corresponding PDB code (https://www.rcsb.org/search)

- ***Target preparation***

The required target protein structures were accessed from RCSB server in PDB format by using corresponding PDB code (**6lu7, 1mui**, **3rcd**, **1b41**). The co-crystallised ligands and water molecules were removed using PyMOL software to avoid further complications and interactions in docking analysis. Additionally, the non-polar hydrogen bonds were added to the target protein structures. Finally, the AutoDock tools were utilized to convert the target protein from the PDB format to PDBQT format.

- ***Prediction of active site***

In molecular docking approach, Discovery studio 2016 was utilized to predict the active binding sites of target proteins. Binding site of the receptor cavity was analysed and the grid points and their x, y, z coordinate values were determined using Discovery studio.

- ***Ligand preparation***

In molecular docking approach, firstly structures of ligands were sketched in ChemSketch software in mol format. By using the OpenBabel software, the mol format were converted to PDB format. An AutoDock tool was used to convert the PDB format into required PDBQT format for molecular docking. Ligands, A9CNPTDA, ANNPTDA, 3APNPTDA, 2APNPTDA, P2CNPTDA, I3A2AT and T2CDACH were prepared for docking analysis.

- ***Docking***

AutoDock vina software was used for calculating the binding energy of the receptor- ligand interactions.

- ***Protein- ligand complex interaction visualization***

Docking of synthesised compounds with the prepared proteins and their interactions were visualised using the BioVia Discovery Studio 2016 software. Three dimensional visualisation of receptor-ligand interaction and the hydrogen bonds established between the ligand and aminoacid residues of active binding site were presented with the interaction distance. Two dimensional structure visualization facilitated to recognize the amino acid present in the receptor bound to the ligands. The protein-ligand interactions is stabilized by hydrogen bonding, hydrophobic and electrostatic interactions. The hydrophobic interactions involve pi-stacked, pi-alkyl, alkyl, pi-T shaped interactions and electrostatic interactions involve pi-cation and pi-anion interactions.

In the present work, four different target proteins accessed from RCSB Protein Data Bank using the corresponding PDB codes (**6lu7, 1mui**, **3rcd**, **1b41**) were selected for the docking studies. Additionally, PyMOL viewer 1.7 was used for preparing protein for docking and Open babel GUI 2.4.1 was used to convert the ligand to required PDB format.

Covid 19-SARS-CoV-2- Main Protease

The COVID-19 main protease (M^{pro}) consists of 306 amino acid residues. In previous studies, it was observed that the N_3 inhibitor complexed with main protease is the potential irreversible inhibitor of the M^{pro} of n-CoVs with perfect covalent bonding interactions and which is suggested as the most prominent antiviral target for the drug discovery against COVID-19. The structure of viral protein sequences of 2019 n-CoVs were accessed from the protein database bank (PDB). The recent publications had suggested the crystal structure of the M^{pro} complexed with the N_3 inhibitor with a resolution of $2.16A^0$ by X-ray method and this structure can be accessed using the PDB code **6lu7** [44]**.** The development of novel corona involves proteolytic processing actions on polyproteins to control viral gene expression and replication. Precursor polyproteins involve cleavage in maturing virus and which is mediated by the CoV main protease (M^{pro}), which is also named as the 3C-like protease. Hence CoV M^{pro} has become an attractive target for anti-CoV drug design, due to its role in the maturation of coronavirus and for key functional enzymes such as: replicase and helicase. The 3D structure of **6lu7** receptor and the crystallographic features are provided in Fig. 2.11 (a) and Table 2.1 respectively.

HIV/AIDS - HIV-1 Protease

HIV-1 protease is the enzyme that plays a significant role in the viral entry, DNA replications and generations of the new infectious virions. For the docking studies, selected the crystal structure of HIV-1 protease, complexed with Lopinavir (PDB code: **1mui**) which was accessed from the protein database bank [35]. Based on the earlier studies on the HIV infections, researchers keenly focus on the envelope proteins of the virus for anti-viral drug development. These envelope glycoproteins initiate the attachment of host CD4 cells or white blood cells that play major role in protecting the

human cell from infections. Envelope protein contains two non-covalently associated subunits gp120 and gp41 which are generated by proteolytic cleavage of precursor polypeptide gp160. Gp120 helps in fusing with the host cell receptor. The receptor cells of the white blood cells provide chances for the viral entry. Fusion of the HIV virus with the host cell membrane and reverse transcription of HIV-RNA to HIV-DNA enhance the entry of HIV-DNA genetic material into the CD4 cell nucleus. After the entry into the nucleus of the cell, integrase enzyme released by the HIV leads helps in inserting HIV-DNA genetic material into the CD4 cell DNA. The replications leads to the generation of long proteins and assembling of new HIV proteins and HIV-DNA on the surface and new immature HIVs are formed and this process generates new virions. One of the essential enzyme for the DNA replication is known as HIV-I PR or HIV-I protease. The production of mature and infectious viral particles is depended on the proteolytic activity of the HIV-1 PR. Because of this activity, HIV–I protease is the best anti-viral target. And for the docking studies, the crystal structure of HIV-1 protease complexed with Lopinavir (PDB co**: 1mui)** is selected [45]. The 3D structure of **1mui** is given in Fig. 2.11 (b) and the crystallographic data is presented in Table 2.1. A potential inhibitor inhibits the activity of HIV- I protease thereby leading to immature and infectious viral particles.

Breast Cancer - HER2 Protease

HER2 protease considered as the target protein due to its gene overexpression which leads to deadly tumour cell growth and breast cancer. X-ray crystal structure of HER2 Kinase complexed with TAK-285 was obtained from protein database bank (PDB code: **3rcd**) with a resolution of 3.21 Å (Ishikawa et al., 2011) [26]. Fig. 2.11 (c) depicts the 3D structure of **3rcd** receptor: The crystallographic data of the receptor is given in Table 2.1. There are several factors that enhance the tumour growth and human

epidermal growth factor receptor (HER2) plays important role in pathogenesis of several human cancers. They regulate cell growth, cell differentiation, cell survival, cell proliferations and in signal transduction pathways. This family consist of four members such as HER1, HER2, HER3, and HER4. All four HER receptors comprise a cysteine-rich extracellular ligand-binding site, a transmembrane lipophilic segment, and an intracellular domain with tyrosine kinase catalytic activity. HER2 up regulates the uncontrollable cell growth and tumorigenesis and it is mostly discussed throughout this work and it is the best target protein for therapeutic approach. The neu oncogene or HER2 was discovered by a group of scientists at Massachusetts Institute of Technology, Rockefeller, and Harvard University. The HER2 receptor is a 1255 amino acid, 185-kD transmembrane glycoprotein located at the long arm of human chromosome. Anti-HER2 drugs blocks the extracellular ligand binding region of the receptor, thereby interfering with its activation and hence inhibits the tumour cell growth [46,47]

Alzheimer's Disease- AChE Enzyme

Acetylcholinesterase (AChE) is the suitable target to inhibit the breakdown of the neurotransmitter and resultant damage of memory and cognitive functions. X-ray crystallographic structure of human acetylcholinesterase complexed with fasciculin-II glycosylated with a resolution $2.76A^0$ is obtained from protein data bank (PDB code: **1b41**) (Kryger et al., 2000). 3D structures of this protein was accessed from the RCSB protein databank in pdb format and is given in Fig. 2.11 (d) and their crystallographic features are illustrated in Table 2.1. Alzheimer's is clinically explained by neuronal decreases linked to deficient synthesis of acetylcholine (ACh) involved in memory, learning, and SNA (Suspected non-Alzheimer's disease). Acetylcholine is an organic substance transfer of neuronal signals to brain. Its hydrolysis into a cholineacetyl group is catalysed by the acetylcholinesterase which plays an important role in central nervous

system. In Alzheimer's patients, the activity of the acetylcholinesterase increases and leads to the augmented breakdown of the neurotransmitter acetylcholine and causes the decline in the acetylcholine level in the brain. AChE over-expression and extracellular accumulation of "mysterious" β-amyloid plaques are the trademark of this disease. AChE promotes the aggregation of β amyloid peptide, protein which is toxic to nerve cells, which is the major cause of the disease and these β-amyloid peptide fragments by forming a complex with the growing fibrils which can damage the neurons. These complexes have been shown to be more cytotoxic than β amyloid fibrils alone. β-amyloid peptide production is initiated by the enzyme β-secretase, BACE1 and it involves in cleavage of the amyloid precursor protein (APP) and it is one of the drug target considered for the treatment of Alzheimer's disease [48].

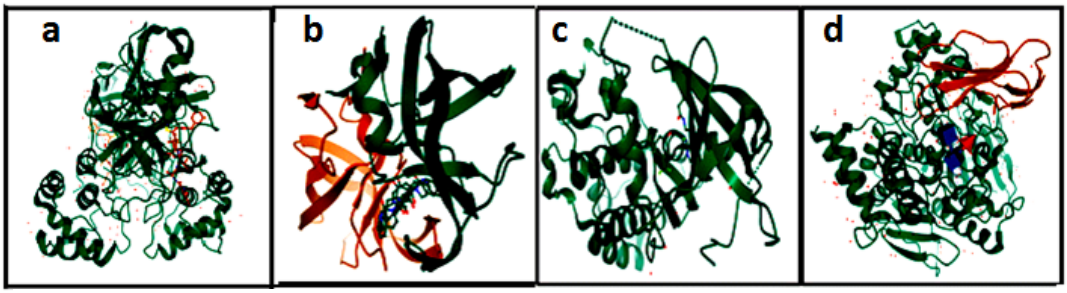

Fig. 2.11: Structures of target proteins **(a) 6lu7 (b) 1mui (c) 3rcd and (d) 1b41**

Table 2.1: Crystallographic features of proteins by X-ray diffraction

Proteins	PDB Code	Classification	Organism	Expression system	Resolution	DA	Chain
SARS-CoV-2 main protease in complex with an inhibitor N_3	**6lu7**	Viral protein	SARS CoV-II	Escherichia coli BL21(DE3)	2.16 Å	34506.34	A
HIV-1 protease complexed with Lopinavir	**1mui**	Hydrolase	HIV-1	Escherichia coli	2.80 Å	22240	A, B
HER2 Kinase complexed with TAK-285	**3rcd**	Transferase/ Transferase inhibitor	Homo sapiens	Spodoptera frugiperda	3.21 Å	154010	A,B,C,D
AChEcomplexed with fasciculin-II	**1b41**	Hydrolase/toxin	Homo sapiens	Dendroaspis angusticeps	2.76 Å	66660	A

CHAPTER 8

IN VITRO ANTIBACTERIAL STUDIES ON SULPHUR CONTAINING SCHIFF BASES AND THEIR METAL COMPLEXES

The inhibitory power of seven novel 'S' containing Schiff base ligands, A9CNPTDA, P2CNPTDA, 3APNPTDA, 2APNPTDA, ANNPTDA, I3A2AT, T2CDACH and their metal complexes with transition elements were established by antibacterial studies against two gram-positive strains *Staphylococcus aureus*, *Bacillus subtilis* and three gram-negative bacterial strains *Klebsiella pneumonia*, *Escherichia coli, Proteus vulgaris,* using disc diffusion method. DMSO was the solvent used for preparing solutions having different concentrations 50µgdisc^{-1}, 200µgdisc^{-1} and 500µgdisc^{-1}. The antibacterial performances of these Schiff bases and their transition metal chelates compared with the inhibition efficiency of standard antibiotics. The standard antibiotics used for the screening studies are Vancomycin, Erythromycin, Chloramphenicol, Streptomycin, Tetracycline, Ampicillin, Gentamicin etc. The results of zone of inhibition (mm) of antibiotics recorded after 24h against each bacterial strains at different concentrations are tabulated in Table 2.2. Antibacterial activity of these seven 'S' containing Schiff base ligands against gram-positive strains *Staphylococcus aureus*, *Bacillus subtilis* and gram-negative bacterial strains *Escherichia coli, Proteus vulgaris, Klebsiella pneumonia* at a concentration 200µgdisc^{-1} are showed in Fig. 2.12 and Fig. 2.13 respectively.

In vitro Antibacterial Studies of A9CNPTDA and its Transition Metal Chelates

The 'S' containing polynuclear Schiff base A9CNPTDA and its transition metal chelates were screened for *in vitro* antibacterial studies and the results are listed in Table 2.3. The ligand A9CNPTDA showed appreciable results against gram-positive

pathogen *Staphylococcus aureus* and gram-negative pathogens *Klebsiella pneumonia, Escherichia coli* and *Proteus vulgaris.* Results obtained for this ligand was comparable to the standard antibiotic Vancomycin. Transition metal chelates of A9CNPTDA exhibit significant antibacterial activities against all the studied microbes. Antibacterial activity of Cr^{3+}, Mn^{2+}, Cu^{2+}, Zn^{2+} complexes of A9CNPTDA against *Escherichia coli* and *Klebsiella pneumonia* at a concentration 50µgdisc^{-1}are represented in Fig. 2.14.

Mn(II) complex of this heterocyclic ligand was notably active against the growth of the *Klebsiella pneumonia* and this complex showed marked zone of inhibition of 17mm even at a concentration 50µgdisc^{-1} which was comparable to the growth preventing efficiency of standard antibiotics such as Vancomycin, Tetracycline, Chloramphenicol, Gentamicin, Ampicillin etc. Zn(II) and Cu(II) complexes displayed enhanced activity against the bacterial strain *Escherichia coli* and *Klebsiella pneumonia.* Cr(III) chelate displayed good inhibition efficiency on the growth against the pathogen *Staphylococcus aureus* which was comparable to the efficiency of standard antibiotics such as Vancomycin and Tetracycline. Fe(III), Ni(II) and Zr(IV) complexes exhibit considerable antibacterial performance against studied pathogens. Except few, almost all complexes of A9CNPTDA showed remarkable antibacterial performance against five antibacterial strains. *Staphylococcus aureus*, *Bacillus subtilis, Proteus vulgaris, Escherichia coli, Klebsiella pneumonia*. The increased activity of the complexes compared to ligands can be explained by Tweed's chelation theory and Overtone's concept of cell permeability. According to these theories, "On chelation, the polarity of metal ion will be reduced to a greater extent due to the overlap of ligand orbital and more number of donor atoms would influence the polarity of metal ion. Further, this would increase the delocalisation of π-electrons in the chelate ring and this will increase the

lipid solubility (lipophilicity) and it helps to the penetration of complex into lipid membrane and thus blocks the binding sites of the microbes and inhibits its growth".

***In vitro* Antibacterial Studies of P2CNPTDA and its Transition Metal Chelates**

Table 2.4 shows the antibacterial screening results of pyridine derivative P2CNPTDA and its metal chelates. They exhibit fair inhibition efficiency against the tested pathogens. P2CNPTDA showed enhanced antibacterial performance against gram-positive pathogen *Bacillus subtilis* and two gram-negative pathogens *Klebsiella pneumonia* and *Escherichia coli.* P2CNPTDA-Cd^{2+} complex showed superior antibacterial activity against *Staphylococcus aureus* and gram-negative pathogens *Klebsiella pneumonia* and *Escherichia coli.* This complex showed a marked zone of inhibition of 26mm at a concentration 500µgdisc^{-1} against *Staphylococcus aureus*, which was comparable and higher than the standard antibiotics such as Vancomycin, Erythromycin and Chloramphenicol, Tetracycline, Ampicillin, Gentamicin etc. Antibacterial activity of P2CNPTDA-Cd^{2+} at different concentrations against *S. aureus* is showed in Fig. 2.20. *Staphylococcus aureus* is a spherical and gram-positive bacterium that causes a broad range of acute diseases like endocarditis, osteomyelitis, toxic shock syndrome and pneumonia. Symptoms of toxic shock syndrome are sudden onset of high fever, diarrhoea, muscle aches and vomiting followed by hypotension etc. Antibacterial activity of Ni^{2+} and Cu^{2+} complexes of P2CNPTDA at 50µgdisc^{-1} concentration against *Staphylococcus aureus* and *Klebsiella pneumonia* are shown in Fig. 2.15. P2CNPTDA-Cu^{2+} complex showed notable activity against *Klebsiella pneumonia* (23mm). P2CNPTDA-Cd^{2+} and P2CNPTDA-Ni^{2+} displayed appreciable activity against this pathogen. *Klebsiella* is a gram-negative bacteria leads to acute disease states notably septicemia, pneumonia, biliary tract infection, soft tissue infections, liver abscess and infection of the lower and upper and respiratory tract etc. Infection by *E. coli* leads to

kidney failure and bloody diarrhoea. P2CNPTDA-Cd^{2+} and P2CNPTDA-Cu^{2+} exhibited fair antibacterial performance against the strain *Escherichia coli.*

***In vitro* Antibacterial Studies of 3APNPTDA and its Transition Metal Chelates**

The 3APNPTDA ligand displayed excellent antibacterial activity against the growth of bacterial strains *Escherichia coli, Staphylococcus aureus, Klebsiella pneumonia* and *Proteus vulgaris* etc. more than standard antibiotics like Vancomycin, Tetracycline and Ampicillin. Fig. 2.16 represents the antibacterial activity of Cr^{3+}, Mn^{2+}, Cu^{2+}, Zn^{2+} complexes of 3APNPTDA against *Staphylococcus aureus*, *Escherichia coli, Proteus vulgaris* and *Klebsiella pneumonia* at a concentration 50 $\mu g disc^{-1}$. At 500 $\mu g disc^{-1}$ the complex 3APNPTDA-Zn^{2+} displayed excellent antibacterial activity (27 mm) against *Klebsiella pneumonia* and appreciable activity against *Staphylococcus aureus (*20mm). 3APNPTDA-Cu^{2+}, 3APNPTDA-Ni^{2+} and 3APNPTDA-Mn^{2+} complexes displayed excellent antibacterial performances against *Staphylococcus aureus*, *Escherichia coli, Klebsiella pneumonia* and *Proteus vulgaris.* 3APNPTDA-Fe^{3+} and 3APNPTDA-Zr^{2+} exhibited considerable antibacterial activity against almost all studied microbes. These results are summarized in Table 2.5.

***In vitro* Antibacterial Studies of 2APNPTDA and its Transition Metal Chelates**

A comparative study on the account of the results of antibacterial efficiency against the selected microbes showed that the ligand 2APNPTDA and four of its transition metal chelates $Cu^{2+,}$ Mn^{2+}, Zn^{2+}, Zr^{2+} exhibit reasonable activity against *Escherichia coli*. 2APNPTDA-Ni^{2+} complexes displayed excellent antibacterial performances against *Bacillus subtilis*, *Staphylococcus aureus*, *Klebsiella pneumonia* and *Escherichia coli.* Transition metal complexes $Cu^{2+,}$ Mn^{2+}, Zn^{2+}, Zr^{2+} showed reasonable antibacterial activity against all pathogens (Fig. 2.17). The highest antibacterial action has been observed for 2APNPTDA-Zn^{2+} complex against *Klebsiella*

pneumonia (24mm). Co(II) complex of the 2APNPTDA didn't exhibit significant antibacterial inhibitory activity and this complex show low zone of inhibition. The results were reported in Table 2.6.

***In vitro* Antibacterial Studies of ANNPTDA and its Transition Metal Complexes**

The growth inhibition results of studied bacterial strains with polynuclear S' containing Schiff base ANNPTDA and its transition metal complexes are listed in Table 2.7. It is clear that from the data that the ligand ANNPTDA and its complexes inhibited the growth of antibacterial strains effectively. ANNPTDA displayed more activity towards *Bacillus subtilis* and *Klebsiella pneumonia*. ANNPTDA exhibited 15mm (maximum zone of inhibition) towards the gram-positive bacterial strain *Bacillus subtilis* at a concentration of 500µgdisc^{-1}. A zone of 23mm were exhibited by Mn(II) complex against the bacterial strain *Bacillus subtilis* and showed slightly higher activity (23.5mm) against *Klebsiella pneumonia* at a concentration of 500µgdisc^{-1}compared to other metal complexes. Ni(II) complex displayed maximum zone of inhibition value (19mm) towards *Staphylococcus aureus* and *Escherichia coli* at high concentration (500µgdisc^{-1}). ANNPTDA-Cr^{3+} complex showed notable activity against *Klebsiella pneumonia.* Cu(II) complex exhibited 21mm of zone of inhibition against *Klebsiella pneumonia*. Fig. 2.18 showed the antibacterial performances of Cr^{3+}, Mn^{2+}, Ni^{2+} of ANNPTDA against *Bacillus subtilis* at a concentration 50µgdisc^{-1}

***In vitro* Antibacterial Studies of I3A2AT and its Transition Metal Chelates**

Thiazole derivative of Schiff base ligand I3A2AT displayed antibacterial activity against the growth of *Klebsiella pneumonia, Escherichia coli* and *Proteus vulgaris* and observed as inactive against other bacterial strains. The Cu(II) complex showed the highest activity against *Staphylococcus aureus* and *Escherichia coli.* The Cr(III) complex was slightly active against *Bacillus subtilis,* whereas the Zn(II) complex displayed a

maximum zone of inhibition against *Klebsiella pneumonia* and *Proteus vulgaris.* Cr(III), Mn(II), Ni(II) and Cu(II) complexes were moderately active against *Klebsiella pneumonia.* All metal complexes had higher antibacterial activity than the ligand 13A2AT against all studied bacterial strains. The detailed report of zone of inhibition data of I3A2AT and their transition metal chelates are tabulated in Table 2.8.

***In vitro* Antibacterial Studies of T2CDACH and its Transition Metal Chelates**

Thiophene derivative of Schiff base ligand T2CDACH and its transition metal complexes established abilities to hinder growth of bacteria. The ligand T2CDACH have high zone of inhibition against the bacterial strain *Proteus vulgaris* and inactive against *Klebsiella pneumonia.* Research has revealed that the ligand upon coordination with the potential (metal) evokes the ability to inhibit bacterial growth. Antibacterial activities of the metal complexes increase with concentration. Even if the ligand is inactive against the pathogen *Klebsiella pneumonia*, all its complexes displayed high inhibition zones at all concentrations which were comparable to standard antibiotic Vancomycin, Tetracyclin and gentamycin etc. The diameter of growth zone inhibition values of Mn(II), Cu(II) complexes were comparable with the growth inhibition values of standard antibiotics like Vancomycin, Tetracyclin towards microorganism *S. aureus* at every concentration. Besides, the performances of Zn(II) and Cu(II) complexes towards *E. coli* was comparable with the inhibitive capability of almost all studied standard antibiotics at all concentrations. The results are listed in Table 2.9. Fig. 2.19 shows the antibacterial performances of Cr(III), Mn(II), Cu(II) and Zn(II) complexes of T2CDACH against *S. aureus* at a concentration 50µgdisc^{-1}

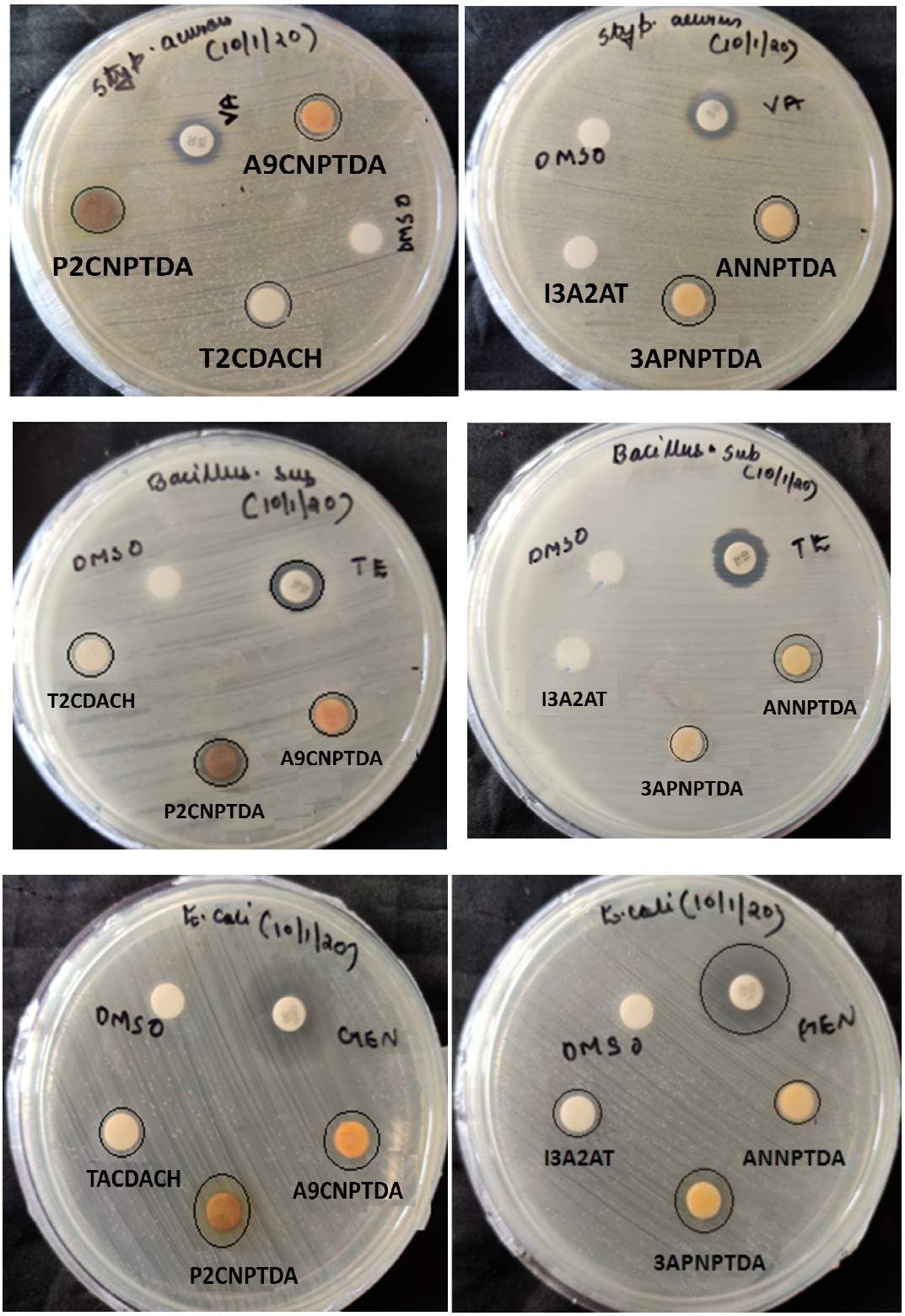

Fig. 2.12: Antibacterial activity of 'S' containing heterocyclic Schiff bases against gram-positive strains *Staphylococcus aureus*, *Bacillus subtilis* and gram- negative bacterial strain *Escherichia coli* at a concentration 200µgdisc^{-1}

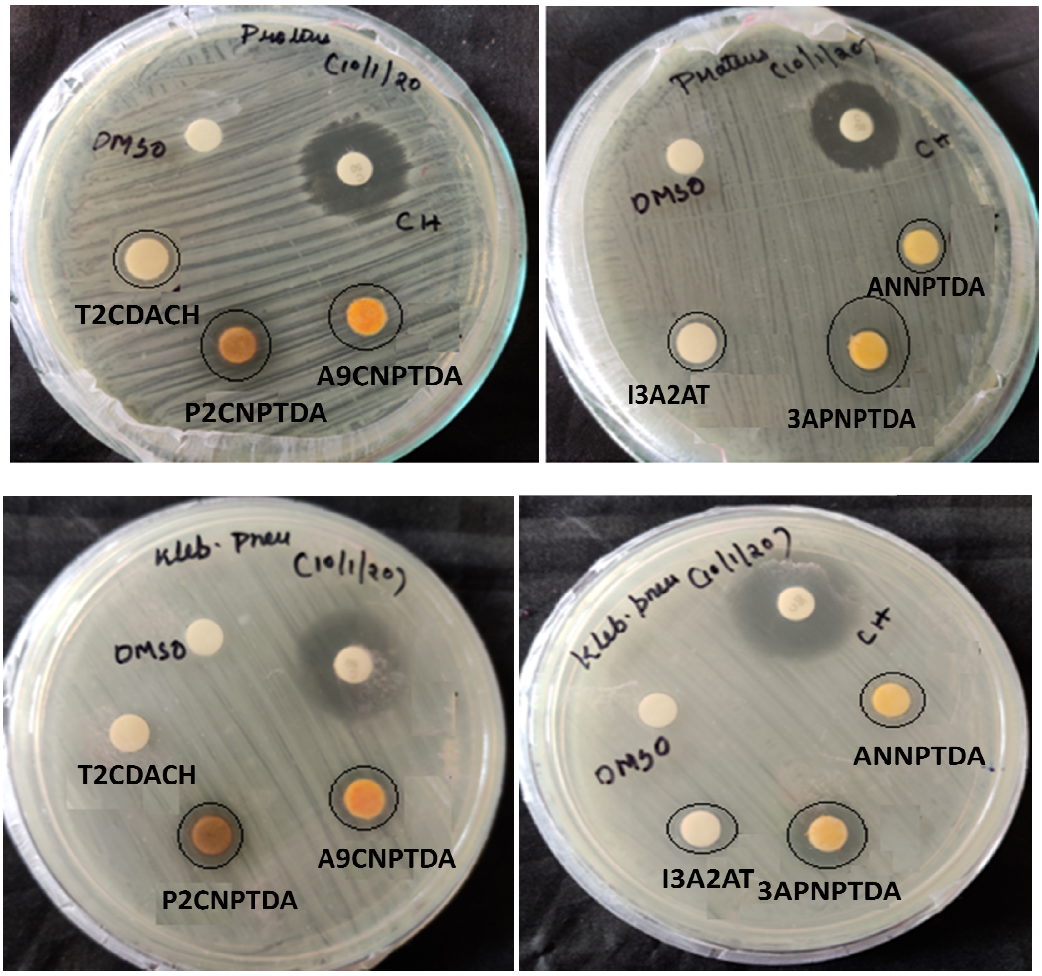

Fig. 2.13: Antibacterial activity of 'S' containing heterocyclic Schiff bases against gram-negative bacterial strains *Proteus vulgaris, Klebsiella pneumonia* at a concentration 200µgdisc^{-1}

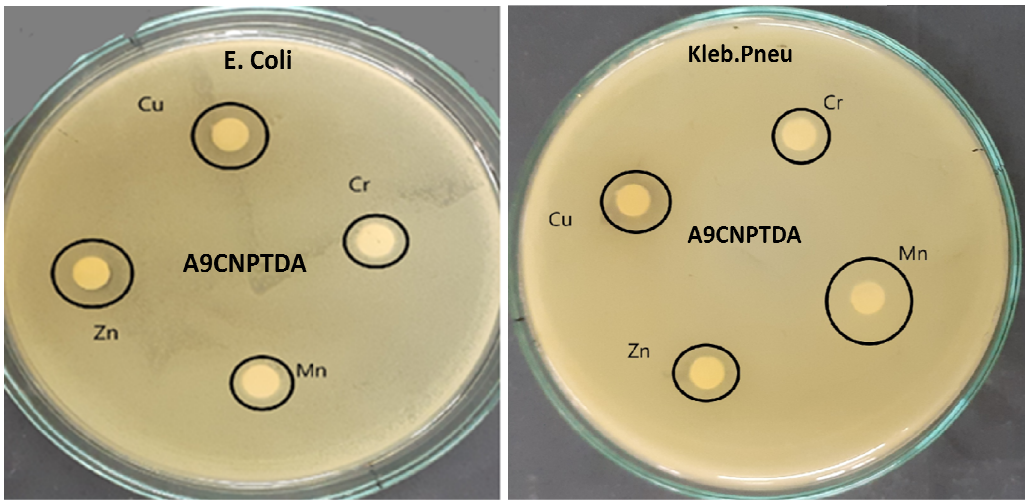

Fig. 2.14: Antibacterial activity of transition metal complexes of A9CNPTDA against *Escherichia coli* and *Klebsiella pneumonia* at a concentration 50µgdisc^{-1}

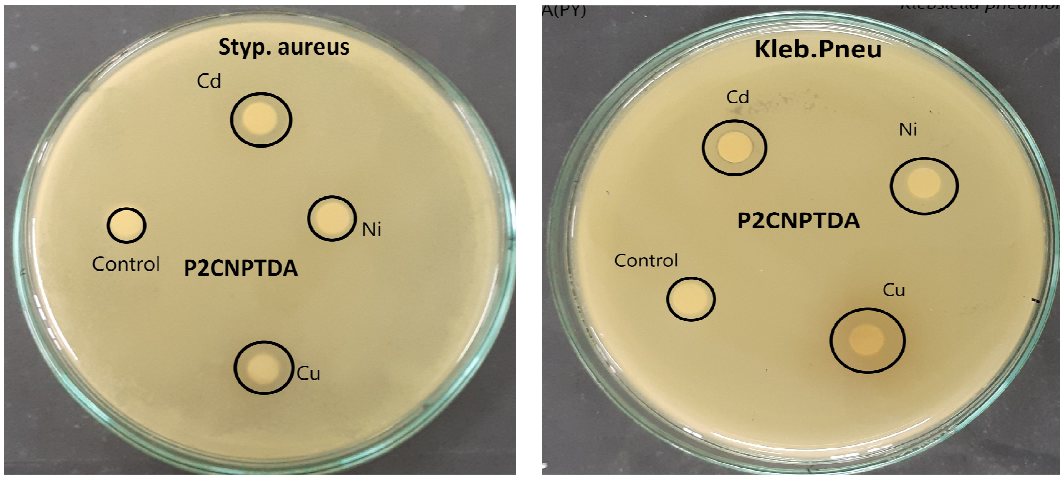

Fig. 2.15: Antibacterial activity of transition metal complexes of P2CNPTDA against *Staphylococcus aureus* and *Klebsiella pneumonia* at a concentration 50µgdisc^{-1}

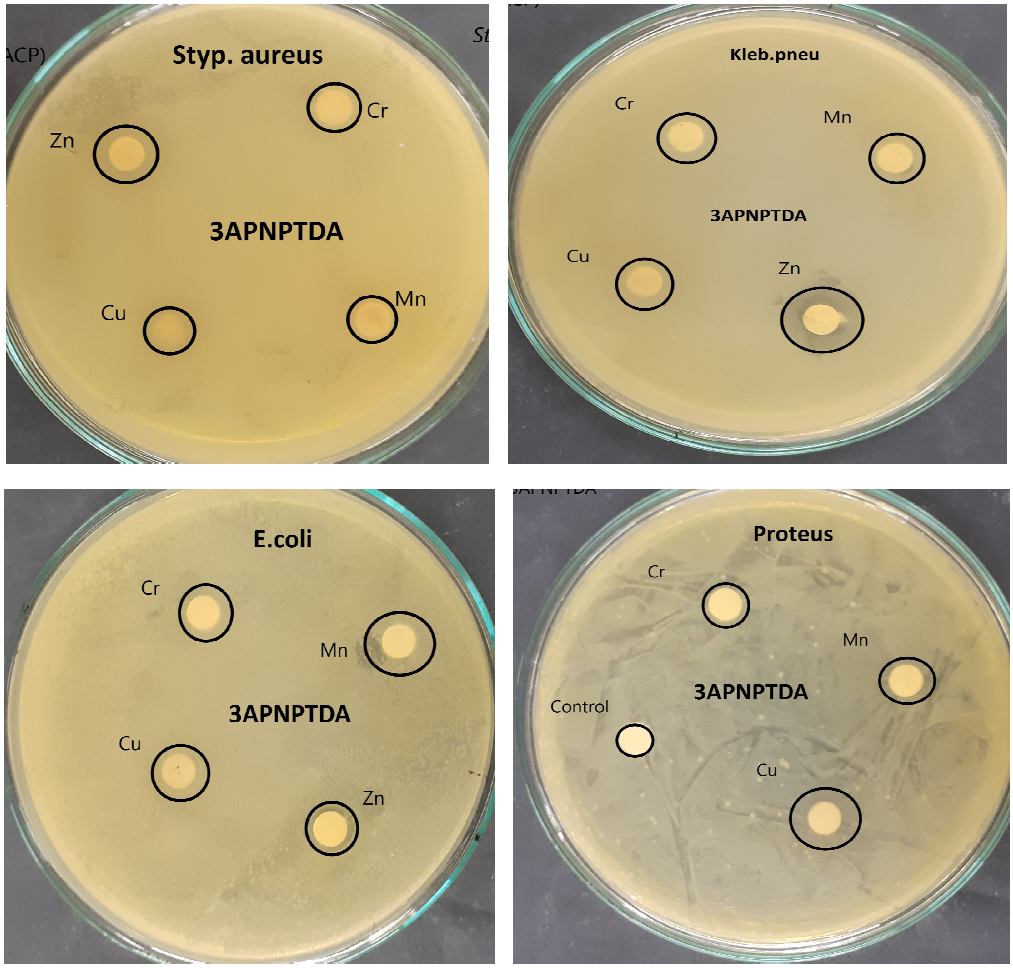

Fig. 2.16: Antibacterial activity of transition metal complexes of 3APNPTDA against *Staphylococcus aureus*, *Escherichia coli, Proteus vulgaris* and *Klebsiella pneumonia* at a concentration 50µgdisc^{-1}

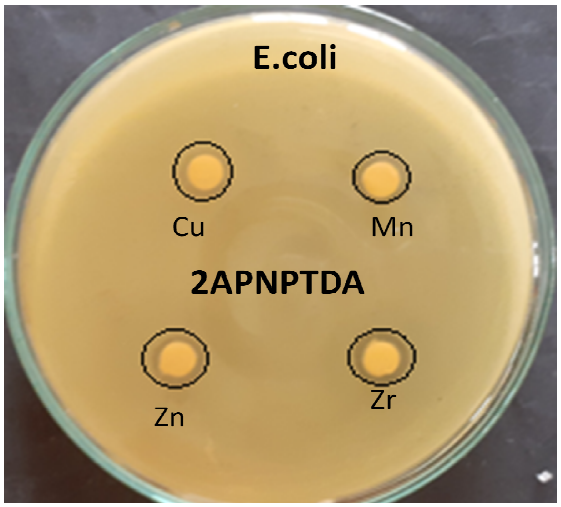

Fig. 2.17: Antibacterial activity of transition metal complexes of 2APNPTDA against *Escherichia coli* at a concentration 50µgdisc^{-1}

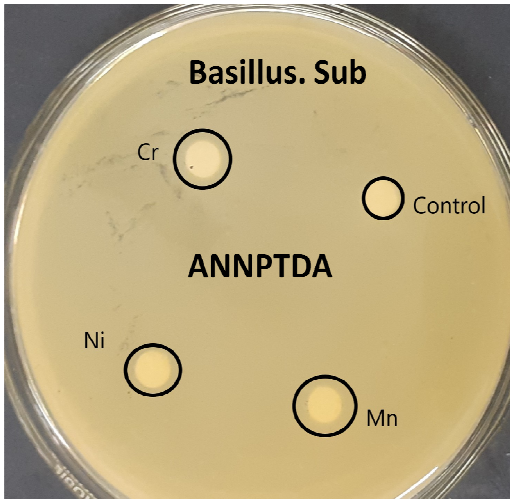

Fig. 2.18: Antibacterial activity of transition metal complexes of ANNPTDA against *Bacillus subtilis* at a concentration 50µgdisc^{-1}

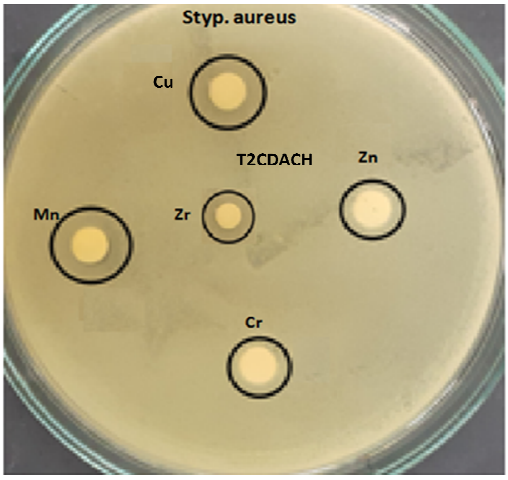

Fig. 2.19: Antibacterial activity of transition metal complexes of T2CDACH against *S. aureus* at a concentration 50µgdisc^{-1}

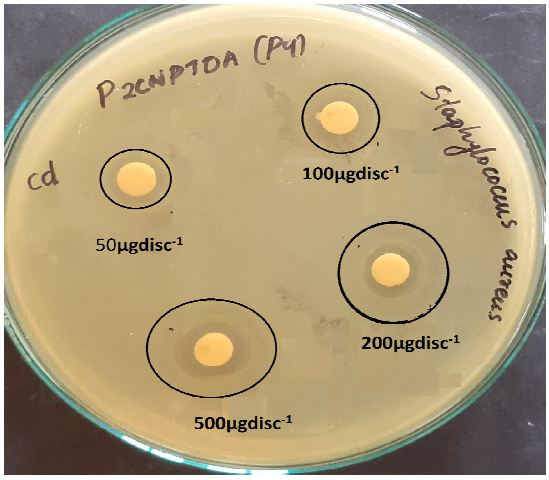

Fig. 2.20: Antibacterial activity of P2CNPTDA-Cd^{2+} at different concentrations against *S. aureus*

Table 2.2: Antibacterial activity of standard antibiotics and the solvent DMSO

Antibiotics	Diameter of the zone (mm) of inhibition at different concentrations (µgdisc^{-1})														
	S. aureus			*B. subtilis*			*K. pneumonia*			*E. coli*			*P. vulgaris*		
	50	200	500	50	200	500	50	200	500	50	200	500	50	200	500
DMSO	0	1	2	0	1	2	0	0	0	0	0	0	0	0	0
Vancomycin	12	12	12	10	13	14	10	12	14	10	12	13	14	16	20
Erythromycin	15	18.5	24	11	14	15	22	25	28	10	11	11	22	24	32
Chloramphenicol	15	20	23	15	17	18	18	20	19	8	10	11	19	20	20
Streptomycin	22	25	26.5	24	29	30	19	27	29	7	9	9	19	25	32
Tetracycline	8	13	17	11	10	11	9	12	13	10	14	17	9	11	16
Ampicillin	15	21	27	0	0	0	0	0	0	12	19	21	25	0	0
Gentamycin	22	24	25	24	25	27	11	13	14	20	19	20	22	15	28

Table 2.3: Antibacterial activity of 'S' containing heterocyclic Schiff base, (E)-(N-anthracene-9-ylmethylene)-5-(4-nitrophenyl)-1,3,4-thiadiazol-2-amine (A9CNPTDA) and its transition metal complexes

Compound	Diameter of the zone (mm) of inhibition at different concentrations (µgdisc^{-1})														
	S. aureus			*B. subtilis*			*K. pneumonia*			*E. coli*			*P. vulgaris*		
	50	200	500	50	200	500	50	200	500	50	200	500	50	200	500
A9CNPTDA (L)	8	9	9	7	7.5	8	10	12	13	9	11	14	9	9.5	10
$[CrL(Ac)_3H_2O]$	12	16	19	8	11	14	10	13	14	11	14	17	9	11	13
$[MnL(Ac)_2(H_2O)_2]$	11	12	13	8	8.5	10	17	23	25	11	13	16	8	9	10
$[FeLCl_3(H_2O)]$	10	11	16	9	13	15	12	13	15	10	12.5	14.5	9	11	15
$[CoL(NO_3)_2(H_2O)_2]$	12	12.5	14	11	13	14	10	11	13	11	13	13.5	7	10	12
$[NiL(Ac_2)_2(H_2O)_2]$	11	14	15	7	10	13	12	14	18	11	13	15	9	10	14
$[CuL(Ac)_2(H_2O)_2]$	11	13	14	6	10	10	13	16	21	14	19	23	8	14	14
$[ZnLCl_2]$	9	12	15	7	8	10	12	14	19	15	20	21	10	12	12
$[ZrOL(NO_3)_2]$	11	13	15	12	14	15	11	13	14	10	14	15	9	10.5	14

Table 2.4: Antibacterial activity of 'S' containing heterocyclic Schiff base, (E)-5-(4-nitrophenyl)-N-((pyridine-2-yl) methylene)-1,3,4-thiadiazol-2-amine (P2CNPTDA) and its transition metal complexes

Compound	Diameter of the zone (mm) of inhibition at different concentrations (µgdisc^{-1})														
	S. aureus			*B. subtilis*			*K. pneumonia*			*E. coli*			*P. vulgaris*		
	50	200	500	50	200	500	50	200	500	50	200	500	50	200	500
P2CNPTDA (L)	8	9.5	10	9	9,5	10	11	12	13	11.5	13	14	11	12	12.5
$[FeLCl_3(H_2O)]$	9	12	13	8	11	14	9	13	14	8	12	14	7	9	13
$[NiL(Ac)_2(H_2O)_2]$	9	12	14	7	10	13	10	13	18	11	13	15	4	10	13
$[CuL(Ac)_2(H_2O)_2]$	11	14	19	6	10	10	14	20	23	12	15	20	8	14	14
$[CdL(NO_3)_2]$	12	21	26	11	13	15	10	14	17	12	16	21	7	10	12
$[ZnL(Ac)_2]$	9	12	15	9	10	10.5	12	13	15	9	9.5	11	9	13	13.5
$[ZrOL(NO_3)_2]$	10	10.5	12	12	13	14	10	12	14	11	12	14.5	9	12	13

Table 2.5: Antibacterial activity of 'S' containing heterocyclic Schiff base, (E)-5-(4-nitrophenyl)-N-(1(pyridine-3-yl)ethylidene)-1,3,4-thiadiazol-2-amine (3APNPTDA) and its transition metal complexes

Compound	Diameter of the zone (mm) of inhibition at different concentrations (µgdisc^{-1})														
	S. aureus			*B. subtilis*			*K. pneumonia*			*E. coli*			*P. vulgaris*		
	50	200	500	50	200	500	50	200	500	50	200	500	50	200	500
3APNPTDA (L)	9	12	13	7	7.5	8	12	12.5	13	11	13	14	13	14	14.5
$[CrL(Ac)_3H_2O]$	9	12	13	9	11	14	9	12	14.5	10	13	15	7	9	11
$[MnL(Ac)_2(H_2O)_2]$	9	12	15	8	8.5	10	9	11.5	14	13	19	24	8	12	14
$[FeLCl_3(H_2O)]$	9	11	14	7.5	9	11	10	11	13	10	11	14	9	12	12.5
$[NiL(Ac)_2(H_2O)_2]$	9	13	14	7	10	13	10	13	18	11	13	15	8	10	13
$[CuL(Ac)_2(H_2O)_2]$	8	12	15	6	10	10	9.5	13	15	10	15	19	12.5	17	20
$[ZnLCl_2]$	12	16	20	4	7	10	13.5	22	27	11	13.5	15	6	9	10
$ZrOL(NO_3)_2]$	8	13	14	8	10	11	10	12	13	10	12	14	10	11	13

Table 2.6: Antibacterial activity of 'S' containing heterocyclic Schiff base, (E)-5-(4-nitrophenyl)-N-(1(pyridin-2-yl)ethylidene)-1,3,4-thiadiazol-2-amine (2APNPTDA) and its transition metal complexes

Compound	Diameter of the zone (mm) of inhibition at different concentrations (µgdisc^{-1})														
	S. aureus			*B. subtilis*			*K. pneumonia*			*E. coli*			*P. vulgaris*		
	50	200	500	50	200	500	50	200	500	50	200	500	50	200	500
2APNPTDA (L)	6	7	8	6	7	8	7	7.5	8	7	7.5	8	8	8.5	8.5
$[CrL(Ac)_3H_2O]$	9	12	13	9	12	13	9	13	14	9	12	13	7	9	13
$[MnL(Ac)_2(H_2O)_2]$	9	12.5	14	9	12.5	14	12	13	15	9	12.5	14	9	9	15
$[CoL(NO_3)_2(H_2O)_2]$	5	5.5	8	6	7.5	7	7	7	8	6.5	7	8	7	8	8.5
$[NiL(Ac)_2(H_2O)_2]$	11	13	19	11	15	19	10	13	18	11	15	19	4	10	13
$[CuL(Ac)_2(H_2O)_2]$	11	15	18	9	10	14	14	18	19	9	10	14	8	14	14
$[ZnL(Ac)_2]$	9	12	14	9	12	14	12	13	24	9	14	20	9	9.5	14.5
$[ZrOL(NO_3)_2]$	11	14	16	9	10.5	11	11	12	15	10	12	13	8	10	14

Table 2.7: Antibacterial activity of 'S' containing heterocyclic Schiff base N(anthracen-9(10H)-ylidene)-5-(4-nitrophenyl)-1,3,4-thiadiazol-2-amine (ANNPTDA) and its transition metal complexes

Compound	Diameter of the zone (mm) of inhibition at different concentrations (µgdisc^{-1})														
	S. aureus			*B. subtilis*			*K. Pneumonia*			*E. coli*			*P. vulgaris*		
	50	200	500	50	200	500	50	200	500	50	200	500	50	200	500
ANNPTDA (L)	7	9	10	11	13	15	10	11	13	7	7.5	8	8	9	9.5
$[CrL_2(Ac)_3H_2O]$	9	12	13	9	12	13	10.5	13	17	9	12	13	7	9	13
$[MnL_2(Ac)_2(H_2O)_2]$	9	12.5	14	12	15	23	12	14	23.5	9	12.5	14	6	9	10
$[NiL_2(Ac)_2(H_2O)_2]$	11	15	19	10	15	16	11	12.5	17	12	15	18	7	10	13
$[CuL_2(Ac)_2(H_2O)_2]$	9	10	14	11	10	16	14	20	21	9	10	14	8	14	14
$[ZnL(Ac)_2(H_2O)]$	9.5	12	14	10	12	14	12	13	15	9	12	14	6	9	10
$[ZrOL(NO_3)_2(H_2O)]$	8	12	13	10	13	15	10	12	14	10	11	12	8	8.5	11

Table 2.8: Antibacterial activity of 'S' containing heterocyclic Schiff base, N-((1H-indol-3-yl)methylene)thiazol-2-amine (I3A2AT) and its transition metal complexes

Compound	Diameter of the zone (mm) of inhibition at different concentrations (µgdisc^{-1})														
	S. aureus			*B. subtilis*			*K. Pneumonia*			*E. coli*			*P. vulgaris*		
	50	200	500	50	200	500	50	200	500	50	200	500	50	200	500
I3A2AT (LH)	0	0	0	0	0	0	10	11	12	7	7	8	8	8.5	9
$[CrL(Ac)_2(H_2O)]$	7	8	9	8	11	12	12	13	13	8	11	12.5	8	9	11
$[MnLAc(H_2O)_3]$	8	9	9.5	9	11	11	10	12	14	9	11	13	8	8.5	10
$[NiLCl(H_2O)_3]$	9	9.5	10	8	11	11	11	13	14	8	10.5	12	4	7	9
$[CuLAc(H_2O)_3]$	9	12	13	6	8	11	11	12	13	9	10	15	5	6	9
$[ZnLAc(H_2O)]$	7	9	10	5	6	9	12	13	15	8	13	14	8	10	11
$[ZrOLNO_3(H_2O)]$	8	9	11	6	7	10	12	13.5	16	7	8	8	8.5	9	9.5

Table 2.9: Antibacterial activity of 'S' containing heterocyclic Schiff base, (13E)-N1,N2-bis((thiophene-2-yl)methylene)cyclohexane-1,2-diamine (T2CDACH) and its transition metal complexes

Compound	Diameter of the zone (mm) of inhibition at different concentrations (µgdisc^{-1})														
	S. aureus			*B. subtilis*			*K. pneumonia*			*E. coli*			*P. vulgaris*		
	50	200	500	50	200	500	50	200	500	50	200	500	50	200	500
T2CDACH (L)	7	7.5	8	6.5	7	7.5	0	0	0	7	7.5	8	9	9.5	10
$[MnL(Ac)_2(H_2O)_2]$	15	21	25	8	8.5	10	11	13	16	12	13	17	9.5	10	13.5
$[NiL(Ac)_2(H_2O)_2]$	11	14	15	15	17	21	12	14	18	11	13	15	10	16	17
$[CuL(Ac)_2(H_2O)_2]$	15	17	22	6	10	10	12	16	23	14	19	23	8	14	14
$[ZnL(Ac)_2]$	12	13	18	7	9	10	13	14	16	19	21	24	10	12	12.5
$[ZrOL(NO_3)_2]$	13	18	20	12	13	15	11	13.5	15	10	14	15	9	10.5	14

CHAPTER 9
IN SILICO MOLECULAR DOCKING STUDIES ON SULPHUR CONTAINING SCHIFF BASES

In this chapter, much attention was given on the evaluation of inhibition competency of the synthesized Schiff bases (E)-(N-anthracene-9-ylmethylene)-5-(4-nitrophenyl)-1,3,4-thiadiazol-2-amine (A9CNPTDA), (E)-5-(4-nitrophenyl)-N-((pyridine -2-yl)methylene)-1,3,4-thiadiazol-2-amine (P2CNPTDA), (E)-5-(4-nitrophenyl)-N-(1 (pyridine-3-yl)ethylidene)-1,3,4-thiadiazol-2-amine (3APNPTDA), (E)-5-(4-nitrophenyl) -N-(1(pyridin-2-yl)ethylidene)-1,3,4-thiadiazol-2-amine (2APNPTDA), N-(anthracen-9 (10H)-ylidene)-5-(4-nitrophenyl)-1,3,4-thiadiazol-2-amine (ANNPTDA), N-((1H-indol-3-yl)methylene)thiazol-2amine (I3A2AT) and (13E)-N1,N2-bis((thiophene-2-yl) methylene)cyclohexane-1,2-diamine (T2CDACH) on SARS-CoV-2 main protease (PDB code: **6lu7**) causing Covid 19, HIV-1 protease (PDB code: **1mui**) responsible for HIV/ADS, human epidermal growth factor receptor, HER2 protease (PDB code: **3rcd**), target protein in Breast cancer and human acetylcholinesterase (AChE) (PDB code: **1b41**) in Alzheimer's disease. The drug likeness of these studied molecules was checked using Lipinski rule of five.

Druglikeness and Toxicity of Schiff Bases

Drug-like properties were examined using Lipinski's rule of five. As per this rule, a drug-like compound must have molecular mass less than 500 Dalton. Molecules with high lipophilicity and molar refractivity values ranging from 40-130 possess good drug ability. The number of hydrogen bond donors must be less than 5 and there should be less than 10 hydrogen bond acceptors.

From the evaluation of Lipinski's parameters, it is clear that lipophilicity, molecular mass, molar refractivity, number of donor and acceptor hydrogen bonds for

the Schiff bases, A9CNPTDA, P2CNPTDA, 3APNPTDA, 2APNPTDA, ANNPTDA, I3A2AT and T2CDACH are within the limits of Lipinski's rule and are depicted in Table 2.10. The above results show that the possibility to act as drug for these Schiff bases are very significant.

Table 2.10: Lipinski's parameters for analysing druglikeness of Schiff bases

Lipinski parameter	Schiff bases						
	A9CNPTDA	P2CNPTDA	3APNPTDA	2APNPTDA	ANNPTDA	I3A2AT	T2CDACH
Molecular mass	410	311	325	325	398	218	302
H-donor	0	0	0	0	0	0	0
H-acceptor	5	6	6	6	4	3	2
Log P	5.129	3.258	3.459	3.459	4.314	0.868	4.658
Molar refractivity	120.02	83.49	87.45	87.45	110.85	58.29	89.87

***** Limiting value of drug like property: Molecular mass < 500; H-donor < 5; H-acceptor < 10; LogP < 5; Molar refractivity 40-130

Further, molecular docking studies were carried out for the above mentioned Schiff base ligands. Upcoming sections explain the interactions of these studied ligands with PDB codes **6lu7, 1mui**, **3rcd** and **1b41**. This chapter is divided into four sections. First section includes the molecular docking studies of SARS-CoV-2 main protease (M^{pro}) with these synthesized Schiff bases. Second section depicts discussion of these Schiff bases docked with HIV-1 main protease. Section III includes the molecular docking studies of HER2 protein with these studied molecules. Studies on interaction between the synthesized sulphur containing Schiff bases with acetylcholinesterase (AChE) are well documented in Section IV.

SECTION-I

MOLECULAR DOCKING STUDIES OF SARS-CoV-2 MAIN PROTEASE (COVID-19) WITH SULPHUR CONTAINING SCHIFF BASES

The current global outbreak, COVID-19 has brought up the dreadful situation which urges for eventual medications to confront this epidemic that lacks explicit treatment. Currently, active drug designing is possible by adopting the structure-based computational docking treatment. In our present study, we selected seven novel 'S' containing Schiff bases and examined their drug-likeness using Lipinski's rule of five. Accordingly, the studies were extended to identify the potential inhibitors of novel coronavirus by utilizing the computational treatment for drug designing. Recent biological studies provided an extensive feature of M^{pro} protease or main protease in novel coronavirus as a potential drug target for precise treatment for COVID-19. We profoundly focus on synthesized compounds, A9CNPTDA, P2CNPTDA, 3APNPTDA, 2APNPTDA, ANNPTDA, I3A2AT and T2CDACH docked into the active binding cavity of SARS-CoV-2 main protease (M^{pro}) (PDB code: **6lu7**). Strong inhibition of the molecules on the main protease will lead to the prevention of transcription and translation process of viral RNA. This will cause to cease the multiplication of new virions appreciably. In drug designing, ligand-receptor complex stability is a significant factor that is decided by the stronger interactions established within the complex and is shown in Table 2.11.

A9CNPTDA-6lu7 Complex

In molecular docking treatment, the thiadiazole derivative of polynuclear Schiff base A9CNPTDA formed stable conformation by interacting with a binding energy of -8.3kcal/mol with hydrophobic bonds. Here the anthracene moiety present in the molecule has established pi-alkyl and pi-pi stacked T-shaped interaction with active

Met165 and His41 residues of **6lu7** receptor. Besides, the thiadiazole ring present in the compound has actively participated in pi-alkyl interactions with Leu27 and Cys145 as represented in Fig. 2.21 (a and b).

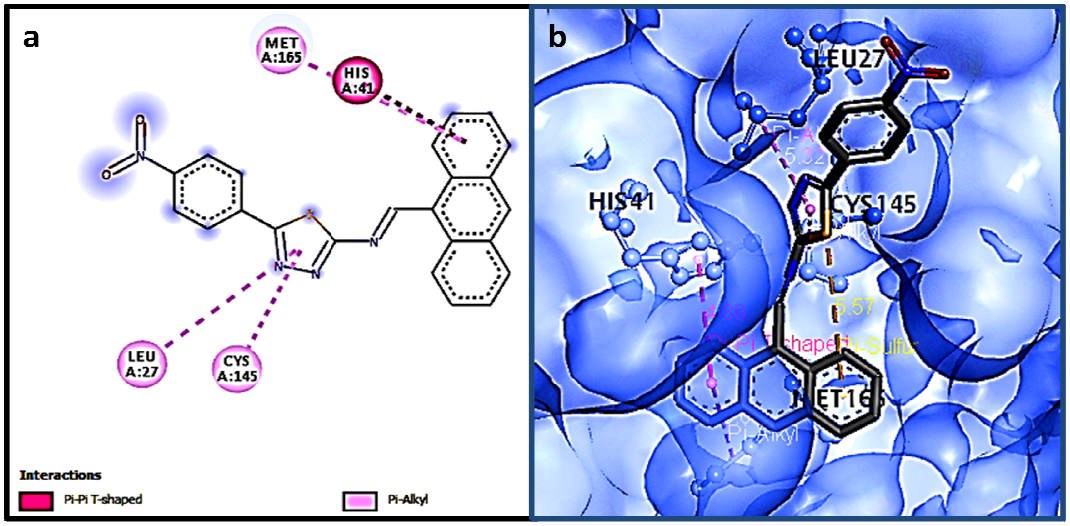

Fig. 2.21: (**a**) 2D and (**b**) 3D interaction diagrams of A9CNPTDA with M^{pro} **(6lu7)**

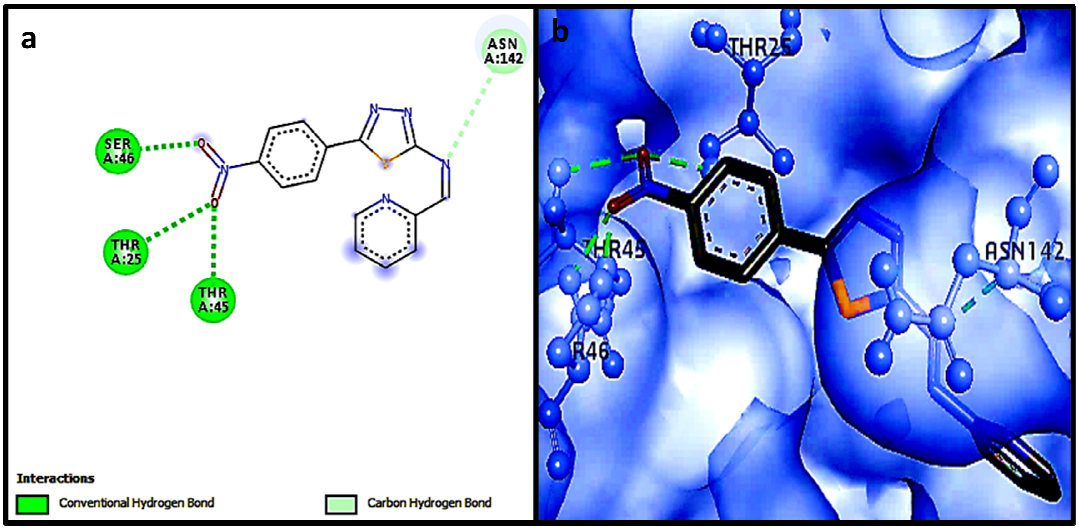

Fig. 2.22: (**a**) 2D and (**b**) 3D interaction diagrams of P2CNPTDA with M^{pro} **(6lu7)**

P2CNPTDA-6lu7 Complex

In complex, P2CNPTDA-main protease, stability is due to the presence of stronger interactions with a binding score of -7.0 kcal/mol. Here the complex involves several hydrogen bonding interactions where active Thr25, Thr45, and Ser46 moieties

are engaged in conventional hydrogen bonding with the electron-withdrawing nitro group as demonstrated in Fig. 2.22 (a and b). The azomethine linkage formed a carbon-hydrogen bonding with the Asn42 and these interactions interpret the competence of the drug in inhibiting the main protease (M^{pro}).

3APNPTDA-6lu7 Complex

On examining the complex 3APNPTDA-main protease, it showed hydrogen bond interactions with Ser46, His163, Asn142, and Gly143 along with hydrophobic, pi alkyl and alkyl interactions with Cys145. A docking score of -7.0 kcal/mol was displayed by this complex. From Fig. 2.23 (a and b) it is clear that the ligand molecule shows a conventional H-bond with the benzene ring and nitro group. Additionally, the azomethine linkage formed a carbon-hydrogen bonding with the Asn142 and Gly143 residue forms pi-donor hydrogen bonding interaction with the sulphur atom present in the thiadiazole ring.

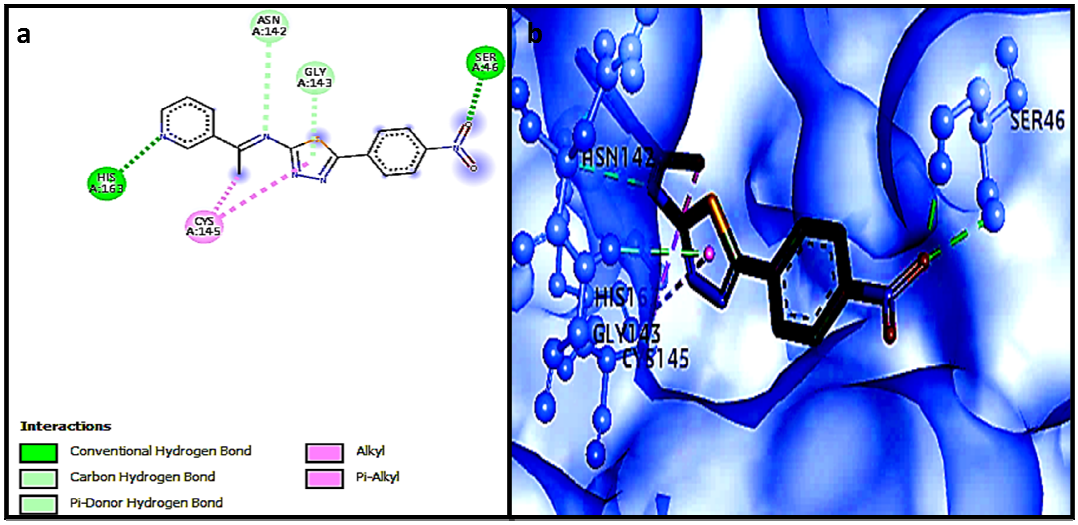

Fig. 2.23: (**a**) 2D and (**b**) 3D interaction diagrams of 3APNPTDA with M^{pro} **(6lu7)**

2APNPTDA-6lu7 Complex

Similarly, from computational evaluation, it was observed that the pyridine derivative of Schiff base, 2APNPTDA less firmly bonded with the main protease with a

binding energy of -6.9 kcal/mol. Here the Schiff base complex with the main protease formed is further stabilized due to the presence of several other interactions such as electrostatic and π-sulfur along with the hydrogen bonding and hydrophobic interactions. In the complex, Gly143 and Glu166 residue of main protease receptor initiated in binding with a benzene ring and nitrogen atom present in thiadiazole ring present in the compound. Moreover, the extra stabilization of the complex is attained by π-cation and π-sulphur interactions with active His41 and Met165 residues, respectively, as illustrated in Fig. 2.24 (a and b).

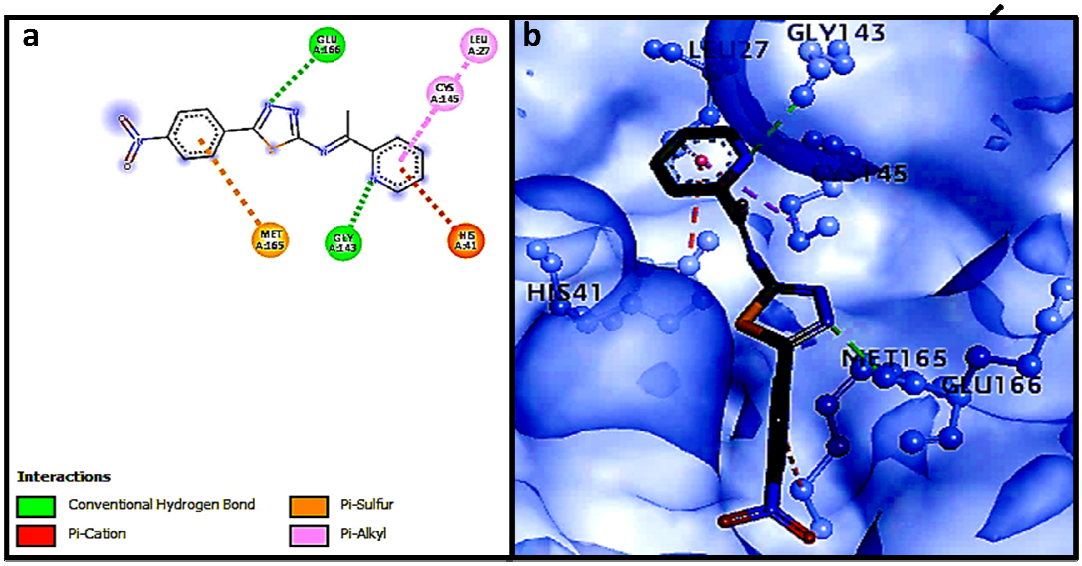

Fig. 2.24: (**a**) 2D and (**b**) 3D interaction diagrams of 2APNPTDA with M^{pro} **(6lu7)**

ANNPTDA-6lu7 Complex

Polynuclear thiadiazole derivative of Schiff base ANNPTDA showed greater stabilized conformations with active amino acid groups present in the main protease and displayed binding energy of -8.4 kcal/mol with hydrogen bonding and hydrophobic interactions as depicted in Fig. 2.25 (a and b). In the ligand-receptor complex, amino acid residue, Thr26 has made conventional hydrogen bonding interaction apart from non-conventional hydrogen bond with the electron-withdrawing nitro group. The conformation of compound ANNPTDA complexed with the main protease acquired

extra stabilization with hydrophobic interactions such as pi-pi T shaped, pi- alkyl, and alkyl interactions. The active, His41 motif established a pi-pi T shaped interaction while Met165 actively formed a pi- alkyl interaction with anthracene ring moiety.

As per results, the thiadiazole pyridine derivatives 3APNPTDA, 2APNPTDA, and P2CNPTDA are moderately inhibited the main protease M^{pro} (**6lu7**) when compared with polynuclear thiadiazole derivatives of Schiff bases A9CNPTDA and ANNPTDA ligands.

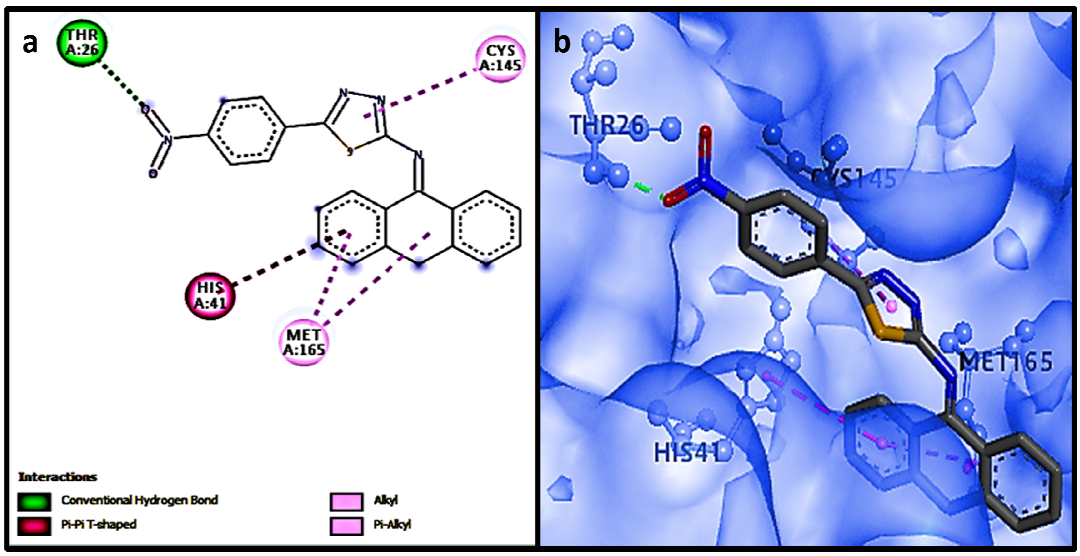

Fig. 2.25: (**a**) 2D and (**b**) 3D interaction diagrams of ANNPTDA with the M^{pro} **(6lu7)**

I3A2AT-6lu7 Complex

As per the studies carried out the the thiazole derivative of Schiff base, I3A2AT show binding energy value -6.3kcal/mol during the interaction with the Main protease. As in the Fig. 2.26 (a and b), the thiazole derivative of Schiff base I3A2AT has involved in two hydrophobic interactions with Met149 and Met49 along with other non-bonding pi-sulfur with Cys145 active amino acid residue of main protease. The benzene ring moiety of the I3A2AT involves in hydrophobic interaction with Met149 residue while heterocyclic five membered nitrogen containing ring system get involved in pi alkyl hydrophobic interaction with Met49.

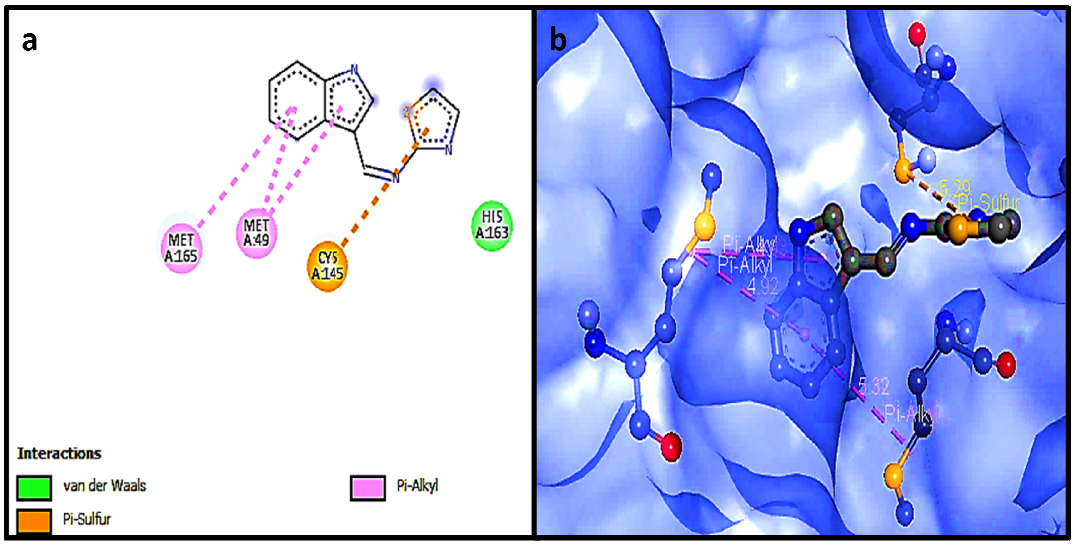

Fig. 2.26: (**a**) 2D and (**b**) 3D interaction diagrams of I3A2AT with the M^{pro} **(6lu7)**

T2CDACH-6lu7 Complex

At the same time the thiophene derivative T2CDACH show binding energy value -6.3kcal/mol during the interaction with the Main protease shown as given in the Fig. 2.27 (a and b), has involved in one conventional hydrogen bonding interaction with His41 along with varying hydrophobic interactions like pi-pi stacked interaction with His41, amide pi stacked interactions with active Met165 and Glu166 and alkyl interactions with Cys145.

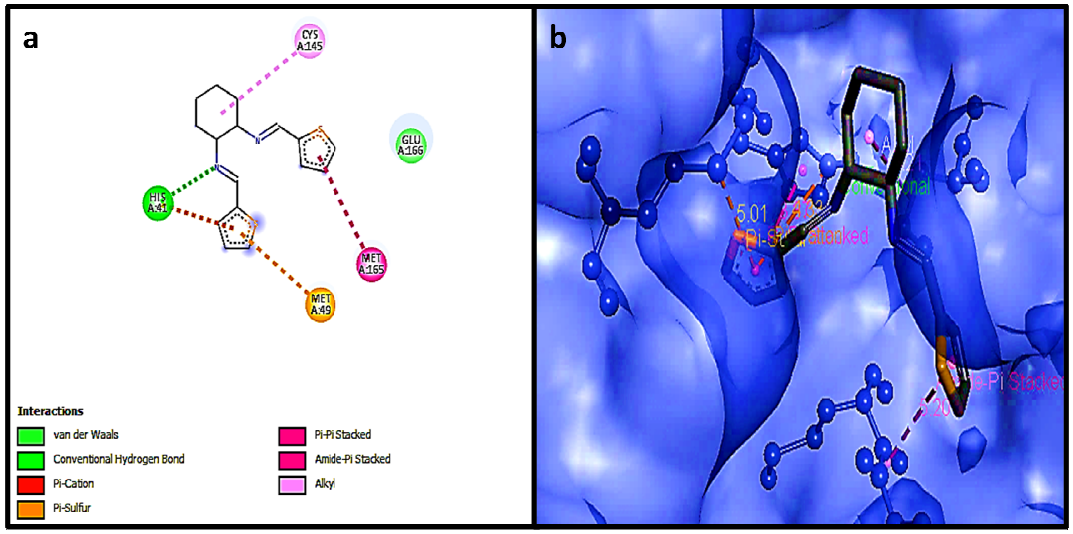

Fig. 2.27: (**a**) 2D and (**b**) 3D interaction diagrams of T2CDACH with the M^{pro} **(6lu7)**

Here, azomethine group of the T2CDACH involved in conventional hydrogen bonding with His41 residue. Moreover, the stability of the complex formed is further established due to the involvement of pi-cation electrostatic interactions along with pi-sulfur interactions are shown in this Fig. 2.27.

Among the studied molecules, the polynuclear thiadiazole derivatives of Schiff bases, A9CNPTDA and ANNPTDA show appreciable binding affinity with stabilizing suitable interactions with active pockets of main protease receptor, leading to the dysfunctioning of target protein leading to the interfering of the viral life cycle in the host cell and which can be further analysed by clinical trials. The binding affinities of ligands follows the order ANNPTDA > A9CNPTDA > 3APNPTDA ~ P2CNPTDA ~ T2CDACH > 2APNPTDA > I3A2AT.

Table 2.11: Binding energies and interactions of seven novel 'S' containing heterocyclic Schiff bases with SARS CoV-2 main protease (PDB code: **6lu7**)

Schiff base	B.E*(ΔG)	Category of interaction	Types of interactions	Amino acid residues
A9CNPTDA	-8.3	Hydrophobic	π – alkyl	Leu27, Cys145, Met165
			π – π T shaped	His41
P2CNPTDA	-7.0	Hydrogen bonding	HB*	Thr25, Thr45, Ser46
			C-H bonding (NHB*)	Asn142
3APNPTDA	-7.0	Hydrogen bonding	HB*	Ser46, His163
			C-H bonding (NHB*)	Asn142
			π-donor H- bonding (NHB*)	Gly143
		Hydrophobic	π –alkyl	Cys145
			alkyl	Cys145
2APNPTDA	-6.9	Hydrogen bonding	HB*	Gly143, Glu166
		Hydrophobic	π –alkyl	Leu27, Cys145
		Electrostatic	π –cation	His41
		Other	π –sulfur	Met165
ANNPTDA	-8.4	Hydrogen bonding	HB*	Thr26
		Hydrophobic	π – π T shaped	His41
			π –alkyl	Met165, Cys145
			alkyl	Met165
I3A2AT	-6.3	Hydrophobic interactions	π- alkyl	Met145, Met49
		Others	π- sulphur	Cys145
T2CDACH	-7.0	Hydrogen bonding	HB*	His41
		Hydrophobic	π- π stacked	HIS41
			Amide π- stacked	Met165,Glu166
			Alkyl	Cys145
		Electrostatic	π-cation	His41
		Others	π- sulfur	Met49

B.E* Binding Energy in kcal/mol; HB* Conventional H bond; NHB* Non-Conventional H-bond

SECTION-II

MOLECULAR DOCKING STUDIES OF HIV-1 PROTEASE (HIV/AIDS) WITH SULPHUR CONTAINING SCHIFF BASES

Acquired immunodeficiency syndrome caused by the HIV virus is continuous to be a global health issue as per the reports of world health organisation. However, currently the disease has been raised to be a manageable chronic illness due to the currently available medications provided globally. Presently advanced technology has contributed its maximum to determine the affordable and appropriate medications to infected patients. In our current study, structure based molecular docking methods were adopted to evaluate the binding affinity of Schiff bases by analysing the drug interaction with the target receptor. The studies shows that seven novel sulphur based Schiff bases, A9CNPTDA, P2CNPTDA, 3APNPTDA, 2APNPTDA, ANNPTDA, I3A2AT and T2CDACH has drug like properties which takes out its wide chances in discovering a proper medication for HIV/AIDS.

In molecular docking studies, a target protein is suitably selected. From the earlier studies carried out, HIV-1 protease is considered to be suitable target protein and the crystal structure HIV-1 protease complexed with Lopinavir were accessed from protein database bank by using corresponding PDB code, **1mui.** Newly synthesized Schiff bases showed high dock scores with hydrogen bonding interactions and thus acted as highly potential inhibitors.

The binding score of a protein with ligand establishes the stability of protein-ligand complex. Ligand-protein complexes have numerous interactions which are very crucial in determining their stability. These interactions are mainly stabilized by conventional hydrogen bonding. Additionally, the extended stability of ligand-receptor complex is decided by carbon-hydrogen bond interactions and hydrophobic interactions

(π-alkyl, π-sigma, Van der Waals, alkyl and π-sulfur). Electrostatic interactions, π-anion and π-cation were also established between the receptor and ligand which resulted in additional stability

Binding energy score and the nature of the interaction of A9CNPTDA, P2CNPTDA, 3APNPTDA, 2APNPTDA, ANNPTDA, I3A2AT and T2CDACH with the amino acid residues of the HIV-1 protease are represented in Table 2.12. Results showed that HIV-1 protease has high binding energy value with the synthesised Schiff bases.

A9CNPTDA-1mui Complex

As in Fig. 2.29, HIV-1 protease (**1mui**) complexed with thiadiazole derivative of polynuclear Schiff base, A9CNPTDA showed binding energies of -10.7 kcal/mol. The ligand was found to be firmly interacted with the HIV-1 protease (**1mui**).

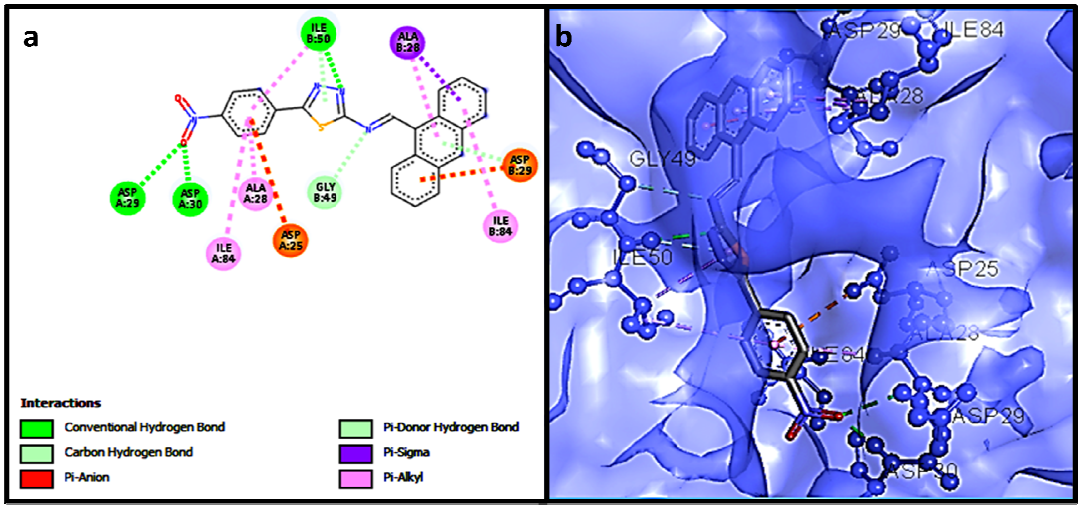

Fig. 2.28: (**a**) 2D and (**b**) 3D interaction diagrams of A9CNPTDA with HIV-1 protease

On examining the structure of the complex, it is clear that nitro group, azomethine and the nitrogen atom of thiadiazole ring system were involved in the hydrogen bonding interactions with the amino acid residues. Here the nitro group made two conventional hydrogen bonding interactions with the Asp29 and Asp30 residues and thiadiazole ring is stabilized through one conventional hydrogen bonding interaction

with Ile50 residue. Nitrogen atom of azomethine linkage is stabilized through C-H bonding with Gly49 residue. Hydrophobic interactions also existed between aromatic rings and the amino acid residues Ala28, Ile47, Ile50 and Ile84. In addition to these bonds, amino acid residues, Asp25 and Asp29 made π-anion bonds with the benzene and anthracene ring system

P2CNPTDA-1mui Complex

Thiadiazole derivative of pyridine Schiff base, P2CNPTDA complexed with HIV-1 protease was stabilized with a binding energy of -8.6kcal/mol. The complex involves various interactions that ensures the excellent stabilization that includes three hydrogen bonding interactions and five hydrophobic interactions. As shown in the Fig. 2.30, nitro group attached to the ring nucleus established a conventional hydrogen bonding with the Asp29, Asp30 while the nitrogen atom present in the thiadiazole ring made a carbon-hydrogen bond with the Gly29 amino acid residue. Further complex stabilization is obtained by the hydrophobic pi-alkyl and pi-sigma interactions. In hydrophobic interactions, Ile50, Ala28, Ile84, Ile50 and Ile47 are the active residues which form stable interaction with the drug molecule.

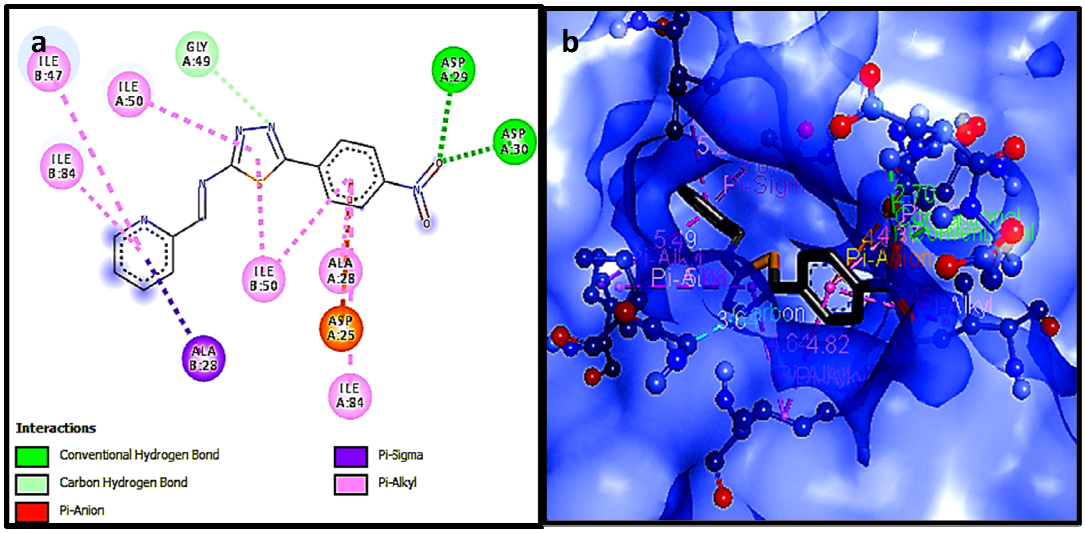

Fig. 2.29: (**a**) 2D and (**b**) 3D interaction diagrams of P2CNPTDA with HIV-1 protease

3APNPTDA-1mui Complex

When consider the complex formed between 3APNPTDA and **1mui**, we can see the stabilized structure with a binding energy of -10.7kcal/mol. As shown in Fig. 2.31, the complex is stabilized by several numbers of interactions, like hydrogen bonding, hydrophobic and electrostatic interactions. The nitro groups attached to the benzene ring nucleus and nitrogen atom in thiadiazole ring moiety of drug molecule establishes strong interactions with the Ile50, Asp29 and Asp30. Additional stabilisation is attained by the hydrophobic interactions formed by pi- alkyl and pi- sigma interactions with the Ala28, Ile84 and Ile50 residue of **1mui** receptor molecule and electrostatic interactions involves pi-anion interactions established between target receptor and benzene ring along with anthracene ring moieties of drug molecule.

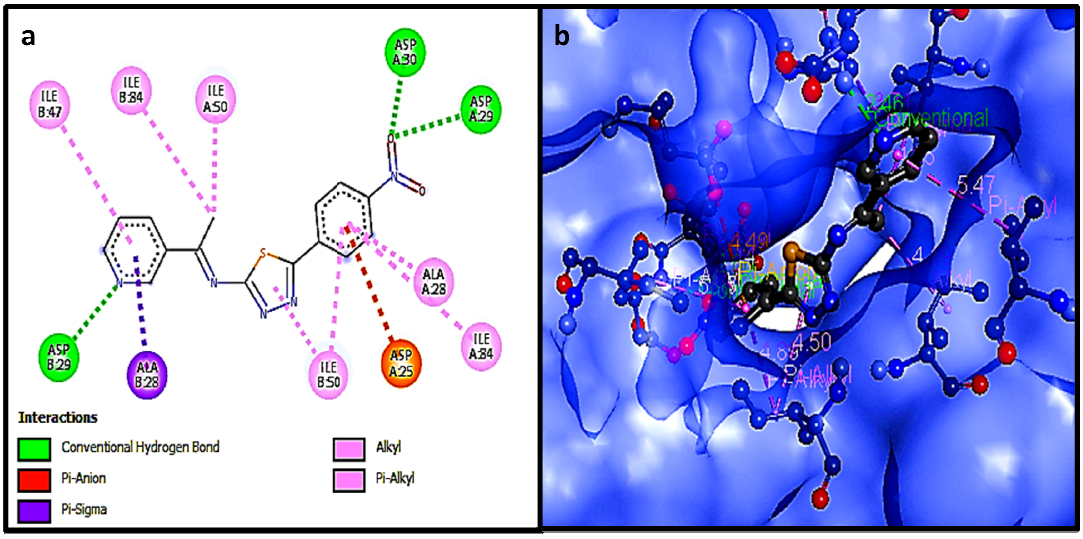

Fig. 2.30: (**a**) 2D and (**b**) 3D interaction diagrams of 3APNPTDA with HIV-1 protease

2APNPTDA-1mui Complex

2APNPTDA-**1mui** complex showed a binding energy of -8.7kcal/mol and showed strong interactions. The interactions established are hydrogen bonding interaction, hydrophobic interaction and electrostatic interaction. Here conventional hydrogen bonds were formed between the nitro group attached to the benzene ring

moiety of the drug molecule with the active Asp29 and Asp30 residues. Ile47,1le50, Ala28 and Ile84 involved in hydrophobic alkyl and pi- sigma interactions with Schiff base molecule while the electrostatic interactions are established within the benzene ring of drug molecule and Asp25 of the amino acid residues as depicted in Fig. 2.32.

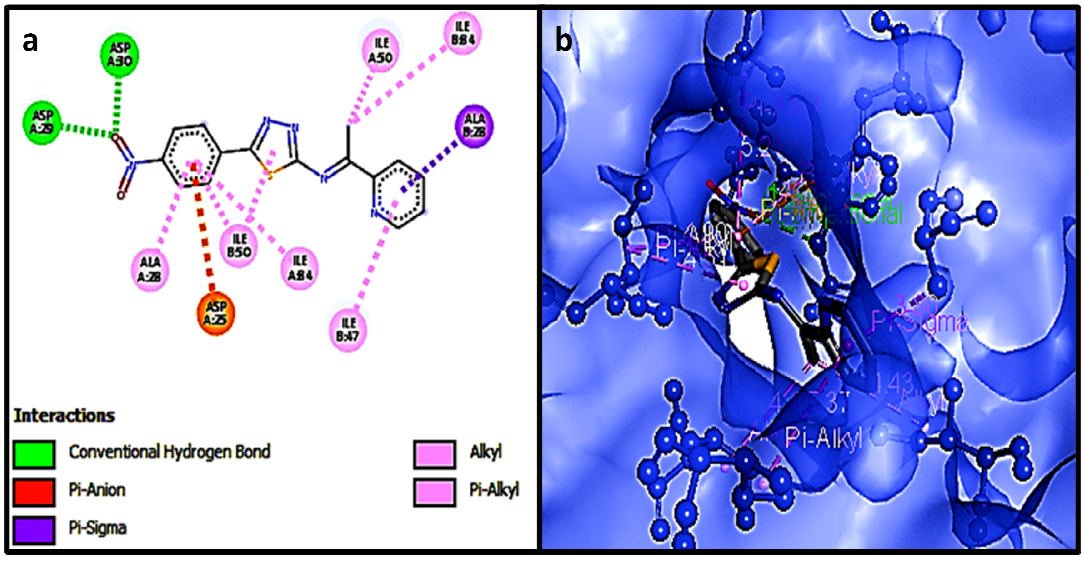

Fig. 2.31: (**a**) 2D and (**b**) 3D interaction diagrams of 2APNPTDA with HIV-1 protease

ANNPTDA-1mui Complex

The complex formed between ANNPTDA and HIV-1 protease is stabilized with a binding energy of -11.7kcal/mol. The nitro group present in the molecule ANNPTDA is involved in two hydrogen bonding interactions with the Asp29 and Asp30 residues. Moreover, the ligand-receptor interactions involved C-H bonding between the Gly49 residue and nitrogen atom of the thiadiazole moiety. This stabilization was further extended due to the presence of hydrophobic interactions like π-alkyl, π-anion and alkyl interactions. In this complex, thiadiazole, benzene and anthracene rings are mostly stabilized by the hydrophobic interactions with the Ala28, Ile47, Ile50 and Ile84, which are the crucial interactions for the ligand. Benzene rings attained extra stability by electrostatic π- anion interactions with active Asp25 residue of HIV-1 protease. All these

interactions are depicted in Fig. 2.33 and these interactions support the stability of conformation of the ligand in the binding pocket of HIV-1 protease (**1mui**).

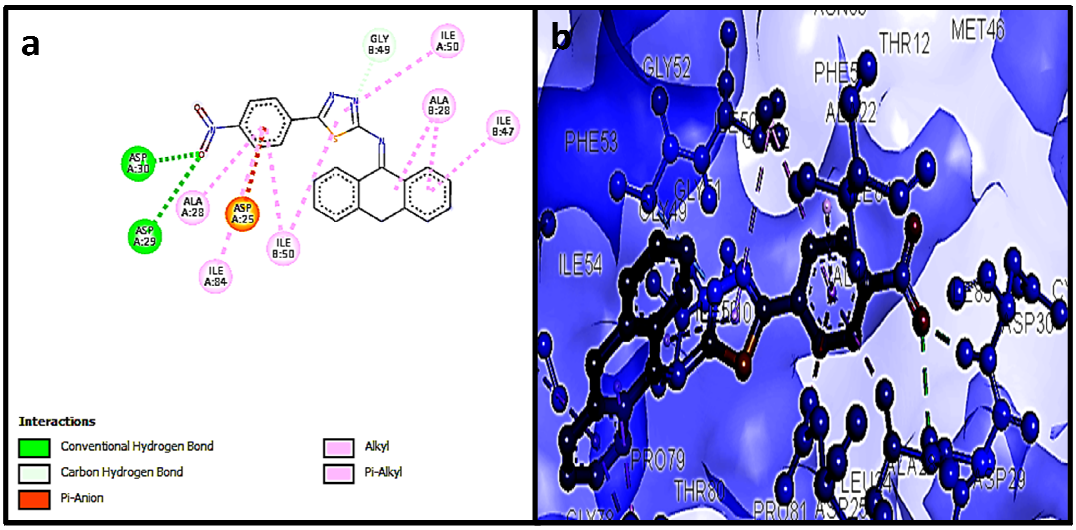

Fig. 2.32: (**a**) 2D and (**b**) 3D interaction diagrams of ANNPTDA with HIV-1 protease

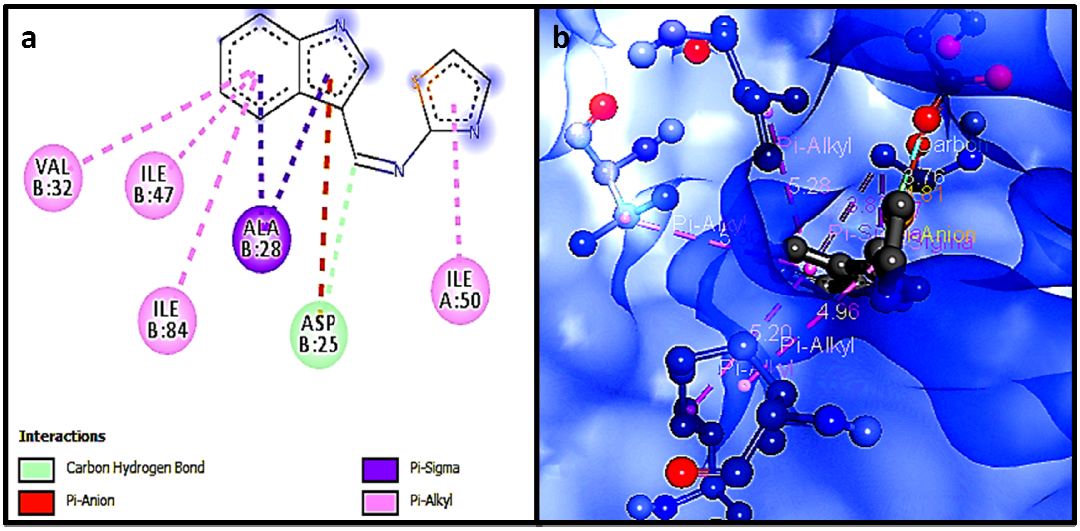

Fig. 2.33: (**a**) 2D and (**b**) 3D interaction diagrams of I3A2AT with HIV-1 protease

I3A2AT-1mui Complex

I3A2AT-**1mui** complex showed a binding energy of -6.7kcal/mol. As given in the Fig. 2.33 the thiazole derivative I3A2AT forms a stabilized binding conformation by hydrogen bonding, hydrophobic and electrostatic interactions. I3A2AT established one carbon- hydrogen bonding interaction within the indole ring moiety and Asp25 whereas electrostatic π-anion interaction is formed between Asp25 and indole ring moiety of this

molecule. Additionally, the azomethine linkage formed a carbon-hydrogen bonding with Asp25. The complex is surrounded by pi-sigma hydrophobic interactions (Ala28, Val32, Ile47, Ile84 and Ile50) as depicted Fig. 2.33

T2CDACH-1mui Complex

The complex of thiophene based Schiff base T2CDACH with **1mui** receptor shows a binding energy of -7.0kcal/mol and showed strong interactions. T2CDACH shows two types of hydrophobic interactions (alkyl and pi- alkyl) with Ala28, Ile47, Val82 and Ile50.

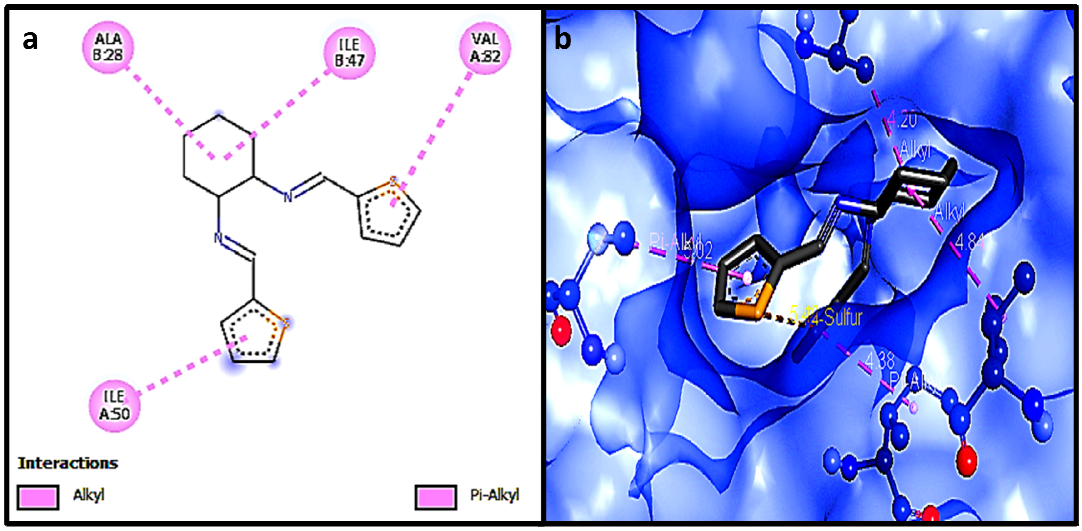

Fig. 2.34: (**a**) 2D and (**b**) 3D interaction diagrams of T2CDACH with HIV-1 protease

Thus according to *in silico* studies, it can be concluded that all seven 'S'containing Schiff bases are potential inhibitors of HIV-1 protease and may hinder the HIV life cycle in human beings. Among the studied molecules, the polynuclear thiadiazole derivative of Schiff base ANNPTDA show appreciable binding affinity -11.4 kcal/mol. The other polynuclear derivative A9CNPTDA and the pyridine derivative 3APNPTDA exhibit binding affinity of -10.7kcal/mol with stabilizing suitable interactions with active pockets of main protease receptor **1mui**. The binding affinities of

studied molecules follows the order ANNPTDA > A9CNPTDA ~ 3APNPTDA > 2APNPTDA > P2CNPTDA ~ T2CDACH > I3A2AT.

Table 2.12: Binding energies and interactions of seven novel 'S' containing heterocyclic Schiff bases with HIV-1 protease (PDB code: **1mui**)

Schiff base	B.E*(ΔG)	Category of interaction	Type of interactions	Amino acid residues
A9CNPTDA	-10.7	Hydrogen bonding	HB*	Ile50, Asp29, Asp30
			C-H bonding (NHB*)	Gly49
		Hydrophobic	π –donor	Asp29, Ile50
			π – sigma	Ala29, Ile50
			π – alkyl	Ile50, Ala28, Ile 84, Ala28, Ile84
		Electrostatic	π –anion	Asp29, Asp25
P2CNPTDA	-8.6	Hydrogen bonding	HB*	Asp29, Asp30
			C-H bonding (NHB*)	Gly29
		Hydrophobic	π -sigma	Ala28
			π – alkyl	Ile50, Ala28, Ile84, Ile50, Ile47
3APNPTDA	-10.7	Hydrogen bonding	HB*	Ile50, Asp29, Asp30
			C-H bonding (NHB*)	Gly49
		Hydrophobic	π – donor	Asp29, Ile50
			π – sigma	Ala28, Ile50
			π –alkyl	Ala28, Ile84, Ile50
		Electrostatic	π- anion	Asp29, Asp25
2APNPTDA	-8.7	Hydrogen bonding	HB*	Asp29,Asp30
		Electrostatic	π – anion	Asp25
		Hydrophobic	π –sigma	Ala28
			Alkyl	Ile47, 1le50, Ala28, Ile84
ANNPTDA	-11.4	Hydrogen bonding	HB*	Asp29, Asp30
			C-H bonding	Gly49
		Hydrophobic	Alkyl	Ala28
			π –alkyl	Ala8, Ile47, Ile50, Ile50, Ile50, Ala28, Ile84
		Electrostatic	π –anion	Asp25
I3A2AT	-6.7	Hydrogen bonding	C-H bonding (NHB*)	Asp25
		Hydrophobic	π- sigma	Ala28, Val32,Ile47, Ile84,Ile50
		Electrostatic	π -anion	Asp25
T2CDACH	-7.0	Hydrophobic	alkyl	Ala28, Ile47
			π- alkyl	Val82, Ile50

B.E* Binding Energy in kcal/mol; HB* Conventional H bond; NHB* Non-Conventional H-bond

SECTION-III

MOLECULAR DOCKING STUDIES OF HER2 PROTEASE (BREAST CANCER) WITH SULPHUR CONTAINING SCHIFF BASES

The chance for breast cancer has been increased in this developing world due to the increased life expectancy, urbanization and adoption of western lifestyles. Breast cancer is a life threatening disease where breast cells grow out of control. Earlier diagnosis and proper medications helps to reduce the risk chances of breast cancer. Failure in proper strategies taken by health systems in breast cancer incidence is relatively low and the majority of women are diagnosed in late stages where they are not provided by adequate awareness about the symptoms, earlier diagnosis and treatment. In our work we keenly focuses on adopting structure based drug designing in order to determine the suitable therapeutic specifics. Presently we had developed seven sulphur based Schiff bases A9CNPTDA, P2CNPTDA, 3APNPTDA, 2APNPTDA, ANNPTDA, I3A2AT and T2CDACH. HER2 protease considered as the target protein due to its gene overexpression which leads to deadly tumour cell growth and breast cancer. X-ray crystal structure of HER2 Kinase complexed with TAK-285 was obtained from protein database bank (PDB code: **3rcd**) selected as the suitable target for this study.

A9CNPTDA-3rcd Complex

Firstly, the complex, HER2 protease-A9CNPTDA complex exhibits binding energy of -9.4kcal/mol. Stable and energetically favourable ligand-receptor conformations with better interactions contribute to the ligand efficiency on binding with the receptor. In the spatial orientation of the compound, A9CNPTDA showed two hydrogen bonds and several hydrophobic interactions. Asn764 and Asp863 residues formed conventional hydrogen bonds and C-H bonding interactions with the compound. Anthracene ring system formed hydrophobic π-π T shaped interaction with Phe864

residue whereas benzene ring made π–sigma interaction with Ile767 residue and these interactions intensified the stability of A9CNPTDA–receptor complex (Fig. 2.35).

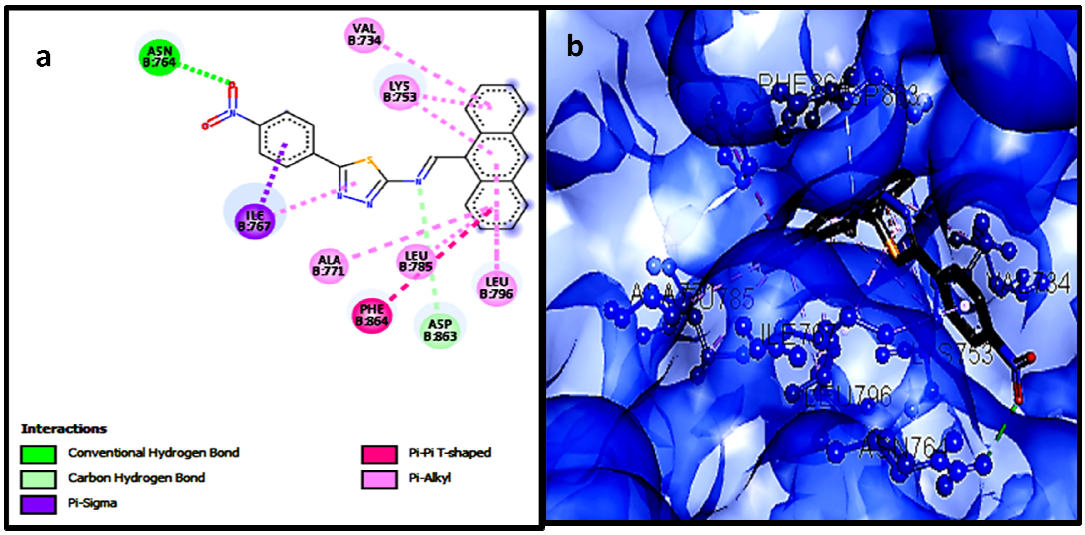

Fig. 2.35: (**a**) 2D and (**b**) 3D interaction diagrams of A9CNPTDA with HER2 protease

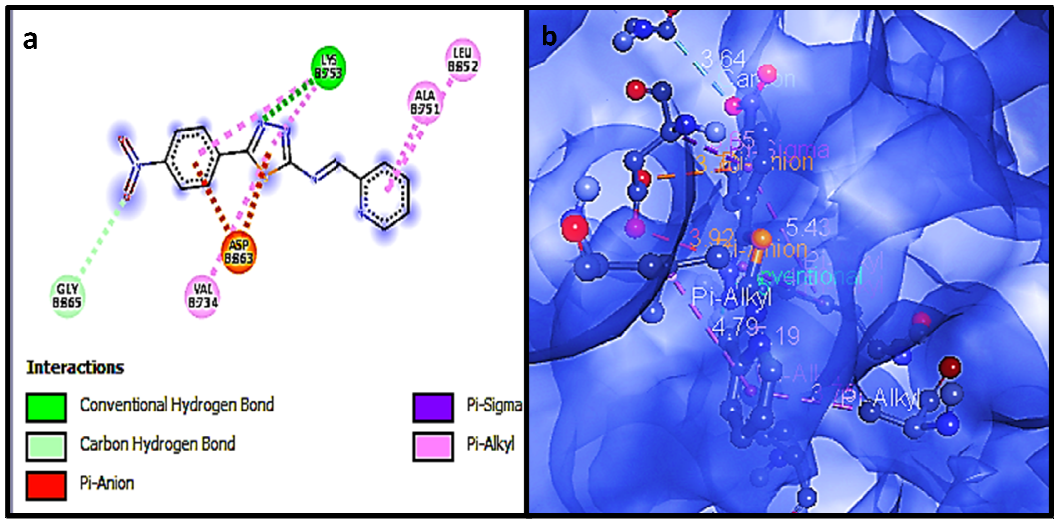

Fig. 2.36: (**a**) 2D and (**b**) 3D interaction diagrams of P2CNPTDA with HER2 protease

P2CNPTDA-3rcd Complex

The complex formed between P2CNPTDA and **3rcd** was stabilized with a binding energy of -7.0 kcal/mol. Stabilization of the complex is attained by several interactions, most commonly, hydrogen bonding, hydrophobic and electrostatic interaction. In the complex, nitrogen atom of thiadiazole ring system interacts with Lys753 and nitro group attached to benzene ring establishes a bond with active Gly865.

Further stabilization is initiated by the electrostatic interaction which is formed between benzene ring and thiadiazole ring with the active Asp863, whereas, Ala751, Val734 and Leu852 residue also involved in hydrophobic interaction with benzene rings as given in Fig. 2.36.

3APNPTDA-3rcd Complex

In the complex, 3APNPTDA-**3rcd**, involves three types of interactions where clearly visible and it was they are stabilized with binding energy of -8.2kcal/mol. As in Fig. 2.37 active Gly865 residue established a bond with nitro group attached to benzene nucleus, while Lys753, Val734, Ala751 and Leu852 surrounds the ligand molecule with hydrophobic interactions mostly by alkyl and pi-alkyl interactions. Additionally, electrostatic π-anion interaction with Asp863 is also observed in the molecule.

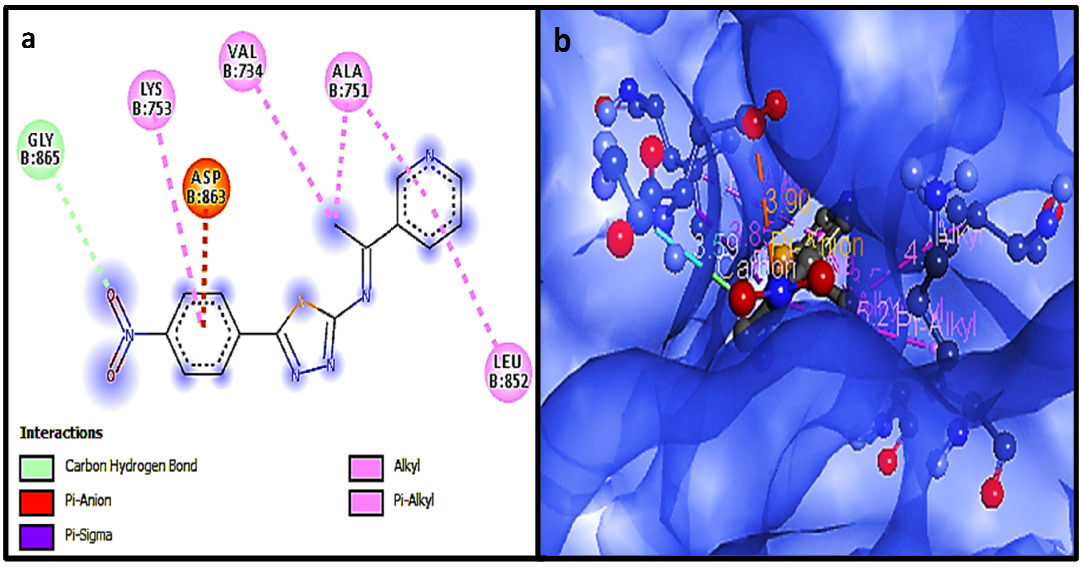

Fig. 2.37: (**a**) 2D and (**b**) 3D interaction diagrams of 3APNPTDA with HER2 protease

2APNPTDA-3rcd Complex

The complex 2APNPTDA-**3rcd** shows similar interactions like 3APNPTDA-**3rcd**. The complex with 2APNPTDA shows stabilized binding energy of -8.3kcal/mol as shown in Fig. 2.38.

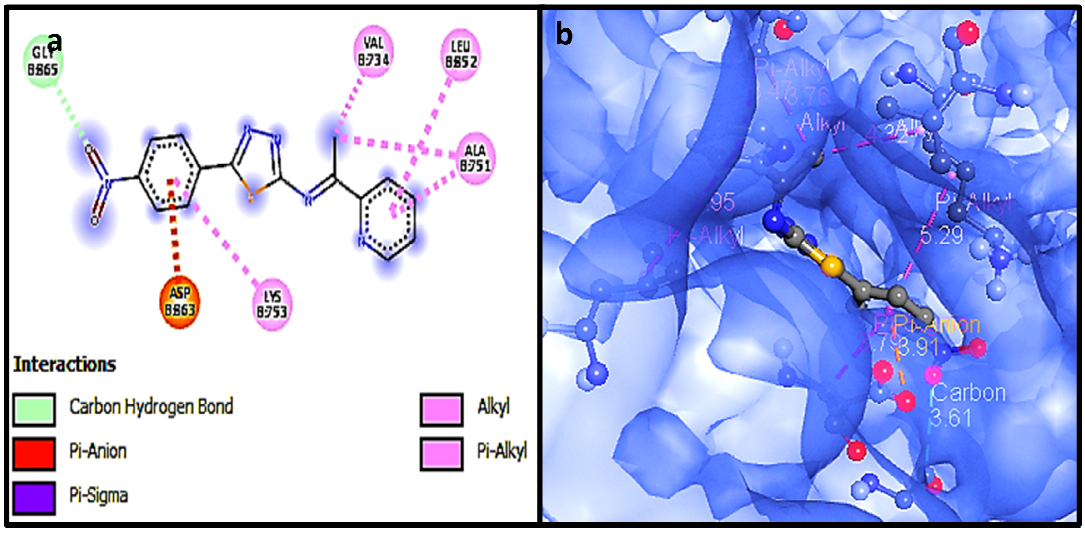

Fig. 2.38: (**a**) 2D and (**b**) 3D interaction diagrams of 2APNPTDA with HER2 protease

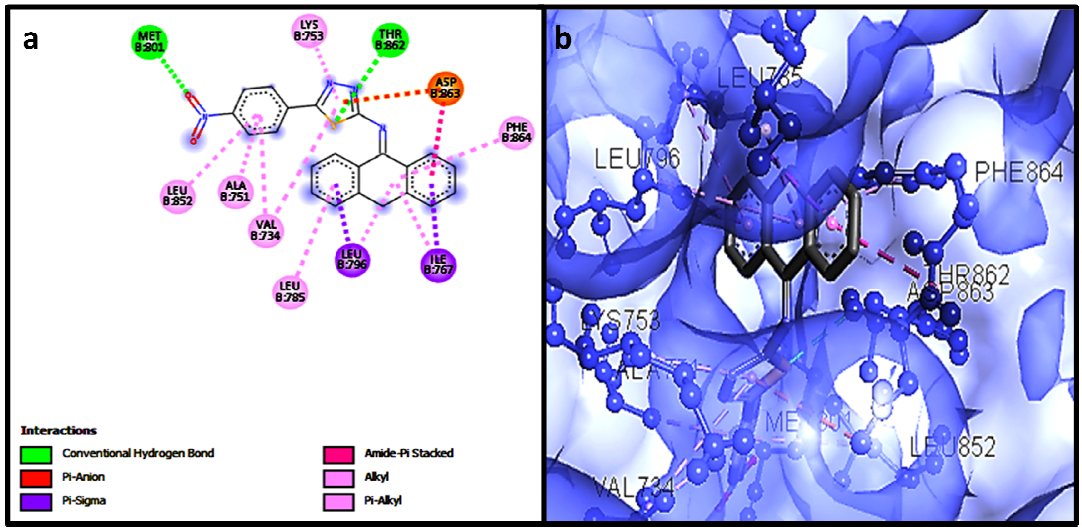

Fig. 2.39: (**a**) 2D and (**b**) 3D interaction diagrams of ANNPTDA with HER2 protease

ANNPTDA-3rcd Complex

ANNPTDA-HER2 protease complex consisted of two conventional hydrogen bonding interactions. Nitro group and oxygen atom of thiadiazole moiety participated in H-bonding with amino acid residues Met801 and Thr862. Fig. 2.39 (a & b), depicts the structure of ligand-receptor complexes and it is revealed that the complex structure includes an exceptional hydrophobic amide π- stacked interaction of thiadiazole ring system with the Asp863 residue. Anthrone ring system was surrounded by Ile767 and

Leu796 residues through π–sigma interactions. Similarly, the benzene and anthrone rings participated in other hydrophobic alkyl and π–alkyl interactions with the amino acid residues. Interactions of all studied Schiff bases are represented in Table 2.13. The involvement of π–alkyl, alkyl, and amide π-stacked interactions enhanced the stability of the ANNPTDA-HER2 protease complex.

I3A2AT-3rcd Complex

Complex formed between I3A2AT and **3rcd** involves several interactions where they are stabilized with a binding energy of -7.0 kcal/mol. Mostly the complex involves electrostatic and hydrophobic interactions. Here active Lys753 residue in the target receptor protein establishes a pi-cation electrostatic interaction while Ile767, Ala771, Leu796 and Leu785 surround the ligand by π-alkyl hydrophobic interaction. Further stabilisation of complex was initiated by pi-pi-T-shaped interaction with active Phe864 residue as shown in Fig. 2.40.

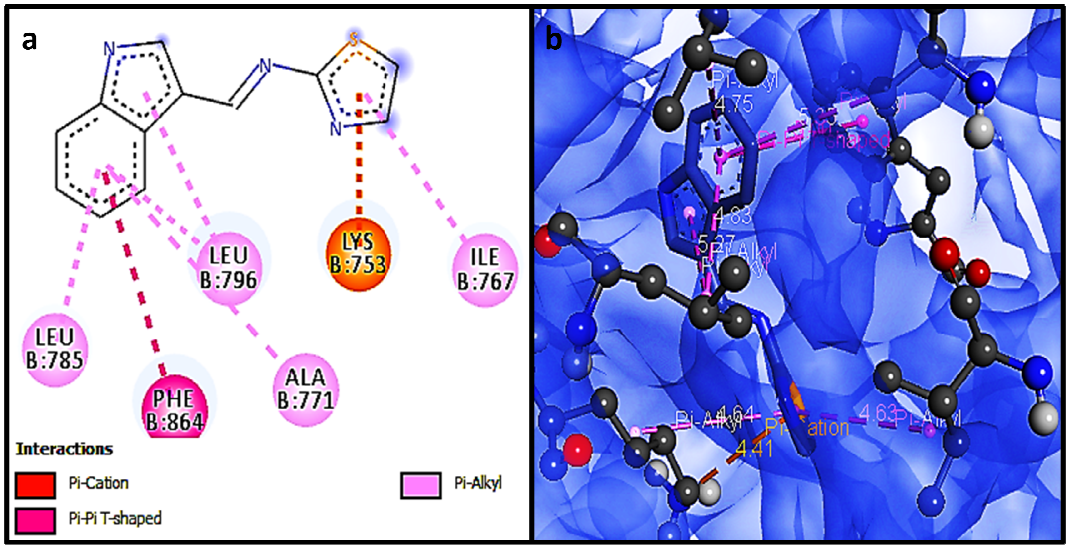

Fig. 2.40: (**a**) 2D and (**b**) 3D interaction diagrams of I3A2AT with HER2 protease

T2CDACH-3rcd Complex

Three different interactions exist in the complex T2CDACH-**3rcd** which is stabilized with a binding energy of -6.5 kcal/mol. Similar to other complexes analysed,

the complex T2CDACH-**3rcd** involves a hydrogen bonding interaction which is established between azomethine group and Ser792. While active Glu717 residue involves in pi-anion interaction in addition to hydrophobic interaction as shown in Fig. 2.41. As per the results, the above series of Schiff bases, found to exhibit remarkable binding affinities with stable conformations which indicate their potential ability to inhibit HER2 protease involved in breast cancer metabolism. Hence the compounds may be considered for therapeutic studies for breast cancer.

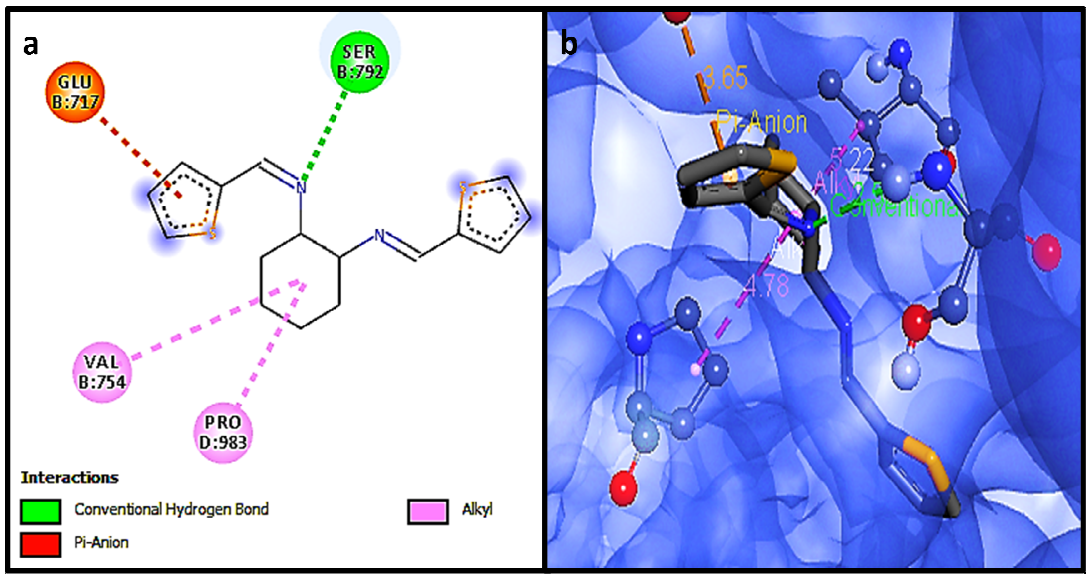

Fig. 2.41: (**a**) 2D and (**b**) 3D interaction diagrams of T2CDACH with HER2 protease

Polynuclear thiadiazole derivative of Schiff base ANNPTDA show significant binding affinity -10.8kcal/mol. The other polynuclear derivative A9CNPTDA exhibit binding affinity of -9.4 kcal/mol with stabilizing suitable interactions with active pockets of HER2 protease. The binding affinities of studied Schiff base molecules follows the order ANNPTDA > A9CNPTDA > 2APNPTDA > 3APNPTDA > P2CNPTDA ~ I3A2AT > T2CDACH

Table 2.13: Binding energies and interactions of seven novel 'S containing heterocyclic Schiff bases with HER2 protease (PDB code: **3rcd**)

Schiff base	B.E*(ΔG)	Category of interaction	Types of interactions	Amino acid residue
A9CNPTDA	-9.4	Hydrogen bonding	HB*	Asn764
			C-H bonding (NHB*)	Asp863
		Hydrophobic	π – sigma	Ile767
			π –π T shaped	Phe864
			π – alkyl	Ile764, Lys753, Leu796, Ala771, Leu785, Val734
P2CNPTDA	-7	Hydrogen bonding	HB*	Lys753
			C-H bonding (NHB*)	Gly865
		Electrostatic	π-anion	Asp863
3APNPTDA	-8.2	Hydrogen bonding	C-H bonding	Gly865
		Electrostatic	Pi anion	Asp863
		Hydrophobic	π –sigma	Asp863
			Alkyl	Ala751, Val734
			π –alkyl	Ala751, Leu852, Lys753
2APNPTDA	-8.3	Hydrogen bonding	C-H bonding (NHB*)	Gly865
		Electrostatic	π-anion	Asp863
		Hydrophobic	π –sigma	Asp863
			Alkyl	Ala751, Val734
			π –alkyl	Ala751, Leu852, lys753
ANNPTDA	-10.8	Hydrogen bonding	HB*	Met801, Thr862
		Hydrophobic	π – sigma	Ile67, Leu796
			Alkyl	Ile767, Leu796
			Amide π – stacked	Asp863
			π –alkyl	Phe864, Leu785, Val 764, Lys753, Val 734, Ala751, Leu852
		Electrostatic	π – anion	Asp863
I3A2AT	-7	Electrostatic	π – cation	Lys753
		Hydrophobic	π – π- T-shaped	Phe864
			π –alkyl	Leu796, Ala771, leu785, Lys753, Ile767
T2CDACH	-6.5	Hydrogen bonding	HB*	Ser792
		Electrostatic	π – anion	Glu717
		Hydrophobic	Alkyl	Val754, pro983

B.E* Binding Energy in kcal/mol; HB* Conventional H bond; NHB* Non-Conventional H-bond

SECTION-IV

MOLECULAR DOCKING STUDIES OF ACETYLCHOLINESTERASE (ALZHEIMER'S DISEASE) WITH SULPHUR CONTAINING SCHIFF BASES

Alzheimer's disease is an irreversible, progressive brain disorder which adversely affects the cognitive functioning in human being by gradual memory loss which interfere the daily routine. This disease leads to the losing of thinking skills, remembering, reasoning and behavioural abilities. From recent studies carried out, it is caused due to the combination of genetics, environmental and lifestyle. Most commonly, disease symptoms are exhibited at the age of 60s. Currently, there is no appropriate treatment available for Alzheimer's disease but proper medications can be provided to reduce the symptoms in Alzheimer's patients. Based on earlier studies, the researchers are engaged in developing cholinesterase inhibitors that might reduce the cognitive dysfunctioning in Alzheimer's patients. In our studies we had extensively established the chances of developing cholinesterase inhibitors where they are sulphur based Schiff bases. As from the initial studies, we had keenly accessed humanacetylcholinesterase (AChE) complexed with fasciculin-ii, glycosylated protein by using PDB code: **1b41** as target receptor. Our studies directs towards the interactions established between each Schiff bases with the acetylcholinesterase enzyme when they are taken for molecular docking treatment and thereby the druggability to Schiff bases are analysed.

A9CNPTDA-1b41 Complex

Binding interactions of acetylcholinesterase (**1b41**) with these novel 'S' containing Schiff bases showed that the compound A9CNPTDA possesses highest binding energy. Here, A9CNPTDA-acetylcholinesterase complex showed binding energy of -7.9kcal/mol with three hydrogen bonding interactions. Nitro group and

azomethine moiety formed one conventional hydrogen-bonding interaction with ArgA247 and two non-conventional H-bonding interactions in the Arg A296 and Gln A291 residues. Additionally, thiadiazole ring made π–sigma hydrophobic interactions, whereas the benzene groups present in the compound were stabilized by electrostatic interactions with two amino acid residues, Glu A243 and Arg A247 which have led to extra stability and binding strength of the complex, as illustrated in Fig. 2.42 (a & b).

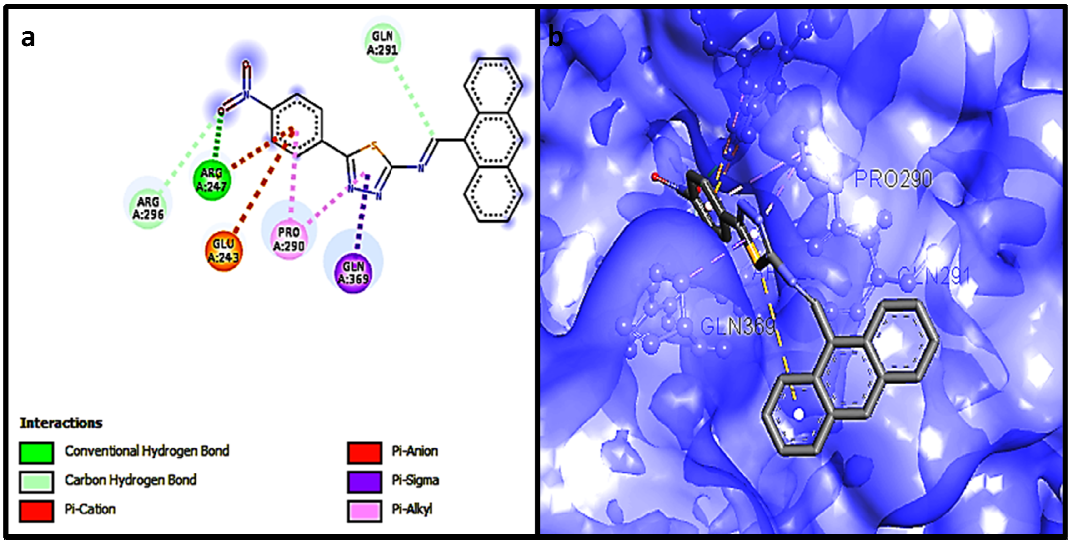

Fig. 2.42: (**a**) 2D and (**b**) 3D interaction diagrams of A9CNPTDA with acetylcholinesterase

P2CNPTDA-1b41 Complex

The complex P2CNPTDA-**1b41** as shown in Fig. 2.43, was stabilized with a binding energy of -6.3 kcal/mol. However, the complex involves several number of interactions that ensures stability. This complex, P2CNPTDA- **1b41** involves a hydrogen bonding. Here the conventional hydrogen bonding interactions were established in between the nitro group attached to the benzene ring and active Ala127 and Tyr133 residues. Sulfur present in the thiadiazole ring interacts with the active Tyr124 residue of the receptor. Specially, a pi-donor hydrogen bond is made within thiadiazole ring moiety of ligand and Phe295 residue of the target receptor. Further stabilization is attained by

the pi-sulfur and sulfur-x interaction made along with amide-pi- stacked and pi-alkyl interactions.

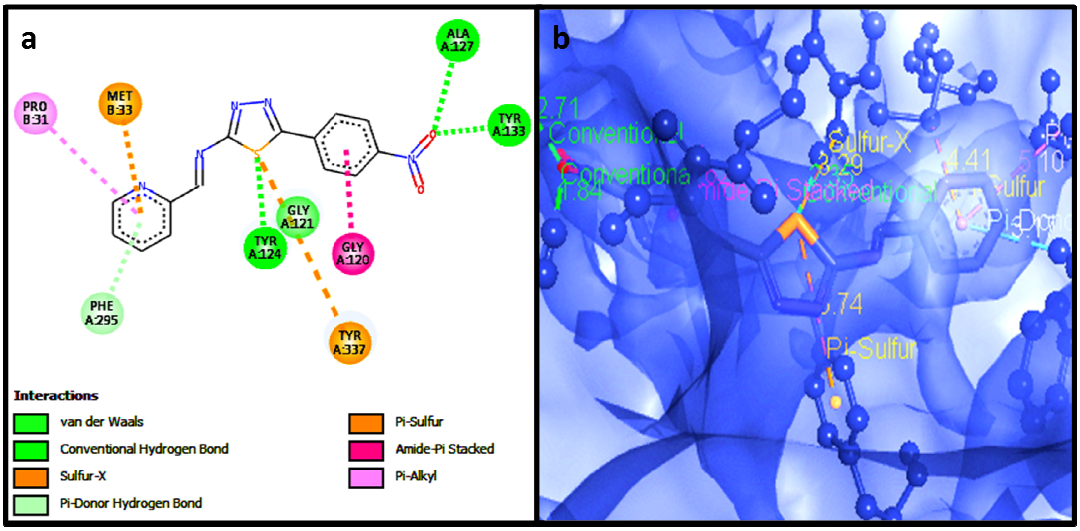

Fig. 2.43: (**a**) 2D and (**b**) 3D interaction diagrams of P2CNPTDA with acetylcholinesterase

3APNPTDA-1b41 Complex

3APNPTDA interacted with **1b41** and displayed a binding energy -5.8kcal/mol and stabilized by conventional hydrogen bonding and carbon- hydrogen bonding. Here three conventional hydrogen bonding is made by the nitro group attached to the benzene ring moiety and sulphur atom present in the thiadiazole ring moiety (Arg296, Gln369 and Arg247). Arg247 residue involves in pi-cation electrostatic interaction. Additionally, two hydrophobic interactions were involved in the complex as shown in Fig. 2.44

2APNPTDA-1b41 Complex

As in Fig.2.45, the complex, 2APNPTDA-**1b41** exhibited binding energy of -5.8 kcal/mol. Here, the complex involves two hydrogen bonding and two hydrophobic interactions. The nitro group attached to the benzene ring moiety of the ligand established a conventional hydrogen bond with active Arg296 residue of the receptor. Whereas Gln369 and Pro290 residue establishes a pi-sigma and pi-alkyl interactions respectively.

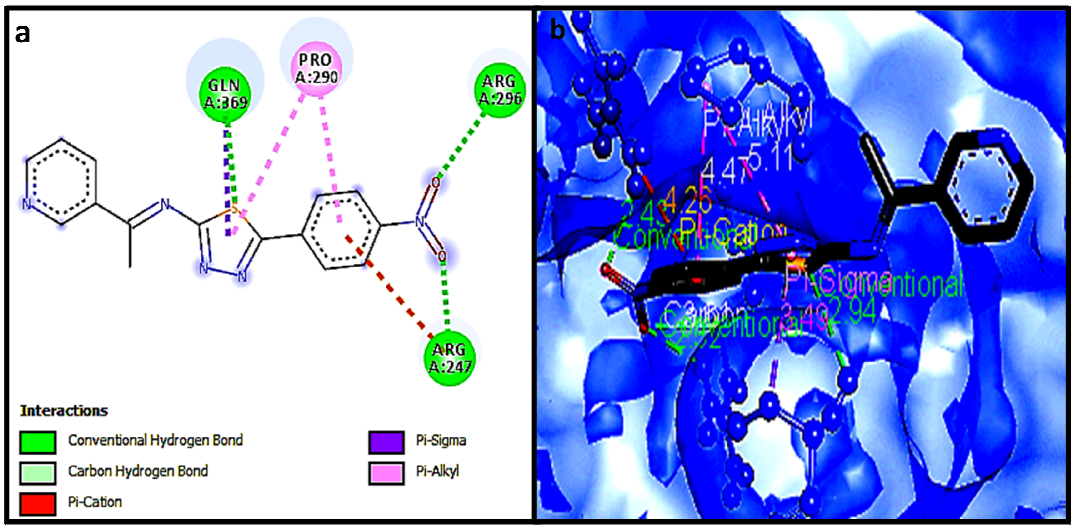

Fig. 2.44: (**a**) 2D and (**b**) 3D interaction diagrams of 3APNPTDA with acetylcholinesterase

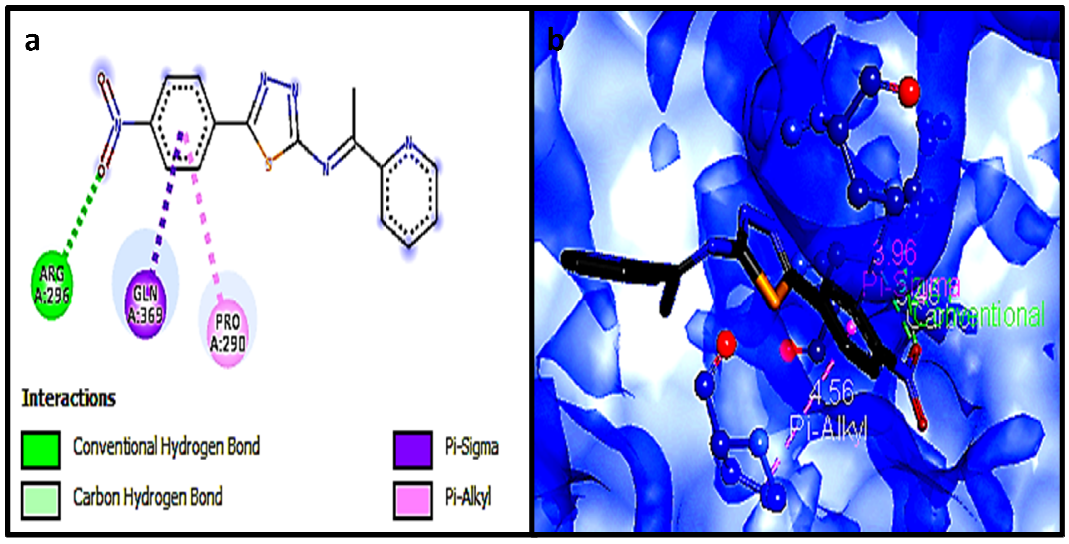

Fig. 2.45: (**a**) 2D and (**b**) 3D interaction diagrams of 2APNPTDA with acetylcholinesterase

ANNPTDA-1b41 Complex

ANNPTDA-acetylcholinesterase complex displayed binding energy of -7.1 kcal/ mol with two hydrogen-bonding interactions. In this complex, the nitro group present in the compound made conventional hydrogen bonding interactions and C-H bonding with Arg296 residue (Table 2.14). Mostly, anthracene ring involved in hydrophobic (π–sigma and π–alkyl) with Gln291, whereas benzene rings involved in electrostatic

interaction with Glu292, as shown in Fig. 2.46 (a & b). Involvement of such interactions stabilized the conformations of the ANNPTDA-acetylcholinesterase complex. From these results, it is inferred that both the compounds fairly inhibited the growth of AChE. *In vivo* toxicological studies and clinical trials have to be performed to claim the actual drug ability of these molecules against Alzheimer's disease.

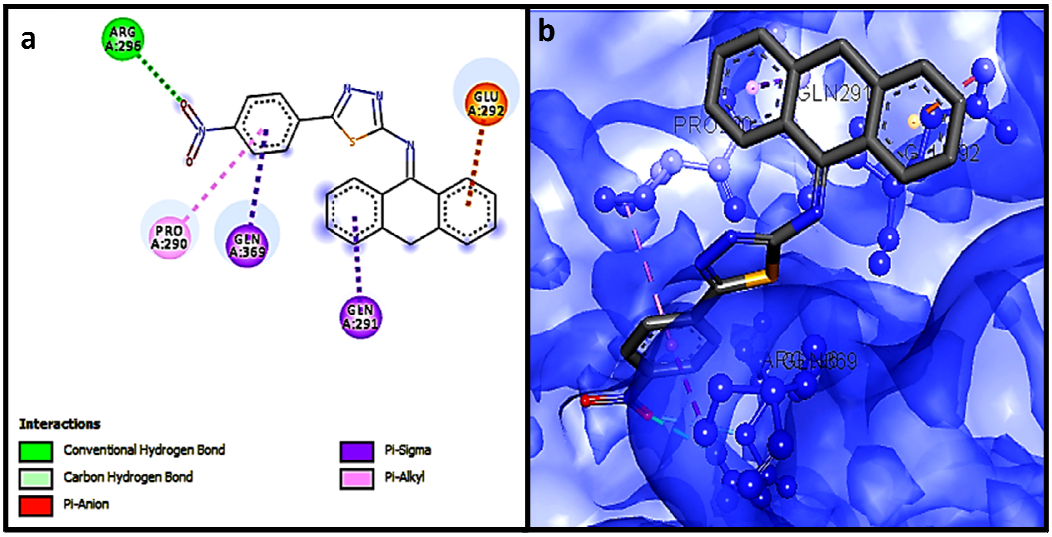

Fig. 2.46: (**a**) 2D and (**b**) 3D interaction diagrams of ANNPTDA with acetylcholineesterase

I3A2AT-1b41 Complex

I3A2ATshowed an excellent interaction with **1b4**1 and displayed binding energy (-8.3 kcal/mol) which was higher than among six Schiff bases (Fig. 2.47 (a and b)). It involved sufficient number of interaction that supports its stability. Most commonly ligand, I3A2AT made hydrogen bonding interaction (conventional and C-H bonding) with Gly121, Ser203 and Tyr337. While Trp86, His447, Tyr124 and Tyr341 active residues formed pi-pi-T-shaped interactions along with pi-cation electrostatic interaction. Additionally, the complex involves other strong interactions, like pi- sulphur interaction with active residues, Tyr124, Phe297 and Phe338.

T2CDACH- 1b41 Complex

Certainly, in complex T2CDACH- **1b41** (Fig. 2.48 (a and b)) exhibits binding energy of -7.2kcal/mol. Here the complex involved three pi-alkyl hydrophobic interactions (Tyr337, Pro31 and Met33) along with the π-sulphur interactions (Phe297 and Tyr124).

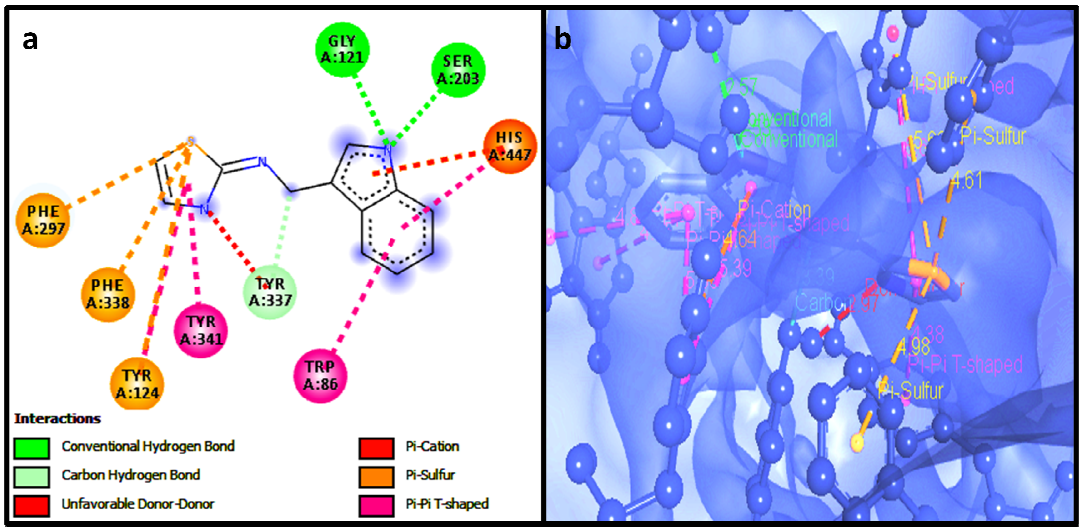

Fig. 2.47: (**a**) 2D and (**b**) 3D interaction diagrams of I3A2AT with acetylcholinesterase

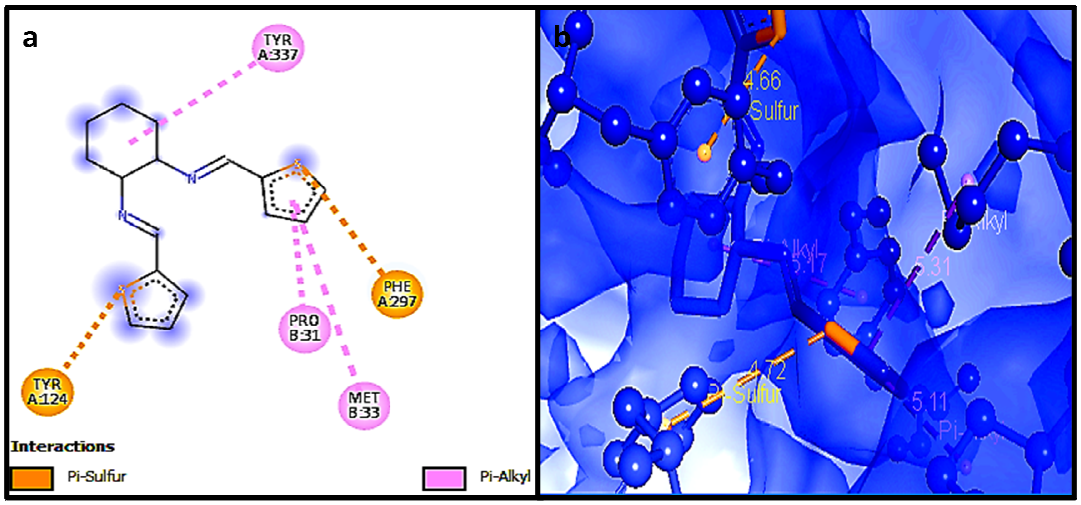

Fig. 2.48: (**a**) 2D and (**b**) 3D interaction diagrams of T2CDACH with acetylcholinesterase

Among other complexes, the complex, I3A2AT-AChE shows a greater binding energy (-8.3kcal/mol) and with higher stability from molecular docking studies. Here the

stability of the complex is due to the hydrogen bonding and non-hydrogen bonding interactions. The binding affinities of studied Schiff base molecules follows the order I3A2AT > A9CNPTDA > T2CDACH > ANNPTDA > P2CNPTDA > 3APNPTDA ~ 2APNPTDA.

Table 2.14: Binding energies and interactions of seven novel 'S' containing heterocyclic Schiff bases with Acetylcholinesterase (AChE) (PDB code: **1b41**)

Schiff base	B.E*(ΔG)	Category of interaction	Types of interactions	Amino acid residue
A9CNPTDA	-7.9	Hydrogen bonding	HB*	Arg247
			C-H bonding (NHB*)	Arg296, Gln291
		Hydrophobic	π – sigma	Gln369
			π – alkyl	Pro290
		Electrostatic	π – anion	Glu243
			π – cation	Arg247
P2CNPTDA	-6.3	Hydrogen bonding	HB*	Tyr124, Ala127, Tyr133
			π-donor H- bonding (NHB*)	Phe295
		Hydrophobic	Amide-π stacked	Gly120, Gly121
			π – alkyl	Pro31
3APNPTDA	-5.8	Hydrogen bonding	HB*	Arg247, Arg296, Gln369
			C-H bonding (NHB*)	Arg296
		Electrostatic	π – cation	Arg247
		Hydrophobic	π – sigma	Gln369
			π – alkyl	Pro290
2APNPTDA	-5.8	Hydrogen bonding	HB*	Arg296
			C-H bonding (NHB*)	Arg296
		Hydrophobic	π – sigma	Gln369
			π – alkyl	Pro290
ANNPTDA	-7.1	Hydrogen bonding	HB*	Arg296
			C-H bonding (NHB*)	Arg296
		Hydrophobic	π – sigma	Gln369, Gln291
			π –alkyl	Pro290
		Electrostatic	π – anion	Glu292
I3A2AT	-8.3	Hydrogen bonding	HB*	Gly121, Ser203
			C-H bonding (NHB*)	Tyr337
		Hydrophobic	π – π – T shaped	Trp86, His447, Tyr124, Tyr341
		Electrostatic	π – cation	His447
		Other	π – sulphur	Tyr124, Phe297, Phe338
T2CDACH	-7.2	Hydrophobic	π – alkyl	Tyr337, Pro31, Met33
		Other	π – sulphur	Phe297, Tyr124

B.E* Binding Energy in kcal/mol; HB* Conventional H bond; NHB* Non-Conventional H-bond

SUMMARY

In present work, the seven novel 'S' containing Schiff bases, examined for Lipinski's rule of five to verify the druglikeness followed by structure based molecular docking studies. *In vitro* antibacterial activity of these novel Schiff bases and their transition metal complexes were analysed in the solvent (DMSO) with different concentrations of 50µgdisc^{-1}, 200µgdisc^{-1} and 500µgdisc^{-1}. Their antibacterial performances were compared with the inhibition efficiency of standard antibiotics like Vancomycin, Erythromycin, Chloramphenicol, Streptomycin, Tetracycline, Ampicillin and Gentamicin. Except few, almost all 'S' containing Schiff bases and their transition metal complexes showed remarkable antibacterial performance against the studied pathogens.

The polynuclear thiadiazole derivative of Schiff base A9CNPTDA showed appreciable results against gram-positive pathogen *S. aureus and g*ram-negative pathogens *K. pneumonia, E. coli* and *P. vulgaris*. Results obtained for this ligand was comparable to the standard antibiotic Vancomycin. All metal chelates of A9CNPTDA demonstrated exhibited significant antibacterial activities against all the studied microbes. Mn(II) complex of this heterocyclic ligand was notably active against the growth of the *K. pneumonia* which was comparable to the growth preventing efficiency of standard antibiotics such as Vancomycin, Tetracycline, Chloramphenicol, Gentamicin and Ampicillin. Another polynuclear Schiff base ANNPTDA displayed high activity towards *B. subtilis* and *K. pneumonia*. A zone of inhibition (23mm) was exhibited by Mn(II) complex against the bacterial strain *B. subtilis* and showed slightly higher activity (23.5mm) against *K. pneumonia* at a concentration of 500µgdisc^{-1} compared to other metal complexes. Among pyridine derivatives of Schiff bases, P2CNPTDA showed enhanced antibacterial performance against gram-positive pathogen *B. subtilis* and two

gram-negative pathogens *K. pneumonia* and *E. coli.* P2CNPTDA-Cd^{2+} complex showed superior antibacterial activity against *Staphylococcus aureus and G*ram-negative pathogens *K. pneumonia* and *E. coli* which was comparable and higher than the standard antibiotics such as Vancomycin, Erythromycin and Chloramphenicol, Tetracycline, Ampicillin, Gentamicin etc. At 500 µgdisc^{-1} the Schiff base complex derived from 3-acetyl pyridine, 3APNPTDA-Zn^{2+} displayed excellent antibacterial activity (Zone of inhibition: 27 mm) against *K. pneumonia* and appreciable activity against *S. aureus.* The highest antibacterial action has been observed for 2APNPTDA-Zn^{2+} complex against *K. pneumonia* (24mm at 500 µgdisc^{-1}).

The Cu(II) complex I3A2AT showed the highest activity against *S. aureus* and *E. coli.* Thiophene derivative of Schiff base ligand T2CDACH and its transition metal complexes established abilities to hinder growth of bacteria. The ligand T2CDACH have high zone of inhibition against the bacterial strain *P. vulgaris* and inactive against *K. pneumonia.* The diameter of growth zone inhibition values of Mn(II) and Cu(II) complexes were comparable with the growth inhibition values of standard antibiotics like Vancomycin, Tetracyclin towards microorganism *S. aureus* at every concentration

Inhibition competency of these Schiff bases on the target proteins of SARS CoV-2 main protease (PDB code: **6lu7**), HIV-1 protease (PDB code: **1mui**), human epidermal growth factor receptor, HER2 protease (PDB code: **3rcd**) and human acetyl cholinesterase (AChE) (PDB code: **1b41**) which are crucially involved in the diseases, Severe Acute Respiratory Syndrome**-**2 (COVID-19), HIV/AIDS, Breast cancer and Alzheimer's diseases respectively. Stability of protein-ligand complex was evaluated based on (i) B.E and (ii) Number of interactions with active site residues. Three-dimensional binding conformation, binding energy and non bonding interactions of ligand on target proteins were evaluated by a docking technique using Autodock and

Discovery studio software. Studies revealed the efficiency of these molecules on receptor proteins of Covid-19, HIV, Breast cancer and Alzheimer's disease. Analyzed complexes formed between the protein entities with Schiff bases has shown stronger interactions which decides the stability of complexes. The druglikeness of these Schiff bases was also studied and these molecules shows high druggability. Results were analyzed and reported in each section. Section I discusses the disease, Severe Acute Respiratory Syndrome-2 caused by SARS-CoV-2 (Covid 19). Main protease as target protein accessed from protein database bank with their PDB code **6lu7** is selected for the study. The complex formed between ANNPTDA and target protein is highly stable with greater binding energy (-8.4 kcal/mol) with greater number of interactions from docking studies. The other polynuclear Schiff base, A9CNPTDA also show appreciable binding affinity (-8.3kcal/mol) with stabilizing suitable interactions with active pockets of main protease receptor, leading to the dysfunctioning of target protein leading to the interfering of the viral life cycle in the host cell and which can be further analysed by clinical trials. The binding affinities of ligands follows the order ANNPTDA > A9CNPTDA > 3APNPTDA ~ P2CNPTDA ~ T2CDACH > 2APNPTDA > I3A2AT.

Molecular docking studies of HIV-1 protease (PDB code**: 1mui**) complexed with the Schiff bases are narrated in section II. Studies concluded that the complexes with HIV-1 protease and Schiff bases ANNPTDA, A9CNPTDA and 3APNPTDA possess greater stability with higher binding energies of -11.4kcal/mol and -10.7kcal/mol respectively and these complexes show greater number of interactions. Hence such interactions established between the target protein HIV-1 protease and Schiff bases would inhibit the right functioning of this protein. So continually it would minimize the viral infection which leads to acute immunodeficiency syndrome. The binding affinities of Schiff base molecules follows the order ANNPTDA > A9CNPTDA ~ 3APNPTDA >

2APNPTDA > P2CNPTDA ~ T2CDACH > I3A2AT

Section III, discuss of breast cancer and molecular docking of target protein, HER-2 with Schiff bases. Overexpression of the HER2 protein (PDB code**: 3rcd**) leads to breast cancer. So this protein is widely considered a target protein for drug interaction and for discovering specific medications for breast cancer treatment. It is concluded that the complex HER2–ANNPTDA shows great binding energy (-10.8kcal/mol) with a higher number of hydrogen bonding and non-hydrogen bonding interactions from molecular docking studies. The binding energies of other studied Schiff base molecules follows the order A9CNPTDA > 2APNPTDA > 3APNPTDA > P2CNPTDA ~ I3A2AT > T2CDACH.

In section IV, attempts were made to discuss progressive brain disorder, Alzheimer's disease, most commonly diagnosed in adults. In this section, each complexes, formed between the Schiff bases and target protein, AChE (acetylcholinesterase) were analyzed and reported. Studies revealed that, the complex, I3A2AT-AChE has greater binding energy (-8.3 kcal/mol) and higher stability compared to other complexes. The stability of the complex can be explained due to the reason of strong hydrogen bonding and non-hydrogen bonding interactions. Hence, the compound shows a greater inhibition competency, which widely suggests the chances of being drug-specific for Alzheimer's diseases. The binding affinities of Schiff base molecules with Acetylcholinesterase (AChE) (PDB code: **1b41**) follows the order I3A2AT > A9CNPTDA > T2CDACH > ANNPTDA > P2CNPTDA > 3APNPTDA ~ 2APNPTDA.

The above studies and results revealed that the 'S' containing Schiff bases and their transition metal complexes have wider possibility as suitable therapeutic specifics. Successive clinical trials and extensive studies might explore the vast possibilities of drug discovery.

REFERENCES

[1] A.S. Hassan, A.A. Askar, E.S. Nossier, A.M. Naglah, G.O. Moustafa, M.A. Al-Omar, Antibacterial evaluation, in silico characters and molecular docking of Schiff Bases derived from 5-aminopyrazoles, Molecules. 24 (2019) 3130-3144.

[2] W. Qin, S. Long, M. Panunzio, S. Biondi, Schiff bases: A short survey on an evergreen chemistry tool, Molecules. 18 (2013) 12264–12289.

[3] A. Kajal, S. Bala, S. Kamboj, N. Sharma, V. Saini, Schiff bases: a versatile pharmacophore, J. Catal. 8 (2013)1-14.

[4] K.M. Dawood, T.A. Farghaly, Thiadiazole inhibitors: a patent review, Expert Opin. Ther. Pat. 27 (2017) 477–505.

[5] D. Chan, D. Fass, J. Berger, Kim. PS Core structure of gp41 from the HIV envelope glycoprotein., Cell. 89 (1997) 263–273.

[6] P. Banerjee, O.P. Pandey, S.K. Sengupta, Microwave assisted synthesis, spectroscopic and antibacterial studies of titanocene chelates of Schiff bases derived from 3-substituted-4-amino-5-hydrazino-1,2,4-triazoles, Transit. Met. Chem. 33 (2008) 1047-1056.

[7] Y. Prashanthi, K. Kiranmai, N. Subhashini, others, Synthesis, potentiometric and antimicrobial studies on metal complexes of isoxazole Schiff bases, Spectrochim. Acta. A. Mol. Biomol. Spectrosc. 70 (2008) 30–35.

[8] T. Rosu, E. Pahontu, C. Maxim, R. Georgescu, N. Stanica, A. Gulea, Some new Cu (II) complexes containing an ON donor Schiff base: synthesis, characterization and antibacterial activity, Polyhedron. 30 (2011) 154–162.

[9] A. Jha, Y. Murthy, U. Sanyal, G. Durga, Rapid synthesis, characterization, anticancer and antimicrobial activity studies of substituted thiadiazoles and their dinucleating ligand metal complexes, Med. Chem. Res. 21 (2012) 2548–2556.

[10] L. Lekha, K.K. Raja, G. Rajagopal, D. Easwaramoorthy, Synthesis, spectroscopic characterization and antibacterial studies of lanthanide (III) Schiff base complexes containing N, O donor atoms, J. Mol. Struct. 1056 (2014) 307–313.

[11] M. Salehi, F. Rahimifar, M. Kubicki, A. Asadi, Structural, spectroscopic, electrochemical and antibacterial studies of some new nickel (II) Schiff base complexes, Inorganica Chim. Acta. 443 (2016) 28–35.

[12] H. Keypour, M. Mahmoudabadi, A. Shooshtari, M. Bayat, F. Mohsenzadeh, R.W. Gable, Cadmium (II) macrocyclic Schiff-base complexes containing piperazine moiety: Synthesis, spectroscopic, X-ray structure, theoretical and antibacterial studies, J. Mol. Struct. 1155 (2018) 196–204.

[13] N. Turan, K. Buldurun, Y. Alan, A. Savci, N. Çolak, A. Mantarcı, Synthesis, characterization, antioxidant, antimicrobial and DNA binding properties of ruthenium (II), cobalt (II) and nickel (II) complexes of Schiff base containing o-vanillin, Res. Chem. Intermed. 45 (2019) 3525–3540.

[14] Y. Xu, Y. Shi, F. Lei, L. Dai, A novel and green cellulose-based Schiff base-Cu(II) complex and its excellent antibacterial activity, Carbohydr. Polym. 230 (2020) 115671.

[15] A. Mishra, M. Khare, S. Gautam, Synthesis, physico-chemical characterization, and antibacterial studies of some bioactive Schiff bases and their metal chelates, Synth. React. Inorg. Met.-Org. Chem. 32 (2002) 1485–1500.

[16] Z.H. Chohan, A. Scozzafava, C.T. Supuran, Zinc complexes of benzothiazole-derived Schiff bases with antibacterial activity, J. Enzyme Inhib. Med. Chem. 18 (2003) 259–263.

[17] A. Srivastava, O. Pandey, S. Sengupta, Synthesis, spectral and antimicrobial studies of Bis (cyclopentadienyl) titanium(IV) derivatives with schiff bases derived from 2-Amino-5-phenyl-1, 3, 4-thiadiazole, Bioinorg. Chem. Appl. 3 (2005) 287-297.

[18] H.L. Singh, A. Varshney, Synthetic, structural, and biochemical studies of organotin(IV) with Schiff bases having nitrogen and sulphur donor ligands, Bioinorg. Chem. Appl. 2006 (2006)1-7.

[19] G.G. Mohamed, M.M. Omar, A.M. Hindy, Metal complexes of Schiff bases: preparation, characterization, and biological activity, Turk. J. Chem. 30 (2006) 361–382.

[20] K.S.A. Melha, In-vitro antibacterial, antifungal activity of some transition metal complexes of thiosemicarbazone Schiff base (HL) derived from N4-(7′-chloroquinolin-4′-ylamino) thiosemicarbazide, J. Enzyme Inhib. Med. Chem. 23 (2008) 493–503.

[21] M. Alias, H. Kassum, C. Shakir, Synthesis, spectral, thermal and antibacterial studies of Cd(II), Mn(II) and Fe(III) complexes containing trithiocarbonate 1, 3, 4-thiadiazole moiety, J. King Saud Univ.-Sci. 25 (2013) 157–166.

[22] B. Rai, others, Synthesis, structural, spectroscopic and antibacterial studies of Schiff base ligands and their metal complexes containing nitrogen and sulphur donor atom, Orient. J. Chem. 29 (2013) 1163–1167.

[23] M. Sahani, U. Yadava, O. Pandey, S. Sengupta, Synthesis, spectral characterization and antimicrobial studies of nano-sized oxovanadium (IV) complexes with Schiff bases derived from 5-(phenyl/substituted phenyl)-2-hydrazino-1, 3, 4-thiadiazole and indoline-2, 3-dione, Spectrochim. Acta. A. Mol. Biomol. Spectrosc. 125 (2014) 189–194.

[24] D. Bandyopadhyay, M. Layek, M. Fleck, R. Saha, C. Rizzoli, Synthesis, crystal structure and antibacterial activity of azido complexes of cobalt (III) containing heteroaromatic Schiff bases, Inorganica Chim. Acta. 461 (2017) 174–182.

[25] A.C. Fluit, M.R. Visser, F.-J. Schmitz, Molecular detection of antimicrobial resistance, Clin. Microbiol. Rev. 14 (2001) 836–871.

[26] X.-Y. Meng, H.-X. Zhang, M. Mezei, M. Cui, Molecular docking: a powerful approach for structure-based drug discovery, Curr. Comput. Aided Drug Des. 7 (2011) 146–157.

[27] A. Sethi, K. Joshi, K. Sasikala, M. Alvala, Molecular docking in modern drug discovery: Principles and recent applications, Drug Discov. Dev. New Adv. 4 (2019) 27–39.

[28] S.-Y. Huang, S.Z. Grinter, X. Zou, Scoring functions and their evaluation methods for protein–ligand docking: recent advances and future directions, Phys. Chem. Chem. Phys. 12 (2010) 12899–12908.

[29] C. Gan, L. Zhou, Z. Zhao, H. Wang, Benzothiazole Schiff-bases as potential imaging agents for β-amyloid plaques in Alzheimer's disease, Med. Chem. Res. 22 (2013) 4069–4074.

[30] N. Siddiqui, S.B. Andalip, R. Ali, O. Afzal, M.J. Akhtar, B. Azad, R. Kumar, Antidepressant potential of nitrogen-containing heterocyclic moieties: an updated review, J. Pharm. Bioallied Sci. 3 (2011) 194-217.

[31] M. Wu, J. Ma, L. Ji, M. Wang, J. Han, Z. Li, Design, synthesis, and biological evaluation of rutacecarpine derivatives as multitarget-directed ligands for the treatment of Alzheimer's disease, Eur. J. Med. Chem. 177 (2019) 198–211.

[32] V. Salmaso, S. Moro, Bridging molecular docking to molecular dynamics in exploring ligand-protein recognition process: An overview, Front. Pharmacol. 9 (2018) 923.

[33] C. Gan, L. Zhou, Z. Zhao, H. Wang, Benzothiazole Schiff-bases as potential imaging agents for β-amyloid plaques in Alzheimer's disease, Med. Chem. Res. 22 (2013) 4069–4074.

[34] D. Wrapp, N. Wang, K.S. Corbett, J.A. Goldsmith, C.-L. Hsieh, O. Abiona, B.S. Graham, J.S. McLellan, Cryo-EM structure of the 2019-nCoV spike in the prefusion conformation, Science. 367 (2020) 1260–1263.

[35] M.L. Doss, K. Lalitha, Molecular docking studies of thiazole Schiff's bases as HIV1-protease inhibitors, J Curr Chem Pharm Sci. 1 (2011).

[36] J. Sridhar, M.E. Sfondouris, M.R. Bratton, T.-L.K. Nguyen, I. Townley, C.L.K. Stevens, F.E. Jones, Identification of quinones as HER2 inhibitors for the treatment of trastuzumab resistant breast cancer, Bioorg. Med. Chem. Lett. 24 (2014) 126–131.

[37] R. Ujan, A. Saeed, P.A. Channar, F.A. Larik, Q. Abbas, M.F. Alajmi, H.R. El-Seedi, M.A. Rind, M. Hassan, H. Raza, others, Drug-1, 3, 4-thiadiazole conjugates as novel mixed-type inhibitors of acetylcholinesterase: synthesis, molecular docking, pharmacokinetics, and ADMET evaluation, Molecules. 24 (2019) 860.

[38] A. W Bauer, Antibiotic susceptibility testing by a standardized single disc method, Am J Clin Pathol. 45 (1966) 149–158.

[39] J.H. Mueller, J. Hinton, A protein-free medium for primary isolation of the Gonococcus and Meningococcus, Proc. Soc. Exp. Biol. Med. 48 (1941) 330–333.

[40] N.M. O'Boyle, M. Banck, C.A. James, C. Morley, T. Vandermeersch, G.R. Hutchison, Open Babel: An open chemical toolbox, J. Cheminformatics. 3 (2011) 1–14.

[41] Z. Yuan, L. Yu, Q. Wu, Y. Jiang, W. Yang, Q. Hu, M. Zhang, Synthesis and characterization of novel polynuclear Schiff base compounds containing o-aminobenzoic acid [J], Chem. World. 6 (2009) 1-18.

[42] N. El-Hachem, B. Haibe-Kains, A. Khalil, F.H. Kobeissy, G. Nemer, AutoDock and AutoDock Tools for protein-ligand docking: Beta-site amyloid precursor protein cleaving enzyme 1 (BACE1) as a case study, in: Neuroproteomics, 16 (2017) 391–403.

[43] O. Trott, A.J. Olson, AutoDock Vina: improving the speed and accuracy of docking with a new scoring function, efficient optimization, and multithreading, J. Comput. Chem. 31 (2010) 455–461.

[44] Z. Jin, X. Du, Y. Xu, Y. Deng, M. Liu, Y. Zhao, B. Zhang, X. Li, L. Zhang, C. Peng, others, Structure of M pro from SARS-CoV-2 and discovery of its inhibitors, Nature. 582 (2020) 289–293.

[45] T. Hou, W.A. McLaughlin, W. Wang, Evaluating the potency of HIV-1 protease drugs to combat resistance, Proteins Struct. Funct. Bioinforma. 71 (2008) 1163–1174.

[46] T. Ishikawa, M. Seto, H. Banno, Y. Kawakita, M. Oorui, T. Taniguchi, Y. Ohta, T. Tamura, A. Nakayama, H. Miki, others, Design and synthesis of novel human epidermal growth factor receptor 2 (HER2)/epidermal growth factor receptor (EGFR) dual inhibitors bearing a pyrrolo [3, 2-d] pyrimidine scaffold, J. Med. Chem. 54 (2011) 8030–8050.

[47] N. Iqbal, N. Iqbal, Human epidermal growth factor receptor 2 (HER2) in cancers: overexpression and therapeutic implications, Mol. Biol. Int. 2014 (2014)1-14.

[48] M. Singh, M. Kaur, H. Kukreja, R. Chugh, O. Silakari, D. Singh, Acetylcholinesterase inhibitors as Alzheimer therapy: from nerve toxins to neuroprotection, Eur. J. Med. Chem. 70 (2013) 165–188.

PART III

CORROSION INHIBITION STUDIES

CHAPTER 10
INTRODUCTION AND REVIEW

From the day of metal invention, corrosion is a costly crisis in material science. Corrosion is the ongoing degradation/deterioration of the property of metal/material due to environmental circumstance and or by chemical reactions ensuing new and undesirable stuff from the original. The word "corrode" originates from "corrodere", a Latin word which indicates "nibble into pieces". Most of the time, corrosion refers to metals, but other materials such as polymers and glass are also undergone corrosion. This reaction can be electrochemical, as in the case of metals and alloys due to their high conductivity. It can also be a chemical deterioration as in the case of non-conducting materials such as ceramics, plastics and concrete. Protection of different metals and their alloys from corrosion in acidic media is the most demanding work in contemporary period. Corrosion shortens the life and demolishes the lustre and beauty of the materials, especially metals. Electron acceptors in the environment assist oxidation of metals ($M \rightarrow M^{+} + e^{-}$) and thereby corrosion. Metals have a strong affinity to go back to its native (low energy oxide) state because the free energy of pure metal is higher than its metal oxide. The process of this conversion to its native oxide state is described as corrosion. The simple pictorial representation of the corrosion process and the components involved are shown in Fig. 3.1.

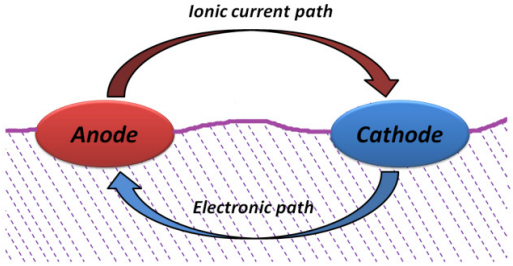

Fig. 3.1: Demonstration of components of corrosion

Corrosion leads to the replacement or repair of the structures, may lead to potential hazards and even becomes a threat to natural resources. Consequences of accidents of the corroded structures direct to damages of resources, safety concerns, loss of life etc. Drinking water is polluted by failed pipelines. Engine corrosion distress ships, aircraft and automobiles. Corrosion to machinery parts negatively influence the production of petrochemicals, mining, defense, food processing and agricultural production. Corrosion also hampers with safety, cause disruptions in industrial operations and poses danger to environment. Corroded bridges may collapse leading to death, public outcry, traffic delays and other crisis. When prosthetic implants like valves, pacemakers, plates and hip joints corrode, serious health problems will occur. Corrosion cause dangerous & expensive damage to highways, bridges, automobiles, home appliances, sewer systems, electrical utilities, ships, aircraft, petroleum refining, food processing, gas transmission, water pipelines etc. Corrosion impacts in different areas are shown in Fig. 3.2.

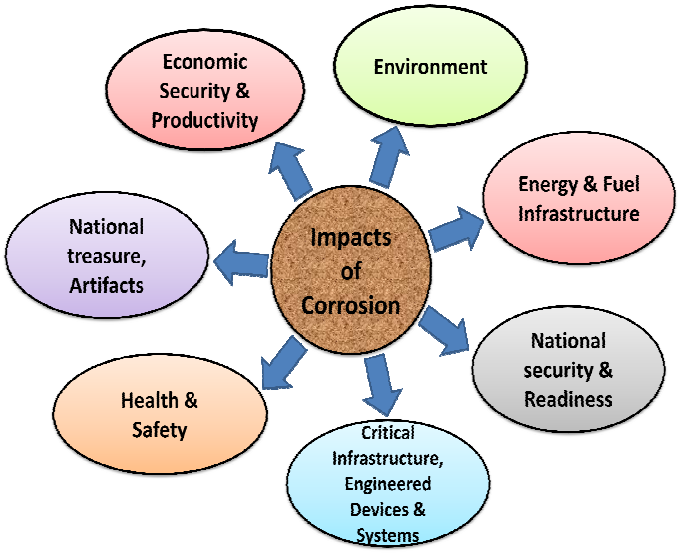

Fig. 3.2: Corrosion impacts in various areas

Economic factor is the major concern for the present studies on corrosion. Corrosion cost in the U.S. was estimated as $276 billion per year which was 3.1% of the

GDP in U.S. as of 1998. The direct cost of corrosion for India estimated during 2011-2012 was 26.1 billion U.S. $ [1].

Pickling is the process of exclusion of any contaminants from the metal surface at a high-temperature range. For the elimination of inorganic impurities like contaminants and any adjacent metal like chromium layer from the stainless steel surface, pickle liquor (acids like hydrochloric acid, nitric acid and sulphuric acid) is used [2]. When steel is exposed to high temperatures in industries, a discolouring oxide scale is developed on its surface and to remove this useless scale from the workpiece (metal) and reinstate the elevated performance of anti-corrosion, it is dished into a case of pickle liquor.

During pickling, addition of inhibitors is advantageous and safe since it protects the surface of metal from the corrosive attack. If inhibitors are not being used, a considerable quantity of metal loss will occur by the corrosive effect of acid on metals. In pickling baths, during corrosion, hydrogen gas is evolved and diffused throughout and makes the metal brittle via hydrogen embrittlement. The addition of inhibitors develops a barrier layer of film on the clean metal surface and decrease metal-acid interaction and thus inhibits surplus release of hydrogen. Consequently, metal becomes less vulnerable to hydrogen embrittlement by the addition of inhibitors in pickling baths [3].

Fig. 3.3: Application of carbon steel/mild steel in various areas

Low carbon steel or mild steel is the cheapest steel type which contains 0.05-0.25% of carbon. These are used in diverse vicinities such as cookware, automobiles, petrochemical industry, oil and gas industry, electrical appliances, agricultural implants, boilers, heat exchangers, marine applications, medical prosthetic implants etc; (Fig. 3.3). It readily undergoes rusting while exposed to environments containing acidic humidity.

Even corrosion looks highly complex, it can be elucidated by three plain electrochemical steps (Fig. 3.4)

a) Loss of metal occurs from the low potential part by oxidation and it acts as anode. In this current illustration, iron gets oxidized from Fe^0 to Fe^{2+}state.

b) Oxygen dissolved in aqueous medium migrate to cathode and completes the electric circuit.

c) Electrons released by Fe reduce oxygen to water at the cathode which is another region of the same metal.

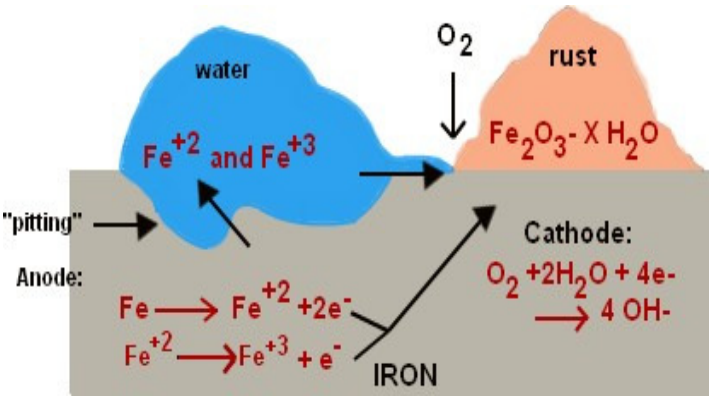

Fig. 3.4: Reactions occurring throughout the corrosion of steel

At anode: $Fe \longrightarrow Fe^{2+} + 2e^-$ (1)

At cathode: $O_2 + 8H^+ + 4e^- \longrightarrow 2H_2O + 4OH^-$ (2)

In the absence of oxygen, hydrogen ions get involved in this reaction at the cathode instead of oxygen and complete the electrical circuit ($2H^+ + 2e^- \longrightarrow H_2$).

Overall reaction is given by the equation:

$$2Fe^{0} + 2O_2 + 4H^{+} \longrightarrow 2Fe^{2+} + 4H_2O \quad (3)$$

In acidic solution, H^+ ions are supplied by H_2CO_3 which is produced by the reaction of carbondioxide from atmosphere and water.

Oxidation of ions of Fe^{2+} as follows:

$$2Fe^{2+}_{(aq)} + O_{2(g)} + (4 + 2x)H_2O_{(l)} \longrightarrow 2Fe_2O_3 \,.\, xH_2O + 4H^{+}_{(aq)} \quad (4)$$

Rust is represented as $2Fe_2O_3.\ xH_2O$. Carbonic acid in water dissociates forming hydronium and bicarbonate ions which causes corrosion. Acidity level is increased by the presence of gaseous pollutants such as SO_2 and NO_2 & aggravates corrosion problems. Prevention of corrosion would be more practical than trying to eliminate it.

Factors Responsible for Corrosion:

- ***Reactivity of the metal:*** More active metals having high oxidation potential values are readily corroded.
- ***Existence of moisture and air:*** Moisture and air content accelerates corrosion phenomena. Gases like CO_2 and SO_2 in the air enhances the process of corrosion. When iron placed in a vacuum, it doesn't rust.
- ***Presence of electrolyte:*** Electrolyte exerts a vital influence in the increasing corrosion rate (e.g.: iron rust sooner in saline water compared to pure water).
- ***Strains in metals:*** Corrosion takes place more rapidly at bends, scratches and cuts in the metal.
- ***Occurrence of impurity:*** Even a small amount of impurities in metal boost the probability of corrosion. Pure metal doesn't corrode easily.

Types of Corrosion

There are different types of corrosions known, but there is no universally conventional classification. Generally, the following categorization is adopted [4,5]

and it depends on the grain structure of metals, its composition or temperature for deformation.

***Galvanic corrosion*:** This is the most commonly found and one of the useful forms of corrosion which tend to arise when metals have dissimilar affinities to corrode when they contact in a corrosive electrolyte (conductive path) or with diverse electrochemical potentials (Fig. 3.5). It can be dry or wet, chemical or electrochemical. In galvanic corrosion cell, the anode is the more active metal (more negative) and its corrosion rate is more. The cathode is the more noble (more positive) metal and its corrosion rate is less. A uniform decrease in the volume of metals takes place at a result of chemical action and soluble corrosion products are formed. When stainless steel is in contact with aluminium alloys (if galvanic corrosion happens) acceleration of corrosion of aluminium occurs. The main principle behind dry cell construction is galvanic corrosion. The negative side is that it may also occur at unwanted vicinity making the metal susceptible to damage.

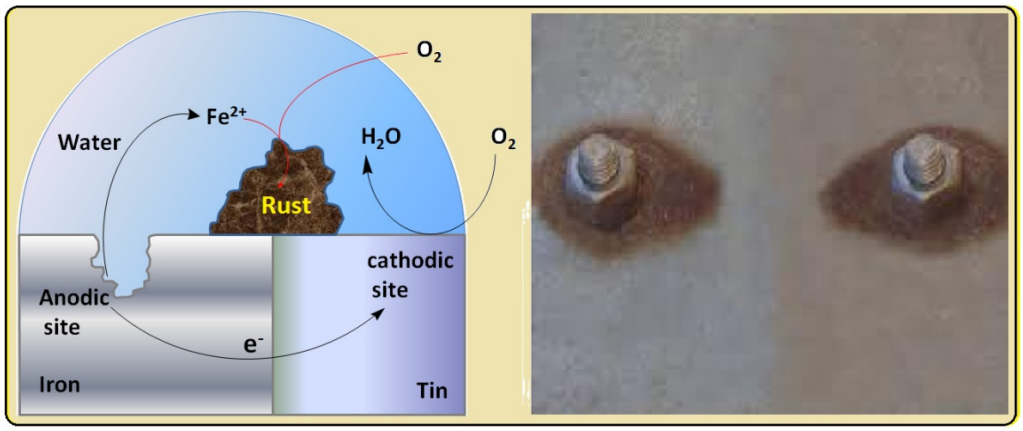

Fig. 3.5: Galvanic corrosion

***Pitting corrosion*:** "Self-nucleating" type crevice corrosion called pitting corrosion (Fig. 3.6), begins at occluded cells. Its prediction, detection and characterization are difficult. A galvanic cell is created on the metal surface because of pinholes, crack,

chemical attack, local straining etc. The crack segment on the metal surface acts as anode. A pit penetrates vertically downward and is developed by the corrosion at the anodic area which penetrates downward and forms a pit, hence named as pitting corrosion. Peripheral impurities such as scale, sand and dust implanted on the surface of metal leads to pitting. Corrosion of stainless steel and aluminium in chloride medium causes pitting.

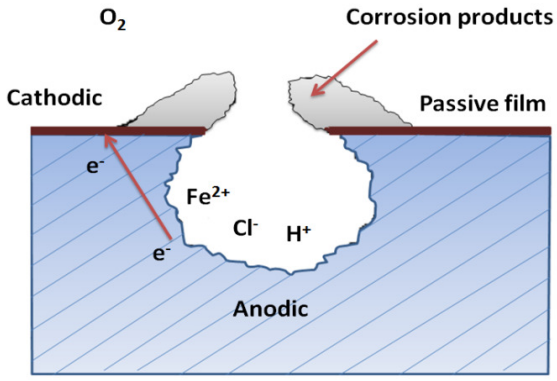

Fig. 3.6: Pitting corrosion in steel

***Crevice corrosion*:** It results from the different concentration of ions between two areas of metal and is a localized form of corrosion. Deviation in the local environment in the crevice i.e., increases in pH, depletion of oxygen and increase in halide ions (Cl^-) may cause the development of this type of corrosion. Proper joint designs minimize crevice corrosion. Usage of materials like plastic, glass, wood, asbestos and wax may contribute to crevice corrosion. Fig. 3.7 shows its mechanism and it is electrochemical in nature.

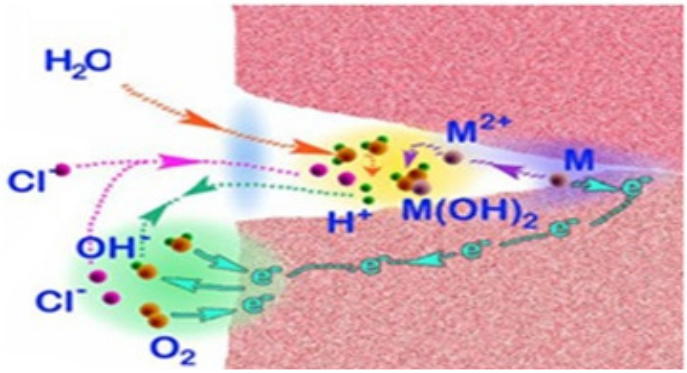

Fig. 3.7: Mechanism of crevice corrosion

***Microbiological corrosion*:** Corrosion caused by the metabolic activity of various microorganisms is called microbiological corrosion and it is commonly referred to as microbiologically influenced corrosion (MIC) or bio-corrosion (Fig. 3.8). In the oil industry, 40% of pipeline metal corrosion is due to microbes. The microorganisms can develop in an environment with or without oxygen and are classified as aerobic and anaerobic respectively. Bacteria, fungi, algae, diatoms etc. are capable of forming films resulting in microbiologically influenced corrosion. Such a film maintains concentration gradients of dissolved salts, gases, acids etc. As a result, local biological concentration cells are developed on the surface leading to microbiological corrosion.

Fig. 3.8: Microbiologically influenced corrosion (MIC) or bio-corrosion

***Inter-granular corrosion*:** This occurs along grain boundaries, especially where the material is sensitive to corrosion attack. Corrosive liquids possess a selective character of attacking only at grain boundaries and leaving the grain interior untouched or only slightly attacked (Fig. 3.9). Material containing grain boundaries shows more anodic electrode potential, undergoes corrosion in the particular corroding medium and affects the mechanical properties of metals while bulk remains intact. This may be due to the precipitation of certain compounds at the grain boundaries.

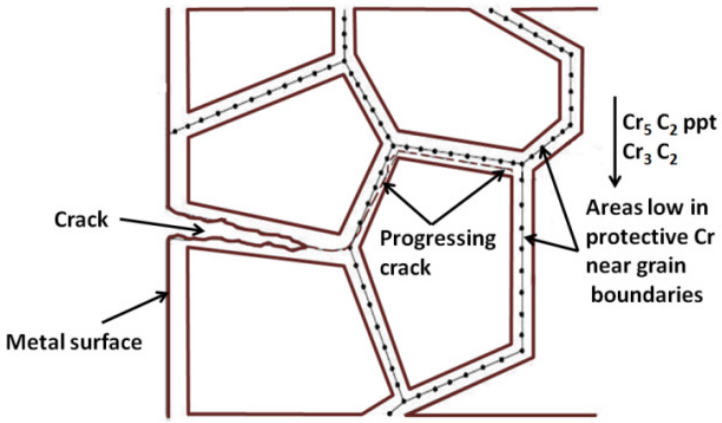

Fig. 3.9: Inter-granular corrosion of stainless steel

***Stress corrosion cracking (SCC)*:** Stress corrosion is a permutation of a corrosive environment and the tensile stress acting on the surface of a metal and this may be external or internal (Fig. 3.10). It may originate from residual stress from welding, machining, grinding etc. and also from external stress. The fraction under stress performs as an anode and the rest as a cathode, developing a galvanic system and resulting in the corrosion of the anodic fraction.

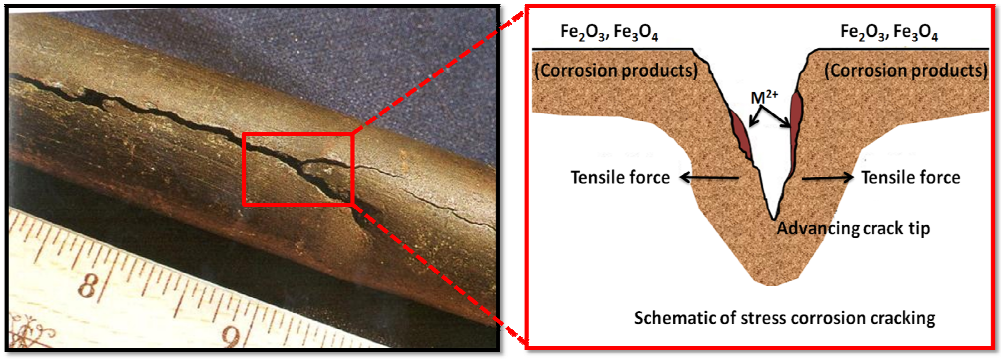

Fig. 3.10: Schematic representation of stress corrosion cracking

Prevention of Corrosion

There are several ways to protect the metal from corrosion.

- ***Barrier protection:*** To prevent corrosion, the metal surface can be protected from direct contact with the surroundings by coating it with paint, oil, enamel or a thin

protective layer of corrosion-resistant metal. Coatings provide a hurdle between moisture from surroundings and metal. E.g. brass tinning.

- ***Sacrificial protection:*** The corrosion of metal can be prevented by covering its surface with the layer of a more active metal like magnesium, zinc or aluminium. The more active metal act as the anode and iron act as cathode in the electrochemical cell set up. The covering metal gets consumed in the course of time, but the nearby exposed surfaces of iron do not rust as long as the sacrificial anode is present.
- ***Cathodic protection:*** Preventing metal surface from corrosion by making its surface as cathode in an electrochemical cell. Fuel pipelines, steel, tanks, ships, offshore oil platforms and steel pier piles are regularly sheltered in this approach.
- ***Anodic protection:*** Protection is done by applying an anodic current on the structure of the metal. Mainly this technique is employed in an aggressive atmosphere and protects the materials exhibiting passivity (e.g. stainless steel).
- ***Avoid exposure to corrosive agents:*** These methods include safeguarding the metal from rainwater or moisture by storing it indoors. Treating the feed water inside water boilers with softener prevent corrosion.
- ***Proper monitoring of metal surface:*** Routine observation for cracks and crevices which can lead to corrosion on the metal surface is to be done and preventive measures are to be adopted because these can lead to corrosion and use corrosion-resistant bars for construction.
- ***By forming insoluble phosphate or chromate coating*:** Treating the surface with phosphoric acid forms an insoluble phosphate coating that prevents corrosion. A thin chromate layer is also used.

- ***Anodization:*** It is another surface treatment, where the metal to be protected is bathed in a specific substance leading to a rigid and resilient film oxide layer and this layer which is thicker than a passivation film resists the corrosion process.
- ***By using corrosion inhibitors:*** Using an inhibitor is one of the best options to fight corrosion. Vast scientific studies have been conducted to develop and explore various corrosion inhibitors [6–12]. They work by making a coating on metal and prevent the access of corrosive agents to the metal surface. Compounds like ethylene glycol, formaldehyde, sodium molybdate, quaternary ammonium salts and glutaraldehyde revealed to restrict biofilm formation and microbial activity. Effectiveness of a corrosion inhibitor primarily depends on the composition of the quantity of H_2O and flow area and characteristics. Inhibition is facilitated by the formation of a coating, most commonly a passivation layer which blocks contact of the corrosive substance onto metal. The inhibitor may be chemically adsorbed onto the metal surface which forms a protective thin film or it may react with a potential corrosive component forming a complex.

Inorganic substances such as chromates, phosphates, silicates etc have been used as effective as inhibitors towards metallic corrosion. Also, organic compounds and natural extracts are used as inhibitors, which diminish metal dissolution rate in acid medium. There are four distinctive mechanisms proposed [13,14] to explain the inhibitory characteristics of organic species viz., (i) electrostatic interactions existing across charged species and the metal (ii) interaction between the π-electrons of the metal and inhibitor (iii) interactions between metal and uncharged electron pairs in the molecule and (iv) a permutation of various mechanism. Greater the affinity of an inhibitor to form a strong coordination bond with the metal, greater is the inhibition efficiency. Molecules

with phosphorous, sulphur, nitrogen and oxygen are found to have a strong tendency to avert corrosion [15].

Organic molecules having electron lone pairs on the heteroatoms such as P, S, N and O atoms have proved, both theoretically and practically, that they can perform as admirable corrosion inhibitors in aggressive solutions by improved adsorption on the metal surface [16,17]. Generally, effectiveness of organic inhibitors depends up on the aromaticity, efficiency (electron density) at the centres of adsorption [18,19], molecular size, number of sites of adsorption on the surfaces [20] etc; Organic molecules bearing sulfur and nitrogen behave as wonderful inhibitors against corrosion in both HCl and H_2SO_4 acidic medium [21]. Inhibitors having heteroatoms in their structures pursue the opposite order of their electronegativities and their efficiencies followed the order O < N < S < P [22,23].

There are different types of inhibitors: Anodic inhibitors form a protective oxide film and cause a large anodic shift. Eg:-molybdates, chromates, tungstates and nitrates. Cathodic inhibitors decrease reaction at cathode by limiting the diffusion of reducing species to steel/ metal surface, eg: Zn and polyphosphate inhibitors and oxygen scavengers. Mixed inhibitors reduce both cathode and anode reactions, eg: phosphates and silicates. Volatile inhibitors of corrosion are carried from source to corrosion site by volatilization, eg: In boilers, hydrazine or morpholine are transported with steam. Green corrosion inhibitors are more economical, easily available and eco-friendly than toxic organic inhibitors. Natural products are a good source, where most of them contain necessary elements such as O, C, S and N which are active in organic compounds and forms a protective film to hinder the corrosion. eg: natural honey, onion, potato, tulsi etc.

Literature survey established that imidazole azo derivatives, benzotriazoles and their derivatives, quaternary imidazoline derivatives, benzaldehyde, quinoline derivatives,

quaternary salts of benzenethiol alkaloids, triazoles, pyridine bases, thiourea, derivatives of chloroanilines, toluidine etc., have noticeable inhibitory action [24–28].

An efficient inhibitor must assure some conditions [29]:

a) It must prove the fine ability of protection while used in very small concentration.

b) It should be long-range effective.

c) It must retain its efficiency in varying conditions of operations like higher velocity and temperature.

d) Inhibitor should have minimum toxicity level.

e) There should not be any severe change in corrosion rate when altering inhibitor dosage.

f) It should be capable to guard the surface of metal from both localized and uniform corrosion.

g) Products formed from inhibitor during reactions or inhibitor itself, must not form any deposits–specially at the areas where heat transfer processes take place.

Schiff Base Corrosion Inhibitors - A Review

Literature survey pointed out that many scientists synthesized and studied different categories of Schiff bases for their inhibition capacity against corrosion of carbon/mild steel in aggressive media. Few of the Schiff bases showed their efficiency in aggressive medium against the corrosion of zinc and copper.

In 2003, M. Hosseini, et al. investigated corrosion inhibition studies of two novel Schiff bases,viz., N,N′-ortho-phenylene(salicylaldimine-2-hydroxy-1-naphthaldimine) and N,N′-ortho-phenylene(salicylaldimine-acetylacetone imine) for mild steel in 0.5M H_2SO_4 by electrochemical impedance spectroscopy (EIS) and Tafel polarization [30]. At

400ppm concentration, these two novel ligands function as good inhibitors with maximum efficiencies of 97–98%.

In 2011, M. T. Muniandy, et al. investigated the corrosion inhibition effect of N, N′-bis(4-bromobenzylidene)-1,3-diaminobenzene,N,N′-bis(2-hydroxy-5-bromobenzylide ne)-1,3-diaminobenzene and N,N′-bis(2-hydroxybenzylidene)-1,3–diamino benzene on aluminium alloy in HCl medium (0.5M) [31]. Inhibition ability of these Schiff bases are approximately similar in this acid medium and was proved by gravimetric weight loss measurements, potentiodynamic polarization (PDP) techniques and scanning electron microscopic (SEM) analysis. The polarization studies exposed that, all inhibitors are mixed type. Predominantly its action was cathodic and inhibition efficiencies were found to enhance linearly with its concentration. On aluminium surfaces, all molecules followed Langmuir adsorption isotherm and SEM studies indicated that a protective layer was developed on the aluminium surface and performance of inhibition strongly depends on the types of functional group substituted on benzene ring.

In 2011, M. D. Shah, et al. revealed the activity of inhibition of tribenzylidene and trisalicylidene derivatives of triethylenetetramine in HCl medium on zinc metal [32]. Molecules showed 96-100% of inhibition efficiency at very low (1%) concentrations in different molar solutions of HCl medium (0.5M and 1M). The efficiency of the trisalicylidene derivatives decreased after 2 hours when temperature increased from 35-65ºC, but the efficiency of other inhibitor remains approximately constant at 99.7%. The activation energies of corrosion were higher in the presence of inhibitors than in the blank. The spontaneity of adsorption of the inhibitor on the metal surface was evident from the negative values of heat of adsorption and free energy of adsorption. Cathodic polarization was found to be predominant in electrochemical studies. Langmuir isotherm was obeyed on both anodic and cathodic sites by these molecules.

M.Q. Mohammed, et al. synthesized three Schiff bases by the condensation reactions of cinnamaldehyde with 2-aminophenol, acrolein with 2-aminophenol and cinnamaldehyde with phenylenediamine in 2011 [33]. These ligands were identified by CHN, ^{1}H NMR, UV-Vis and IR analyses. Studies include the use of these ligands as corrosion inhibitors on carbon steel in 0.5M HCl media.

S.P. Fakrudeenet, et al. evaluated the corrosion inhibition efficiencies of N,N'-bis(3-methoxysalicylidene)-1,4-diaminophenelyne (MSDP), N,N'-bis (salicylidene)-1, 4-diamino phenelyne (SDP) and on an alloy (AA6061) by gravimetric weight loss method and SEM micrography in 1M hydrochloric acid medium in 2012 [34]. From the studies, it is revealed that the inhibition efficiency of these Schiff bases (MSDP, SDP) and alloy (AA6061) increases with increase in concentration. Efficiency of these ligands varied with temperature and time of immersion in solution. The adsorption of these molecules on the surface of alloy followed the Freundlich isotherm and the mechanism of inhibition was suggested based on thermodynamic parameters.

Singh, et al. studied the corrosion inhibition effect of some Schiff base compounds namely, hexane 1,4-diaminebis-isatin (HDBI), ethylenediaminebis-isatin (EDBI), and thiocarbohydrazidebis-isatin (TCBI) by gravimetric weight loss, electrochemical impedance spectroscopy, potentiodynamic polarization, scanning electron microscopy and atomic force microscopy in 2012 [35]. Frumkin isotherm was most suited isotherm for these three inhibitors. TCBI showed highest efficiency followed by EDBI and HDBI and led to a conclusion that a competent corrosion inhibitor should have planarity, large size, and unoccupied d-orbital along with an extensive number of π-electrons.

In 2013, S. Junaedi, et.al., investigated the corrosion inhibitory influence of 1,5 dimethyl-4-((2-methylbenzylidene)amino)-2-phenyl-1*H*-pyrazol-3(2H)-one in aggressive

medium on mild steel employing EIS, PDP, EFM and OCP techniques [36]. Highest occupied molecular orbital energy (E_{HOMO}), lowest unoccupied molecular orbital energy (E_{LUMO}) and dipole moment (μ) were determined and discussed.

In 2015, Kannan, et.al. reported the corrosion inhibitory effect of N,N-bis(2-hydroxyacetophenylidene)-2-hydroxy-1,3-propanediamine (LACOH) and N,N-bis (salicylidene)-2-hydroxy-1,3-propanediamine (LOH) in 2M HCl medium at 303K [37]. These inhibitors appeared to follow the Langmuir adsorption isotherm.

M. R. Vinutha and T.V. Venkatesha reported an article which enumerates numerous inhibitors accustomed to combat corrosion in aggressive medium in 2016 [38]. By economic, technical, safety and environmental terms, corrosion control is an important activity and, in this article, the literature on corrosion inhibitors has been reviewed and discussions were made on their efficiency and properties. They reported the nature of the media and metals along with the physicochemical, electronic and structural properties which having prominent roles while explaining the mechanism. Further, they inferred that the presence of S, O and N heteroatoms in the structure of ligands, surfactants and phytochemicals acting as the most efficient inhibitors within their CMC concentration.

In 2018, D. M. Jamil, et al. studied the inhibition efficiencies of relatively stable and inexpensive Schiff bases, namely 3-((4-(dimethylamino)benzylidene) amino)-2-methylquinazolin-4(3*H*)-one and 3-((4-hydroxybenzylidene)amino)-2-methyl quinazolin-4(3H)-one, by weight loss method in acid medium [39]. To compare the effects of N, N-dimethylamino and hydroxyl substituents on corrosion inhibition efficiency, density functional theory calculations were conducted which provide insight for designing novel molecular structures with improved corrosion inhibition efficiencies.

In 2020, P. Shetty reported a review of the corrosion inhibition activities of a variety of reported Schiff bases on the disintegration of mild steel in aggressive media [40]. During pickling, an undue deterioration of metal happens which can be controlled by the addition of a suitable inhibitor to this pickling solution. The relationship of structure and corrosion inhibition activity of Schiff base ligands are highlighted in this paper which finds valuable practical applications in different industrial fields. It helps the researchers to develop novel corrosion inhibitors for performing inhibitors in acid media.

Heterocyclic Schiff Base Inhibitors- A Review

In 2004, Dhayabaranet, et al. studied tetrazole derivatives, namely, 1-(9′-acridinyl)-5-(4′-hydroxy phenyl) tetrazole, 1-(91-acridinyl)-5-(4′-aminophenyl) tetrazole and 1-(9′-acridinyl)-5-(4′-chlorophenyl) tetrazole as corrosion inhibitors for commercial mild steel in 1M hydrochloric acid medium by weight loss studies [41]. Thermodynamic parameters like entropy of adsorption, heat of adsorption, activation energy and free energy of adsorption have been calculated at 303K, 318K and 333K to study the adsorption characteristics of tetrazole derivatives.

R. Upadhyay and S. Mathur have studied the corrosion inhibitory outcome of novel Schiff bases viz.N-(furfurilidine)-4-methylaniline, N-(furfurilidine)-4-methoxy aniline, N-(salicylidine)-4-methoxyaniline, N-(cinnamalidine)-2-methylaniline and N-(cinnamalidine)-4-methoxy aniline on mild steel in sulphuric acid solutions by thermometric and mass loss methods in 2007 [42]. Results obtained by both methods are in good agreement with each other and maximum inhibition performances were shown at high concentration of the Schiff's base.

In 2008, G. Elewady studied characteristics of corrosion inhibition of 2,6-dimethylpyrimidine-2-amine and its derivatives in HCl medium on carbon steel

corrosion via gravimetric techniques and EIS studies [43]. At 0.005M concentration, N-benzylidene-4,6-dimethylpyrimidine-2-amine displayed highest inhibition efficiency of 92.78 %.

In 2014, Gopi, et al. reported the corrosion inhibition behaviour of phosphano and benzotriazole and their derivatives at various temperatures ranging from 30-60°C in groundwater using PDP, scanning electron microscopy (SEM) and X-ray diffraction on mild steel [44]. At optimum concentration, an excellent inhibition efficiency of 99.59% was reported.

In 2015, L.O. Olasunkanmi et. al., studied mild steel corrosion in hydrochloric acidusing some quinoxaline derivatives namely 1-(3-phenyl-5-(quinoxalin-6-yl)-4,5-di hydro-1H-pyrazol-1-yl)propan-1-one,1-[3-phenyl-5-quinoxalin-6-yl-4,5-dihydro pyrazol -1-yl]butan-1-one and 2-phenyl-1-[3-phenyl-5-(quinoxalin-6-yl)-4,5-dihydro pyrazol-1-yl] ethanol using EIS and PDP techniques [45]. Studies were supported by Monte-Carlo simulation and quantum chemical calculations.

In 2016, P. Singh, et.al.,analysed the inhibition and adsorption effects of quinoline derivatives such as 2-amino-7-hydroxy-4-(p-tolyl)-1,4 dihydroquinoline-3-carbonitrile, 2-amino-7-hydroxy-4-phenyl-1,4-dihydroquinoline-3-carbonitrile, 2-amino-4-(4-(dimethyl amino)phenyl)-7-hydroxy-1,4-dihydroquinoline-3-carbonitrile, 2-amino-7-hydroxy-4-(4-methoxyphenyl)-1,4-dihydroquinoline-3-carbonitrile using gravimetric weight loss studies, EIS and PDP techniques [46]. Among the studied inhibitors, 2-amino-4-(4-(dimethylamino)phenyl)-7-hydroxy-1,4-dihydroquinoline-3-carbonitrile exhibited maximum inhibition efficiency of 98.19 % at 150 mg/L. Surface morphology was studied using SEM, X-ray photoelectron spectroscopy (XPS) and atomic force microscopy techniques.

Tasic, et al. investigated the synergistic inhibition effect of corrosion on benzotriazole with gelatine and potassium sorbate on copper in an acidic sulphate medium by conventional gravimetric and electrochemical studies in 2016 [47]. The maximum inhibition efficiency of 99 % was displayed due to the synergistic effect by the effective adsorption of molecules.

In 2019, I. Benmahammed, et al. studied (1Z)-N′-(4-bromophenyl)-2-oxo-N-quinolin-8-ylpropane hydrazonamide and (1Z)-2-oxo-N′-phenyl-N-quinolin-8-yl propane hydrazonamide as corrosion inhibitors in 1 M HCl medium on carbon steel by conventional gravimetric weight loss techniques, electrochemical studies, energy dispersion X-ray spectroscopy (EDS), scanning electron microscopy (SEM) coupled with atomic force microscopy, AFM studies etc.,[48]. The temperature effect was supported and different thermodynamic parameters were considered along with the synergetic effect and hydrodynamic effect. With increased rotation speed, corrosion inhibitory efficiency was decreased and the used additives adsorb cooperatively by forming a protective layer on the surface of metal. The theoretical calculations by DFT and MD simulation are in good correlation with the results obtained by the experimental measurements.

A. Mishra, et al. reviewed the collection of major investigations which illustrated the anticorrosive effect of imidazole derivatives in different electrolytes in 2020 [49]. Mostly, these derivatives acted on interface and behaved as mixed type corrosion inhibitors. They interact with the metal surface by charge sharing (donor-acceptor) interactions. Their adsorption mechanism obeyed the Langmuir adsorption isotherm.

Sulphur Containing Schiff Base Inhibitors-A Review

In 2004, M. Özcan, et al. investigated the effects of corrosion of mild steel in 0.1M H_2SO_4 using thiourea and its derivatives like phenylthiourea and methylthiourea by considering the concentration of thioamides [50]. These molecules are similar structure on one side (thiocarbonyl group) and altered on the other. Data obtained using the techniques of EIS (electrochemical impedance spectroscopy) and R_p (polarisation resistance) revealed that these molecules showed good corrosion inhibition. Phenylthiourea was the most efficient derivative and thiourea was the least.

In 2004, A. Yurt, et al. revealed the inhibition capacity of ligands containing heterocyclic substituents namely, 2-((1E)-2-az-2-pyrimiadine-2-ylvinyl)thiophene, 2-((1Z)-1-aza-2-(2-pyridyl)vinyl)pyrimidine, 2-((1E)-2-aza-2-(1,3-thiazol-2yl)vinyl) thiophene, 2-((1Z)-1-aza-2-(2-thienyl)vinyl)benzothiazole in 0.1M hydrochloric acid by AC impedance and PDP studies on carbon steel [9]. Adsorption mechanism of inhibitors obeyed the Temkin isotherm.

In 2007, H. H. Hassan, et al. carried out a comparative study of 5-amino-3-mercapto-1,2,4-triazole, 5-amino-1,2,4-triazole, 1-amino-3-methylthio-1,2,4-triazole and 5-amino-3-methylthio-1,2,4-triazole as inhibitors in 0.1M HCl solution for mild steel corrosion at 20°C [51]. To study the metal corrosion behaviour of these inhibitors at different concentrations, potentiodynamic polarization and electrochemical impedance spectroscopy (EIS) techniques were used. Open circuit potential (OCP) was measured as a function of time and these results are in close agreement with the results obtained from impedance and polarisation measurements. These studies were established that 5-amino-3-mercapto-1,2,4-triazole was the most efficient inhibitor.

In 2011, F. Bentiss and M. Lagrenée reported the relationship between corrosion inhibition properties and electronic parameters of thiadiazole, oxadiazole and

triazole derivatives [52]. Results showed that planar compounds have better adsorption than twisted or puckered molecules.

In 2011, S. Issaadi, et al. tested the corrosion inhibition of two thiophene based Schiff bases 4,4′-bis(3-carboxaldehydethiophene)diphenyldiiminoethane and 4,4′-bis (3-carboxaldehydethiophene)diphenyldiimino ether on mild steel in 1M HCl medium using electrochemical studies like EIS and PDP techniques [53]. The polarisation studies and adsorption studies were established that they were performed as mixed type (anodic/cathodic) inhibitors and satisfied the Langmuir's adsorption isotherm.

In 2012, C. Loto, et al. reviewed the inhibitive effect of thiadiazole and thiourea derivatives. Heterocyclic and organosulphur compounds and derivatives have so many practical applications [54]. The effects of these molecules on the corrosion of metallic alloys were appraised in diverse journals by different experimental techniques. It is concluded from the complete discourse presented, thiadiazole and thiourea derivatives fulfil the basic requirements for a competent corrosion inhibitor.

In 2014, Djamel Daoud, et al. analysed the inhibitory action of the molecule (NE)-N-(thiophen-3-ylmethylidene)-4-({4-[(E)-(thiophen-2-ylmethylidene)amino] phenyl}m-ethyl)aniline on the corrosion of mild steel (X52) in 1M sulfuric acid and 1M hydrochloric acid [55]. They have used the methods like weight loss, PDP, EIS, DFT to explain the correlation between inhibition efficiency and quantum chemical calculations of the investigated compounds.

In 2016, A. Aouniti, et al. studied the corrosion inhibition and adsorption behaviour of (*E*)-2-methyl-N-(thiophen-2-ylmethylidene)aniline at mild steel in 1M HCl using gravimetric weight loss and electrochemical methods at 308 K [56]. Inhibition efficiency was increased with increase in the concentration of thiophene Schiff base. The potentiodynamic polarization studies revealed that this novel

thiophene Schiff base acted as a mixed-type inhibitor. The inhibition was proposed to occur due to the adsorption of the components of the thiophene derivatives on the mild steel surface which were approximated by invoking the Langmuir adsorption isotherm model. DFT method, theoretical and experimental correlation results were also discussed.

In 2018, A. Singh, et.al., investigated the corrosion inhibitive action of thiopyrimidine derivatives viz, 5-cyano-2-thioxo-6-(p-tolyl)-2,3dihydropyrimidin-4-one, 6-(4-(dimethylamino)phenyl)-5-cyano-2-thioxo-2,3-dihydropyrimidin-4-one and 5-cyano-6-phenyl-2-thioxo-2,3-dihydropyrimidin-4-one, 5-cyano-6-(4-methoxyphenyl) -2-thioxo-2,3-dihydropyrimidin-4-one on the corrosion of mild steel in aggressive medium using EIS and PDP techniques [57]. Maximum inhibition efficiency of 97% was exhibited by 6-(4-(dimethylamino)phenyl)-5-cyano-2-thioxo-2,3-dihydro pyrimidin-4-one at 200 mg/L. All these inhibitors are mixed type with predominant control of cathodic reaction.

Polynuclear Schiff Base Inhibitors– A Review

In 2011, I. Obot, et. al., synthesized and characterized novel phenanthroline derivative, 2-mesityl-1H-imidazo[4,5-f][1,10]phenanthroline [58]. Its corrosion inhibition performance was studied in sulphuric acid medium on low carbon steel by electrochemical and quantum chemical techniques. UV-visible absorption spectrum of this molecule displayed the formation of an iron-inhibitor peak.

In 2012, Baskar et. al. synthesized three biphenyl compounds namely(2E)-1-(biphenyl-4-yl)-3-(4-hydroxyphenyl)prop-2-en-1-one, (2E)-3-(4-aminophenyl)-1-(biphenyl-4-yl)prop-2-en-1-one and (2E)-1-(Biphenyl-4-yl)-3-(4-nitrophenyl)prop-2-en-1-one, characterised and investigated their inhibition efficiency against corrosion by weight loss, PDP and EIS techniques on low carbon steel [59]. Mechanism was

supported by the surface studies (SEM-EDS) and adsorption isotherms. All biphenyl derivatives were mainly found to be cathodic nature.

In 2014, K. Shaju et al. investigated the inhibitory effect of (s)-2-(anthracene-9 (10H)-ylideneamino)-5-guanidinopentanoic acid on carbon steel (CS) in 0.5M sulphuric acid medium using different corrosion monitoring techniques [60]. Addition of KI to this medium enhances the corrosion inhibition efficiency of this ligand (synergistic effect) and the results established that the ligand acted as a mixed type inhibitor. Surface morphology of the metal (CS) was evaluated by SEM analysis.

Pyridine Derivatives of Schiff Base Inhibitors- A Review

In 1995, Ekpe U. J. et al. studied the corrosion inhibitory action of methyl and phenyl thiosemicarbazone derivatives, 2-acetylpyridine-(4-methylthiosemicarbazone) (2AP4MTSC) and 2-acetylpyridine-(4-phenylthiosemicarbazone) (2AP4PTSC) on mild steel in HCl medium using weight loss and hydrogen evolution techniques [61]. 2AP4PTSC displayed a maximum efficiency of 80.67% than 2AP4MTSC. The kinetic treatment of the results revealed that corrosion resistance found to increase with inhibitor concentration and decrease with temperature. The first-order type of mechanism was deduced and inhibition process was attributed to physisorption.

In 1999, E. Ebenso, et al. reported the effect of functional groups of some thiosemicarbazone and amide derivatives of pyridine on their corrosion inhibition efficiency using hydrogen evolution and weight loss techniques [62]. 2-acetylpyridine-(4-methyl)thiosemicarbazone,2-acetylpyridine-(4phenyl)thiosemicarbazone, urea, thio urea, semicarbazide, thiosemicarbazide, acetamide, thioacetamide, methoxy benzaldehydethiosemicarbazone, benzilthiosemicarbazone and benzointhiosemi carbazone were the compounds employed for this study. Molecules having thiocarbonyl group exhibited higher inhibition efficiency and the corrosion inhibition mechanism

depends on the total molecular structure of the inhibitor, nature and spatial relationship of the different functional groups

In, 2004, M. Lashkari, et al. studied the molecular behaviour of some pyridine derivatives as corrosion inhibitors of aluminium and iron in aggressive media. Three conditions were used for these calculations; metal cluster, isolated inhibitor molecule and polarized-continuum media. The extents of charge transfer (ΔN) and chemical potential (μ) of the inhibitor were determined. A linear correlation between these two parameters and the inhibition efficiencies are also demonstrated in this article [63].

In 2004, P. C. Okafor, et al. established the corrosion inhibition of aluminium in HCl solution by some thiosemicarbazone derivatives; 2-acetylpyridine-(4-phenyl-iso-methylthiosemicarbazone), 2-acetylpyridine-(4-phenylthiosemicarbazone) and 2-acetyl pyridine-(4-phenyl-iso-ethylthiosemicarbazone) by weight loss and hydrogen evolution techniques [25]. This paper elucidates the effects of inhibitor concentration, temperature and the molecular structure on corrosion inhibition efficiency. The inhibition efficiency increased with inhibitor concentration, while their functions get reversed and became accelerators at very low concentration.

In 2005, Abd El-Maksoud and A. S. Fouda, introduced some pyridine derivatives as corrosion inhibitors for carbon steel in acidic medium and their efficiency was studied by electrochemical polarization method (potentiodynamic, Tafel extrapolation) as well as weight loss method [64]. Results established that all these compounds acted as good inhibitors and inhibition efficiency was found to depend on the nature and the concentration of the inhibitor. The presence of substitution in the pyridine ring has significant role in the percentage of inhibition and the adsorption of these compounds obeys Langmuir adsorption isotherm.

In 2007, Kandemirli F. and S. Sagdinc, carried out the quantum chemical and corrosion inhibition studies to examine the relationship between quantum chemical calculations and the efficiencies of urea, thiourea, acetamide, thioacetamide, semicarbazide, thiosemicarbazide, methoxybenzaldehyde-thiosemicarbazone, 2-acetyl pyridine-(4-methyl)-thiosemicarbazone, 2-acetylpyridine(4phenyl)thiosemicarbazone, benzointhiosemicarbazone and benzilthiosemicarbazone [65]. The quantum chemical calculations were employed using DFT, ab-initio molecular orbital and semi-empirical methods to determine various quantum chemical parameters such as highest occupied molecular orbital energy (E_{HOMO}), lowest unoccupied molecular orbital energy (E_{LUMO}), the energy gap between E_{HOMO} and E_{LUMO} ($\Delta E_{HOMO-LUMO}$), dipole moments (μ) etc.

In 2012, Ghazoui A, et al. investigated the corrosion inhibition of imidazo derivatives namely, 2-phenylimidazo[1,2-a]pyridine and 2-(methoxyphenyl)imidazo[1,2-a]pyrimidine and on C38 steel in 1M HCl by weight loss, PDP and EIS techniques [66]. Thermodynamic data for the adsorption progression were discussed and calculated. Kinetic parameters like pre-exponential factor, activation energy, entropy and enthalpy of activation were estimated from the effect of temperature on the inhibition and corrosion processes.

In 2014, V. P. Raphael, et al. investigated the corrosion resisting capacity of 3-acetylpyridine semicarbazone (3APSC) on carbon steel in hydrochloric acid medium using weight loss measurements, electrochemical impedance spectroscopy (EIS) and potentiodynamic polarization studies [67].

In, 2016, P. Mourya, et al. studied the consequence of iodide ions on corrosion inhibition of 1, 4, 6-trimethyl-2-oxo-1, 2- dihydropyridine-3-carbonitrile on carbon steel in sulphuric acid medium using gravimetric and electrochemical techniques and

established that its adsorption followed Langmuir isotherm and showed good protection efficiency [68].

In 2018, W. Zhang, et al. investigated the adsorption and corrosion inhibition properties of pyridine-2-aldehyde-2-quinolylhydrazone for Q235 steel in acid medium by PDP and EIS techniques [69]. The protective layer formed on the steel surface was examined by surface analysis techniques (SEM, EDX, SECM). The adsorption of the compound followed Langmuir adsorption isotherm and contained both physical and chemical adsorptions.

In 2019, N.N. Hazani, et al. synthesised 2-acetylpyridine-4-ethyl-3-thiosemi carbazone and it's tin (IV) complex and investigated their corrosion inhibition behaviour on mild steel in 1M HCl solution by weight loss measurement, potentiodynamic polarization, electrochemical impedance spectroscopy (EIS), and scanning electron microscopy (SEM) [70]. The polarisation study showed that both synthesised compounds are mixed-type inhibitors and the electrochemical impedance study revealed that the presence of inhibitors resulted to increase the charge transfer resistance.

Indole Derivatives of Schiff Base Inhibitors- A Review

In 2008, G. Avci investigated the corrosion inhibition of indole-3-acetic acid on mild steel in 0.5M HCl medium containing the desired concentration of inhibitor at various temperatures using PDP, EIS and PRM measurements [71]. The experimental results indicated that corrosion potential shifted towards a more negative potential region in the presence of indole-3-acetic acid than that of blank solution. Inhibition efficiency was about 77% with 1.7×10^{-3} M inhibitor and increasing to about 93% at 1×10^{-2} M inhibitor concentration. Potentiodynamic polarization measurements showed that in the presence of inhibitor, the current at anodic and cathodic regions have smaller value than that of the blank solution at almost all potentials. Activation

energy (E_a), enthalpy (ΔH_{ads}), Gibbs free energy (ΔG_{ads}) and entropy (ΔS_{ads}) were calculated.

In 2010, M. Lebrini carried out a comparative study of 1-methyl-9H-pyrido [3,4-b]indole (harmane), 9H-pyrido[3,4-b]indole (norharmane) as corrosion inhibitors for C38 steel in 1M HCl medium at 25°C using potentiodynamic polarization and electrochemical impedance spectroscopy (EIS) techniques [72]. The OCP as a function of time was also established. Anodic and cathodic polarization curves showed that harmane and norharmane are mixed-type inhibitors and they followed Langmuir adsorption isotherm model. Potential of zero charge (PZC) of the C38 steel in the inhibited solution was estimated by the EIS technique. Raman spectroscopy established that indole molecules strongly adsorbed on the steel surface.

In 2012, Paul Aby et al. investigated the corrosion inhibition efficiency of 3-formylindole-3-aminobenzoic acid on mild steel (MS) in 1M HCl solution using gravimetric weight loss measurements, electrochemical impedance spectroscopy (EIS) and potentiodynamic polarization (PDP) studies [73]. Even at low concentrations, the ligand exhibited good inhibition on mild steel in HCl medium. The adsorption of inhibitor on the surfaces of the corroding metal followed Langmuir isotherm. Polarization studies revealed that the molecule act as a mixed type inhibitor. Thermodynamic parameters like K_{ads} and ΔG^0_{ads} were calculated using Langmiur adsorption isotherm.

In 2014, A. Fouda, et al. investigated the influence of 2-oxyindole and indole on the rate of corrosion of α-brass in 1M HNO_3 using gravimetric weight loss, potentiodynamic polarization, electrochemical impedance spectroscopy (EIS) and electrochemical frequency modulation (EFM) techniques [2]. It was found that the investigated compounds behave as inhibitors. The adsorption of these ligands on the

α-brass surface followed Langmuir's adsorption isotherm and electrochemical results showed that all the investigated ligands act as mixed-type inhibitors. Results obtained from electrochemical techniques were in good agreement [74].

Scope and Objectives of Present Investigation

Steel with carbon content varying between 0.05 to 2.1 % by weight is termed as carbon steel (CS). It is used in research and development, defence, mega projects, various industries like oil industry, nuclear industry, petro-chemical industry, pulp and paper industry etc. Resistance to wear and tear, toughness and high strength are their important properties. The combination of these properties is utilized in the manufacture of train wheels, railway tracks, crankshafts and gears and machinery parts. The consequences of corrosion which is a serious problem worldwide have escalated rapidly. It is clear from the literature survey that there is great urge for expedited research in the fields of metallic corrosion generally and particularly in carbon steel in attributed to its practical significance. Carbon steel is well prone to corrosion by an environment with aggressive medium, particularly during pickling or acid cleaning. Many additives including organic compounds alter the corrosion rate of metals like iron, copper and aluminium when added to the working media.

Many organic molecules have been extensively screened for their corrosion inhibition efficiencies on various metals in acidic media. The quest for novel potential corrosion inhibitors is still continuing in the present decade. One of the most practical, effective and economic corrosion inhibitors are the organic compounds containing heteroatoms in their molecular structures. The development of novel corrosion inhibitors containing heteroatoms such as sulphur, oxygen and nitrogen is one of prime interests in chemical industries address the problems of corrosion and to diminish the economic liability in the case of equipment. Till now, several review articles have been published

depicting elaborately the application of P, N and O atoms; but, a thorough literature survey revealed that corrosion inhibition studies of organic molecules bearing sulphur atoms are scarce. This part of thesis aims to study the applications of novel sulphur containing Schiff bases as corrosion inhibitors. Sulphur-containing compounds are greatly preferred for preventing the metallic dissolution, due to the high polarisability of the sulphur atom. So the present investigation is intended to realize novel potential sulphur containing organic inhibitors, especially towards carbon steel corrosion.

Seven novel sulphur containing Schiff base inhibitors, (E)-(N-anthracene-9-ylmethylene)-5-(4-nitrophenyl)-1,3,4-thiadiazol-2-amine (A9CNPTDA), (E)-5-(4-nitro phenyl)-N-((pyridine-2-yl)methylene)-1,3,4-thiadiazol-2amine (P2CNPTDA), (E)-5-(4-nitrophenyl)-N-(1(pyridine-3-yl)ethylidene)-1,3,4-thiadiazol-2-amine (3APNPTDA), (E) -5-(4-nitrophenyl)-N-(1(pyridin-2-yl)ethylidene)-1,3,4-thiadiazol-2-amine (2APNPTDA), N-(anthracen-9(10H)-ylidene)-5-(4-nitrophenyl)-1,3,4-thiadiazol-2-amine (ANNPTDA), N-((1H-indol-3-yl)methylene)thiazol-2amine (I3A2AT) and (13E)-N1,N2-bis((thiophene -2-yl)methylene)cyclohexane-1,2-diamine (T2CDACH) were synthesized and a detailed procedure for the synthesis of these inhibitors are explained in chapter 2. The present work was designed in order to explore the inhibition efficiencies of these 'S' containing heterocyclic Schiff bases as corrosion inhibitors on carbon steel (CS) in aggressive medium (1M HCl and 0.5M H_2SO_4). The behaviour of CS in the presence of these heterocyclic compounds was investigated by electrochemical measurements and gravimetric studies. Electrochemical impedance spectroscopy, potentiodynamic polarization and electrochemical noise studies were employed for the detailed analysis. Quantum chemical studies were also performed. The mechanism of corrosion inhibition by these sulphur-containing heterocyclic Schiff bases was another consideration of this part which will be addressed via the evaluation of the adsorption as well as

thermodynamic parameters and was further verified by surface morphological studies using scanning electron microscopy.

The entire work on corrosion inhibition studies are well documented in this part as two chapters. Chapter 12 describes the corrosion inhibition investigations of CS in the presence of 'S' containing heterocyclic Schiff bases in 1M HCl medium. Corrosion inhibition response of these Schiff bases on CS in 0.5M H_2SO_4 are well explained in chapter 13. Both these chapters comprise of the weight loss measurements, electrochemical measurements, surface morphological studies and quantum chemical studies in detail. Lastly a brief summary on these finding is depicted following by important references.

CHAPTER 11
MATERIALS AND METHODS

Corrosion inhibition effectiveness of novel 'S' containing heterocyclic Schiff bases was investigated by adopting conventional mass loss or gravimetric investigations [75], electrochemical methods like Tafel polarization analysis [76], electrochemical impedance spectroscopy (EIS) [77], electrochemical noise studies [78] and theoretical calculations such as quantum chemical studies [79]. Scanning electron microscopy [80], UV spectroscopy [81] and Fourier transform infrared spectroscopy [82] were engaged to analyze the surface morphological studies of the metal specimen.

It is not a monotonous job to craft a natural corrosive environment for the experimental settings in a laboratory. For mimicking the corrosive environment, we have customary to espouse accelerated corrosion environment, since corrosion is not only a natural and slow observable fact and to monitor the decay rate of steel is a very prolonged process. Before execution of corrosion inhibition tests, surface treatments of metal specimens were performed to make them free from grease and oxides are crucial. The preparation of metal specimens, aggressive solutions (acidic medium) and different techniques adopted for the assessment of corrosion inhibition efficiencies of these 'S' containing heterocyclic Schiff bases are specified in detail.

Metal Specimens

Carbon steel (CS) specimen dimensions (1cm long x 1cm breadth x 0.155 thickness) were used for conventional gravimetric experiments. The weight % (Chemical composition; C,0.55%; Mn,0.08%; Si,0.02% ; P,0.04%; S,0.012%) and the remainder Fe (confirmed by EDX method) of the CS worn throughout the investigation. Before weight loss and electrochemical investigations, CS specimen was cleaned underneath running

distilled water and abraded using diverse grades of silicon carbide emery papers (grade 100-1200), washed with detergent and dried. The precise surface area of the carbon steel specimens was exactly measured using screw gauge and vernier callipers. The cleaned specimen was engrossed in acetone for 10s, washed, dried using tissue paper and weighed. The specimens were conserved in desiccators with the intention to keep away from the contact of the environment till use. After immersing carbon steel specimens in aggressive medium in the absence and presence of inhibitors in diverse concentrations for a preset time, metal specimens were carefully removed, dried and then weighed.

Aggressive Solutions

Stock solutions having 1M HCl and 0.5M H_2SO_4 were prepared by the dilution of the accurate quantity of respective concentrated acids (AR grade) and using double distilled water. Stock solutions of each 'S' containing heterocyclic ligands were prepared by weighing precise amounts of these with corresponding acids and diluted to diverse concentrations (0.2mM–1.0mM). 50ml and 100ml acid solutions were used in gravimetric studies and electrochemical investigations respectively.

Methods

Gravimetric measurements were done following ASTM standards. Aggressive solutions having different concentrations of sulphur-containing heterocyclic Schiff base inhibitors were prepared, finely polished carbon steel (CS) specimens were engrossed in these solutions and the weight loss of steel specimens was calculated after 24h A blank trial was also done without the addition of the inhibitors. Duplicate experiments were carried for ensuring the reproducibility of results and the average values were recorded. The corrosion rate of carbon steel and the percentage of inhibition efficiencies of each sulphur-containing heterocyclic Schiff base inhibitors

were estimated by the following equations. The rate of corrosion was expressed in 'mm/y' and the percentage of inhibition efficiencies of each sulphur-containing heterocyclic Schiff base inhibitor were calculated using equations (1) and (2) respectively.

$$\text{Rate of corrosion, } W = \frac{K \times \text{Wt.loss (grams)}}{\text{Area in sq.cm} \times \text{Time in Hrs} \times \text{Density}} \quad (1)$$

where 'K'= 87600 (This factor used to alter cm/hour into mm/year), Density of CS specimen is 7.88g/cc

The inhibition efficiency (η) or Percentage of inhibition is given by

$$\eta = \frac{W - W'}{W} \times 100 \quad (2)$$

where W and W' are the corrosion rate of the CS specimen without and with sulphur-containing heterocyclic Schiff base inhibitors respectively [83].

Comparison studies of the inhibition efficiency of the synthesized heterocyclic Schiff bases with their parent amine for a period of 24 hrs explore the function of azomethine linkage in the corrosion inhibition ability of heterocyclic Schiff bases.

Adsorption Isotherms

The mechanism of action of inhibition of Schiff bases on the metal surface is not entirely disclosed by the researchers and later it was proved that adsorption is the main reason for the inhibitory action of these molecules [84,85]. It may be physical adsorption, chemical adsorption or both. Adsorption isotherms have a significant role in shaping the inhibition mechanism [86,87]. The extend of corrosion inhibition can be explained by considering the adsorption isotherms. These isotherms characterize the molecular interactions with the reactive sites on the specimen surface. Langmuir, Freundlich, Frumkin and Temkin are the common adsorption isotherms. The finest fit isotherm is

accepted with the support of correlation coefficient and all isotherms were tried with the help of following equations

Langmuir adsorption isotherm $\frac{C}{\theta} = \frac{1}{K_{ads}} + C$ (3)

Freundlich adsorption isotherm $\theta = K_{ads}C$ (4)

Temkin adsorption isotherm $e^{f\theta} = K_{ads}\, C$ (5)

Frumkin adsorption isotherm $\frac{\theta}{1-\theta}\exp(f\theta) = K_{ads}\, C$ (6)

where C is the inhibitor concentration, θ is the fractional surface coverage, f is the molecular interaction parameter and K_{ads} is the adsorption equilibrium constant. Among the tried isotherms, most suitable one which has the highest correlation coefficient value (R^2) was considered for explaining the adsorption mechanism.

The relation between adsorption equilibrium constant K_{ads} and the standard free energy of adsorption ΔG^0_{ads} given by the equation,

$\Delta G^0_{ads} = -RT\ln(55.5\, K_{ads})$ (7)

where the constant value 55.5 is the molar concentration of water, R is the ideal gas constant and T is the temperature in Kelvin. The value of K_{ads} and ΔG^0_{ads} were obtained from different adsorption isotherms.

Surface Analysis

The changes in the morphology of the carbon steel surface monitored by surface analysis help to illustrate the mechanism by which the synthesized compounds diminish the rate of corrosion [88]. This was done by taking SEM image (scanning electron microscopic images) of the surfaces of untreated bare metal (CS), metal engrossed in acid medium (24h) and metal engrossed in synthesized inhibitor solution (24 h). For taking SEM-EDAX the Model-JEOL 6390LA/OXFORD XMX N (0.5-30KV) accelerating voltage and Magnification x 300000) was used.

Temperature Studies

The evaluation of thermodynamic corrosion parameters (activation energy (E_a), enthalpy of corrosion (ΔH*), the entropy of corrosion (ΔS*) and Arrhenius parameter (A) in the gravimetric weight loss study was evaluated in different temperatures (30-60°C). The activation energy for the corrosion progression in the absence and presence of these synthesized sulphur containing Schiff bases was assessed by Arrhenius equation.

Rate of Corrosion; $K = A \exp\left(\frac{-Ea}{RT}\right)$ (8)

where A is the frequency factor, E_a is the activation energy, R is the gas constant and T is the temperature (Kelvin). The plot logK Vs 1000/T have to be a straight line. According to this equation, slope of the line will be $-E_a/2.303R$ (activation energy evaluated from this slope) and intercept will be log A.

Transition state theory [89] can be used for the assessment of the enthalpy and entropy of activation (ΔH*, ΔS*), which corresponds to the equation,

$$K = \left(\frac{RT}{Nh}\right) \exp\left(\frac{\Delta S*}{R}\right) \exp\left(\frac{-\Delta H*}{RT}\right) \quad (9)$$

where N is the Avogadro number and h is the Planks constant. This equation can be modified to an equation for straight line (y = mx + c)

$$log\ \frac{K}{T} = log\ \frac{R}{Nh} + \frac{\Delta S}{2.303\ R} - \frac{\Delta H}{2.303\ RT} \quad (10)$$

The enthalpy of the reaction can be obtained from the slope, $-\Delta H/2.303R$ and entropy of the reaction acquired from the intercept, $(\log\frac{R}{Nh} + \frac{\Delta S}{2.303\ R})$ of the line on y axis.

Electrochemical Impedance Spectroscopy

AC impedance methods or electrochemical impedance spectroscopy (EIS) are extensively exploited in modern days for corrosion experiments [90–96] as a

sophisticated and precise method. Mechanistic and kinetic information on inhibition investigations can be attained by impedance measurements. The response of the system offers information concerning the responses occurring at the interface. The detection of electric and dielectric properties of components under inquiry is made viable by the system. By means of suitable equivalent electrical circuits [97], electrochemical scrutinisation can be performed.

Iviumcompactstat-e system associated with a superior version of 'IviumSoft' software was employed for the electrochemical analysis. This makes it easier and possible steps to derive an appropriate equivalent circuit, computation of current densities and resistance. Assemblies of three-electrode was used as the electrochemical cell in which a saturated calomel electrode (SCE) was used as the reference electrode, a platinum electrode of area $1cm^2$ was used as the auxiliary or counter electrode and well-polished metal surface of exposed area ($1cm^2$) towards the corroding medium was employed as the working electrode for analysis.

The dimension of the capacitance (C_{dl}) in the constituency of the electrical double layer formed between oppositely charged ions in the aggressive medium and the charged carbon steel surface can be regarded as correspondent to an electrical capacitor. Corrosion inhibitors in the aggressive medium form an adsorption layer on the electrode (CS) surface. The electrical capacity decreases with an increase in the concentration of the inhibitor.

A small and steady sinusoidal current was applied during the measurement of impedance and along with the phase angle and the resulting current was measured. The real and imaginary fractions of impedance were derived by this method. The real constituent of the impedance, $Z'(\omega)$ corresponds to the resistance and the imaginary constituent, $Z''(\omega)$ corresponds to capacitance and the relation between these two

constituents are

$Z(\omega) = Z'(\omega) + jZ''(\omega)$

where Z(ω) is the impedance, Z'(ω) is given by $Z_0\cos\Phi$ and Z''(ω) is given by $Z_0\sin\Phi$, Z_0 is the magnitude of the impedance and j is the imaginary number √-1

Fig. 3.11: Equivalent circuit

Impedance data can be well represented by diverse forms of plots such as Nyquist (Cole-Cole) plot, Impedance plot and Bode plot and all forms provide considerable benefits for establishing definite characteristics of an exact system. The commonly used Nyquist plots are achieved by plotting the square of the real fraction of impedance against the square of the imaginary part. The ohmic resistance or solution resistance, R_s, is the resistance between the reference electrode and the working electrode, which is given by the impedance at elevated frequencies of the semicircular Nyquist plot. At the leftmost end of the semicircle, the frequency achieves its high limit of the semicircle and at the rightmost end, it achieves its low limit, where the impedance observed is the sum of R_s and R_{ct} (charge transfer resistance at the electrode-solution interface). Subsequently, the inhibition efficiency of the synthesized molecule can be deliberated using equation (11) [30].

$$\eta_{EIS}\,\% = \frac{R_{ct} - R'_{ct}}{R_{ct}} X100 \qquad (11)$$

where R'_{ct} and R_{ct} are the charge transfer resistances of working electrode (CS) in the absence and presence of inhibitor respectively.

In Bode plots, the magnitude of impedance (|Z|) and phase angle (θ), are plotted against frequency. The absolute impedance (Z) is acquired from the equation,

$$|Z| = \sqrt{Z'^2 + Z''^2} \quad (12)$$

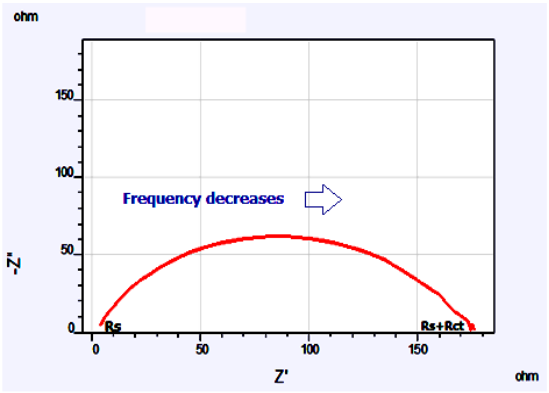

Fig. 3.12: Nyquistplot

The Bode plot is a time-consuming substitute of the Nyquist plot which helps to avoid longer times for the measurement of low frequency. The curve obtained from impedance plot ie log|Z| versus log frequency provides the value of R_s and R_{ct}. The cut-off point of this curve reclines on a straight line which has a slope of -1. Extrapolating this line to the y-axis at logf = 0 or f=1 provides outcome value of C_{dl}.

$$|Z| = \frac{1}{C_{dl}} \quad (13)$$

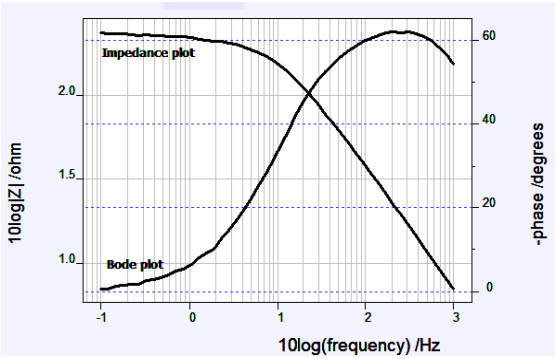

Fig. 3.13: Bode and impedance plots

The plot of 'θ' versus log f, shows a peak which equivalent to f θ^{max} representing the maximum phase shift value and from which C_{dl} can be intended. Frequency breakpoints allied with every step are the trait of impedance and Bode plots.

Potentiodynamic Polarization Studies

Polarization studies can be divided into two i) Linear polarization studies and ii) Tafel extrapolation studies. The Polarization technique associated with the alteration in the potential of the working electrode and the produced current is measured as a function of potential or time [98–100].

Linear polarization technique

The equation analogous to the Butler-Volmer equation can be used to explain the polarization reaction of a metal (carbon steel specimen)

$$i = i_{corr}[e\left(\frac{\eta}{\beta a}\right) - e\left(\frac{\eta}{\beta c}\right)] \quad (14)$$

where 'i' is the net current density across the metal specimen and electrolyte boundary, 'i_{corr}' is the corrosion current density (Acm^{-2}), $'\eta'$ is the overpotential (difference between $E_{measured}$ and E_{corr}). Depending on the mechanism of reaction, β_a and β_c are the anodic and cathodic constants and are specified by

$$\beta_a = \frac{RT}{(1-\propto)nF} \quad (15) \qquad \beta_c = -\frac{RT}{\propto nF} \quad (16)$$

It is established from Equation (14) that the charge transfer process occurred at the interface constituted by the metal and solution is the rate-determining step (slowest step) in the electrochemical process of corrosion. Experimentally this relation is observed between the potential of an electrode under corrosion (in the absence of competing redox reactions) and applied electrochemical current density. The significance of this relationship depends on the single charge transfer controlled anodic

and cathodic reactions. This equation brings the support of the electrode which undergo corrosion where electrochemical polarization method is applied.

Linear polarization mode depends on the practical and theoretical authentication that the applied current density is linear as a function of the potential of the electrode and potentials are very near to $E_{corr,}$ +/- 10mV. This is exemplified in Fig. 3.14.

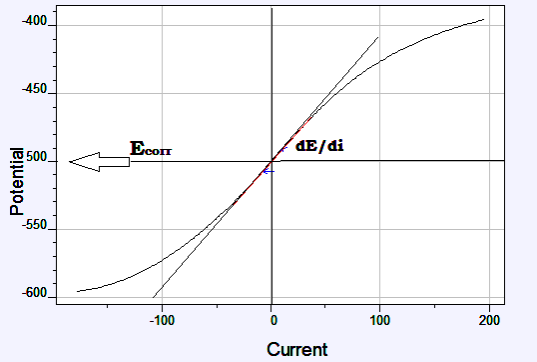

Fig. 3.14: Linear polarization plot

Slope is $\frac{\Delta E}{\Delta i}$ and has the unit of resistance (R_p), which is known as polarization resistance. Thus sometimes this approach is known as polarization resistance technique. When equation (14) undergo mathematical linearization, the famous Stern and Geary equation (11) is obtained, which indicates that the slope is inversely related to i_{corr} and is given by the equation

$$i_{corr} = \left[\frac{b_a b_b}{2.303(b_a b_b)}\right]\frac{\Delta i}{\Delta E} = \frac{B}{R_p} \qquad (17)$$

where 'b_a' and 'b_b' are called Tafel slopes (anodic and cathodic). Current density, i_{corr} in the form of corrosion rate can be measured with the aid of equation 17, where values of R_p and B are identified. For evaluating corrosion inhibition efficiency, linear polarization technique is employed in the manner that, whenever increasing the inhibitor concentration, polarization resistance (R_p) have the affinity to enhance. The rate of charge transfer process decreases on the corroding surface with the adsorption of inhibitors and

this practice boosts the polarization resistance or diminishes the corrosion rate. The polarization resistance values were acquired by the scrutiny of the slope of linear polarization curves in the vicinity of corrosion potential of blank and diverse concentration of the inhibitors [101,102]. The inhibition efficiency was considered from the polarization resistance, using the equation

$$\eta_{R_p}\% = \frac{R'_p - R_p}{R'_p} X100 \quad (18)$$

where 'R'_p' and 'R_p' are the polarization resistances with and without inhibitors respectively.

Tafel extrapolation technique

Tafel equation discloses the relationship between logarithmic value of current density and the applied potential. Using the equation 19, Tafel equation can simply be deduced. For an anodic (metal dissolution) process, the current density (i) is obtained by Tafel's law. The equation must assure the clause $\left(\frac{\eta_a}{\beta_a}\right) \gg 1$

$$i = i_{corr} e \left(\frac{\eta_a}{\beta_a}\right) \quad (19)$$

On taking the logarithm of the equation (19),

$$\eta_a = -\beta_a \ln i_{corr} + \beta_a \ln i_{corr} \quad (20)$$

Converting into logarithm to base 10 and defining the anodic Tafel constants a and b, then $\eta_a = a_a + b_a \log i_a$ (21)

where $a_a = -2.303\beta_a \log i_{corr}$ and $b_a = 2.303\beta_a \log i_a$

Likewise for cathodic process, $\left(\frac{\eta_b}{\beta c}\right) \ll 1$

$$i = -i_{corr} e \left(-\frac{\eta_c}{\beta c}\right) \quad (22)$$

Then $\eta_c = a_c - b_c \log i_c$ (23)

where $a_c = -2.303\beta_c \log i_{corr}$ and $b_c = 2.303\beta_c \log i_c$

The plot of potential of the electrode versus the logarithm of current density confers a straight line and termed as Tafel lines. The slope of a Tafel plot, 'b' provides the mechanism of electrode process and the intercept 'a' at $\eta = 0$ offer the exchange current density. The information of the rate constant is given by this model.

A way to measure i_{corr} value is the method of extrapolating the linear fragments of potential-current density curves. This practice is based on the law that the samplings (specimens) were made to operate as cathode of the electrochemical cell consisting the corrodent. Cathode potential-current density curve was plotted over a potential range E_{corr} to $E_{c.}$ In the same way, anodic potential-current density is attained in the path away from E_{corr} and at this moment the sampling (specimen) performes as anode. The attained cathodic and anodic potential-current density curves consist of linear sectors, regarded as Tafel constituency. By the extrapolation of these linear fragments of cathodic and anodic curves (Fig. 3.15), Tafel lines criss-cross at the point of coordinates E_{corr} and $logi_{corr}$ and thus the value corrosion current density achieved. Subsequently, the percentage of inhibition efficiency is calculated using the equation

$$\eta_{pol}\,\% = \frac{I_{corr} - I'_{corr}}{I_{corr}}\ X100 \qquad (24)$$

where i_{corr} and i'_{corr} are corrosion current densities of uninhibited and inhibited cases respectively.

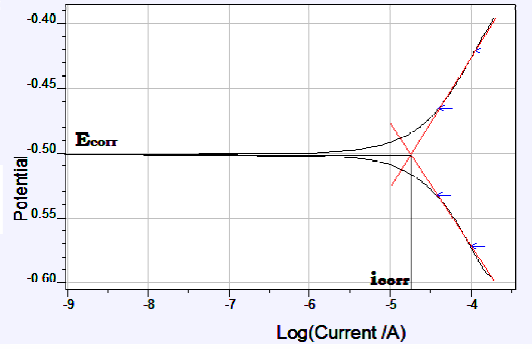

Fig. 3.15: Tafel plot

In the present investigation Tafel polarization studies of carbon steel in 1M HCl and 0.5M H_2SO_4 in the presence and absence of inhibitors conducted by recording both cathodic and anodic potentiodynamic polarization curves using Iviumcompactstat-e electrochemical system.

Electrochemical Noise Measurements

Electrochemical noise (ECN), is a common term which measures the fluctuations of current and potential allies with corrosion progression followed by metal deterioration. This technique also helps to compute the quantity of localized pitting corrosion [103–105]. The experimentation was executed in a three-electrode cell assemblage consisted of two carbon steel electrodes ($1cm^2$) used as working electrode and counter electrode/SCE was used as reference electrode [106,107] in the cell connected to Ivium Compactstat-e electrochemical system (controlled by Iviumsoft software) for a period of 1200s.

Noise is considered as a non-deterministic progression and it is an algebraic expression having random character which depicts the amplitude-time dependence of a source is unfeasible. Usually, deterministic progressions are periodic and this can be described mathematically by a varying function of time. Fluctuations observed in corrosion current values are a non-deterministic process and analysis done by statistics and probability rather than the algebraic method. Fig. 3.16 corresponds to the plot of noise current Vs time and the noise current values provide a design about the corrosion protection power of the molecules. Fig. 3.17 corresponds the pitting index curve of the sample and the amplitude of the curve point out the resistance power of the sample against localized pitting corrosion.

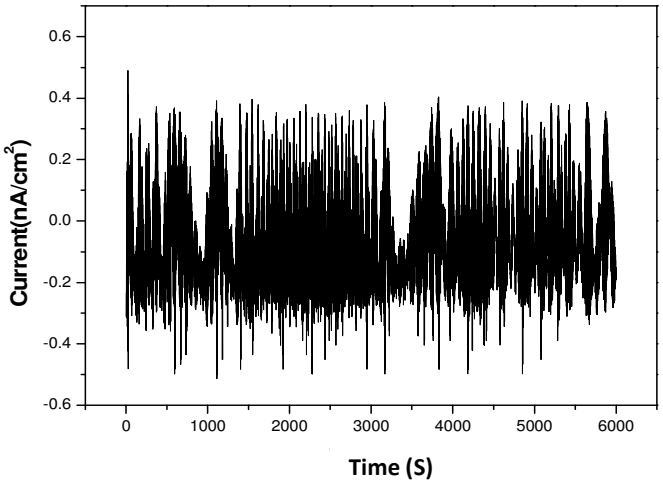

Fig. 3.16: Noise current Vs time

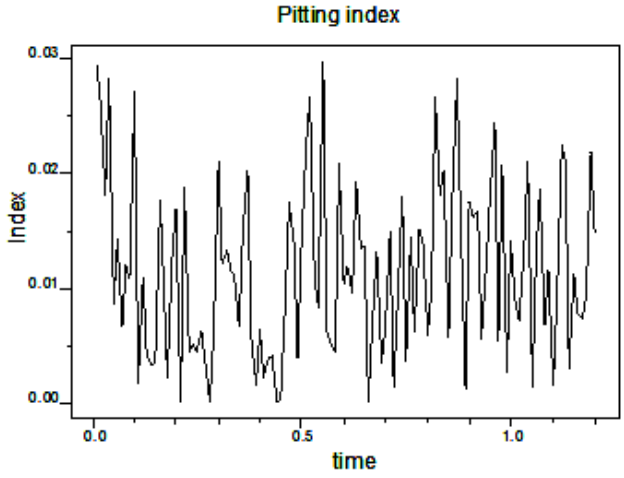

Fig. 3.17: Pitting index curve

Frequency Domain Analysis

It is understood that any complex waveform can be taken as the sum of several sinusoidal waveforms of acceptable amplitudes, periodicity and relative phase[108,109]. A spectrum is the illustration of time depending development in the frequency domain analysis and the corresponding noise measurement analysis gave the Power Spectral Density (PSD) which is given in Fig. 3.18. The PSD has diverse applications in different areas of science and technology which are showing here

- The signals of noise are significant in biomedical purposes like simulation, therapy etc;
- For acoustic measurements.
- Earthquake determination from the spectra obtained from seismographs.
- From the characteristic component analysis of the acoustic noise signals from the engine can detect its malfunction.

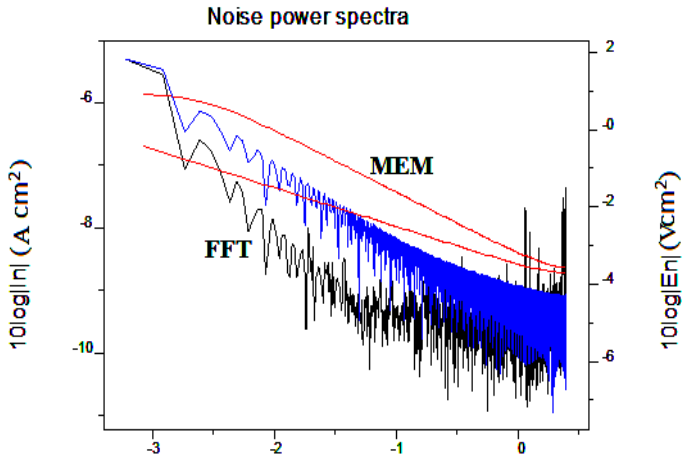

Fig. 3.18: PSD plot

Fast Fourier Transform (FFT)

In the complex Fourier series, Fast Fourier Transform is a machine calculation method and it is significantly quicker than other traditional methods. There are two major difficulties linked with investigation by FFT are aliasing and leakage. Aliasing applies to all spectral analysis methods and it is an error occurs by rate of sampling become too slow. Leakage is resulting by the basic presumption of the Fourier Transform to the fixed time record is said as periodic.

Maximum Entropy Method

In every spectral analysis mode, analysis by Fourier Transform has been measured as a basic tool [110]. It becomes precise only when long record length takes

place. When it is short, conventional spectrum estimation by smoothing may provide poor resolution. The Burg's maximum entropy method helps to improve the spectral resolution of short length records. This is achieved by the extrapolation of auto-correlation function and helps to maximize the entropy of the probability density function in each step of the extrapolation. Burg's method is data dependable method and therefore it is nonlinear. The MEM has applications in various fields in science and technology.

Quantum Chemical Studies

The corrosion inhibition response of organic molecules can be correlated with the energy of frontier molecular orbitals [111–113]. The donor-acceptor interactions (explained by HSAB concept)between the vacant d-orbitals of Fe on the surface atoms and the filled molecular orbitals of the inhibitor molecules are very significant in the preclusion of metal dissolution [114–116]. The high value of E_{HOMO} and the smallest value of E_{LUMO} and the difference in their energy (which should be low) are the vital parameters which assist the strong binding of the compounds on the metal surface. Optimisation of molecular geometry and calculations of quantum chemical studies was performed by DFT method utilizing the GAMMES software. Lee–Yang–Parr nonlocal correlation functional method (B3LYP) and Beck's three-parameter exchange functional was employed in DFT calculations [117]. HOMO (Highest occupied molecular orbital) gives information about the most vigorous (energetic) electrons containing regions and these electrons are generally likely to be donated to the electron-poor species. The LUMO (Lowest unoccupied molecular orbital) has the lowest energy and indicated the locations in a molecule which has the highest tendency to receive electrons from the electron-rich metal species. HSAB parameters such as electronegativity (χ) and chemical hardness (η) of the inhibitors were assessed by the following equations,

$$\chi \approx -1/2\ (E_{HOMO} + E_{LUMO}) \quad (25)$$

$$\eta \approx 1/2\ (E_{HOMO} - E_{LUMO}) \quad (26)$$

The number of electrons transferred (ΔN) implies the propensity of a ligand to donate electrons. Higher the value of ΔN, the superior is the tendency of the compound to donate electrons to the electron-deficient species. For the case of corrosion inhibitors, a higher ΔN signifies a greater tendency of interaction with the metal surface through the adsorption process. The electronegativity and chemical hardness of bulk iron are assumed as 7eV and zero respectively. The number of transferred electrons (approximate) from the molecule to atoms of iron is assessed by the subsequent equation,

$$\Delta N = \frac{\chi_{Fe} - \chi_{inhib}}{2(\eta_{Fe} + \eta_{inhib})} \quad (27)$$

Optimized geometry of newly synthesised molecules can be recognized by quantum mechanical software and this facilitates to forecast the three-dimensional arrangement of atoms in molecules which formulates them most stable form with the lowest energy.

CHAPTER 12

CORROSION INHIBITION STUDIES OF SULPHUR CONTAINING SCHIFF BASES ON CARBON STEEL IN 1M HCl

Corrosion inhibition investigations of seven novel 'S' containing Schiff base inhibitors, (E)-(N-anthracene-9-ylmethylene)-5-(4-nitrophenyl)-1,3,4-thiadiazol-2-amine (A9CNPTDA), (E)-5-(4-nitrophenyl)-N-((pyridine-2-yl)methylene)-1,3,4-thiadiazol-2-amine (P2CNPTDA), (E)-5-(4-nitrophenyl)-N-(1(pyridine-3-yl)ethylidene)-1,3,4-thiadiazol-2-amine (3APNPTDA), (E)-5-(4-nitrophenyl)-N-(1(pyridin-2-yl)ethylidene)-1,3,4-thiadiazol-2-amine (2APNPTDA), N-(anthracen-9(10H)-ylidene)-5-(4-nitrophenyl) -1,3,4-thiadiazol-2-amine (ANNPTDA), N-((1H-indol-3-yl)methylene)thiazol-2amine (I3A2AT) and (13E)-N1,N2-bis((thiophene-2-yl)methylene)cyclohexane-1,2-diamine (T2CDACH) on carbon steel were conducted by preparing inhibitor solutions in the range of 0.2mM-1mM in 1M HCl medium. Carbon steel specimens were prepared as per ASTM standards and employed for this study. To assess the capacity of inhibitors for corrosion inhibition, gravimetric weight loss measurements, potentiodynamic polarization (PDP), electrochemical impedance spectroscopy (EIS), electrochemical noise studies, quantum chemical analysis and surface morphological studies were performed and the results are documented in detail in this chapter.

Gravimetric Weight Loss Investigations

The well-polished specimens of CS were engrossed in the medium of hydrochloric acid in the absence and presence of the Schiff base inhibitors and the weight loss happened for the specimens were noted after 24h. The rate of corrosion was monitored and revealed that each heterocyclic sulphur containing Schiff base inhibitors do possess significant anticorrosive property towards the carbon steel corrosion in IM

HCl medium.

Table 3.1 represents the corrosion rates of the seven heterocyclic 'S' containing Schiff bases A9CNPTDA, P2CNPTDA, 3APNPTDA, 2APNPTDA, ANNPTDA, I3A2AT and T2CDACH in 1M HCl medium at 28^0C for 24h and established that the rates of corrosion of carbon steel specimens were noticeably decreased with the concentration of inhibitor in all cases. In the absence of Schiff bases, carbon steel specimen engrossed in the hydrochloric acid solution showed the corrosion rate of 9.19mmy^{-1}. But these seven 'S' containing Schiff bases inhibited the metallic dissolution appreciably in the acidic medium even at very low concentrations. Fig. 3.19 shows the comparison study of the corrosion rates of carbon steel specimen in the presence of varying concentrations of sulphur-containing heterocyclic Schiff base inhibitors.

Table 3.1: Corrosion rate of carbon steel in mmy^{-1} in the absence and presence of 'S' containing heterocyclic Schiff bases in 1M HCl at 28^0C for 24h

C (mM)	Corrosion rate (mmy^{-1})						
	A9CNPTDA	P2CNPTDA	3APNPTDA	2APNPTDA	ANNPTDA	I3A2AT	T2CDACH
0	9.19	9.19	9.19	9.19	9.19	9.19	9.19
0.2	0.52	1.09	0.86	1.1	1.68	0.72	1.55
0.4	0.47	0.85	0.68	1.04	1.18	0.56	1.16
0.6	0.42	0.65	0.64	0.83	0.92	0.52	0.93
0.8	0.35	0.44	0.44	0.72	0.78	0.42	0.82
1	0.18	0.29	0.35	0.41	0.43	0.22	0.45

On close assessment of the rates of corrosion, it is obvious that the carbon steel specimen exhibited an appreciably low corrosion rate in the presence of the heterocyclic Schiff base inhibitor A9CNPTDA in HCl medium and displayed an elevated value in the presence of T2CDACH. The value of the corrosion rate of CS for A9CNPTDA was 0.18mm/year at a concentration of 1mM and the rate in the presence of T2CDACH was

0.45mm/year. Values of the corrosion rate of heterocyclic corrosion inhibitors A9CNPTDA, P2CNPTDA, 3APNPTDA, 2APNPTDA and ANNPTDA, I3A2AT and T2CDACH were 0.18, 0.29, 0.35, 0.41, 0.43, 0.22 and 0.45mm/year respectively at 1mM concentration in 1M HCl medium.

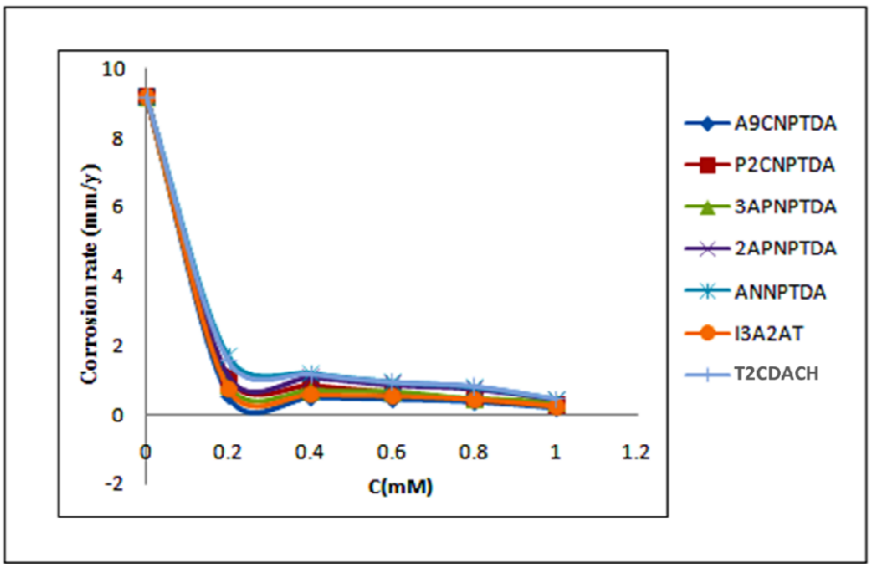

Fig. 3.19: Corrosion rates of CS with different concentration of 'S' containing heterocyclic Schiff base inhibitors in 1M HCl at 28^0C for 24h.

Corrosion inhibition efficiencies of these heterocyclic Schiff bases on carbon steel specimen were investigated in HCl medium which is depicted in Table 3.2 and a comparison of inhibition efficiencies at various concentrations are shown in Fig. 3.20. It is instantly recognizable that all 'S' containing heterocyclic Schiff bases containing azomethine linkage exhibited significant inhibition capacity against the corrosion of metals. These compounds are outfitted with active probes such as azomethine linkage, thiadiazole, thiazole, indole and thiophene moieties and aromatic rings in their structure. Lone pair of electrons on the 'N' atom and highly polarizable sulphur atom makes it a soft base and can contribute its electrons to the vacant'd' orbitals of Fe atoms (which can be considered as soft acid) efficiently. According to Pearson's concept, soft acids

strongly interact with soft bases and this soft-soft interaction is thus possible between the heterocyclic 'S' containing molecules with Fe atoms, which may be accountable for their higher inhibition efficiency. The efficiencies of these heterocyclic inhibitors were increased with the concentration.

Table 3.2: Corrosion inhibition efficiencies of 'S' containing heterocyclic Schiff bases in 1M HCl at 28^0C for 24h

C (mM)	Inhibition Efficiency (η_w%)						
	A9CNPTDA	P2CNPTDA	3APNPTDA	2APNPTDA	ANNPTDA	I3A2AT	T2CDACH
0.2	93.87	88.07	90.68	88.07	81.68	91.38	81.42
0.4	94.26	90.68	92.63	88.64	87.16	93.9	86.59
0.6	95.42	93.88	92.88	90.96	89.98	94.35	89.83
0.8	96.17	95.64	95.19	92.16	91.51	94.94	91.15
1	98.04	96.81	96.22	95.53	95.32	97.61	95.18

On examining Table 3.2, it is quite clear from the data that five heterocyclic 'S' containing Schiff bases A9CNPTDA, P2CNPTDA, 3APNPTDA, 2APNPTDA, ANNPTDA derived from 5-(4-nitro)-1,3,4-thiadiazol-2-amine (NPTDA), the Schiff base I3A2AT, derived from thiazole 2-amine and T2CDACH, which is a thiophene derivative possess excellent corrosion inhibition efficiencies at all concentrations. All of them showed outstanding corrosion inhibition efficiencies and displayed >95.18% of corrosion inhibition efficiency on CS at 1mM concentration at 28^0C.

The potential inhibition efficiency of thiadiazole derivatives of Schiff bases A9CNPTDA, P2CNPTDA, 3APNPTDA, 2APNPTDA and ANNPTDA molecules can be accredited to the presence of heteroatoms especially highly polarizable 'S' atom in the thiadiazole ring, azomethine moiety, electron-rich aromatic rings and planar structure. The highly delocalized electron clouds of the aromatic rings interacted with the metal surface deeply and thus prevent the metallic dissolution appreciably. On approach to the

metal surface, $-NO_2$ group in the heterocyclic Schiff bases derived from NPTDA is replaced by the electron-rich (activating) amino group by the reduction process. In 1854, M.A Bechamp reduced the aromatic nitro compounds into the corresponding amino compounds using Fe/HCl [118] and prepared naphthylamines from nitro naphthalenes and anilinenitrobenzene. The larger electron density around the amino group along with other factors helps the Schiff bases to adsorb on the surface of the metal firmly and can display excellent inhibition efficiency.

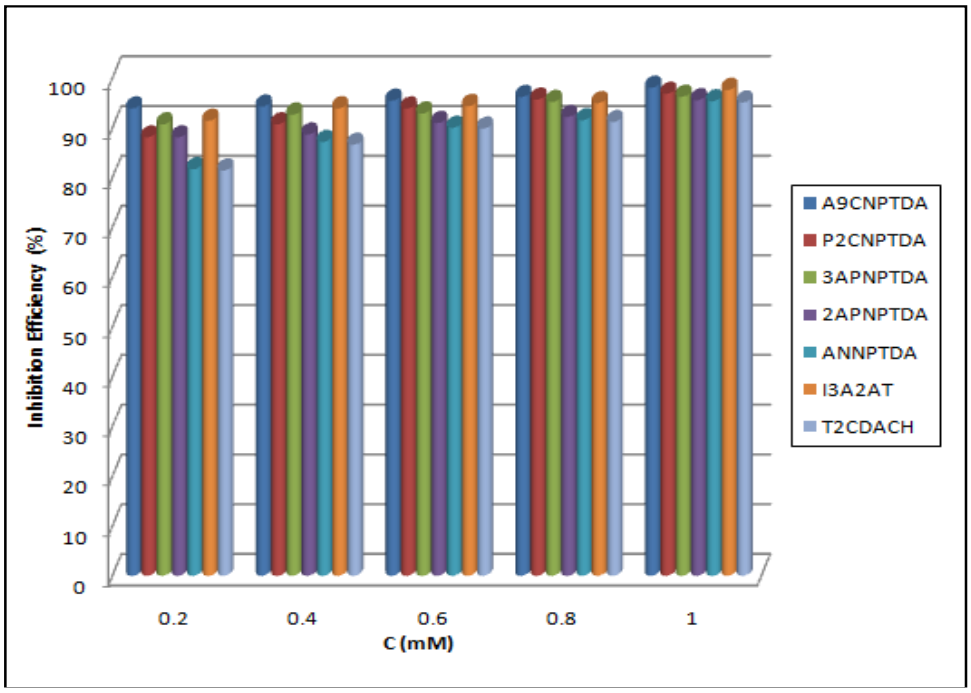

Fig. 3.20: Comparison of corrosion inhibition efficiencies (η_w%) of 'S' containing heterocyclic Schiff bases on CS in 1M HCl at 28^0C for 24h

On the assessment, it is obvious from the data that the heterocyclic polynuclear Schiff base A9CNPTDA showed pronounced corrosion inhibition efficiency compared to all other heterocyclic Schiff bases at every concentration and a maximum efficiency of 98.04% was exhibited at 1mM concentration. The remarkable corrosion preventing ability of this ligand can be interrelated with its molecular structure. Presence of highly delocalized π electron cloud of the aromatic rings in the aldehyde fraction, highly

polarisable ‘S’ atom, lone-pair of electrons of two N atoms of the thiadiazole moiety and one phenyl group attached to it together with highly conjugated azomethine linkage makes A9CNPTDA so electron-rich and help the molecule to bind metal atoms on the carbon steel surface efficiently. In addition to this, the molecule possesses almost planar structure which was deep-rooted by the optimized geometry calculation and favoring strong binding on the carbon steel surface.

Even though there is a structural similarity between the polynuclear heterocyclic Schiff bases A9CNPTDA and ANNPTDA, corrosion inhibition efficiency of ANNPTDA is relatively low compared to that of A9CNPTDA. It is not only due to the presence of an sp^3 carbon atom in the aromatic ring, but also there is a slight deviation from its coplanarity. In addition to the less extensive conjugation and aromatic nature, the presence of strained azomethine linkage also caused to decrease its corrosion inhibition efficiency.

One of the key factors for the elevated inhibition efficiency of heterocyclic pyridine derivatives P2CNPTDA, 3APNPTDA and 2APNPTDA molecules is the presence of pyridine ring in addition to thiadiazole moiety, azomethine linkage and a phenyl group. Maximum inhibition efficiency of 96.81, 96.22 and 95.53% was exhibited by P2CNPTDA, 3APNPTDA and 2APNPTDA respectively at 1mM concentration. On comparing the inhibition efficiencies of P2CNPTDA and 2APNPTDA in HCl medium, 2APNPTDA showed comparatively low η_w%. In these molecules, azomethine linkage starts from the second position of the pyridine ring but a severe steric hindrance is observed in 2APNPTDA due to a bulky methyl group, leading to the loss of coplanarity. But in the case of 3APNPTDA, a methyl group is at the third position with respect to ‘N’ atom of the pyridine ring. There is no steric hindrance in this molecule and planarity is maintained and so high inhibition efficiency showed by this molecule compared to

2APNPTDA.

For a period of 24h, the I3A2AT molecule showed little bit higher inhibition efficiency than the molecule T2CDACH at all concentrations and a maximum efficiency of 97.61% was achieved at a concentration of 1mM. The enhanced efficiency of I3A2AT attributed by the presence of indole and thiazole moieties, extensively conjugated azomethine linkage and electron rich aromatic heterocyclic ring contain highly polarizable 'S' atom. The decreased inhibition efficiency of T2CDACH may be due to its puckered nature of aromatic rings.

Stability of the inhibitor in aggressive medium is very essential if it is to be recommended for long time use. The consequence of time on the corrosion inhibition efficiency of these 'S' containing heterocyclic corrosion inhibitors are represented in Table 3.3.

Table 3.3: Effect of time on the corrosion inhibition efficiency of 'S' containing heterocyclic corrosion inhibitors (1mM) on CS in 1M HCl

Time (h)	Inhibition Efficiency (η_w%)						
	A9CNPTDA	P2CNPTDA	3APNPTDA	2APNPTDA	ANNPTDA	I3A2AT	T2CDACH
24	98.04	96.81	96.22	95.53	95.32	97.61	95.08
48	97.93	94.64	94.01	92.68	94.88	95.12	82.16
72	97.82	94.38	94.30	90.30	94.12	93.34	71.91
96	97.89	93.79	94.27	88.62	92.60	91.18	62.14
120	97.85	93.782	94.64	84.72	90.31	89.83	39.49

Fig. 3.21 represents the variation of corrosion inhibition efficiency with time for the inhibitor molecules at 1mM concentration. The results of gravimetric corrosion studies established that all inhibitor molecules derived from NPTDA and 2-amino thiazole exhibited predominant inhibition efficiency for a long time period. This may be due to their slow hydrolysis rate in acidic medium and prominent adsorption capability by highly active heteroatoms

Even though T2CDACH contain two thiophene ring and two azomethine linkage, its inhibition efficiency decreased with time. It is attributed by its puckered geometry and the tendency to hydrolysis which prevents the molecule to interact with the metal surface. It was confirmed by UV-Visible study that this molecule undergo fast hydrolysis into their parent compounds in 1M HCl medium (Fig. 3.22).

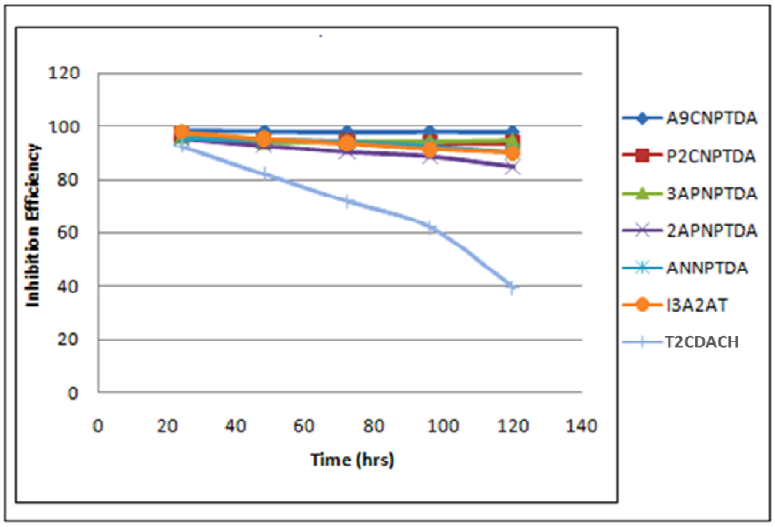

Fig. 3.21: Variation of corrosion inhibition efficiencies of 'S' containing heterocyclic Schiff base inhibitors (1mM) with time on CS in 1M HCl

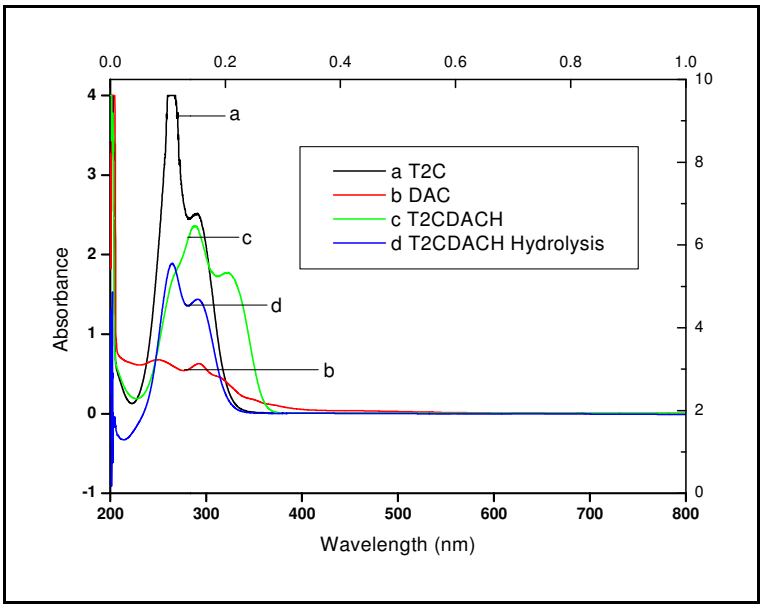

Fig. 3.22: UV-Visible spectra of a) Thiophene 2-carbaldehyde (T2C) b) 1,2 Diaminocyclohexane (DAC) c) T2CDACH at 0h and (d) T2CDACH at 48h 1M HCl

Comparison of Corrosion Inhibition Efficiencies (η_w%) of Schiff Bases With Their Parent Compounds

Corrosion inhibition behaviour of five thiadiazole heterocyclic Schiff base inhibitors A9CNPTDA, P2CNPTDA, 3APNPTDA, 2APNPTDA and ANNPTDA was compared with their parent amine 5-(4-nitrophenyl)-1,3,4-thiadiazol-2-amine (NPTDA) at three different concentrations and revealed that inhibition efficiency was remarkably higher than that of parent amine. Superior inhibitory authorities of these ligands were accredited due to the presence of extensively conjugated azomethine linkage in their structure.

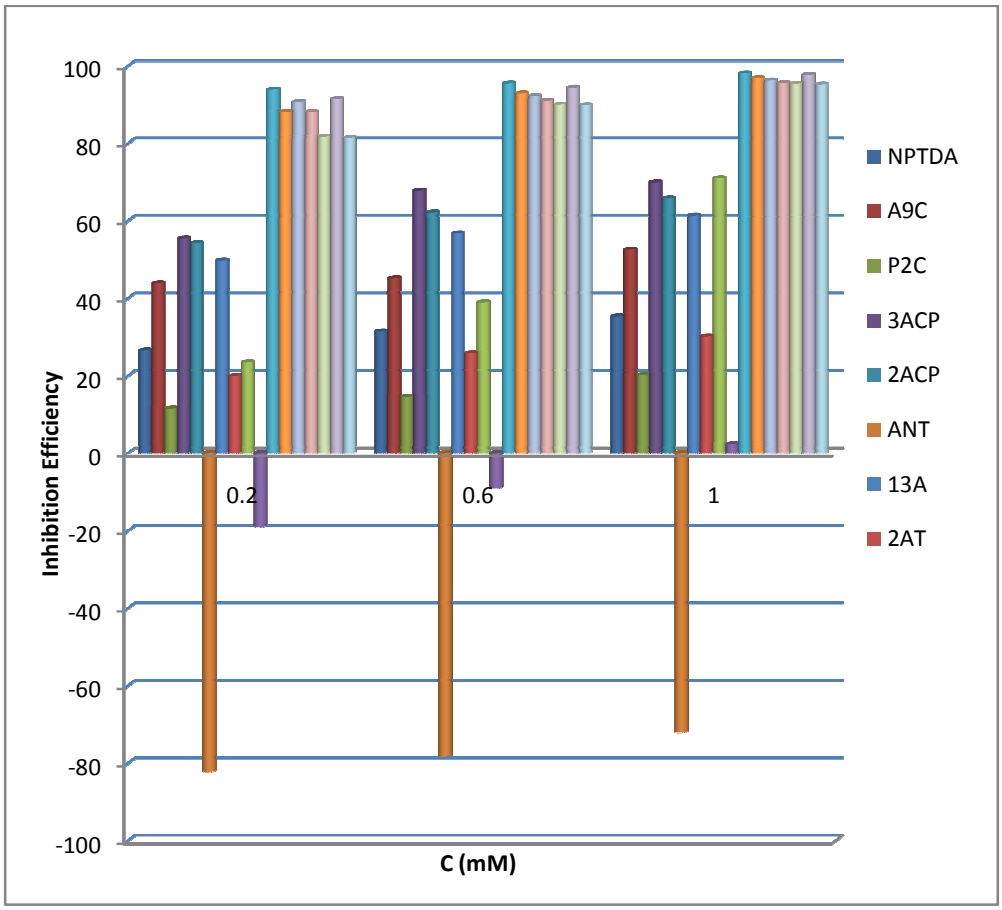

Fig. 3.23: Comparison study of corrosion inhibition efficiencies (η_w%) of 'S' containing heterocyclic Schiff bases with their parent compounds in 1M HCl

It is evident from the Fig. 3.23 and Table 3.4 that all synthesized sulphur-containing heterocyclic Schiff bases exhibit extraordinarily high inhibition efficiencies in comparison with their subsequent parent compounds Anthracene 9-carbaldehyde (A9C), Pyridine-2-carbaldehyde (P2C), 3-acetylpyridine (3ACP), 2-acetylpyridine (2ACP), Anthrone (AN), Indole-3-Carbaldehyde (I3A), 2-Aminothiazole (2AT), Thiophene-2-carbaldehyde (T2C) and 1,2-Diamino cyclohexane (DAC). This substantiates the striking aspect of electron rich azomethine (C=N) moiety present in all sulphur containing Schiff bases which hamper the mechanism of corrosion on the CS surface

Table 3.4: Corrosion inhibition efficiencies (η_w%) of parent compounds NPTDA, A9C, P2C, 3ACP, 2ACP, ANT, I3A, 2AT, T2C and DAC on CS in 0.5M HCl for a period 24h

C (mM)	Inhibition Efficiencies (η_w%)									
	NPTDA	A9C	P2C	3ACP	2ACP	ANT	13A	2AT	T2C	DAC
0.2	26.57	43.87	11.56	55.43	54.28	-82.26	49.74	19.97	23.47	-19
0.6	31.47	45.13	14.5	67.78	62.13	-78.34	56.72	25.78	38.94	-9
1	35.3	52.55	20.16	69.92	65.78	-72.06	61.36	30.17	70.96	2.3

Adsorption Isotherms

The mechanism of inhibition of these sulphur-containing Schiff bases on the surface of the carbon steel specimens can be explained by the adsorption process and the resultant surface modifications on the metal specimen under consideration. The mechanism of adsorption of these organic compounds can be explained by considering different adsorption isotherms; in which the commonly used ones are Langmuir, Freundlich, Temkin, Frumkin, Elawady, and FlorryHuggin etc. The parameters like free energy of adsorption ΔG_{ads} and adsorption equilibrium constant K_{ads} were calculated and its assessment is done by selecting the finest fit isotherm model assisted by the highest correlation coefficient (R^2).

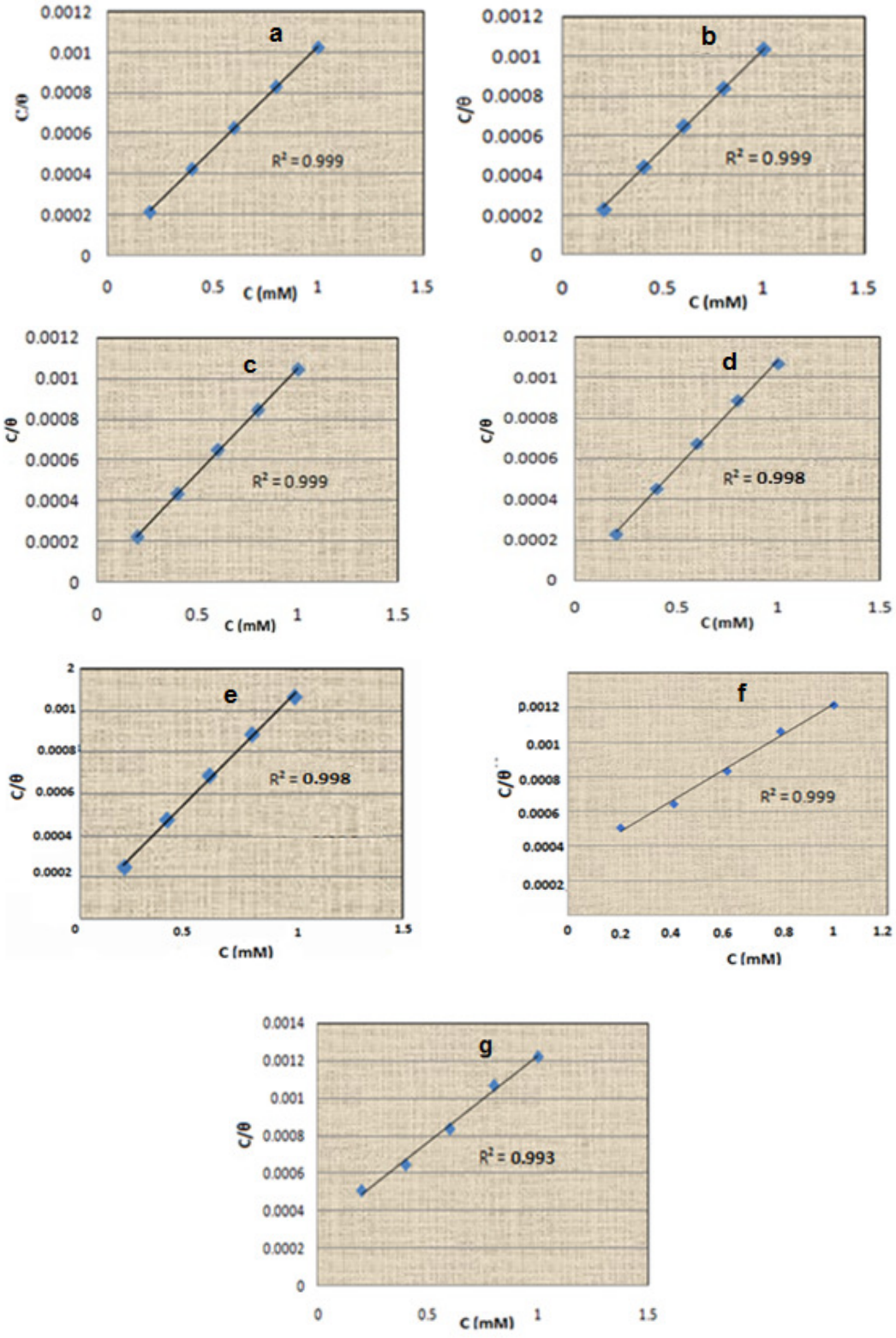

Fig. 3.24: Langmuir adsorption isotherm of (**a**) A9CNPTDA, (**b**) P2CNPTDA, (**c**) 3APNPTDA, (**d**) 2APNPTDA (**e**) ANNPTDA (**f**) I3A2AT (**g**) T2CDACH on CS corrosion in 1M HCl

From the adsorption investigations, it was found that these 'S' containing heterocyclic Schiff base inhibitors A9CNPTDA, P2CNPTDA, 3APNPTDA, 2APNPTDA, ANNPTDA, I3A2AT and T2CDACH followed Langmuir adsorption isotherm on the CS surface of during the process of corrosion inhibition. Isotherms of these inhibitors in 1M HCl are represented from Fig. 3.24 and parameters obtained from investigations are tabulated in Table 3.5

Table 3.5: Adsorption parameters of 'S' containing heterocyclic Schiff bases on CS corrosion in 1M HCl

Adsorption Parameter	Schiff bases						
	A9CNPTDA	P2CNPTDA	3APNPTDA	2APNPTDA	ANNPTDA	I3A2AT	T2CDACH
K_{ads}	58823.5	50000	47619	33334	22222.2	47128.6	3333.3
ΔG^0_{ads} ($kJmol^{-1}$)	-37.56	-37.15	-37.02	-36.14	-35.12	-37.02	-30.37

Negative values of ΔG^0_{ads} for all sulphur containing Schiff bases inhibitors point out the spontaneity of the adsorption on the surface of CS. ΔG^0_{ads} values up to -20kJ/mol indicates the electrostatic interaction between the charged heterocyclic organic inhibitors and the charged metal surface (physisorption). If ΔG^0_{ads} is more negative than -40kJ, shows a well-built adsorption of the inhibitors molecules on the surface of the metal through co-ordinate type bond, which is known as chemisorption [119]. In the present investigation, all the synthesized novel 'S' containing Schiff bases inhibitors exhibited ΔG^0_{ads} ranges between -30.37 and -37.56 kJ/mol on CS specimens in 1M HCl medium which implies that the adsorption behaviour of all the synthesized heterocyclic inhibitor molecules involves both electrostatic and chemical adsorption. The free energy of adsorptions of these heterocyclic Schiff base inhibitors, A9CNPTDA, P2CNPTDA, 3APNPTDA, 2APNPTDA and I3A2AT, were comparatively elevated than that of the other heterocyclic imines ANNPTDA and T2CDACH. The main reason is that these inhibitors are more powerfully adsorbed on the CS surface forming a monolayer through

highly conjugated azomethine linkage, highly polarisable aromatic rings. Planarity of the molecule also helped to adsorb molecules strongly.

The adsorption equilibrium constant K_{ads} also represents the extension of the adsorption happening on the corresponding surface. The above data shows that almost all heterocyclic Schiff base inhibitors derived from 5-(4-nitrophenyl)-1,3,4-thiadiazol-2-amine (NPTDA) except ANNPTDA and the Schiff bases derived from thiazole I3A2AT have relatively high K_{ads} value than heterocyclic sulphur containing Schiff base T2CDACH.

Impact of Temperature

To assess the consequences of temperature of corrosion inhibition process of these 'S' containing heterocyclic Schiff bases, gravimetric weight loss studies were performed at the temperature sequence of 303-333K. The activation energy of corrosion (E_a) with and without these inhibitors was measured by Arrhenius equation,

The rate of corrosion,

$$K = A \exp\left(\frac{-Ea}{RT}\right) \quad (28)$$

where A is the frequency factor, R is the universal gas constant and T the temperature in Kelvin scale.

Linear plots between log K and 1000/T having regression coefficients close to unity point out that the corrosion on CS in aggressive medium can be explained by a simple kinetic model. Fig. 3.25-3.31 represents the plots of log K Vs 1000/T and log (K/T) Vs 1000/T with and without these inhibitors. Enthalpy and entropy of activation (ΔH^*, ΔS^*) were calculated from the transition state theory, which can be represented by the following equation.

$$K = \left(\frac{RT}{Nh}\right) \exp\left(\frac{\Delta S*}{R}\right) \exp\left(\frac{-\Delta H*}{RT}\right) \quad (29)$$

where h is the Planck's constant and N is the Avogadro number.

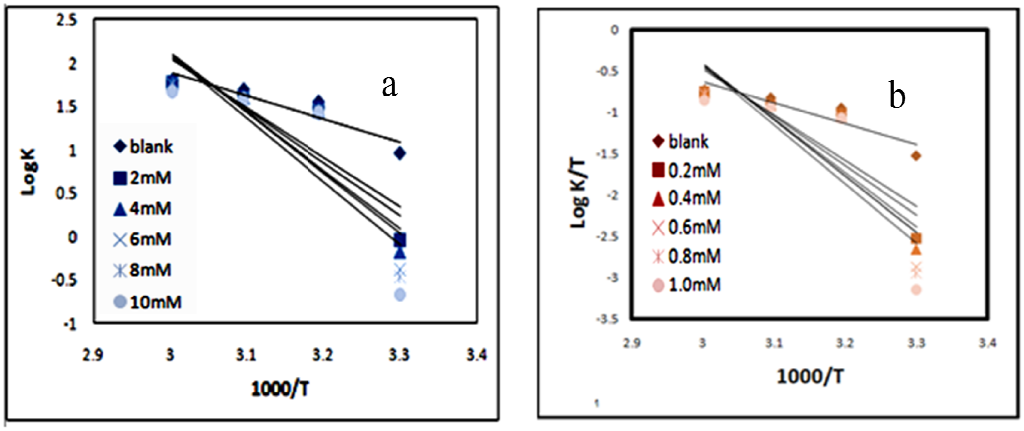

Fig. 3.25: a) Arrhenius plots and **b)** log (K/T) vs 1000/T plots of CS corrosion in the presence and absence of A9CNPTDA in 1M HCl

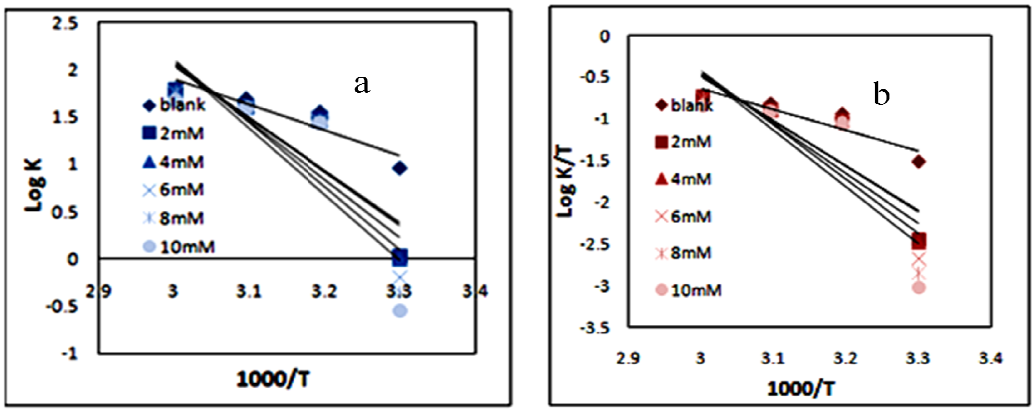

Fig. 3.26: a) Arrhenius plots and **b)** log (K/T) vs 1000/T plots of CS corrosion in the presence and absence of P2CNPTDA in 1M HCl

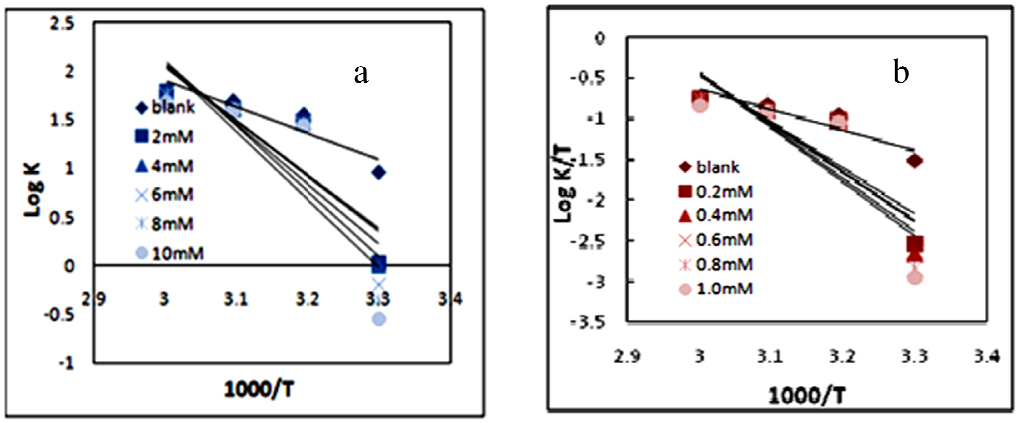

Fig. 3.27: a) Arrhenius plots and **b)** log (K/T) vs 1000/T plots of CS corrosion in the presence and absence of 3APNPTDA in 1M HCl

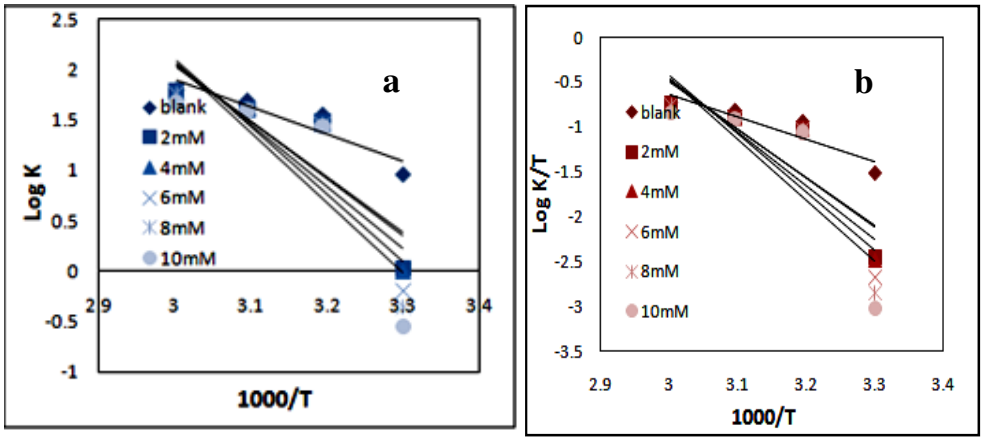

Fig. 3.28: a) Arrhenius plots and **b)** log (K/T) vs 1000/T plots of CS corrosion in the presence and absence of 2APNPTDA in 1M HCl

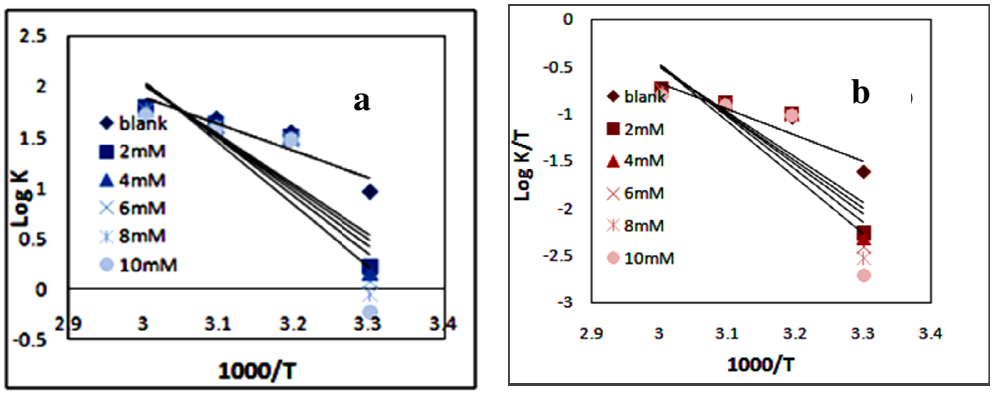

Fig. 3.29: a) Arrhenius plots and **b)** log (K/T) vs 1000/T plots of CS corrosion in the presence and absence of ANNPTDA in 1M HCl

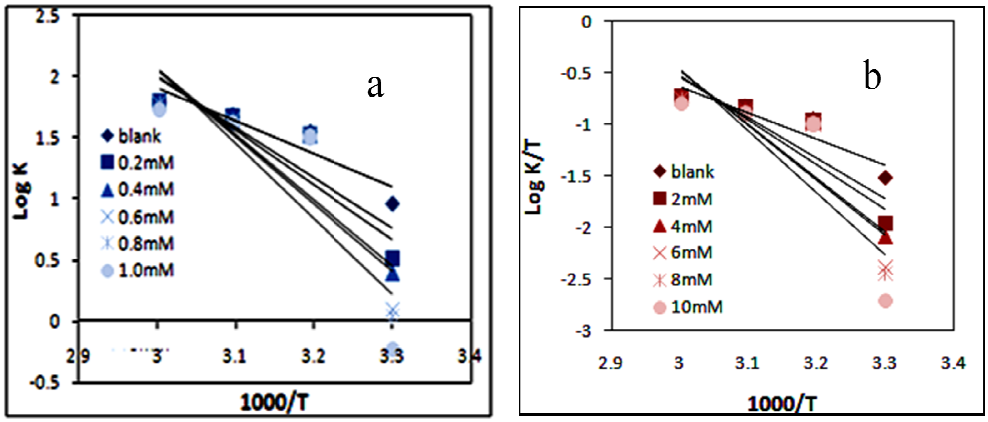

Fig. 3.30: a) Arrhenius plots and **b)** log (K/T) vs 1000/T plots of CS corrosion in the presence and absence of I3A2AT in 1M HCl

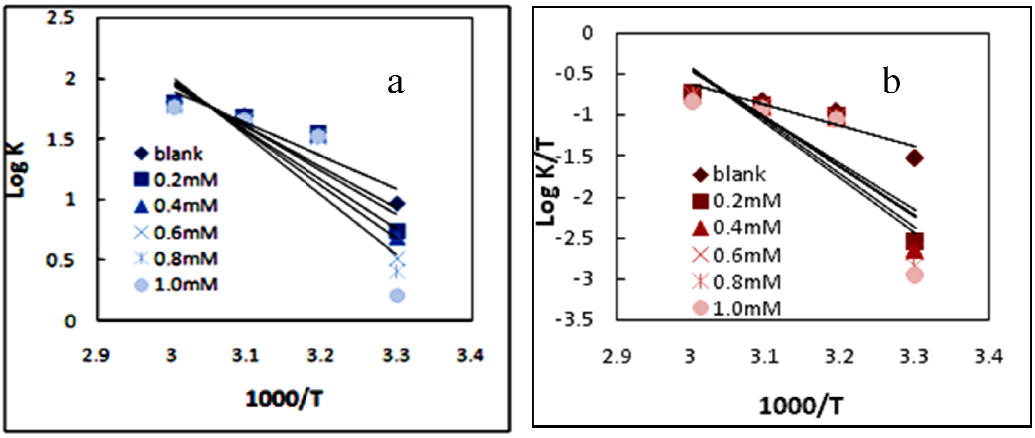

Fig. 3.31: a) Arrhenius plots and **b)** log (K/T) vs 1000/T plots of CS corrosion in the presence and absence of T2CDACH in 1M HCl

Thermodynamic parameters (entropy of activation ad enthalpy of activation) of corrosion in 1M HCl in the presence and absence of these inhibitors A9CNPTDA, P2CNPTDA, 3APNPTDA, 2APNPTDA, ANNPTDA, I3A2AT and T2CDACH are depicted in Table 3.6. Positive signs of enthalpies with a regular rise reflect the endothermic nature of dissolution and the decreasing corrosion tendency with the inhibitor. Increase of entropy values emphasizes that randomness increase for the activated complex take place than the reactant with the concentration of the inhibitor. The raise of entropy and activation energy implies that the reluctance of dissolution of metal increased with the inhibitor concentration, which can be attributed to the considerable intervention of inhibitor molecules during the metallic dissolution.

Table 3.6: Thermodynamic parameters of CS corrosion, in the presence and absence of 'S' containing heterocylic Schiff bases in 1M HCl

Schiff base	C (mM)	E_a (kJ mol^{-1})	A	ΔH* (kJ mol^{-1})	ΔS* (J mol-1 K^{-1})
Blank	0	51.33	8.73×10^{9}	48.7	-56.51
A9CNPTDA	0.2	109.23	1.48×10^{19}	107	107.29
	0.4	117.00	2.34×10^{20}	114	110.16
	0.6	128.7	1.91×10^{22}	126	113.04
	0.8	132.00	8.71×10^{22}	130	121.26
	1	140.00	1.2×10^{24}	138	133.33
P2CNPTDA	0.2	104.92	3.01×10^{18}	102	106.99
	0.4	107.33	7.24×10^{18}	105	114.37
	0.6	117.69	3.44×10^{20}	115	142.14
	0.8	127.32	1.12×1^{22}	125	175.26
	1	133.41	9.55×10^{22}	131	193.07
3APNPTDA	0.2	111.19	3.02×10^{19}	109	126.06
	0.4	117.14	2.69×10^{20}	114	144.25
	0.6	118.62	3.47×10^{20}	115	146.35
	0.8	127.62	1.26×10^{22}	125	176.22
	1	129.88	2.63×10^{22}	127	194.78
2APNPTDA	0.2	105.02	1.41×10^{18}	111	107.29
	0.4	105.96	1.68×10^{18}	114	110.16
	0.6	106.95	6.44×10^{18}	119	113.03
	0.8	109.69	1.56×10^{19}	122	121.26
	1	117.25	5.24×10^{20}	125	144.00
ANNPTDA	0.2	94.45	6.46×10^{16}	92	75.12
	0.4	97.57	2×10^{17}	95	84.51
	0.6	102.82	1.38×10^{18}	100	100.39
	0.8	109.10	1.39×10^{19}	106	119.55
	1	116.83	2.69×10^{20}	117	142.71
I3A2AT	0.2	77.70	1.45×10^{9}	55	-34.39
	0.4	112.87	2.38×10^{19}	111	143.13
	0.6	114.73	3.47×10^{19}	119	148.75
	0.8	120.5	1.16×10^{20}	121	160.22
	1	123.44	2.04×10^{20}	128	174.47
T2CDACH	0.2	64.04	9.33×10^{9}	61.4	-17.64
	0.4	67.64	3.47×10^{11}	65	-6.82
	0.6	76.01	8.13×10^{13}	73.7	19.59
	0.8	82.58	9.55×10^{14}	80	38.74
	1	93.17	3.98×10^{16}	90.5	60.18

Surface Morphological Investigations

In order to establish the mechanism of action of these heterocyclic Schiff bases A9CNPTDA, P2CNPTDA, 3APNPTDA, 2APNPTDA, ANNPTDA, I3A2ATand T2CDACH on CS surface, SEM experiments were conducted. The SEM micrographs of (a) bare CS surface (b) CS specimen immersed in 1M HCl and CS specimen immersed in 1M HCl containing 1mM concentration of (c) A9CNPTDA and (d) T2CDACH after 48 hrs of immersion time are shown in Fig. 3.32. The pits and cracks appearing in the SEM image of the bare metal specimen were due to the polishing effects. Some cracks are observed on the CS surface in T2CDACH solution. This is due to the fast hydrolysis nature of this molecule. On close examination of these images, it was clear that the CS surface undergoes severe corrosion in blank HCl solution and smoother surface was displayed by metal specimens immersed in 1M HCl in the presence of heterocyclic inhibitor A9CNPTDA at 1mM concentration. This can be attributed to the prevention of CS corrosion in aggressive medium by the formation of a protective barrier of inhibitors through adsorption process.

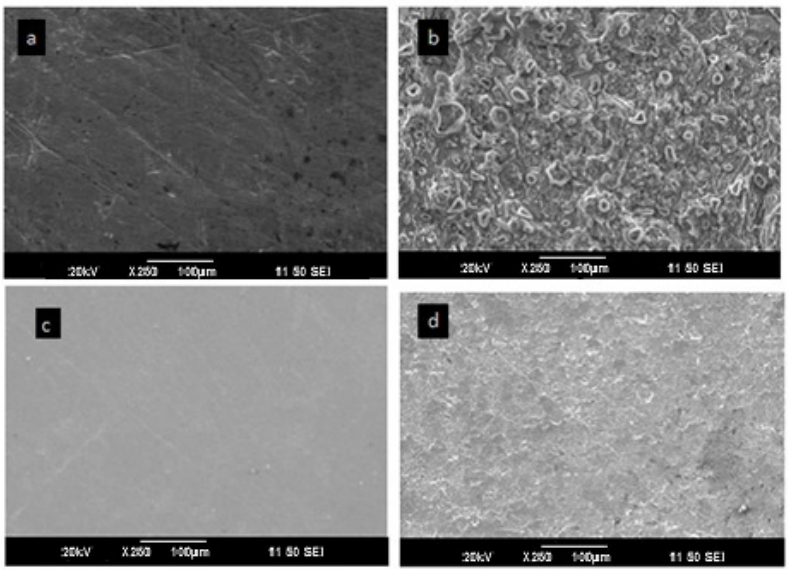

Fig. 3.32: SEM images of (a) bare CS (b) CS treated with 1M HCl (c) CS treated with A9CNPTDA (1mM) (d) CS treated with T2CDACH (1mM) for 48h.

Electrochemical Impedance Spectroscopic Studies (EIS)

The behavior of corrosion on CS in 1M HCl with and without the heterocyclic inhibitors was studied by employing impedance spectroscopic analysis. To make clear the inhibitory action of these organic ligands, CS specimens were engrossed in 1M HCl medium in the presence and absence of the inhibitors for 30 minutes prior to the experiment at 303K. Fig. 3.33 to Fig. 3.39 corresponding to the Nyquist plots and Bode plots of the sulphur-containing heterocyclic Schiff bases A9CNPTDA, P2CNPTDA, 3APNPTDA, 2APNPTDA, ANNPTDA, I3A2AT and T2CDACH respectively. The impedance (EIS) parameters such as charge transfer resistance (R_{ct}), solution resistance (R_s), double layer capacitance (C_{dl}) and percentage of inhibition efficiency ($\eta_{EIS\%}$) were calculated from these plots and documented in Table 3.7. From R_{ct} values, the percentage of inhibition efficiency was evaluated using the subsequent equation

$$\eta_{EIS}\% = \frac{Rct - R'ct}{Rct} \times 100 \quad (30)$$

where R'_{ct} and R_{ct} are the charge transfer resistances of the working electrode in acid medium in the absence and presence of the heterocyclic Schiff bases respectively.

R_{ct} is a measure of electron transfer between the acidic solution and exposed area of CS and the corrosion rate is inversely proportional to it. From Nyquist plots, it was observed that the diameter of semicircle increases with the concentration of inhibitors indicating that these 'S' containing inhibitors self-assemble on the CS surface by forming protective layer and resist the corrosion. The monolayer of inhibitors obstructs the charge transfer between the carbon steel and the acidic solution and charge transfer resistance increases with inhibitor concentration. The diminishing nature of capacitance values (C_{dl}) with the concentration of inhibitor, mainly indicates the increase in the thickness of the electrical double layer and/or decrease in local dielectric constant.

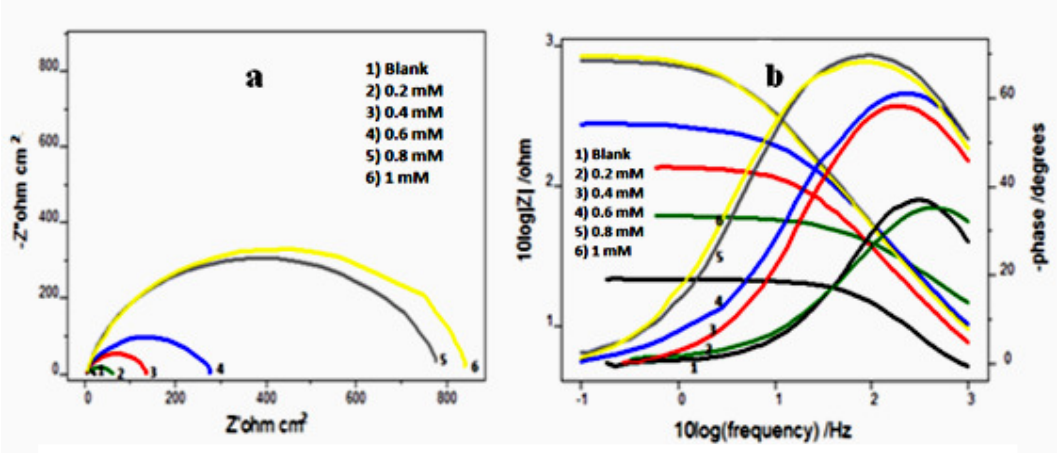

Fig. 3.33: a) Nyquist plots and **b)** Bode plots of CS corrosion in the presence and absence of A9CNPTDA in 1M HCl

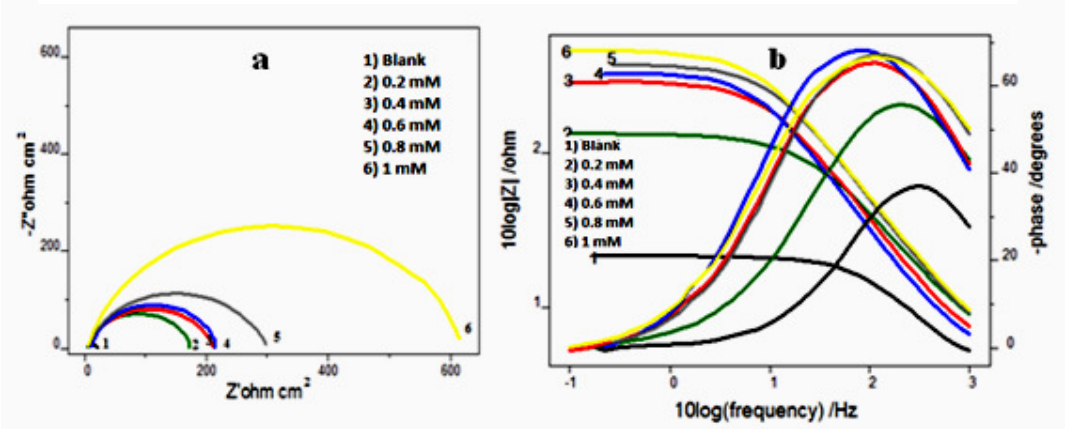

Fig. 3.34: a) Nyquist plots and **b)** Bode plots of CS corrosion in the presence and absence of P2CNPTDA in 1M HCl

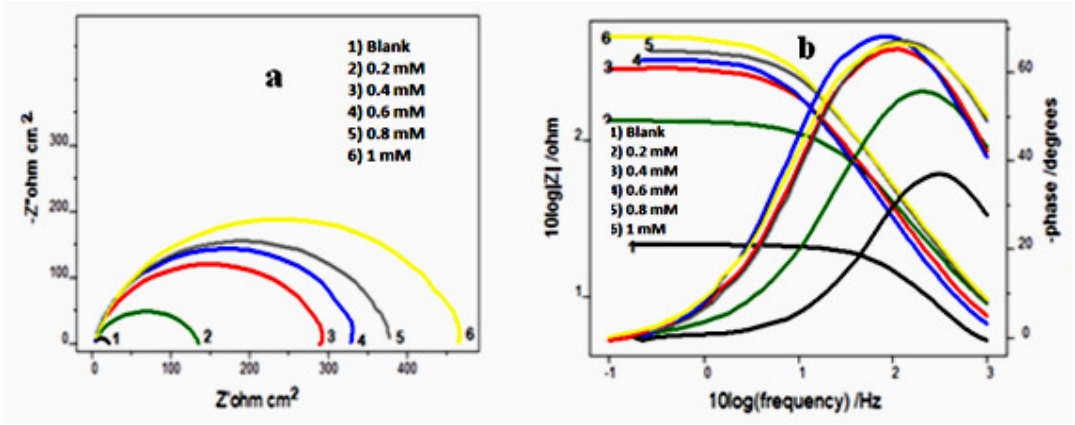

Fig. 3.35: a) Nyquist plots and **b)** Bode plots of CS corrosion in the presence and absence of 3APNPTDA in 1M HCl

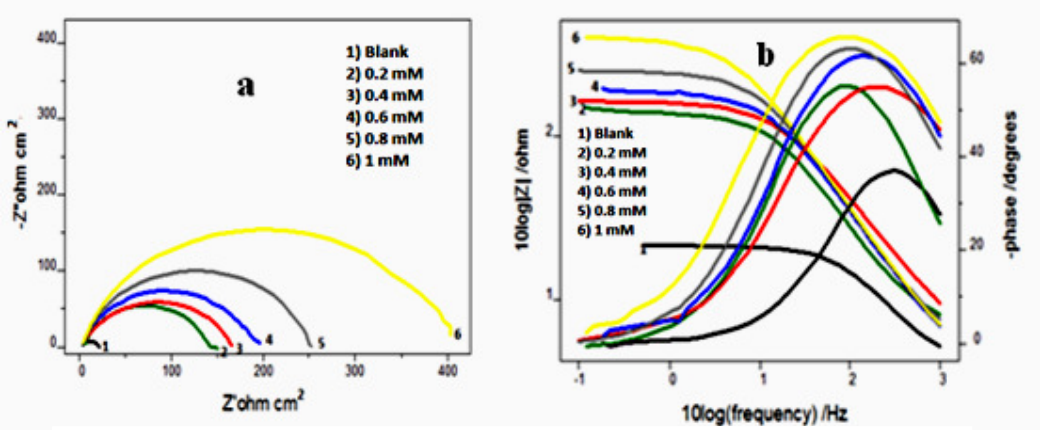

Fig. 3.36: a) Nyquist plots and **b)** Bode plots of CS corrosion in the presence and absence of 2APNPTDA in 1M HCl

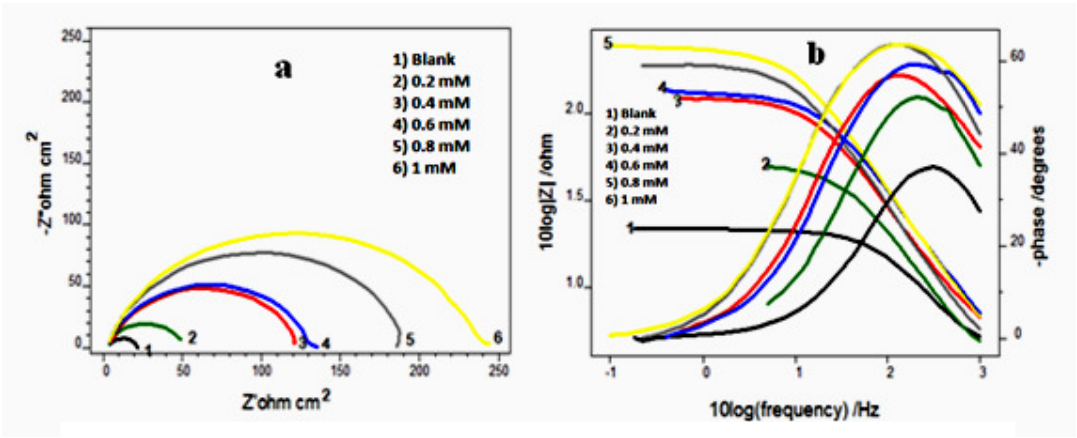

Fig. 3.37: a) Nyquist plots and **b)** Bode plots of CS corrosion in the presence and absence of ANNPTDA in 1M HCl

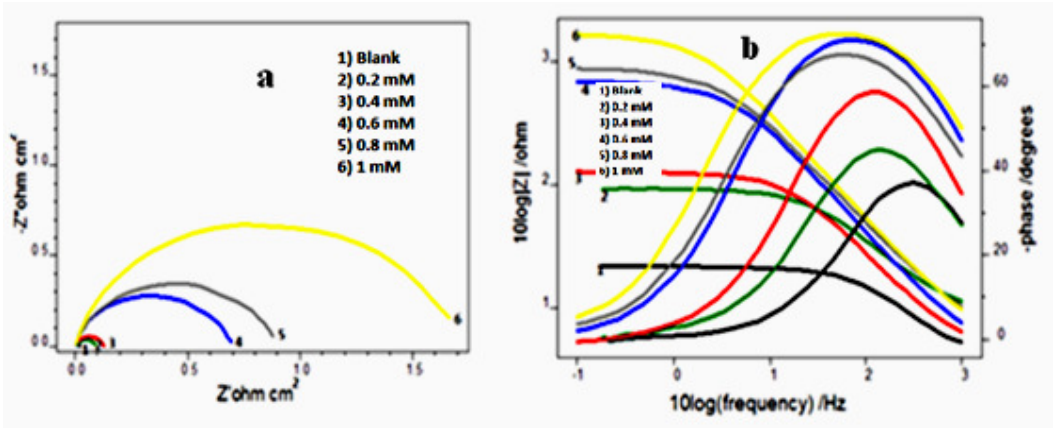

Fig. 3.38: a) Nyquist plots and **b)** Bode plots of CS corrosion in the presence and absence of I3A2AT in 1M HCl

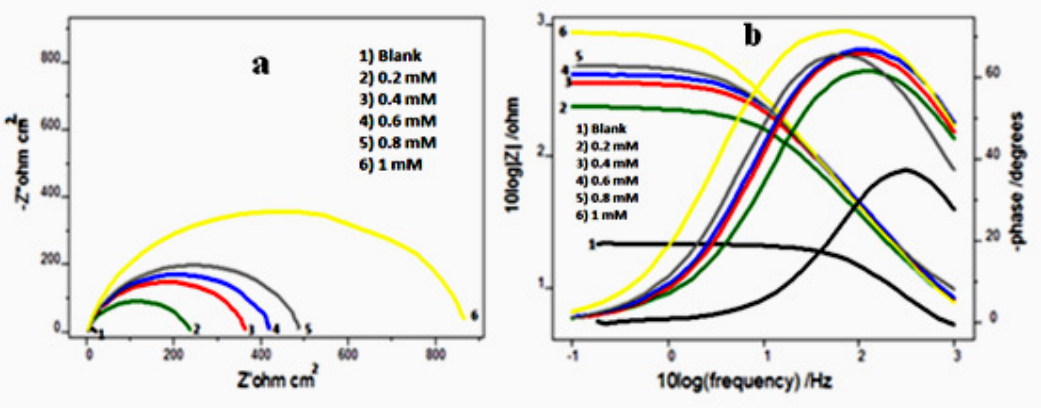

Fig. 3.39: a) Nyquist plots and b) Bode plots of CS corrosion in the presence and absence of T2CDACH in 1M HCl

From these plots, it is obvious that the impedance response of CS specimens showed a marked difference in the presence and absence of inhibitors. On examining Table 3.7, all synthesized 'S' containing Schiff base inhibitors displayed remarkable inhibition efficiency on CS even at low concentration. The weight loss results of heterocyclic Schiff bases derived from the parent amine NPTDA were in good agreement with EIS measurements. Presence of highly polarized sulphur atom from the thiadiazole moiety and the presence of azomethine linkage which is bridged through two aromatic systems enhance the delocalization of π electron cloud in these molecules and favour the interaction with CS surface. Among thiadiazole derivatives, the Schiff base inhibitor A9CNPTDA exhibited notable inhibition efficiency compared to others. Maximum efficiency of 97.9% was obtained at 1mM concentration of the inhibitor. Even at lowest concentration of 0.2mM, thiadiazole derivative A9CNPTDA exhibited 89.74% inhibition potency.

Table 3.7: Electrochemical Impedance parameters of CS corrosion in the presence and absence of 'S' containing heterocyclic Schiff base inhibitors in 1M HCl at 303K

Schiff bases	C (mM)	C_{dl} ($\mu F\ cm^{-2}$)	R_{ct} ($\Omega\ cm^{-2}$)	η_{EIS}%
Blank	0	101	16.1	-
A9CNPTDA	0.2	83.9	157	89.74
	0.4	53.0	187	91.39
	0.6	45.7	239	93.23
	0.8	47.5	712	97.73
	1.0	53.1	768	97.90
P2CNPTDA	0.2	55.5	120	86.50
	0.4	51.0	182	91.15
	0.6	83.0	194	91.70
	0.8	66.3	262	93.85
	1.0	55.2	567	97.16
3APNPTDA	0.2	52.4	115	86.00
	0.4	59.5	271	94.01
	0.6	65.7	312	94.83
	0.8	42.6	347	95.36
	1.0	45.4	431	96.26
2APNPTDA	0.2	80.3	125	87.12
	0.4	56.6	140	88.50
	0.6	62.6	167	90.35
	0.8	63.8	228	92.94
	1.0	72.2	359	95.51
ANNPTDA	0.2	84.3	29	61.80
	0.4	46.0	38.8	83.50
	0.6	73.1	68.6	85.09
	0.8	74.9	131	90.69
	1.0	73.6	208	92.47
I3A2AT	0.2	61.4	76.3	78.9
	0.4	76.7	114	85.87
	0.6	57.8	633	97.45
	0.8	57.3	800	97.98
	1.0	51.5	1540	99.6
T2CDACH	0.2	64.9	211	92.37
	0.4	55.3	334	95.17
	0.6	53.1	386	95.82
	0.8	58.1	449	96.41
	1.0	59.7	811	98.01

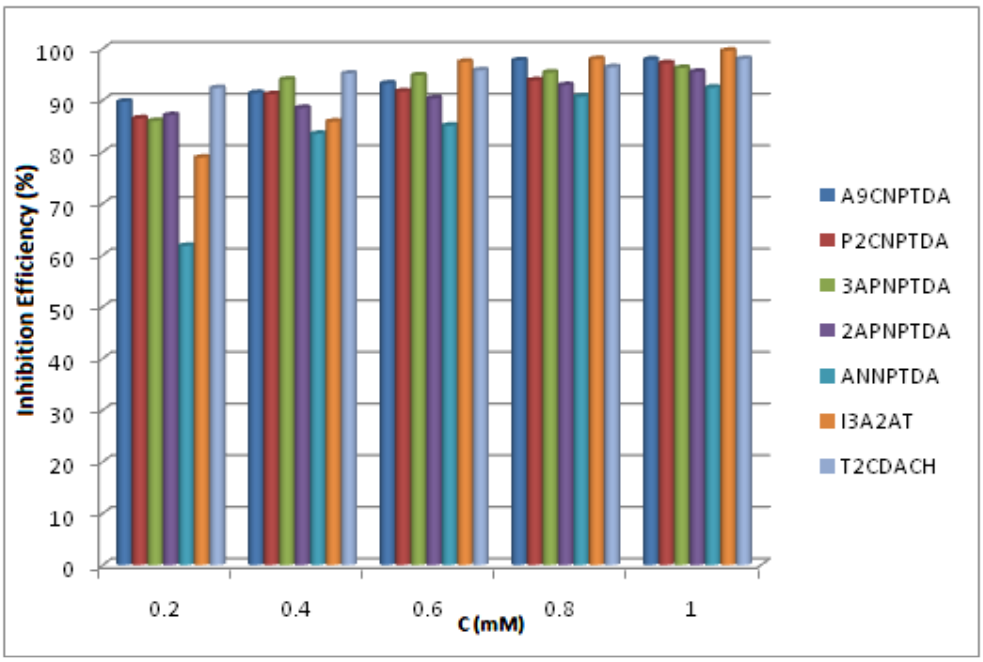

Fig. 3.40: Comparison of the corrosion inhibition efficiencies ($\eta_{EIS\%}$) of 'S' containing heterocyclic Schiff bases in 1M HCl at 28^0C

The electrochemical analysis is a quick corrosion monitoring procedure and displays the corrosion inhibition potencies of inhibitors in the early hours of treatment. Fig. 3.40 illustrate the assessment of the corrosion inhibition efficiencies of seven heterocyclic Schiff base inhibitors by EIS measurements. It is noticeable from the figure that the inhibition efficiency of the five heterocyclic Schiff base inhibitors derived from NPTDA follows the order A9CNPTDA < P2CNPTDA < 3APNPTDA < 2APNPTDA < ANNPTDA respectively. This tendency finds good harmony with the outcome obtained from the gravimetric weight loss studies. Thiazole derivative of Schiff base I3A2AT and thiophene derivative T2CDACH showed outstanding inhibition efficiency and maximum efficiency of 99.6% was obtained for I3A2AT and 98.01% for T2CDAC at 1mM concentration. The highest R_{ct} value 1540 exhibited by I3A2AT can be attributed to the presence of thiazole moiety, indole ring and azomethine linkage. As per gravimetric studies, the heterocyclic Schiff base T2CDACH exhibited low inhibitive

response on CS surface but showed outstanding inhibition by EIS measurements. From the UV-visible spectral studies, it was confirmed that T2CDACH undergo fast hydrolysis and I3A2AT undergo slow hydrolysis in hydrochloric acid medium.

Potentiodynamic Polarization Studies

To emphasize the corrosion inhibitory role of the novel 'S' containing Schiff bases on carbon steel and to verify the electrochemical site of interaction, potentiodynamic polarization studies including Tafel extrapolation analysis and Linear polarization studies were conducted. Corrosion potential (E_{corr}), corrosion current density (i_{corr}) and polarization resistance (R_p) were calculated in every analysis and by means, determined the inhibition efficiency. Tafel plots and linear polarization curves of CS in 1M HCl medium in the presence and absence of these heterocyclic Schiff base inhibitors are depicted from Fig. 3.41 to 3.47. Tafel and Linear polarization data including corrosion current density (I_{corr}), corrosion potential (E_{corr}), anodic slope (b_a), cathodic slope (b_c) and corrosion inhibition efficiency were obtained by potentiodynamic polarization studies and tabulated in Table 3.8.

On scrutiny, it was revealed that the corrosion current densities of steel specimens decreased appreciably with the concentration of inhibitors. This is because of these organic molecules obstruct the metal dissolution progression appreciably by either prevailing in the cathodic or anodic process of corrosion or they acted as mixed type inhibitors [120]. On the evaluation of Tafel and Linear polarization curves, it was established that the slope of the Tafel curves of uninhibited solution entirely different from the slope obtained in the presence of inhibitors. The outcome obtained by the potentiodynamic polarization studies were in good harmony with the electrochemical impedance studies.

Table 3.8: Potentiodynamic polarization parameters of CS corrosion in the presence and absence of 'S' containing heterocyclic inhibitors in 1M HCl

Inhibitors	Tafel Data						Polarization data	
	C (mM)	$-E_{corr}$ (mV/SCE)	I_{corr} ($\mu A/cm^2$)	$-b_a$ (mV/dec)	b_c (mV/dec)	η_{pol} %	R_p (ohm)	η_{Rp} %
Blank	0	451	1115	110	184	-	26.86	-
A9CNPTDA	0.2	471	77	70	134	93.1	259.6	90.00
	0.4	469	37.8	63	119	96.6	475.2	94.34
	0.6	479	36	61	123	96.8	494.6	94.56
	0.8	470	30.3	66	115	97.3	601.6	95.53
	1	476	12.2	52	103	98.9	1239	97.83
P2CNPTDA	0.2	444	132	76	197	88.2	175.9	84.72
	0.4	441	70.5	72	134	93.7	227.7	88.20
	0.6	448	37.3	61	132	96.7	417	93.55
	0.8	463	36.3	68	145	96.8	461.3	94.17
	1	456	21.2	68	136	98.1	882.3	96.95
3APNPTDA	0.2	453	92.2	76	164	91.7	227	88.16
	0.4	454	80.2	75	123	92.8	302	91.10
	0.6	455	66.6	72	157	94.1	320	91.60
	0.8	461	97.1	87	133	91.3	322	91.65
	1	457	22.9	58	164	97.9	785	96.57
2APNPTDA	0.2	427	204	98	185	81.7	143	81.20
	0.4	482	81	86	122	92.8	323.1	91.68
	0.6	463	84	81	121	92.5	376.2	92.90
	0.8	487	64	84	123	94.3	425.3	93.68
	1	443	48	78	128	95.7	505.4	94.68
ANNPTDA	0.2	473	492	93	151	55.9	71.88	62.63
	0.4	468	161	83	153	85.7	158.4	83.04
	0.6	472	125	73	142	88.8	193.5	86.11
	0.8	453	105	62	138	90.6	258.3	89.60
	1	483	70.4	79	125	93.7	284	90.54
I3A2AT	0.2	473	284	112	208	74.52	97.05	71.90
	0.4	467	110	73	205	90.04	216.6	87.59
	0.6	474	12.5	43	111	98.86	878.7	97.00
	0.8	460	11.1	61	116	98.99	1097	97.55
	1	480	7.6	82	102	99.31	1708	98.42
T2CDACH	0.2	471	79	73	130	93.07	285.6	90.60
	0.4	468	37.8	63	119	96.65	495.2	94.60
	0.6	469	36	61	124	96.77	512.6	94.77
	0.8	470	30.3	66	117	97.28	621.6	95.60
	1	476	12.2	52	103	98.87	1274	97.90

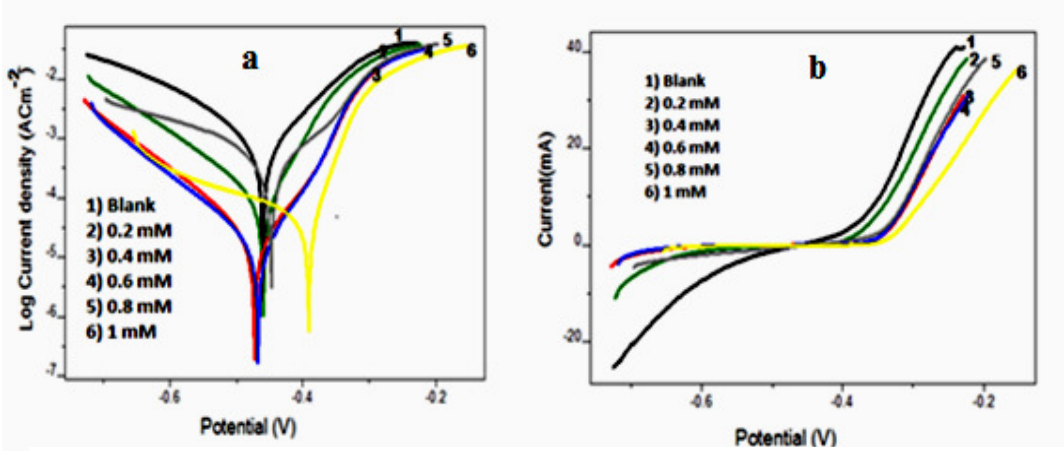

Fig. 3.41: a) Tafel plots and **b)** Linear polarization plots of CS corrosion in the presence and absence of A9CNPTDA in 1M HCl.

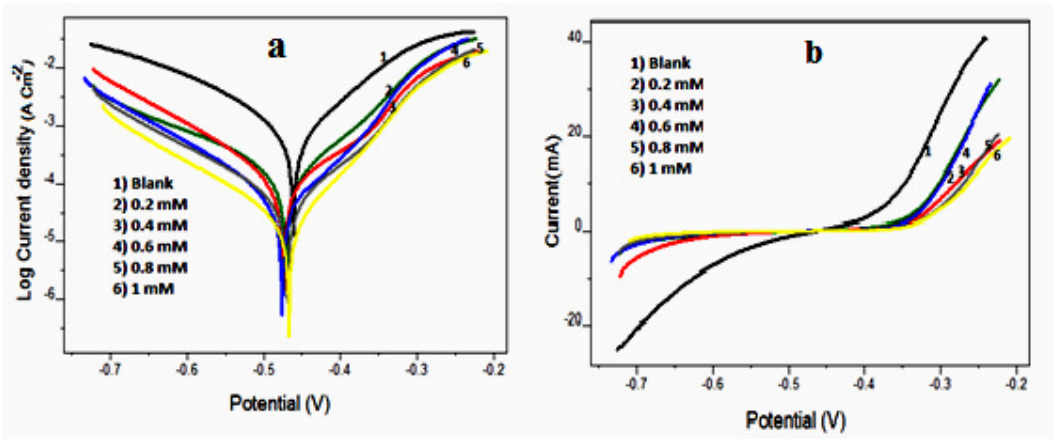

Fig. 3.42: a) Tafel plots and **b)** Linear polarization plots of CS corrosion in the presence and absence of P2CNPTDA in 1M HCl

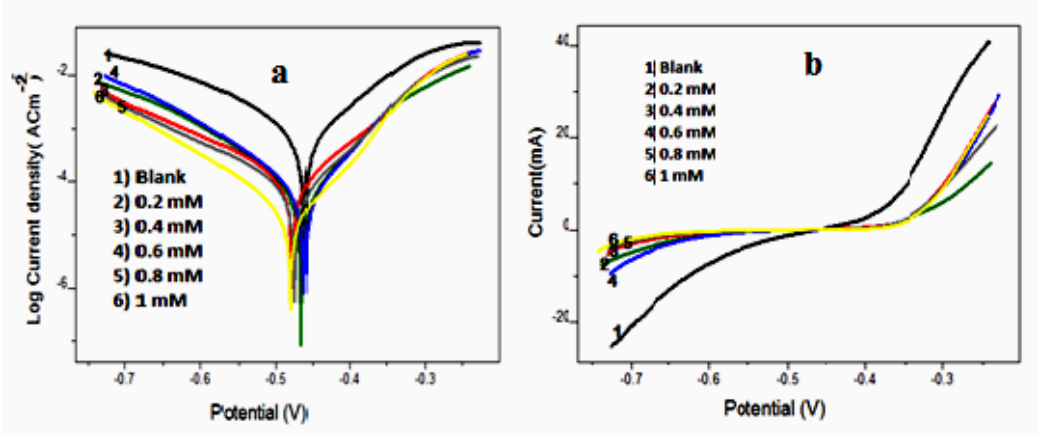

Fig. 3.43: a) Tafel plots and **b)** Linear polarization plots of CS corrosion in the presence and absence of 3APNPTDA in 1M HCl

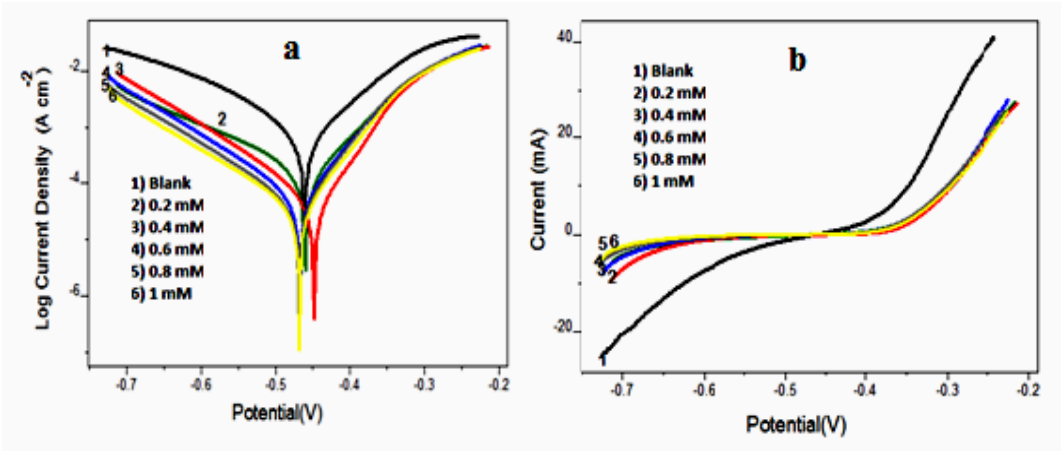

Fig. 3.44: a) Tafel plots and **b)** Linear polarization plots of CS corrosion in the presence and absence of 2APNPTDA in 1M HCl

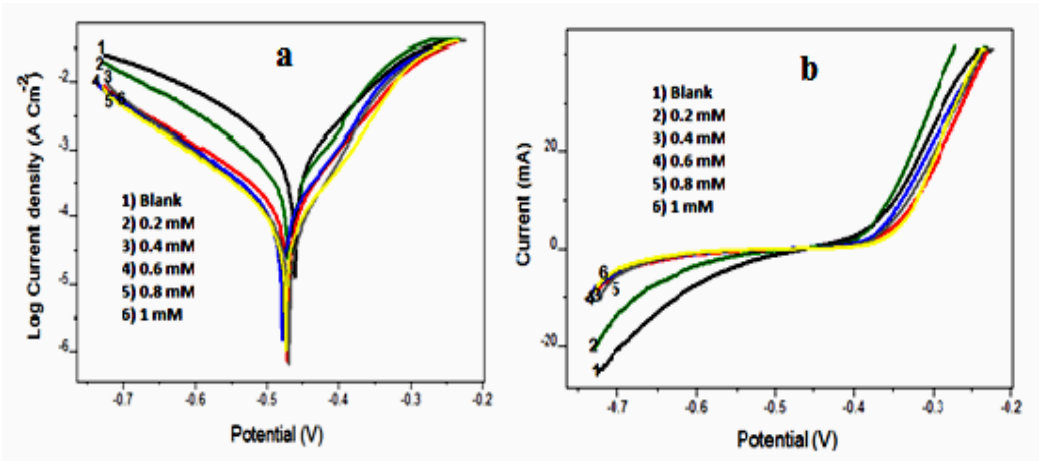

Fig. 3.45: a) Tafel plots and **b)** Linear polarization plots of CS corrosion in the presence and absence of ANNPTDA in 1M HCl

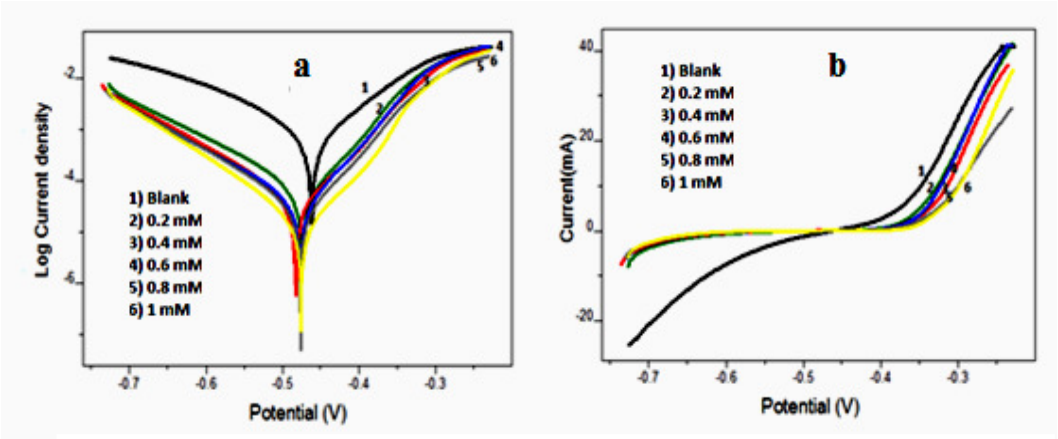

Fig. 3.46: a) Tafel plots and **b)** Linear polarization plots of CS corrosion in the presence and absence of I3A2AT in 1M HCl

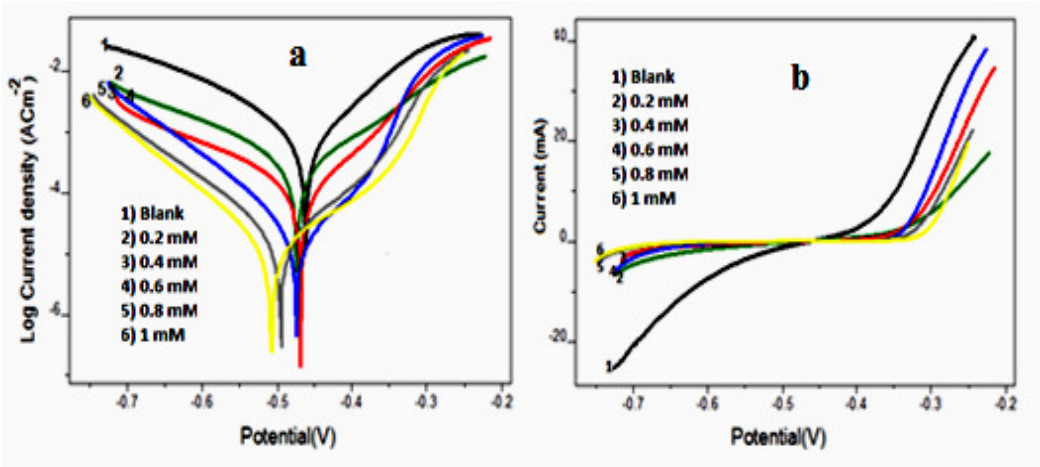

Fig. 3.47: a) Tafel plots and **b)** Linear polarization plots of CS corrosion in the presence and absence of T2CDACH in 1M HCl

A comparison between the inhibition efficiencies of these sulphur containing heterocyclic Schiff base inhibitors was done and portrayed in Fig. 3.48. Among thiadiazole derivatives, the heterocyclic Schiff base, A9CNPTDA exhibited the maximum inhibition efficiency of 98.9% at 1mM concentration. The heterocyclic Schiff bases, I3A2AT and T2CDACH, also exhibited excellent inhibition efficiencies (99.31% in the case of I3A2AT and 98.87% in the case of T2CDACH, which is higher than that obtained from the gravimetric weight loss studies. This is because, in electrochemical investigations, the contact time between the acid solution and the working electrode is about 30 minutes only whereas in the later the contact time is 24h. Generally, if the shift of E_{corr} is greater than 85 and a significant change is observed in cathodic or anodic slopes, the inhibitor can be considered as cathodic or anodic. In the present investigation, the seven heterocyclic Schiff bases namely A9CNPTDA, P2CNPTDA, 3APNPTDA, 2APNPTDA, ANNPTDA, I3A2AT and T2CDACH affects the anodic and cathodic slopes uniformly and E_{corr} values didn't alter considerably with respect to the blank (>85) and therefore these molecules can be regarded as mixed-type inhibitors.

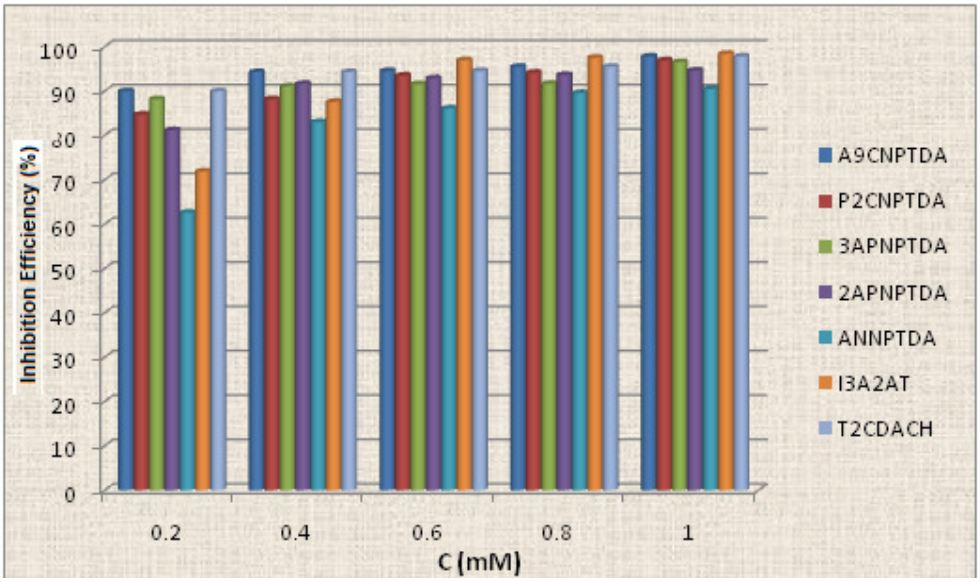

Fig. 3.48: Comparison study of corrosion inhibition efficiencies ($\eta_{pol\%}$) of 'S' containing heterocyclic Schiff base inhibitors on CS in 1M HCl at 28^0C

Mechanism of Inhibition

Organic inhibitors can prevent the metal dissolution by forming a hydrophobic film through adsorption process on the metal surface. The Capability of the inhibitor molecule mainly depends on its molecular structure and chemical composition.

The mechanism anodic dissolution of iron can be represented as follows.

i) In aqueous solutions

$$Fe + H_2O \rightarrow [FeOH]_{ads} + H^+ + e^- \quad (31)$$

$$[FeOH]_{ads} \rightarrow [FeOH]^+_{ads} + e^- \quad (32)$$

$$[FeOH]^+_{ads} + H^+ \rightarrow Fe^{2+} + H_2O \quad (33)$$

ii) In aqueous solution containing A^- (A= Cl^-, or SO_4^{2-}) ions

$$Fe + H_2O + A^- \rightarrow [FeAOH]^-_{ads} + H^+ + e^- \quad (34)$$

$$[FeAOH]^-_{ads} \rightarrow [FeAOH]_{ads} + e^- \quad (35)$$

$$[FeAOH]_{ads} + H^+ \rightarrow Fe^{2+} + A^- + H_2O \quad (36)$$

where $[FeOH]_{ads}$ and $[FeAOH]^-_{ads}$ are the adsorbed molecules which are intermediates

involved in the rate determining step of the reaction (equations 32 and 35, respectively). The following equations are the mechanism of the evolution of hydrogen in the cathode

$$Fe + H^{+} \rightarrow (FeH^{+})_{ads} \quad (37)$$

$$(FeH^{+})_{ads} + e^{-} \rightarrow (FeH)_{ads} \quad (38)$$

$$(FeH)_{ads} + H^{+} + e^{-} \rightarrow Fe + H_2 \quad (39)$$

The protonated inhibitor molecules adsorb at cathodic sites and hence reduce the H_2 gas evolution. Generally, the surface of the metal tends to have a positively charged environment in acidic media. The adsorption of negatively charged Cl^- ion will lead to the allocation of more and more negative charge and make easy the adsorption of the protonated Schiff bases on the metal surface, preventing the reduction of Fe to Fe^{2+} [121]. If one observes the features of these heterocyclic Schiff base inhibitors, many potential areas of metal–inhibitor interaction can be recognized. In this case, the binding of the compound on the metallic surface can be associated with the pi-electron cloud containing aromatic rings. In addition to this electrostatic interaction between the metal surface and the protonated inhibitor, the presence of heteroatoms which provide lone pair of electrons, interaction of π-electron cloud containing aromatic rings, azomethine moiety etc, will affect the adsorption progression. Highly polarisable sulphur atom and the unpaired electrons on the N atoms were the key factors for making a coordinate bond with the metal surface.

Besides, the highly conjugated azomethine linkage in the heterocyclic inhibitors allows the back donation of metal ‘d’ electrons to the antibonding π* orbital of the ligand and this type of interaction cannot be observed in the parent compounds. This can be defensible by the lower inhibition efficiency of the parent compounds. Fig. 3.49 illustrates the interaction of the inhibitor A9CNPTDA on the metal surface.

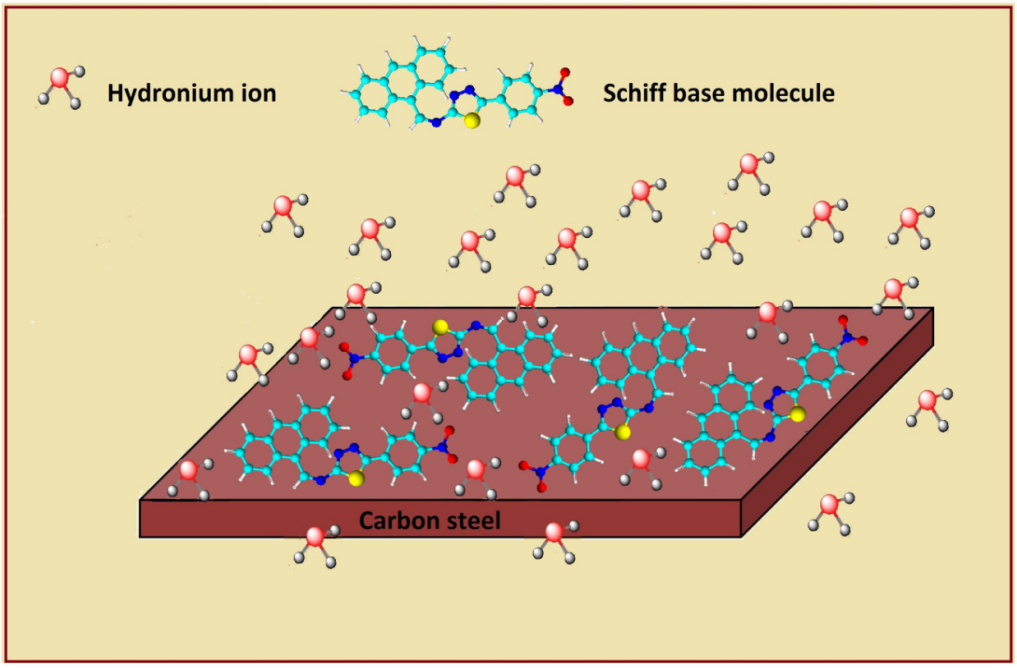

Fig. 3.49: Corrosion inhibition mechanism of A9CNPTDA molecules on CS surface

Electrochemical Noise Studies

Electrochemical noise experiments (ECN) were performed by a three-electrode cell system, which consists of SCE as a reference electrode, two carbon steel electrodes of 1cm^2 area used as working electrode and counter electrode. All ECN analyses were performed for 1200s using Ivium Compactstat-e electrochemical system.

Fig. 3.50 represents the noise current of carbon steel specimen engrossed in the acid solution with and without inhibitors. From the figure, it is obvious that at all frequencies, the noise current in the presence of inhibitors has very low value than the blank carbon steel specimen, which shows the protective corrosion power of these 'S' containing Schiff base ligands. Higher values of noise current for carbon steel specimen in uninhibited acid medium indicates appreciable localized corrosion takes place on the surface of the metal [122].

The frequency-domain analysis of noise measurement gave the Power Spectral

Density (PSD) of different systems, which are depicted in Fig. 3.51. It doesn't affect signal statistics and time. In the Ivium software, the time-dependent noise parameters were converted into PSD plots by FFT (Fast Fourier Transformation) technique. MEM (Maximum entropy method) for better spectral resolution was introduced by Burge. PSD plots in Figures revealed that the magnitude of the signals is higher for blank metal than metals with studied molecules in 1M HCl medium. These results pointed out a considerable amount of localised corrosion on carbon steel surface in the absence of these inhibitors.

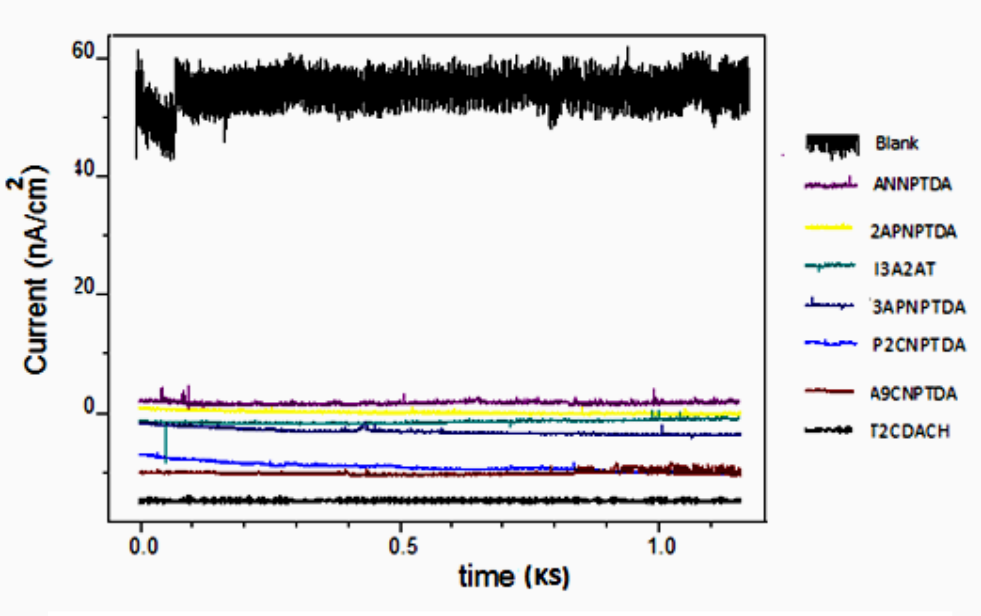

Fig. 3.50: Noise current of CS corrosion in the presence and absence of 'S' containing heterocyclic inhibitors in 1M HCl solution

Pitting Resistance Equivalent Number (PREN) or pitting index is the measurement of resistance against pitting corrosion. On analyzing the pitting index plots represented in Fig. 3.52, it is established that the amplitude of pitting index curves corresponding to the blank carbon steel specimen is lower than the specimen treated with heterocyclic Schiff base demonstrating their higher resistance towards pitting corrosion. These results are in close agreement with other electrochemical studies.

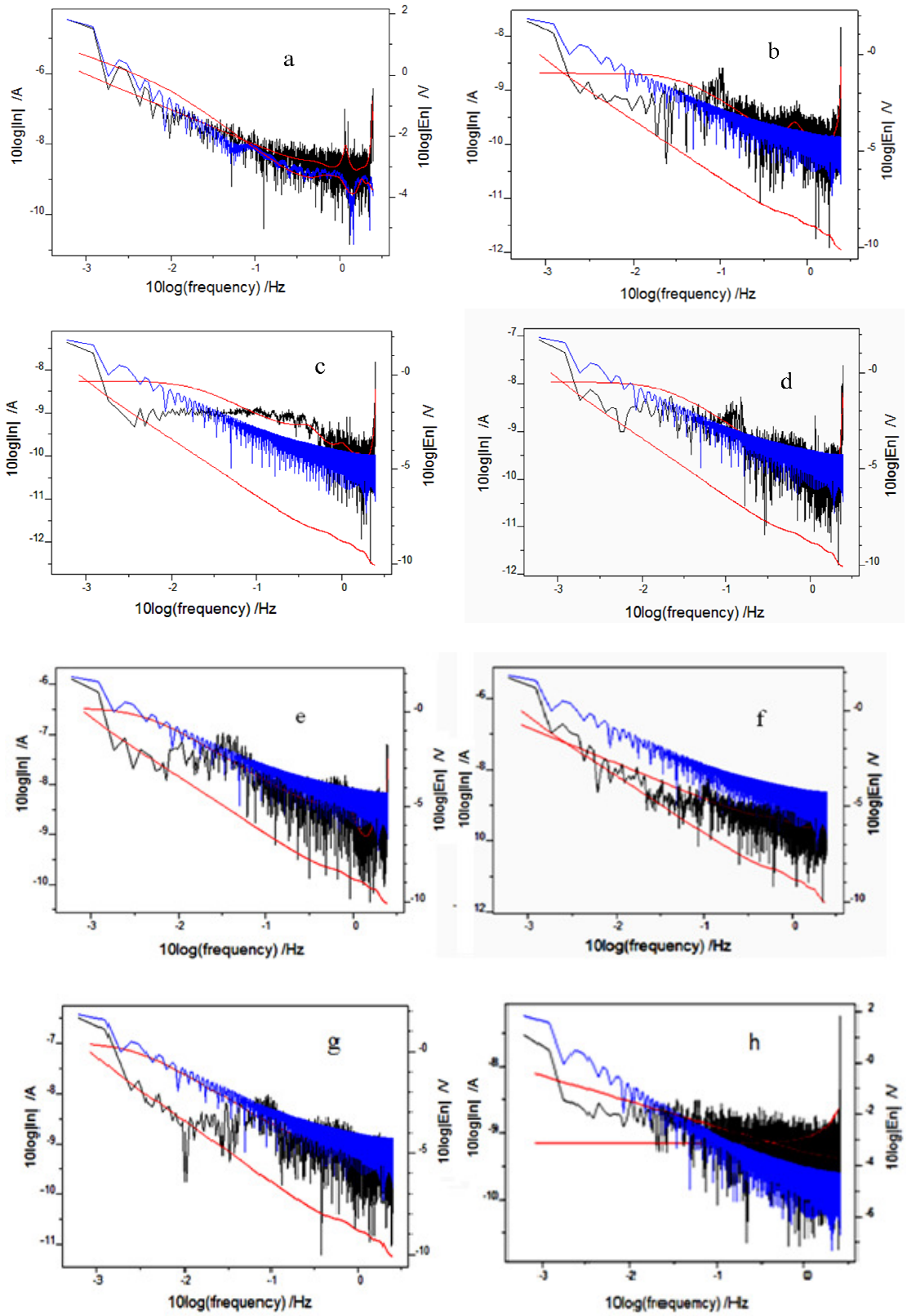

Fig. 3.51: PSD curves of CS corrosion in a) blank b) A9CNPTDA c) P2CNPTDA d) 3APNPTDA e) 2APNPTDA f) ANNPTDA g) I3A2AT h) T2CDACH at 1mM concentration in 1M HCl

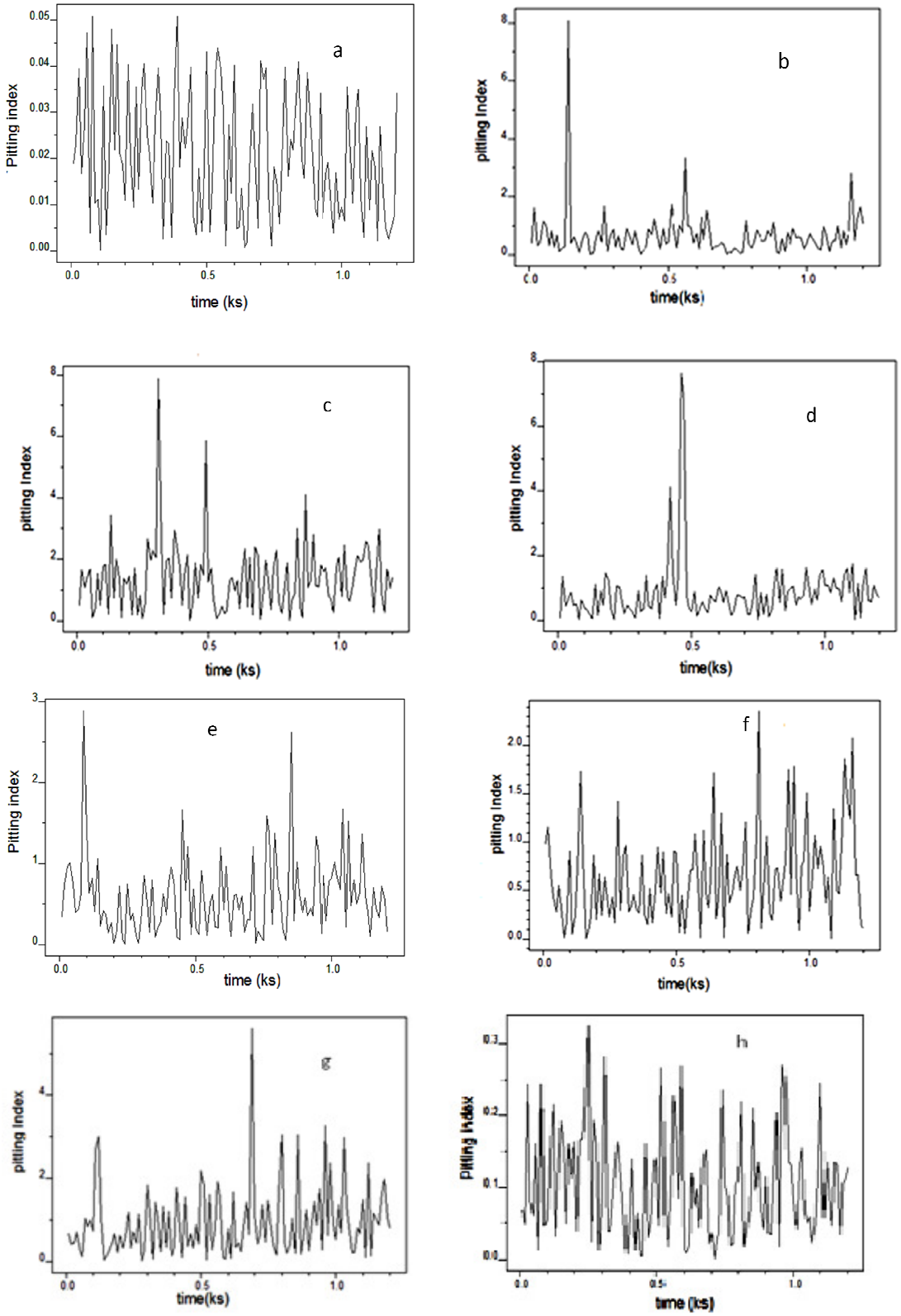

Fig. 3.52: Pitting index curves of CS corrosion in a) blank b) A9CNPTDA c) P2CNPTDA d) 3APNPTDA e) 2APNPTDA f) ANNPTDA g) I3A2AT and h) T2CDACH in IM HCl

Quantum Chemical Studies

The corrosion inhibition efficiency of these 'S' containing heterocyclic Schiff bases can be interrelated with the energies of Frontier molecular orbitals. The HSAB concept (donor-acceptor interactions) between the vacant d-orbitals of Fe atoms on the surface and the filled molecular orbitals of the molecules (inhibitors) have significant role in the prevention mechanism of metal disintegration. The highest value of E_{HOMO}, the lowest value of E_{LUMO} and the energy difference between the HOMO and the LUMO (ΔE) are the significant quantum chemical parameters which facilitate strong binding of the inhibitor molecules on the surface of metal. Energy of HOMO (E_{HOMO}) provides information about the tendency of a molecule to donate electrons to an electron-poor species. The higher E_{HOMO} indicates the greater tendency of a molecule to donate its electrons to the electron-poor species. The lowest $E_{LUMO} - E_{HOMO}$ (ΔE) value of inhibitors is an important quantum chemical parameter, it helps the ligands to bind on the metal surface strongly. Quantum chemical evaluations and Optimization of geometries of these inhibitors were carried out using DFT method by GAMMES software and B3LYP method was employed in DFT calculations. Calculated quantum mechanical parameters like E_{HOMO}, E_{LUMO}, Energy gap (ΔE), electronegativity (χ), hardness (η) and number of transferred electrons (ΔN) for the investigated inhibitors are tabulated in Table 3.9. HOMO and LUMO of inhibitors are depicted from Fig. 3.53 – Fig. 3.59 and optimized geometry of compounds established quantum mechanically represented in Fig. 3.60.

The energy gap between the Frontier orbitals ΔE, it helps to describe the static molecular reactivity. Low values of ΔE imply that the polarization and the adsorption of the molecule on the metal surface were takes place easily. Chemical hardness (η) is an important property to measure the reactivity molecular stability. A soft molecule has the small energy gap (ΔE) and they can offer electrons to the acceptor. The ΔE between

HOMO and LUMO is comparably low (2.68eV) for A9CNPTDA than other 'S' containing heterocyclic Schiff base inhibitors, implied that A9CNPTDA has high ability to accept electrons from the d-orbital of iron and high stability of the [Fe–L] complexes. It is also observed from the data that the Schiff base A9CPTDA has a low chemical hardness value (η = 1.361eV) compared to other studied molecules and thus, by being a soft molecule A9CNPTDA would enhance adsorption on the steel surface.

Table 3.9: Quantum chemical parameters of 'S' containing heterocyclic inhibitors

Inhibitors	E_{HOMO} (eV)	E_{LUMO} (eV)	ΔE (eV)	χ (eV)	η (eV)	Δ N
A9CNPTDA	-3.53	-0.843	2.68	2.204	1.361	0.836
P2CNPTDA	-3.619	-0.841	2.77	2.231	1.388	0.811
3APNPTDA	-3.592	-0.707	2.88	2.149	1.442	0.808
2APNPTDA	-3.538	-0.626	2.91	2.082	1.456	0.814
ANNPTDA	-3.565	-0.544	3.02	2.041	1.497	0.815
I3A2AT	-2.395	1.551	3.94	0.422	1.973	1.029
T2CDACH	-3.673	1.016	4.68	1.333	2.341	0.672

Table 3.8 shows that the hardness order of thiadiazole derivatives are as follows: A9CNPTDA > P2CNPTDA > 3APNPTDA > 2APNPTDA > ANNPTDA, which is in close agreement with the experimentally obtained inhibition potency. It is reported from the studies that electron transfer from an inhibitor to metal takes place easily when the N value is > 0 and < 3.6.

Among investigated compounds, it can be concluded that thiadiazole derivatives A9CNPTDA and thiazole derivative I3A2AT have the highest E_{HOMO} and ΔN value implied that they have the greater tendency to donate their electrons to the metal surface and therefore bind strongly on the metal surface. The higher value of ΔE (4.68 eV), high chemical hardness (η= 2.341eV) and low ΔN (0.672) value for thiophene based Schiff base T2CDACH which could be recognized to its lesser corrosion inhibition efficiency. These results are in good agreement with the results obtained from the gravimetric

weight loss studies.

The calculations are conducted using following equations,

$$\chi \approx -1/2\ (E_{HOMO} + E_{LUMO})$$

$$\eta \approx 1/2\ (E_{HOMO} - E_{LUMO}) \qquad \Delta N = \frac{\chi_{Fe} - \chi_{inhib}}{2(\eta_{Fe} + \eta_{inhib})}$$

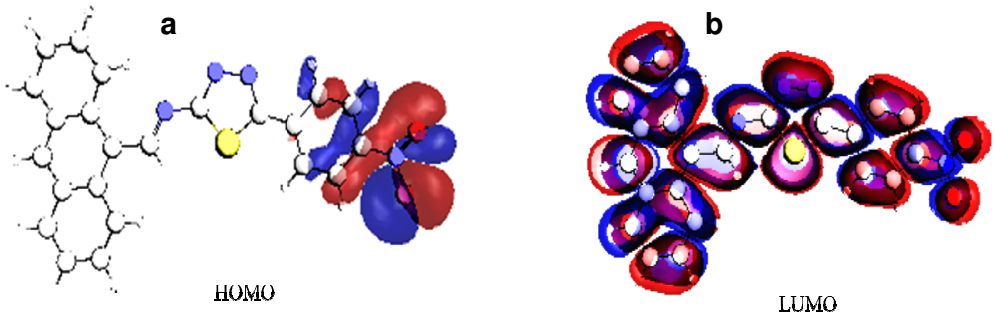

Fig. 3.53: a) HOMO and **b**) LUMO of A9CNPTDA

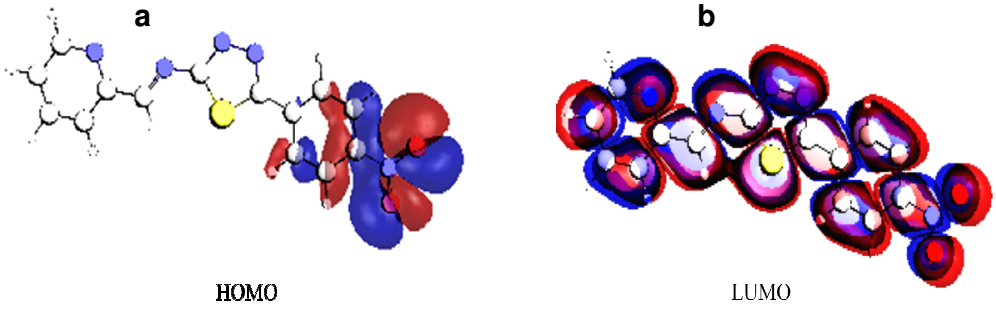

Fig. 3.54: a) HOMO and **b**) LUMO of P2CNPTDA

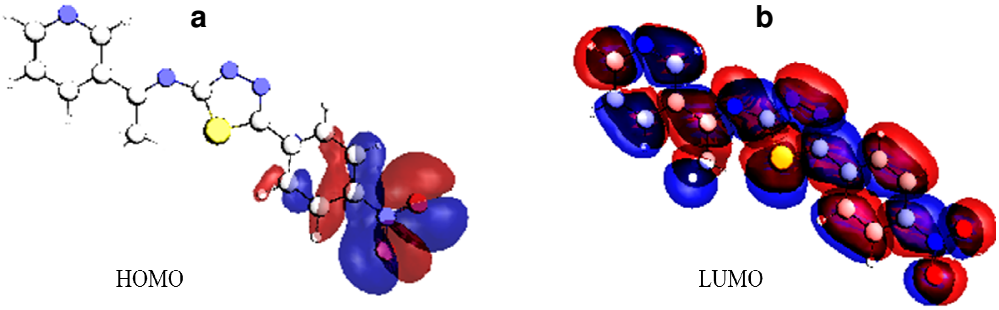

Fig. 3.55: a) HOMO and **b**) LUMO of 3APNPTDA

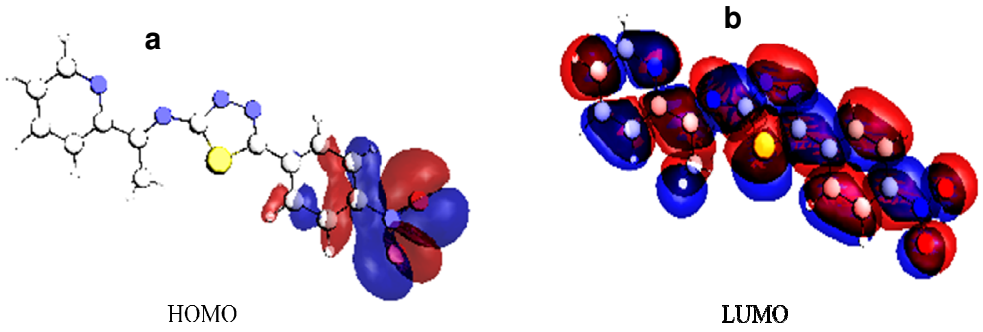

Fig. 3.56: a) HOMO and **b**) LUMO of 2APNPTDA

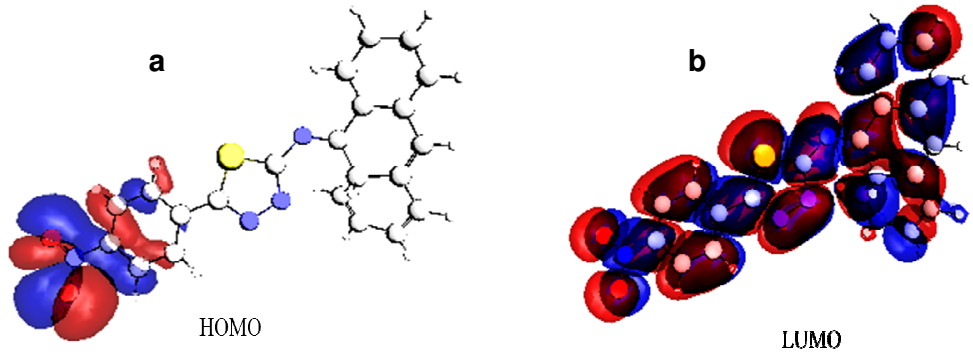

Fig. 3.57: a) HOMO and **b**) LUMO of ANNPTDA

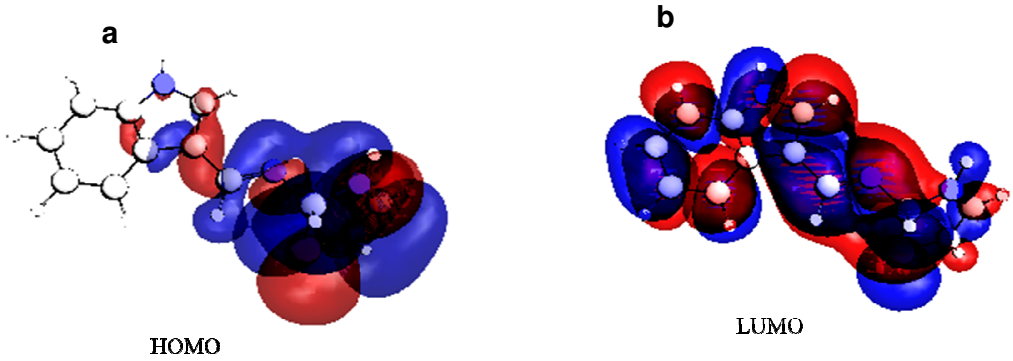

Fig. 3.58: a) HOMO and **b**) LUMO of I3A2AT

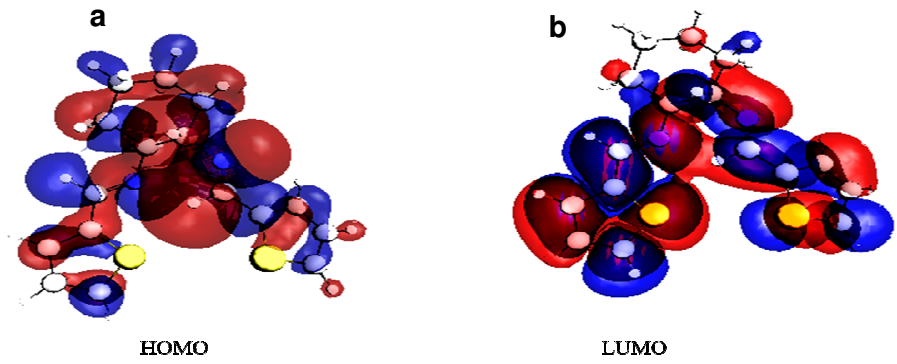

Fig. 3.59: a) HOMO and **b**) LUMO of T2CDACH

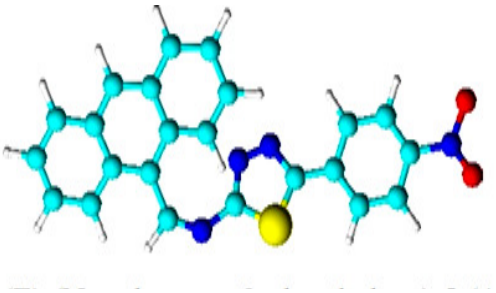

(E)-(N-anthracene-9-ylmethylene)-5-(4-nitrophenyl)-1,3,4-thiadiazol-2-amine (A9CNPTDA)

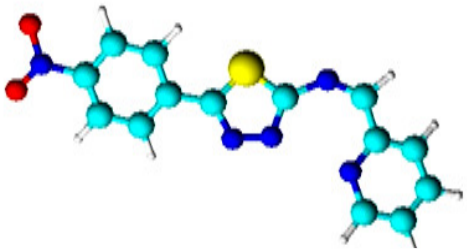

(E)-5-(4-nitrophenyl)-N-((pyridine-2-yl)methylene)-1,3,4- thiadiazol-2 amine (P2CNPTDA)

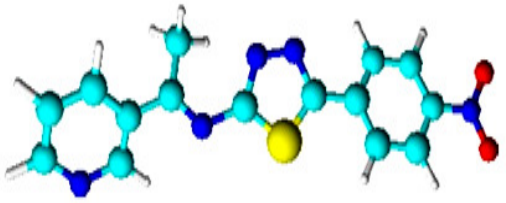

(E)-5-(4-nitrophenyl)-N-(pyridine-3-yl) ethylidene)-1,3,4-thiadiazol-2-amine (3APNPTDA)

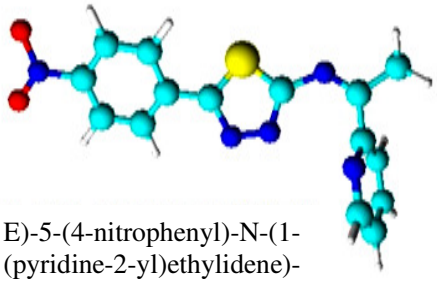

E)-5-(4-nitrophenyl)-N-(1-(pyridine-2-yl)ethylidene)-1,3,4-thiadiazol-2-amine (2APNPTDA)

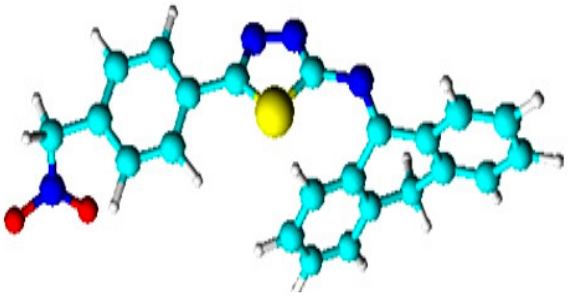

N-(anthracen-9(10H)-ylidene)-5-(4-nitrophenyl)-1,3,4-thiadiazol-2-amine (ANNPTDA)

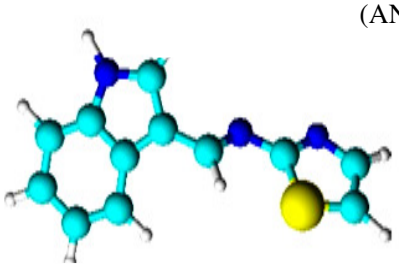

N-((1H-indol-3-yl)methylene)thiazol-2amine (I3A2AT)

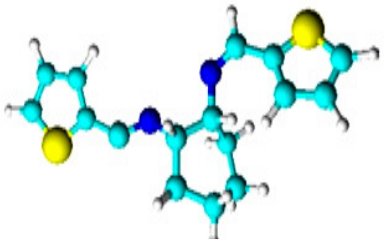

(13E)-N1,N2-bis((thiophene-2-yl)methylene)cyclohexane-1,2-diamine (T2CDACH)

Fig. 3.60: Optimized geometries of 'S' containing Schiff bases

CHAPTER 13

CORROSION INHIBITION STUDIES OF SULPHUR CONTAINING SCHIFF BASES ON CARBON STEEL IN 0.5M H_2SO_4

Investigations of corrosion inhibition response of seven heterocyclic Schiff bases including thiazole derivative, thiophene derivative and thiadiazole derivatives on carbon steel specimens in 0.5M sulphuric acid medium was established. Most adopted methods like gravimetric weight loss measurements, electrochemical impedance studies (EIS), potentiodynamic polarization studies (PDP), theoretical studies like quantum chemical calculations and surface morphological studies (SEM) were carried out for the investigation of corrosion inhibition capacity and to explain the mechanism of inhibition. In general, the inhibition competence of these heterocyclic Schiff base inhibitors in 0.5M H_2SO_4 medium was not that much prominent as in the HCl medium and it may be due to the highly aggressive nature of sulphuric acid lead to high corrosion rate of carbon steel specimens.

Gravimetric Weight Loss Measurements

Carbon steel specimens were engrossed in 0.5M sulphuric acid medium for 24h at 303K in the absence and presence of heterocyclic inhibitors. The rate of corrosion (W) and inhibition efficiencies (η_w%) are the characteristics of each heterocyclic Schiff base inhibitor which are displayed in Table 3.10 and Table 3.11 respectively. Variation of corrosion rate and the comparison of percentage of inhibition efficiency (η_w%) with concentration of heterocyclic Schiff bases are depicted in Fig. 3.61 and Fig. 3.62 respectively.

On the assessment, it is obvious that a corrosion rate of 40.64mm/y was observed for carbon steel specimens in 0.5M H_2SO_4 (blank) whereas CS in the presence of

investigated inhibitors displayed low corrosion rate. The heterocyclic poly nuclear thiadiazole Schiff base A9CNPTDA showed pronounced corrosion inhibition efficiency and low corrosion rate compared to all other heterocyclic Schiff bases at every concentration and a maximum efficiency of 90.7% was exhibited at 1mM concentration.

Table 3.10: Corrosion rates (mmy^{-1}) of CS in the presence of 'S' containing heterocyclic Schiff bases, in 0.5 M H_2SO_4 at 28^0C for 24h

C (Mm)	Corrosion rate (mmy^{-1})						
	A9CNPTDA	P2CNPTDA	ANNPTDA	3APNPTDA	2APNPTDA	I3A2AT	T2CDACH
0	40.64	40.64	40.64	40.64	40.64	40.64	40.64
0.2	11.4	13.9	23.51	22.55	24.98	12.68	19.19
0.4	9.28	12.24	20.09	21.66	23.48	10.21	11.45
0.6	7.81	10.21	16.04	20.76	22.58	6.96	7.84
0.8	6.04	8.13	15.76	19.2	20.96	6.23	6.89
1	3.74	5.23	14.76	18.82	19.59	3.95	6.04

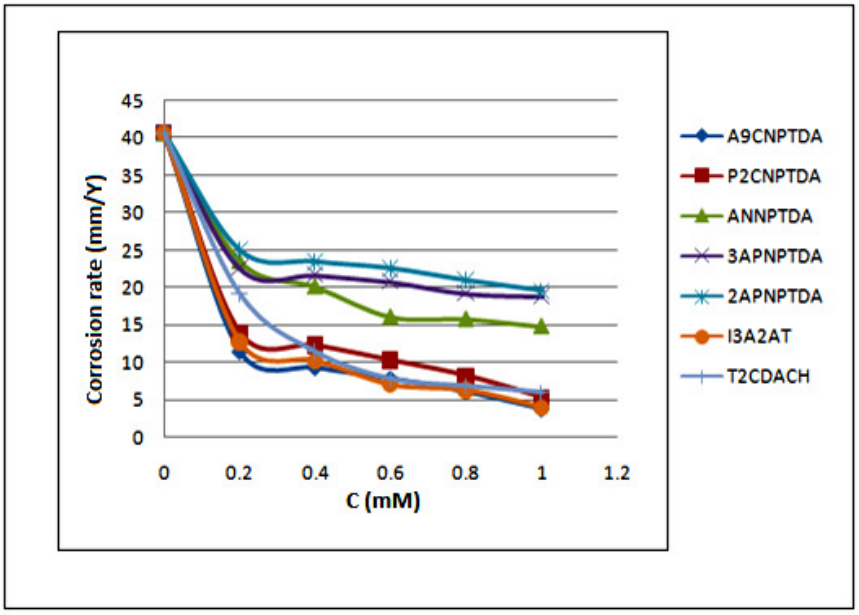

Fig. 3.61: Variation of corrosion rates of CS with the concentration of 'S' containing heterocyclic Schiff base inhibitors, in 0.5M H_2SO_4 for 24h

Table 3.11: Corrosion inhibition efficiencies (η_w%) of 'S' containing heterocyclic Schiff bases on CS corrosion in 0.5M H_2SO_4 at 28^0C for 24h

C (mM)	Inhibition efficiency (η_w%)						
	A9CNPTDA	P2CNPTDA	3APNPTDA	2APNPTDA	ANNPTDA	I3A2AT	T2CDACH
0.2	71.95	65.8	44.52	38.54	42.16	68.7	52.77
0.4	77.16	69.88	46.71	42.23	50.57	74.88	71.82
0.6	80.91	74.89	48.92	44.44	60.54	82.8	80.68
0.8	85.13	79.99	52.66	48.43	61.22	84.67	83.04
1	90.7	87.14	53.69	51.8	63.68	90.28	85.13

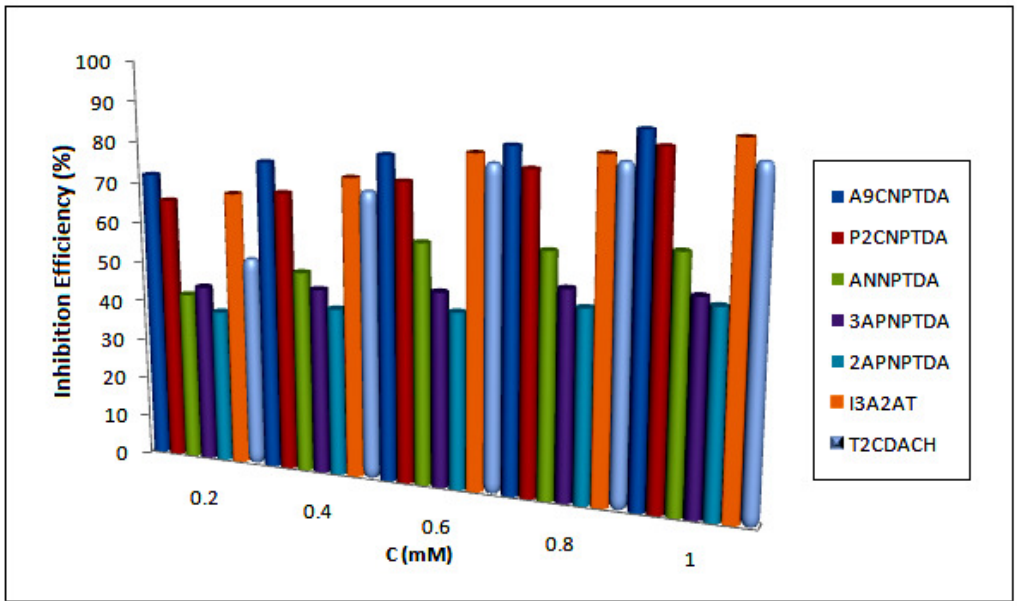

Fig. 3.62: Comparison of corrosion inhibition efficiencies (η_w%) of 'S' containing heterocyclic Schiff base inhibitors on CS corrosion in 0.5M H_2SO_4 for 24h

Among thiadiazole Schiff base inhibitors, 3APNPTDA, 2APNPTDA and ANNPTDA showed moderately low corrosion inhibition efficiency and high corrosion rate on CS surface in aggressive solution. Even though these organic molecules have dynamic corrosion inhibition probes such as a highly polarisable sulphur atom, azomethine linkage, heteroatoms and aromatic rings, they exhibited low corrosion inhibition performance, which may be recognized to i) vibrant corrosive behaviour of

H_2SO_4 medium and ii) possibility of slow hydrolysis rate of the molecules in H_2SO_4 medium.

The Heterocyclic Schiff base I3A2AT which is derived from indole-3-carbaldehyde and 2-aminothiazole and T2CDACH which is a derivative of thiophene 2aldehyde showed elevated inhibition efficiency in H_2SO_4 medium. Maximum η_w% shown by I3A2AT molecule at a concentration of 1mM was 90.28%. The maximum inhibition efficiency of I3A2AT is attributed by its adsorption employing between the electrons of the indole rings and CS surface, and it acts as a bidentate ligand in which surface coordination taking place via both the amino group and the –S– moiety from the thiazole ring. The Schiff base derived from thiophene-2-aldehyde i.e., T2CDACH showed elevated corrosion inhibition efficiency than thiadiazole pyridine derivatives and anthrone derivatives in sulphuric acid medium. The η_w% varied from 52.77 to 85.13% for concentrations 0.2 to 1mM respectively. Like other Schiff bases, T2CDACH also undergo hydrolysis but one of the hydrolysed product, thiophene 2-aldehyde exhibited higher inhibition efficiency in H_2SO_4 medium (Table 3.11).

Corrosion inhibition potencies of the 'S' containing Schiff base inhibitors were compared with their parent compounds 5-(4-nitrophenyl)-1,3,4-thiadiazol-2-amine (NPTDA), Anthracene-9-carbaldehyde (A9C), Pyridine-2-carbaldehyde (P2C), 3-Acetylpyridine (3ACP), 2-Acetylpyridine (2ACP), Anthrone (AN), Indole-3-Carbaldehyde (I3A), 2-Aminothiazole (2AT), Thiophene-2-carbaldehyde (T2C) and 1,2-Diamino cyclohexane (DAC) in 0.5M H_2SO_4 for a period 24h at different concentrations and are tabulated in Table 3.12. It can be inferred from the comparison studies that higher corrosion inhibition potencies of these heterocyclic Schiff base inhibitors were because of the presence of highly conjugated azomethine linkage.

Table 3.12: Corrosion inhibition efficiencies (η_w%) of parent compounds NPTDA, A9C, P2C, 3ACP, 2ACP, ANT, I3A, 2AT, T2C and DAC on CS in 0.5M H_2SO_4 for a period 24h

C (Mm)	Inhibition Efficiencies (η_w%)									
	NPTDA	A9C	P2C	3ACP	2ACP	ANT	13A	2AT	T2C	DAC
0.2	12.43	15.9	7.35	0.82	0.73	-85.78	38.92	12.28	22.16	-28
0.6	30.17	18.53	11.18	1.49	1.18	-80.09	43.54	14.64	34.72	-16
1	32.84	20.58	16.47	1.82	1.59	-74.93	48.65	21.87	70.03	1.68

On comparing the inhibition efficiencies of these heterocyclic Schiff bases in HCl and H_2SO_4 medium, it is obvious that they show higher inhibition efficiency in HCl medium. It is supposed that the Cl^- ions can more strongly adsorb on the metal surface than SO_4^{2-} ions and builds an excess negative charge on the carbon steel surface. It will facilitate the adsorption of protonated heterocyclic Schiff bases and reduce iron dissolution.

Adsorption Isotherms

The mechanism of interaction of these heterocyclic Schiff bases on the surface of CS specimens was demonstrated with the aid of adsorption isotherms. By considering different adsorption isotherms and the best fit model was selected with the support of correlation coefficient. Isotherms of these inhibitors in 0.5M H_2SO_4 are represented from Fig. 3.63 and parameters obtained from investigations are tabulated in Table 3.13.

From the adsorption investigations, it was found that these 'S' containing heterocyclic Schiff base inhibitors A9CNPTDA, P2CNPTDA, 3APNPTDA, 2APNPTDA, ANNPTDA, I3A2AT and T2CDACH followed Langmuir adsorption isotherm on the CS surface of during the process of corrosion inhibition in 0.5M H_2SO_4. Negative values of ΔG^0_{ads} for all sulphur containing Schiff bases inhibitors point out the spontaneity of the adsorption process. ΔG^0_{ads} values up to -20kJ/mol indicates the electrostatic interaction between the charged metal surface (physisorption) and the charged heterocyclic organic inhibitors.

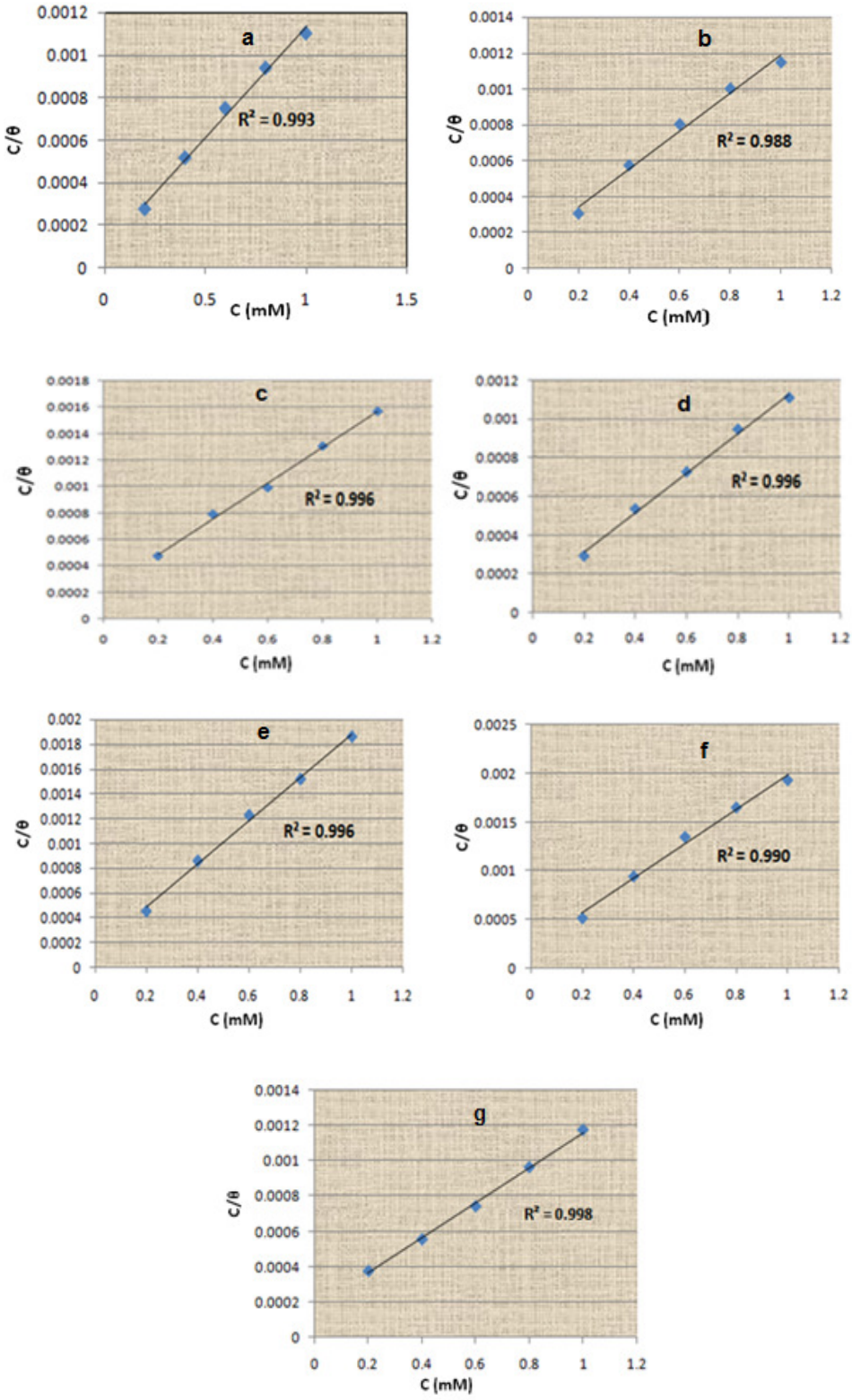

Fig. 3.63: Langmuir adsorption isotherms of (**a**) A9CNPTDA (**b**) P2CNPTDA (**c**) 3APNPTDA (**d**) 2APNPTDA (**e**) ANNPTDA (**f**) I3A2AT (**g**) T2CDACH on CS in 0.5M H_2SO_4

Table 3.13: Adsorption parameters of 'S' containing heterocyclic Schiff base inhibitors on CS corrosion in 0.5M H_2SO_4

Adsorption Parameter	Schiff bases						
	A9CNPTDA	P2CNPTDA	3APNPTDA	2APNPTDA	ANNPTDA	I3A2AT	T2CDACH
K_{ads}	10000	7633.58	7352.94	5000	4672	9090.90	6250
ΔG^0_{ads} ($kJmol^{-1}$)	-33.12	-32.44	-32.35	-31.38	-31.12	-32.88	-31.94

ΔG^0_{ads} ranges between -31.94 and -33.12kJ/mol on CS specimens in 0.5M H_2SO_4 medium which implies that the adsorption behaviour of all the synthesized heterocyclic inhibitor molecules involves both electrostatic and chemical adsorption. The free energy of adsorptions of these heterocyclic Schiff base inhibitors, A9CNPTDA and I3A2AT were comparatively elevated than that of the other heterocyclic imines. The main reason is that these inhibitors are more powerfully adsorbed on the CS surface forming a monolayer through highly conjugated azomethine linkage, highly polarisable aromatic rings etc.

Surface Morphological Investigations

In order to establish the mechanism of action of these heterocyclic Schiff base inhibitors A9CNPTDA, P2CNPTDA, 3APNPTDA, 2APNPTDA, ANNPTDA, I3A2AT and T2CDACH, SEM experiments were conducted in 0.5M H_2SO_4 on CS surface. The SEM micrographs of (a) bare CS surface (b) CS specimen immersed in 0.5M $H_2SO_4$and containing 1mM concentration of (c) A9CNPTDA and (d) ANNPTDA after 24 h of immersion time are shown in Fig. 3.64. Surface morphology of these images were clearly established that in presence of inhibitors, the damage occurred on the CS surfaces was fairly decreased whereas the surface was dangerously destroyed in the absence of inhibitor.

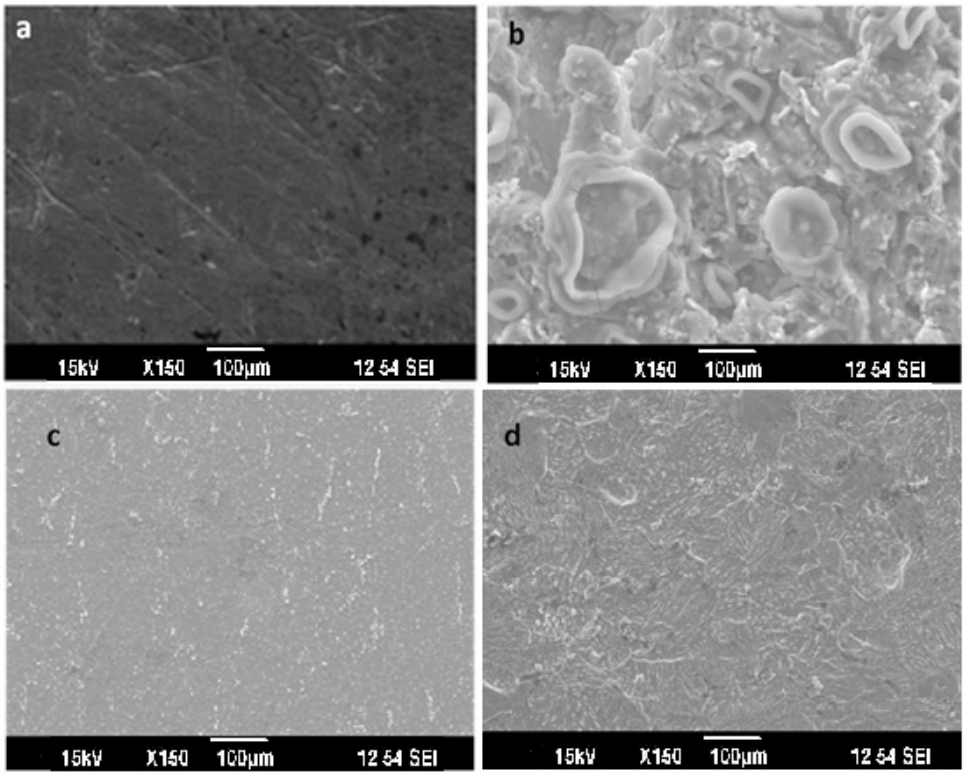

Fig. 3.64: SEM images of (**a**) bare CS (**b**) CS treated with 0.5M H_2SO_4 (**c**) CS treated with A9CNPTDA (1mM) (**d**) CS treated with ANNPTDA (1mM) for 24h

Electrochemical Impedance Spectroscopic Studies (EIS)

Iviumcompactstat-e system associated with a superior version of 'IviumSoft' software was employed for the electrochemical analysis. Assemblies of three-electrode was used as the electrochemical cell in which a saturated calomel electrode (SCE) was used as the reference electrode, a platinum electrode of area $1cm^2$ was used as the auxiliary or counter electrode and well-polished metal surface of exposed area ($1cm^2$) towards the corroding medium was employed as the working electrode for analysis.

The corrosion behaviour of CS in 0.5M H_2SO_4 with and without these 'S' heterocyclic inhibitors was studied by employing impedance spectroscopic analysis. To make clear the inhibitory action of these organic ligands, CS specimens were engrossed in 0.5M H_2SO_4 medium in the presence and absence of the inhibitors for 30 minutes prior to the experiment at 303K.

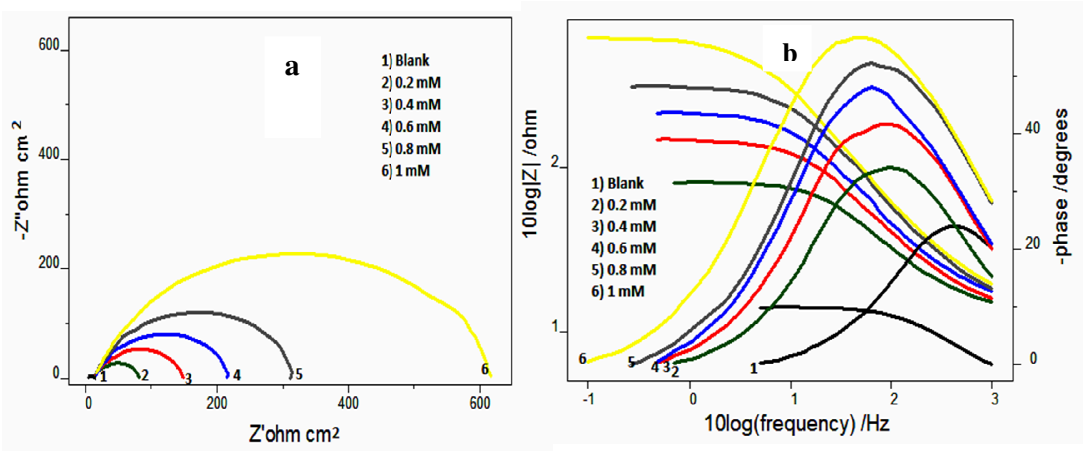

Fig. 3.65: a) Nyquist plots and **b)** Bode plots of CS corrosion in the presence and absence of A9CNPTDA in 0.5M H_2SO_4

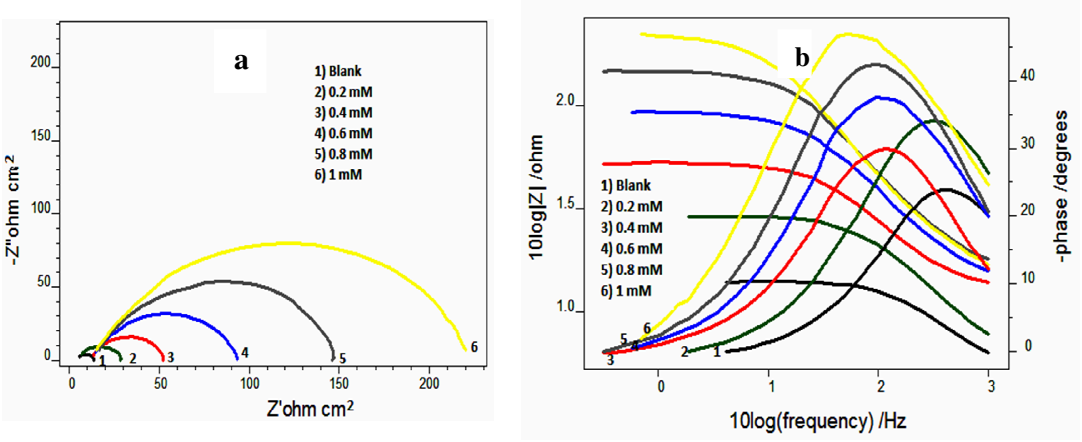

Fig. 3.66: a) Nyquist plots and **b)** Bode plots of CS corrosion in the presence and absence of P2CNPTDA in 0.5M H_2SO_4

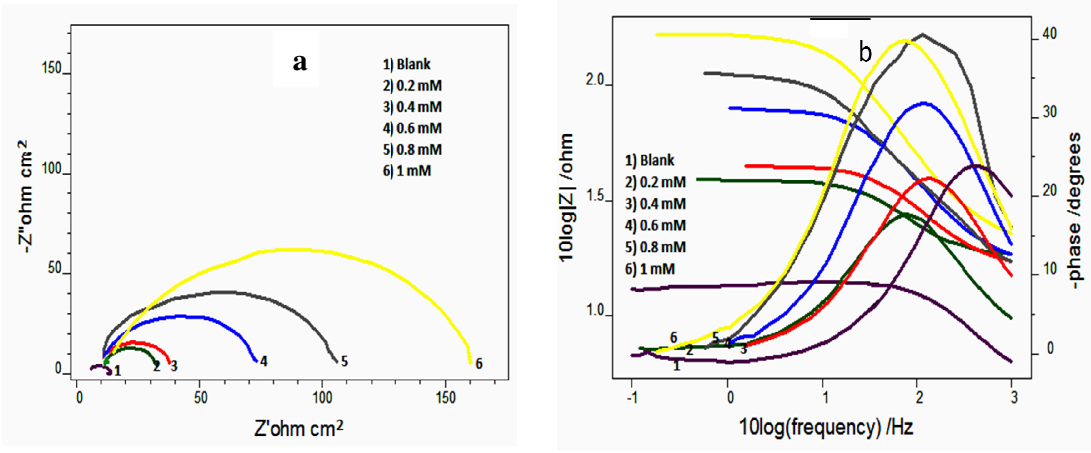

Fig. 3.67: a) Nyquist plots and **b)** Bode plots of CS corrosion in the presence and absence of 3APNPTDA in 0.5M H_2SO_4

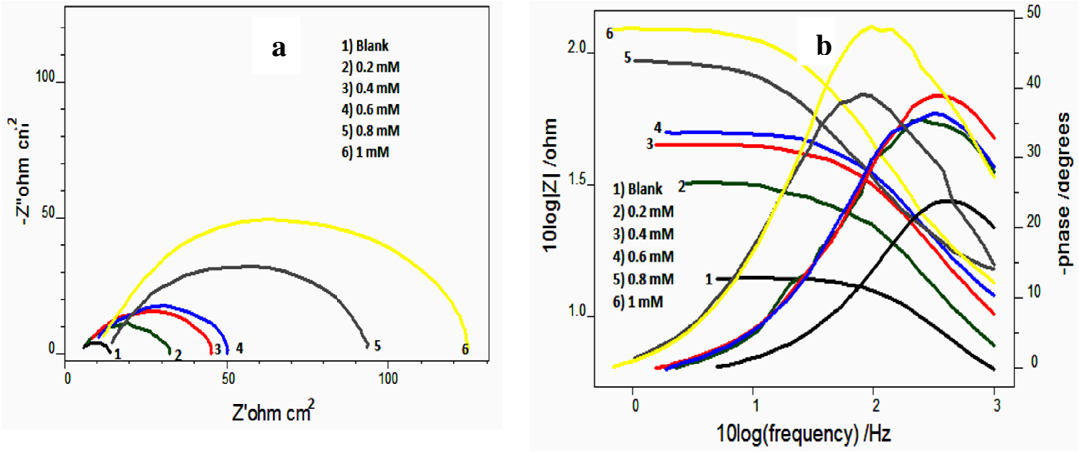

Fig. 3.68: a) Nyquist plots and **b)** Bode plots of CS corrosion in the presence and absence of 2APNPTDA in 0.5M H_2SO_4

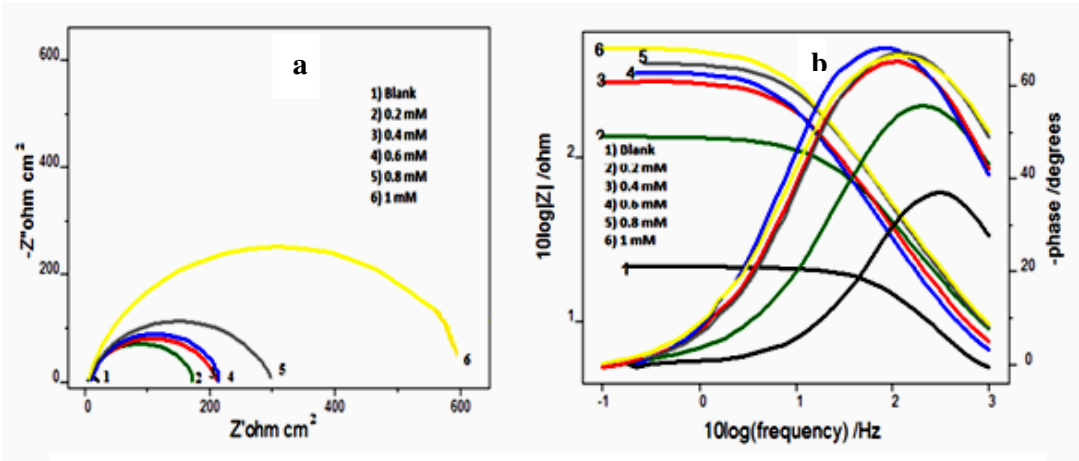

Fig. 3.69: a) Nyquist plots and **b)** Bode plots of CS corrosion in the presence and absence of ANNPTDA in 0.5M H_2SO_4

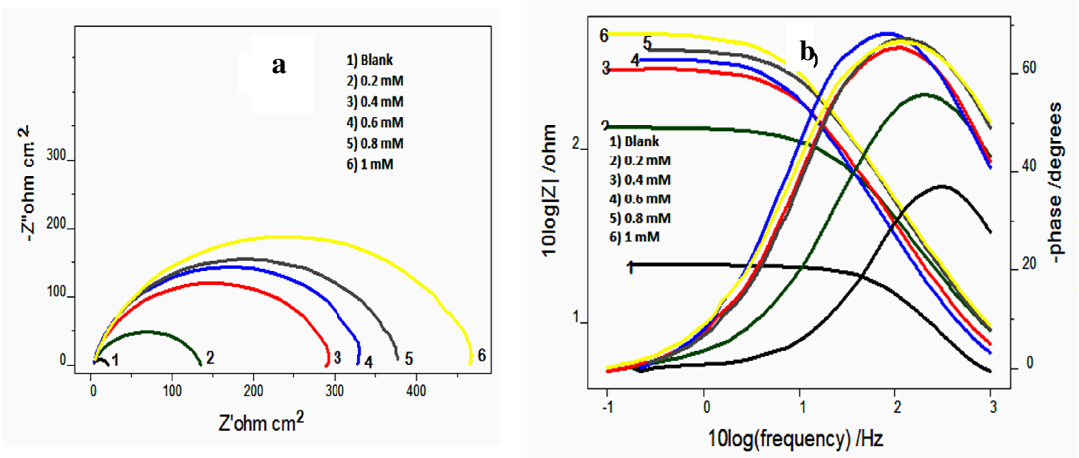

Fig. 3.70: a) Nyquist plots and **b)** Bode plots of CS corrosion in the presence and absence of I3A2AT in 0.5M H_2SO_4

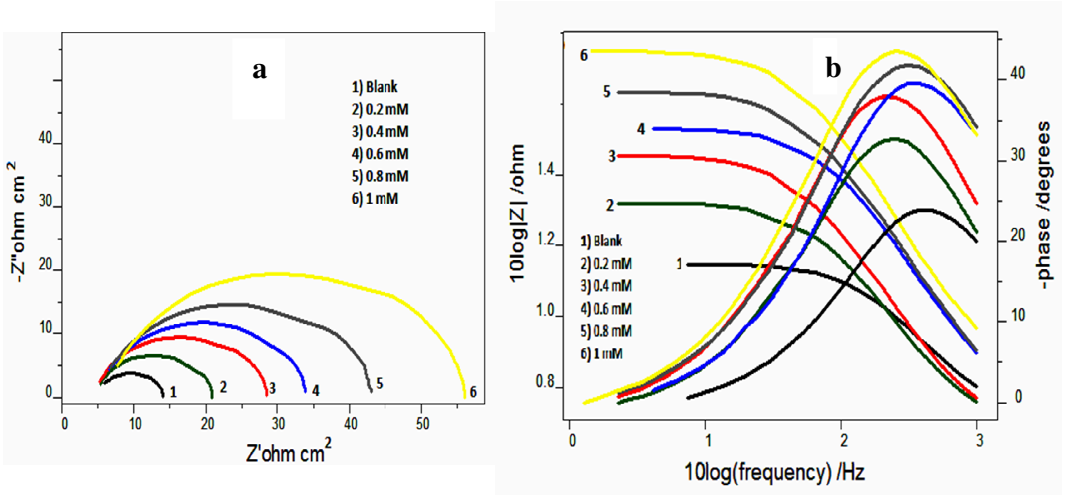

Fig. 3.71: a) Nyquist plots and **b)** Bode plots of CS corrosion in the presence and absence of T2CDACH in 0.5M H_2SO_4

Fig. 3.65 to Fig. 3.71 corresponding to the Nyquist plots and Bode plots of the 'S' containing heterocyclic Schiff bases A9CNPTDA, P2CNPTDA, 3APNPTDA, 2APNPTDA, ANNPTDA, I3A2AT and T2CDACH respectively. The impedance (EIS) parameters such as charge transfer resistance (R_{ct}), double layer capacitance (C_{dl}), solution resistance (R_s)and percentage of inhibition efficiency ($\eta_{EIS\%}$) were calculated from these plots and documented in Table 3.14. From R_{ct} values, the percentage of inhibition efficiency was evaluated using the subsequent equation

$$\eta_{EIS}\% = \frac{Rct - R'ct}{Rct} \times 100 \qquad (40)$$

where R'_{ct} and R_{ct} are the charge transfer resistances of the working electrode in acid medium in the absence and presence of these heterocyclic Schiff base indicators respectively

The value of R_{ct} is a measure of electron transfer between acidic solution and the exposed area of CS and the rate of corrosion is inversely proportional to it. From Nyquist plots, it was observed that the diameter of semicircle increases with the concentration of inhibitors indicating that these 'S' containing inhibitors undergo self-assembly on the CS

surface for forming a protective layer and resist the corrosion process. Highest value of R_{ct} is shown by thiadiazole Schiff base A9CNPTDA and a maximum efficiency of 97.81% was obtained at 1mM concentration of the inhibitor. The monolayer formation of inhibitors obstructs the charge transfer between the carbon steel and the acidic solution and charge transfer resistance increases with inhibitor concentration. The decreasing nature of capacitance values C_{dl} with the inhibitor concentration mainly indicates the increase in the thickness of the electrical double layer and/or decrease in local dielectric constant. The trend of increasing percentage of inhibition efficiency with the concentration is depicted in Fig. 3.72.

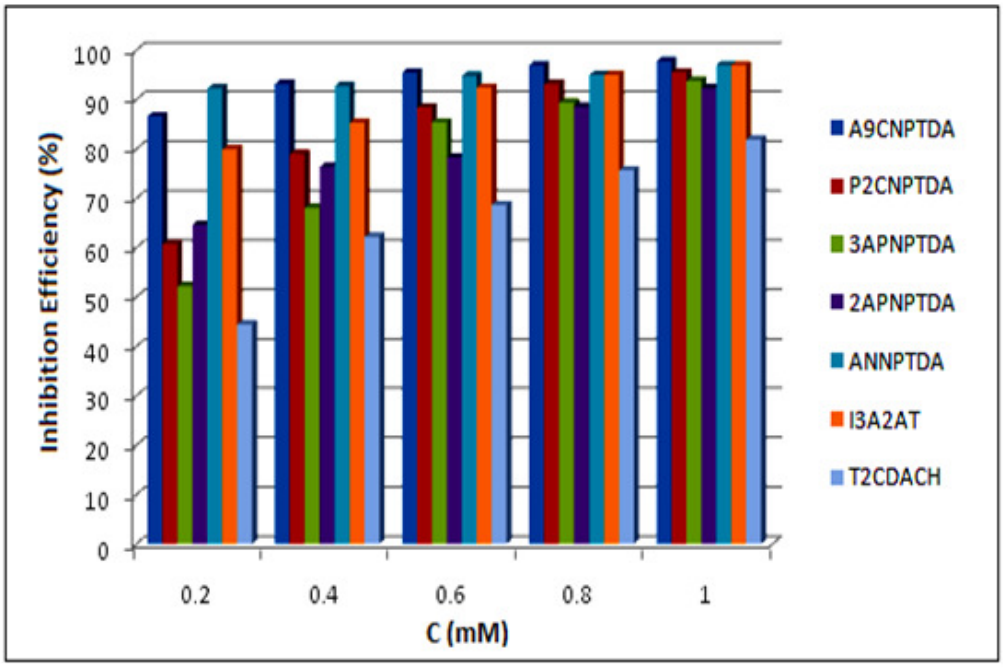

Fig. 3.72: Comparison of Corrosion inhibition efficiencies ($\eta_{EIS\%}$) of 'S' containing heterocyclic Schiff base inhibitors on CS in 0.5M H_2SO_4 at 28^0C

Table 3.14: Electrochemical impedance parameters of CS corrosion in the presence and absence of 'S' containing heterocyclic Schiff bases in 0.5M H_2SO_4

Inhibitors	C (mM)	C_{dl} ($\mu F\ cm^{-2}$)	R_{ct} ($\Omega\ cm^{-2}$)	η_{EIS}%
Blank	0	90	8.16	-
A9CNPTDA	0.2	79.2	61.2	86.66
	0.4	65.2	120	93.22
	0.6	58.3	181	95.49
	0.8	43.6	273	97.01
	1	39.5	374	97.81
P2CNPTDA	0.2	66.9	20.8	60.76
	0.4	89.9	35.9	79.03
	0.6	62.1	70.5	88.42
	0.8	52.7	120	93.2
	1	60.7	184	95.56
3APNPTDA	0.2	64.0	19.1	52.27
	0.4	87.3	25.6	68.12
	0.6	63.9	56.1	85.45
	0.8	64.7	77.4	89.45
	1	55.0	133	93.86
2APNPTDA	0.2	69.6	23.1	64.67
	0.4	43.9	34.6	76.41
	0.6	43.0	37.6	78.29
	0.8	80.7	72.0	88.60
	1	46.7	106	92.35
ANNPTDA	0.2	68.7	106	92.30
	0.4	65.1	113	92.77
	0.6	70.0	158	94.83
	0.8	71.0	164	95.02
	1	66.3	359	97.02
I3A2AT	0.2	80.0	60.9	80.00
	0.4	68.8	101	85.41
	0.6	69.7	146	92.50
	0.8	118	159	95.05
	1	59.2	312	97.01
T2CDACH	0.2	106	14.7	44.55
	0.4	97.7	21.6	62.26
	0.6	52.8	25.9	68.70
	0.8	57.0	33.6	75.74
	1	49.8	45.0	82.00

Inhibition efficiency obtained from gravimetric weight loss studies and results gained from EIS analysis are not comparable. Results from EIS studies are higher than the results obtained from gravimetric weight loss studies. Electrochemical analysis is a quick corrosion monitoring procedure and it will only show the corrosion inhibition potencies in the early hours stage of treatment. In H_2SO_4 medium, these ligands have a tendency to hydrolyze into their parent compounds and they exhibit poor inhibition efficiency for a long period of 24h. This is the main reason for the poor results of gravimetric corrosion inhibition studies than the electrochemical analysis results. Comparatively least efficiency was reported in the case of inhibitor T2CDACH and these results are similar to gravimetric weight loss studies. This is because of the inhibitor T2CDACH undergoes faster hydrolysis in H_2SO_4 medium in the early hours stage. Heterocyclic inhibitors ANNPTDA and I3A2AT showed high results in EIS analysis, but the performance of ANNPTDA in gravimetric studies are very low. The results also show the fast hydrolytic nature of this molecule in aggressive medium. Order of performances of the studied S containing heterocyclic Schiff base inhibitors in H_2SO_4 medium on can be given as A9CNPTDA > ANNPTDA > I3A2AT > P2CNPTDA > 3APNPTDA >2APNPTDA > T2CDACH.

Potentiodynamic Polarization Studies

To emphasize the corrosion inhibitory role of the novel 'S' containing Schiff bases on carbon steel and to recommend the electrochemical site of interaction, potentiodynamic polarization studies including Tafel extrapolation analysis and Linear polarization studies were conducted. Corrosion potential (E_{corr}), corrosion current density (i_{corr}) and polarization resistance (R_p) were calculated in every analysis and by means, the inhibition efficiency was determined. Tafel plots and linear polarization curves of CS in 0.5M H_2SO_4 medium in the presence and absence of these heterocyclic Schiff base

inhibitors are depicted from Fig. 3.73 to Fig. 3.79. Tafel and Linear polarization data including corrosion potential (E_{corr}), corrosion current density (I_{corr}), anodic slope (b_a), cathodic slope (b_c) and inhibition efficiency were obtained by potentiodynamic polarization studies and tabulated in Table 3.15. A comparison between the inhibition efficiencies of these sulphur containing heterocyclic Schiff base inhibitors was done and portrayed in Fig. 3.83.

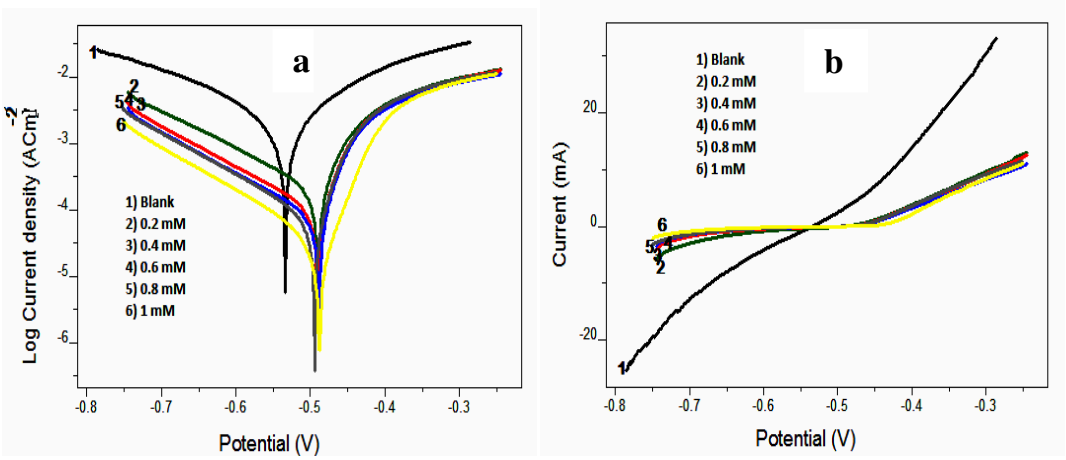

Fig. 3.73: a) Tafel plots and **b)** Linear polarization curves of CS corrosion in the presence and absence of A9CNPTDA in 0.5M H_2SO_4

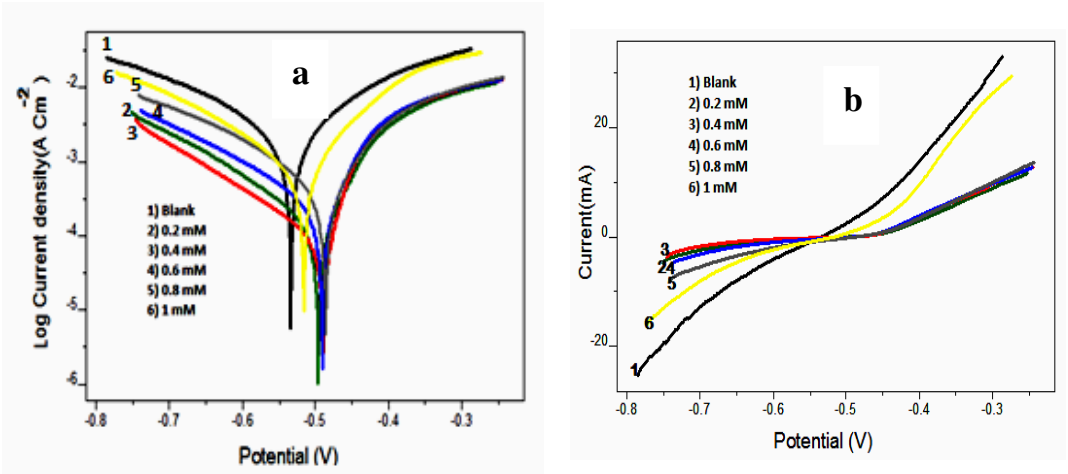

Fig. 3.74: a) Tafel plots and **b)** Linear polarization curves of CS corrosion in the presence and absence of P2CNPTDA in 0.5M H_2SO_4

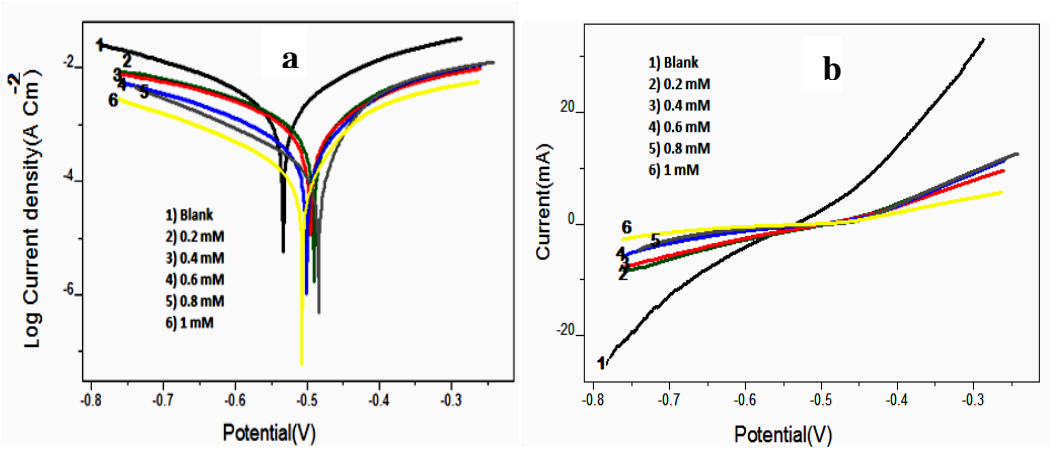

Fig. 3.75: a) Tafel plots and **b)** Linear polarization curves of CS corrosion in the the presence and absence of 3APNPTDA in 0.5M H_2SO_4

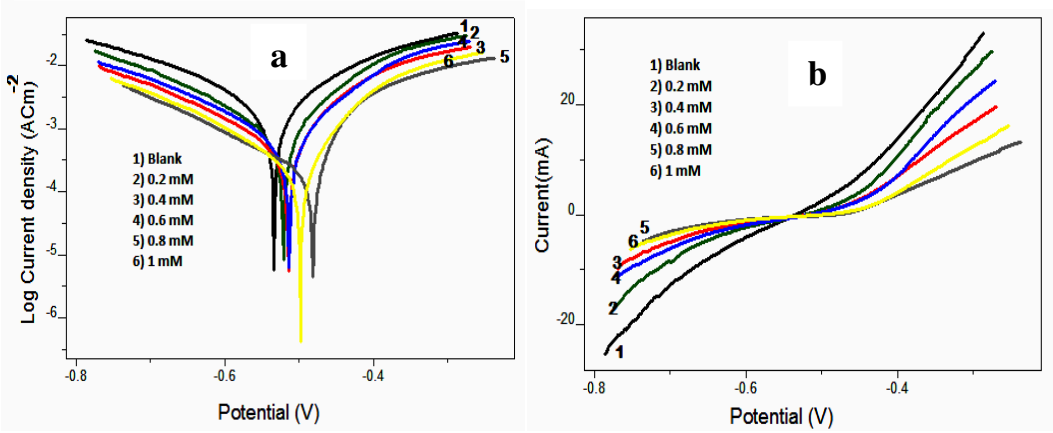

Fig. 3.76: a) Tafel plots and **b)** Linear polarization curves of CS corrosion in the presence and absence of 2APNPTDA in 0.5M H_2SO_4

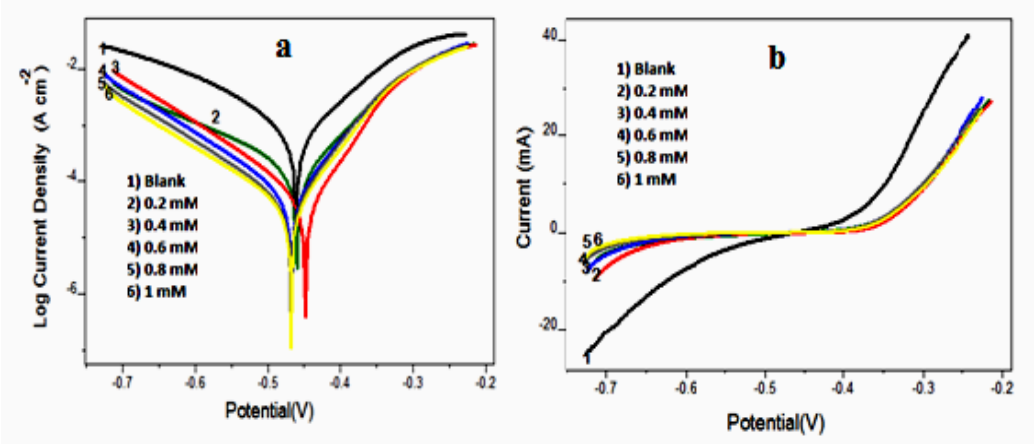

Fig. 3.77: a) Tafel plots and **b)** Linear polarization curves of CS corrosion in the presence and absence of ANNPTDA in 0.5M H_2SO_4

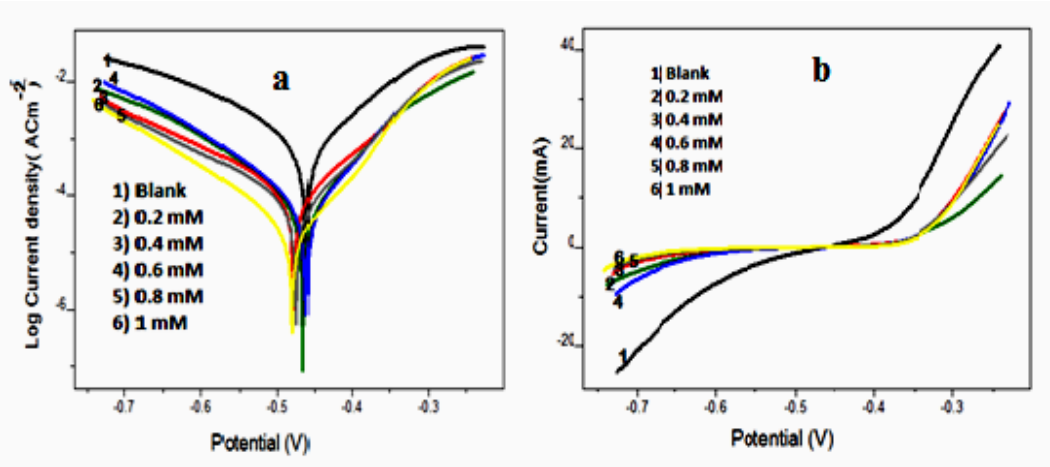

Fig. 3.78: a) Tafel plots and **b)** Linear polarization curves of CS corrosion in the presence and absence of I3A2AT in 0.5M H_2SO_4

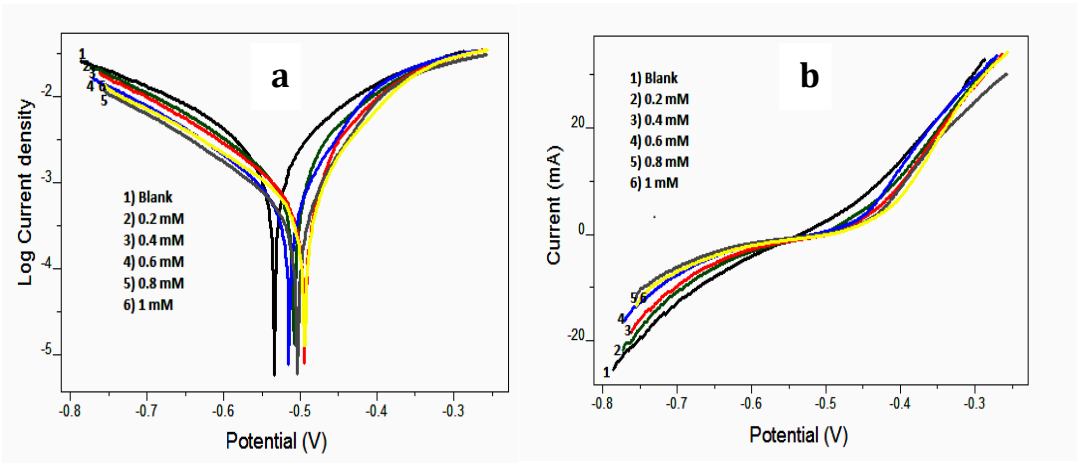

Fig. 3.79: a) Tafel plots and **b)** Linear polarization curves of CS corrosion in the presence and absence of T2CDACH in 0.5M H_2SO_4

Table 3.15: Potentiodynamic polarization parameters of CS corrosion in the presence and absence of 'S' containing heterocyclic Schiff bases in 0.5M H_2SO_4

Inhibitor	Tafel Data						Polarization data	
	C (mM)	$-E_{corr}$ (mV/SCE)	I_{corr} ($\mu A/cm^2$)	$-b_a$ (mV/dec)	b_c (mV/dec)	η_{pol}%	R_p(ohm)	η_{Rp}%
Blank	0	541	2705	205	234	-	15.23	-
A9CNPTDA	0.2	577	602	225	177	77.74	82.17	81.46
	0.4	606	479	232	165	82.29	130	88.28
	0.6	612	402	233	161	85.13	161	90.54
	0.8	608	368	214	158	86.39	204.1	92.53
	1	583	149	154	156	94.49	611.5	97.50
P2CNPTDA	0.2	536	1140	151	190	57.8	30.45	49.98
	0.4	529	893	211	205	66.9	58.35	73.89
	0.6	573	724	232	192	73.23	88.88	82.86
	0.8	562	391	182	167	85.54	142.6	89.32
	1	608	490	233	163	81.88	164.9	90.76
3APNPTDA	0.2	499	1217	211	271	55	36.08	57.78
	0.4	497	1072	212	269	60.36	40.08	62.00
	0.6	528	611	179	220	77.41	76.7	80.14
	0.8	574	610	224	179	77.46	108.8	85.92
	1	564	335	214	199	87.6	172.3	91.16
2APNPTDA	0.2	545	1241	161	186	54.12	29.52	48.40
	0.4	560	927	187	189	65.73	44.83	66.02
	0.6	533	886	150	196	67.25	39.64	61.57
	0.8	583	701	244	170	74.1	69.18	77.98
	1	550	544	172	175	79.88	87.87	82.66
ANNPTDA	0.2	601	456	235	163	83.14	132.7	88.52
	0.4	559	318	180	172	88.24	160.9	90.53
	0.6	558	302	178	161	88.88	184.9	91.76
	0.8	527	189	236	253	93.01	216.6	92.96
	1	474	71.1	163	138	97.37	258.3	94.10
I3A2AT	0.2	580	631	225	179	76.67	71.17	78.60
	0.4	606	483	232	166	82.14	129.9	88.27
	0.6	612	417	233	161	84.58	157.4	90.32
	0.8	608	386	216	160	85.73	199.5	92.36
	1	583	158	155	156	94.15	605.18	97.48
T2CDACH	0.2	543	1674	180	190	37.49	22.75	33.05
	0.4	544	1390	173	181	48.41	33.89	55.06
	0.6	558	1241	165	167	53.65	37.33	59.20
	0.8	555	960	164	174	64.15	46.54	67.27
	1	527	881	139	187	67.10	64.15	76.25

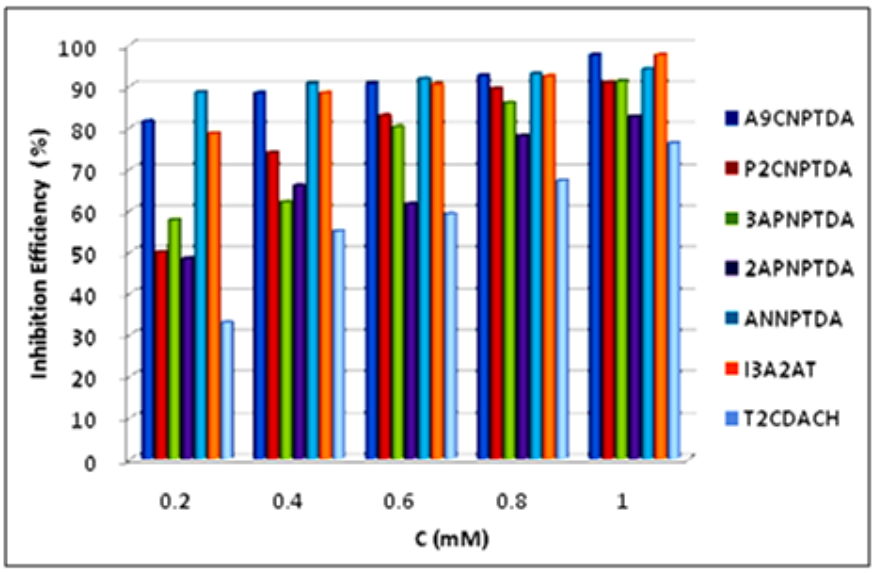

Fig. 3.80: Comparison study of corrosion inhibition potencies (η_{pol}%) of 'S' containing heterocyclic Schiff bases on CS in 0.5M H_2SO_4 at 28^0C

On scrutiny, it was revealed that the corrosion current densities of steel specimens decreased appreciably with the concentration of inhibitors. This is because of these organic molecules obstruct the metal dissolution progression appreciably by either prevailing in the cathodic or anodic process of corrosion or they acted as mixed type inhibitors. On the evaluation of Tafel and Linear polarization curves, it was established that the slope of the Tafel curves of uninhibited solution entirely different from the slope obtained in the presence of inhibitors. The outcome obtained by the potentiodynamic polarization studies were in good harmony with the electrochemical impedance studies.

Among thiadiazole derivatives, the polynuclear heterocyclic Schiff base inhibitor, A9CNPTDA exhibited the maximum inhibition efficiency of 97.50% at 1mM concentration. The heterocyclic Schiff bases, I3A2AT and ANNPTDA, also exhibited excellent inhibition efficiencies (97.48% in the case of I3A2AT and 94.10% in the case of ANNPTDA). But the performance of ANNPTDA in gravimetric studies is very low. Even if the Schiff base inhibitors 3APNPTDA and 2APNPTDA showed poor inhibitive performance as per gravimetric weight loss studies in 0.5M H_2SO_4 at 24h, their corrosion

inhibitory power in accordance with the polarization techniques were very much higher than that of expected. This is because of that, in electrochemical investigations, the contact time between the acid solution and the working electrode is about 30 minutes only whereas in the later the contact time is 24h and more.

Generally, if the shift of E_{corr} is greater than 85 and a significant change is observed in cathodic or anodic slopes, the inhibitor can be considered as cathodic or anodic inhibitors. In the present investigation, the seven heterocyclic Schiff bases namely A9CNPTDA, P2CNPTDA, 3APNPTDA, 2APNPTDA, ANNPTDA, I3A2AT and T2CDACH affects the anodic and cathodic slopes uniformly and E_{corr} values didn't alter considerably with respect to the blank (>85) and therefore these molecules can be regarded as mixed-type inhibitors.

SUMMARY

The corrosion inhibition efficiencies of newly synthesized sulphur containing heterocyclic Schiff base inhibitors namely (E)-(N-anthracene-9-ylmethylene)-5-(4-nitrophenyl)-1,3,4-thiadiazol-2-amine (A9CNPTDA), (E)-5-(4-nitrophenyl)-N-((pyridine -2-yl)methylene)-1,3,4-thiadiazol-2-amine (P2CNPTDA), (E)-5-(4-nitrophenyl)-N-(1 (pyridine-3-yl)ethylidene)-1,3,4-thiadiazol-2-amine (3APNPTDA), (E)-5-(4-nitrophenyl) -N-(1(pyridin-2-yl)ethylidene)-1,3,4-thiadiazol-2-amine (2APNPTDA), N-(anthracen-9(10H)-ylidene)-5-(4-nitrophenyl)-1,3,4-thiadiazol-2-amine (ANNPTDA), N-((1H-indol-3-yl)methylene)thiazol-2amine (I3A2AT) and (13E)-N1,N2-bis((thiophene-2-yl)methylene)cyclohexane-1,2-diamine (T2CDACH) against CS specimens in 1M HCl and 0.5M H_2SO_4 solutions were analysed using weight loss studies and electrochemical investigations like electrochemical impedance spectroscopy (EIS), potentiodynamic polarization studies (PDP) and electrochemical noise measurements. It was found that all these 'S' containing Schiff base ligands exhibited excellent corrosion inhibition efficiency on carbon steel in HCl medium. Generally the corrosion inhibition efficiency was lower in H_2SO_4 medium than in HCl medium. The corrosion inhibition mechanism of the compounds was confirmed by adsorption studies and surface morphological analysis and the effect of temperature and time on the corrosion inhibition efficiency of the compounds was also established. Quantum chemical investigations were performed using Gammess software and optimized geometries were formulated.

According to the weight loss studies in HCl medium, the inhibition efficiencies were increased with the inhibitor concentrations for all the compounds. At a maximum concentration of 1mM, all the studied inhibitors displayed 95.18 - 98.04% inhibition efficiencies by the gravimetric weight loss studies. A9CNPTDA showed pronounced

corrosion inhibition efficiency compared to all other heterocyclic Schiff bases at every concentration and a maximum efficiency of 98.04% was exhibited at 1mM concentration

All the inhibitors were performed very potential anticorrosive activity (92.47-99.6%) towards CS at 1mM concentration during electrochemical studies. The highly delocalized electron clouds of the aromatic rings, interacted with the metal surface deeply and thus prevent the metallic dissolution appreciably. Presence of heteroatoms especially highly polarizable 'S' atom, azomethine moiety, electron-rich aromatic rings and planarity are the root causes by which the molecule showed higher inhibition efficiency. The stability of the inhibitor in aggressive medium is very essential if it is to be recommended for long time use. All synthesized heterocyclic inhibitors except T2CDACH are excellent inhibitors for long time use. This is because of the puckered geometry and the tendency of hydrolysis which prevents the molecule to interact with the metal surface. It was confirmed by UV-Visible study that the molecule undergoes fast hydrolysis into their parent compounds in 1M HCl medium.

Adsorption studies revealed that Langmuir isotherm was the best fit isotherm for all synthesized molecules 1M HCl medium. The values of thermodynamic parameters suggested that adsorption process was spontaneous and the interaction between the metal and inhibitor molecules involves both electrostatic-adsorption and chemisorptions. The role of azomethine group in the inhibitory action was proved when the parent compounds of the Schiff base inhibitors were taken for corrosion studies. The activities were higher for the Schiff bases than the parent compounds. The corrosion inhibition performances of the compounds at elevated temperatures were also studied in HCl medium. Data obviously established that the rate of corrosion is increased at elevated temperatures.

Temperature-dependent gravimetric analysis showed that the activation energy of corrosion was high in 1M HCl solution containing Schiff base molecules. Also it was

observed that activation energy increased with rise in concentration of Schiff bases. Positive value of enthalpy of corrosion reflects the endothermic nature of corrosion. Both Nyquist plot and Bode plot analysis were utilized to get much density on the inhibitory action of these novel Schiff bases by EIS method. During polarization analysis, Tafel extrapolation method and Linear polarization method were performed separately. Surface morphological study established the protective nature of Schiff bases on mild steel surface. Electrochemical noise measurement was also carried out to examine the inhibition capacity. These results are in close agreement with other electrochemical studies. The results obtained from quantum chemical studies are also in close agreement the gravimetric weight loss studies.

In 0.5M sulphuric acid medium, the gravimetric studies gave a different order of corrosion inhibition efficiency for the Schiff base inhibitors, i.e. A9CNPTDA > I3A2AT > P2CNPTDA > T2CNPTDA > ANNPTDA > 3APNPTDA > 2APNPTDA. A maximum of 90.7% was obtained by A9CNPTDA at 1mM concentration. The inhibition efficiencies were lesser than that in HCl medium, which can be explained with the aggressive nature of the sulphuric acid and possibility of hydrolysis in this medium. Weight loss measurements on both Schiff base inhibitors and their corresponding parent compounds were performed and compared. Langmuir isotherm was the best fit one for all the studied molecules. The ΔG^0_{ads} values for all the molecules suggested that the adsorption involved both physisorption and chemisorption. Electrochemical impedance and potentiodynamic investigations in 0.5M H_2SO_4 gave higher corrosion inhibition efficiencies compared to gravimetric studies because it is quick monitoring technique. A9CNPTDA and I3A2AT expressed inhibition efficiency greater than 90% in both experiments. Comparatively least efficiency was reported by T2CDACH. This is because faster hydrolysis nature of this molecule in the early hours stage. One of the polynuclear

derivative ANNPTDA exhibit high inhibition efficiency in EIS analysis (97.02%), but its gravimetric performance is less because its hydrolyzed products (parent compounds) showed less inhibition efficiency in H2SO4 Medium. Polarization studies revealed that the Schiff bases affected cathodic and anodic sites of corrosion (mixed type inhibitor).

REFERENCES

[1] G. Koch, Cost of corrosion, Trends Oil Gas Corros. Res. Technol. 1(2017) 3–30.

[2] E. Sherif, S.-M. Park, Inhibition of copper corrosion in acidic pickling solutions by N-phenyl-1, 4-phenylenediamine, Electrochimica Acta. 51 (2006) 4665–4673.

[3] S. Muralidharan, R. Chandrasekar, S. Iyer, Effect of piperidones on hydrogen permeation and corrosion inhibition of mild steel in acidic solutions, J. Chem. Sci. 112 (2000) 127–136.

[4] M.G. Fontana, N.D. Greene, Corrosion engineering, McGraw-hill, 3 (2018) 1-465.

[5] C. Jomdecha, A. Prateepasen, P. Kaewtrakulpong, Study on source location using an acoustic emission system for various corrosion types, Ndt E Int. 40 (2007) 584–593.

[6] L. Elkadi, B. Mernari, M. Traisnel, F. Bentiss, M. Lagrenee, The inhibition action of 3, 6-bis (2-methoxyphenyl)-1, 2-dihydro-1, 2, 4, 5-tetrazine on the corrosion of mild steel in acidic media, Corros. Sci. 42 (2000) 703–719.

[7] S. Sharma, R. Chaudhary, Inhibitive action of methyl red towards corrosion of mild steel in acids, Bull. Electrochem. 16 (2000) 267–271.

[8] L. Garverick, Corrosion in the petrochemical industry, ASM international, 1994.

[9] A. Yurt, A. Balaban, S.U. Kandemir, G. Bereket, B. Erk, Investigation on some Schiff bases as HCl corrosion inhibitors for carbon steel, Mater. Chem. Phys. 85 (2004) 420–426.

[10] M. Cisse, B. Zerga, F. El Kalai, M.E. Touhami, M. Sfaira, M. Taleb, B. Hammouti, N. Benchat, S. El Kadiri, A.T. Benjelloun, Two dipodal pyridin-pyrazol derivatives as efficient inhibitors of mild steel corrosion in HCl solution—part I: electrochemical study, Surf. Rev. Lett. 18 (2011) 303–313.

[11] Z. Cao, Y. Tang, H. Cang, J. Xu, G. Lu, W. Jing, Novel benzimidazole derivatives as corrosion inhibitors of mild steel in the acidic media. Part II: theoretical studies, Corros. Sci. 83 (2014) 292–298.

[12] J.M. Gaidis, Chemistry of corrosion inhibitors, Cem. Concr. Compos. 26 (2004) 181–189.

[13] H. Shokry, M. Yuasa, I. Sekine, R. Issa, H. El-Baradie, G. Gomma, Corrosion inhibition of mild steel by Schiff base compounds in various aqueous solutions: part 1, Corros. Sci. 40 (1998) 2173–2186.

[14] A. Fekry, M. Ameer, Corrosion inhibition of mild steel in acidic media using newly synthesized heterocyclic organic molecules, Int. J. Hydrog. Energy. 35 (2010) 7641–7651.

[15] C. Verma, D.K. Verma, E.E. Ebenso, M.A. Quraishi, Sulfur and phosphorus heteroatom-containing compounds as corrosion inhibitors: An overview, Heteroat. Chem. 29 (2018) 1-20.

[16] A.A. Al-Amiery, A.A.H. Kadhum, A.H.M. Alobaidy, A.B. Mohamad, P.S. Hoon, Novel corrosion inhibitor for mild steel in HCl, Materials. 7 (2014) 662–672.

[17] A. Asan, S. Soylu, T. Kıyak, F. Yıldırım, S. Öztaş, N. Ancın, M. Kabasakaloğlu, Investigation on some Schiff bases as corrosion inhibitors for mild steel, Corros. Sci. 48 (2006) 3933–3944.

[18] T. Ahamad, S.M. Alshehri, Thermal, microbial, and corrosion resistant metal-containing poly (Schiff) epoxy coatings, J. Coat. Technol. Res. 9 (2012) 515–523.

[19] B. Clubby, Chemical inhibitors for corrosion control, Royal Soc, Chem Camb. 141 (1990).

[20] M. Gojic, L. Kosec, Corrosion inhibition on iron with propargylic alcohol in acid solutions, ISIJ Int. 37 (1997) 685–690.

[21] M. Metikos-Hukovic, R. Babić, Z. Grubać, S. Brinć, Inhibition of the hydrogen evolution reaction on aluminium covered by ‘spontaneous’ oxide, J. Appl. Electrochem. 24 (1994) 325–331.

[22] H. Awad, S.A. Gawad, Mechanism of inhibition of iron corrosion in hydrochloric acid by pyrimidine and series of its derivatives, Anti-Corros. Methods Mater. (2005).

[23] A.Y. Musa, A.A.H. Kadhum, A.B. Mohamad, M.S. Takriff, Experimental and theoretical study on the inhibition performance of triazole compounds for mild steel corrosion, Corros. Sci. 52 (2010) 3331–3340.

[24] B. Joseph, S. John, A. Joseph, B. Narayana, Imidazolidine-2-thione as corrosion inhibitor for mild steel in hydrochloric acid, 14 (2010) 366-374.

[25] P.C. Okafor, Y. Zheng, Synergistic inhibition behaviour of methylbenzyl quaternary imidazoline derivative and iodide ions on mild steel in H2SO4 solutions, Corros. Sci. 51 (2009) 850–859.

[26] M. Abdel Aal, A. Abdel Wahab, A.E. Saied, A study of the inhibiting action of benzene thiols and related compounds on the corrosion of zinc in acidic media, Corrosion. 37 (1981) 557–563.

[27] M. Desai, J. Talati, N. Shah, Schiff bases of ethylenediamine/triethylenetetramine with benzaldehyde/cinnamic aldehyde/salicylaldehyde as corrosion inhibitors of zinc in sulphuric acid, Anti-Corros. Methods Mater. (2008).

[28] A.S. El Din, A. El Hosary, R. Saleh, J.A. El Kader, Peculiarities in the Behaviour of Thiourea as corrosion-inhibitor, Mater. Corros. 28 (1977) 26–31.

[29] M. Benabdellah, A. Tounsi, K. Khaled, B. Hammouti, Thermodynamic, chemical and electrochemical investigations of 2-mercapto benzimidazole as corrosion inhibitor for mild steel in hydrochloric acid solutions, Arab. J. Chem. 4 (2011) 17–24.

[30] M. Hosseini, S.F. Mertens, M. Ghorbani, M.R. Arshadi, Asymmetrical Schiff bases as inhibitors of mild steel corrosion in sulphuric acid media, Mater. Chem. Phys. 78 (2003) 800–808.

[31] M. Muniandy, A.A. Rahim, H. Osman, A.M. Shah, S. Yahya, P.B. Raja, Investigation of some schiff bases as corrosion inhibitors for aluminium alloy in 0.5 M hydrochloric acid solutions, Surf. Rev. Lett. 18 (2011) 127–133.

[32] M. Shah, A. Patel, G. Mudaliar, N. Shah, Schiff bases of triethylenetetramine as corrosion inhibitors of Zinc in Hydrochloric acid, Port. Electrochimica Acta. 29 (2011) 101–113.

[33] M.Q. Mohammed, Synthesis and characterization of new Schiff bases and evaluation as Corrosion inhibitors, J. Basrah Res. 37 (2011) 116–130.

[34] S.P. Fakrudeen, A. Murthyh , V. Raju , Corrosion inhibition of AA6061 and AA6063 alloy in hydrochloric acid media by Schiff base compounds, J. Chil. Chem. Soc. 57 (2012) 1364–1370.

[35] A.K. Singh, M. Quraishi, Study of some bidentate schiff bases of isatin as corrosion inhibitors for mild steel in hydrochloric acid solution, Int J Electrochem Sci. 7 (2012) 3222–3241.

[36] S. Junaedi, A.A. Al-Amiery, A. Kadihum, A.A.H. Kadhum, A.B. Mohamad, Inhibition effects of a synthesized novel 4-aminoantipyrine derivative on the corrosion of mild steel in hydrochloric acid solution together with quantum chemical studies, Int. J. Mol. Sci. 14 (2013) 11915–11928.

[37] K.C. Emregül, A.A. Akay, O. Atakol, The corrosion inhibition of steel with Schiff base compounds in 2M HCl, Mater. Chem. Phys. 93 (2005) 325–329..

[38] M. Vinutha, T. Venkatesha, Review on mechanistic action of inhibitors on steel corrosion in acidic media, Port. Electrochimica Acta. 34 (2016) 157–184.

[39] D.M. Jamil, A.K. Al-Okbi, S.B. Al-Baghdadi, A.A. Al-Amiery, A. Kadhim, T.S. Gaaz, A.A.H. Kadhum, A.B. Mohamad, Experimental and theoretical studies of Schiff bases as corrosion inhibitors, Chem. Cent. J. 12 (2018) 1–9.

[40] P. Shetty, Schiff bases: An overview of their corrosion inhibition activity in acid media against mild steel, Chem. Eng. Commun. 207 (2020) 985–1029.

[41] V.V. Dhayabaran, I.S. Lydia, J.P. Merlin, P. Srirenganayaki, Inhibition of corrosion of commercial mild steel in presence of tetrazole derivatives in acid medium, Ionics. 10 (2004) 123–125.

[42] R. Upadhyay, S. Mathur, Effect of Schiff's bases as corrosion inhibitors on mild steel in sulphuric acid, E-J. Chem. 4 (2007) 408-414.

[43] G. Elewady, Pyrimidine derivatives as corrosion inhibitors for carbon-steel in 2M hydrochloric acid solution, Int J Electrochem Sci. 3 (2008) 1149.

[44] D. Gopi, E.-S.M. Sherif, V. Manivannan, D. Rajeswari, M. Surendiran, L. Kavitha, Corrosion and corrosion inhibition of mild steel in groundwater at different temperatures by newly synthesized benzotriazole and phosphono derivatives, Ind. Eng. Chem. Res. 53 (2014) 4286–4294.

[45] L.O. Olasunkanmi, I.B. Obot, M.M. Kabanda, E.E. Ebenso, Some quinoxalin-6-yl derivatives as corrosion inhibitors for mild steel in hydrochloric acid: experimental and theoretical studies, J. Phys. Chem. C. 119 (2015) 16004–16019.

[46] P. Singh, V. Srivastava, M. Quraishi, Novel quinoline derivatives as green corrosion inhibitors for mild steel in acidic medium: electrochemical, SEM, AFM, and XPS studies, J. Mol. Liq. 216 (2016) 164–173.

[47] Z.Z. Tasic, M.M. Antonijevic, M.B.P. Mihajlovic, M.B. Radovanovic, The influence of synergistic effects of 5-methyl-1H-benzotriazole and potassium sorbate as well as 5-methyl-1H-benzotriazole and gelatin on the copper corrosion in sulphuric acid solution, J. Mol. Liq. 219 (2016) 463–473.

[48] I. Benmahammed, T. Douadi, S. Issaadi, M. Al-Noaimi, S. Chafaa, Heterocyclic Schiff bases as corrosion inhibitors for carbon steel in 1 M HCl solution: hydrodynamic and synergetic effect, J. Dispers. Sci. Technol. (2019) 1–20.

[49] A. Mishra, J. Aslam, C. Verma, M. Quraishi, E.E. Ebenso, Imidazoles as highly effective heterocyclic corrosion inhibitors for metals and alloys in aqueous electrolytes: A review, J. Taiwan Inst. Chem. Eng. 114 (2020) 341-358.

[50] M. Özcan, İ. Dehri, M. Erbil, Organic sulphur-containing compounds as corrosion inhibitors for mild steel in acidic media: correlation between inhibition efficiency and chemical structure, Appl. Surf. Sci. 236 (2004) 155–164.

[51] H.H. Hassan, E. Abdelghani, M.A. Amin, Inhibition of mild steel corrosion in hydrochloric acid solution by triazole derivatives: Part I. Polarization and EIS studies, Electrochimica Acta. 52 (2007) 6359–6366.

[52] F. Bentiss, M. Lagrenée, Heterocyclic compounds as corrosion inhibitors for mild steel in hydrochloric acid medium-correlation between electronic structure and inhibition efficiency, J Mater Env. Sci. 2 (2011) 13–17.

[53] S. Issaadi, T. Douadi, A. Zouaoui, S. Chafaa, M.A. Khan, G. Bouet, Novel thiophene symmetrical Schiff base compounds as corrosion inhibitor for mild steel in acidic media, Corros. Sci. 53 (2011) 1484–1488.

[54] C. Loto, R. Loto, A. Popoola, Corrosion inhibition of thiourea and thiadiazole derivatives: a review, J. Mater. Environ. Sci. 3 (2012) 885–894.

[55] D. Daoud, T. Douadi, S. Issaadi, S. Chafaa, Adsorption and corrosion inhibition of new synthesized thiophene Schiff base on mild steel X52 in HCl and H2SO4 solutions, Corros. Sci. 79 (2014) 50–58.

[56] A. Aouniti, H. Elmsellem, S. Tighadouini, M. Elazzouzi, S. Radi, A. Chetouani, B. Hammouti, A. Zarrouk, Schiff's base derived from 2-acetyl thiophene as corrosion inhibitor of steel in acidic medium, J. Taibah Univ. Sci. 10 (2016) 774–785.

[57] A. Singh, K. Ansari, J. Haque, P. Dohare, H. Lgaz, R. Salghi, M. Quraishi, Effect of electron donating functional groups on corrosion inhibition of mild steel in hydrochloric acid: Experimental and quantum chemical study, J. Taiwan Inst. Chem. Eng. 82 (2018) 233–251.

[58] I. Obot, N. Obi-Egbedi, A. Eseola, Anticorrosion potential of 2-mesityl-1H-imidazo [4, 5-f][1, 10] phenanthroline on mild steel in sulfuric acid solution: experimental and theoretical study, Ind. Eng. Chem. Res. 50 (2011) 2098–2110.

[59] R. Baskar, M. Gopiraman, D. Kesavan, I.S. Kim, K. Subramanian, Synthesis, characterization, and electrochemical studies of novel biphenyl based compounds, Ind. Eng. Chem. Res. 51 (2012) 3966–3974.

[60] K. Shaju, V.P. Raphael, others, Effect of iodide on the corrosion inhibitive behaviour on carbon steel by an azomethine compound derived from anthracene-9 (10 H)-one, Orient. J. Chem. 30 (2014) 807–813.

[61] U. Ekpe, U. Ibok, B. Ita, O. Offiong, E. Ebenso, Inhibitory action of methyl and phenyl thiosemicarbazone derivatives on the corrosion of mild steel in hydrochloric acid, Mater. Chem. Phys. 40 (1995) 87–93.

[62] E. Ebenso, U. Ekpe, B. Ita, O. Offiong, U. Ibok, Effect of molecular structure on the efficiency of amides and thiosemicarbazones used for corrosion inhibition of mild steel in hydrochloric acid, Mater. Chem. Phys. 60 (1999) 79–90.

[63] M. Lashkari, M. Arshadi, DFT studies of pyridine corrosion inhibitors in electrical double layer: solvent, substrate, and electric field effects, Chem. Phys. 299 (2004) 131–137.

[64] S. Abd El-Maksoud, A. Fouda, Some pyridine derivatives as corrosion inhibitors for carbon steel in acidic medium, Mater. Chem. Phys. 93 (2005) 84–90.

[65] F. Kandemirli, S. Sagdinc, Theoretical study of corrosion inhibition of amides and thiosemicarbazones, Corros. Sci. 49 (2007) 2118–2130.

[66] A. Ghazoui, R. Saddik, N. Benchat, M. Guenbour, B. Hammouti, S. Al-Deyab, A. Zarrouk, Comparative study of pyridine and pyrimidine derivatives as corrosion inhibitors of C38 steel in molar HCl, Int J Electrochem Sci. 7 (2012) 7080–7097.

[67] V.P. Raphael, K.J. Thomas, K. Shaju, A. Paul, Corrosion inhibition investigations of 3-acetylpyridine semicarbazone on carbon steel in hydrochloric acid medium, Res. Chem. Intermed. 40 (2014) 2689–2701.

[68] P. Mourya, P. Singh, R. Rastogi, M. Singh, Inhibition of mild steel corrosion by 1, 4, 6-trimethyl-2-oxo-1, 2-dihydropyridine-3-carbonitrile and synergistic effect of halide ion in 0.5 M H2SO4, Appl. Surf. Sci. 380 (2016) 141–150.

[69] W. Zhang, H.-J. Li, Y. Wang, Y. Liu, Y.-C. Wu, Adsorption and corrosion inhibition properties of pyridine-2-aldehyde-2-quinolylhydrazone for Q235 steel in acid medium: Electrochemical, thermodynamic, and surface studies, Mater. Corros. 69 (2018) 1638–1648.

[70] N.N. Hazani, Y. Mohd, S.A.I.S.M. Ghazali, Y. Farina, N.N. Dzulkifli, Electrochemical Studies on Corrosion Inhibition Behaviour of Synthesised 2-acetylpyridine 4-ethyl-3-thiosemicarbazone and Its Tin(IV) Complex for Mild Steel in 1 M HCl Solution, J. Electrochem. Sci. Technol. 10 (2019) 29–36.

[71] G. Avci, Corrosion inhibition of indole-3-acetic acid on mild steel in 0.5 M HCl, Colloids Surf. Physicochem. Eng. Asp. 317 (2008) 730–736.

[72] M. Lebrini, F. Robert, H. Vezin, C. Roos, Electrochemical and quantum chemical studies of some indole derivatives as corrosion inhibitors for C38 steel in molar hydrochloric acid, Corros. Sci. 52 (2010) 3367–3376.

[73] A. Paul, K. Joby Thomas, V.P. Raphael, K. Shaju, Electrochemical and Gravimetric Corrosion Inhibition Investigations of A Heterocyclic Schiff Base Derived From 3-Formylindole., Rct. 100 (2012) 3.

[74] A. Fouda, K. Shalabi, H. Elmogazy, Corrosion inhibition of α-brass in HNO3 by indole and 2-oxyindole, J Mater Env. Sci. 5 (2014) 1691.

[75] X. Ma, X. Jiang, S. Xia, M. Shan, X. Li, L. Yu, Q. Tang, New corrosion inhibitor acrylamide methyl ether for mild steel in 1 M HCl, Appl. Surf. Sci. 371 (2016) 248–257.

[76] C. Li, P. Wang, S. Sun, K. Voisey, D. McCartney, Corrosion behaviour of Al86. 0Co7. 6Ce6. 4 glass forming alloy with different microstructures, Appl. Surf. Sci. 384 (2016) 116–124.

[77] Z. He, F. Mansfeld, Exploring the use of electrochemical impedance spectroscopy (EIS) in microbial fuel cell studies, Energy Environ. Sci. 2 (2009) 215–219.

[78] A. v Homborg, E. Van Westing, T. Tinga, X. Zhang, P. Oonincx, G. d Ferrari, J. De Wit, J. Mol, Novel time–frequency characterization of electrochemical noise data in corrosion studies using Hilbert spectra, Corros. Sci. 66 (2013) 97–110.

[79] T.K. Chaitra, K.N.S. Mohana, H.C. Tandon, Thermodynamic, electrochemical and quantum chemical evaluation of some triazole Schiff bases as mild steel corrosion inhibitors in acid media, J. Mol. Liq. 211 (2015) 1026–1038.

[80] M. Goyal, R. Kumar, O.S. Yadav, R. Sharma, G. Singh, others, Experimental, surface characterization and computational evaluation of the acid corrosion inhibition of mild steel by methoxycarbonylmethyltriphenylphosphonium bromide (MCMTPPB), Indian J. Chem. Technol. IJCT. 24 (2017) 256–268.

[81] Y. Wang, Y. Zuo, X. Zhao, S. Zha, The adsorption and inhibition effect of calcium lignosulfonate on Q235 carbon steel in simulated concrete pore solution, Appl. Surf. Sci. 379 (2016) 98–110.

[82] N. Vlachos, Y. Skopelitis, M. Psaroudaki, V. Konstantinidou, A. Chatzilazarou, E. Tegou, Applications of Fourier transform-infrared spectroscopy to edible oils, Anal. Chim. Acta. 573 (2006) 459–465.

[83] V. Kuz'min, V. Lozitsky, G. Kamalov, R. Lozitskaya, A. Zheltvay, A. Fedtchouk, D. Kryzhanovsky, Analysis of the structure-anticancer activity relationship in a set of Schiff bases of macrocyclic 2, 6-bis (2-and 4-formylaryloxymethyl) pyridines., Acta Biochim. Pol. 47 (2000) 867–875.

[84] H. Hamani, T. Douadi, D. Daoud, M. Al-Noaimi, S. Chafaa, Corrosion inhibition efficiency and adsorption behavior of azomethine compounds at mild steel/hydrochloric acid interface, Measurement. 94 (2016) 837–846.

[85] B. Ateya, B. El-Anadouli, F. El-Nizamy, The adsorption of thiourea on mild steel, Corros. Sci. 24 (1984) 509–515.

[86] T. Zhao, G. Mu, The adsorption and corrosion inhibition of anion surfactants on aluminium surface in hydrochloric acid, Corros. Sci. 41 (1999) 1937–1944.

[87] N. Soltani, H. Salavati, N. Rasouli, M. Paziresh, A. Moghadasi, Adsorption and corrosion inhibition effect of Schiff base ligands on low carbon steel corrosion in hydrochloric acid solution, Chem. Eng. Commun. 203 (2016) 840–854.

[88] M. Bedair, M. El-Sabbah, A. Fouda, H. Elaryian, Synthesis, electrochemical and quantum chemical studies of some prepared surfactants based on azodye and Schiff base as corrosion inhibitors for steel in acid medium, Corros. Sci. 128 (2017) 54–72.

[89] M. Bouklah, N. Benchat, B. Hammouti, A. Aouniti, S. Kertit, Thermodynamic characterisation of steel corrosion and inhibitor adsorption of pyridazine compounds in 0.5 M H2SO4, Mater. Lett. 60 (2006) 1901–1905.

[90] J.R. Macdonald, E. Barsoukov, Impedance spectroscopy: theory, experiment, and applications, History. 1 (2005) 1–13.

[91] A. Xu, X. Wu, H. Xu, F. Jin, G. Wang, Electrochemical impedance spectroscopy (EIS) study of vehicle protective coating performance, in: ICCTP 2011 Sustain. Transp. Syst., 2011: pp. 3827–3834.

[92] B.M. Mistry, N.S. Patel, M.J. Patel, S. Jauhari, Corrosion inhibition performance of 1, 3, 5-triazinyl urea derivatives as a corrosion inhibitor for mild steel in 1 N HCL, Res. Chem. Intermed. 37 (2011) 659–671.

[93] F. Mansfeld, M. Kendig, Evaluation of Protective Coatings with Impedance Measurements, in: F Mansfeld M Kendig Rockwell Int. Sci. Cent. Thousand Oaks CA 91360 Intl Congr. Met. Corr, 1984.

[94] G. Reinhard, U. Rammelt, Discussion and application of impedance testing in corrosion protection investigations, Corrosion. 15 (1984) 175–193.

[95] T. Strivens, C. Taylor, An assessment of A/C impedance as a basic research and routine testing method for studying corrosion of metals under paint films, Mater. Chem. 7 (1982) 199–220.

[96] F. Mansfeld, M. Kendig, Concerning the choice of scan rate in polarization measurements, Corrosion. 37 (1981) 545–546.

[97] A. Mohamed, H. Mostafa, G. El-Ewady, A. Fouda, 10. DD Macdonald, Transient Techniques in Electrochemistry, Plenum Press, New York, Port. Electrochimica Acta. 18 (2000) 99–111.

[98] K.C. Emregül, O. Atakol, Corrosion inhibition of iron in 1 M HCl solution with Schiff base compounds and derivatives, Mater. Chem. Phys. 83 (2004) 373–379.

[99] F. Bentiss, M. Lagrenee, M. Traisnel, J. Hornez, Corrosion inhibition of mild steel in 1 M hydrochloric acid by 2, 5-bis (2-aminophenyl)-1,3,4-oxadiazole, Corrosion. 55 (1999) 968–976.

[100] P.G. Grützmacher, F.J. Profito, A. Rosenkranz, Multi-scale surface texturing in tribology—Current knowledge and future perspectives, Lubricants. 7 (2019) 95-112.

[101] D. Gopi, K. Govindaraju, L. Kavitha, Investigation of triazole derived Schiff bases as corrosion inhibitors for mild steel in hydrochloric acid medium, J. Appl. Electrochem. 40 (2010) 1349–1356.

[102] K.C. Emregül, R. Kurtaran, O. Atakol, An investigation of chloride-substituted Schiff bases as corrosion inhibitors for steel, Corros. Sci. 45 (2003) 2803–2817.

[103] J. Smulko, K. Darowicki, A. Zieliński, Pitting corrosion in steel and electrochemical noise intensity, Electrochem. Commun. 4 (2002) 388–391.

[104] S. Abd El Wanees, M.I. Alahmdi, M. Abd El Azzem, H.E. Ahmed, 4, 6-Dimethyl-2-oxo-1, 2-dihydropyridine-3-carboxylic acid as an inhibitor towards the corrosion of C-steel in acetic acid, Inter J Electrochem Sci. 11 (2016) 3448–3466.

[105] J. Chen, W. Bogaerts, The physical meaning of noise resistance, Corros. Sci. 37 (1995) 1839–1842.

[106] Y. Tan, S. Bailey, B. Kinsella, The monitoring of the formation and destruction of corrosion inhibitor films using electrochemical noise analysis (ENA), Corros. Sci. 38 (1996) 1681–1695.

[107] F. Mansfeld, Z. Sun, C. Hsu, A. Nagiub, Concerning trend removal in electrochemical noise measurements, Corros. Sci. 43 (2001) 341–352.

[108] H. Ashassi-Sorkhabi, D. Seifzadeh, M. Raghibi-Boroujeni, Analysis of electro chemical noise data in both time and frequency domains to evaluate the effect of ZnO nanopowder addition on the corrosion protection performance of epoxy coatings, Arab. J. Chem. 9 (2016)1320–S1327.

[109] A. Homborg, P. Oonincx, J. Mol, Wavelet transform modulus maxima and holder exponents combined with transient detection for the differentiation of pitting corrosion using electrochemical noise, Corrosion. 74 (2018) 1001–1010.

[110] S.F. Burch, S.F. Gull, J. Skilling, Image restoration by a powerful maximum entropy method, Comput. Vis. Graph. Image Process. 23 (1983) 113–128.

[111] D.K. Yadav, M. Quraishi, B. Maiti, Inhibition effect of some benzylidenes on mild steel in 1 M HCl: an experimental and theoretical correlation, Corros. Sci. 55 (2012) 254–266.

[112] S. Benabid, T. Douadi, S. Issaadi, C. Penverne, S. Chafaa, Electrochemical and DFT studies of a new synthesized Schiff base as corrosion inhibitor in 1 M HCl, Measurement. 99 (2017) 53–63.

[113] H. Hamani, T. Douadi, M. Al-Noaimi, S. Issaadi, D. Daoud, S. Chafaa, Electrochemical and quantum chemical studies of some azomethine compounds as corrosion inhibitors for mild steel in 1 M hydrochloric acid, Corros. Sci. 88 (2014) 234–245.

[114] V. Sastri, J. Perumareddi, Molecular orbital theoretical studies of some organic corrosion inhibitors, Corrosion. 53 (1997) 617–622.

[115] M. Shahraki, M. Dehdab, S. Elmi, Theoretical studies on the corrosion inhibition performance of three amine derivatives on carbon steel: Molecular dynamics simulation and density functional theory approaches, J. Taiwan Inst. Chem. Eng. 62 (2016) 313–321.

[116] A. Fouda, M. Ismail, G. EL-ewady, A. Abousalem, Evaluation of 4-amidinophenyl-2, 2′-bithiophene and its aza-analogue as novel corrosion inhibitors for CS in acidic media: experimental and theoretical study, J. Mol. Liq. 240 (2017) 372–388.

[117] P. Senet, Chemical hardnesses of atoms and molecules from frontier orbitals, Chem. Phys. Lett. 275 (1997) 527–532.

[118] A. Béchamp, De l'action des protosels de fer sur la nitronaphtaline et al nitrobenzine;: nouvelle méthode de formation des bases orgnaiques artificielles de zinin, (1854) 1-25.

[119] E. Cano, J. Polo, A. La Iglesia, J. Bastidas, A study on the adsorption of benzotriazole on copper in hydrochloric acid using the inflection point of the isotherm, Adsorption. 10 (2004) 219–225.

[120] D.P. Schweinsberg, G.A. George, A.K. Nanayakkara, D.A. Steinert, The protective action of epoxy resins and curing agents—inhibitive effects on the aqueous acid corrosion of iron and steel, Corrosion Science. 28 (1988) 33–42.

[121] H. Shokry, M. Yuasa, I. Sekine, R. Issa, H. El-Baradie, G. Gomma, Corrosion inhibition of mild steel by Schiff base compounds in various aqueous solutions: part 1, Corrosion Science. 40 (1998) 2173–2186.

[122] A. v Homborg, E. Van Westing, T. Tinga, X. Zhang, P. Oonincx, G. d Ferrari, J. De Wit, J. Mol, Novel time–frequency characterization of electrochemical noise data in corrosion studies using Hilbert spectra, Corrosion Science. 66 (2013) 97–110.

LIST OF PUBLICATIONS

1. **Reeja Johnson,** Joby Thomas Kakkassery K, Vinod Raphael Palayoor, Ragi Kooliyat and Vidhya Thomas Kannanaikkal, "Experimental and Theoretical Investigations on the Corrosion Inhibition Action of Thiadiazole Derivatives on Carbon Steel in 1M HCl medium", *Oriental Journal of Chemistry,* 36(6), 1179-1188, 2020.
   doi: http://dx.doi.org/10.13005/ojc/360624
2. Vidhya Thomas K; Joby Thomas. K; Vinod P Raphael; A S Sabu; K Ragi; **Reeja Johnson,"** *Tinospora cordifolia* Extract as an Environmentally Benign Green Corrosion Inhibitor in Acid Media: Adsorption, Surface Morphological, Quantum Chemical and Statistical Investigations", *Materials Today Sustainability,* 13, 100076, 2021 doi: https://doi.org/10.1016/j.mtsust.2021.100076
3. Vidhya K Thomas, Joby K Thomas, Vinod P Raphael, Ragi K, **Reeja Johnson** and Ramesh Babu "Green Corrosion Inhibition Properties of *Croton Persimilis* Extract on Mild Steel in Acid Media" *Journal of Bio and Tribo corrosion,* 7(121),1-19, 2021 doi: https://doi.org/10.1007/s40735-021-00554-z)
4. Ragi K, Joby Thomas Kakkassery, Vinod P. Raphael, **Reeja Johnson** and Vidhya Thomas K "*In vitro* Antibacterial and *In Silico* Docking Studies of Two Schiff Bases on *Staphylococcus aureus* and its Target Proteins". *Future Journal of Pharmaceutical Sciences*, 7(1), 1-9, 2021 doi: https://doi.org/10.1186/s43094-021-00225-3
5. Ragi K**,** Joby Thomas Kakkassery, Vinod P. Raphael, Binsi M. Paulson and **Reeja Johnson**, "Corrosion Inhibition of Mild steel by N,N'-(5,5-dimethylcyclohexane-1,3-diylidene)dianiline in Acid Media: Gravimetric and Electrochemical Evaluations", *Current Chemistry Letters*, 9, 1-14, 2020 doi: 10.5267/j.ccl.2020.8.001
6. M. Paulson Binsi, Thomas K. Joby, K. Ragi, Varghese C. Sini and **Johnson Reeja**. "Interaction of Two Heterocyclic Schiff Bases Derived from 2-acetyl pyridine on Mild

Steel in Hydrochloric acid: Physicochemical and Corrosion Inhibition Investigations", *Current Chemistry Letters,* 9, 19-30, 2019 doi: 10.5267/j.ccl.2019.6.005

7. Vidhya Thomas K, Joby Thomas K, Vinod P Raphael, Ragi K and **Reeja Johnson,** "*Ixora coccinea* Extract as an Efficient Eco-Friendly Corrosion Inhibitor in Acidic Media: Experimental and Theoretical Approach", *Current Chemistry Letters,* 10(3), 139-50, 2021 doi: http://dx.doi.org/10.5267/j.ccl.2020.12.001
8. Aby Paul, Joby Thomas K, **Reeja Johnson** and Sini Varghese C, "Transition Metal Complexes of (z)-4-((1H-indole-3-yl)methyleneamine)benzoic acid: Synthesis, Structural and Antibacterial studies" *Chemical Science Reviews and Letters*, 4(13), 292-298, 2015
9. Paul. A, Thomas J and **Johnson R,** "Thermal Decomposition Kinetics and mechanism on Mn(II), Ni(II) and Cu(II) complexes of 3-Formyl Indole-2-amino5-Bromo Benzoic acid", *International Journal of Engineering, Science and Mathematics*, 7(2), 25-30, 2018
10. Aby Paul, Joby Thomas K, Sini Varghese C and **Reeja Johnson** "Evaluation on Structural and Thermoanalytical Properties of a Novel Heterocyclic Schiff base Derived from 3-formylindole and Its Metal Chelates" *Chemical Science Reviews and Letters*, 4(13), 278-284, 2015
11. Aby Paul, Joby Thomas K, Sini Varghese C and **Reeja Johnson** "Chelating competency and Antibacterial Properties of (E)-2-((1H-indol-3-yl)metheneamino)-5-bromobenzoic acid and Its Metal Chelates" *International Journal of Research in Chemistry and Environment*, 6(2), 50-54, 2016

LIST OF CONFERENCE PAPERS

1. **Reeja Johnson** and Joby Thomas K, "Electrochemical Corrosion Investigations on

(13E)-N1,N2-bis((thiophen-2-yl)methylene)cyclohexane-1,2-diamine on Mild steel in 1.0M HCl", International Conference on Chemistry and Physics of Materials ICCPM, St.Thomas' College (Autonomous), Thrissur, Dec 19-21, 2018

2. **Reeja Johnson**, Aby Paul, Joby Thomas K, Binsi M. Paulson and Sini Varghese C, "Synthetic, Structure and Antibacterial Analysis of Ni(ll), Cu(ll) and Cd(ll) Complexes of (z)-3-((1H-Indol-3-yl)methyleneamino) benzoic acid", UGC Sponsored National Seminar on Organic Synthesis at St. Joseph's College, Irinjalakuda, Jan 22-23, 2015
3. **Reeja Johnson**, Joby Thomas K and Sangeetha M, "Electrochemical investigations on the "Corrosion Inhibition Properties of N-(Anthracene-9(10H)-Ylidene)-5-(4-nitrophenyl)-1,3,4-Thiadiazole-2-amine on Mild Steel", UGC Sponsered National Seminar on Recent Trends in Chemical Science in Carmel College, Mala, Aug 13-14, 2014
4. Jaicy Joy K, Joby Thomas K., **Reeja Johnson** and Sini Varghese C, "Synthesis and Characterisation of Novel Schiff Base, N-(Anthracen-9(10H)-ylidene)-5-(4-nitrophenyl)-1,3,4-thiadiazol-2-amine and its Transition Metal Complexes", National Seminar on Recent Trends in Chemical Sciences, Carmel College, Mala, Aug 13-14, 2014
5. Shafna Jose, Joby Thomas K, **Reeja Johnson** and Sini Varghese C, "Gravimetric Weight Loss Studies on Imine Derivatives of 5-(4-nitrophenyl)-1,3,4-thiadiazol-2-amine in Acid Medium", UGC sponsored National Seminar on Recent Trends in Chemical Science, Carmel College, Mala, Aug 13-14, 2014
6. Aby Paul, Joby Thomas K, **Reeja Johnson** and Sini Varghese C, "Studies on Physicochemical and Thermal properties of Mn(II) and Cu(II) Chelate of 3-Formyl indole-2-amino-5-nitro benzoic acid", UGC Sponsored National Seminar Advanced Topics in Chemistry, Sree Narayana College, Nattika, Aug 19-20, 2015 (**Best Poster Award**)

7. Aby Paul, Joby Thomas K, Sini Varghese C, **Reeja Johnson** and Binsi M Paulson, "Evaluation of Anticorrosive Properties of 3-Formylindole-2-amino Benzoic Acid and 3-Formylindole-3-amino Benzoic Acid: on Copper in HCl Media," UGC Sponsored National Seminar on Advanced Topics in Chemistry, Sree Narayana College, Nattika, Aug 19-20, 2015
8. Aby Paul, Joby Thomas K, Binsi M Paulson,Sini Varghese C and **Reeja Johnson,** "Vo(ll), Cr(ll) and Fe(lll) Complexes of (Z)-3-((1H-indol-3-yl)methyleneamino) Benzoic Acid," UGC Sponsored National seminar on Green Technologies for Green Environment, S.N.M. College Maliankara, Dec 3-4, 2015
9. Binsi M Paulson, Joby Thomas K, Ragi K, Sini Varghese C and **Reeja Johnson**, "Corrosion Inhibition Efficacy of 2-Acetylpyridine Phenyl Hydrazone on Mild Steel in Acid Media: Physicochemical and Electrochemical investigations", DST Sponsored International Conference on Materials for the Millennium MATCON 2019, Cochin University of Science and Technology, Mar 14-16, 2019
10. Vidhya Thomas K, Joby Thomas K, Ragi. K and **Reeja Johnson**, "Excellent Eco-friendly Corrosion Inhibition Behaviour of *Croton Persimilis* Extract (CPE) for Mild Steel in Acidic Media: Physicochemical, Electrochemical and Surface Morphological Studies", National Seminar on Current Trends in Chemistry (CTriC 2020), Cochin University of Science and Technology, Feb 6-7, 2020
11. Aby Paul, Joby Thomas, Binsi M Paulson, **Reeja Johnson** and Sini Varghese, "Preparation, Chacterisation and Antimicrobial Studies on Transition Metal Complexes of (Z)-2-(1H-indol-3-yl)methyleneamino)-5-nitrobenzoic acid" UGC Sponsered National Seminar on Recent Trends in Chemistry, St. Mary's College, Thrissur, Aug 19-20, 2015

PAPERS COMMUNICATED

1. **Pharmaceutical Chemistry Journal-Springer**

   Reeja Johnson, Joby Thomas Kakkassery, Vinod Raphael Palayoor, Deeya Kuriakose, Vidhya Thomas Kannanaikkal and Binsi M. Paulson, "Inhibitory Competency of Novel Thiadiazole Derivatives on HIV-1 Protease, Human Epidermal Growth Factor Receptor and Acetylcholinesterase: An *In Silico* Analysis" (**Communicated**)

2. **Portugaliae Electrochimica Acta (Elsevier Database / Scopus indexed)**

   J. Reeja, K. Joby Thomas, K. Ragi and M. P. Binsi, "Screening of Corrosion Inhibition Properties of Two Sulphur Containing Schiff Bases on Carbon Steel: Electrochemical and Quantum Chemical Studies" (**Communicated**)